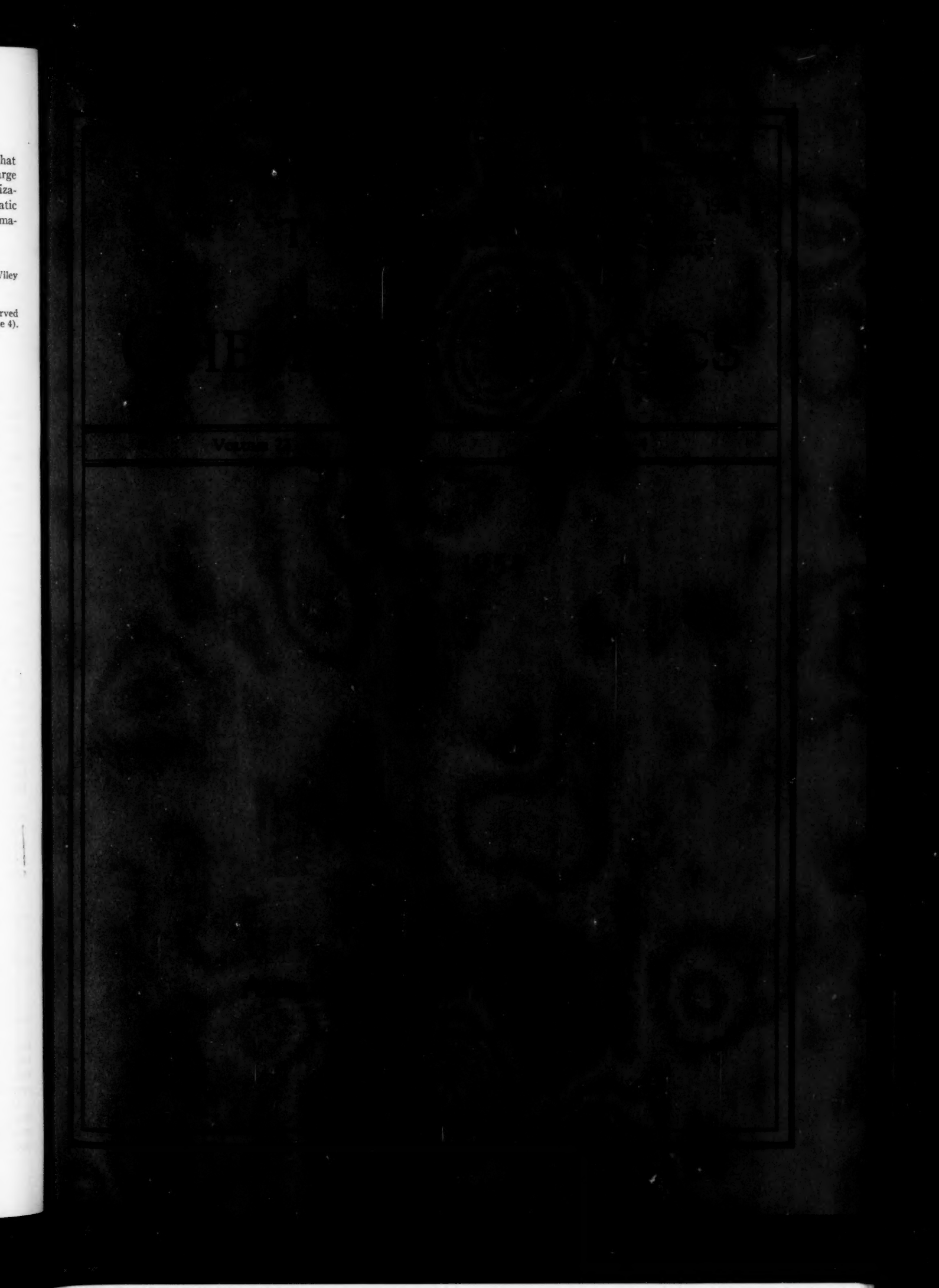

THE JOURNAL
OF
CHEMICAL PHYSICS

VOLUME 22, NUMBER 4 APRIL, 1954

The Rate Constant of the Reaction between Hydrogen Peroxide and Ferrous Ions

TYSON RIGG, WILLIAM TAYLOR, AND JOSEPH WEISS
University of Durham, King's College, Newcastle upon Tyne, England
(Received October 9, 1953)

The rate constant of the reaction between hydrogen peroxide and ferrous ions has been measured in sulfuric acid solutions, by direct spectrophotometric observations of the ferric salt produced at $\lambda=304$ mμ. It has been confirmed that the rate is independent of acidity (measurements were carried out from 0.05 N to 0.8 N H_2SO_4) and that the reaction is bimolecular within a wide range of the concentrations of the reactants; the hydrogen peroxide concentration was varied in the ratio 1:25 and the ferrous sulfate in the ratio 1:20. The rate constant, which has been measured within the temperature range of 15° to 40°C, can be represented by the equation

$$k_1=1.05\times10^8\times\exp(-8460/RT)1 \text{ moles}^{-1} \text{ sec}^{-1}.$$

IT has been shown by Haber and Weiss[1] that the reaction between hydrogen peroxide and ferrous ions can, under certain conditions, be described by the following two consecutive reactions:

$$Fe^{2+}+H_2O_2\rightarrow Fe^{3+}+OH^-+OH \quad (k_1), \qquad (1)$$

$$Fe^{2+}+OH \rightarrow Fe^{3+}+OH^-, \qquad (2)$$

which correspond to the simple stoichiometry

$$2Fe^{2+}+H_2O_2\rightarrow 2Fe^{3+}+2OH^-. \qquad (3)$$

In this case, the rate of the reaction, in the stationary state, is given by the simple differential equation

$$-d(Fe^{2+})/dt=d(Fe^{3+})/dt=2k_1[Fe^{2+}][H_2O_2] \qquad (4)$$

corresponding to the bimolecular reaction between hydrogen peroxide and ferrous ions according to Eq. (1). It is thus possible to measure the rate constant k_1 directly. This constant has been the object of several investigations, but up to the present no concordant results have been obtained. The first measurements of Haber and Weiss,[1] in the temperature range from 6° to 45°C, were carried out by means of a simple flow apparatus. The measurements reported subsequently[2,3] employed a colorimetric method and involved stopping of the reaction with α, α'dipyridyl.

More recently, some preliminary measurements have been reported by Taylor and Weiss,[4] who followed the course of the reaction by measuring the light absorption of the ferric salt produced in a silica cell which also served as the reaction vessel. This method appeared to be very satisfactory, particularly because the course of the reaction can be followed continuously. Unfortunately, the values which were given in this preliminary note[4] were marred by an arithmetical error in one of the initial concentrations.

We have reinvestigated this reaction over a wide range of concentration and temperature, and we have also checked the stoichiometry of this reaction, as it had been suggested previously[3] that, particularly at a low concentration of the reactants, side reactions with impurities in the water are liable to occur, which influence the accuracy of the results.

EXPERIMENTAL

The course of the reaction was followed by spectrophotometric measurement of the ferric salt formed at $\lambda=304$ mμ. The instrument used was a "Unicam" spectrophotometer ("S.P. 500"), which had been modified so that the absorption cells (in this case also the reaction cell) could be maintained at any desired temperature, in this case in the range from 15° to 40°C.

[1] F. Haber and J. Weiss, Proc. Roy. Soc. (London) **A147**, 332 (1934).
[2] Baxendale, Evans, and Park, Trans. Faraday Soc. **42**, 155 (1946).
[3] Barb, Baxendale, George, and Hargrave, Trans. Faraday Soc. **47**, 462 (1951).
[4] W. Taylor and J. Weiss, J. Chem. Phys. **21**, 1419 (1953).

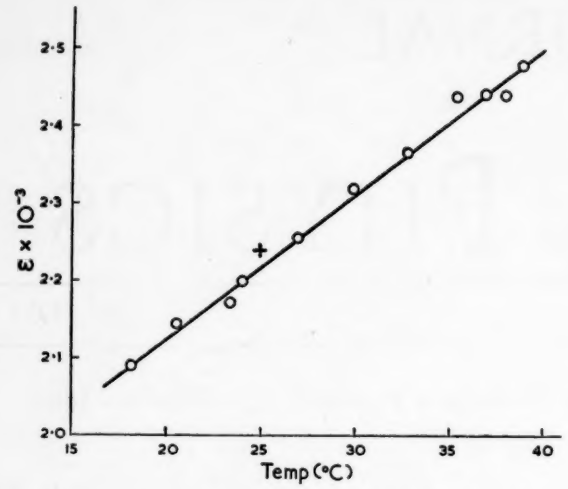

FIG. 1. Temperature dependence of the molar extinction coefficient at $\lambda = 304$ mμ. Ferric sulfate in 0.80 N sulfuric acid.
(+) corresponds to the value obtained by Hochanadel and Ghormley (see reference 7).

This was achieved by circulating water, from a thermostated tank, at a relatively high rate of flow, around the cells in a specially constructed cell carriage. The temperature of the reaction cells could be determined by placing a thermometer directly into the liquid in the cells.

The solutions used were prepared from specially distilled (stabilizer-free) hydrogen peroxide and ferrous sulfate, "AnalaR," which contained less than 0.1 percent ferric salt. Stock solutions (about millimolar) were prepared and diluted for use as required. It was found that ferrous sulfate in acid solution was completely stable; hydrogen peroxide (acidified) showed only a slight decrease in several weeks. The latter was standardized with potassium permanganate, the ultimate standard being oxalic acid. Ferrous salt was determined by titration with ceric ammonium sulfate, using α,α′-dipyridyl as indicator;[5] the standard in this case was arsenious oxide. Some of the diluted hydrogen peroxide solutions were checked with the titanium sulfate (colorimetric) method of Eisenberg.[6] The sulfuric acid ("AnalaR") was standardized with sodium hydroxide previously checked against oxalic acid. The water used was prepared by triple distillation; ordinary distilled water was distilled from alkaline permanganate and then again from dilute phosphoric acid in an all-glass still.

TABLE I.

Temp. (°C)	Conc. of sulfuric acid (normality)	Initial conc. (moles/l) ×10⁶ $[Fe^{2+}]_0$	$[H_2O_2]_0$	k_1 (l mole^{-1} sec^{-1})
15.1	0.5	273	88.4	40.8
15.1	0.5	191	66.7	41.6
18.6	0.8	51.5	26.3	47.8
20.0	0.5	273	160	50.6
20.0	0.5	136	64.7	51.4
20.6	0.05	49	12.3	59
23.8	0.8	12.8	6.6	64
23.8	0.8	52.25	26.5	63.5
25.1	0.5	273	64.7	63.5
25.1	0.5	273	102	64.6
29.1	0.8	50.15	25.4	82.5
33.7	0.8	50.15	25.4	100
35.5	0.5	262	105	101.2
40.0	0.5	136	64	127.4
40.0	0.5	273	142	123

[5] C. J. van Nieuwenburg and A. B. Blumendal, Mikrochem. **18**, 39 (1935).

Rapid mixing of the ferrous salt and hydrogen peroxide in appropriately acidified solutions was carried out by pouring 50 ml of each simultaneously into a 250-ml beaker, stirring, and pouring some of the mixture into the absorption cell. Readings of the optical density could be obtained 30 sec after mixing and could then be made as frequently as desired, up to completion of the reaction. The solutions were thermostated before use and the mixing beaker and silica cells were warmed up to the required temperature.

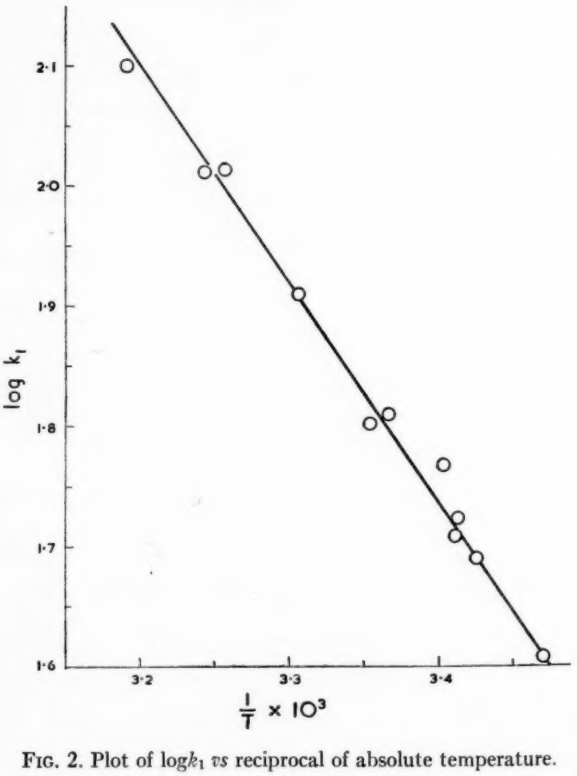

FIG. 2. Plot of logk_1 *vs* reciprocal of absolute temperature.

Ferric standards were prepared by treating an accurately known quantity of ferrous salt with excess hydrogen peroxide, boiling to decompose the excess, and diluting to a known volume. The extinction coefficient (ϵ) of ferric sulfate in sulfuric acid (0.8 N) was found to vary with temperature in the manner shown in Fig. 1. The molar extinction coefficient was found to be about 4 percent lower in 0.05 N acid and showed a variation parallel to that in the more strongly acid solutions, in

[6] G. M. Eisenberg, Ind. Eng. Chem. (Anal. Ed.) **15**, 327 (1943).

the temperature range 18° to 25°C. The wavelength of maximum absorption (at $\lambda=304$ mμ) was not appreciably affected by change in the acidity. The value of ϵ in 0.8 N acid at 25°C is in good agreement with the value given by Hochanadel and Ghormley.[7]

RESULTS

Some of the experimental results are listed in Table I and the mean values of k_1 for different temperatures are given in Table II. The Arrhenius plot of these results is shown in Fig. 2. The values of k_1 in Table I have been derived from logarithmic plots, using the equation

$$k_1 t=\frac{2.3}{(2a-b)}\log\frac{b(a-x/2)}{a(b-x)}, \tag{5}$$

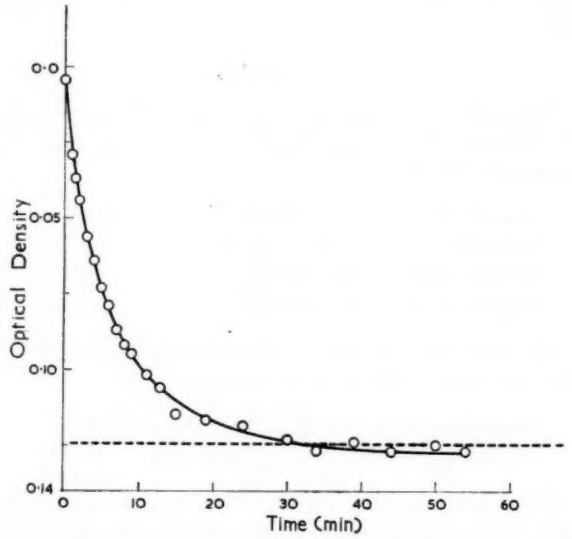

FIG. 3. Increase of the optical density at $\lambda=304$ mμ. (2-cm silica cell) for initial concentrations. $[H_2O_2]_0=1.325\times10^{-5}$ moles/1 and $[Fe^{2+}]_0=5.15\times10^{5}$ moles/1 in 0.8 N sulfuric acid solutions at 23.8°C. The straight line corresponds to the theoretical amount of ferric salt produced according to the simple stoichiometry [Eq. (3)].

where $[H_2O_2]_{t=0}=a$, $[Fe^{2+}]_{t=0}=b$, $[Fe^{3+}]_{t=t}=x$. In those cases where $b=2a$, the time of half-change ($t_{\frac{1}{2}}$) or the time between half- and three-quarter change was used to determine k_1 according to the equation

$$k_1 t=\frac{1}{2a}.$$

[7] C. J. Hochanadel and J. A. Ghormley, J. Chem. Phys. **21**, 880 (1953).

TABLE II.

Conc. of sulfuric acid (normality)	Temp. °C	k_1 (mean) (1 moles^{-1} sec^{-1})
0.5	15.1	40.5±2.0
0.8	18.6	48.9±2.5
0.8	19.75	52.8±2.5
0.5	20.0	51.0±2.5
0.05	20.6	58.8±3.0
0.8	23.8	64.4±3.0
0.5	25.1	63.4±3.0
0.8	29.1	81.2±4.0
0.8	33.7	102.8±5.0
0.5	35.5	102.5±5.0
0.5	40.0	125.2±6.0

DISCUSSION

Barb *et al.*[3] had some difficulty in obtaining the stoichiometric ratio $(\Delta Fe^{II}/\Delta H_2O_2)=2.0$, corresponding to Eq. (3) and at initial concentrations of the reactants, similar to some of those used in the present work, they reported values for this ratio up to 4.

In the present work no such difficulty was experienced and this ratio was always found to be 2.0, within the limits of experimental error. An example of this is given in Fig. 3, which shows that the amount of ferric salt produced, when the reaction is followed to completion, corresponds very closely to the hydrogen peroxide used up, according to Eq. (3). Water from three different stills did not affect either the values of k_1 or the stoichiometry.

From Fig. 2 it is found that the rate constant can be represented, in the temperature range 15° to 40°C, by

$$k_1=1.05\times10^{8}\exp(-8460/RT)\ 1\ \text{mole}^{-1}\ \text{sec}^{-1}. \tag{7}$$

In the range 20° to 25°C this is in closer agreement with the earlier results of Baxendale, Evans, and Park[2] than with the more recent measurements of Barb *et al.*[3]

From Eq. (7) a value of $E=8460$ cal follows for the energy of activation: this is rather lower than the values 10 100 cal and 9400 cal given by the aforementioned authors,[2,3] respectively, but is in good agreement with the older value of Haber and Weiss (8500 cal)[1] although, in the latter case, there is a difference of about a factor of two in the nonexponential factor.

In a very recent publication[8] values for the rate constant at 18° and 25°C have been reported; these were determined by stopping the reaction with *o*-phenanthroline and colorimetric determination of the ferrous salt. While the value for 25°C is in very good agreement with the value given in this work, that at 18°C is lower by nearly 20 percent.

[8] F. S. Dainton and H. C. Sutton, Trans. Faraday Soc. **49**, 1011 (1953).

The Dielectric Properties of Some Long-Chain Fatty Acids and Their Methyl Esters in the Microwave Region

T. J. BUCHANAN
Department of Physics Applied to Medicine, Middlesex Hospital Medical School, London
(Received September 29, 1953)

Measurements were made of the dielectric constant and loss of stearic, palmitic, and some other acids in the solid and liquid states between wavelengths of 1 and 50 cm. The loss was small in the solid state, and there was no absorption peak in the wavelength range covered; in the liquid state the loss was greater with evidence of a small absorption peak near 3 cm. The methyl esters show an absorption peak in the microwave region in both the solid and liquid states. The measurements on the liquid methyl esters indicate that resonance absorption is occurring at a frequency of about 6000 Mc/sec. Some ethyl esters were measured and were found to show a relaxation loss in the microwave region of the same order as the relaxation loss of the methyl esters but they showed no sign of resonance absorption loss. An attempt is made to explain both the relaxation loss and the resonance loss on the basis of a model which has already been used by Hoffman and Smyth.

INTRODUCTION

A CONSIDERABLE amount of work has been done, particularly by Smyth and his collaborators,[1–3] on the dielectric properties of long-chain aliphatic compounds. This work has shown that restricted rotation is of frequent occurrence in these substances, the molecule turning around its long axis from one equilibrium position to another. Hoffman[1] has proposed a model for those long-chain compounds which crystallize as double molecules, and from this model he derives many of their dielectric and thermal properties. We use Hoffman's model to explain the dielectric properties of the acids and the esters in the solid state and, on the basis that a considerable degree of short-range order exists at the lower temperatures in the liquid state, the model is also used to explain the dielectric properties of the liquid acids and esters just above the melting point.

The curves for the methyl esters indicate that resonance absorption occurs at a frequency of about 6000 Mc/sec. This frequency is between 100 and 1000 times smaller than one would expect on the basis of the calculations advanced by Frohlich.[4] An attempt is made to explain the resonance absorption as resulting from an almost free rotation of the molecule about the long-chain axis.

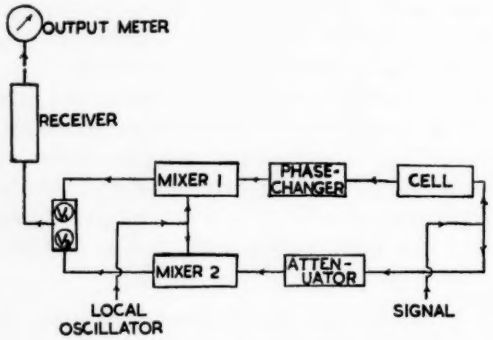

FIG. 1. Schematic diagram of apparatus.

MATERIALS

The acids were supplied by the Research Laboratories of Unilever. They are listed below along with the measured melting points.

Stearic acid ($C_{17}H_{35}COOH$)	69°C
Palmitic acid ($C_{15}H_{31}COOH$)	62.5°C
Lauric acid ($C_{11}H_{23}COOH$)	43.5°C
Capric acid ($C_9H_{19}COOH$)	31°C

The methyl esters were obtained from the same source and were estimated to be 99.9 percent pure.

Methyl stearate ($C_{17}H_{35}COOCH_3$)	39°C
Methyl palmitate ($C_{15}H_{31}COOCH_3$)	29.5°C

Ethyl stearate and ethyl palmitate were also measured. They were obtained commercially and an attempt was made to purify them by fractional distillation. This was not very successful and those ethyl esters must be considered as of very uncertain composition.

EXPERIMENTAL

Measurements were made, as a function of the temperature, at wavelengths of 1.26, 3.2, 4.0, 4.5, 5.0, 6.5, 10, 17, and 50 cm. The measurements at 1.26 cm and 3.2 cm, on both the solid and liquid materials, were obtained by the Roberts-von Hippel method using wave-guide equipment;[5] and the measurements on the solids at the longer wavelengths were also obtained by this method, but in this case using coaxial line equipment. The measurements on the liquids at the longer wavelengths were obtained by a phase and amplitude balance method which is an extension of one already described by the author and the apparatus is similar to that described by Branin and Smyth.[6,7] A schematic diagram of the apparatus is shown in Fig. 1.

[1] J. D. Hoffman, J. Chem. Phys. **20**, 541 (1952).
[2] C. P. Smyth, Faraday Soc. Discussion on Dielectrics (1946).
[3] Crowe, Hoffman, and Smyth, J. Chem. Phys. **20**, 550 (1952).
[4] H. Frohlich, *Theory of Dielectrics* (Clarendon Press, Oxford, 1949).
[5] S. Roberts and A. Von Hippel, J. Appl. Phys. **17**, 610 (1946).
[6] F. H. Branin and C. P. Smyth, J. Chem. Phys. **20**, 1121 (1952).
[7] T. J. Buchanan, Proc. Inst. Elec. Engrs. Pt. III, **99**, 61 (1952).

The cell (Fig. 2) is in the form of a coaxial line, closed at the top by a brass plug, and fitted with a central conductor which is made from telescopic tubing to allow the tube holding the output cable to move along the axis of the cell. The output cable passes down inside the central conductor and ends in a fine probe which is bent to project into the cell through a small hole in the central conductor. When the central conductor moves it carries the cable with it and the probe can then sample the electric field at any desired point along the axis of the cell. The relative phase and amplitude of the field at points along the axis of the cell can then be measured by obtaining a null-balance at the receiver by adjustment of the cut-off attenuator and the phase changer (Fig. 1).

There is a wide range of possible methods of measurement with this form of apparatus, the most suitable method depending on the substance being examined. Three methods were used for the measurements on the

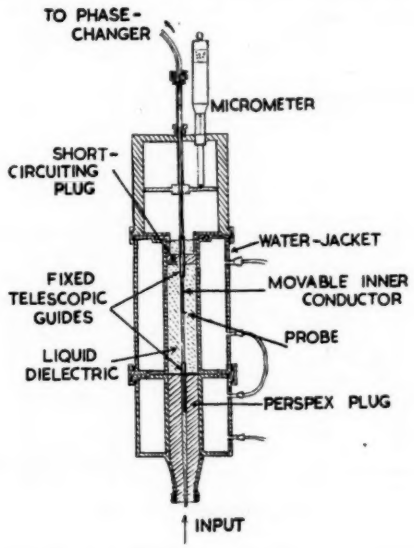

FIG. 2. Sketch of coaxial-line cell.

acids and esters. These can be illustrated by Fig. 3 which represents a typical distribution of the amplitude of the electric vector along the axis of the cell. If measurements are made at any points P and Q which are related by the condition that $OQ=2OP$ then it can be shown that[7]

$$\cosh\alpha x_1=\frac{k^2}{4}+\left\{\left(1-\frac{k^2}{4}\right)^2+k^2\sin^2\theta\right\}^{\frac{1}{2}}, \qquad (1)$$

$$\cos\beta x_1=\frac{k^2}{4}-\left\{\left(1-\frac{k^2}{4}\right)^2+k^2\sin^2\theta\right\}^{\frac{1}{2}}, \qquad (2)$$

where $x_1=OQ$, and $\alpha+j\beta$ is the propagation constant of the liquid and $ke^{i\theta}$ is the ratio of the vector at Q to that at P. k is measured by the cut-off attenuator and θ by the phase changer. Maximum accuracy is obtained when Q is near a minimum which is an odd number of

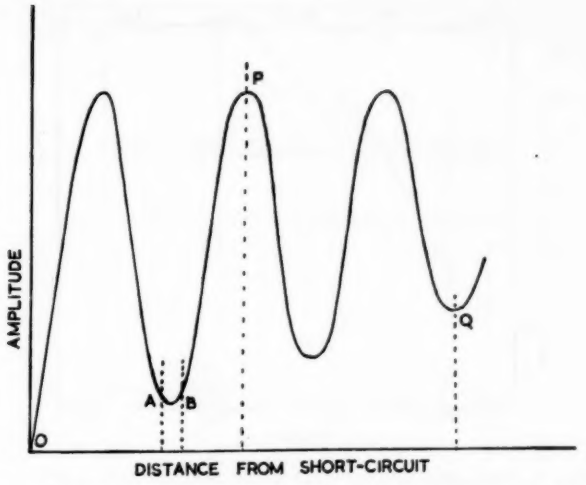

FIG. 3. Typical amplitude distribution of electric vector along axis of cell.

half-wavelengths from the short circuit. Equations (1) and (2) involve no approximations and this method, in theory, can be used for any liquid. If α and β are found from (1) and (2) then ϵ' and ϵ'' can be found from

$$\epsilon'=(\lambda/2\pi)^2(\beta^2-\alpha^2), \qquad (3)$$

$$\epsilon''=2(\lambda/2\pi)^2\alpha\beta, \qquad (4)$$

where $\epsilon'-j\epsilon''$ is the complex permittivity and λ is the free space wavelength.

In the second method the ratio of the vectors at points A and B close to and on opposite sides of a minimum are measured. The following approximate formula can then be derived for the case where the amplitudes of the vectors at A and B are equal.

$$\tanh\alpha d=\frac{\tan\beta\xi}{\tan(\theta/2)}, \qquad (5)$$

where $2d=OA+OB$, $2\xi=OB-OA$, and θ is the phase-difference between the vectors at A and B. To ensure that the vectors at A and B are equal a balance is established when the probe is at A, and the cut-off attenuator is then fixed in position. The probe is now moved through the minimum to a point roughly the same distance from the minimum on the other side. By small alternative adjustments of the probe position and the phase changer a second balance point can be found. The movement of the phase changer gives a measure of θ. A first approximation to the value of β can be found with sufficient accuracy from the positions of the minima in the cell and then from (5) a first approximation to the value of α can be found. If greater accuracy is required, then β can be found more accurately from the approximate formula

$$\beta\simeq\frac{n\pi}{x}\left(1-\frac{\alpha^2}{\beta^2}\right), \quad n=1,2,3,\cdots, \qquad (6)$$

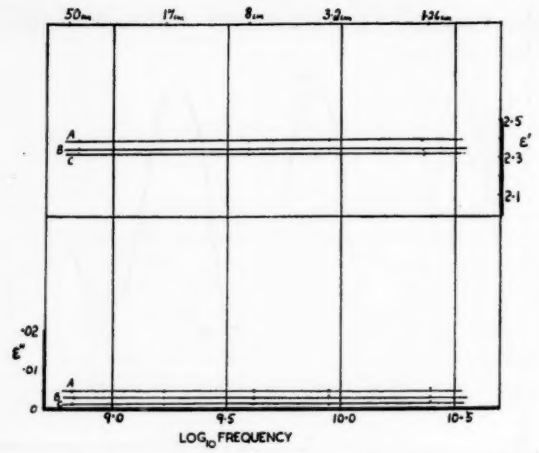

FIG. 4. Dielectric properties of three acids in the solid state: *A*: Capric acid. *B*: Palmitic acid. *C*: Stearic acid.

where x is the distance of the nth minimum from the short circuit. Since α/β is small (for the acids and esters examined) it is sufficient to take the first approximations to α and β for use in the second member of (6). The more accurate value of β, so derived, can then be used in (5) to obtain a more accurate value of α. It was found that, with the acids and esters, the use of this more accurate approximation was scarcely justified by the experimental accuracy.

The third method was used to determine α alone. If k is the ratio of the amplitude at any minimum to the amplitude at any maximum then the following approximate formula can be derived

$$\alpha \simeq \frac{k}{x_1} \cdot \frac{1+(k^2/2)(x_2/x_1)^2}{1+(k^2/6)}, \qquad (7)$$

where x_1 and x_2 are the distances of the minimum and the maximum from the short circuit, respectively. The amplitudes at the successive maxima and minima can be recorded during one movement of the probe along the axis of the cell, and Eq. (7) can then be applied to each pair of readings to give a good average reading and to check that the apparatus is working properly.

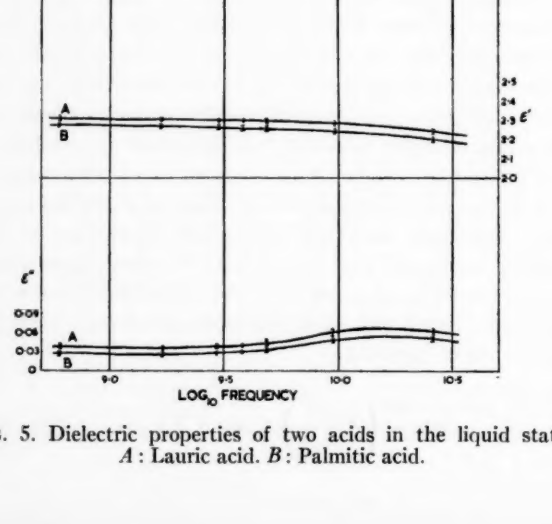

FIG. 5. Dielectric properties of two acids in the liquid state: *A*: Lauric acid. *B*: Palmitic acid.

RESULTS

The results for the acids in the solid state (Fig. 4) show no sign of a loss maximum in the microwave region and the loss and the dielectric constant were low and constant from 50 cm to 1.26 cm. The dielectric constant at 50 cm is already low so that no appreciable loss of the Debye type can occur at the lower frequencies. A direct comparison with the static dielectric constant will verify this conclusion. The results for liquid palmitic acid and lauric acid (Fig. 5) were similar but showed a higher loss and a suggestion of a region of relaxation loss between 1 and 3 cm.

The measurements on ethyl palmitate are shown in Fig. 6. The ϵ' and ϵ'' curves are relaxation loss curves

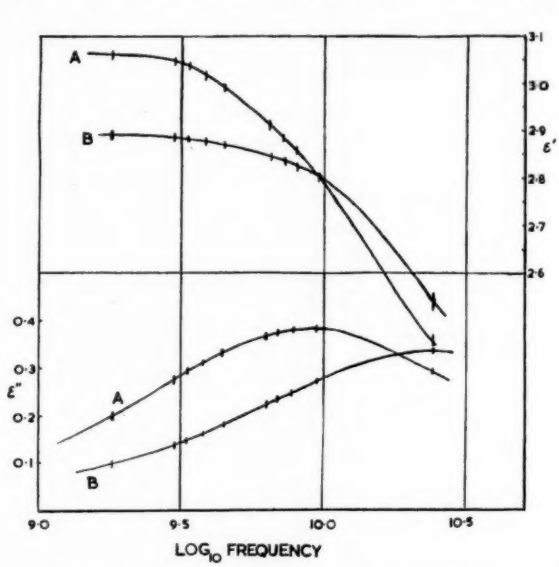

FIG. 6. Dielectric properties of ethyl palmitate. *A*: 26°C; *B*: 75°C.

with a spread of relaxation times. The static dielectric constant of ethyl palmitate is 3.09 which is just slightly greater than the dielectric constant at 17 cm so that this substance can possess no other region of relaxation loss at lower frequencies. Similar results were obtained with ethyl stearate. No measurements were made on the solid ethyl esters.

The measurements of Dryden and Welsh[8] on the loss of methyl stearate over a wide frequency range and at three different temperatures are shown in Fig. 7. The dielectric constant measurements in the same figure are the author's own measurements. The curves of Fig. 7 are required later in the discussion. The measurements of Fig. 7 refer to the solid methyl ester. Dryden and Welsh have obtained similar results for methyl palmitate and methyl behenate in the solid state.

[8] J. S. Dryden and H. K. Welsh, Australian J. Sci. Research 4, 616 (1951).

The author's results for liquid methyl palmitate are shown in Fig. 8. Similar curves were obtained with methyl stearate and a mixture of methyl stearate and methyl palmitate. These curves for the liquid esters show marked irregularities in both ϵ' and ϵ''.

DISCUSSION

X-ray measurements on long-chain compounds have shown that there exists, at temperatures just above the melting point, a considerable degree of short-range order in which the molecules tend to lie parallel to their near neighbors.[9–13] As the temperature rises the degree of order diminishes and the molecules tend to bend and crumple due to rotation of the parts of the molecule about the C—C bonds.[14]

In the solid state the acids and the methyl esters of the even acids crystallize as double molecules in the monoclinic system. The angle of tilt of the unit cell to

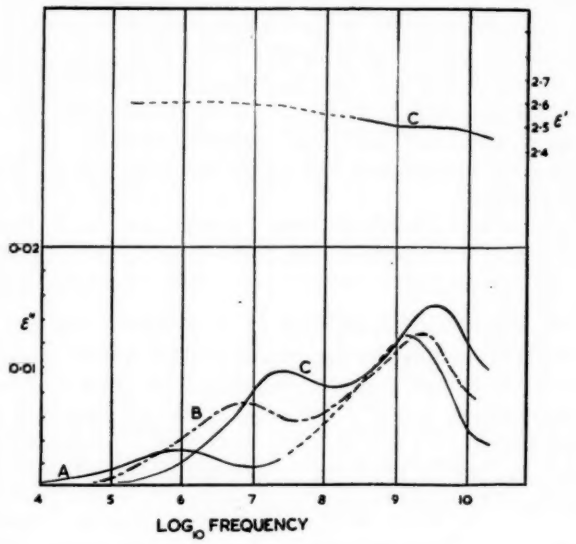

FIG. 7. Dielectric properties of solid methyl stearate: A: −18°C; B: 2°C; C: 25°C.

the basal plane may be capable of assuming different values thus giving rise to different polymorphic forms. The ethyl esters crystallize as single molecules.

Hoffman[1] has considered a model which is applicable to a crystalline lattice of double molecules. He pictures the molecules in the ground state as oriented with the polar groups adjacent to each other and with the dipole moments antiparallel. If one component of the double molecule is now considered to rotate while its neighbors remain fixed then we obtain the potential diagram shown in Fig. 9, where ϕ is the angle the half-molecule rotates from the ground state position, i.e. the position

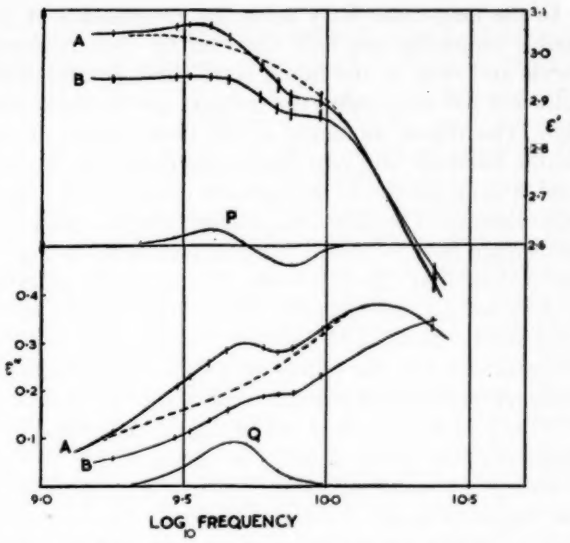

FIG. 8. Dielectric properties of methyl palmitate: A: 31°C; B: 65°C. The dashed curves and curves P and Q illustrate the evidence for resonance absorption (see text).

where the dipoles are antiparallel. The ground state corresponds to the deep potential minimum and the shallower minima are due to the effects of the near neighbors. This arrangement of potential minima gives rise to two different relaxation times τ_{12} and τ_{22}, the former corresponding to transitions from the deep minimum to the shallower minima and the latter to transitions between the shallow minima. Hoffman writes for these relaxation times

$$\tau_{12} = Be^{(V_1+V_2)/kT}. \quad (8)$$

$$\tau_{22} = Be^{V_2/kT}. \quad (9)$$

Little can be known about B but it seems reasonable to assume that it will be the same for each relaxation process.

On the basis of this model let us consider the dielectric properties of the fatty acids, the ethyl, and methyl esters which have been measured. On the basis of the existence of a state of short-range order in the liquid at temperatures just above the melting point it will be assumed that the model can be applied in that temperature range as well as in the solid.

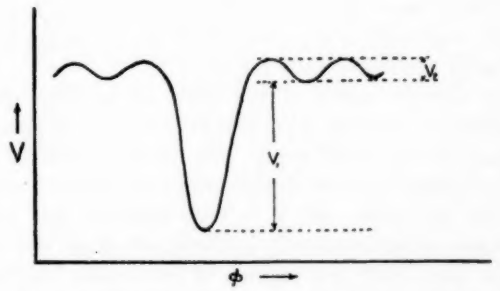

FIG. 9. Potential energy diagram for rotation around long axis of the molecule.

[9] P. Debye and H. Menke, Physik. Z. **31**, 797 (1930).
[10] G. W. Stewart and R. M. Morrow, Phys. Rev. **30**, 232 (1927).
[11] G. W. Stewart, Phys. Rev. **31**, 10 (1928).
[12] J. J. Trillat, Z. Physik. **64**, 191 (1930).
[13] J. J. Trillat, Compt. rend. **190**, 858 (1930).
[14] A. R. Ubbelohde and J. C. McCoubrey, Faraday Society Discussion on Hydrocarbons, p. 94 (1951).

In the long-chain fatty acids the components of the double molecules are held together by two hydrogen bonds and even in the liquid state these double molecules will still exist unless the temperature becomes very high. The dipole moments of the constituents of the double molecule will practically cancel out so that the double molecule would be expected to behave as a nonpolar element. The dielectric constant and the relaxation loss should both be small. The measurements in Figs. 4 and 5 show that this is the case. If we consider palmitic acid we see that the measured dielectric constants in the solid and liquid are 2.34 and 2.27, respectively, and this difference may be due to a density difference. The static dielectric constant of palmitic acid in the liquid state at 71°C is 2.34 so that there can be only a very small low-frequency loss if any at all. The curves of Fig. 5 show evidence of a small relaxation loss in the liquid acids in the region of about 3 cm and this may be due to the separation of a small proportion of the double molecules into their constituent single molecules. We can interpret this behaviour in terms of the potential diagram of Fig. 9 by saying that, in the case of the acids, the potential minimum is very deep and well populated while the upper shallow minima are almost completely empty. In the liquid state the upper minima may acquire a small population because of increased thermal agitation and this could lead to a small relaxation loss in both the high- and the low-frequency regions.

The ethyl esters do not form double molecules in either the solid or the liquid state but they crystallize in a similar form to the acids and might therefore be expected to show a potential diagram, for rotation around the long axis, lacking the deep potential minimum of Fig. 9 and consisting of only a series of shallow potential minima due to near neighbors. There would then be only one relaxation time corresponding to transitions between the shallow minima and we would expect only one region of relaxation loss in both the solid and liquid states. The measurements on the liquid ethyl esters show a pronounced relaxation loss peak in the microwave region and the dielectric constants of ethyl palmitate and ethyl stearate at 36°C and 17 cm (3.03 and 3.02) are very little different from the static dielectric constants (3.09 and 3.03) so that there cannot be any appreciable relaxation loss at lower frequencies. We have no measurements on the solid ethyl esters but we deduce from the model that there will be only one region of relaxation loss and that this loss region should also be in the microwave region.

The methyl esters of the even acids form double molecules in the solid state and in this case the potential diagram of Fig. 9 will apply. The binding force between the components of the double molecule is much weaker than in the acids, and it is very unlikely that double molecules occur frequently in the liquid state. We would expect then that two regions of relaxation loss would occur in the solid and only one region of relaxation loss in the liquid. Because of the similarity in molecular size and molecular surroundings we would expect the relaxation loss in the liquid methyl ester to be of the same magnitude and of roughly the same frequency as in the ethyl esters and a comparison of Figs. 6 and 8 shows this to be so. The measurements of Dryden and Welsh, Fig. 7, clearly show the two regions of relaxation loss in solid methyl stearate and these authors have reported[8] similar results with methyl palmitate and methyl behenate. No measurements are available at lower frequencies for the liquid methyl esters but we deduce that no relaxation loss can occur at frequencies lower than 600 Mc/sec. This deduction again depends on the assumption that the model can be applied at temperatures just above the melting point of the ester.

Because of the weaker binding of the components of the double molecules in the methyl esters the deep potential minimum will not be so deep as in the acids and the populations of the upper minima will be relatively much greater. If we now confine our attention to the methyl esters in the solid state and consider the effects of temperature we can draw some conclusions from the model and compare them with the results of Dryden and Welsh. The model predicts two relaxation-loss regions and these are clearly shown in Fig. 7. Following Hoffman we can derive from Eqs. (8) and (9) the relation

$$\log_e \tau_{22} - \log_e \tau_{12} = -\frac{V_1}{kT}. \tag{10}$$

This relation indicates that as T increases and if V_1 remains constant the maxima of the two relaxation loss curves should move closer together. This point again is clearly shown in Fig. 7. We can also use relation (10) to find whether V_1 is a function of temperature since the first member of (10) can be derived directly from the curves. For methyl stearate we obtain

$$V_1 = 4.1 \text{ kcals/mole at } -18°\text{C},$$
$$V_1 = 3.2 \text{ kcals/mole at } \quad 2°\text{C},$$
$$V_1 = 2.8 \text{ kcals/mole at } \quad 25°\text{C}.$$

By measuring the area under the low-frequency loss curves at different temperatures Dryden and Welsh have obtained 2.9 as the mean value of V_1 for methyl stearate between the temperatures of 25°C and 2°C. This is in good agreement with the values obtained from (10). From the measurements on solid methyl palmitate and methyl behenate given in the paper by Dryden and Welsh[8] a similar drop in V_1 can be established as the temperature rises towards the melting point. Hoffman[1] and Frohlich[4] have shown that this drop in V_1 should occur. Frohlich shows that as the temperature increases from very low values V_1 will at first remain constant. But as the subsidiary equilibrium positions are occupied (the upper minima in Fig. 9) the energy of interaction of the dipoles increases and V_1 will therefore decrease and a critical temperature T_0 will exist at which V_1 will vanish. It appears therefore that we have made our measure-

ments in the temperature range over which V_1 is continuously diminishing, i.e., V_1 is a function of the temperature.

If we plot $\log_e \tau_{12}$ or $\log_e \tau_{22}$ as a function of $1/T$ we find that the points do not lie on a straight line but on a curve which is concave to the $1/T$-axis. This shows that we cannot assume V_1 or V_2 to be independent of temperature, and in the absence of a knowledge of the absolute value of B the exact form of the temperature dependence of V_1 and V_2 cannot be derived. We have already shown that V_1 decreases with increasing temperature and the curvature of the $\log_e \tau_{22}$ curves could be consistent with a similar drop in V_2, but we cannot be certain. Muller,[15] by x-ray analysis of some of the long-chain aliphatic compounds, has shown that when the temperature in the solid approaches the melting point the lattice becomes looser and the symmetry of the unit cell tends to become hexagonal. The molecule then has more room in which to rotate and the barriers between the subsidiary equilibrium positions therefore probably become considerably smaller than those in the rigid lattice at the lower temperatures.

By considering the relative populations of the shallow and the deep potential minima of Fig. 9 some conclusions may be drawn concerning the value of the maximum loss ϵ'' as a function of temperature. It can be shown that the maximum loss in the low-frequency relaxation-loss region should be proportional to the expression

$$\frac{\Omega e^{-V_1/kT}}{(1+\Omega e^{-V_1/kT})^2},$$

where Ω is the total number of shallow potential minima in the potential diagram of Fig. 9. By substituting the experimental values of V_1 we can derive values which should be proportional to the maximum value of the low-frequency loss at each temperature. These derived values increase much more rapidly than the experimental values.

A similar attempt to calculate the maximum loss as a function of temperature in the high-frequency loss region leads to the same result: the experimental rate of increase is much less than the calculated rate of increase. These results were calculated with a value of $\Omega=12$ which Hoffman derived from thermodynamical considerations and to obtain agreement with the experimental results an impossibly high value of Ω would be required. It is likely that the model assumed is too simple and, in particular, it may be that B in Eqs. (8) and (9) should be a different quantity for each relaxation time and also a function of the temperature.

We conclude then that the model predicts well the qualitative dielectric properties of the solid methyl esters but fails to provide a satisfactory quantitative basis.

When the methyl ester crystal melts the components of the double molecules separate and long-range order disappears. In the liquid the single molecules tend to lie parallel with each other in a form of short-range order which the x-ray evidence shows to be most apparent just above the melting point and to diminish as the temperature rises. The potential diagram for this state of short-range order should consist of a series of minima due to the effects of the near neighbors, and the deep potential minimum of Fig. 9 will be absent. The only form of transition would then be from one potential minimum to another of equal depth, the transitions from a deep minimum to an upper series of minima, as in Fig. 9, would be absent. We would then expect only a single region of relaxation loss and that in the higher frequency region. The author knows of no measurements on the liquid methyl esters in the frequency region below 600 Mc/sec but from the measurements at higher frequencies (Fig. 8), which show a pronounced relaxation loss in the microwave region, we conclude that there can be no other region of relaxation loss at the lower frequencies.

On the basis of our model we regard the relaxation loss in the microwave region, in both the solid and the liquid esters, to be due to the same mechanism, *viz.*, the transition of the molecule from one to another of a series of equilibrium positions separated from each other by potential barriers caused by the presence of near neighbors. The loss in the liquid state is considerably higher than in the solid state, and this we consider to be due to the elimination of the deep potential minimum in the liquid and the consequent increase in the population of the upper minima. As the temperature rises the state of short-range order gives place to a state of complete disorder (pure liquid) in which our model has no validity. We would expect the character of the relaxation loss to be considerably affected by this disappearance of short-range order but neither our temperature nor frequency range is high enough to enable us to draw any definite conclusions on this point. However, as an examination of Fig. 8 will show, the loss curve in the liquid methyl esters is due to a spread of relaxation times, and this spread seems to increase as the temperature increases.

RESONANCE ABSORPTION

In addition to the obvious loss in the microwave region the methyl esters show, in the liquid, another region of loss in the neighborhood of 5 cm. The ϵ'' curves (Fig. 8) show a very decided shoulder at this wavelength, and as the temperature rises this shoulder becomes less marked but occurs at the same frequency. The ϵ' curves show a corresponding irregularity which again diminishes as the temperature rises but remains at approximately the same frequency. In Fig. 8 the dashed lines indicate the results one would expect from a pure relaxation mechanism. If we subtract these dashed curves from the experimental curves we obtain the curves P and Q which have the form of typical resonance

[15] A. Muller, Proc. Roy. Soc. (London) **A127**, 417 (1930).

curves. There is, of course, some latitude in the choice of the dashed curves, but any reasonable choice will have little effect on the shape of curves P and Q. The width of Q is roughly one-fifth of the width of an ϵ'' curve resulting from a single relaxation time.

There seems to be justification for accepting these results as evidence of some form of resonance absorption. The central frequency of this absorption is lower by a factor between 100 and 1000 than would be expected from the process discussed by Frohlich[4] in which the molecule is considered to oscillate about a position of equilibrium. We suggest as a provisional hypothesis that the resonance is due to an almost free rotation of the molecule about its long axis. For this to occur the molecule must remain straight and must lie parallel with its near neighbors, i.e., a state of short-range order in the liquid would be essential for the appearance of this form of resonance absorption. This would account for the experimental fact that this absorption decreases rapidly as the temperature of the liquid rises because it is known, from infrared measurements,[14] that as the temperature rises an increasing number of molecules crumple by rotation about the C—C bonds and no longer retain the straight configuration. This feature and the consequent decrease in the short-range order would effectively prevent any free rotation of the type envisaged. This picture fits in with the extension of Hoffman's model which we have used to explain the relaxation phenomena in the liquid. Relaxation occurs when the molecule moves from one potential minimum to another; resonance occurs when the molecule, owing to a concurrence of steric and energetic circumstances, rotates almost freely through a large angle around its axis of rotation. If this rotation were completely free the absorption line width would be small, but in the liquid the state of short-range order is transient and the total angle of rotation will be finite and of varying magnitude. The absorption will then occupy a comparatively wide frequency band which the experimental results show to be the case.

Pauling[16] has treated the problem of free rotation in diatomic molecules and has suggested the extension of the treatment to long-chain aliphatic molecules rotating about the long axis. His treatment can be applied to the present case if an adjustment is made to take account of the large number Ω of potential minima. A knowledge of the height of the potential barrier is required in order to calculate the energy levels, and this height is precisely what the experimental results have failed to disclose. An examination of Pauling's curves relating energy levels and barrier height shows that the experimental central frequency of resonance could be obtained, for the molecules in question, with barrier heights of the order of a few hundred cal/mole. Barriers of this height may possibly occur in very favorable circumstances in the liquid near the melting point where short-range order prevails. These barriers will presumably be of very variable magnitude in both space and time because of thermal motion, and suitable barrier heights may occur infrequently, and even more infrequently as the temperature rises. The conventional procedure of plotting $\log\tau$ as a function of $1/T$ cannot be applied to the relaxation loss curves in Fig. 8 because our measurements do not extend to a high enough frequency, and we are therefore unable to obtain an estimate of the barrier height in the region of importance, *viz.*, just above the melting point of the liquid.

From the above discussion we would expect the ethyl esters to show a similar resonance absorption. They do not. It seems likely that the ethyl group projects sufficiently far from the long axis of the molecule to present a steric hindrance to sustained rotational motion. Smyth[2] has found that the substitution of an ethyl group for a methyl group in some compounds is sufficient to suppress restricted rotation.

The acids are bimolecular in the liquid state and the two dipoles tend to cancel and make the double molecule nonpolar. We have seen that they do not show relaxation effects, and we would not expect them to show this form of resonance absorption.

CONCLUSION

Hoffman's model gives a good qualitative prediction of the dielectric behavior of the long-chain molecules which we have measured, but the failure to determine the height of the potential barriers from the experimental data makes it impossible to test the model for a more detailed and quantitative agreement.

The measurements on the liquid methyl esters indicate the existence of a resonance absorption with a central frequency at approximately 6000 Mc/sec.

ACKNOWLEDGMENTS

Thanks are due Professor J. E. Roberts for providing the facilities for this work and for permission to publish. The construction of the apparatus was due to Mr. J. Tierney and Mr. F. Hart. We are indebted to the Research Laboratories of Unilever for the provision of the pure methyl esters and the acids.

[16] L. Pauling, Phys. Rev. **36**, 430 (1930).

The Onsager Thermodynamics of Galvanic Cells with Liquid-Liquid Junctions

RICHARD J. BEARMAN
Department of Chemistry, Stanford University, Stanford, California
(Received October 5, 1953)

The general theory of galvanic cells with liquid-liquid junctions, including gravitational effects, is discussed by means of the Onsager thermodynamics of irreversible processes.

I. INTRODUCTION

THE pseudothermostatic theory of galvanic cells with liquid-liquid junctions was reviewed and generalized by Koenig.[1] Using essentially only one pseudothermostatic postulate, the "qrc assumption," he derived a key equation—the so-called "qrc condition"—which, combined with reasonable assumptions, resulted in a general theory (including gravitational effects) of galvanic cells with liquid-liquid junctions.[2]

Since then, the thermodynamics of irreversible processes has been applied in a limited way to cells of this type. De Groot[3] only briefly discussed galvanic cells and he did not mention the qrc condition. Denbigh[4] found a form of the equation for the special case of cylindrical symmetry, but his treatment was not completely rigorous and he neglected gravity. Furthermore, vital to his proof was the restriction that, in the absence of current between the electrodes, there is no current in the diffusing solution. In a discussion of the general case, this assumption cannot be made.[5]

Our object is to rigorously derive the qrc condition, including the effects of gravity, by means of the Onsager thermodynamics of irreversible processes.

II. ASSUMPTIONS AND DEFINITIONS

We accept Koenig's definition 1, except that we omit his restrictions ii, iii, iv (a), and iv (b).

We also require his definitions 2, 3, 4, 6, and 7.

We further adopt his auxiliary assumptions 1, 3, and 4. The word "auxiliary" will prove unnecessary and will hereafter be omitted.

We shall retain several assumptions made by Koenig in the section entitled, "The Assumption of Quasi-Reversible Conduction" and we shall reject the remainder. We therefore repeat (with some changes) that part we wish to keep and we make it our assumption 1.[6,7]

Assumption 1

In the system postulated by definition 1 (k), let the electric current between the electrodes α and α' be zero and let diffusion proceed spontaneously. At each instant the system is in a definite state characterized by (i) a definite configuration, (ii) a definite electrochemical state at each point, (iii) a definite chemical state at each point, and (iv) definite values of the flow vectors $\mathbf{\Phi}_i$ and current vector $\mathbf{I}$ at each point. We select the system at an arbitrary instant and let Z^{spont} denote its state at this instant, as characterized by i, ii, iii, and iv.

Now we consider the system when a steady, arbitrarily small current is flowing through the solution from α to α', while at the same time spontaneous diffusion is proceeding. We assume that the flow of current is brought about by the continual isothermal transfer of electrons externally from the metal in α to the metal in α' or vice versa. Under these conditions there is a continual change of composition at each point of the solution due to (i) spontaneous diffusion, (ii) transference of components by the current, and (iii) change in chemical content of the solution by the electrode processes. We now assume the system can be so arranged such that at some instant it passes through a state Z^* which has exactly the same configuration as the state Z^{spont} and exactly the same chemical state at each point as Z^{spont}. Since the electrode current is arbitrarily small, Z^* will differ infinitesimally from Z^{spont} in (i) the electrochemical state at each point and (ii) the vectors $\mathbf{\Phi}_i$ and $\mathbf{I}$ at each point.

We now replace the qrc assumption itself by the following two assumptions.

Assumption 2

The phenomonological relations,

$$\mathbf{\Phi}_i = -\sum_k L_{ik}\,\mathbf{grad}\mu_k, \tag{1}$$

and the Onsager reciprocal relations,

$$L_{ik} = L_{ki}, \tag{2}$$

are valid in the solution.

Assumption 3

At each point, the L_{ik} are functions only of the chemical state.

This assumption is rendered plausible by consideration of a cylindrically symmetrical, isothermal, chemi-

[1] F. O. Koenig, J. Phys. Chem. **44**, 101 (1940).
[2] F. O. Koenig and S. W. Grinnell, J. Phys. Chem. **44**, 463 (1940).
[3] S. R. de Groot, *Thermodynamics of Irreversible Processes* (North-Holland Publishing Company, Amsterdam, 1951).
[4] K. G. Denbigh, *The Thermodynamics of the Steady State* (Methuen and Company, Ltd., London, 1951) pp. 78–81.
[5] F. Dolezalek and F. Krüger, Z. Elektrochem. **12**, 669 (1906).
[6] In order to avoid confusion, the assumptions and definitions of reference 1 will henceforth be denoted by their number followed by the letter "k" in parentheses.
[7] Assumption 1 should be read before assumptions 3 (k) and 4 (k) and definition 7 (k).

cally uniform, ohmic electrolyte solution in the absence of a gravitational field. The following equation holds:

$$\mathbf{I}=\sum_i z_i\mathbf{\Phi}_i=-\sum_i\sum_k z_iL_{ik}\,\mathbf{grad}\mu_k, \tag{3}$$

where

$$\mu_k=\tau_k+z_k\mathfrak{F}\psi \tag{4}$$

(see assumption 5 following). But since the solution is chemically uniform,

$$\mathbf{grad}\tau_k=0. \tag{5}$$

Thus

$$\mathbf{I}=-\mathfrak{F}(\mathbf{grad}\psi)\sum_i\sum_k z_iz_kL_{ik}. \tag{6}$$

But the summation appearing in Eq. (6) is, in appropriate units, the conductivity which empirically is a function of chemical state alone. This empirical fact would clearly result from the assumption that the L_{ik} are functions of chemical state only.

The following two assumptions were also used by Koenig, but he did not state them as assumptions.

Assumption 4

At the electrodes, no matter enters (or leaves) the diffusing solution except when current is flowing in the external circuit.

Assumption 5

For each component:

$$\mu_k=\tau_k+z_k\mathfrak{F}\psi+M_k\varphi, \tag{7}$$

where $\mathfrak{F}$ is Faraday's number and M_k is the molecular weight and at each point, τ_k is a function of the chemical state there, ψ is the electric potential, and φ is the gravitational potential.

III. DEDUCTION OF THE QRC CONDITION

The general form of the qrc condition is

$$\int_v \partial\mathbf{I}\cdot\sum_k\frac{l_k}{\bar{z}_k}\,\mathbf{grad}\mu_k\,\delta V=0. \tag{8}$$

Accordingly, we proceed to find an expression for the left-hand side ("lhs") and show that it is, indeed, identically zero.

By definition 6 (k),

$$\mathbf{I}^{\text{spont}}=\sum_i z_i\mathbf{\Phi}_i{}^{\text{spont}}. \tag{9}$$

Likewise,

$$\mathbf{I}^*=\sum_i z_i\mathbf{\Phi}_i{}^*. \tag{10}$$

Substituting Eq. (1) into Eq. (9), we obtain

$$\mathbf{I}^{\text{spont}}=-\sum_i\sum_k z_iL_{ik}{}^{\text{spont}}\,\mathbf{grad}\mu_k{}^{\text{spont}}$$

$$=-\sum_k l_k{}^{\text{spont}}\,\mathbf{grad}\mu_k{}^{\text{spont}}. \tag{11}$$

$$l_k\equiv\sum_i z_iL_{ik} \tag{12}$$

was defined by Denbigh.[4] Similarly, we obtain from Eqs. (1) and (10),

$$\mathbf{I}^*=-\sum_k l_k{}^*\,\mathbf{grad}\mu_k{}^*. \tag{13}$$

Substituting Eq. (7) into Eqs. (11) and (13) gives

$$\mathbf{I}^{\text{spont}}=-\sum_k z_k\mathfrak{F}l_k{}^{\text{spont}}\,\mathbf{grad}\psi^{\text{spont}}$$

$$-\sum_k l_k{}^{\text{spont}}\,\mathbf{grad}(\tau_k{}^{\text{spont}}+M_k\varphi^{\text{spont}}). \tag{14}$$

$$\mathbf{I}^*=-\sum_k z_k\mathfrak{F}l_k{}^*\,\mathbf{grad}\psi^*$$

$$-\sum_k l_k{}^*\,\mathbf{grad}(\tau_k{}^*+M_k\varphi^*). \tag{15}$$

But assumptions 1, 3, and 5 imply

$$L_{ik}{}^*=L_{ik}{}^{\text{spont}}\equiv L_{ik}, \tag{16}$$

$$\tau_k{}^*=\tau_k{}^{\text{spont}}. \tag{17}$$

Further,

$$\varphi^*=\varphi^{\text{spont}}, \tag{18}$$

since Z^* and Z^{spont} have the same configuration. Subtracting Eq. (14) from Eq. (15) and utilizing assumption 3 (k) and Eqs. (16), (17), and (18), we find

$$\partial\mathbf{I}\equiv\mathbf{I}^*-\mathbf{I}^{\text{spont}}=-\mathfrak{F}(\mathbf{grad}\partial\psi)\sum_k z_kl_k, \tag{19}$$

where

$$\partial\psi\equiv\psi^*-\psi^{\text{spont}} \tag{20}$$

by definition. Similarly,

$$\partial\mathbf{\Phi}_i=-\sum_k L_{ik}\,\mathbf{grad}\partial\mu_k=-\mathfrak{F}(\mathbf{grad}\partial\psi)\sum_k z_kL_{ik}, \tag{21}$$

$$=-\mathfrak{F}l_i\,\mathbf{grad}\partial\psi. \tag{22}$$

Equation (22) follows from Eq. (21) by use of Eqs. (2) and (12). This is the only point where the reciprocal relations are utilized. By definition 7 (k),

$$\frac{\bar{z}_i\partial\mathbf{\Phi}_i}{t_i{}^{[0]}}=\partial\mathbf{I}, \tag{23}$$

where $t_i{}^{[0]}$ denotes the transference number defined under the convention

$$\partial\mathbf{v}=0.$$

Substituting Eqs. (19) and (22) into Eq. (23) and rearranging yields

$$\frac{t_i{}^{[0]}}{\bar{z}_i}=\frac{l_i}{\sum_k z_kl_k}. \tag{24}$$

Equation (24) is consistent with assumption 3 by virtue of assumption 4 (k).

We shall hereafter only consider the state Z^{spont} and therefore we shall omit the superscript "spont." By

Eq. (11),

$$\mathbf{I}=-\sum_k l_k \,\mathbf{grad}\mu_k. \tag{25}$$

From Eqs. (24) and (25),

$$\sum_k \frac{t_k^{[0]}}{\bar{z}_k}\,\mathbf{grad}\mu_k=-\frac{\mathbf{I}}{\sum_i z_i l_i}, \tag{26}$$

whence, integrating over the volume of the solution,

$$\int_v \partial\mathbf{I}\cdot\sum_k \frac{t_k^{[0]}}{\bar{z}_k}\,\mathbf{grad}\mu_k\,\delta V=-\int_v \frac{\mathbf{I}\cdot\partial\mathbf{I}}{\sum_i z_i L_i}\delta V. \tag{27}$$

The lhs of Eq. (27) is in the form of the qrc condition. We shall prove that the right-hand side ("rhs") is zero.

Substituting Eq. (19) into the rhs of Eq. (27), then using an elementary identity and finally Gauss' theorem, gives

$$\begin{aligned}\int_v \partial\mathbf{I}\cdot\sum_k \frac{t_k^{[0]}}{\bar{z}_k}\,\mathbf{grad}\mu_k\,\delta V&=\mathfrak{F}\int_v \mathbf{I}\cdot\mathbf{grad}\partial\psi\,\delta V\\ &=-\mathfrak{F}\int_v \partial\psi\,\mathrm{div}\mathbf{I}\,\delta V+\mathfrak{F}\int_v \mathrm{div}(\partial\psi\mathbf{I})\delta V\\ &=-\mathfrak{F}\int_v \partial\psi\,\mathrm{div}\mathbf{I}\,\delta V+\mathfrak{F}\int_\sigma \partial\psi\mathbf{I}\cdot\boldsymbol{\delta\sigma},\end{aligned} \tag{28}$$

where σ denotes the boundary surface of the solution.

From the equation of continuity we know that

$$\mathrm{div}\boldsymbol{\Phi}_i=-\frac{dc_i}{dt}. \tag{29}$$

Therefore, by Eq. (9) and assumption 1 (k),

$$\mathrm{div}\mathbf{I}=\sum_i z_i\,\mathrm{div}\boldsymbol{\Phi}_i=-\sum_i z_i\frac{dc_i}{dt}=0. \tag{30}$$

This implies that the first term on the rhs of Eq. (28) is zero.

As a consequence of definition 1 (k) and assumption 4, no matter enters or leaves the solution in the state Z^{spont}. Therefore—because of restriction iv (c) of definition 1 (k)—at all points of the boundary, the component of current normal to the boundary surface of the solution is zero. The second term on the rhs of Eq. (28) is then zero. Thus

$$\int_v \partial\mathbf{I}\cdot\sum_k \frac{t_k^{[0]}}{\bar{z}_k}\,\mathbf{grad}\mu_k\,\delta V=0. \tag{31}$$

We now derive the final form of the qrc condition. Since

$$\sum_k c_k\,\mathbf{grad}\mu_k=0,^{8} \tag{32}$$

we may add zero to Eq. (31) as follows,

$$\begin{aligned}\int_v \sum_k\left(\frac{\partial\mathbf{I}t_k^{[0]}+\bar{z}_k c_k\partial\mathbf{v}}{\bar{z}_k}\right)\cdot\mathbf{grad}\mu_k\,\delta V&\\ =\int_v \partial\mathbf{I}\cdot\sum_k \frac{t_k}{\bar{z}_k}\,\mathbf{grad}\mu_k\,\delta V=0.&\end{aligned} \tag{33}$$

Equation (33) is equivalent to Eq. (8), the desired form of the qrc condition.

The removal of restriction iv (c) of definition 1 (k) (which, in practice, always holds approximately) is not so easily accomplished as Koenig suggests.[9] In general, Eq. (33) holds exactly when, at the boundary surface of the solution, the component of $\mathbf{I}^{\text{spont}}$ normal to the boundary is zero.

If we accept the assumptions of this paper, then all of the conclusions of Koenig are valid in so far as restrictions ii and iii of definition 1 (k) and definitions 5 (k), 8 (k), 9 (k), and 10 (k) and assumptions 2 (k), 5 (k), and 6 (k) are correct.

ACKNOWLEDGMENT

The author extends his thanks to Professor F. O. Koenig for suggesting the problem and for his helpful comments.

[8] Reference 1, p. 119. The "work" terms associated with the presence of an electric field inside of the diffusing solution are neglected in the Gibbsian equation used by Koenig to derive Eq. (32). It is possible that the exact Gibbsian equation would yield the same result. At the worst, Eq. (32) is a very good approximation.

[9] Reference 1, p. 121.

Random Walk with Semiadsorbing Barrier

FRANK C. GOODRICH
California Research Corporation, Richmond, California
(Received September 8, 1953)

The problem of random walk in the presence of a semiadsorbing barrier is formulated and discussed. The results are applied to a study of the kinetics of adsorption in colloidal systems.

I. INTRODUCTION

THE Smoluchowski theory of the kinetics of colloid coagulation as a diffusion controlled process[1] has been recently re-examined by Collins and Kimball[2] in the light of a new and more flexible boundary condition. The original Smoluchowski theory considered a single colloid particle as a small spherical sink of radius R into which the remaining particles of the system were diffusing. Under the assumption that every colloid particle impinging upon the reaction surface would react, Smoluchowski solved the diffusion equation

$$\frac{\partial C}{\partial t}=D\nabla^2 C, \tag{1}$$

with the boundary condition

$$C=0, \tag{2}$$

over the surface of a sphere of radius R. Here C represents concentration, t the time, and D the diffusion constant.

For our purposes, it will be more convenient in the following discussion to restrict our attention to simple diffusion in one dimension along a coordinate x measured perpendicular to a planar reaction surface. Equation (1) then becomes

$$\frac{\partial}{\partial t}C(x,t)=D\frac{\partial^2}{\partial x^2}C(x,t), \tag{3}$$

with the boundary condition

$$C=0 \tag{4}$$

at $x=0$. For the case of uniform initial concentration C_0, the solution to (3) and (4) is

$$C/C_0=\operatorname{erf}\frac{x}{(4Dt)^{\frac{1}{2}}}. \tag{5}$$

A more general problem in the kinetics of colloid coagulation is one in which one relinquishes the assumption that every particle striking the reaction surface reacts, and instead assigns a nonzero probability to the event that the particle is reflected unchanged. It is this problem which Collins and Kimball have considered in a series of papers,[2,3] showing how the boundary condition (4) must in this case be replaced by

$$\Phi=kC(0,t), \tag{6}$$

where Φ is the flux across the reaction surface and k has the nature of a specific rate constant. The solution to (3) under the boundary condition (6) is

$$C/C_0=\operatorname{erf}\frac{x}{(4Dt)^{\frac{1}{2}}}+\exp(\sigma x+D\sigma^2 t)\times\operatorname{erfc}\left(\frac{x}{[4Dt]^{\frac{1}{2}}}+\sigma[Dt]^{\frac{1}{2}}\right), \tag{7}$$

where $\sigma=k/D$. Analyzing the diffusion process as consisting of a series of random jumps performed by the diffusing particles, Collins and Kimball conclude that k is given by

$$k=\tfrac{1}{2}\nu\mu\alpha, \tag{8}$$

in which μ is the mean jump length, ν the jump frequency, and α is the probability that a particle entering the reaction surface will react. (6) and (8) are presumed valid for $0\leq\alpha\leq 1$, i.e., even for a perfectly adsorbing surface, so that (6) represents a departure from the original Smoluchowski boundary condition (4).

II. THE INITIAL FLUX

The argument by which Collins and Kimball arrive at Eq. (8) is not entirely free from objection. Because the main purport of this paper is to modify their interpretation of the rate constant k as well as to reestablish the original Smoluchowski boundary condition for a perfect adsorber, it becomes necessary to examine their analysis in some detail.

Placing the particles to the right of the adsorbing wall, they show that the rate at which the particles strike the wall, and hence the rate of adsorption for a perfect adsorber is given by

$$\Phi=\nu\int_{-\infty}^{0}\varphi(s)\int_{0}^{s}C(x,t)\,dx\,ds. \tag{9}$$

Here, $\varphi(s)$ is the probability that a particle execute a jump of length s. To find the initial flux, they expand

[1] M. v. Smoluchowski, Z. physik. Chem. **92**, 129 (1917).
[2] F. C. Collins and G. E. Kimball, J. Colloid Sci. **4**, 425 (1949).
[3] F. C. Collins, J. Colloid Sci. **5**, 499 (1950).

the concentration in a MacLaurin series in the time.

$$C(x,t)=C_0+t\left(\frac{\partial C}{\partial t}\right)_{t=0}+\tfrac{1}{2}t^2\left(\frac{\partial^2 C}{\partial t^2}\right)_{t=0}+\cdots \quad (10)$$

and substitute (10) into (9).

$$\Phi=\nu\int_{-\infty}^{0}\varphi(s)\left[sC_0+t\int_0^s\left(\frac{\partial C}{\partial t}\right)_{t=0}dx+\cdots\right]ds. \quad (11)$$

Now letting $t\to 0$, they neglect all terms in the series except the first to find

$$\Phi=\tfrac{1}{2}\nu\mu C_0, \quad (12)$$

for the initial flux. μ is defined by

$$\mu=2\int_0^\infty s\varphi(s)ds, \quad (13)$$

(12) is, of course, just (6) and (8) with α set equal to 1.

This argument is valid only if the limiting processes involved are valid, and it is here that certain weaknesses appear. For consider the expansion (10). After substitution into (9), the coefficients of the various powers of t appear as integrals, of which we select the term linear in t as typical

$$\int_0\left(\frac{\partial C}{\partial t}\right)_{t=0}dx=\lim_{t\to 0}\frac{\partial}{\partial t}\int_0^s C(x,t)dx. \quad (14)$$

It will be noted that this integral has itself the nature of an initial flux, because it represents the limiting rate of decrease of matter in the neighborhood of the boundary as $t\to 0$. In short, by assuming in (11) that

$$\lim_{t\to 0}t\frac{\partial}{\partial t}\int_0^s C(x,t)dx=0, \quad (15)$$

Collins and Kimball have effectively assumed the result they set out to prove—that the initial flux is finite. To put the matter in other words, if the initial flux is finite, then the expansion (10) will be valid; but if the initial flux is infinite, (10) is invalid since a discontinuity will have been introduced into $C(x,t)$ at $x=t=0$.

The present paper is concerned with deriving the boundary condition for a semiadsorbing barrier on the basis of a discrete random-walk model. It will appear that the boundary condition is identically (6), (8); but with this difference, that α be in every case an infinitesimal of $O(\mu)$, i.e., α cannot be interpreted as a normalized transition probability $0\leq\alpha\leq 1$. With this understanding, there is no difficulty in showing that the original Smoluchowski boundary condition (4) for a perfect adsorber is correct. In fairness to Collins and Kimball, it must be said that the infinitesimal nature of α is implied by their Eq. (53) of reference 1. Their subsequent discussion, however, seems to have overlooked this property.

The final portion of this communication will be devoted to a discussion of the kinetics of reversible adsorption in colloidal systems.

III. DISCRETE RANDOM WALK MODEL

We consider a linear random walk starting at the origin $z=0$ in the presence of a semiadsorbing barrier at $z=m$. The barrier has a probability α of adsorbing an incident particle and a probability $\beta=1-\alpha$ of reflecting it. We permit the particle to make discrete flights of unit length with probability $\frac{1}{2}$ in either direction along the z axis. At the end of n such flights we require the probability $P(z,n)$ that the particle shall have coordinate z.

In solving this problem, it is convenient to break up the totality of possible successful paths to z into nonoverlapping sets H_j depending upon the number of contacts the particle has made with the barrier. That is, H_0 is the set of successful paths to z in which no contact is made with the barrier, H_1 is the set of successful paths in which exactly one contact is made with the barrier; and in general, the set H_j includes all possible paths to z in which exactly j contacts are made with the barrier. We may then write $P(z,n)$ in the form

$$P(z,n)=h_0(z,n)+\beta h_1(z,n)+\beta^2 h_2(z,n)+\cdots \quad (16)$$
$$=\sum_j \beta^j h_j$$

where $h_j(z,n)$ is the conditional probability that a path selected at random belongs to the set H_j, given that the particle is reflected at each contact with the barrier. Equation (16) follows from the fact that in a successful passage to z with j contacts with the barrier, the particle must have been reflected j times. In order to evaluate the quantities h_j we shall need several well-known formulas from the general theory of unrestricted one-dimensional random walks.[4]

a. The Unrestricted Walk

The probability $Q(z,n)$ that a particle initially at $z=0$ shall be at $z=z$ after n flights along an infinite line in the absence of any barriers is

$$Q(z,n)=(\tfrac{1}{2})^n\binom{n}{\frac{1}{2}(n+z)}. \quad (17)$$

b. The First Passage Time

The probability $W(z,n)$ that the particle achieves the coordinate z for the first time on the nth flight is

$$W(z,n)=\frac{z}{n}Q(z,n). \quad (18)$$

[4] W. Feller, *An Introduction to Probability Theory and Its Applications* (John Wiley and Sons, Inc., New York, 1950), Chapter 14.

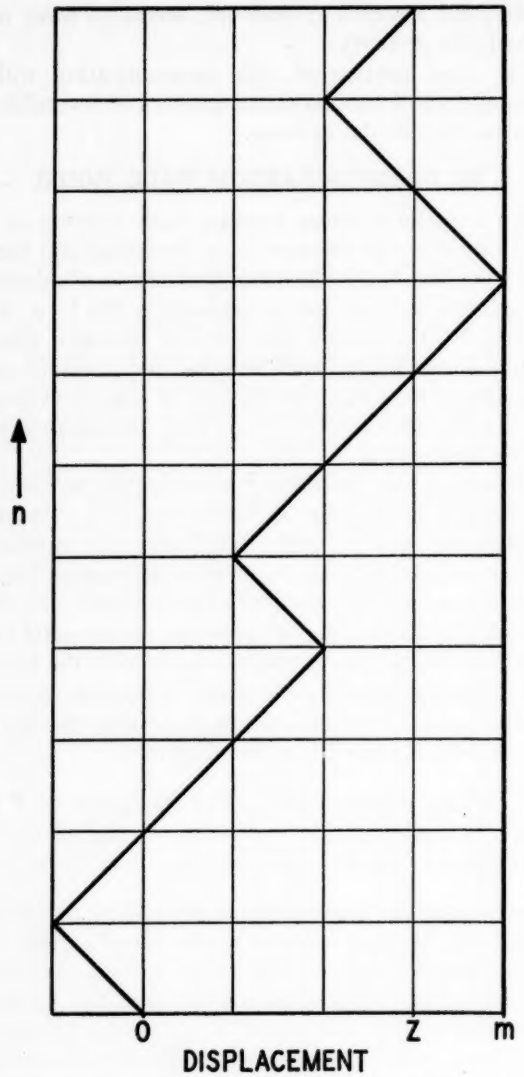

FIG. 1. A member of the set H_1, for $m=4$, $z=3$, $i=8$.

c. The First Return

The probability $Y(n)$ that the particle return to the origin for the first time on the nth flight is

$$Y(n)=W(1,n-1). \tag{19}$$

d. The Flight Without Return

Given that the direction of the first flight is towards z, the probability $Z(z,n)$ that the particle achieve the coordinate z on the nth flight without ever returning to the origin is

$$Z(z,n)=2W(z,n). \tag{20}$$

Given these quantities, the evaluation of the h_j becomes a relatively simple matter.

Fixing our attention on H_0, we consider the totality of paths to z in the absence of any barrier and eliminate from them all those paths which intersect the point $z=m$. This is best done by the method of images,[5] and leads to a well-known result:

$$h_0=Q(z,n)-Q(2m-z,n). \tag{21}$$

Referring to Fig. 1, we now suppose that the particle strikes the barrier for the first time on the ith flight. If the path is to belong to the set H_1, the particle must then achieve z from m in $n-i$ flights without return to m. The probability that it does this may consequently be expressed as a sum of products of the type $W(m,i)Z(m-z,n-i)$, and, in fact, summing over all possible i we have

$$h_1=\sum_{m}^{n-(m-z)}{}_i\ W(m,i)Z(m-z,n-i). \tag{22}$$

For members of the set H_2, we suppose that after striking m for the first time on the ith flight, the particle makes its first return to m in r additional flights. It must then proceed to z from m without return to m in $n-i-r$ flights, so that summing over all possible i,r we have

$$h_2=\sum_i \sum_r W(m,i)Y(r)Z(m-z,n-i-r). \tag{23}$$

In performing the summations in (23), note that to be included in the set H_2 a path can have no value of r less than $r=2$, and no value of i greater than $i=n-(m-z)-2$, since otherwise less than two contacts will have been made with the barrier. In a similar way, h_3 can be constructed as a triple sum of products of the type $W(m,i)Y(r)Y(s)Z(m-z,n-i-r-s)$, taking due precaution to let r and s take no values less than 2. The generalization to higher h_j follows easily.

The sums (22) and (23) are of the convolution type and are conveniently evaluated by use of an addition formula proved in the appendix.

$$\sum_{i=z}^{n-y} W(z,i)W(y,n-i)=W(z+y,n). \tag{24}$$

Substituting (19) and (20) into (22) and (23), successive application of (24) yields

$$\begin{aligned} h_1&=2W(2m-z,n),\\ h_2&=2W(2m-z+1,n-1), \end{aligned} \tag{25}$$

and, in general,

$$h_{j+1}=2W(2m-z+j,n-j);\quad j\geqslant 0. \tag{26}$$

To complete the problem we have merely to substitute (21) and (26) into (16), whence finally

$$P(z,n)=Q(z,n)-Q(2m-z,n)+2\beta\sum_{j=0}\beta^j W(2m-z+j,n-j). \tag{27}$$

It is worth pointing out that if $\beta=0$,

$$P(z,n)=Q(z,n)-Q(2m-z,n), \tag{28}$$

known to be correct if the barrier is a perfect adsorber,

[5] S. Chandrasekhar, Revs. Modern Phys. **15**, 1 (1943).

while if $\beta=1$, a simple induction shows readily that

$$P(z,n)=Q(z,n)+Q(2m-z,n), \tag{29}$$

known to be correct if the barrier is a perfect reflector.[5]

IV. PROBABILITY OF ADSORPTION ON THE nth STEP

A problem of supplementary interest is that of finding the probability $R(m,n)$ that the particle starting from the origin will be adsorbed on exactly the nth step. This will be α times the probability that the nth step takes the particle into the barrier, and as such may be computed by the methods used in Sec. 3.

We break up all possible paths to the barrier into sub sets H_j' depending on the total number of contacts made with the barrier, including that in which the particle is adsorbed. To each sub set we assign a conditional probability $h_j'(m,n)$ equal to the probability that a path selected at random belongs to the set H_j', given that the particle has been reflected on its first $j-1$ contacts with the barrier. In this scheme H_0' is necessarily empty, and $h_0'=0$. It follows that

$$\begin{aligned}R(m,n)&=\alpha h_1'(m,n)+\alpha\beta h_2'(m,n)\\&\qquad+\alpha\beta^2 h_3'(m,n)+\cdots\\&=\alpha\sum_{j=0}\beta^j h_{j+1}'.\end{aligned}\tag{30}$$

The evaluation of the h_j' is almost identical with that of the h_j, the only difference being that none of the terms of our summations will contain the factor Z. We find

$$\begin{aligned}h_1'&=W(m,n),\\h_2'&=\sum_{i=m}^{n-2}W(m,i)Y(n-i),\\h_3'&=\sum_{i=m}^{n-4}\sum_{r=2}^{n-i-2}W(m,i)Y(r)Y(n-i-r)\\&\cdots\cdots\cdots\cdots\cdots\cdots.\end{aligned}\tag{31}$$

Substitution of (19) into (31) followed by application of (24) leads to

$$h_j'(m,n)=W(m+j,n-j), \tag{32}$$

whence introducing (32) into (30) we have

$$R(m,n)=\alpha\sum_{j=0}\beta^j W(m+j,n-j). \tag{33}$$

As an important corollary to (27) and (33), note that at $z=m$, $P(z,n)$ satisfies the boundary condition

$$R(m,n)=\frac{1}{2}\frac{\alpha}{\beta}P(m,n). \tag{34}$$

Before passing on to the significance of these results with regard to colloid statistics, two other results of general interest will be obtained by the method of generating functions. These are the total probability of adsorption as $n\to\infty$ and the mean adsorption time. We define a generating function $F(m,s)$ for the terms $R(m,n)$ by

$$F(m,s)=\sum_{n=0}^{\infty}s^n R(m,n). \tag{35}$$

To obtain an explicit expression for $F(m,s)$, recall that the terms $W(m,n)$ possess a generating function $G^m(s)$ known to be[4]

$$G^m(s)=\sum_{n=0}^{\infty}s^n W(m,n)=\left\{\frac{1}{s}[1-(1-s^2)^{\frac{1}{2}}]\right\}^m. \tag{36}$$

The equations

$$\begin{aligned}G^m(s)&=W(m,0)+sW(m,1)+s^2W(m,2)+\cdots\\G^{m+1}(s)&=W(m+1,0)+sW(m+1,1)+\cdots\\G^{m+2}(s)&=W(m+2,0)+sW(m+2,1)+\cdots\\&\cdots\cdots\cdots\cdots\cdots\cdots\end{aligned}\tag{37}$$

are therefore valid; and in fact, multiplying the second by $\alpha\beta s$, the third by $\alpha(\beta s)^2$, the fourth by $\alpha(\beta s)^3$, etc., and adding all the equations, the coefficient of s^n in the resulting series is seen to be identical with (33). We have, therefore,

$$\begin{aligned}F(m,s)&=\alpha\sum_{n=0}^{\infty}(\beta s)^n G^{m+n}(s)\\&=\alpha G^m(s)\sum_{n=0}^{\infty}[\beta s G(s)]^n\\&=\frac{\alpha G^m(s)}{1-\beta s G(s)},\end{aligned}\tag{38}$$

whence on substitution from (36)

$$F(m,s)=\left(\frac{1}{s}\right)^m\frac{\alpha[1-(1-s^2)^{\frac{1}{2}}]^m}{\alpha+\beta(1-s^2)^{\frac{1}{2}}}. \tag{39}$$

Letting $s\to1$ in the usual way, examination of (39) shows that $F(m,s)$ approaches the total probability that the particle will be adsorbed in a random walk of infinite duration. If $\alpha=0$, this probability will be zero. For all other values of α, however small, the probability of eventual adsorption is 1, so that we may speak of eventual adsorption as a certain event whatever the specifications of the barrier only provided that it is not perfectly reflecting. This is a not unexpected result, for it is known from a theorem due to Polya[4] that a particle performing a random walk on the line or plane will pass infinitely often through every point. We must therefore expect infinitely many contacts with the barrier and, hence, eventual adsorption unless the barrier is impermeable.

The mean adsorption time is given by

$$\langle n\rangle=\sum_{n=0}^{\infty} nR(m,n), \tag{40}$$

recognizable as

$$\lim_{s\to 1}\frac{d}{ds}F(m,s).$$

Differentiating (39) and letting $s\to 1$, it follows that the mean adsorption time is infinite, independent of the nature of the barrier.

V. PASSAGE TO THE LIMIT

The analysis of the Brownian motion on the basis of a random-walk model is a classical procedure. It is well known that the diffusion equations may be obtained from the discrete random-walk formulas by letting the latter pass to the limit of infinite jump frequency ν and zero-path length μ. Generally speaking, the only restriction on this limiting process in the case of symmetric random walks is that $\nu\mu^2$ shall remain finite. The case in hand, however, forms an interesting exception, for it appears in the analysis that sensible results are obtainable only in the case that the additional restriction is adopted that the ratio $\sigma=\alpha/\mu$ remain finite as $\mu\to 0$. The actual details of the limiting process are well known[4,5] and need not be discussed here. In (27) we replace z by x/μ and n by νt with x and t continuous space and time coordinates, respectively. As $\mu\to 0$ and $\nu\to\infty$, the terms in $P(x/\mu, \nu t)$ can with increasing exactness be approximated by the normal approximation to the binomial distribution. The final result is a continuous distribution function $C(x,t)dx$ which represents the limiting probability that a particle starting at the origin will be between x and $x+dx$ at time t. We have

$$P(z,n)\to C(x,t)dx=\frac{dx}{(4\pi Dt)^{\frac{1}{2}}}\times\left\{\exp\left(-\frac{x^2}{4Dt}\right)+\exp\left[-\frac{(2m-x)^2}{4Dt}\right]\right\}-dx\sigma\exp[\sigma(2m-x)+D\sigma^2t]\times\operatorname{erfc}\left[\frac{2m-x}{(4Dt)^{\frac{1}{2}}}+\sigma(Dt)^{\frac{1}{2}}\right], \tag{41}$$

where we have written $D=\frac{1}{2}\nu\mu^2$.

Equation (41) can easily be shown to satisfy the diffusion Eq. (3) with the boundary condition

$$-\left(\frac{\partial C}{\partial x}\right)_{x=m}=\sigma C(m,t). \tag{42}$$

Multiplying both sides through by D, (42) becomes identical with (6) if we take $k=D\sigma$, or more specifically

$$k=\tfrac{1}{2}\nu\mu\alpha. \tag{43}$$

VI. DISCUSSION

With this derivation of the Collins-Kimball boundary condition, the difficulty mentioned at the beginning of this paper of treating $0\leq\alpha\leq 1$ as a simple adsorption probability is removed. α is shown necessarily to be an infinitesimal of $O(\mu)$. The magnitude of the constant k is shown to depend upon the quantity σ, which is to say upon the way in which α/μ behaves as both numerator and denominator approach zero. σ is consequently not restricted to lie between zero and some finite value for perfectly reflecting and perfectly adsorbing barriers, respectively, as required in the theory of Secs. I and II. Rather it may and does become infinite for the latter case. From this fact we can readily show that the original Smoluchowski boundary condition for a perfect adsorber may be obtained from (41) by letting $\sigma\to\infty$. Introducing into (41) the asymptotic expansion[6]

$$\operatorname{erfc}\xi=\frac{1}{(\pi)^{\frac{1}{2}}}\exp(-\xi^2)\left(\frac{1}{\xi}-\frac{1}{2\xi^3}+\cdots\right), \tag{44}$$

(41) reduces to

$$C(x,t)dx=\frac{dx}{(4\pi Dt)^{\frac{1}{2}}}\left\{\exp\left(-\frac{x^2}{4Dt}\right)-\exp\left[-\frac{(2m-x)^2}{4Dt}\right]\right\}, \tag{45}$$

as $\sigma\to\infty$. (45) satisfies the boundary condition

$$C(m,t)=0. \tag{46}$$

On the other hand, as $\sigma\to 0$, (41) becomes simply

$$C(x,t)dx=\frac{dx}{(4\pi Dt)^{\frac{1}{2}}}\left\{\exp\left(-\frac{x^2}{4Dt}\right)+\exp\left[-\frac{(2m-x)^2}{4Dt}\right]\right\}, \tag{47}$$

which satisfies the boundary condition

$$\left(\frac{\partial C}{\partial x}\right)_{x=m}=0, \tag{48}$$

known to be correct for a perfectly reflecting surface. Equations (28), (29), (34) show an obvious correlation with (45), (47), (42), respectively.

VII. ADSORPTION KINETICS

The simplest application of the boundary condition (6) to problems in kinetics is the case of irreversible adsorption of a diffusing substance at a boundary wall.

[6] B. O. Pierce, *A Short Table of Integrals* (Ginn and Company, Boston, 1929), p. 120.

This is essentially the problem discussed by Collins and Kimball and needs no further treatment here. The solution is given by (7) for the case of diffusion in one dimension. If the wall is perfectly adsorbing, $\sigma\to\infty$ and through use of (44), one can show that (7) reduces to (5), representing complete diffusion control. It is worth pointing out that this problem has been incorrectly treated by Sveshnikoff[7] and by Blair.[8] Both these authors have assumed that the flux into the reaction surface in the presence of an activation energy barrier to adsorption can be derived from the flux for complete diffusion control by merely multiplying the latter by a probability factor less than unity.

A problem of corresponding interest is that of reversible adsorption, in which we assume that the adsorption reaction is opposed by a desorption reaction and that at equilibrium part of the diffusing material will be in the adsorbed state and part in the bulk solution. This is of interest, for instance, in the kinetics of accumulation of matter at phase boundaries.[9]

As in Sec. I, we suppose that the solution containing the diffusing substance is to the right of the origin with the adsorbing wall located at $x=0$, where x is distance measured perpendicular to the wall. At the start of the reaction the concentration is uniform and equal to C_0. The flux Φ per unit area leftward through the barrier will be

$$\Phi=D\left[\frac{\partial}{\partial x}C(x,t)\right]_{x=0},$$

whence we may write the surface concentration Γ of adsorbed material at any time t as

$$\Gamma=D\int_0^t\left[\frac{\partial}{\partial x}C(x,t')\right]_{x=0}dt'. \tag{49}$$

Two cases of interest now arise: I. The reaction is diffusion controlled. II. There exists an activation energy for adsorption at the barrier.

Case I implies that the adsorbed layer is in instantaneous equilibrium with the layer of solution immediately adjacent to it, and that the sole rate process in the system consists in the diffusion of solute up to the boundary. The kinetics will, of course, be dependent upon the form of the equilibrium relationship between Γ and the concentration of the adjacent layer $C(0,t)$. To fix our ideas, we shall treat the special case of a linear isotherm,

$$C(0,t)=K\Gamma \tag{50}$$

with K an equilibrium constant. This might represent, for example, the first term in the low concentration expansion of the Langmuir adsorption isotherm. We have, therefore, to solve (3) with the boundary condition (50) for the case of uniform initial concentration C_0. The solution is well known.[10]

$$C/C_0=1-\exp(Kx+DK^2t)\,\mathrm{erfc}\left[\frac{x}{(4Dt)^{\frac{1}{2}}}+K(Dt)^{\frac{1}{2}}\right]. \tag{51}$$

From (51) the reaction rate is readily calculated to be

$$\Phi/C_0=\left(\frac{D}{\pi t}\right)^{\frac{1}{2}}-DK\exp(DK^2t)\,\mathrm{erfc}K(Dt)^{\frac{1}{2}}. \tag{52}$$

For Case II, we take both adsorption and desorption reactions at the boundary to be first order with rate constants k_1 and k_2, respectively. The flux leftward through the boundary will then be

$$\Phi=k_1C(0,t)-k_2\Gamma. \tag{53}$$

With this boundary condition, the solution to (3) for uniform initial concentration is[10]

$$C/C_0=1-\frac{k_1/D}{b-a}\Big[\exp(ax+Da^2t)\times\mathrm{erfc}\left\{\frac{x}{(4Dt)^{\frac{1}{2}}}+a(Dt)^{\frac{1}{2}}\right\}-\exp(bx+Db^2t)\times\mathrm{erfc}\left\{\frac{x}{(4Dt)^{\frac{1}{2}}}+b(Dt)^{\frac{1}{2}}\right\}\Big], \tag{54}$$

where

$$a=-\frac{1}{2}\frac{k_1}{D}[1+(1-\lambda)^{\frac{1}{2}}],$$

$$b=-\frac{1}{2}\frac{k_1}{D}[1-(1-\lambda)^{\frac{1}{2}}],$$

$$\lambda=4k_2D/k_1^2.$$

The boundary flux or reaction rate derived from (54) is

$$\Phi/C_0=\frac{k_1}{a-b}[a\exp(Da^2t)\,\mathrm{erfc}a(Dt)^{\frac{1}{2}}-b\exp(Db^2t)\,\mathrm{erfc}b(Dt)^{\frac{1}{2}}]. \tag{55}$$

The forms (52) or (55) are not particularly useful for practical calculations but are easily approximated by simple expressions for both small and large values of the time. Introducing the expansion[11]

$$\mathrm{erfc}\xi=1-\frac{2}{\sqrt{\pi}}\exp(-\xi^2)(\xi+\tfrac{2}{3}\xi^3+\cdots). \tag{56}$$

Eq. (52) at small $K(Dt)^{\frac{1}{2}}$ reduces to

$$\Phi/C_0=\left(\frac{D}{\pi t}\right)^{\frac{1}{2}}, \tag{57}$$

[7] B. Sveshnikoff, Acta Physicochim. U.R.S.S. **3**, 257 (1935).
[8] C. M. Blair, J. Chem. Phys. **16**, 113 (1948).
[9] K. L. Sutherland, Australian J. Sci. Research **A5**, 683 (1952).
[10] Carslaw and Jaeger, *Conduction of Heat in Solids* (Oxford University Press, London, 1947), pp. 248, 249.
[11] E. P. Adams, *Smithsonian Mathematical Formulae and Tables of Elliptic Functions* (Washington, 1947), p. 133.

which becomes infinite as $t\to 0$. At large $K(Dt)^{\frac{1}{2}}$ we use (44) to find for Case I

$$\Phi/C_0=K^{-2}(4\pi Dt^3)^{-\frac{1}{2}}. \tag{58}$$

In a similar way, the small time approximation to (55) can be shown to be

$$\Phi/C_0=k_1\left[1-2k_1\left(\frac{t}{\pi D}\right)^{\frac{1}{2}}+\cdots\right], \tag{59}$$

while at large times (55) reduces to

$$\Phi/C_0=\left(\frac{k_1}{k_2}\right)^2(4\pi Dt^3)^{-\frac{1}{2}}-\cdots. \tag{60}$$

It is of interest to compare these asymptotic formulas with the corresponding approximations for irreversible adsorption. The boundary flux for complete diffusion control is derived from (5) and is at all times

$$\Phi/C_0=\left(\frac{D}{\pi t}\right)^{\frac{1}{2}}. \tag{61}$$

If a first-order process at the boundary also contributes to the over-all rate, the flux is obtained from (7) and has small and large time approximations, respectively,

$$\Phi/C_0=k\left[1-2k\left(\frac{t}{\pi D}\right)^{\frac{1}{2}}+\cdots\right], \tag{62}$$¶

$$\Phi/C_0=\left(\frac{D}{\pi t}\right)^{\frac{1}{2}}-\sigma^{-2}(4\pi Dt^3)^{-\frac{1}{2}}+\cdots. \tag{63}$$

Examination of Eqs. (57) through (63) reveals that reversible and irreversible adsorption kinetics on a plane surface are experimentally distinguishable only for large values of the time. On the other hand, it is precisely at large values of the time that the asymptotic flux for both reversible and irreversible adsorption becomes independent of the presence of an activation energy at the adsorbing wall. Any attempt to study such activation energies must consequently be based on measurements of the initial flux. This point has already been made by Collins.[3]

¶ Equation (62) is quoted as Eq. (16) in reference 3, but with a misprint.

VIII. SUMMARY

The Smoluchowski theory of adsorption kinetics as a diffusion controlled process is modified to include the case in which not all particles entering the reaction surface are adsorbed. It is shown that the proper boundary condition for the diffusion equation in this case is $\Phi=kC$, in which Φ is the flux across the reaction surface and C is the boundary concentration. k is given by $k=\sigma D$, where D is the diffusion constant and $\sigma=\alpha/\mu$ is the limiting ratio of the adsorption probability to the jump length of the diffusing particle as both quantities approach zero.

In a study of reversible adsorption kinetics in colloidal systems, it is shown that for diffusion in one dimension, the asymptotic flux at large values of the time is independent of k. This is in agreement with the known result for irreversible adsorption.

APPENDIX

We have to prove the convolution formula

$$\sum_{i=z}^{n-y} W(z,i)W(y,n-i)=W(z+y,n), \tag{64}$$

where $W(z,n)$ is defined by

$$W(z,n)=\left(\frac{1}{2}\right)^n\frac{z}{n}\binom{n}{\frac{1}{2}(n+z)}. \tag{65}$$

It is known[4] that $W(z,n)$ is the coefficient of s^n in the power series expansion of

$$G^z(s)=\left\{\frac{1}{s}[1-(1-s^2)^{\frac{1}{2}}]\right\}^z=\sum_{n=0}^{\infty}s^nW(z,n). \tag{66}$$

Multiplying the series for $G^z(s)$ by that for $G^y(s)$ and collecting the coefficients of like powers of s we have

$$G^z(s)G^y(s)=W(z,0)W(y,0)+s[W(z,0)W(y,1)+W(z,1)W(y,0)]+\cdots. \tag{67}$$

But

$$G^z(s)G^y(s)=G^{z+y}(s)=\sum_{n=0}^{\infty}s^nW(z+y,n). \tag{68}$$

Comparing coefficients in (67) and (68) the theorem follows.

Exchange Energy of Electrons in Metals and Ionic Crystals

JOHN R. REITZ*
U. S. Office of Naval Research, American Embassy, London, England
(Received November 16, 1953)

The exchange energy of valence electrons in both monatomic and diatomic crystals is computed in the Bloch approximation for the case where the lowest electronic wave function in the band shows considerable spatial variation. Only ground-state wave functions which are spherically symmetric in each atomic cell are considered, but within this limitation two types of spatial variation are considered: radial variation in the unit cell, and the variation in a diatomic lattice due to the wave function being more concentrated on one of the atomic species than on the other. The results of the calculation show that, for a monatomic solid, deviations from uniformity in the wave function have a relatively small effect on the exchange energy; in highly ionic diatomic solids, however, the exchange energy may be increased up to 50 percent in magnitude over the free-electron value as a result of the electron density in anion cells being different from that of cation cells.

I. INTRODUCTION

IN the one-electron approximation of quantum mechanics, there are two fundamental approaches for calculating the properties of solids, namely, the *Bloch scheme* in which the individual electron valence functions extend throughout the entire crystal and the *Heitler-London* or *valence bond scheme*, in which the starting point is the atomic wave functions associated with the atoms making up the crystal. The Bloch scheme, particularly in the form developed by Wigner and Seitz,[1] has proved especially suited to calculations of the cohesion of metals and has also been used, with moderate success, for investigating the cohesive energy of ionic crystals.[2] Only the Bloch approximation will be considered in the present paper.

In the treatment of the cohesive energy of metallic sodium by Wigner and Seitz,[1] calculation of the exchange energy of the valence electrons was facilitated by the fact that the lowest wave function in the band is practically constant over most of the unit cell, and the other wave functions in the band differ from this distribution only by the exponential factor $e^{2\pi i\mathbf{k}\cdot\mathbf{r}}$. Thus the exchange energy was approximated by that of a system of perfectly free electrons. Seitz[3] has shown that under certain conditions, in particular those applying to the valence band in alkali metals, the wave function corresponding to the wave vector $\mathbf{k}$ may be expressed in the form

$$\psi_{\mathbf{k}}=V^{-\frac{1}{2}}e^{2\pi i\mathbf{k}\cdot\mathbf{r}}[f(r)+i\mathbf{k}\cdot\mathbf{r}g(r)], \qquad (1)$$

where f and g are radial functions having spherical symmetry in the unit cell and V is the volume of the system. $f(r)$ is thus the lowest wave function in the band, and $g(r)$ is related to the effective mass of the electrons. In his treatment of the cohesive energy of lithium[4,5] Seitz calculated the exchange energy of the system (1) under the assumption that both f and g are constants, with the result that the exchange energy is increased slightly in magnitude over the free electron value. Herring,[6] however, has stated that Seitz's calculation involves a computational error and has found a *decrease* of about 2.2 kcal/mole in the magnitude of the exchange energy for lithium. Recently Wohlfarth[7] investigated the exchange energy of nearly free electrons in metals as a function of the effective mass of the electrons. His results, strictly applicable in the limit of low electron density, but based on two analyses using differing one-electron wave functions, show that the exchange energy is much less sensitive to changes of the effective mass of the electrons than is the Fermi energy.

So far no attempts have been made to evaluate the exchange energy when the lowest wave function in the band $f(r)$ cannot be approximated by a constant value; it is the purpose of the present analysis to make this evaluation. The calculation will be carried out in Wigner-Seitz approximation with the analysis restricted to spherically-symmetric distributions of charge in each cell. Two types of spatial variation of the wave function will be considered: radial variation in the unit cell and the variation in a diatomic lattice due to the electron wave function being more concentrated on one of the atomic species than on the other. This last variation is especially important since the periodicity of the variation is of the same order of magnitude as the "range of interaction" of the exchange forces.

II. EXCHANGE ENERGY OF A MONATOMIC SOLID

In this section the exchange energy of valence electrons in a monatomic solid will be evaluated. The calculation will be made for the case where there is one electron per atom in the valence band although conclusions will also be drawn about the more general case. It will be assumed that the wave function corre-

* The opinions or assertions in this article are the private ones of the writer and are not to be construed as official or as reflecting the views of the United States Navy.

[1] E. Wigner and F. Seitz, Phys. Rev. **43**, 804 (1933); **46**, 509 (1934).

[2] W. Shockley, Phys. Rev. **50**, 754 (1936); D. H. Ewing and F. Seitz, Phys. Rev. **50**, 760 (1936); S. R. Tibbs, Trans. Faraday Soc. **35**, 1471 (1939); D. G. Bell *et al.*, Proc. Roy. Soc. (London) **A217**, 71 (1953).

[3] F. Seitz, *Modern Theory of Solids* (McGraw-Hill Book Company, Inc., New York, 1940), p. 353.

[4] F. Seitz, Phys. Rev. **47**, 400 (1935).

[5] See reference 3, p. 359.

[6] C. Herring, Phys. Rev. **82**, 282 (1951).

[7] E. P. Wohlfarth, Phil. Mag. **44**, 281 (1953).

sponding to the wave vector $\mathbf{k}$ may be written as

$$\psi_{\mathbf{k}} = V^{-\frac{1}{2}} e^{2\pi i \mathbf{k}\cdot\mathbf{r}} f(\mathbf{r}), \tag{2}$$

where f is a function with spherical symmetry in the unit cell; f is normalized so that

$$\int_v f^2(\mathbf{r}) d\tau = v, \tag{3}$$

where v is a volume made up of an integral number of cells, the unit cell in turn being defined as a spherical volume v_c containing one atom. Here we have written $f^2(\mathbf{r})$ for $|f(\mathbf{r})|^2$.

The quantities occurring in the exchange integral have the same $\mathbf{k}$ dependence as in the free-electron case, so that the integrations over $d\mathbf{k}$ and $d\mathbf{k}'$ can be performed immediately. Turning now to the volume integral, we find that the volume element may be written[8]

$$d\tau_1 d\tau_2 = r_1 dr_1 r_2 dr_2 r_{12} dr_{12} \sin\theta_1 d\theta_1 d\varphi_1 d\chi, \tag{4}$$

where $\mathbf{r}_1$ and $\mathbf{r}_2$ are position vectors of $\psi_{\mathbf{k}}(\mathbf{r}_1)$, etc., measured from a fixed origin (in this case from one of the atomic nuclei in the crystal), r_1 and r_2 are the magnitudes of $\mathbf{r}_1$ and $\mathbf{r}_2$, respectively, $r_{12} = |\mathbf{r}_1 - \mathbf{r}_2|$, θ_1 is the angle between $\mathbf{r}_1$ and the z axis through the origin, φ_1 is an azimuthal angle around this z axis, and χ is an azimuthal angle around the direction of $\mathbf{r}_1$. Because of the symmetry of the problem, the integrations over θ_1, φ_1, and χ can be performed at once. The exchange energy of the valence electrons then becomes

$$\begin{aligned} J &= -(e^2/V^2) \int e^{2\pi i(\mathbf{k}'-\mathbf{k})\cdot(\mathbf{r}_1-\mathbf{r}_2)} \\ &\qquad \times f^2(r_1) f^2(r_2) r_{12}^{-1} V^2 d\mathbf{k}' d\mathbf{k} d\tau_1 d\tau_2 \\ &= -(128/9)\pi^4 e^2 k_0^6 N_a \int_0^R f^2(r_1) r_1 dr_1 \\ &\qquad \times \int_0^\infty dr_{12} Q(\zeta) \int_{|r_1-r_{12}|}^{r_1+r_{12}} f^2(r_2) r_2 dr_2, \end{aligned} \tag{5}$$

where the integration of dr_1 over the linear dimension of the crystal has been replaced by N_a integrations over the unit cell, N_a being the number of atoms in the system. Here k_0 is the wave number belonging to the top of the Fermi distribution, namely $k_0 = (3N/8\pi V)^{\frac{1}{3}}$ with N equal to the number of electrons in the system; the radius of the cell R is given by

$$R = (3v_c/4\pi)^{\frac{1}{3}} = (3V/4\pi N)^{\frac{1}{3}}\alpha, \tag{6}$$

where α^3 is the number of electrons per atom (in this case $\alpha = 1$). The exchange function

$$Q(\zeta) = 9(\zeta\cos\zeta - \sin\zeta)^2/\zeta^6, \tag{7}$$

where

$$\zeta = 2\pi k_0 r_{12} = (9\pi/4)^{\frac{1}{3}}\alpha r_{12}/R. \tag{7a}$$

[8] H. Margenau and G. M. Murphy, *The Mathematics of Physics and Chemistry* (D. Van Nostrand Company, Inc., New York, 1943), p. 366.

Before proceeding with the evaluation of Eq. (5), let us examine the exchange function in some detail. $Q(\zeta)$ is plotted in Fig. 1, and it is seen that the range of interaction between two regions of charge is essentially restricted to $\zeta \cong 4.5$, or to $r_{12} \cong 2R$ for the case of $\alpha = 1$ (one electron per atom in the valence band). Thus the exchange interaction is fairly short ranged, and interactions of the charge distribution inside a unit cell with itself are expected to make up a substantial fraction of the exchange energy. $Q(\zeta)$ has further subsidiary maxima beyond $\zeta = 4.5$, but these are relatively unimportant; direct computation shows that the loop containing the first subsidiary maximum (i.e., the part of the function between its first and second zero) contributes only three percent to the exchange energy. The combined contribution of all other loops is about one percent.

In order to carry out the integrations of Eq. (5) in the case where $f(r)$ is neither a constant nor given by the same analytic expression inside and outside the unit cell, it is desirable to approximate $Q(\zeta)$ by a simpler function. Accordingly,

$$Q(\zeta) \cong Q_1(\zeta) + Q_2(\zeta), \tag{8}$$

where

$$\begin{aligned} Q_1 &= \cos^2[(\pi/4)(4/9\pi)^{\frac{1}{3}}\zeta] \quad \text{for} \quad \zeta \leq 2(9\pi/4)^{\frac{1}{3}}, \\ Q_2 &= 0.005, \quad \text{for} \quad 4.75 \leq \zeta \leq 7.25. \end{aligned}$$

$Q_1(\zeta)$ and $Q_2(\zeta)$ are also shown graphically in Fig. 1. As a check on this approximation, the exchange energy of an assembly of free electrons was computed using expression (8) for the exchange function, with the result that $J = 1.007 J_0$ ($J_0 = -4\pi e^2 k_0^4 V$, i.e., the free-electron value). The term in Q_1 contributes 0.974 to J/J_0, and the term in Q_2 contributes 0.033. The contribution of the Q_1 term is about two percent larger than the corresponding part of the $Q(\zeta)$ term; this source of error could be reduced by changing the coefficient of ζ in $Q_1 = \cos^2[(\pi/4)(4/9\pi)^{\frac{1}{3}}\zeta]$, but our choice is particularly convenient, in the case where $\alpha = 1$, since Q_1 reduces to

$$Q_1 = \cos^2[(\pi/4) r_{12}/R],$$

and the subsequent integrations over r_1 are greatly simplified. Furthermore, these errors essentially drop out of the final comparison of the exchange energies.

The calculation of the exchange energy of anything but an assembly of free electrons quickly becomes a rather complicated problem in algebra; thus only the simplest type of wave function $f(r)$ could be investigated. Nevertheless it is desirable to study a case where the wave function deviates markedly from a constant value. Accordingly, the following expression was chosen for $f(r)$:

$$\left.\begin{aligned} f(r) &= (A/r)^{\frac{1}{3}} \quad \text{for} \quad r \leq R, \\ f(r) &= 1 \quad\quad\;\; \text{for} \quad r \geq R. \end{aligned}\right\} \tag{9}$$

Our expression for $f(r)$ inside the unit cell may be

considered to be an approximation to $A^{\frac{1}{2}}/(r+\eta)^{\frac{1}{2}}$, where η is a length very small compared to R; there are no divergence difficulties with any of the configurational integrals when expression (9) is used. The normalization condition Eq. (3) gives $A=(2/3)R$.

The exchange energy (5) will now be evaluated for the case where $f(r)$ is given by (9); for convenience the approximate expression (8) will be used for $Q(\zeta)$. The r_2 integration can be readily performed, yielding since $r_1 \leq R$:

$$\int_{|r_1-r_{12}|}^{r_1+r_{12}} f^2(r_2) r_2 dr_2$$

$$= 2r_1 r_{12} \quad \text{if} \quad R \leq |r_{12}-r_1|,$$

$$= A[R-|r_1-r_{12}|] + \tfrac{1}{2}r_1^2 + r_1 r_{12} + \tfrac{1}{2}r_{12}^2 - \tfrac{1}{2}R^2$$

$$\text{if} \quad |r_{12}-r_1| \leq R \leq r_1+r_{12},$$

$$= A[r_1+r_{12}-|r_1-r_{12}|] \quad \text{if} \quad R \geq r_1+r_{12}. \tag{10}$$

The subsequent integration over r_{12} yields the following sum of integrals (note again that $r_1 \leq R$):

$$\int_{R+r_1}^{\infty} 2r_1 r_{12} Q(\zeta) dr_{12}$$

$$+ \int_{R-r_1}^{R+r_1} [AR - \tfrac{1}{2}R^2 + \tfrac{1}{2}r_1^2 + r_1 r_{12} + \tfrac{1}{2}r_{12}^2] Q(\zeta) dr_{12}$$

$$- \int_{R-r_1}^{R+r_1} A(r_{12}-r_1) Q(\zeta) dr_{12} \quad (\text{for } r_1 \leq R/2)$$

$$- \int_{R-r_1}^{r_1} A(r_1-r_{12}) Q(\zeta) dr_{12} \quad (\text{for } r_1 \geq R/2)$$

$$- \int_{r_1}^{R+r_1} A(r_{12}-r_1) Q(\zeta) dr_{12} \quad (\text{for } r_1 \geq R/2)$$

$$+ \int_{0}^{R-r_1} 2A r_{12} Q(\zeta) dr_{12} \quad (\text{for } r_1 \geq R/2)$$

$$+ \int_{0}^{r_1} 2A r_{12} Q(\zeta) dr_{12} \quad (\text{for } r_1 \leq R/2)$$

$$+ \int_{0}^{R-r_1} 2A r_1 Q(\zeta) dr_{12} \quad (\text{for } r_1 \leq R/2). \tag{11}$$

These are all elementary integrals which can be performed, and the final integration over r_1 can be carried out in a straightforward fashion, yielding

$$J/J_0 = 1.0904(A/R)^2 + 0.8628(A/R)$$
$$= 0.4846 + 0.5752$$
$$= 1.060, \tag{12}$$

where $J_0 = -4\pi e^2 k_0^4 V$, the free-electron value of the exchange energy. Thus it is seen that a charge distribution $f^2(r)$, which is peaked about the ion cores and which falls to two-thirds of the uniform charge distribution at the edge of the unit cell, has only increased the magnitude of exchange energy by five to six percent. Since the $(A/R)^2$ term in (12) represents interactions of the charge distribution in a cell with itself, and the (A/R) term interactions between cells, it is observed that the former type of interaction contributes almost one-half of the exchange energy.

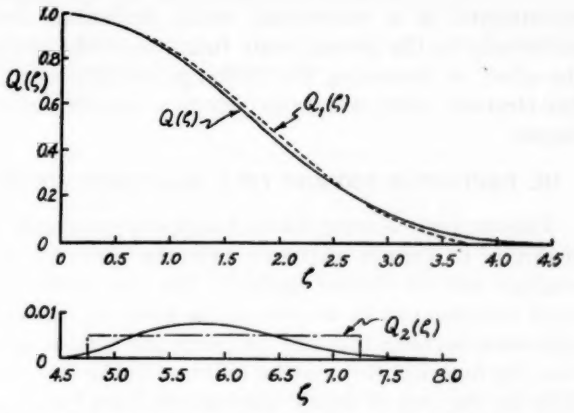

FIG. 1. Plot of the exchange function, $Q(\zeta)$, as defined in Eq. (7), along with the functions $Q_1(\zeta)$ and $Q_2(\zeta)$ of Eq. (8). ——$Q(\zeta)$, - - - - - -$Q_1(\zeta)$, — - —$Q_2(\zeta)$.

The above calculation was made for the case of one electron per atom in the valence band. Let us now consider the case where there are more than one electron per atom ($\alpha^3>1$) but still restrict ourselves to a spherically-symmetric distribution of charge in the unit cell. The exchange interaction is unchanged in terms of the variable ζ, and from Eq. (7a) it may be seen that the range of interaction is given by $r_{12} \cong 2R/\alpha$. Thus the range of the exchange forces has been reduced relative to the radius R of the cell. As a result, a larger percentage of the exchange energy arises from interactions of the nonuniform charge distribution with itself, and J/J_0 will be slightly increased relative to the case described above. This cannot be a large effect, however, amounting perhaps to only one or two percent for $\alpha^3=2$.

Other types of spatial variation of the wave function might be investigated. For instance, one might consider a wave function which reached its maximum near the boundary of the cell, such as $f^2(r)=Br^{\frac{1}{2}}$ for $r \leq R$. The exchange energy would also in this case be slightly larger in magnitude than the free-electron value, since any deviation from uniformity in the wave function tends to increase the energy (another example of this will be given in Sec. III). The presence of a large number of radial nodes in the wave function will probably not affect the exchange energy very much, since this type of spatial variation is of rather short wavelength compared to the range of the exchange interaction. It thus appears that, for the type of wave function normally

encountered in a monatomic solid, deviations from uniformity in the ground state function, while having the effect of increasing the exchange energy over the free electron value, will do so only to a relatively small degree.

III. EXCHANGE ENERGY OF A DIATOMIC SOLID

This section will treat the exchange energy of valence electrons in certain diatomic crystals, although the analysis will be limited again to the case where the wave function can be written in the form (2), the only difference between this and the preceding section being that the function $f(r)$ may be different in the two cells. Now for the case of nearly filled bands, even Eq. (1) is not a satisfactory representation of wave functions near the top of the band, except in certain cases where this band strongly overlaps an empty one. Thus the results of this section might properly be applied to ordered diatomic alloys but would have to be applied with considerable caution to ionic crystals. On the other hand, an approximate treatment of this type might be justified for ionic crystals in that some of the features of a more accurate analysis will come into evidence. Within the limitations set out above, then, the calculation is applicable to the valence band of monovalent metal hydrides ($\alpha=1$), and, since $f(r)$ enters the integrals only as f^2, to the filled p band (Γ_4' band)[9] in ionic crystals ($\alpha^3=3$) where the valence functions are approximated by

$$\psi_k=3^{\frac{1}{2}}V^{-\frac{1}{2}}e^{2\pi i\mathbf{k}\cdot\mathbf{r}}f(r)\cos\theta, \tag{13}$$

etc.

The exchange energy of valence electrons in diatomic crystals will now be calculated for the case where $\alpha=1$. This evaluation can be carried out fairly easily in terms of the result of the previous section. The crystal is divided into cells such that an *equal* volume, $v_c=V/N=V/(N_1+N_2)$, is assigned to each ion core in the lattice, and the cell is considered to be spherically symmetric, with a radius R given by Eq. (6). The ground-state wave function $f(r)$ is assumed to have the same basic shape but different magnitude in the two kinds of cells, i.e.,

$$\left.\begin{aligned} &f(r)=(A_1/r)^{\frac{1}{2}} \text{ in anion cells} \\ &f(r)=(A_2/r)^{\frac{1}{2}} \text{ in cation cells} \end{aligned}\right\} \quad \text{for } r\leq R, \qquad f(r)=1 \quad \text{for } r\geq R, \tag{14}$$

and the normalization condition is such that

$$A_1+A_2=(4/3)R. \tag{15}$$

The exchange energy is calculated in similar fashion to that in the preceding section, except that interactions of the charge distribution in a cell with itself give rise to two types of terms, namely, to terms in $(A_1/R)^2$ and in $(A_2/R)^2$. Similarly, the interaction of a cell with the charge distribution outside of it is either of the form (A_1/R) or (A_2/R). Thus

$$\begin{aligned} J/J_0&=0.5452[(A_1/R)^2+(A_2/R)^2] \\ &\quad +0.4314[(A_1/R)+(A_2/R)] \\ &=0.5452[(A_1/R)^2+(A_2/R)^2]+0.5752, \end{aligned} \tag{16}$$

the last expression being obtained through the use of the normalization condition.

Now for $\alpha=1$, there are two valence electrons per molecule; if we assign x electrons to the cation and y to the anion, subject to $x+y=2$, then Eq. (16) reduces to

$$J/J_0=0.2423(x^2+y^2)+0.5752. \tag{16a}$$

It is observed that in a strongly ionic crystal, in which all of the valence electrons are concentrated around the anions, the quantity J/J_0 is increased almost 50 percent over the case where the electrons are equally distributed between the two types of cells.

It should be pointed out that nearly the same result, (16a), is obtained when $f(r)$ is a constant, but of different magnitude in the two types of cells.

IV. DISCUSSION OF RESULTS

The results of the preceding sections have shown that the exchange energy of valence electrons in monatomic metals is not altered very much because of spatial variations of the ground-state wave functions; thus if the wave function ψ_k can be expressed in the form (1), the approximation, $f(r)=$constant, certainly appears to be justified in the exchange energy term. The effect of a spatial variation in $g(r)$ has not been investigated, but the entire contribution due to terms in g is in general small.[6,7]

In diatomic solids the exchange energy may be increased considerably in magnitude due to differences in the wave function in the two types of cells. This type of spatial variation has a periodicity of the same order of magnitude as the range of the "exchange interaction," and is therefore capable of producing a large effect. The largest effect is to be expected in highly ionic solids, but in these solids, with filled valence bands, the above analysis is not so accurate since the neglected nonspherical terms in the wave functions will alter the exchange energy somewhat; Eq. (1) can only be regarded as a good approximation to wave functions in the lower part of the band. On the other hand, it should be emphasized that the exchange energy depends only on the integral properties of these wave functions, and deviations from spherical symmetry in ψ_k near the boundary of the cell will probably produce a similar effect to that of radial variation of ψ_k inside one cell (i.e., the effect on the exchange energy will be small).

V. ACKNOWLEDGMENT

The author would like to thank Professor Hans Bethe for several stimulating discussions concerning this calculation and related problems.

[9] The notation is that of Bouckaert, Smoluchowski, and Wigner, Phys. Rev. 50, 58 (1936). See also D. G. Bell *et al.* (reference 2) for a list of "Kubic harmonics" in ionic crystals of this type.

The Far Ultraviolet Absorption Spectra of the Isomeric Butenes*

JULIA T. GARY AND LUCY W. PICKETT
Department of Chemistry, Mount Holyoke College, South Hadley, Massachusetts

(Received August 27, 1953)

Measurements of the intensity and position of absorption from 45 000 to 64 000 cm^{-1} of butene-1, *cis*-butene-2, *trans*-butene-2, and 2-methylpropene were made on flowing vapors. All show a broad intense band which is most intense in the case of the *cis*-isomer, and superimposed systems of narrow bands, both at shorter and longer wavelengths. Whereas the position of the last named is dependent on the number of alkyl groups adjacent to the double bond, the broad band maximum is not similarly displaced but rather depends on the molecular shape and seems related to the dipole moment vector. The vibrational structure of the bands is consistent with infrared and Raman data.

INTRODUCTION

THE four butenes constitute a simple complete group of isomeric compounds suitable for a study of the influence of molecular symmetry and alkyl substitution on transitions of the π electrons of doubly bonded carbon atoms. An investigation of the absorption spectra of butene-1, *cis*-butene-2, *trans*-butene-2, and 2-methylpropene or isobutylene in the Schumann ultraviolet region was undertaken to obtain position and intensity of absorption bands and to correlate the data with the structure and symmetry properties of the molecules. Carr and Stücklen[1,2] have made a systematic study of alkyl-substituted ethylenes which included the butenes, but were unable to make measurements of intensity. Price and Tutte[3] observed the spectrum of *trans*-butene-2 in a study of derivatives of ethylene. A study of the isomeric pentenes similar to the present work has recently been made in this laboratory.[4]

EXPERIMENTAL

Compounds

Samples of the four isomeric butenes were obtained from the API Research Project through the courtesy of Dr. Frederick D. Rossini. The samples were research grade materials prepared by Phillips Petroleum Company. A second sample of *cis*-butene-2 of higher specified purity than the first was supplied directly by the Phillips Petroleum Company. Purity data for the compounds used are shown in Table I.

Spectral Measurements

Measurements of flowing vapor were made with a Hilger fluorite-prism vacuum spectrograph using a hydrogen discharge as light source. The Pyrex absorption cell with fluorite windows was 32.4 cm in length. A modified McLeod gauge was used to measure pressures of the compounds, which ranged from 0.016 to 1.5 mm. The spectra were recorded on Ilford Q–1 plates. The Schwarzschild constant was taken as unity on the basis of previous experiments.[5,6] Optical densities were calculated from microphotometer records of the plates with timed exposures of the light source for calibration purposes. Positions of sharp bands were measured with a comparator, using as standards the emission lines of a copper spark, a mercury-absorption line (54 065 cm^{-1}), nitrogen-emission lines, and the line spectrum of molecular hydrogen. The experimental procedures have been described in previous papers.[6,7]

Modifications of the apparatus for low-temperature studies were made by packing the absorption tube in dry ice and precooling the entering gas. These measurements were only qualitative.

RESULTS

The absorption curves of the four compounds are shown in Figs. 1 and 2, where $\log\epsilon$ is shown as a function of wave number. The molar extinction coefficient ϵ is defined as $(1/cl)\log(I_0/I)$ where c is the concentration of the absorbing material in moles/liter calculated through the assumption of perfect gas law and l is the length of the absorbing path in cm. The precision of the determination of band position depended on the spectral region and type of band and in favorable cases could be duplicated to 10 cm^{-1}. The average deviation in $\log\epsilon$ was in most cases of the order of 0.02, but because of lack of standards in the region, the accuracy of the intensity measurements cannot be determined. Because

TABLE I.

Compound	Purity in mole percent	Most probable impurities
Butene-1	99.88	Isobutane, *n*-butane
Cis-butene-2	96.18	*Trans*-butene-2
(high boiling)	99.82	*Trans*-butene-2
Trans-butene-2	98.92	*Cis*-butene-2
2-methylpropene	99.44	*n*-butane

* This work has been supported by The National Science Foundation (Research Grant NSF-G226).

[1] E. P. Carr and H. Stücklen, J. Chem. Phys. **4**, 760 (1936).
[2] E. P. Carr and H. Stücklen, J. Am. Chem. Soc. **59**, 2138 (1937).
[3] W. C. Price and W. T. Tutte, Proc. Roy. Soc. (London) **A174**, 207 (1940).
[4] Semenow, Harrison, and Carr (to be published).
[5] L. E. Jacobs and J. R. Platt, J. Chem. Phys. **16**, 1137 (1948).
[6] Harrison, Gaddis, and Coffin, J. Chem. Phys. **18**, 221 (1950).
[7] Pickett, Muntz, and McPherson, J. Am. Chem. Soc. **73**, 4862 (1951).

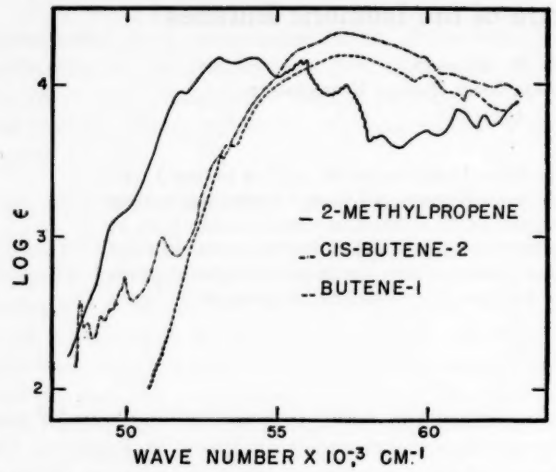

FIG. 1. Far ultraviolet absorption curves of isomeric butenes.

the continuum of hydrogen diminishes and the many-line spectrum begins near 1650A, measurements beyond 59 500 cm^{-1} are more difficult and probably less accurate than those at longer wavelengths.

Each curve represents more than a hundred experimental points taken from 10 to 15 plates for each compound.

DISCUSSION

General Characteristics of Spectra

In the butenes, as in ethylene and the other alkyl derivatives, the spectra in this region are with little doubt a superposition of two types of bands of quite different structure, corresponding to different electronic transitions. The more intense appears as a broad intense band. Superimposed on this at longer wavelengths is a series of narrow bands which has been designated as $N \rightarrow R$ or Rydberg type,[8] while the intense band has previously been ascribed to an $N \rightarrow V$ transition.[9] Evidence of an electronic transition on the short-wavelength side of the broad band, whose structure indicates that it is also of a Rydberg type, is especially marked in 2-methylpropene and in *trans*-butene-2.

The position of the first Rydberg band, found in this study to be 53 390 cm^{-1} for butene-1, 49 750 cm^{-1} for isobutylene, 49 470 cm^{-1} for *trans*-butene-2, and 48 400 cm^{-1} for *cis*-butene-2, was reported by Carr and Stücklen[1] to be a function of the number of alkyl groups substituted on carbon atoms of the double bond. This study supports the earlier conclusions.

The position of maximum absorption, however, exhibits no such rule. In fact, a most interesting characteristic of both butenes and pentenes is the displacement of the broad band maxima from one compound to another. Isobutylene exhibited maximum absorption at 53 100 cm^{-1}, *trans*-butene-2 at 56 270 cm^{-1}; but butene-1 and *cis*-butene-2 showed highest molar-extinction coefficients at 57 100 and 57 000 cm^{-1}, respectively, although the band center appeared to be perhaps 200 cm^{-1} larger. While no explanation for this displacement can be offered with certainty, it was of interest to observe that there is a correlation with the direction of polarity of the molecules which is consistent through butene and pentene isomers. If *trans*-butene-2, where no dipole moment would be expected because of cancellation of dipole vectors, is taken as the norm, the remaining butene isomers fit into a pattern on the basis of the relation of the dipole vector of the molecule to the double bond and hence direction of charge displacement during the transition. Butene-1 has a dipole moment of 0.30*D* [10] whose largest component would be perpendicular to the double bond. *Cis*-butene, whose moment is not on record, would reasonably have a net moment only in this perpendicular direction; and in both compounds the band maximum is displaced to higher frequencies in

TABLE II.

Type	Vector	Butenes Name	Butenes Band max. (cm^{-1})	Pentenes[a] Name	Pentenes[a] Band max. (cm^{-1})
	0	*trans*-butene-2	56 270	*trans*-pentene-2	55 500
	→	2-methylpropene	53 100	2-methyl-1-butene	53 220
	↑	*cis*-butene-2	57 000	*cis*-pentene-2	56 600
	↑→	butene-1	57 100	pentene-1 3-methyl-1-butene	56 600 56 800
	↑→			2-methyl-2-butene	56 575

[a] See reference 4.

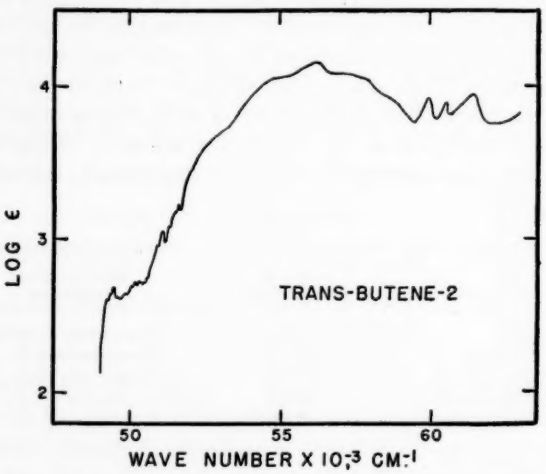

FIG. 2. Far ultraviolet absorption curve of *trans*-butene-2.

[8] E. P. Carr and H. Stücklen, J. Chem. Phys. **7**, 631 (1939).
[9] R. S. Mulliken, J. Chem. Phys. **7**, 20 (1939).
[10] H. E. Watson and K. L. Ramaswamy, Proc. Roy. Soc. (London) **A156**, 130 (1936).

TABLE III.

Wave number in cm^{-1}	*Cis*-butene-2 $\Delta\nu$	Infrared or Raman[a]	Motion	Wave number in cm^{-1}	*Trans*-butene-2 $\Delta\nu$	Infrared or Raman[a]
				49 250 w.	−220	
				49 370 w.	−100	
48 400 v.s.	0			49 470 v.s.	0	
				49 640 v.w.	170	
48 635 v.w.	235	304	Skeletal deformation	49 935 v.w.	465	507
				50 165 v.w.	695	
49 100 w.	700	876	C−C stretching	50 220 v.w.	750	870
				50 320 m.	850	1080
49 365 m.	965	1018	CH_3 wagging	50 440 m.	970	1309
49 650 m.	1250	1267	CH wagging	50 735 w.	1265	
				50 935 v.w.	1465	
49 905 s.	1505	1672	C−C stretching	51 050 m.s.	1580	1680
50 215 w.	1815			51 370 v.w.	1900	
50 575 w.	2175					
51 200 broad	2800	3000 approx	C−H stretching	52 230 broad	2760	3000 approx

[a] See reference 14.

relation to the *trans*-isomer. Addition of the dipole vectors of 2-methylpropene gives a resultant moment in the bond direction only, which has been measured as 0.49*D*,[10] while here the band is displaced to lower frequencies. In the case of the pentenes, as measured by Semenow, Harrison, and Carr,[4] *trans*-pentene-2 is again intermediate, with 2-methyl-1-butene at lower and the other four isomers at higher frequencies. Inspection of the structural formulas, as shown in Table II, will show that only in the case of the 2-methyl-1-butene is the resultant vector in the direction of the bond; in the others the resultant vector or its larger component would reasonably be normal to the bond direction. If these observations, which will be tested on the isomeric hexenes, are supported, it will indicate that when there is a dipole vector in the direction of the bond, less energy is required to excite the transition, while a moment which is greater in the perpendicular direction will increase the excitation energy.

When the spectra of the four compounds are compared, a striking feature observed is the higher intensity of the band of the *cis*-isomer. All four compounds have values of molar extinction coefficient of over 10 000, indicating allowed transitions and showing consistency with other olefins observed. It is difficult to estimate the oscillator strengths of the transitions with reliability because of the overlapping transitions. The following values of $f=4.32\times10^{-9}\int\epsilon d\nu$, where the integral was evaluated from the product of the maximum value of ϵ and the band width at the half maximum value,[11] were obtained: butene-1, 0.39; *cis*-butene-2, 0.59; *trans*-butene-2, 0.32; 2-methylpropene, 0.39. These are consistent with the range of values obtained for other olefins.[4,12] In comparison with the isomeric pentenes as a group,[4] the bands of the butene isomers are slightly more intense, slightly displaced to shorter wavelengths, and have more marked vibrational structure.

[11] R. S. Mulliken, J. Chem. Phys. **7**, 14 (1939).
[12] Platt, Klevens, and Price, J. Chem. Phys. **17**, 466 (1949).

Any theoretical assignment of the electronic band systems and the vibrational structure involves a consideration of symmetry. While butene-1 has at most a plane of symmetry, each of the other three isomers may be considered as a symmetrically substituted dimethylethylene. There is immediately difficulty in the assignment of axes, since the axis of symmetry, conventionally termed the z axis, bears a different relation to the double bond direction in each isomer. Thus for *cis*-butene-2, of C_{2v} symmetry, the z axis is in the molecular plane normal to the double bond, while in 2-methylpropene, also C_{2v}, the z axis is along the bond. In the application of the Herzberg tables,[13] the y axis is taken in the molecular plane for both molecules, and hence the motions symmetrical to the molecular plane are of species A_1 and B_2. In the *trans*-butene-2, the symmetry is C_{2h} and modes of motion symmetrical to the molecular plane would be termed A_g and B_u.

In these terms the electronic transitions from a bonding to antibonding state involving the π electrons of the double bond may be described as follows:

butene-1 $(2a'')^2$, $^1A'\rightarrow(2a'')(2a'')$, $^1A'$;
cis-butene-2 $(2b_1)^2$, $^1A_1\rightarrow(2b_1)(2a_2)$, $^1B_1$;
trans-butene-2 $(2a_u)^2$, $^1A_g\rightarrow(2a_u)(2b_g)$, ^1B_u;
2-methylpropene $(2b_1)^2$, $^1A_1\rightarrow(2b_1)(2b_1)$, $^1A_1$.

In all cases it would be reasonable to expect that totally symmetrical (a', a_1 or a_g) vibrations would accompany the electronic change. Group theory considerations lead to the conclusion that ten of the thirty normal modes of vibration of *cis*- or *trans*-butene-2 or 2-methylpropene would be totally symmetrical, while butene-1 (C_s) would have 19 such.

The vibrational structure of the bands of all of the compounds show prominently a separation near 1500

[13] G. Herzberg, *Infrared and Raman Spectra of Polyatomic Molecules* (D. Van Nostrand Company, Inc., New York, 1945), p. 106.

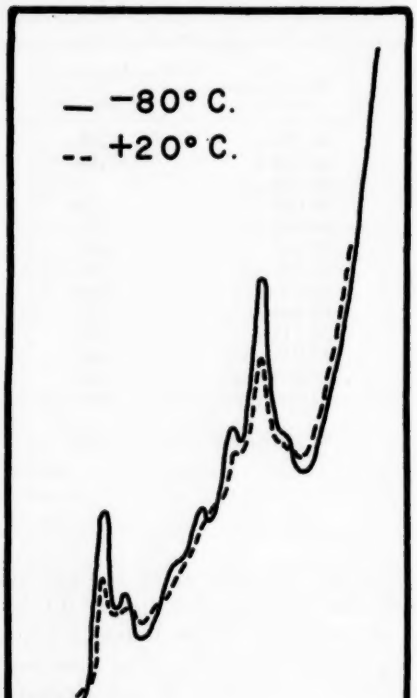

FIG. 3. Microphotometer records of first bands of *cis*-butene-2 superimposed to show temperature effects.

cm^{-1} which is certainly due to the stretching vibration of the double bond in the upper electronic state. In the case of butene-1 this is the only vibrational separation to be detected. This is reasonable since the number of allowed transitions is so large as to obscure any but the strongest.

In the case of the other three compounds there is a distinctive vibrational pattern which reveals other frequencies. The pattern of *cis*- and *trans*-isomers is very different, with more narrow bands evident in the latter, as was pointed out by Carr and Stücklen,[2] who noted that the *cis*-isomer resembled cyclohexane, which is also a *cis*-substituted compound. Furthermore, both isomers give evidence of upper state vibrations of comparable but lower frequencies than those found in Raman and infrared regions and assigned by Kilpatrick and Pitzer[14] as totally symmetrical vibrations. The bands of each of these compounds are listed in Table III in such a way as to bring out the correspondences noted. The separation from the band believed to be the O—O transition is shown together with the lower state frequency and the nature of the motion as indicated by Kilpatrick and Pitzer. The unassigned bands are all very weak and may be other fundamentals or combination frequencies. In some cases their positions were uncertain because they appeared as changes of slope only, and there may be other bands so weak that they could not be detected with certainty. It will be noted that few overtones may be seen; it is believed that they are obscured by the more intense band previously discussed. In the case of *trans*-butene-2, a third transition with well-marked bands, somewhat obscured because of the hydrogen-line background, shows something of the same vibrational pattern.

The *cis*-butene-2 was measured at two temperatures and the records of the two spectra are superimposed; although the data are qualitative only, it may be seen in Fig. 3 that the O—O band and the band involving the double-bond stretching frequency are especially sharpened.

The vibrational pattern of 2-methylpropene differs from the others and from most hydrocarbons studied here. The first narrow bands are diffuse, although there was some indication that there may be very weak bands on the upward slope which could not be shown on the curve. The first peaks of the charge transfer band are similar to those observed in other hydrocarbons, but above 55 000 cm^{-1} is a peak with closely spaced narrow bands followed by others with similar narrow banded structure. The change in appearance of these bands suggests a new electronic transition in which the double-bond stretching frequency is again prominent. The existence of a third transition shifted appreciably to lower frequencies as compared with the other butenes is paralleled in the pentenes by 2-methyl-1-butene,[4] the only pentene like 2-methylpropene in that one carbon is bonded to two alkyl groups while the other has hydrogen atoms only.

[14] J. E. Kilpatrick and K. S. Pitzer, J. Research Natl. Bur. Standards 38, 191 (1947).

The Viscoelastic Properties of Plastics

F. BUECHE *
Department of Physics, University of Wyoming, Laramie, Wyoming
(Received September 2, 1953)

A general method has been devised to predict the viscoelastic behavior of plastics. A simplified model of the molecule is assumed and its general motion is treated by the method of normal coordinates. General equations have been developed such that when the manner of application of external forces to the molecule is known, the molecule's general behavior may be found in a convenient and straightforward fashion.

This method has been used to obtain theoretical curves for the viscoelastic behavior of cross-linked polymers subjected to sinusoidal forces. Also, the similar problem for linear material has been solved together with the creep and stress relaxation problems. It is shown that the temperature-time superposition procedure of Ferry and Tobolsky has a firm theoretical basis. In general, the theoretical curves appear to agree with the limited experimental data available. The method is also applied to the case of dilute solutions and comparison is made with the result obtained by Rouse using a different approach.

INTRODUCTION

DURING the past several years there has been an increasing interest in the viscoelastic properties of solid and semiliquid polymers. Although two notable attempts have been made to provide a theoretical basis for this phenomena, neither is completely satisfactory. The first, due to Alfrey,[1] can be no more than qualitatively correct since it assumes an incorrect expression for the viscosity of a chain molecule and its segments. The second, due to Kirkwood,[2] is restricted to the case of the response of a network polymer to a sinusoidal force. This method has not been extended, apparently because the formalism employed is not easily adapted to other problems. However, compare a paper by W. G. Hammerle (reference 9). Very recently Rouse treated the case of the response of a linear molecule in dilute solution to a sinusoidal driving force.[3]

Since it has recently been found feasible to interpret the Newtonian flow properties of polymers in at least a semiquantitative fashion,[4,5] the extension of the theory to the viscoelastic behavior of both linear and cross-linked polymers now seems possible.

In this paper we show how a simple model of an average polymer molecule in a viscous medium gives rise to the observed viscoelastic behavior found by experiment. Working equations are found which predict the observed shape and superposition properties found by means of sinusoidal vibration methods and from creep and stress relaxation measurements. It has not been possible (or at least practical) to work the problem out exactly. Instead, rather drastic but well-defined plausible approximations have been made in order to arrive at a useful result. In Part I we obtain the general equations which apply to any physical experiment performed on the specimen. After that, in Part II, we apply the result to experimental methods actually in use and make comparisons with available experimental data.

PART I. GENERAL EQUATIONS

From the beginning we shall assume a fictitious molecule which is particularly amenable to calculation. Furthermore, in order to reduce the complexity of the problem we shall assume the molecule to have a particular direction in space. The latter approximation will make our relaxation-time spectrum discrete but it should not alter its over-all characteristics.

Consider a special chain having $3N$ links each having an average length l. Also, we assume the bond angle to be 90 degrees with steric hindrances such that the first link must point in either the $\pm x$ direction, the second in the $\pm y$ direction, the third in the $\pm z$ direction, the fourth in the $\pm x$ direction, etc. Furthermore, we assume any applied force to be in the x direction and so we will not be concerned with the y and z directions. For that reason, taking each link to have a mass m_0, each x link is associated with a mass $3m_0=m$. Let us now find the dynamical behavior of such a molecule by making the assumption that each segment (3 links) acts like a molecular spring. When such a spring of length l is stretched to $l+\Delta$, the restoring force will be $\alpha\Delta$. It is shown in Appendix I that this model will actually give a good picture of the behavior of a polymer molecule, provided we take $\alpha=3kT/l^2$ and stipulate that the mean-square end-to-end chain distance is Nl^2.

Take as an origin of coordinates a system such that x_0 is the distance in the x direction that the zeroeth segment has been displaced from its equilibrium position. Also, x_1 is the displacement of the first segment from *its* equilibrium position, and so on for the rest. Using this definition, the origins of the various x coordinates trace out the equilibrium configuration of the molecule.

The x component of the nonviscous force acting on the ith segment will be

$$F_{xi}=(x_{i+1}-x_i)\alpha-(x_i-x_{i-1})\alpha=\alpha(x_{i+1}-2x_i+x_{i-1}). \quad (1)$$

* Now at the Rohm and Haas Research Laboratories, 5000 Richmond Street, Philadelphia, Pennsylvania.

[1] T. Alfrey, J. Chem. Phys. **12**, 374 (1944).
[2] J. G. Kirkwood, J. Chem. Phys. **14**, 51 (1946).
[3] P. Rouse, J. Chem. Phys. **21**, 1272 (1953).
[4] F. Bueche, J. Chem. Phys. **20**, 1959 (1952).
[5] F. Bueche, J. Chem. Phys. **21**, 1850 (1953).

Since we shall solve our dynamical problem by the normal coordinate method, it will be advantageous to introduce the viscous and driving forces later and merely calculate the resonant frequencies of our molecule at this point. Equating force to mass times acceleration gives

$$m\ddot{x}_i=\alpha(x_{i+1}-2x_i+x_{i-1}).$$

The boundary conditions are that, when we are at the end of the chain, there is no restoring force on one end of the segment. Therefore, for the two chain ends we have

$$m\ddot{x}_0=\alpha(x_1-x_0),$$
$$m\ddot{x}_N=\alpha(x_N-x_{N-1}).$$

The solutions of these equations are of the form

$$x_{in}=\exp(j\omega_n t)\cos(ik_n), \tag{2}$$

with

$$\omega_n^2=2\alpha(1-\cos k_n)/m,$$

and

$$k_n=n\pi/N,$$

where

$$\alpha=3kT/l^2 \quad \text{and} \quad n=0, 1, 2, \cdots, N.$$

The ω_n are the resonant frequencies of the free molecule. There are N such frequencies varying from 0 to $(4\alpha/m)^{\frac{1}{2}}$. Had we not oriented our molecule to begin with we should have had three times this number but the distribution and limits of the frequencies would remain the same. k_n is the parameter defined above and it should not be confused with Boltzmann's constant k.

It turns out that our problem is now nearly mathematically identical to the vibration of N similar masses equally spaced on a string. The solution to this problem is well known[6] and will not be carried through here. In the notation of the normal coordinates q_n the solution is

$$x_i=\sum_{n=1}^{N}[2q_n/(2mN)^{\frac{1}{2}}]\cos(ik_n). \tag{3}$$

The normal coordinates are to be determined from the differential equation

$$\ddot{q}_n+(f/m)\dot{q}_n+\omega_n^2 q_n=F_n, \tag{4}$$

where $-f\dot{x}_i$ is the viscous force on the ith segment because of its motion through the medium and F_n is a function of the external forces applied to the segments $\Phi(i,t)$, as defined by the relation

$$F_n=\sum_{i=0}^{N}[2\Phi(i,t)/(2mN)^{\frac{1}{2}}]\cos(ik_n). \tag{5}$$

In any practical problem the method of procedure is now as follows. Find out how the applied force is transmitted to the molecule ignoring all viscous forces due to the motion of the molecule itself; the applied force to the ith segment is called $\Phi(i,t)$. Using Eq. (5), compute F_n, substitute F_n into Eq. (4), and compute q_n. Once this is done, the displacement of the ith segment can be found using Eq. (3).

Therefore, we have a general solution for the behavior of our polymer molecule in a viscous liquid. The friction factor f is essentially equivalent to the similar factor used in the treatment of the viscosity of solid polymers.[4] For any given method of excitation of the sample we can compute its behavior, provided we can determine $\Phi(i,t)$, the forces acting on the segments because of the applied forces. We shall treat several practical examples in the next section. First, however, we shall investigate the qualitatively obvious meaning of our results.

It is informative to compare our general result with the qualitative considerations usually proposed. The common view is to accept the molecular motion as being the result of the numerous relaxation times associated with varied lengths of the molecule. For example, short-range strains involving only a few segments of a chain are generally considered to relax more quickly than the long-range strains. The exact manner in which these relaxation times should depend upon the number of segments involved has been a matter of considerable speculation. We believe the above relations clarify this point. This may be seen as follows.

Each normal coordinate represents a mode of motion of the polymer chain. The case (or mode) of $n=0$ represents a pure translation of the whole chain. This is true since for $n=0$ we have $k_0=0$, and, therefore, we see from Eqs. (3) and (5) that all the x_i are equal. For the mode $n=1$ the values of x_i are negatively symmetric about $i=N/2$, and if the molecule were a stretched string, we would say that in this mode it oscillates in two segments with a node at its center. Similarly, the nth mode is very roughly analogous to a string vibrating in $n+1$ segments.

Just as the motion of a string depends upon a superposition of the motion in many separate modes, each with its own amplitude depending upon the method of excitation, so, too, the motion of the molecule may be analyzed into the component motion of its many modes. The segments defined by these modes clearly indicate the nature of the relaxing elements so often used in qualitative discussions. The damping or relaxation time for each mode may be calculated from Eq. (4). It is the damping out of these various modes which gives rise to a relaxation time distribution.

Since the relaxation times involved are those assigned to the various modes of motion of the chain, we see at once that the relaxation time distribution will depend upon the experiment being performed. For example, most mechanical measurements will predominantly excite the lower modes of motion since in general the forces will vary slowly along the chain. However, in dielectric measurements on a polar polymer the forces are localized along the chain and so we should expect the higher-frequency modes to be most active. In this

[6] See for example J. Slater and N. Frank, *Mechanics* (McGraw-Hill Book Company, Inc., New York, 1947), first edition, p. 157.

latter case we should expect the whole relaxation-time spectrum to differ from that found by mechanical excitation.

PART II. EXAMPLES

Example A. Constant Force Applied to a Network Polymer; Steady-State Solution

Obviously the external force of the previous section is applied to the two ends of the molecule (or network segment) and the other forces are viscous in nature. Therefore, $\Phi(0,t)=-\mathfrak{F}$, $\Phi(N,t)=\mathfrak{F}$, and all the other Φ are zero. Substitution into (5) gives

$$F_n=0 \quad \text{for } n \text{ even}$$
$$=-2\mathfrak{F}/(mN/2)^{\frac{1}{2}} \quad \text{for } n \text{ odd}.$$

The differential Eq. (4) is for steady state,

$$-\omega_n^2 q_n=F_n.$$

Using this result in Eq. (3) gives

$$x_N-x_0=\sum_{n \text{ odd}} 8\mathfrak{F}/mN\omega_n^2.$$

Replacing ω_n^2 by its value from Eq. (2) and making the approximation that $1-\cos k_n=k_n^2/2$ gives

$$x_N-x_0=\mathfrak{F}R^2/3kT,$$

where $R^2=Nl^2$.

To relate $\mathfrak{F}$, the force on a chain end, to F, the force acting on the sample, we make use of two facts. First, the work done by the external force must equal the energy stored in the ν network chains,

$$\nu\mathfrak{F}(\Delta x)=F(\Delta L).$$

The second relation available is that

$$(\Delta L/L)=(\Delta x/R).$$

Using these relations, one finds that

$$F=3\nu kT(\Delta L/L), \tag{6}$$

and

$$\mathfrak{F}=(F/\nu R). \tag{7}$$

Equation (6) agrees with the result obtained from the well-known theories of rubber-like elasticity.

Example B. Sinusoidal Force on a Network Polymer

If we assume as in example A that a force of frequency ω is applied to the ends of the network chains, we find at once that

$$F_n=0 \text{ for } n \text{ even},$$
$$=[4\mathfrak{F}/(2mN)^{\frac{1}{2}}]\exp(j\omega t) \text{ for } n \text{ odd}.$$

In this case it turns out that

$$x_N-x_0=(8\mathfrak{F}/mN)\exp(j\omega t)\sum_{n \text{ odd}}[\omega_n^2-\omega^2+j\omega f/m]^{-1}.$$

If we make the same approximation as we used in example A, we find that (after dropping the small inertia terms)

$$\frac{\Delta L}{L}=\frac{8F\exp(j\omega t)}{3\pi^2\nu kT}\sum_{n \text{ odd}}\frac{1-j\omega\tau_n}{n^2(1+\omega^2\tau_n^2)}, \tag{8}$$

where

$$\tau_n=fNR^2/3\pi^2kTn^2.$$

TABLE I. Response of a cross-linked polymer to a sinusoidal driving force.

$\omega\tau_1$	0	0.010	0.100	1.000	10.00	100.0
$(\Delta L/L)(3\nu kT/F)_{\text{real}}$	1.000	1.000	0.992	0.594	0.187	0.045
$(\Delta L/L)(3\nu kT/F)_{\text{imag.}}$	0.000	0.010	0.099	0.409	0.107	0.045

In the limit of ω approaching zero, Eq. (8) reduces to the classical expression for the equilibrium extension of a cross-linked sample under constant load. For all other driving frequencies $\Delta L/L$ will be complex. The real part of the displacement represents a response in phase with the force. The imaginary part gives rise to a displacement in phase with the velocity (90 degrees out of phase from the force) and leads to viscous losses. The variation of these two components is shown in Table I as a function of $\omega\tau_1$.

There are several features which should be mentioned about this result. Since $\tau_1\sim N^2$ there is a marked dependence upon N. Because of this, data on randomly cross-linked sample must actually be a superposition of a large number of such curves which will give rise to a very wide dispersion region. This fact may well far overshadow the inherent nonsymmetrical nature of the curves. Spurious maxima may easily arise purely because of the distribution of segment lengths.

Except for the minor temperature dependence of $\Delta L/L$ resulting from the factor T in Eq. (8), the temperature enters only in the quantity τ_1. The factor f contained in τ_1 is extremely temperature sensitive, especially near the glass temperature[5] but it is apparent that any variation of f can be balanced by a change in ω. This gives a firm foundation to the superposition method used so successfully by Ferry.[7]

Example C. Creep under Constant Load; Linear Polymer

For the case of a linear polymer we can no longer assume the external force to be applied at the chain ends alone. Actually the force will be distributed along the entire chain. It is reasonable to assume that the applied force will be a function of position in the polymer since the force acting on the segments of the molecule will actually be the result of the flow of the surrounding polymer through the molecule. We can split this motion into two distinct parts: (1) the velocity of the center of mass of the molecule and (2) the velocity of the surrounding polymer relative to the center of mass.

[7] J. D. Ferry, J. Am. Chem. Soc. **72**, 3746 (1950).

TABLE II. Response of a linear polymer subjected to a constant load.

t/τ_1	0.010	0.100	0.500	1.000	5.000	10.00
$(\Delta L/L)(3\nu kT/F)$	0.011	0.104	0.403	0.638	0.993	1.000

If the flow is in the x direction, then this latter velocity will vary linearly with x and will be zero at the center of mass of the molecule. Therefore, if the ith segment is at a x distance r_x from the center of the molecule, it will experience an average force proportional to r_x. It is shown in Appendix II that the average force is the force required.

If one considers the middle segment of the molecule to be at the center of mass, it may be shown that the average x displacements of the other segments are directly proportional to $i-N/2$. In view of this and the fact that the average force is the force required, we shall take

$$\Phi(i,t)=\mathfrak{F}(i-N/2)/N \quad t\geqslant 0,$$
$$=0 \quad t<0.$$

Using Eq. (5) we find that

$F_n=0$ for n even,

$F_n=[2\mathfrak{F}/N(2mN)^{\frac{1}{2}}][(N/2)+(1-\cos k_n)^{-1}]$ for n odd.

This result should be substituted into Eq. (4). When this is done, it is found that the inertia terms are negligible and may be dropped. The result obtained is

$$q_n=(F_n/\omega_n^2)[1-\exp(-m\omega_n^2 t/f)].$$

By use of Eq. (3) one finds that

$$x_N-x_0=(4\mathfrak{F}/mN^2)\sum_{n\ \text{odd}}(1/\omega_n^2)$$
$$\times[(N/2)+(1-\cos k_n)^{-1}]\cdot[1-\exp(-m\omega_n^2 t/f)]. \quad (9)$$

To find the value of $\mathfrak{F}$ we use the fact that it is defined to be one-half the force on the chain end. But since the force on any chain segment is fv where v is the relative velocity of the surrounding liquid, we have

$$\mathfrak{F}=RfF/\eta,$$

where η is the tensile viscosity of the sample.

Upon placing this result in Eq. (9), we find

$$(\Delta L/L)=(4F/\eta N^2)\sum_{n\ \text{odd}}\tau_n$$
$$\times[(N/2)+(1-\cos k_n)^{-1}][1-\exp(-t/\tau_n)], \quad (10)$$

where τ_n is the same as in Eq. (8). However, by making use of the value found for η in reference 4 (and confirmed in example E of this paper), we find

$$\eta=(1/12)\nu fNR^2, \quad (11)$$

so

$$\tau_1=4\eta/\pi^2\nu kT.$$

By making the further assumption that N is large, we can neglect N with respect to $N^2/n^2\pi^2$ and rewrite (10) as

$$(\Delta L/L)=(32F/\pi^4\nu kT)$$
$$\times\sum_{n\ \text{odd}}(1/n)^4[1-\exp(-t/\tau_n)]. \quad (12)$$

The general behavior of $\Delta L/L$ is shown in Table II.

The above expression for $\Delta L/L$ has no unknown factors and could conceivably be tested quite readily. However, certain difficulties present themselves. First, the maximum value for $\Delta L/L$ predicted by (12) is the same as one would obtain for a network polymer of ν network chains, namely, $F/3\nu kT$. Because of this, either low molecular wieghts or large elongations must be used. Secondly, the true viscous flow turns out to be exactly equal to the initial elastic flow and so the sample will never recover completely from the flow treated by this theory which increases the practical difficulties involved. Thirdly, an initial elastic deformation is always observed which is not accounted for here. It is the result of our neglect of very short relaxation times by using a molecular model which does not actually take into account the steric effects of the polymer chain. In spite of these difficulties, experiments are now in progress which indicate that the foregoing ideas are essentially correct.

Again it should be noticed that the results are severely dependent upon the molecular weight through the quantity τ_1. For this reason, quantitative interpretation of data on nonfractionated samples will be impossible unless the molecular weight distribution is known. It is also clear that since the important quantity entering into the equations is t/τ_1, a time-temperature superposition procedure should be possible. This has been observed experimentally by many investigators.

Example D. Stress Relaxation; Linear Polymer

The experimental method used for this type of measurement consists of applying a sudden stress to the sample and measuring the tension required to hold the sample at fixed elongation as a function of time. In accordance with this we take

$$\Phi(i,t)=\mathfrak{F}(i-N/2)/N \quad \text{for} \quad 0\geqslant t\geqslant\delta,$$
$$=0 \quad \text{for} \quad t>\delta.$$

During the period from 0 to δ the elongation will behave approximately according to the results of the previous example. So when $t=\delta$ we have as a boundary condition that q_n must be as given in that section. After that time the molecule is described by Eqs. (3) and (4), with F_n equal to zero. Proceeding as before, we find that for $t>\delta$

$$x_N-x_0=(4\mathfrak{F}/N^2m)$$
$$\times\sum_{n\ \text{odd}}(1/\omega_n^2)[(N/2)+(1-\cos k_n)^{-1}]$$
$$\cdot[1-\exp(-\delta\omega_n^2 m/f)]\exp(-\omega_n^2 mt/f). \quad (13)$$

It is obvious that the magnitude of δ/f will greatly influence the results. It appears that in most of the experiments made to date, δ has been small enough so that the exponential may be expanded in a series, keeping only the first terms. We certainly cannot say that the exponent is always large, since that would mean that the sample had reached an equilibrium elongation (neglecting permanent flow) before the stress was removed. However, the exponent varies by a factor of N^2 from the beginning to the end of the series, and so probably the approximation of δ small is not valid for short relaxation times.

Making the assumption indicated and replacing $1-\cos k_n$ as before leads to the result that

$$F/F_0=\sum_{n\ \text{odd}}[(N/2)+2N^2/n^2\pi^2]\times\exp(-t/\tau_n)/\sum_{n\ \text{odd}}[(N/2)+2N^2/n^2\pi^2], \quad (4)$$

where

$$\tau_n=4\eta/\pi^2n^2\nu kT.$$

At relatively long times we can neglect those terms in the sum for which n is large and, therefore, safely neglect $(\frac{1}{2})N$ in comparison to the second term in the brackets. This gives

$$F/F_0=(8/\pi^2)\sum_{n\ \text{odd}}(1/n^2)\exp(-t/\tau_n). \quad (15)$$

The behavior of this function is illustrated in Table III.

The inclusion of the $N/2$ term from Eq. (13) leads to a rise in F when going to small t/τ values. It is in that region where the assumption made concerning δ is no longer valid. The effect of a finite size for δ needs further investigation, but it is clear that its magnitude must seriously affect the short-time stress relaxation behavior. Although this fact will seriously complicate the analysis of short-time relaxation, the long-time portion of relaxation should be insensitive to δ.

Again we see that the important quantity determining the relaxation of stress is the quantity t/τ. Because of this the validity of a time-temperature superposition is indicated. The experiments of Tobolsky and his associates confirm both this fact and the prediction that the stress will relax slowly over many decades of time.[8] It is also apparent that the molecular weight enters into the result in a sensitive fashion. For this reason, experiments on nonfractionated polymers will be difficult to interpret unless the molecular weight istribution is known.

Example E. Sinusoidal Force; Dilute Polymer Solution

P. Rouse[3] has recently given an interesting treatment of this problem. However, since his method of approach is completely different from our own, we feel that a comparison of the results obtained by the two methods applied to the same problem would be extremely interesting.

[8] R. Andrews and A. Tobolsky, J. Polymer Sci. **7**, 221 (1951); J. McLoughlin and A. Tobolsky, *ibid.* **8**, 543 (1952).

TABLE III. Stress relaxation.

t/τ_1	0.000	0.010	0.100	0.500	1.000	2.000	5.000
F/F_0	1.000	0.928	0.773	0.493	0.298	0.110	0.0054

We wish to find the complex viscosity of a dilute polymer solution subjected to a sinusoidal driving force giving rise to a tensile velocity gradient $v=v_0\exp(j\omega t)$ in the x direction. By definition, if a force F is required per unit cross section to produce a velocity gradient in the solution equal to v, then $F=v\eta^*$, where η^* is the complex tensile viscosity. The rate of doing work per unit volume is just Fv, and so

$$W=v_0^2\eta^*\exp(j\omega t). \quad (16)$$

To find η^* we need, therefore, to calculate the work done on a unit volume of solution due to the velocity gradient. This work results from viscous losses in the solvent plus the friction losses between the chain segments and the solvent.

If we consider the ith chain segment at a x distance r_{xi} from the center of mass of the molecule, the velocity of the solvent with respect to the segment will be $(vr_{xi}-\dot{x}_i)$, since the center of mass of the molecule will be at rest and since the ith segment will have a velocity $\dot{x}_i$ with respect to it. The force on this segment will be $f(vr_{xi}-\dot{x}_i)$ and so the work done on this segment is $f(vr_{xi}-\dot{x}_i)^2$. We need now to sum this work over all segments of the molecule and multiply by the number of molecules in order to obtain W.

To carry out this calculation we must notice two things. First, the force $\Phi(i,t)$ in our general equations is just fvr_{xi} since it was defined in such a way as to exclude the forces due to the motion of the segment itself. Second, we will here be interested in the square of $(vr_{xi}-\dot{x}_i)$ so that the quantities entering are the average values of the products of the Φ's not the Φ's alone. We show in Appendix III that

$$\langle r_pr_q\rangle=(1/9)R^2[1-(3q/N)+(\tfrac{3}{2}N^2)(q^2+p^2)]=(1/f^2v^2)\langle\Phi_p\Phi_q\rangle \quad (17)$$

for $p\leqslant q$. This result agrees with the well-known value of $\langle r_p^2\rangle$ for the case $p=q$.

Making use of Eqs. (3), (4), (5), and (17), one finds that the work done on a single polymer molecule of the solution is

$$W_p=\frac{\alpha^2NfR^2}{18}\left[1-\frac{12}{\pi^2}\sum_1^N\frac{j\omega\tau_n}{n^2(1+j\omega\tau_n)}-\frac{6}{\pi^2}\sum_1^N\frac{\omega^2\tau_n^2}{n^2(1+j\omega\tau_n)^2}\right], \quad (18)$$

where

$$\tau_n=f/m\omega_n^2.$$

TABLE IV. A comparison of the real part of the viscosity as predicted by two theories.

$\omega\tau_1$	$(\eta_1-\eta_s)/(\eta_0-\eta_s)$ This paper	Rouse	% difference from average
0.10	0.98	0.98	0
0.20	0.93	0.90	+2
0.40	0.76	0.73	+2
1.00	0.37	0.48	−14
2.00	0.25	0.33	−14
4.00	0.18	0.24	−14
10.00	0.12	0.15	−14
20.00	0.075	0.10	−14

Actually this result should be corrected by multiplying by a factor $\frac{3}{2}$. This factor is needed to take care of the fact that flow is also taking place in the y and z directions, so as to keep the density of fluid constant as flow takes place in the x direction. It is easily shown that the gradients in the y and z directions are equal to $\frac{1}{2}$ of that in the x direction. Since the quantity which enters is the square of the gradient, this gives rise to an additional term $\frac{1}{2}$ as large as the original.

The total work done on the solution is, therefore, $(\frac{3}{2})\nu W_p+v^2\eta_s$, where η_s is the viscosity of the solvent. From this

$$\eta^*=(3\nu W_p/2v^2)+\eta_s. \tag{19}$$

If we represent the steady-flow tensile viscosity by η_0 and the real part of the viscosity by η_1, we have

$$\eta_1=\eta_s+(\eta_0-\eta_s)\left\{1-\frac{6}{\pi^2}\sum_1^N\left[\frac{2\omega^2\tau_1^2}{n^2(n^4+\omega^2\tau_1^2)}+\frac{\omega^2\tau_1^2(n^4-\omega^2\tau_1^2)}{n^2(n^4+\omega^2\tau_1^2)^2}\right]\right\}, \tag{20}$$

where

$$\tau_1=(4/\pi^2)(\eta_0-\eta_s)/\nu kT.$$

A similar expression may be written down for the imaginary part of η^*.

Since the tensile viscosity is three times larger than the shear viscosity, it is easily seen that our τ_1 is larger by a factor of two than the similar quantity defined by Rouse. Keeping this in mind we compare the two theories by listing the values of $(\eta_1-\eta_s)/(\eta_0-\eta_s)$ each would predict as a function of the variable $\omega\tau_1$ as defined in this paper. The results are listed in Table IV.

In view of the fact that Rouse's theory has been found to agree with the available experimental data, the substantial agreement between the two theories is quite gratifying, particularly since neither theory contains adjustable parameters. A close scrutiny of the results for both parts of η^* indicates that our result does not appear to agree with the data Rouse quotes quite as well as his own result. However, the agreement is good enough to indicate the essential validity of our approach to the problem.

Example F. Sinusoidal Force; Linear Polymer

The results of the previous example may be applied with but little modification to the case of a solid polymer. A treatment similar to example C could also be given. Without repeating the arguments given in reference 4 to justify such a procedure, we state only that Eq. (19) applies to the bulk polymer, provided we set $\eta_s=0$. With this modification, Eq. (20) states the result for a bulk polymer. Of course, the friction factor f has the more complex meaning outlined in reference 4.

CONCLUSION

It should be mentioned that we have presented only a survey of the types of problems to which this method may be applied. Such problems as strain relaxation, action under impulsive forces, and many others are equally amenable to study. Because of the simplicity of the model needed for the calculation and because of its striking analogy to the more familiar problems of vibrating strings and springs, valid qualitative conclusions may often be drawn without performing any calculations.

We believe the approximate picture of the viscoelastic behavior of plastics presented here is accurate enough to show the important features of such behavior except in the region of very short times. It has the advantage that starting from a rather simple basic set of equations, the results of viscoelastic experiments may be predicted, subject only to the condition that we are able to ascertain the type of external forces acting on the molecule.

There are two obvious directions in which improvements to this theory should proceed. First, as previously mentioned, the situation at short times is unsatisfactory because of the neglect of the actual structure of the segments of the chain. Second, the friction factor f cannot be a true constant. This arises from the fact that it represents not only the rubbing friction force between segments but also contains the effect of chain entanglements.

Very recently an attempt was made by Hammerle[9] to account for this latter effect as applied to the problem of stress relaxation using a modification of Kirkwood's[2] method. Hammerle presents an interesting procedure for taking care of the fact that the value of f for the chain ends will not be the same as for the central segments. We might also mention that f should be amplitude-sensitive, since the effect of entanglements will depend upon the degree of distortion of the molecules.

APPENDIX I

The model used for the calculation is actually much more realistic than might be expected from its simplicity. This may be seen most easily by comparing the results of the basic concepts of such a model with those to be

[9] W. G. Hammerle, paper presented at the meeting of the Society of Rheology, New York, October 30, 1953.

found from a more conventional type. For convenience we compare our model with the often used exponential segment chain; i.e., the probability for a segment length equal to r is proportional to $\exp(-\gamma r^2)$ where $\gamma=\frac{3}{2}l^2$. Such a chain is obtained by splitting a true chain into a group of subchains. It has an average square end-to-end distance R^2 equal to Nl^2.

We first justify the assumption of a chain composed of elastic elements complying with Hooke's law. Consider the exponential chain in a force field such that each segment is subjected to a x-directed tension F. This tensile force may be represented by a potential such that $\partial V/\partial x=-2F$. The factor 2 occurs because both ends of the segment experience a force. Using this fact together with Boltzmann's relation leads to the result that the probability that a segment will have an end-to-end distance of r is proportional to $\exp(-\gamma r^2+2Fr_x/kT)$. For small forces one easily finds that the effect of this potential is to increase the average value of r_x by an amount $\Delta r_x=Fl^2/3kT$. This shows that a chain segment actually behaves like an elastic Hookian spring with a spring constant $\alpha=3kT/l^2$.

The total x end-to-end displacement of a true molecule can also be calculated quite rigorously using the exponential chain. It turns out that the total x displacement is merely the sum of the average x displacements of the chain elements and so the second assumption inherent in our model is justified.

Since the model chain used in the body of this paper is composed of nonrotating "bonds," it might be assumed that rotations in an actual chain are not considered. We see from the above considerations that such is not the case. The elasticity constant α actually includes this factor. By this device we have considerably reduced the apparent complexity of the problem. It is for that reason that such a chain was used in preference to the exponential chain. It is apparent from the foregoing results that both chains will give the same results for small forces. Because of this, the model will prove inadequate where the actual character of the segments becomes important, that is, at high frequencies of excitation or at equivalent short observation times.

APPENDIX II

In our calculations we are interested in quantities such as

$$x_0=(\tfrac{1}{2}mN)\textstyle\sum_n q_n=(\tfrac{1}{2}mN)\sum_n F_nQ_n;$$

but

$$F_n=\textstyle\sum_i\Phi(i,t)\cos(ik_n),$$

where $\Phi(i)$ is the force applied to the ith segment.

Really we desire the value of x_0 averaged over all molecules and so we have

$$x_0=(\tfrac{1}{2}mN\nu)\textstyle\sum_n Q_n[F_{n1}+F_{n2}+\cdots+F_{n\nu}],$$

where ν is the number of molecules in the sample.

Substitution of the above expression for F_n leads to

$$x_0=(\tfrac{1}{2}mN\nu)\textstyle\sum_n Q_n\{[\Phi_1(1)+\Phi_2(1)+\cdots+\Phi_\nu(1)]\cos k_n +\text{similar terms}\}.$$

But the quantity in square brackets when divided by ν is the average force on the first segment and similarly for the others. Therefore,

$$x_0=(\tfrac{1}{2}mN)\textstyle\sum_n[Q_n\sum_i\langle\phi(i)\rangle\cos(ik_n)],$$

and the average force is the quantity which enters.

APPENDIX III

It is needed to calculate the average value of the product r_pr_q where r_p is the distance of the pth segment from the center of mass of the chain. This is a rather involved computation if one uses the customary chain models. However, even the use of the usual chain models gives a result for the comparatively simple average of r_p^2, which is uncertain as regards the length of a statistical chain segment. For that reason, nothing of importance is lost by choosing the particularly advantageous model used here. We assume that each chain segment is l units long. The first segment can point in either the $\pm x$ direction, the second in the $\pm y$, the third in the $\pm z$, and so on. Take the chain to have $3N$ segments.

From the definition of the center of mass and counting segments from a chain end, one has

$$r_{px}=\sum_{n=1}^{p} l_{nx}-(1/N)\sum_{j=1}^{N}\sum_{n=1}^{j} l_{nx}.$$

Taking the product $r_{px}r_{qx}$ and noticing that for our model the average value of the product is zero for $p\neq q$, we have at once that

$$\langle r_{px}r_{qx}\rangle=(Nl^2/3)[1-(3q/N)+(\tfrac{3}{2}N^2)(q^2+p^2)].$$

The factor $Nl^2/3$ depends upon the particular chain model used. Since in the text we have adjusted our chain so as to correspond to the freely orienting segment model we must also be sure that our constant here fits such a model. By comparing our result with the known result for the special case $p=q$, we find that our constant is actually a factor three too large to agree with the freely orienting segment model we are using. Therefore,

$$\langle r_pr_q\rangle=(R^2/9)[1-(3q/N)+(\tfrac{3}{2}N^2)(q^2+p^2)].$$

Network Theory of the Gel Point and the "Incestuous" Polymerization of Diallyl Phthalate

MANFRED GORDON
Technical Chemistry Department, Royal Technical College, Glasgow, Scotland
(Received August 12, 1953)

The status of the gel point equation, advanced by Flory, Stockmayer, and Walling for polyfunctional reactions, is briefly discussed. Two complicating factors in the chain polymerization of divinyl compounds, to which this equation has been applied, are reviewed: the admixture of a monovinyl compound of comparable reactivity, and the "incestuous" tendency for the two double bonds in a divinyl compound to enter the same polymerization chain. Contrary to the treatment by Simpson and co-workers, these two factors are found to demand different theoretical approaches. The progress of polymerization enriches the monomer mixture in the monovinyl compound, while the incestuous tendency remains constant. Kinetic derivations are given for the gel point condition in both cases. The gel point in the "incestuous" polymerization of diallyl phthalate is calculated to lie at conversions 40 percent higher than estimated by Simpson and co-workers, and much better agreement is thus achieved with their experimental measurements.

A simple network theory suffices to predict the gel point in two chain polymerization reactions. Substantial delays of the gel point, predicted by Walling's theory of diffusion control in such reactions, are not encountered.

1. INTRODUCTION

FLORY[1] first postulated that the gel point in polyfunctional reactions occurs when the weight average molecular weight (and hence the viscosity) becomes infinite; i.e., when in an infinite sample of the reaction mixture the weight fraction of infinite networks first exceeds zero. A simple general equation has geen deduced in various ways[1–3] for determining this critical condition (subscript c) in terms of the fraction α of the functionalities which have reacted, *viz.*,

$$\alpha_c = 1/(f_w - 1), \tag{1}$$

where f_w is the weight average functionality of the molecules present initially, when $\alpha = 0$. The equation is intended to apply only if all the functionalities are equally reactive, in particular equally reactive irrespective of the reacted or unreacted status of other functionalities in a molecule, so that chain reactions are excluded. None of the general and direct arguments advanced for the derivation of Eq. (1), and based on probability arguments concerning randomly chosen cross links[1–3] are satisfactory, as they contain various concealed approximations which cancel out somewhat fortuitously. However, when a complete distribution function of the initial functionalities ($\alpha = 0$) has been given, the distribution functions for all values of α become statistically determinate, and have been computed in many individual cases.[1,2] In all these cases Eq. (1) has been verified, in that the current weight average functionality reaches infinity at the value of α_c specified by Eq. (1).

In the particular case of vulcanization reactions, where the initial polyfunctional material consists of chains of units each bearing a single functionality (cross-linking position), f_w signifies merely the weight average degree of polymerization DP_w of the initial material

$$\alpha_c = 1/(DP_w - 1). \tag{2}$$

Although Eqs. (1) and (2) cannot in general be applied to chain reactions, (2) has been extended[2] to the special case of the chain polymerization of symmetrical divinyl monomers. This is done by allowing DP_w to stand for the weight average polymerization degree of the chains which would result, if all the cross links in the networks at the gel point were severed. Each such cross link arises quite clearly from a monomer unit both of whose double bonds happen to have reacted. By this device, the case is reduced to the gel point in the vulcanization of pre-existent chains. Two generalizations arising in practice have been considered in connection with divinyl polymerizations. The first[2] is the admixture of a monovinyl monomer of a structure closely related to the divinyl one (e.g., methyl methacrylate to ethylene dimethacrylate[3]), so that all double bonds present have the same reactivity. As shown again below, this merely introduces a factor ρ into (2), which denotes the fraction of all double bonds residing on divinyl units in the initial system

$$\alpha_c = 1/\rho(DP_w - 1). \tag{3}$$

The other generalization concerns a complicating factor recently observed in the polymerization of diallyl phthalate by Simpson, Holt, and Zetie.[4] This is the tendency for two allyl groups belonging to the same monomer unit to be incorporated into the same polymerization chain, a kind of reaction here termed "incestuous." This leads to cyclic structures, and since such structures are normally rare, and are explicitly discounted in the derivation of Eq. (2), the question arises how to allow for the effect. An incestuous reaction is fruitless as regards the production of cross links, and Simpson *et al.* allowed for the fraction $(1-r)$ of in-

[1] P. J. Flory, J. Am. Chem. Soc. **63**, 3083, 3091, 3096 (1941).
[2] W. H. Stockmayer, J. Chem. Phys. **12**, 125 (1944).
[3] C. Walling, J. Am. Chem. Soc. **67**, 441 (1945).
[4] Simpson, Holt, and Zetie, J. Polymer Sci. **10**, 489 (1953).

cestuously reacted units by treating them as monovinyl units, i.e., essentially by using Eq. (3) with $\rho=r$. It is shown below that this is only an approximation, and that a more accurate treatment gives results in much better agreement with the gel point measurements by Simpson *et al.* The problem of the legitimacy of any simple network theory when applied to fast chain reactions, in the face of possible interference with cross linking caused by the slowness of the diffusion rate of active radical chain ends, which was raised by Walling,[3] will then be touched on in the concluding section.

2. VINYL/DIVINYL COPOLYMERIZATION

It is well known that there are two fully equivalent ways of computing molecular distributions, *viz.*, by a set of differential kinetic equations, or by direct statistical analysis. This equivalence may be found exemplified in Stockmayer's first paper[5] on the theory of cross-linking reactions, and in the kinetic derivation by the author[6] of Flory's statistical treatment[7] of certain intramolecular cyclizations in polymers. It turns out that the "incestuous" polymerization of diallyl phthalate, treated in the next section, is handled more readily on a kinetic basis. For the sake of uniformity, the same kinetic treatment is first applied to the simple copolymerization under consideration.

Two important concepts, which coincide for the case of vulcanization of pre-existent chains, need separate symbolization for copolymerization studies. Contrary to previous usage, it appears desirable always to denote by α the variable which is significant for the gel point theory, namely, in this case, the proportion of reacted double bonds which belong to bridge units. A reacted double bond is one that has been converted to a single bond by polymerization, and a bridge unit is a divinyl unit both of whose double bonds have thus reacted. We shall name β the variable, called α by Stockmayer, which is significant in the chemical analysis of unsaturation, namely, the proportion of all double bonds originally present which have reacted. A and B will denote the concentrations of mono- and divinyl monomer, respectively, so that $\rho=2B_0/(A_0+2B_0)$. The proportion of all divinyl units which have doubly reacted, and have thus become bridge units, will be denoted by c. The following relation follows directly from these definitions:

$$\alpha=\rho c/\beta. \tag{4}$$

The rates of incorporation into the polymer of the two kinds of units are given in terms of the concentration fractions $a(=A/A_0)$ and $b(=B/B_0)$, thus

$$da/dt=-kRa, \tag{5}$$

$$db/dt=-2kRb, \tag{6}$$

where R is the current concentration of growing free radical chain ends. The factor 2 in Eq. (6) corresponds to the presence of two double bonds in the divinyl molecule, while the identity of the rate constant k in (5) and (6) betokens the assumed equality of reactivity ("true" copolymerization) of the units. From the two rate equations the time is eliminated, to obtain the equation given by Walling:[3]

$$d(\log a)/d(\log b)=\tfrac{1}{2} \quad \text{or} \quad a^2=b. \tag{7}$$

To evaluate α according to Eq. (4), we next obtain c and β. By the law of mass action, the rate of cross-link formation will be proportional to the fraction $(1-b-c)$ of the concentration B_0 consisting of singly reacted divinyl units:

$$dc/dt=k(1-b-c)R. \tag{8}$$

The second double bond being assumed equally reactive as the first, the same rate constant k figures again in (8). Eliminating the time between Eqs. (6) and (8) gives

$$dc/db=-(1-b-c)/2b. \tag{9}$$

The solution of this differential equation which obeys the initial condition ($c=0$ for $b=1$) is simply

$$c=(1-\sqrt{b})^2. \tag{10}$$

The fraction β of all double bonds which have reacted is

$$\beta=((1-a)A_0+(1-b)B_0+cB_0)/(A_0+2B_0) \tag{11}$$

which, with the aid of (7) and (10) reduces to the statistically obvious results:

$$\beta=(1-b-c)/2=1-a. \tag{12}$$

Collecting Eqs. (4), (10), and (12), we obtain

$$\alpha=\rho(1-\sqrt{b})=\rho(1-a). \tag{13}$$

We have merely to substitute the critical value of α from (13) in (2), to obtain the solution derived statistically by Stockmayer, and by Walling, in our notation

$$\beta_c=1-a_c=1/\rho(DP_w-1) \tag{14}$$

for the gel point.

3. THE "INCESTUOUS" POLYMERIZATION OF DIALLYL PHTHALATE

Simpson, Holt, and Zetie,[4] in the most elegant and thorough investigation so far made, polymerized this divinyl compound in the absence of monovinyl compound ($\rho=1$). The rather low number average degree of polymerization DP_n was measured cryoscopically with considerable accuracy on the polymer chains in the network after cutting all the cross links by saponification. Certain side reactions, which might interfere with the simple network theory, were shown to be absent by critical experiments. However, a strong "incestuous" tendency for the two allyl groups in one monomer molecule to become linked together in the same polymer chain was convincingly demonstrated by these authors,

[5] W. H. Stockmayer, J. Chem. Phys. **11**, 45 (1943).
[6] M. Gordon, Proc. Roy. Soc. (London) **A204**, 569 (1951).
[7] P. J. Flory, J. Am. Chem. Soc. **61**, 1518 (1939).

TABLE I. Analytical results on diallyl phthalate (Simpson *et al.*).

% conversion on monomer basis	6.7	15.6	22.2	
Fraction r polymerized normally	0.569	0.575	0.577	Average 0.574
DP_n of chains	13.6	14.0	14.2	Average 13.9

and is further confirmed by the agreement with the gel-point theory based on this factor given below. To evaluate quantitatively the delay of the gel point occasioned by this tendency, the simplest theory would predict that the fraction r of monomer units in the polymer which are found to have reacted normally, i.e., *not* incestuously, should be independent of the progress of the reaction, especially in the early stages up to the gel point. This can be verified from Simpson and co-workers' data as shown in Table I. The DP_n of the chains is there also found remarkably constant.

It is preferred to express DP_n (and later DP_w) in terms of monomer units per chain. Simpson *et al.* express it in terms of reacted double bonds per chain, thus using $DP_n'=(2-r)DP_n$ and $r'=r/(2-r)$. Because of the manner in which DP_n and r enter the gel-point theory (as a product) this change of basis has negligible effects on the results.

We can now show that Simpson and co-workers' treatment of the incestuous units as so many monovinyl units present at the start, underrates the critical conversion of double bonds β_c, or of monomer units b_c, by about 40 percent, thereby prejudicing the comparison with their gel-point measurements. The reason may be stated first in chemical kinetic terms, and then in statistical terms.

Chemically, the inces uous reaction differs from the admixture of a monovinyl compound in that the relative rates of entry into the polymer of a monovinyl and a divinyl compound change in the course of the reaction [Eq. (7)], while a constant fraction of diallyl phthalate monomer enters the polymer incestuously, irrespective of the reaction progress (Table I). It would be a correct chemical analogy to say that the diallyl phthalate behaves kinetically as if it were engaged in an equilibrium between its tetra- and difunctional forms, an equilibrium so rapidly adjusted as to be maintained during the polymerization reaction.

In the statistical derivation of the gel point, it is assumed that the fraction of pendent vinyl groups ($c/\beta=1-a$ above) is equal to the fraction of all double bonds reacted ($\beta=1-a$ above). But in diallyl phthalate this equality is destroyed. The fraction β of all double bonds reacted contains many which have reacted incestuously, while the pendent vinyl groups, once formed, have no opportunity of reacting incestuously. Thus, fewer pendent vinyl groups are found reacted to form cross links, and the true gel point will occur later than predicted on Simpson and co-workers' basis.

The kinetic scheme of Eqs. (4) to (14) must be modified as follows. Equation (4) is adapted by putting $\rho=1$, and replacing the fraction β of all double bonds reacted, by the fraction β' of all double bonds reacted *non-incestuously*. Thus any monomer unit whose second double bond has incestuously entered the same chain as its brother, has this second double bond discounted. However, it is obvious that β' is still given by $(1-b+c)/2$, as was β in Eq. (12). Thus (4) becomes

$$\alpha=2c/(1-b+c). \tag{15}$$

Equation (6) accounts, as before, for the rate of incorporation of monomer units into the polymer. The rate of cross-link formation [Eq. (8)] needs adjustment to allow for the incestuous units, thus,

$$dc/dt=k(r(1-b)-c)R. \tag{16}$$

Eliminating the time now between (6) and (16), we obtain

$$dc/db=-(r(1-b)-c)/2b, \tag{17}$$

which is to be compared with (9). The solution which satisfies the same initial condition as (9) is now

$$c=r(1-\sqrt{b})^2. \tag{18}$$

By comparison with (10), this shows that c, at least, can be corrected for the incestuous reaction by the mere factor r. This is statistically obvious. Combining (15) and (18), the solution analogous to (13) is obtained, which is most easily written when solved for b,

$$b=[(2r-\alpha(1+r))/(2r+\alpha(1-r))]^2. \tag{19}$$

For the critical case ($b=b_c$, $\alpha=\alpha_c$), substitution from Eq. (2) yields

$$b_c=\left[\frac{r(2DP_w-3)-1}{r(2DP_w-3)+1}\right]^2. \tag{20}$$

Equation (19) agrees with (13), i.e., the divinyl/monovinyl case, if and only if $\rho=r=1$; which serves as a check, for the two cases are identical when there is neither addition of monovinyl compound nor any incestuous tendency.

The over-all fraction β of reacted double bonds (both normally and incestuously reacted) is readily shown to be

$$\beta=1-b-r(\sqrt{b}-b), \tag{21}$$

from which the critical conversion β_c, on a double-bond basis, may be calculated with the aid of Eq. (20).

TABLE II. Gel point of diallyl phthalate.

		Eq. (2)	(correct) Eq. (20)	Found
Critical conversion $1-b_c$	Uniform chains ($DP_w=DP_n$)	0.18	0.25	0.25
	Random chains ($DP_w=2DP_n-1$)	0.09	0.13	

Simpson *et al.* found the gel point of diallyl phthalate experimentally at 25 percent monomer conversion. Their calculation according to Eq. (2) is contrasted in Table II with our calculation according to Eq. (20). As DP_n has been measured, while DP_w is required for the calculation, the two limiting laws $DP_w = DP_n$ and $DP_w = 2DP_n - 1$ are considered. These correspond to uniform polymerization chains, and randomly distributed polymerization chains, and the true value of DP_w is strongly expected to lie between these limits. The table shows that the range of the critical conversion $(1-b_c)$ calculated on our basis lies 40 percent higher than on Simpson and co-workers', and just stretches to the observed value. It is not suggested that the chains are, in fact, precisely uniform, because of the agreement of our calculation with the observed value on this assumption. However, when it is remembered that theoretical gel point calculations, which ignore cyclic structures (other than incestuous ones), normally give values for the critical conversion just below the true figure, it must be admitted that this study of diallyl phthalate gelation by Simpson and co-workers furnishes a new buttress for the Flory space network theory.

4. SIMPLE NETWORK THEORY AND WALLING'S DIFFUSION CONTROL THEORY

Walling[3] attempted to check Eq. (2) against his experiments on methyl methacrylate/ethylene dimethacrylate and on vinyl acetate/divinyl adipate. He found that the gel point was always observed at higher conversions than predicted by Eq. (2), and this departure became increasingly serious as ρ was raised from 10^{-3} to unity. When ρ was unity, the observed critical conversion ($\beta_c = 0.029$) was over 100 times that calculated from Eq. (2). Walling measured the DP_w of the polymer chains (always in the high range 400 to 5000) viscosimetrically in the absence of divinyl compound ($\rho = 0$), and assumed it to be unaffected when divinyl compound was added. Serious deviations of the observed gel points at high values of ρ from gel points calculated on this assumption, were explained by a special theory. This theory proposed that the reaction mixture consists of discrete swollen polymer molecules, spherical in shape, whose rate of cross-linking falls below the value deduced from a simple network theory,[1,2] because of their slow rate of diffusion. Thus a given sphere has, during its brief period of growth, opportunities to be cross-linked to no more than those immediately neighboring spheres which it happens to be touching. A model calculation, involving many simplifying assumptions, gave Walling rough agreement with his observed gel points.

It is noteworthy that slow diffusion causes no substantial delay on the gel point of diallyl phthalate, since the calculations here derived from the simple network theory give fair agreement with Simpson and co-workers' measurements. The absence of any marked delay has also been noted in experiments in these laboratories (to be published), on the copolymerization of polyethylene maleate and methyl methacrylate. This system would be expected to be particularly sensitive to the delaying action covered by Walling's theory, because of the high functionality of the maleate ester, and the high chain length of the polymerization chains. One may, therefore, justifiably examine alternative explanations of the retardation of gelling observed by Walling on his systems. Because of the strong dependence of the ratio β_c (observed)/β_c(calculated) on ρ, the retardation cannot be explained by the occurrence of an incestuous reaction involving the divinyl compound, nor by errors in the viscosimetric determinations of DP_w. It does seem possible, however, that contrary to Walling's assumption, DP_w fell with increasing ρ. Indeed, the progressive introduction of the divinyl compounds involved the addition of more and more $R-\mathbf{CH_2}-O\cdot CO-$ groups, and such methylene groups might lower the DP_w through chain transfer reactions. Qualitative support for this tentative suggestion is found in the fact that the viscosity was unaffected by changes in ρ until the gel point was approached. A rise in viscosity with increasing ρ (but at constant β) would be expected, if DP_w was constant.

ACKNOWLEDGMENTS

It is a pleasure to acknowledge valuable criticisms offered by Professor P. D. Ritchie, and a valuable discussion with Mr. W. Simpson and Mr. T. Holt of the Metropolitan Vickers Electric Company, Ltd.

The Crystal and Molecular Structure of B_5H_{11}

LOUIS R. LAVINE* AND WILLIAM N. LIPSCOMB
School of Chemistry, University of Minnesota, Minneapolis 14, Minnesota

(Received October 9, 1953)

The molecular structure of B_5H_{11} has been determined from 299 x-ray diffraction maxima which have been analyzed by three-dimensional Fourier and least-squares methods. There are four molecules in a monoclinic unit cell, in the space group $P2_1/n$, having parameters $a=6.76$, $b=8.51$, $c=10.14$A, and $\beta=94.3°$.

Although no molecular symmetry is demanded by the space group, the molecular dimensions indicate C_s symmetry for the isolated molecule. The boron skeleton is a fragment of the icosahedronlike arrangement in $B_{10}H_{14}$, and can also be derived from the tetragonal pyramid in B_5H_9 by opening up one of the basal B—B bonds. The apex boron B_I is "singly" bonded to two hydrogens, one of which H_{VII}, is very weakly bonded to the two outer borons B_{III}. Each B_{III} is "singly" bonded to two hydrogen atoms. Each of the remaining two borons B_{II} is "singly bonded" to one hydrogen atom, and there are three bridge hydrogens, one bridging the B_{II}—B_{II} bond and two bridging the B_{II}—B_{III} bonds. Molecular parameters are two B_I—$B_{III}=1.86_5$, two B_{II}—$B_{III}=1.75$, two B_I—$B_{II}=1.72$, one B_{II}—$B_{II}=1.77$A, seven B—H$=1.0_7$, six B—H (bridge) $=1.2_4$A, one B_I—$H_{VII}=1.0_0$ and two B_{III}—$H_{VII}=1.6_7$A. The B_{III}—B_I—B_{III} angle is 107°. Bond angles to hydrogen strongly resemble those in the other known boron hydrides.

INTRODUCTION

RECENT studies of the molecular structures of B_2H_6,[1] $B_{10}H_{14}$,[2] B_5H_9,[3,4] and B_4H_{10}[5,6] have made clear many of the structural principles of the boron hydrides, both with respect to molecular geometry and chemical binding. Spectroscopic, x-ray diffraction and recent electron diffraction methods have been employed with success. Although no one of the recent electron diffraction studies yields unambiguous results, these studies partly elucidate and partly are derived from a set of consistent principles based on the structures of B_2H_6, $B_{10}H_{14}$, and the borides. They also prove the incorrectness of the earlier electron diffraction studies. Nevertheless, except for the establishment of the B_2H_6 structure by spectroscopic techniques, the certainty with which all of the known structures are established is due to the complete x-ray diffraction results. We therefore considered an investigation of the molecular structure of B_5H_{11} by the x-ray diffraction method highly desirable.

EXPERIMENTAL

Samples of pure B_5H_{11}, mp[7] −129°C, were vacuum-distilled into thin-walled Pyrex capillaries about 1 mm in diameter, which were then mounted on the x-ray cameras. Only during this distillation and mounting were the samples allowed to be above −80°C. Single crystals were grown and maintained at about −140°C during photography by the usual procedure.[8] Growth occurred without supercooling, and almost always with the monoclinic b axis along the capillary axis. No transition was observed in any of the experiments. The 23 most densely populated 0-level nets, containing $0k0$ reflections in common, were photographed with MoKα radiation at a precession angle of 30° in the Buerger camera. All nets were photographed from one to four times using varying exposure times up to 30 hours in length. In addition, the zero, first, and second level Weissenberg photographs about the b axis were taken in order to obtain additional reflections and to correlate the precession photographs. Multiple films, interleaved with brass foil, were used for the Weissenberg photographs, which were also taken with MoKα radiation ($\lambda=0.7107$A).

Integrated intensities were estimated visually with the aid of standard scales prepared from single crystal reflections. Estimates of 299 reflections were considered sufficiently reliable to use in the structure determination. Forty-one additional reflections, observed on the precession photographs of sparsely populated nets, were identified as reflections on adjacent nets only a few degrees away; these additional reflections had the expected slightly out-of-focus appearance of maxima on misaligned photographs, and all were less intense than the lower 25 percent of the 299 reflections which were estimated more reliably. These 41 additional reflections were not used in the structure determination, because we were unsure of their reliability until the final model was obtained. Their agreement with the calculated values, discussed below, is satisfactory but probably significantly poorer than that shown by the 299 more reliable reflections. Besides providing support of the correctness of the molecular structure, these reflections are of interest in connection with the experimental problem of complete coverage of reciprocal space with the use of fewer photographs.

* Present address: Gates and Crellin Laboratories of Chemistry, Pasadena 4, California.

[1] W. C. Price, J. Chem. Phys. **15**, 614 (1947); **16**, 894 (1948).

[2] Kasper, Lucht, and Harker, Acta Cryst. **3**, 436 (1950).

[3] W. J. Dulmage and W. N. Lipscomb, J. Am. Chem. Soc. **73**, 3539 (1951); Acta Cryst. **5**, 260 (1952).

[4] Hedberg, Jones, and Schomaker, J. Am. Chem. Soc. **73**, 3538 (1951); Proc. Natl. Acad. Sci. U. S. **38**, 679 (1952).

[5] C. E. Nordman and W. N. Lipscomb, J. Am. Chem. Soc. **75**, 4116 (1953); J. Chem. Phys. **21**, 1856 (1953).

[6] Jones, Hedberg, and Schomaker, J. Am. Chem. Soc. **75**, 4116 (1953).

[7] A. Stock, *Hydrides of Boron and Silicon* (Cornell University Press, Ithaca, 1933), p. 73.

[8] T. B. Reed and W. N. Lipscomb, Acta Cryst. **6**, 45 (1953).

The usual[9,10] Lorentz and polarization factors were applied, and the complete data were correlated to a single scale with the use of reflections common to the various films.

STRUCTURE DETERMINATION

The reciprocal lattice symmetry of C_{2h} and the monoclinic cell parameters, $a=6.76\pm0.02$, $b=8.51\pm0.03$, $c=10.14\pm0.03$A, and $\beta=94.3\pm0.3°$, were obtained. The presence of $h0l$ only with $h+l$ even and of $0k0$ only with k even indicates uniquely that the space group is $C_{2h}^5-P2_1/n$. Assumption of four molecules in the unit, cell leads to a volume of 581A^3 per molecule, which is very reasonable in comparison with similar data[3,5] for B_5H_9 and B_4H_{10}.

The three-dimensional Patterson function, sharpened by the use of $F^2/\Sigma f_j^2$ as coefficients, was calculated as a series of sections, $P(u,v,w)$, on the X-RAC. The sections had constant values of v, from 0 to $\frac{1}{4}$ at intervals of 1/60 of the b axis. They were analyzed by an analytical analog of the Patterson superposition method. Because it was expected that B_5H_{11} formed a molecular crystal, all the vectors in Patterson space less than 2A were assumed to include all the intramolecular B−B bond vectors and no others. Indeed, it was highly doubtful from the peak heights and general resolution that any other interactions would be evident. All possible pairs of these vectors were checked to see if the sum or difference was equal to some other vector in the maps. This procedure did, indeed, give a unique arrangement for five boron atoms projected on (010). Then the Patterson-Harker section $P(u,\frac{1}{2},w)$ was calculated. It was possible to assign rough x and z parameters to the boron atoms, and to explain tentatively all non-Harker peaks on $P(u,\frac{1}{2},w)$ from a consideration of the related peaks on $P(u,0,w)$. This model was then refined in the usual way by the use of alternate $h0l$ Fourier projections and structure factor calculations.

In order to obtain approximate y parameters for the boron atoms, the Patterson line section $P(\frac{1}{2},v,\frac{1}{2})$ was calculated and compared with the vectors in Patterson space from which the $h0l$ model had been obtained. Reasonable y parameters which were consistent with the non-Harker peaks found on $P(u,\frac{1}{2},w)$ were readily obtained in this fashion. Refinement was then continued using both $0kl$ and $hk0$ Fourier projections.

It was necessary to use all three principal projections for refinement because at least two atoms overlap in each of these projections. Since some atoms are involved in overlaps occurring on more than one projection, it was impossible to obtain good values for the parameters of all boron atoms from projections alone. To overcome these difficulties the X-RAC was used once more for the calculation of Fourier sections with constant values of y ranging from 0 to $\frac{1}{4}$ at intervals of 1/60 of the b axis. Two sets of these Fourier sections along with the prior calculation of all hkl structure factors were sufficient to give good values for all boron parameters and to show that there were no significant additional peaks.

These boron positions were then refined using two successive least-squares refinements in which the off-diagonal terms were ignored, a procedure which is partly justifiable because the axes were nearly orthogonal and the parameters were sufficiently close to the final values. The function minimized was $\Sigma w_{hkl}(F_0-F_c')^2$ where F_0 is the observed structure factor with the sign of the calculated one, F_c' is the calculated structure factor including scale and temperature factors, and w_{hkl} is the weighting factor for the particular reflection. The scale and temperature factors were treated as quantities to be determined by the least-squares calculation, along with the atomic parameters. The weighting factors were slightly modified from those recommended by Hughes,[11] i.e., $w_{hkl}^{\frac{1}{2}}=1/|F_0|$ if $|F_0|\geq 4|F_{\min}|$ and $w_{hkl}^{\frac{1}{2}}=|F_0|/16|F_{\min}|^2$ if $|F_0|\leq 4F_{\min}$, where $|F_{\min}|^2$ is the smallest corrected intensity observed. It may be demonstrated that this procedure, using the particular function and weighting factors mentioned, is roughly equivalent to minimizing the function $\Sigma w'(F_0^2-F_c'^2)^2$, using the proper weighting factors for this case.

Further refinement without considering hydrogens would have been pointless. Examination of the three-dimensional Fourier sections from which boron parameters were obtained indicated some peaks that might have been interpreted as hydrogen atoms, but it was not possible to assign positions for all of the hydrogen atoms from these sections. Consequently, a three-dimensional difference synthesis was calculated, in which the coefficients were the observed structure factors minus the contributions of borons only. Sixteen sections with constant values of y from 0 to $\frac{1}{4}$ at intervals of 1/60 of b were computed. Unfortunately, these maps showed more than eleven peaks in the asymmetric unit, and there was no grouping of the heights of the peaks into the eleven highest, and a group of much smaller peaks. Nevertheless, it was still possible to examine them in the order of decreasing peak heights, and to decide from a consideration of distances to the nearest boron atoms whether any given peak was a likely candidate for a hydrogen position. It was found that the eleven highest peaks were, indeed, located in positions that would correspond to chemically reasonable boron-hydrogen distances. These peaks varied from ten to eight on a relative scale of electron density. The highest false peak was seven on the same scale. None of the peaks of heights seven and six gave chemically reasonable boron-hydrogen distances, and lower peaks were not examined.

In order to investigate this model further, two successive least-squares calculations starting with the boron positions found previously and the hydrogen

[9] J. Waser, Rev. Sci. Instr. **22**, 567 (1951).
[10] Chia-Si Lu, Rev. Sci. Instr. **14**, 331 (1943).
[11] E. W. Hughes, J. Am. Chem. Soc. **63**, 1737 (1941).

TABLE I. Atomic parameters.

Atom	Type	x	y	z
B_1	III	0.290	0.106	0.318
B_2	II	0.133	0.105	0.175
B_3	I	0.024	0.047	0.317
B_4	II	0.891	0.164	0.208
B_5	III	0.880	0.216	0.376
H_1	IV	0.395	0.019	0.331
H_2	III	0.324	0.204	0.383
H_3	II	0.161	0.031	0.108
H_4	I	0.961	0.932	0.334
H_5	II	0.764	0.112	0.152
H_6	III	0.986	0.303	0.423
H_7	IV	0.738	0.173	0.414
H_8	VI	0.274	0.182	0.218
H_9	V	0.015	0.206	0.144
H_{10}	VI	0.847	0.300	0.262
H_{11}	VII	0.069	0.107	0.398

positions found from the three-dimensional synthesis were carried out. At the end of the second least-squares refinement it was found that the borons had not moved appreciably from their previous positions and that the hydrogen positions had refined so that they were in somewhat better positions from a chemical point of view than the positions which had been found on the difference synthesis. From the magnitude of the shifts found on the last refinement and from the small decrease of 5 percent in $\Sigma w(F_0-F_c')^2$, it was assumed that the atomic parameters and temperature scale factor found were the best possible with the data available, and the structure determination was considered to have been completed.

As a further check on the correctness of the positions assigned to hydrogen atoms, a three-dimensional difference synthesis using observed structure factors minus the final calculated structure factors was computed in the same manner as before. Only two peaks as high as five, on the same scale used above, occurred. Neither of these peaks was close enough to any boron atom to correspond to a B—H distance. If any of the hydrogen atoms had been incorrectly placed, we would have expected much higher peaks, and at positions corresponding to reasonable B—H distances.

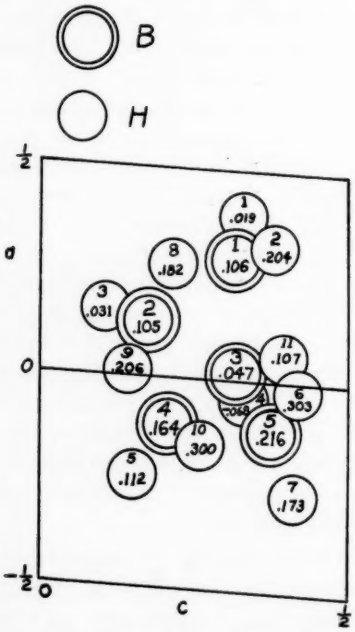

FIG. 1. Atomic positions for one molecule of B_5H_{11} as projected on a-c plane. Atom numbers and y coordinates are indicated.

FINAL MODEL AND DISCUSSION OF THE RESULTS

The final least-squares refinement gave a value for B, the empirical constant in the temperature factor, of 2.9_5A^2. The atomic parameters are listed in Table I. It appears that, within the experimental error, the molecule possesses C_s symmetry not required by the space group. The Roman numerals indicating the types of atoms in Table I are assigned assuming that C_s symmetry is present. Figure 1 is a line drawing of the unit cell showing the atomic positions listed in Table I.

Table II gives the bond distances calculated from the parameters in Table I, with the average deviation where equivalent bonds have been averaged. Figure 2 is a drawing of the molecule which indicates these bonds and the C_s symmetry.

TABLE II. Bond distances.

B—B bonds

$B_2-B_3 = 1.74$A
$B_3-B_4 = 1.70$A
Ave. $B_I-B_{II} = 1.72\pm0.02$A

$B_1-B_3 = 1.87$A
$B_3-B_5 = 1.86$A
Ave. $B_I-B_{III} = 1.86_5\pm0.00_5$A

$B_1-B_2 = 1.73$A
$B_4-B_5 = 1.77$A
Ave. $B_{II}-B_{III} = 1.75\pm0.02$A
$B_2-B_4 = B_{II}-B_{II} = 1.77$A

B—H ("single") bonds

$B_1-H_1 = 1.03$A
$B_1-H_2 = 1.08$A
$B_2-H_3 = 0.96$A
$B_3-H_4 = 1.09$A
$B_4-H_5 = 1.09$A
$B_5-H_6 = 1.11$A
$B_5-H_7 = 1.12$A
Ave. B—H ("single") bonds $= 1.0_7\pm0.04$A

B—H (bridge) bonds

$B_1-H_8 = 1.20$A
$B_2-H_8 = 1.21$A
$B_2-H_9 = 1.20$A
$B_4-H_9 = 1.15$A
$B_4-H_{10} = 1.32$A
$B_5-H_{10} = 1.36$A
Ave. B—H (bridge) bonds $= 1.2_4\pm0.0_7$A

B—H ("long bridge") bonds

$B_3-H_{11} = B_I-H_{VII} = 1.00$A

$B_1-H_{11} = 1.75$A
$B_5-H_{11} = 1.58$A
Ave. $B_{II}-H_{VII} = 1.6_7\pm0.0_9$A

A rigorous calculation of the errors to be expected in the various bond lengths can be made, but this is laborious. However, using an averaged value for all borons and for all hydrogens and assuming that errors in one atomic parameter are independent of all others makes possible a rapid but crude error calculation which is certain to give too low a value. If the results of such a crude calculation are doubled, they give a probable error of 0.02A for the B−B distances and a probable error of 0.09A in the B−H distances. These appear to be reasonable values.

Table III gives various angles found in the molecule along with the average deviation where equivalent angles have been averaged.

Figure 3 is included to give some indications of the nature of the peaks observed on the three-dimensional Fourier maps showing borons. It is probable that the very slight differences in peak heights are caused primarily by the fact that the real maxima for the various atoms lie at varying distances from the planes of the sections calculated.

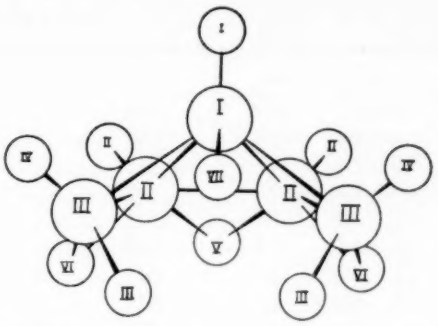

FIG. 2. B_5H_{11} molecule. Atom types are taken from Table I. Larger circles are borons; smaller ones are hydrogens.

All of the contacts between different molecules are

TABLE III.[a] Bond angles.

B−B−B angles

$B_2-B_1-B_3 = 59°$
$B_4-B_5-B_3 = 56°$
Ave. $B_{II}-B_{III}-B_I = 57.5\pm1.5°$

$B_1-B_2-B_3 = 66°$
$B_5-B_4-B_3 = 64°$
Ave. $B_{III}-B_{II}-B_I = 65\pm1°$

$B_1-B_2-B_4 = 112°$
$B_5-B_4-B_2 = 112°$
Ave. $B_{III}-B_{II}-B_{II} = 112\pm0°$

$B_3-B_2-B_4 = 56°$
$B_3-B_4-B_2 = 62°$
Ave. $B_I-B_{II}-B_{II} = 60\pm2°$

$B_1-B_3-B_2 = 55°$
$B_5-B_3-B_4 = 59°$
Ave. $B_{III}-B_I-B_{II} = 57\pm2°$

$B_1-B_3-B_4 = 109°$
$B_5-B_3-B_2 = 108°$
Ave. $B_{III}-B_I-B_{II}' = 108.5\pm0.5°$

$B_1-B_3-B_5 = B_{III}-B_I-B_{III} = 107°$
$B_2-B_3-B_4 = B_{II}-B_I-B_{II} = 62°$

B−B−H angles
B−B_{III}−H angles

$B_3-B_1-H_1 = 115°$
$B_3-B_5-H_7 = 111°$
Ave. $B_I-B_{III}-H_{IV} = 113\pm2°$

$B_3-B_1-H_2 = 111°$
$B_3-B_5-H_6 = 111°$
Ave. $B_I-B_{III}-H_{III} = 111\pm0°$

$B_3-B_1-H_8 = 96°$
$B_3-B_5-H_{10} = 93°$
Ave. $B_I-B_{III}-H_{VI} = 94.5\pm1.5°$

$B_2-B_1-H_1 = 116°$
$B_4-B_5-H_7 = 110°$
Ave. $B_{II}-B_{III}-H_{IV} = 113\pm3°$

$B_2-B_1-H_2 = 128°$
$B_4-B_5-H_6 = 125°$
Ave. $B_{II}-B_{III}-H_{III} = 126.5\pm1.5°$

B−B_{II}−H angles

$B_3-B_2-H_3 = 118°$
$B_3-B_4-B_5 = 121°$
Ave. $B_I-B_{II}-H_{II} = 119.5\pm1.5°$

$B_3-B_2-H_8 = 103°$
$B_3-B_4-H_{10} = 112°$
Ave. $B_I-B_{II}-H_{VI} = 108\pm5°$

$B_3-B_2-H_9 = 94°$
$B_3-B_4-H_9 = 101°$
Ave. $B_I-B_{II}-H_V = 98\pm4°$

$B_1-B_2-H_3 = 118°$
$B_5-B_4-H_5 = 121°$
Ave. $B_{III}-B_{II}-H_{II} = 119.5\pm1.5°$

B−B_I−H angles

$B_1-B_3-H_4 = 127°$
$B_5-B_3-H_4 = 114°$
Ave. $B_{III}-B_I-H_I = 120\pm7°$

$B_1-B_3-H_{II} = 71°$
$B_5-B_3-H_{II} = 58°$
Ave. $B_{III}-B_I-H_{VII} = 64\pm7°$

$B_2-B_3-H_4 = 121°$
$B_4-B_3-H_4 = 115°$
Ave. $B_{II}-B_I-H_I = 118\pm3°$

$B_2-B_3-H_{II} = 115°$
$B_4-B_3-H_{II} = 109°$
Ave. $B_{II}-B_I-H_{VII} = 112\pm3°$

H−B−H angles

$H_1-B_1-H_2 = 108°$
$H_7-B_5-H_6 = 126°$
Ave. $H_{IV}-B_{III}-H_{III} = 117\pm9°$
$H_4-B_3-H_{II} = H_I-B_I-H_{VII} = 116°$

[a] Table III does not include all angles present but does furnish sufficient information for the construction of a unique model.

TABLE IV.[a] Comparison of structure factors.

hkl	F_c	F_0	hkl	F_c	F_0	hkl	F_c	F_0	hkl	F_c	F_0
002	−42.7	40.2	$21\bar{8}$	−3.3	3.1	320	2.6	1.8	630	5.4	5.6
004	−16.4	15.6	310	3.8	2.7	321	−14.4	15.0	$\bar{6}32$	2.5	2.6
006	12.3	11.8	$\bar{3}11$	6.5	7.9	$\bar{3}21$	3.2	4.0	737	−4.2	3.2
008	−7.9	9.0	312	−5.8	4.7	322	4.2	3.1			
0,0,10	5.1	5.8	$\bar{3}13$	−4.9	6.3	$\bar{3}22$	13.0	14.0	040	−8.4	8.2
101	−15.1	14.4	316	4.3	6.0	323	8.5	7.9	042	8.1	8.9
$\bar{1}01$	4.7	4.0	410	−2.9	1.9	$\bar{3}23$	9.0	10.5	043	2.6	2.1
$\bar{1}03$	−5.8	5.6	411	−7.1	7.1	324	−7.5	6.5	046	−5.0	5.3
105	13.0	11.1	413	9.2	7.3	$\bar{3}24$	−14.1	14.4	047	−7.3	7.3
107	−11.4	10.6	$\bar{4}13$	8.6	9.4	$\bar{3}25$	−4.7	4.5	048	6.7	6.5
$\bar{1}07$	6.1	6.0	414	−5.3	6.5	326	4.8	4.7	0,4,11	3.1	2.9
202	−16.4	16.6	$\bar{4}14$	−7.1	7.6	$\bar{3}26$	6.4	7.6	0,4,13	−3.8	3.4
$\bar{2}02$	18.2	17.6	$\bar{4}15$	−10.4	11.0	$\bar{3}$,2,10	−6.5	6.5	140	−11.8	12.6
206	8.4	8.5	416	6.0	6.3	$\bar{3}$,2,12	5.1	4.8	141	2.1	2.3
$\bar{2}06$	−7.3	6.8	$\bar{4}16$	9.9	11.0	420	7.2	7.7	$\bar{1}41$	−11.0	10.3
208	−5.5	7.1	510	−4.2	2.9	421	7.5	6.6	142	5.8	5.8
$\bar{3}01$	−15.3	16.3	511	10.4	10.5	$\bar{4}22$	−6.4	7.7	143	8.1	9.0
303	10.4	11.0	$\bar{5}15$	−2.9	2.9	423	−6.6	5.3	$\bar{1}43$	8.5	9.5
$\bar{3}03$	18.5	19.0	610	−2.3	2.4	$\bar{4}23$	6.8	5.8	$\bar{1}44$	−7.5	8.4
305	−9.9	10.0	710	5.3	5.2	424	−3.6	3.1	145	−9.3	8.2
$\bar{3}05$	−12.7	12.9	$\bar{7}17$	−4.1	3.1	$\bar{4}25$	−5.8	5.6	240	7.5	7.6
$\bar{3}07$	6.0	6.6	810	−3.7	2.6	620	2.8	2.9	242	−5.4	5.8
309	4.8	3.9				626	4.3	3.5	244	−5.3	5.8
$\bar{3}09$	5.5	5.6	020	−4.8	3.7	720	−4.0	3.7	246	6.9	7.4
$\bar{3}$,0,11	−9.5	9.8	021	−45.2	36.1	$\bar{7}27$	2.7	3.1	$\bar{2}48$	−6.8	7.7
400	−5.9	6.6	022	−4.4	4.7				$\bar{2}$,4,10	6.0	4.8
402	8.9	7.6	023	3.8	3.9	032	−5.0	4.5	340	−8.7	8.1
404	−4.8	5.3	024	2.0	2.1	033	9.1	9.2	$\bar{3}41$	4.9	5.6
$\bar{4}04$	9.3	9.5	025	10.4	9.7	034	−4.3	5.0	342	12.0	10.5
406	4.8	4.8	026	7.7	7.6	035	−13.0	13.5	$\bar{3}43$	−10.8	10.8
4,0,12	4.3	3.9	027	−9.0	9.4	036	6.3	5.6	442	−5.6	4.4
505	−5.4	4.4	028	−7.0	7.1	037	5.2	5.3	444	5.3	3.2
$\bar{5}05$	−6.6	7.7	029	6.1	6.0	0,3,10	−3.5	2.7	$\bar{4}48$	−3.4	3.1
$\bar{6}02$	−3.9	3.1	0,2,12	3.8	3.1	130	−5.3	5.8	545	0.8	2.9
$\bar{6}06$	5.7	4.5	120	−12.5	11.5	$\bar{1}31$	−8.5	8.7	$\bar{5}45$	−3.8	3.1
800	4.9	3.7	121	−12.2	10.2	$\bar{1}33$	10.1	10.5	$\bar{6}42$	−3.5	2.6
			$\bar{1}21$	16.0	16.6	137	−4.8	4.2			
011	−6.9	6.6	$\bar{1}22$	−14.3	13.7	$\bar{1}37$	−5.6	6.3	052	7.1	7.3
012	11.5	11.0	$\bar{1}23$	5.9	7.3	230	−13.5	13.1	054	−8.0	9.2
013	8.1	7.9	124	8.2	7.4	231	−13.7	11.8	055	4.3	3.2
014	9.1	10.0	$\bar{1}24$	6.3	6.0	232	3.9	4.5	056	3.6	3.2
016	−8.2	9.0	125	−4.3	5.2	233	6.8	6.3	151	−3.0	3.1
019	2.2	2.6	$\bar{1}25$	−10.9	10.2	$\bar{2}33$	5.6	6.0	$\bar{1}53$	−4.6	3.4
110	28.1	27.9	126	−11.0	9.2	234	6.0	4.5	$\bar{1}55$	3.8	2.4
111	−28.1	26.9	128	5.5	4.7	$\bar{2}34$	−6.3	6.6	250	−3.3	2.7
$\bar{1}11$	−21.7	21.3	220	4.9	6.6	330	5.7	7.1	251	7.2	7.3
112	−9.2	13.5	$\bar{2}21$	9.5	11.0	$\bar{3}31$	−4.4	4.0	$\bar{2}51$	−6.2	6.0
$\bar{1}12$	−16.3	16.9	$\bar{2}22$	−7.5	9.2	$\bar{3}32$	−6.0	7.4	252	7.9	7.9
113	−3.3	3.2	223	6.7	5.8	$\bar{3}36$	6.2	6.3	253	4.2	2.4
114	−9.3	9.7	$\bar{2}23$	−4.8	4.8	430	−4.9	5.3	254	−7.5	7.6
115	9.7	8.9	224	4.2	4.2	432	12.2	10.3	258	3.1	3.4
116	9.3	9.4	$\bar{2}24$	−3.4	3.2	$\bar{4}32$	7.0	8.1	351	−4.5	2.9
210	16.7	17.9	226	−3.9	3.4	434	−6.1	4.2	$\bar{3}51$	−2.8	2.4
212	−8.1	7.9	$\bar{2}26$	8.2	9.5	$\bar{4}34$	−8.5	9.8	$\bar{3}52$	−3.4	3.2
213	2.2	2.1	$\bar{2}27$	6.7	6.0	530	9.9	9.4	353	3.5	2.6
$\bar{2}13$	7.6	9.4	$\bar{2}28$	−2.5	2.9	535	4.1	2.9	356	5.7	4.0
$\bar{2}14$	3.8	4.8	$\bar{2}29$	−4.5	4.4	$\bar{5}35$	−4.7	3.9			

[a] The ten unobserved reflections having the largest values of $|F_c|$ are $\bar{1}09$, $\bar{2}04$, $\bar{2}08$, $\bar{4}02$, $\bar{5}01$, 212, $\bar{3}15$, $\bar{1}28$, 057, and 266. Of these, six have values corresponding to intensities greater than the smallest observable intensity on the photographs on which they might have been observed. Only one of these six unobserved reflections has a value (2.2) of $|F_c| > 2F_0$.

TABLE IV—*Continued.*

hkl	F_c	F_o	*hkl*	F_c	F_o	*hkl*	F_c	F_o	*hkl*	F_c	F_o
$\bar{3}59$	5.5	5.8	$\bar{2}63$	3.9	3.5	$\bar{2}74$	−5.1	6.5	283	−5.3	4.5
750	−2.4	2.6	264	−5.6	6.3	$\bar{2},7,10$	−2.9	2.4	$\bar{2}83$	8.6	8.9
060	−2.5	2.9	$\bar{2}64$	6.1	7.3	$\bar{3}71$	−4.5	4.0	284	3.6	3.2
063	−3.5	3.2	361	3.2	2.4	372	4.6	2.6	286	−4.4	3.9
064	4.3	3.5	$\bar{3}61$	−1.6	2.4	373	−6.5	7.3	$\bar{2}88$	2.5	2.9
066	−4.5	5.2	$\bar{3}62$	−4.5	4.4	$\bar{3}73$	5.9	6.0			
067	3.4	2.3	363	−4.7	4.4	$\bar{5}75$	3.9	3.7	099	−2.9	3.1
160	5.2	5.2	369	−3.6	3.7	670	−6.0	6.3	$\bar{1}92$	4.4	2.9
161	7.0	7.3	$\bar{4}64$	−3.4	3.7	672	5.6	4.5	$\bar{2}93$	−5.7	6.3
$\bar{1}61$	−4.7	3.5	560	−4.1	3.2	$\bar{6}76$	4.8	4.2	392	−4.8	3.1
162	4.3	2.9	760	−3.1	2.6				$\bar{3}92$	5.4	5.0
$\bar{1}62$	8.1	8.4				085	−4.0	2.7	396	−2.6	2.3
163	−4.5	3.5	071	3.6	3.2	180	3.5	4.0	590	−2.9	2.9
164	−9.1	8.7	073	−5.0	4.5	$\bar{1}81$	4.5	3.9			
$\bar{1}64$	−3.1	2.9	0,7,10	0.0	2.4	$\bar{1}82$	3.9	3.7	$\bar{1},10,1$	3.6	3.5
$\bar{1}67$	−5.5	3.9	170	−2.9	2.4	$\bar{1}83$	−3.5	3.9	$\bar{1},10,3$	−3.8	3.7
261	−6.8	6.3	$\bar{1}74$	4.3	2.9	$\bar{1}84$	−4.0	3.2	2,10,0	−3.6	3.4
$\bar{2}61$	−4.6	3.5	270	3.5	2.4	280	−3.7	4.4	$\bar{2},10,2$	6.6	6.0
262	3.7	4.2	$\bar{2}72$	6.0	5.2	$\bar{2}81$	−7.9	8.5	2,10,4	3.8	2.9
$\bar{2}62$	−6.9	6.0	273	−5.2	4.0	$\bar{2}82$	4.4	4.4	2,10,6	−3.2	2.7
									3,11,3	3.4	3.2

between hydrogen atoms. The five shortest intermolecular H···H distances, and the symmetry operation relating the adjacent molecules between which they occur, are $H_4\cdots H_{10}(2_1-b)=2.50$A, $H_4\cdots H_{11}(\bar{1})=2.74$A, $H_1\cdots H_9(2_1-b)=2.74$A, $H_1\cdots H_{10}(2_1-b)=2.76$A, and $H_2\cdots H_3(2_1)=2.78$A. In view of the fact that the intramolecular B−H distances are, in reality, probably slightly longer than indicated by our results, these appear quite reasonable.[12]

A comparison of the 299 observed structure factors with those calculated from the final parameters is shown in Table IV, and a similar comparison of the 41 additional, presumably less reliable, reflections from nets not properly lined up for the precession photography is shown in Table V. The value of $R=\Sigma||F_o|-|F_c||/\Sigma|F_o|$ is 0.11 for the 299 reflections in Table IV, and 0.19 for the 41 reflections in Table V.

With all honesty it must be stated that the hydrogen positions found in the B_5H_{11} structure are not sufficiently accurate to justify the use of the B−H distances in theoretical calculations. The number of diffraction maxima observed is somewhat low for a very accurate determination of hydrogen positions. It is to be expected that more nearly complete data would give larger values for the B−H distances; this phenomenon has been observed previously in the structure of B_4H_{10} in which there were relatively more data available and, therefore, probably, less shortening of these distances.[5]

There is just one feature of the B_5H_{11} structure which had not been previously observed in the structures of other boron hydrides which have been investigated. This is the unique hydrogen H_{VII}. Obviously, H_{VII} must be considered as forming a "single" bond to B_I. However, the close approach of H_{VII} to the two B_{III} atoms seems to indicate that it is also very weakly bonded to these two atoms, even more weakly than the usual bridge bonds previously observed for hydrogens in boron hydrides. This "long bridge," although never observed previously, appears to be quite similar to previously observed unsymmetrical bridges established[2,5] in $B_{10}H_{14}$ and B_4H_{10}.

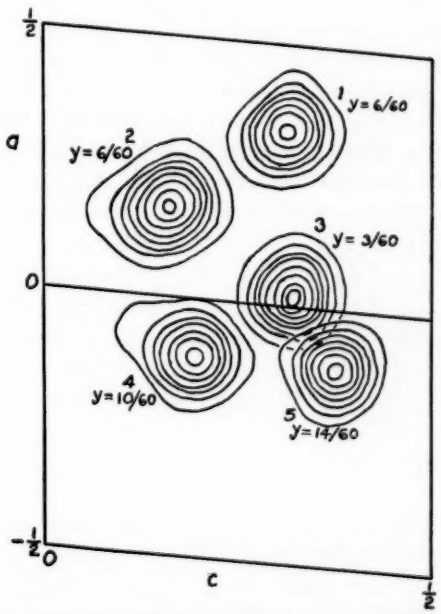

FIG. 3. Traces of sections perpendicular to *b* as presented on X-RAC. Boron atoms are shown with atom numbers and section numbers.

[12] The "normal" van der Waals contact is 2.4A. See L. Pauling, *Nature of the Chemical Bond* (Cornell University Press, Ithaca, 1940), second edition, p. 189.

TABLE V. Structure factors not used in calculations.

hkl	F_c	F_o	*hkl*	F_c	F_o
$\bar{3}$,0,13	4.0	8.4	$\bar{1}$56	−2.9	4.2
			255	−6.6	4.2
$\bar{1}$16	2.0	3.9	354	−5.0	4.2
118	−4.9	4.0	$\bar{3}$54	7.6	9.4
$\bar{1}$18	−3.5	4.0	451	6.7	7.9
$\bar{2}$,1,11	−2.8	4.5	$\bar{4}$53	−5.3	5.3
317	−6.4	5.8	$\bar{5}$53	5.7	6.6
$\bar{4}$,1,11	−3.9	5.0			
512	7.4	6.0	265	8.7	7.7
$\bar{7}$12	−5.4	6.5	267	−5.5	5.6
			$\bar{2}$69	6.2	6.8
227	−3.1	4.5	$\bar{2}$,6,11	−3.1	3.4
229	3.2	3.5	375	6.6	7.3
3,2,11	−3.0	4.5			
			$\bar{1}$88	6.0	3.4
$\bar{1}$36	3.9	2.9	582	5.1	5.6
$\bar{3}$38	−5.3	4.8	394	6.3	6.6
532	−5.7	4.2			
$\bar{5}$32	−4.8	4.5			
533	−6.3	4.7			
$\bar{1}$46	9.1	8.1			
245	−7.0	5.6			
$\bar{2}$45	6.6	6.0			
$\bar{2}$47	−5.2	6.6			
$\bar{3}$44	−5.6	6.8			
441	−3.8	4.5			
$\bar{4}$41	−7.6	9.2			
$\bar{4}$43	3.9	4.0			
$\bar{4}$,4,11	−4.1	4.4			

The structure found for B_5H_{11} may be considered in a number of ways which indicate its close relationship with the structures of other boron hydrides. By moving the two B_{III} atoms toward each other along the line connecting their centers until they are close enough to form a B−B bond, the B_5H_{11} structure can be distorted into an arrangement very close to that found for B_5H_9. In this distortion, of course, the two H_{III} atoms and the unique H_{VII} atoms are eliminated and one bridge hydrogen inserted between the two B_{III} atoms. The other hydrogens present already bear a striking geometrical resemblance to those observed in the B_5H_9 structure. There are three bridge hydrogens, two H_{VI} and one H_V, present; the remaining hydrogens, two H_{IV}, two H_{II}, and one H_I, have their counterparts in the hydrogens "singly" bonded to borons in the B_5H_9 structure.

B_4H_{10} and B_5H_{11} are most readily compared by imagining one of the two B_{III} atoms removed from B_5H_{11} along with the two hydrogens H_{IV} and H_{III}, which are "singly" bonded to it. The H_{VI} forming a bridge to this B_{III} will now be "singly" bonded to the B_{II} on this side. The gap left by the removal of the boron must be filled in with a hydrogen bridge between B_I and this B_{II}, and H_{VII} must be moved over slightly to form an unsymmetrical bridge to the B_{III} which was not disturbed. The result of this imaginary rupture and subsequent rearrangement of a few hydrogen atoms is a molecule of B_4H_{10}.

The relationship between the structures of $B_{10}H_{14}$ and B_5H_{11} is also not very remote. The five borons in the B_5H_{11} molecule are arranged approximately in the form of a fragment of a regular icosahedron as are the borons in $B_{10}H_{14}$; in addition, although naturally H_{VII} is at a smaller distance from B_I than would be expected for a boron, it lies in the same general direction in which one would expect to find a boron if this were a molecule of $B_{10}H_{14}$. Thus, the structure of the molecule of B_5H_{11} gives additional evidence that the geometrical properties of boron hydrides investigated previously appear in other members of the group.

It is a pleasure to acknowledge support of this research by the U. S. Office of Naval Research, and by a predoctoral fellowship (to L.R.L.) from the General Electric Company. Dr. L. V. McCarty very kindly prepared a sample of pure B_5H_{11}, and Professor A. E. Finholt of St. Olaf's College, as well as Dr. McCarty, gave valuable advice in the handling of this unstable material. The computations were carried out on the X-RAC at The Pennsylvania State College and at the Computing Center of the University of Minnesota. Dr. Christer E. Nordman, Dr. Richard M. Curtis, and Mr. Masao Atoji assisted in the experimental work.

Free Radicals by Mass Spectrometry. V. The Ionization Potentials of Methyl, Allyl, and Benzyl Radicals*

F. P. Lossing, K. U. Ingold† and I. H. S. Henderson†
Division of Pure Chemistry, National Research Council, Ottawa, Canada
(Received July 10, 1953)

The ionization potentials of methyl, allyl, and benzyl radicals have been measured directly by electron impact. The values found were methyl 9.95±0.03 ev, allyl 8.16±0.03 ev, and benzyl 7.73±0.08 ev. The radicals were produced by thermal decomposition of suitable compounds in a mass spectrometer designed for the study of free radicals. Reactions of the radicals after formation led to the expected dimers, but the disproportionation reactions were found to be negligibly slow.

INTRODUCTION

CONSIDERABLE information about the bond dissociation energies of hydrocarbons and other compounds has been obtained from electron impact measurements carried out over the last few years. Two methods of obtaining bond dissociation energies from appearance potentials have been used with considerable success by Stevenson and others. These methods have been recently summarized.[1] The first, or direct, method is based on the following relationship

$$A(R_1^+)=D(R_1-R_2)+I(R_1)+E,$$

where $A(R_1^+)$ is the appearance potential of the ion R_1^+ from the compound R_1R_2, $D(R_1-R_2)$ is the bond dissociation energy of the R_1-R_2 bond, $I(R_1)$ is the ionization potential of the radical R_1, and E is energy which may in some cases be associated with the formation of the ion R_1^+ from the parent molecule. In many cases E can be shown to be very small or zero.[1] The second, or indirect, method compares two bond dissociation energies, eliminating $I(R_1)$ from two equations similar to the above. By a combination of these methods with heats of formation, Stevenson and others have been able to obtain a number of bond dissociation energies which are self consistent and generally in good agreement with values obtained from kinetic measurements.[1–7] A much fuller use of the direct method could be made if more were known about the ionization potentials of hydrocarbon radicals. In addition, the thermochemical cycles used in the indirect method, which are often of necessity rather roundabout, could be considerably strengthened if more cross checks could be made with known radical ionization potentials.

A rough estimate of the ionization potential of methyl was first made by Mulliken[8] who suggested 8.5 ev on the basis of molecular orbital considerations. The first direct measurement of the ionization potentials of hydrocarbon radicals was that of Fraser and Jewitt,[9] who directed a molecular beam of radicals, formed by decomposing the appropriate lead tetra-alkyl, into an ionization gauge detector. In this way they obtained $I(CH_3)=11.2\pm0.8$ and $I(C_2H_5)=10.6\pm0.8$ ev. These values were undoubtedly too high because of the presence of other reaction products such as methane and ethylene, which were probably formed in large amounts.

A number of estimates of radical ionization potentials have been made from appearance potentials and bond dissociation energies. Smith [10] estimated the ionization potential of methyl to be ≤ 9.9 ev and that of methylene ≤ 12.0 ev. These values were obtained from the appearance potentials of CH_3^+ and CH_2^+ in the mass spectrum of methane and are in excellent agreement with more recent values. In the same way Hipple[11] estimated $I(CH_3)\leq 10.4$ ev and $I(C_2H_5)\leq 9.8$ ev from the appearance potentials of CH_3^+ and $C_2H_5^+$ in the mass spectrum of ethane. Stevenson and Hipple[12] estimated $I(C_2H_5)=8.6$ ev from the appearance potential of $C_2H_5^+$ in ethane.

The ionization potentials of CH_3 and C_2H_5 were measured directly by Hipple and Stevenson[13] on a stream of radicals produced in a quartz capillary furnace opening into the ionization chamber of a mass spectrometer. The radicals were produced from lead tetra-alkyls. This method was similar in many respects to that of Fraser and Jewitt, with the great advantage that only ions of the proper mass to charge ratio were collected. They obtained $I(CH_3)=10.07\pm0.1$ ev and $I(C_2H_5)=8.67\pm0.1$ ev. These ionization potentials in conjunction with the appearance potentials of CH_3^+ and $C_2H_5^+$ from methane and ethane lead to values of $D(CH_3-H)$ and $D(C_2H_5-H)$, which are in agreement with kinetic measurements of these bond dissociation

* National Research Council Contribution No. 3225.
† National Research Council Postdoctorate Fellow.
[1] D. P. Stevenson, Discussions Faraday Soc. **10**, 35 (1951).
[2] D. P. Stevenson, J. Chem. Phys. **10**, 241 (1942).
[3] D. P. Stevenson and J. A. Hipple, J. Am. Chem. Soc. **64**, 1588 2766, 2769 (1942).
[4] D. P. Stevenson, J. Am. Chem. Soc. **65**, 209 (1943).
[5] J. A. Hipple and D. P. Stevenson, Phys. Rev. **63**, 121 (1943).
[6] V. Dibeler, J. Research Natl. Bur. Standards **38**, 329 (1947).
[7] D. P. Stevenson, J. Chem. Phys. **18**, 1347 (1950).
[8] R. S. Mulliken, J. Chem. Phys. **1**, 492 (1933).
[9] R. G. J. Fraser and T. N. Jewitt, Proc. Roy. Soc. (London) **A160**, 563 (1937). See also Phys. Rev. **50**, 1091 (1936).
[10] L. G. Smith, Phys. Rev. **51**, 263 (1937).
[11] J. A. Hipple, Phys. Rev. **53**, 530 (1938).
[12] D. P. Stevenson and J. A. Hipple, J. Am. Chem. Soc. **64**, 1588 (1942).
[13] J. A. Hipple and D. P. Stevenson, Phys. Rev. **63**, 121 (1943).

energies.[14] McDowell and Warren[15] have recently redetermined the appearance potential of CH_3^+ from CH_4 by a more precise method, and from this value they calculate $I(CH_3)$ to be $\leq 9.96 \pm 0.05$ ev. No direct measurements of the ionization potential of the allyl radical have been made. Evans and Szwarc[16] have estimated this ionization potential to be 9.05 ev, based on the appearance potential of allyl from 1-butene[4] and the value of 2.6 ev for $D(CH_2{:}CH{\cdot}CH_2{-}CH_3)$ obtained from the pyrolysis of 1-butene.[14]

The authors are not aware of any value, predicted or measured, for the ionization potential of the benzyl radical.

EXPERIMENTAL

The free radical mass spectrometer used in this work has been described.[17,18] The reactor was fitted with a retractable furnace[19] in addition to a fixed furnace with a heating element 3.5 cm long.

Production of Radicals

Methyl radicals were obtained from the decomposition of mercury dimethyl carried at a partial pressure of about 15 microns in a stream of helium at 7 mm pressure. The decomposition of the mercury dimethyl was almost complete at 950°C, and the amount of methyl accounted for over 90 percent of the mercury dimethyl decomposed, the other products being methane and ethane.

Allyl radicals have previously been detected with a mass spectrometer by reacting methyl radicals with propylene.[20] In the present work they were prepared by the pyrolysis of allyl iodide,[14,21] the iodide being almost completely decomposed at 750°C in a contact time of 0.8 millisecond.

The production of allyl appeared to be almost quantitative, the only other hydrocarbon product of any importance being the dimerization product 1,5 hexadiene. This was identified by comparing the spectrum with that of a NBS sample of 1,5 hexadiene. Peaks corresponding to iodine atoms and HI were also found. The products formed by the reaction of allyl radicals with each other and with iodine were determined by the use of the retractable furnace. With this furnace at a temperature sufficient to decompose the allyl iodide completely, it was withdrawn from the leak to a distance of 6 cm and the spectra of the products in the two positions were compared. The products were mainly 1,5 hexadiene and allyl iodide formed by the combination of the allyl radicals with each other and with iodine atoms, respectively. Propylene and allene, the products of disproportionation of allyl radicals, were not found and, if present, amounted to less than 1 percent of the amount of 1,5 hexadiene. A small amount of another hexadiene was found; the spectrum analysis indicated that it was most probably 2,3 dimethyl butadiene.

In order to reduce the interference of the 41 peak from 1,5 hexadiene with the 41 peak for allyl, the possibility of operating at a reactor temperature where the 1,5 hexadiene was also decomposed was considered. The decomposition of pure 1,5 hexadiene was examined, and it was found that it started to decompose at 690°–700°C and was completely decomposed at 890°C. The main products were radicals of parent mass 41, presumably allyl, with a small amount of hydrogen and methyl radicals. No trace of vinyl radicals, C_4H_7 radicals, or of the dehydrogenation product hexatriene could be found.

The ionization efficiency curves for allyl radicals produced from allyl iodide were obtained under two sets of conditions: at 766°C where the iodide was about 95 percent decomposed, and at 915°C where both the iodide and the 1,5 hexadiene were decomposed. The second set of conditions is open to question, since the 1,5 hexadiene may isomerize to 2,3 dimethyl butadiene or 2,4 hexadiene. These could then decompose to give $CH_3{\cdot}\dot{C}{:}CH_2$ or $CH_3{\cdot}CH{:}\dot{C}H$ radicals, respectively.

Allyl radicals were also produced by the thermal decomposition of 1-butene at about 1000°C, the other major product being methyl radicals. There may also have been present a trace of propylene and allene. A value for the ionization potential of allyl was obtained in this experiment by comparing the ionization efficiency curve of mass 41 with that of the methyl radicals formed simultaneously.

Benzyl radicals were produced by the pyrolysis of benzyl iodide.[14,21] Small amounts of toluene and dibenzyl were also produced. On use of the retractable furnace to study the combination products of benzyl, no increase in the amount of toluene was found, but the amounts of dibenzyl and benzyl iodide increased with the distance of withdrawal. The main reactions, as with allyl, were the combination of the radicals with each other and with iodine atoms to form dibenzyl and to reform the iodide. This experiment indicates that the disproportionation of benzyl radicals is much slower than the combination reaction.[22]

Measurement of the Ionization Potential

Various methods have been employed for measuring an unknown ionization potential by comparing it with

[14] For a review see M. Szwarc, Chem. Rev. **47**, 75 (1950).
[15] C. A. McDowell and J. W. Warren, Discussions Faraday Soc. **10**, 53 (1951).
[16] M. G. Evans and M. Szwarc, J. Chem. Phys. **19**, 1322 (1951).
[17] F. P. Lossing and A. W. Tickner, J. Chem. Phys. **20**, 907 (1952).
[18] Lossing, Ingold, and Tickner, Discussions Faraday Soc. **14**, 34 (1953).
[19] K. U. Ingold and F. P. Lossing, J. Chem. Phys. **21**, 1135 (1953).
[20] G. C. Eltenton, J. Chem. Phys. **15**, 455 (1947).
[21] E. T. Butler and M. Polanyi, Trans. Faraday Soc. **39**, 19 (1943).
[22] C. Horrex and S. E. Miles, Discussions Faraday Soc. **10**, 187 (1951). See also the discussion by W. A. Waters and by M. Szwarc, Discussions Faraday Soc. **10**, 231 (1951).

a reference standard whose ionization potential is known from spectroscopic data. These methods have been discussed in a number of publications.[23–27] The method of extrapolated voltage differences suggested by Warren[28] has been used by McDowell and Warren,[15] who obtained bond dissociation energies in good agreement with reliable kinetic data. The method seems to be less subject to personal error than the initial break method. The ionization efficiency curves for the ion to be studied and for the molecular ion of the reference standard are plotted with the linear portions of the curves parallel. The voltage difference (δV) between the two curves at a given ion current is plotted as a function of the ion current (I), and the resulting curve or straight line is extrapolated to zero ion current. The voltage difference at I=0 is added algebraically to the spectroscopic ionization potential of the reference standard to obtain the ionization potential of the ion in question. For many ions, particularly molecular ions (ionization potentials), the δV curves are straight lines almost perpendicular to the voltage axis. For these ions, the "1 percent method" used for the deuterated methanes[25] is seen to be a special case of the method of extrapolated voltage differences.

In the case of methyl and allyl in the present work, the δV *vs* I relation was a straight line almost perpendicular to the voltage axis, but a small curvature (about 0.06 ev) was found for the benzyl ion. With the use of benzyl iodide as a source of benzyl radicals, very little toluene was produced, and the benzyl radical could be detected by the low electron energy method. The low resolution of the mass spectrometer (1 in 100) and the relatively large amounts of toluene present (mass 92 as against 91 for benzyl) were found to be the reasons for the previous failure to detect benzyl radicals at low electron energies.[29]

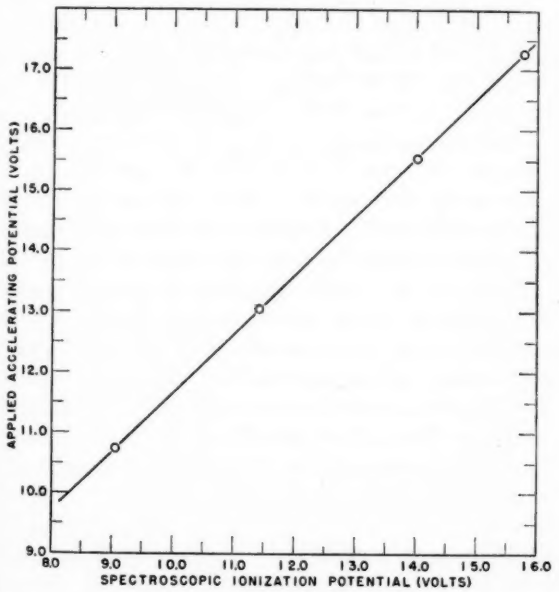

FIG. 1. Calibration line relating observed and spectroscopic ionization potentials. Spectroscopic values used were: argon 15.77 ev, krypton 14.01 ev, acetylene 11.41 ev, and furane 9.05 ev.

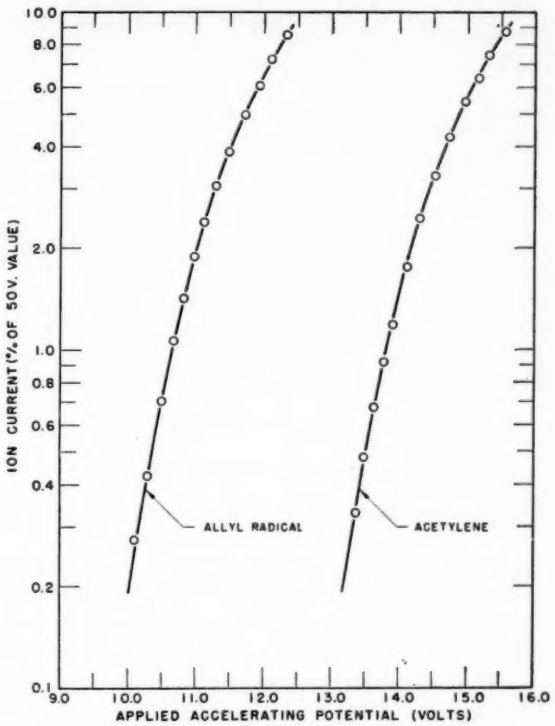

FIG. 2. Lower portions of typical ionization efficiency curves obtained for a radical and for the acetylene standard.

Some authors[23,26] find that the use of one reference standard, usually argon or krypton, yields ionization potentials for other rare gases and for certain compounds such as acetylene, nitrogen, water, carbon disulfide, hydrogen sulfide, and furane, which are in good agreement with the spectroscopic values. This corresponds to a calibration relation between observed and spectroscopic values which is a straight line with a slope of unity. Others find the calibration line to be curved[24] or a straight line with a slope slightly different from unity.[25] In the present work four reference standards, argon, krypton, acetylene, and furane were used to construct a calibration line, whose slope was 0.969_3. This line is shown in Fig. 1. All the points were in a straight line within ± 0.02 ev, the precision of measurement. One reference standard, acetylene, was introduced into the helium carrier gas together with the substance used as a source of radicals. In order to have the conditions as nearly as possible the same for the standard and for the radical ion to be measured, the quantities entering the helium stream were adjusted to make

[23] R. E. Honig, J. Chem. Phys. **16**, 105 (1948).
[24] J. J. Mitchell and F. F. Coleman, J. Chem. Phys. **17**, 44 (1949).
[25] Lossing, Tickner, and Bryce, J. Chem. Phys. **19**, 1254 (1951).
[26] J. D. Morrison, J. Chem. Phys. **19**, 1305 (1951).
[27] J. D. Waldron and K. Wood, *Mass Spectrometry* (Institute of Petroleum, London, 1952), p. 16.
[28] J. W. Warren, Nature **165**, 810 (1950).
[29] K. U. Ingold and F. P. Lossing, Can. J. Chem. **31**, 30 (1953).

TABLE I. The ionization potentials of methyl, allyl, and benzyl radicals.

Radical	Source	Individual values	Average	Ionization potential (ev) Literature value	Method of determination	Reference number
Methyl	mercury dimethyl	9.95 9.94	9.95±0.03	10.07±0.1	direct measurement	5
		9.95 9.96		≤9.96±0.05	$A(CH_3^+)$ from CH_4	15
Allyl	allyl iodide at 766°C	8.16 8.16	8.16±0.03	9.05	$A(C_3H_5^+)-D(C_3H_5-CH_3)$ from 1-butene	16
	at 916°C	8.05[a] 8.05[a]				
	1-butene at 1000°C	8.15	8.15±0.07			
Benzyl	benzyl iodide	7.73 7.72 7.77 7.69	7.73±0.08			

[a] See text.
The limits of error shown in the Table were estimated from the permissible latitude in the extrapolation of the δV *vs* I curves.

the peak height of the standard equal to that of the radical ion. In the case of methyl, the height of the mass 15 peak with 50-ev electrons was corrected for contributions from the methane produced. The 41 peak for allyl was corrected for the contribution from 1,5 hexadiene. The 91 peak for benzyl was corrected for toluene and dibenzyl contributions. In all cases it was found that these corrections were negligible below an electron voltage at which the height of the radical peak was 8–10 percent of the height at 50 ev. For this reason the contributions from these fragments could not affect the shape of the ionization efficiency curves in the region below 5 percent where the δV measurements were made. Similar corrections to the mass 26 peak were made to prevent interference with the acetylene standard. The ion efficiency curves were drawn with the ion currents expressed as a percentage of the net height at 50 volts.

RESULTS

A typical ionization efficiency curve, that for the allyl radical, is shown in Fig. 2 for comparison with the curve obtained for the acetylene standard. The ionization potentials for the three radicals obtained from the calibration line are given in Table I.

DISCUSSION

The value of 9.95±0.03 ev found for the ionization potential of methyl appears to be significantly lower than the 10.07±0.1 ev found by Hipple and Stevenson[5] although it is hard to estimate the experimental error involved in both measurements. The predicted value of ≤9.96±0.05[15] is in good agreement with the result presented here.

For the reasons given earlier, the ionization potential of allyl measured at 915°C is believed to be too low. The possible presence of an isomeric radical cannot be ruled out. The other two values are in good agreement, although the error involved in the experiment with 1-butene is larger owing to the method of measurement. Both values are lower by almost a volt than the ionization potential predicted by Evans and Szwarc[16] from the appearance potential of the mass 41 ion from 1-butene as found by Stevenson[4] and confirmed by Mitchell and Coleman.[24]

A serious discrepancy must exist in the relation

$$A(C_3H_5^+)=D(C_3H_5-CH_3)+I(C_3H_5).$$

It will be shown in a later paper that the ionization potential of allyl obtained in this work is consistent with the appearance potentials of $C_3H_5^+$ and the known bond dissociation energies for the allyl halides. This suggests that the appearance potential of $C_3H_5^+$ from 1-butene includes an excess energy term as is found for the appearance potential of CH_3^+ from ethane.[11,24,30] In view of the suggested[16] higher value for the ionization potential of allyl, it is of importance to be certain that the ion of mass 41 examined in the present work was actually allyl and not one of the isomeric radical ions. The observation that the combination of the radicals formed the expected dimer (1,5 hexadiene) to the virtual exclusion of other hexadienes is a conclusive proof that the allyl radical was not isomerized to any appreciable extent. The possibility of the formation of an isomeric ion of lower ionization potential in the ionization process itself seems unlikely.

As far as the authors are aware, there are no values with which to compare the 7.73±0.08 ev found for the ionization potential of benzyl.

The appearance potentials of the methyl, allyl, and benzyl ions from a number of compounds including the halides have been measured. The relation of these values to the ionization potentials reported here will be discussed in a later publication.

Reactions of the Radicals

As mentioned in a previous section, no products of disproportionation reactions were found for any of the three radicals, although the products of dimerization were present in large amounts in the experiments with

[30] M. B. Koffel and R. A. Lad, J. Chem. Phys. **16**, 420 (1948).

the retractable furnace. The absence of disproportionation can hardly be attributed to higher activation energies than for the combinations in view of the elevated temperatures but is more probably the result of low steric factors for such reactions.

ACKNOWLEDGMENT

The authors wish to thank Dr. L. C. Leitch, Mr. A. T. Morse, and Mr. R. Renaud of these laboratories for preparing the mercury dimethyl, allyl iodide, and benzyl iodide used in this work. The assistance of Dr. J. B. Farmer in the determination of the ionization potential of benzyl is gratefully acknowledged.

Note added in proof.—In view of the difference of 0.18 ev found between the ionization potentials of CH_4 and CD_4[25], it was of interest to compare the ionization potentials of CH_3 and CD_3 radicals. The CD_3 radicals were produced from the pyrolysis of $Hg(CD_3)_2$ and values of 9.96 and 9.95 were obtained for the ionization potential. It may be concluded that the ionization potentials of CH_3 and CD_3 are the same within 0.03 ev. The ionization potentials of CD_4 and CH_4 were redetermined under comparable conditions and $I_{CD_4}-I_{CH_4}=0.12\pm0.03$ ev. This may be compared with the difference of 0.18 ± 0.03 ev found previously.[25] It is interesting to note that a similar difference has been found between I_{ND_3} and I_{NH_3}.[31] In this case $I_{ND_3}-I_{NH_3}=0.22$ ev.

[31] H. Neuert, Z. Naturforsch **7A**, 293 (1952).

THE JOURNAL OF CHEMICAL PHYSICS VOLUME 22, NUMBER 4 APRIL 1954

Schlieren Studies of the Critical Region*†

HOWARD B. PALMER‡
University of Wisconsin, Naval Research Laboratory, Madison, Wisconsin
(Received September 21, 1953)

The critical regions of ethane, carbon dioxide, and xenon have been studied, using a Schlieren optical system. The material to be studied was confined in a thermostatted high pressure cell having optically flat windows, and placed in the test section of the optical system. At temperatures over a range of about two degrees, in the critical region, refractive index gradients within the cell were determined as a function of height along the cell. From these data were calculated the density distribution, the pressure distribution, and the shapes of the pressure-volume isotherms at the various temperatures. The technique permitted detailed study of the isotherms over a narrow range of pressures, too small to be observed by usual experimental methods. Extensive visual observations were made throughout the course of the experiments. Particular attention was devoted to the question of the equilibrium state in the critical region and the process of equilibrium attainment.

I. INTRODUCTION

IN recent years, numerous attempts have been made to obtain accurate experimental data concerning the properties of a pure substance in its critical region. The experiments have dealt principally with the density distribution within a cell containing a fluid in its critical region,[1,2] the detailed shapes of pressure-volume isotherms near the critical temperature,[3,4] the shape of the coexistence curve as the critical temperature is approached,[5,6] and the structure of a fluid in its critical region.[7,8] Interpretation of the experimental results has rested chiefly upon the concepts of molecular clustering in gases and local order in liquids, and upon knowledge of the effect of gravity upon a compressible fluid. The magnitude of the effect of gravity in causing such phenomena as flat tops on coexistence curves has only recently begun to be appreciated, although the theoretical basis for such phenomena has been established for some time.[9,10] The theoretical treatment of condensation by Mayer,[11] with its controversial prediction[12,13] of a temperature region of anomalous behavior, near the critical temperature, has provided much of the impetus for many of the experimental investigations.

The present study was undertaken in hopes of elucidating further the problem of the equilibrium behavior of a fluid in its critical region, particularly as

* Based on a thesis presented by Howard B. Palmer in partial fulfillment of the requirements for the Ph.D. degree, the University of Wisconsin, 1952. The thesis has appeared as University of Wisconsin CM-740, October 30, 1952.

† The work reported here was supported by the U. S. Navy Bureau of Ordnance Contract NOrd 9938, University of Wisconsin, Naval Research Laboratory.

‡ Present address: Metcalf Research Laboratory, Brown University, Providence, Rhode Island.

[1] O. Maass, Chem. Revs. **23**, 17 (1938).
[2] M. A. Weinberger and W. G. Schneider, Can. J. Chem. **30**, 847 (1952).
[3] R. H. Wentorf, dissertation, University of Wisconsin (1951). Portions of this thesis have appeared as University of Wisconsin CM-724, May 12, 1952.
[4] Weinberger, Habgood, and Schneider, Can. J. Chem. **30**, 815 (1952).
[5] M. A. Weinberger and W. G. Schneider, Can. J. Chem. **30**, 422 (1952).
[6] S. G. Whiteway and S. G. Mason, Can. J. Chem. **31**, 569 (1953).
[7] R. L. Wild, J. Chem. Phys. **18**, 1627 (1950).
[8] H. A. Cataldi and H. G. Drickamer, J. Chem. Phys. **18**, 650 (1950).
[9] M. Gouy, Compt. rend. **115**, 720 (1892).
[10] R. Ruedy, Can. J. Research **16A**, 89 (1938).
[11] J. E. Mayer and M. G. Mayer, *Statistical Mechanics* (John Wiley and Sons, Inc., New York, 1940).
[12] B. H. Zimm, J. Chem. Phys. **19**, 1019 (1951).
[13] J. E. Mayer, J. Chem. Phys. **19**, 1024 (1951).

manifested in the density distribution within a cell under the influence of gravity. The use of a Schlieren technique permitted detection of density gradients, with high sensitivity, without perturbing the fluid.[14]

II. EXPERIMENTAL DETAILS

A. The Cell Assembly

The material to be studied was confined in a cell 3 in. high, which had been cut out of a block of steel 6 in. square by $1\frac{1}{4}$ in. thick. The block was recessed so that the thickness of the cell was only $\frac{3}{8}$ in. Its width was also $\frac{3}{8}$ in. The cell windows were of "Crystallex" plate glass, a very clear glass which permitted accurate visual observation of the cell contents. Use of plate glass was possible because the small sections used for windows were found to be flat to the order of a few wavelengths of light, at worst. Because of glass breakage, the final configuration of the cell had one window of $\frac{1}{2}$-in. glass and the other of $\frac{3}{4}$-in. glass. The windows were pulled against the cell block by means of $\frac{1}{2}$-in. steel plates, tightened down by bolts which threaded into the cell block. Lead gaskets were used between the windows and the cell block. For access to the cell, $\frac{1}{16}$-in. holes were drilled into the cell from the top and bottom of the cell block, and their openings at the block surface were machined to take standard $\frac{1}{4}$-in. Aminco "superpressure" fittings. The bottom outlet was used only for preliminary cleaning of the cell. The top outlet was provided with a valve which permitted the cell to be filled with the material being studied and which then could close off the outlet at the surface of the cell block. This was necessary in order to insure that the entire body of fluid under study would be subject to the thermostatting action of the large steel cell block.

Cylindrical brass vacuum housings attached to the cell block prevented the cell windows and the portions of the block in the vicinity of the cell from being subjected to fluctuations in the surrounding air temperature. The windows on the vacuum housings were of $\frac{1}{4}$-in. Crystallex. The cell assembly was supported on four wheels, made to fit the circular flanges on the ends of the vacuum housings. The wheels were mounted on a small frame of iron pipe, which was in turn mounted on a wooden base. The entire assembly stood within an air thermostat which had double windows of Crystallex. Strings, attached to the vacuum housings and running out of the thermostat, permitted inversion of the cell. A $\frac{5}{16}$-in. steel ball bearing inside of the cell assured vigorous stirring during inversion. This type of stirring had the asset of being entirely internal, with no possibility of energy exchange between the exterior and the cell contents during the stirring process. The cell assembly was insulated thoroughly with asbestos before being placed in the thermostat.

The volume of the cell was measured by a gas expansion method. It was found to be 7.53 cc, accurate to about $1\frac{1}{2}$ percent. For calculations, it was necessary to know the volume of the cell from the top of the ball bearing in the bottom to the highest point visible, namely the bottom edge of the portion of the lead gasket running across the top of the cell. This volume was calculated to be 6.66 cc, with a probable error of 3 to 4 percent.

The temperature along the height of the cell was measured by means of five copper-constantan thermocouples, located in wells which extended into the cell block to within $\frac{3}{16}$ in. of the cell wall. Readings were taken on a Rubicon Type B high-precision potentiometer, in conjunction with a Rubicon 3201 wall galvanometer having a sensitivity of 0.1 microvolt per mm at one meter. The sensitivity was increased by moving the galvanometer scale to a distance of about five meters. A detectable deflection at this distance corresponded to a temperature change of around 0.001°C. Each of the thermocouples was calibrated against a Leeds and Northrup platinum resistance thermometer which had in turn been calibrated at the National Bureau of Standards. The absolute accuracy of measurement with the thermocouples was approximately ±0.01°C, with an available precision of about ±0.001°C in the measurement of temperature differences.

The temperature of the air thermostat was controlled by a Western Electric thermistor, type D-169604, connected as one arm of a wheatstone bridge, the balance of which controlled a relay in the heating circuit. The heater consisted of 60 feet of No. 18 nichrome wire, distributed over the two sides of the thermostat furthest from the cell. Stirring of the air was provided by a combination of convection currents and the action of two small fans in the top of the thermostat. The temperature of the air was found to fluctuate as much as 0.2°C about its mean value. The thermostatting action of the insulated steel cell block evened out this variation to the extent that no fluctuations in the cell temperature could be detected as accompanying the periodic changes in air temperature. Thus, the fluctuations due to this cause were of the order of ±0.001°C or less. However, changes in room temperature, plus changes in the line voltage, placed a limit upon the regulation over long periods of time. With some manual attention to the regulation, the cell temperature could be preserved constant to about ±0.01°C over periods of several hours. The temperature remained constant to about ±0.05°C without any supervision, e.g., overnight.

B. Substances Studied

The substances studied were carbon dioxide, ethane, and xenon. The carbon dioxide was prepared from reagent grade sulfuric acid and sodium carbonate, the liberated gas being bubbled through several sulfuric acid traps and passed over a dry ice trap before being

[14] After the work was begun, it was discovered that Ruedy (reference 10) suggested the use of a Schlieren method in critical studies.

collected. Analysis by absorption in 6 N KOH showed it to be about 99.997 percent pure, the 0.003 percent impurity probably being air. The ethane was "research grade" ethane, obtained from the Phillips Petroleum Company. Its purity was specified by them to be 100.00 percent. The xenon was the "reagent grade" product, purchased from the Air Reduction Sales Company. The average purity of the xenon in the several flasks in which it was shipped was about 99.9 percent, according to the report of mass spectrographic analysis which accompanied the shipment. The 0.1 percent impurity was composed primarily of krypton and nitrogen or carbon monoxide. No attempt was made to purify the gas further.

The materials were introduced into the cell by condensation. To facilitate this, use was made of the loading bomb designed by Wentorf.[3] The bomb could be weighed on an analytical balance, which yielded the sample weight to an accuracy of about 0.1 percent. The cell contents were also weighed at the end of each study. It was discovered that the cell had a very slow leak, giving rise to a loss of contents at the rate of about 0.01 percent per hour. Mean densities of loading were calculated for each day by using the average rate of leakage.

C. Optics

A Z-type Schlieren system[15] was used to study the refractive index gradients in the fluid. An excellent discussion of Schlieren systems may be found in the monograph by Schardin.[16] The light source was an Ediswan "Pointolite" tungsten arc lamp. It emitted essentially white light. The light was not filtered, since error from other causes far exceeded error from variation of refractive index with wavelength.

For a Z-type system

$$\Delta a = \epsilon f, \tag{1}$$

where Δa is the deflection of the source image at the knife edge, ϵ is the angular deviation given the ray in passage through the test section, and f is the focal length of the mirror nearest the knife edge. For the sort of test section employed, *viz.*, one of rather small and virtually constant thickness, the relation

$$\epsilon = W d\mu/dz \tag{2}$$

holds to a good approximation in most instances. W is the thickness of the cell and $d\mu/dz$ is the change of refractive index with height. The relation is not valid when $d\mu/dz$ is extremely large, e.g., at a meniscus. The Lorenz-Lorentz equation can be differentiated to give

$$d\rho/dz = [6M\mu/([R](\mu^2+2)^2)]d\mu/dz, \tag{3}$$

where $[R]$ is the molar refractivity, μ is the refractive index, M is the molecular weight, and ρ is the density. Substitution into (2) yields

$$d\rho/dz = \{6M\mu/([R](\mu^2+2)^2 W f)\}\Delta a. \tag{4}$$

Over the range of densities of interest in a study of the critical region, the expression in brackets is constant to within 3 percent.[17] In this work, it was treated as a constant, for the sake of simplicity in calculations.

The values of Δa were found, for the most part, by using a grid, i.e., a "multiple knife edge," as the Schlieren stop. A continuous distribution of refractive index gradients in the cell yielded a series of bands in the cell image on the camera back. Knowledge of the grid constant and the position of the undeviated source image at the knife edge, plus one or often two values of the deflection at particular points in the cell made it possible to read the values of $d\rho/dz$ at all points along the cell directly from a single photograph. The grid employed was made by photographing a series of black and white lines of equal widths and printing them on a lantern slide. The grid constant was 0.0332 in. The grid and knife edge mounting was raised and lowered by a screw having a scale which permitted the height of the mounting to be read to ± 0.001 in. An obvious limit to the measurable refractive index gradients was presented by the size of the mirrors and the aperture of the camera. As an auxiliary means of deflection measurement, used when extremely steep gradients were present in the fluid, one of a series of thin prisms was sometimes placed in the light path in such a way that light deflected downward by the steep gradient would be redeflected upward by the prism and enter the camera.

Experimental data were recorded in the form of photographs of the fringe pattern in the cell image. The films were read by means of a Gaertner comparator. It permitted the location of a fringe in the cell to be determined to within ± 0.01 cm.

D. Procedures and Calculations

Observations were made, for the most part, over a range of about a degree, commencing around 0.2°C below the temperature of meniscus disappearance. Below this point, gradients in the liquid and vapor extended over too small a distance to be analyzable, while at temperatures from about 0.8° to 1.0°C above the meniscus disappearance point, gradients throughout the cell became too slight to study.

The criterion taken for equilibrium was the constancy of appearance of the Schlieren pattern on the camera back over several hours' time or the return of contents to their former appearance after thorough shaking.

[15] Designed and assembled by H. L. Olsen, H. Rubin, and A. Ingersoll, at the University of Wisconsin Naval Research Laboratory, in 1947. The parabolic mirrors in the system were first surface, aluminized mirrors, 12 in. in diameter, having a surface accuracy of $\frac{1}{10}$ wavelength of sodium light and a focal length of 100 ± 1 inches. They were manufactured by the Perkin-Elmer Corporation.

[16] H. Schardin, "Toepler's Schlieren Method," U. S. Navy Department, David Taylor Model Basin, Washington, D. C., 1949.

[17] A. Michels and J. Hamers, Physica 4, 995 (1937), provide data on the constancy of the molar refractivity of carbon dioxide. In the present study, it was assumed that the molar refractivities of ethane and xenon have constancies similar to that of carbon dioxide.

At temperatures at or below about 0.2°C beneath the meniscus disappearance temperature, equilibrium was established in at most a few minutes. Above this temperature, it was established much more slowly upon cooling or shaking, but appeared to be continuously established, in the absence of stirring, upon slow and continuous rise in temperature. Therefore, heating rates not over 0.03°C per hour were generally employed. When the temperature reached the level at which gradients could no longer be observed, it was allowed to fall slowly to a temperature below the condensation point. The rate of fall was made extremely small as the condensation point was approached. It was observed that at temperatures higher than a point about 0.05°C above the temperature of reappearance of the meniscus, the rate of fall of temperature made no perceptible difference in the establishment of gradients.

Photographs of the gradients were usually taken at intervals of a few hundredths of a degree. The cell contents were also observed visually, and occasionally some direct photographs were taken of the cell, for example, to show opalescence or fogging. A number of miscellaneous experiments were performed to test the stability of the gradients and to check upon reappearance of gradients after vigorous stirring.

Visual observation was employed in determining the temperature of disappearance of the meniscus. The criterion used for the existence of a meniscus was the ability to distinguish reflection of light from a surface within the fluid. The light source for this was a 100-watt bulb, turned on briefly in order to prevent heating of the fluid by radiation. It was located outside the air thermostat. It was found that reflection was observed to the highest temperature when the angles of incidence and reflection were about 60 degrees. The lowest temperature at which a reflection could no longer

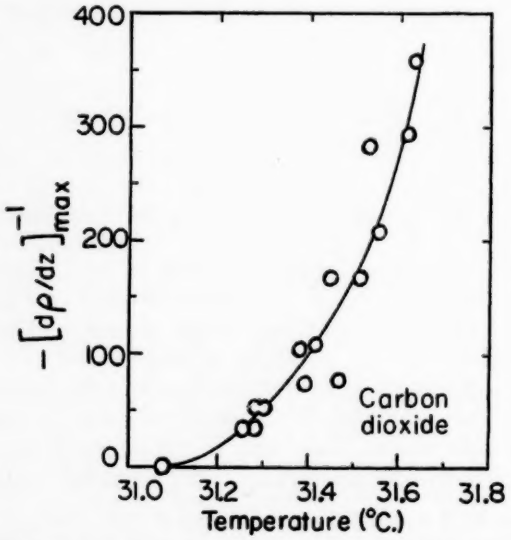

FIG. 1. Plot of the reciprocal of the maximum density gradient in carbon dioxide, at temperatures above the temperature of meniscus disappearance.

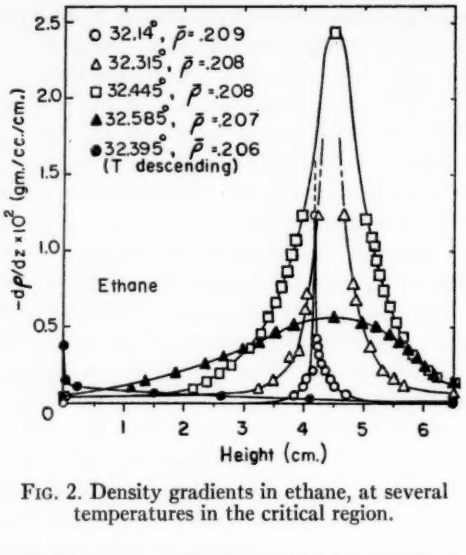

FIG. 2. Density gradients in ethane, at several temperatures in the critical region.

be distinguished was taken to be the temperature of meniscus disappearance.

The values of the density at various points in the cell were calculated by numerical integration of the function $d\rho/dz$ over the cell. For this purpose, all the density gradient data were plotted, and values at intervals of 0.25 cm in the height z were tabulated, so that integration could be performed over equal intervals. Integration could only be carried out over the entire cell at temperatures somewhat above the temperature of meniscus disappearance, since at lower temperatures, and in particular at temperatures below the meniscus disappearance point, values of $d\rho/dz$ could not be measured over the entire cell. In order to make an estimate, however crude, of the density distribution at temperatures only slightly above the meniscus disappearance temperature, values of the reciprocal of the maximum density gradient present in the fluid at higher temperatures were plotted as a function of temperature and extrapolated smoothly to a value of zero at the temperature of meniscus disappearance. Such a plot is shown for carbon dioxide in Fig. 1. Values of the maximum gradients in the region of immeasurability were then estimated from this graph. For these cases, using the estimated value of the maximum gradient, the integral of the density gradient was calculated over the immeasurable region in the cell, on the assumption that the gradient distribution had a Gaussian shape in the unknown region. This assumption was apparently quite good at temperatures 0.1°C or more above the meniscus disappearance temperature, as evidenced by a fit at a slightly higher temperature to a gradient distribution which was known in its entirety; but the assumption became very poor at temperatures only a few hundredths of a degree above the meniscus disappearance point. This fact was apparent from the calculation of negative densities in the upper part of the cell, in the case of xenon at a temperature 0.025°C above the meniscus disappearance point.

The known portions of the density gradient distributions—i.e., the entire curves, at the majority of temperatures—were integrated over each 0.25 cm interval in z, using the partial-range formula[18]

$$\int_{z_i}^{z_{i+1}} f dz = h/24[-f_{i-1}+13f_i+13f_{i+1}-f_{i+2}], \quad (5)$$

where h is the length of the interval, and the subscripts refer to the regularly-spaced values of the independent variable z. The integration performed in this manner gave the value of the change in density, $\Delta\rho$, from the value at the bottom of the cell, as a function of the height. This function was then integrated over the cell height, using Simpson's rule, to permit calculation of the density at the bottom of the cell from the relation

$$\bar{\rho}H=\rho_0 H+\int_0^H \Delta\rho(z)dz, \quad (6)$$

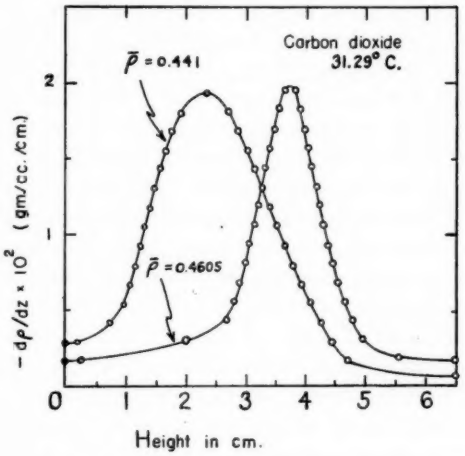

FIG. 3. Density gradients in carbon dioxide, at two mean densities.

where ρ_0 is the density at the cell bottom and $\bar{\rho}$ is the mean density of loading of the cell. Absolute values of the density in the cell at regular intervals in z could then be found from the sum of ρ_0 and $\Delta\rho(z)$.

To find the pressure distribution in the cell, the change in pressure from the pressure at the bottom of the cell was calculated by integration of the equation

$$dp=-g\rho(z)dz, \quad (7)$$

over each of the 0.25-cm intervals in z. The same partial-range formula (5) was used in these integrations. Since no absolute value of the pressure at any point in the cell was known, it was not possible to calculate any absolute pressures. The shapes of pressure-volume isotherms could, however, be found by plotting the values of the molar volume, corresponding to the various density values, *versus* the change in pressure from the value at the cell bottom.

[18] W. G. Bickley, Math. Gazette 23, 352 (1939).

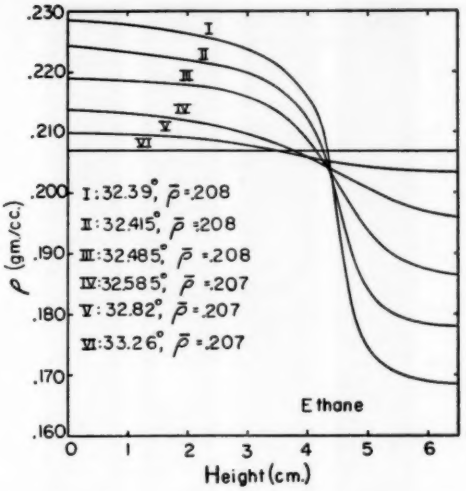

FIG. 4. Density distributions in ethane, at several temperatures.

III. RESULTS

The results for the three substances studied were qualitatively very similar. The distributions of density observed under conditions of rising temperature were all sigmoid in character, and a complete hysteresis was observed in all three cases; i.e., no sigmoid distributions were found under conditions of descending temperature. Because of the similar behavior, and for the sake of brevity, the pressure-volume isotherms found for all three substances are presented, but typical data for only one of the three are selected to show the other characteristics.

The observed meniscus disappearance temperatures were 31.08°C for carbon dioxide, 32.315°C for ethane, and 16.485°C for xenon, all with uncertainties of about ±0.02°C. The respective temperatures of reappearance of the meniscus observed were 31.09°C, 32.325°C, and 16.475°C, again with probable uncertainties of ±0.02°C. Thus, the temperatures of disappearance and reappearance coincided, within the experimental uncertainty, for all three substances, in the absence of stirring. The uncertainty was composed of a ±0.01°C uncertainty in temperature measurement, plus an observational uncertainty of approximately ±0.01°C.

Representative density gradient data for ethane are shown in Fig. 2, which contains plots of the gradient in

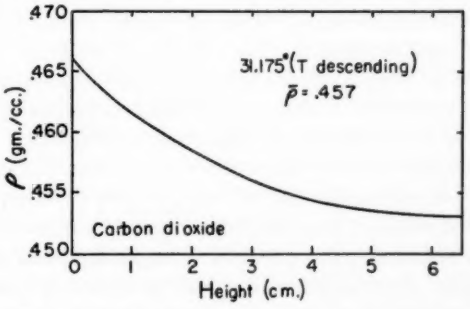

FIG. 5. A typical density distribution in carbon dioxide, under descending temperature conditions.

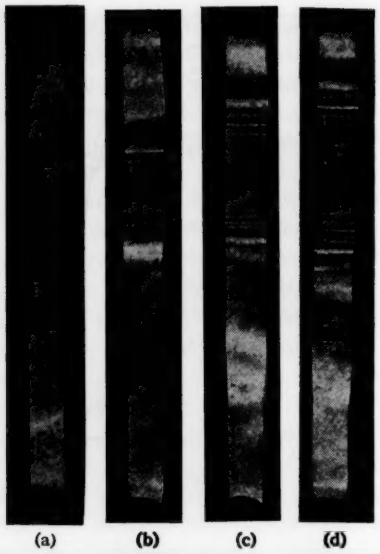

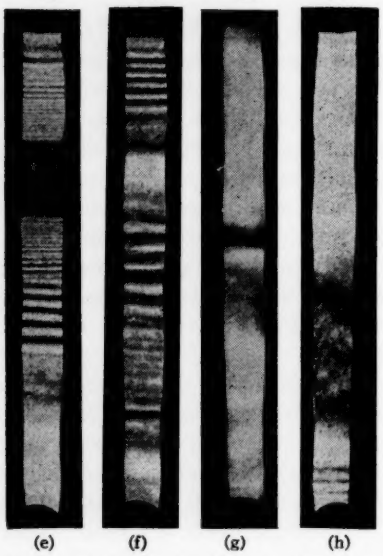

FIG. 6. Schlieren photographs of ethane in the critical region. (a) 31.57°C, (b) 32.21°C, (c) 32.29°C. An extremely flat and thin meniscus is still visible. (d) 32.32°C. No meniscus is distinguishable. (e) 32.445°C, (f) 32.585°C, (g) 33.235°C, (h) 32.41°C. T descending.

the fluid as a function of height, at several temperatures. The curve at 32.315°C shows the data at the observed temperature of meniscus disappearance. It will be noted that the data at 32.395°C (T descending) are the type one would expect if the gradient resulted from a simple sedimentation equilibrium of large molecular clusters in a medium of density somewhat smaller than that of a cluster. This sort of curve was typical of those observed under falling temperature conditions.

The approximate reproducibility of results is shown by Fig. 3, which is a plot of the gradient distribution in carbon dioxide at two different mean densities. The two curves also show the effect of changes in mean density upon the distribution. The peak gradient is the same in the two cases, within experimental error, as would be expected.

Several plots of the calculated density distributions in ethane at various temperatures, under conditions of slowly rising temperature, are shown in Fig. 4. The curves for the temperatures 32.39°C and 32.415°C were calculated with the aid of the assumption that the center portions of the gradient distributions had Gaussian shapes. Figure 5 shows the density distribution calculated for carbon dioxide at the temperature 31.175°C under conditions of slowly descending temperature.

It is felt that photographs of the cell as it underwent changes in temperature may be of interest. Therefore, in Fig. 6 are presented eight Schlieren photographs of ethane in the critical region. Each fringe across the cell represents an equal increment in the density gradient. From Fig. 6(c), it can be seen that at a temperature at which a meniscus was still visible, the gradient became large (indicated by the edges of the blacked-out region) at points well above and well below the meniscus. In xenon, this fact was emphasized by the use of prisms in estimating the values of the large gradients; e.g., it was found that at a temperature 0.045°C below the meniscus disappearance temperature in xenon the density gradient went to the extremely large value of 0.7 gm/cc/cm at points 0.5 mm above and below the meniscus. This may possibly indicate that in fact the density gradient at such a temperature proceeds continuously to a value of infinity at the meniscus, or to whatever maximum value is characteristic of the liquid-vapor transition region at this temperature, instead of undergoing a discontinuity. At lower temperatures a discontinuity was observed, within the limitations of the experimental measurements.

The fluid shown in Fig. 6(c) was in a condition of some interest visually, in that casual inspection of the cell revealed only a blur in the meniscus region; but closer examination showed that one could see by light reflection an extremely thin and flat meniscus within the blurred region.

Another phenomenon of visual interest in the critical region is opalescence. Two photographs of opalescence in carbon dioxide are shown in Fig. 7, for temperatures 0.01°C and 0.06°C above the meniscus disappearance

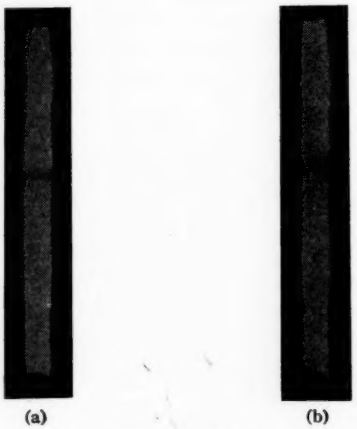

FIG. 7. Opalescence in carbon dioxide. (a) 31.09°C, (b) 31.14°C.

temperature. These were taken with a diffuse white light background. The temperature range in which opalescence was observed in all three substances was from perhaps 0.01°C below the meniscus disappearance temperature to 0.1°C or 0.15°C above that temperature. The range was approximately the same for both ascending and descending temperature conditions, but the opalescence was concentrated in a band in the former case and was distributed throughout the cell in the latter. Under rising temperature conditions, the band of opalescence became broader and less intense as the temperature rose. One unusual feature was noted in the study of xenon. At a temperature about 0.01°C above the condensation temperature, under conditions of descending temperature, the opalescence seemed to commence concentrating into a band about halfway up the cell. Unfortunately, the temperature fell to the condensation point before it could be found whether or not the concentration would become identical to that observed under rising temperature conditions. The opalescence was so pronounced at this temperature that no Schlieren pictures could be taken. Because of difficulties in temperature control, the experiment could not be repeated.

Isotherms calculated from the data for the three substances studied are shown in Figs. 8, 9, and 10. Several isotherms are included which were calculated using the assumption of a Gaussian shape in the center portions of gradient distributions. These are the isotherms at 31.14°C and 31.18°C for carbon dioxide, at 32.415°C for ethane, and at 16.69°C for xenon. The principal significance of the isotherms perhaps lies in their showing qualitatively the state behavior of the system over a range of pressures too small for measurement by ordinary experimental techniques. Their quantitative validity is not felt to be great. More will be said concerning this in discussing experimental errors.

The minimum slope of each isotherm was read graphically and plotted *versus* temperature in the hope of determining the validity of a linear extrapolation to

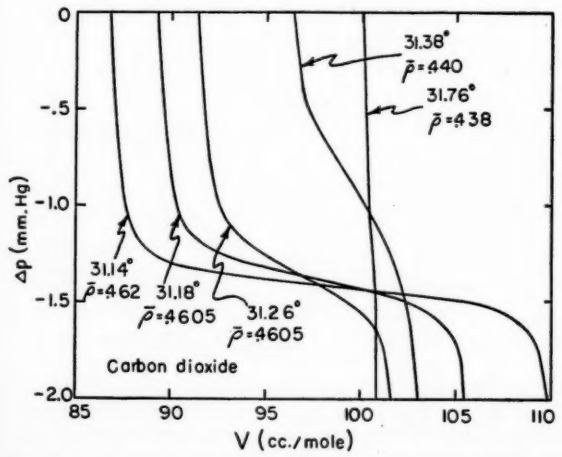

FIG. 8. Isotherms for carbon dioxide, at several temperatures.

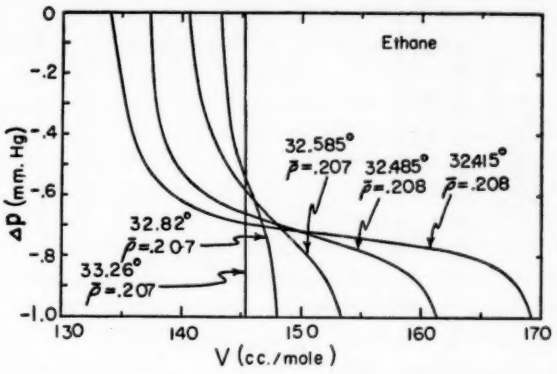

FIG. 9. Isotherms for ethane, at several temperatures.

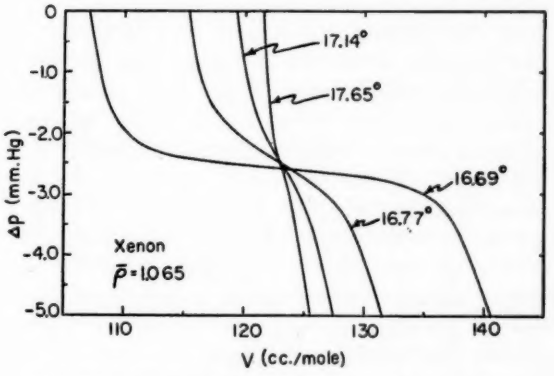

FIG. 10. Isotherms for xenon, at several temperatures.

zero of a plot of this quantity, used by some workers[3,19] as a method of estimating the critical temperature. Such a plot is shown for xenon in Fig. 11. The point at 16.56°C is an upper limit to the minimum slope, estimated by using prisms; it was not possible at this temperature actually to measure the largest gradient. The point at 16.625°C was also found by using the prisms; at this temperature it was possible to determine the value of the largest gradient in the cell, which permitted a good estimate to be made of the minimum value of $(\partial p/\partial V)_T$ from the relation

$$(\partial p/\partial V)_T = g\rho^3/[M(d\rho/dz)], \qquad (8)$$

where g is the gravitational constant, M is the molecular weight, and ρ is the density. If one assumes the minimum slope of the isotherm at the temperature of meniscus disappearance to be zero, then it appears from the figure that the plot of the minimum slopes has a pronounced curvature, instead of being linear.

The importance of pressure corrections in PVT measurements in the critical region suggested that a plot of the calculated change in pressure, from the value at the bottom of the cell, as a function of height, would be significant. This quantity is plotted for ethane at a temperature of 32.37°C, 0.055°C above the observed meniscus disappearance temperature, in Fig. 12. This is a temperature for which the assumption of a Gaussian

[19] Michels, Blaisse, and Michels, Proc. Roy. Soc. (London) **A160**, 358 (1937).

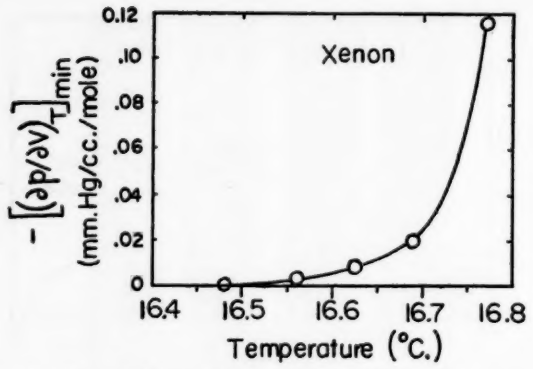

FIG. 11. The minimum slopes of the isotherms for xenon, at temperatures above the meniscus disappearance temperature.

gradient distribution was made, and it is virtually certain that the deviation of the change in pressure from linearity is quite exaggerated, as a consequence. This case was deliberately chosen, to show that within the present accuracy of pressure measurements in the critical region, a linear correction is generally adequate. The maximum difference between a linear curve and the calculated curve for xenon, at a temperature of 16.56°C (also an exaggerated case), was found to be 1.2 mm of mercury, just about the limit of present experimental accuracy in pressure measurements in the critical region. Of course, the maximum difference between the true curve and a straight line is a function of the height of the cell, so that for longer cells the maximum difference might exceed the experimental error. This would also be the case at lower temperatures.

The stability of the sigmoid gradients observed under rising temperature conditions was tested by raising ethane to a temperature of 32.42°C and retaining it there, within about ±0.05°C, for a period of about 40 hours. At the end of that time, the gradient configuration was approximately the same as that observed at 32.50°C, under conditions of slow and steady rise in temperature. That is, the final gradient was probably that which was characteristic of the highest temperature to which the cell was carried by temperature fluctuation.

Stirring of a fluid containing a sigmoid gradient was observed to destroy the gradient and fill the cell with turbulent regions of inhomogeneity. If opalescence was originally present, it became immediately distributed throughout the cell. The inhomogeneity tended to decrease upon continued stirring, but the Schlieren camera still clearly showed it to be present. In carbon dioxide the cell was retained at constant temperature (within ±0.05°C) for a period of 24 hours after stirring, at a mean temperature 0.1°C above the meniscus disappearance temperature, without any sign being observed of the return of a sigmoid density distribution.

The gradients observed under descending temperature conditions showed no tendency to become sigmoid. More than 48 hours were devoted to the cooling process in the study of carbon dioxide, 52 hours in the case of ethane, and 24 hours in xenon. The data for Fig. 5 were taken after the cell had been retained at constant temperature (within ±0.05°C) for some 24 hours.

IV. ERRORS AND UNCERTAINTIES

The uncertainty in measuring deflections at the Schlieren knife edge was estimated to be about 0.005 in. This figure was confirmed by a check of the system using a plano-convex lens of 20-meter focal length, ground to very exact optical specifications by the Naval Gun Factory Optical Shop. The assumptions implicit in the derivation and use of Eq. (4) introduced errors of about 2 percent in the measured density gradients, for moderately large gradients. For extremely large gradients, the error approached 6 percent. Uncertainties in the cell width and in the focal length of the Schlieren mirror contributed a relative error of perhaps 3 percent in the measured density gradients. In reading the photographs, there may occasionally have been a counting error of a fringe. Possibility of such an error was minimized by the requirement that the total number of fringes counted had to agree with the value of the maximum deflection visible, as determined by adjusting the knife edge or by allowing the source image to fall upon a piece of ruled paper held at the knife edge. If a fringe counting error occurred, the error in a gradient of average value was about 10 percent.

A possibly reasonable estimate of the total relative error in the measured density gradients, exclusive of counting errors, might be about 12 percent for a small gradient value and a smaller error of 8 or 9 percent for a gradient of large magnitude. Error in the function $\Delta\rho(z)$ was of the same order, aside from errors introduced in the numerical integration process. The consequent error in the calculated value of the density at the cell bottom, ρ_0, was around 2 or 3 percent for cases in which there was a large difference in density between the bottom and top of the cell, and much less for cases in which the distribution of densities extended over a small range. The uncertainty in the measured values of the mean densities of loading increased the error in the

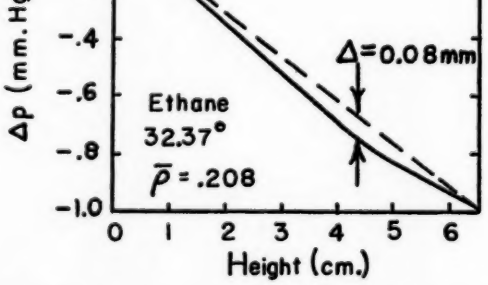

FIG. 12. The change in pressure, from the value at the bottom of the cell, as a function of height, for ethane at a temperature somewhat above the meniscus disappearance temperature. Solid line: calculated from the experimental data. The maximum deviation from simple linearity is 0.08 mm Hg.

calculated density values by about 1.5 percent. For the extreme density distributions, then, the density at the cell bottom may have been in error by 4 percent, and that at the top by 7 or 8 percent. For narrow distributions, all calculated density values should have been accurate within 2 or 3 percent. The relative error in the calculated values of the change in pressure from the value at the bottom of the cell was of the order of magnitude of the error in the density values.

V. DISCUSSION

The average temperature of meniscus disappearance-reappearance found for carbon dioxide, 31.085±0.02°C, may be compared with the values 31.045°C, 31.04°C, and 31.04°C, found, respectively, by Wentorf,[3] Michels, Blaisse, and Michels,[19] and Meyers and Van Dusen.[20] The higher temperature observed in the present work may well be a consequence of the use of reflected light as a criteron for the existence of a meniscus. The average temperature for ethane, 32.32±0.02°C, may be compared with the value of 32.27°C listed in the tables of the American Petroleum Institute,[21] and with the values 32.23°C and 32.167°C reported by Whiteway and Mason.[6] The difference between the latter two values and that found in the present work seems too large to be accounted for by differences in the technique of observing the meniscus. The temperature observed in the case of xenon, 16.48±0.02°C, is 0.11°C below the value 16.59°C reported by Weinberger and Schneider[2] and by Whiteway and Mason[6] for very pure xenon. A crude calculation of the expected effect of 0.06 percent krypton and 0.04 percent nitrogen upon the observed meniscus disappearance temperature of xenon, assuming a linear dependence relation and taking 16.59°C as the correct value, yields a predicted temperature of 16.48°C. The agreement is partly accidental.

The results of the present study seem to indicate that equilibrium in the critical region can be continuously achieved under conditions of very slowly rising temperature. Stirring destroys equilibrium, which is not reattained in any reasonable length of time, except possibly at temperatures very slightly above the meniscus disappearance temperature. Similarly, the approach to equilibrium under descending temperature conditions appears to be imperceptibly slow, except perhaps at temperatures within a few hundredths of a degree of the meniscus reappearance temperature. These observations are consistent with the concept that a fluid in the critical region possesses a degree of order intermediate between that of a gas and that of a liquid, and that within the fluid there is a near equality of the energies of motion and of attraction.

The quantitative agreement between the density distributions and isotherms found in this study and the results of Wentorf[3] for carbon dioxide, and of Weinberger and Schneider[2] for xenon, is not very good. The high quality of these studies cited for comparison suggests that the results reported here probably should be regarded as being largely of qualitative and heuristic interest. This casts some doubt upon the results shown in Fig. 11; however, in their defence it may be added that a tangential approach to the value zero at the critical temperature of the minimum value of the slopes of isotherms above this temperature seems far more reasonable than the sort of discontinuous break necessitated by a straight-line approach; furthermore, the results of Wentorf[3] for sulfur hexafluoride fit the tangential condition much better than they do a straight-line approach.

It seems to the author that at present there is no experimental evidence to support the making of a distinction between the "meniscus disappearance" temperature and the "critical" temperature of a substance, so long as experiments on the critical region are performed in a gravitational field. An initial reason for saying this is that the meniscus disappearance temperature of carbon dioxide, observed in the present work, corresponds within the experimental uncertainty to the highest temperature for which Wentorf[3] observed a flat portion in the isotherm. Use of reflected light in observing the meniscus probably accounts for the ability to see a meniscus in this work at a temperature for which Wentorf was unable to see one. Thus it appears that, for carbon dioxide at least, the meniscus disappearance temperature and the critical temperature coincide, in a gravitational field.

The theory of Mayer,[11] which has provided the theoretical basis for making a distinction between the two temperatures, says nothing as to whether or not gravity may create a meniscus which otherwise would not exist, in a fluid having a region in which $(\partial p/\partial V)_T$ is zero. In Mayer's anomalous region, the predicted condition of the fluid is that its isotherms have flat portions, but no condensation into a bulk liquid phase can occur (thus creating a meniscus). However, it is seen from Eq. (8) that when $(\partial p/\partial V)_T$ is zero, $d\rho/dz$ is infinite. This is the condition for the existence of a meniscus, and implies that even if the anomalous region exists, gravity will create a meniscus in the fluid in this region. The implication should be qualified, however, by pointing out that the actual ability to see the meniscus in this region (or in the critical region in general) is complicated by the thickening of the liquid-vapor transition region as the critical temperature is approached.[22,23,24]

If Mayer's prediction is correct, but gravity causes a coincidence of the meniscus disappearance temperature and the critical temperature, it should still be possible to detect a lower characteristic temperature (Mayer's

[20] C. H. Meyers and M. S. Van Dusen, J. Research Natl. Bur. Standards **10**, 381 (1933).
[21] A.P.I. Research Project 44, Carnegie Institute of Technology, "Selected Values of Properties of Hydrocarbons," Natl. Bur. Standards. Washington, D. C.
[22] G. Bakker, Z. physik. Chem. **171** (Ser. A), 49 (1934).
[23] T. L. Hill, J. Chem. Phys. **20**, 141 (1952).
[24] P. S. Epstein, Proc. Natl. Acad. Sci. U. S. **16**, 627 (1930).

T_m) at which the meniscus would disappear in the absence of gravity. The results of the present study lead to the tentative conclusion that there may be such a temperature, lying a few hundredths of a degree below the critical temperature. In a gravitational field, this temperature could be determined by finding the temperature at which $(\partial p/\partial V)_T$ commences proceeding continuously, instead of discontinuously, to the value zero as the isotherms enter the liquid-vapor equilibrium region. In the present work, the possible evidence for such a temperature was the increase of density gradients to a very large value at points well away from the meniscus, commencing at temperatures the order of 0.05°C below the temperature of meniscus disappearance.

An interesting implication of the above conclusions is that investigators looking for Mayer's anomalous region at temperatures above the temperature of meniscus disappearance have probably been looking for it in the wrong temperature region, and should instead have been looking for it below the meniscus disappearance temperature. The possibility of making critical studies in the absence of gravity at some time in the future, which could clear up the entire question of an anomalous region, is an intriguing prospect.

VI. CONCLUSIONS

The Schlieren optical technique has proven to be a very useful tool in studying the critical region. Its most striking potentialities appear to be its use in studies of the attainment of equilibrium and in determining the isotherms, at temperatures above the critical temperature, as they behave over pressure intervals too small to be studied by ordinary experimental methods. The improvements which should be incorporated into any future work of this sort are extremely refined temperature control, plus a means of measuring the very steep density gradients which occur just above the critical temperature. A detailed study of the reflection of light by liquid-vapor interfaces should also be made, in order to provide a sound basis for decisions regarding the existence of a meniscus.

The author wishes to acknowledge with pleasure and gratitude the advice and encouragement of Dr. J. O. Hirschfelder, Dr. C. A. Boyd, Dr. Paul Bender, Dr. C. F. Curtiss, and Dr. R. H. Wentorf. Sincere thanks for their manifold contributions to this work are also due Miss Gertrude Heyer, Mrs. Anita Olsen, Mr. Lloyd Lincoln, Mrs. Bjarni Steingrimsson, and the computing staff of the University of Wisconsin Naval Research Laboratory.

THE JOURNAL OF CHEMICAL PHYSICS VOLUME 22, NUMBER 4 APRIL 1954

Magnetic Susceptibilities of K_3MoCl_6 and $RuCl_3$†

CHARLES EPSTEIN* AND NORMAN ELLIOTT
Chemistry Department, Brookhaven National Laboratory, Upton, New York
(Received November 18, 1953)

Magnetic susceptibilities of K_3MoCl_6 and $RuCl_3$ were measured in the temperature range 76°–297°K. Curie's law is obeyed by both salts. The magnetic moments 3.83β and 2.07β are calculated for the ions Mo^{3+} and Ru^{3+}, respectively.

THE palladium and platinum transition elements are structurally similar to the iron group. They contain an unfilled 4*d* and 5*d* shell of electrons, respectively. With wider multiplets than the iron series, it might be expected that the magnetic properties of compounds of the palladium and platinum groups would conform more closely to theory than those of the iron group. This is not the case, however, and the existing data are too scanty to permit an understanding of these elements at present. More low temperature measurements and, if possible, investigations of magnetically dilute salts are needed.

Extrapolation of published data for the magnetic susceptibilities of K_3MoCl_6[1–3] and of $RuCl_3$[4–6] suggest that these salts obey Curie's law. The data are insufficient for this conclusion to be drawn with certainty though, and we have prepared the compounds and extended the measurements down to liquid nitrogen temperatures.

K_3MoCl_6 was prepared by the electrolytic reduction of a solution of MoO_3 (starting material Eimer and

TABLE I. Magnetic susceptibility of K_3MoCl_6.

Temp.°K	77°	195°	295°
$\chi_{atom}\times10^6$	6175	9300	23 100

Table II. Magnetic susceptibility of $RuCl_3$.

Temp.°K	64°	76°	161°	191°	296°
$\chi_{atom}\times10^6$	8400	7240	3330	2790	1810

† Research carried out under the auspices of the U. S. Atomic Energy Commission.
* Present address: Harvard University, Cambridge, Massachusetts.
[1] P. Ray and H. Bhar, J. Indian Chem. Soc. **5**, 497 (1928).
[2] B. Th. Tjabbes, Proc. Acad. Sci. Amsterdam **35**, 693 (1932).
[3] W. Klemm and H. Steinberg, Z. anorg. u. allgem. Chem. **227**, 193 (1936).
[4] D. M. Bose and H. G. Bhar, Z. Physik **48**, 716 (1928).
[5] A. N. Guthrie and L. T. Bourland, Phys. Rev. **37**, 303 (1931).
[6] B. Cabrera and H. Fahlenbrach, Ann. Physik **21**, 832 (1934).

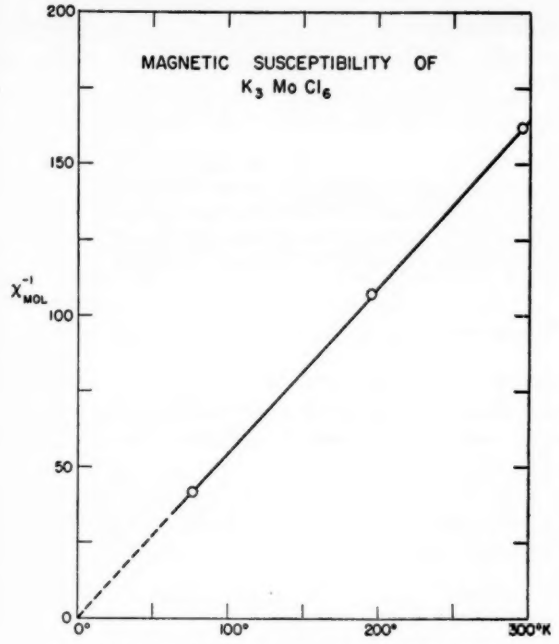

FIG. 1. Magnetic susceptibility of K_3MoCl_6.

Amend Molybdenum Metal) in 8N HCl and the addition of KCl.[7–9]

$RuCl_3$ was obtained commercially (Variacoid Chemical Company). It was dried in a Cl_2 atmosphere at 600°C. Black, lustrous crystals were obtained.

Both the K_3MoCl_6 and the $RuCl_3$ were found to be very pure by chemical and spectroscopic analysis, and contained less than 0.01 percent of any impurity which could interfere with the magnetic measurements.

Magnetic susceptibility measurements were made on K_3MoCl_6 by the Gouy method, and on $RuCl_3$ by the Faraday method. Three samples of each salt were examined. The average deviation in the measurements was less than ± 1.7 percent. The data are given in Tables I and II. The susceptibilities have been corrected

[7] A. Rosenheim and H. I. Braun, Z. anorg. u. allgem. Chem. **46**, 320 (1905).
[8] A. Rosenheim and T. H. Li, Ber. deut. chem. Ges. **56B**, 2228 (1923).
[9] W. R. Bucknall, S. R. Carter, and W. Wardlaw, J. Chem. Soc. 512 (1927).

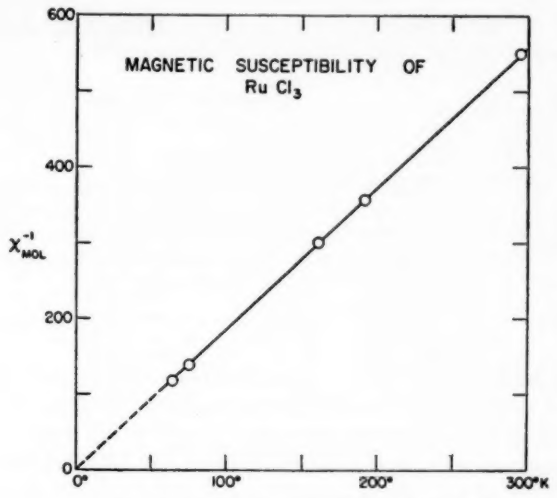

FIG. 2. Magnetic susceptibility of $RuCl_3$.

for diamagnetism using Angus' values.[10] Both compounds follow Curie's law. For K_3MoCl_6,

$$\chi_{\text{atom}} = 1.82/T,$$

and for $RuCl_3$,

$$\chi_{\text{atom}} = 0.536/T.$$

The magnetic moments of Mo^{3+} and Ru^{3+}, calculated from these data, are 3.83 and 2.07 Bohr magnetons, respectively. For the case of K_3MoCl_6 this result is in close agreement with the theoretical moment for three unpaired electron spins 3.87β and is similar to the values found for the Cr^{3+} ion.

If Ru^{3+} in the salt $RuCl_3$ were in a $^6S_{\frac{1}{2}}$ state, the anticipated moment would be 5.92β. The experimental value, 2.07β suggests that it is covalently bonded, analogous to the ion Fe^{3+} in such compounds as $K_3Fe(CN)_6$. The observed magnetic moment is then due to a single electron spin 1.73β plus a small orbital contribution.

ACKNOWLEDGMENT

We wish to thank Dr. Max Wolfsberg for placing at our disposal his profound knowledge regarding chemical bonds.

[10] W. R. Angus, Proc. Roy. Soc. (London) **A136**, 569 (1932).

Electron Affinity of Fluorine

JOHN L. MARGRAVE*
Department of Chemistry, University of Wisconsin, Madison, Wisconsin
(Received October 16, 1953)

Various theoretical and semi-empirical methods for determining electron affinities of atoms have been applied to fluorine. All results indicate a low value of the electron affinity consistent with recent experimental data, and with the value implied by the recently determined dissociation energy of the fluorine molecule. An extrapolation of the type suggested by Hellmann and Mamotenko appears to give the most reliable value and indicates $E_F = 83.2 \pm 0.3$ kcal/mole.

EXPERIMENTAL determinations now indicate without doubt that the electron affinity of fluorine is in the range 82–83 kcal/mole.[1,2,3,4] This value is consistent with that implied through the new determinations of the dissociation energy of F_2[5] and a Born-Haber cycle involving alkali fluorides. Pritchard[6] in a recent review has discussed experimental methods and also various theoretical and semiempirical approaches for calculating the electron affinity. Unfortunately many of the extrapolation procedures appear not to give values for the electron affinity near that determined experimentally. In several cases apparently reasonable extrapolations of ionization potentials or other properties of fluorine and neighboring atoms or ions have yielded high values for the electron affinity consistent with the old, high value for $D(F_2)$.[7,8,9] These references have been reviewed and new calculations carried out with available spectroscopic data. In every case a low value for the electron affinity is indicated.

EXTRAPOLATIONS OF IONIZATION POTENTIALS

Glockler[7] suggested the determination of electron affinities by extrapolation of the ionization potentials of a series of isoelectronic ions. Recent work by Bates[10] and Johnston[11] using essentially this method but with newer data and, in the latter case, a more refined extrapolation, indicates a value for the electron affinity of fluorine of 67–73 kcal/mole. Similar extrapolations for oxygen also give values definitely lower than that found experimentally.

The problem of determining ionization potentials by extrapolation methods has also been considered in detail by Finkelnberg and Stern[12] who have shown the importance of the quantity Δs (the difference in effective atomic numbers between the atom or ion being considered and the atom or ion having an atomic number one less) in analyzing trends throughout the periodic table. For the series of ions and atoms isoelectronic with the fluoride ion, they find that Δs varies from 0.72 for $(S_{PVI} - S_{SiVI})$ to 0.75 for $(S_{NeI} - S_{FI})$. Extrapolation indicates 0.78 for $(S_{O^-} - S_{F^-})$ and, using the experimental value for the ionization potential of O^-,[13] one calculates 86 ± 2 kcal/mole as the electron affinity of fluorine.

EXTRAPOLATIONS INVOLVING REMOVAL ENERGIES FOR p ELECTRONS

The ratio of the removal energies for corresponding p electrons from the outer electronic shells of various halogen atoms and fluorine is a quantity which increases continuously as p electrons are added to the outer shell. A consideration of trends in this ratio and the extension to the filled shell case for fluoride ion indicates that an electron affinity of fluorine equal to 83 kcal/mole would not be inconsistent, but that the possibility of a higher value for the electron affinity cannot be definitely excluded.

Hellmann and Mamotenko[8] proposed an extrapolation method involving the average removal energy of one p electron from the various fluorine ions F I (s^2p^5), F II (s^2p^4), F III (s^2p^3), F IV (s^2p^2), and F V (s^2p). They suggest the quantity e/n (where e is the energy difference between the center of gravity of the various atomic states possible for the given electronic configuration and the ^1S_O states of the F VI ion formed by removal of all

TABLE I. Average removal energy of p electrons.

Species	Number of p electrons	$(e/n)_{exptl.}$ K	$(e/n)_{calc.}$ K
F V	1	920 953	920 932
F IV	2	806 492	806 487
F III	3	699 370	699 450
F II	4	600 690	600 583
F I	5	510 647	510 648
F^-	6	430 379[a]	430 407

[a] By taking $E_F = 83$ kcal/mole.

* Portions of this work were performed while the author was a U. S. Atomic Energy Commission postdoctoral fellow at the University of California at Berkeley, 1951–2.

[1] G. Kimball and M. Metlay, J. Chem. Phys. **16**, 779 (1948).
[2] N. Ionov and V. Dukelskii, Fiz. Zhur. **10**, 248 (1940).
[3] J. L. Margrave, thesis, University of Kansas, 1950; R. Bernstein and M. Metlay, J. Chem. Phys. **19**, 612 (1951).
[4] T. Bailey, thesis, University of Chicago, 1953.
[5] R. N. Doescher, J. Chem. Phys. **19**, 1070 (1951); **20**, 330 (1952); H. Wise, J. Chem. Phys. **20**, 927 (1952); P. W. Gilles and J. L. Margrave, J. Chem. Phys. **21**, 381 (1953).
[6] H. O. Pritchard, Chem. Rev. **52**, 529 (1953).
[7] G. Glockler, Phys. Rev. **46**, 111 (1934).
[8] H. Hellmann and M. Mamotenko, Acta Physicochim. URSS **7**, 127 (1937).
[9] T. Y. Wu, Phil. Mag. **22**, 837 (1936).
[10] D. Bates, Proc. Roy. Irish Acad. **A51**, 151 (1947).
[11] R. Johnston, J. Chem. Phys. **19**, 1391 (1951).
[12] W. Finkelnberg and F. Stern, Phys. Rev. **77**, 303 (1950).
[13] M. Metlay and G. Kimball, J. Chem. Phys. **16**, 774 (1948).

the p electrons, and n is the number of p electrons) as the one to be extrapolated. These energy differences have been evaluated from the data of Moore[14] and fitted with a third degree least-squares equation:

$$e/n = 920\,932 - 117\,895\,(n-1) + 3323(n-1)^2 + 127\,(n-1)^3 K$$

where n = the number of p electrons. The comparison of experimental and calculated results is given in Table I. This extrapolation indicates the electron affinity of fluorine to be 83.2 kcal/mole with an uncertainty of ±0.3 kcal/mole.

CALCULATION OF THE ELECTRON AFFINITY FROM ATOMIC ENERGY LEVELS

Wu[9] has calculated the electron affinity of fluorine by the method of Bacher and Goudsmit[15] in which the energy of an n-electron atom or ion may be determined from term values for various energy levels in the $n-1$, $n-2$, $\cdots$ electron atoms or ions. Wu found a value for the electron affinity of 94.5 kcal/mole in his calculation using the spectroscopic data of Edlen.[16]

Moore[14] has tabulated new and important extensions of the data on fluorine ions made possible by additional work of Edlen as yet unpublished elsewhere. Term values for various energy levels computed from these data and referred to the energy of F VIII ($1s^2\,{}^1S$) as zero are listed in Table II. It will be noted that in the terms of F I, F II, F III, and F IV there is a discrepancy of approximately 720K (cm^{-1}) between these values and those given by Wu. Other variations from the data used by Wu include the rather large shift of 1176K in the position of the quartet system of F V with respect to the doublet system and some minor shifts for individual energy levels. Intercombination lines necessary to place the quartet and doublet systems of F V absolutely have not been observed and Edlen has estimated their position from observed series.

TABLE II. Experimental energy levels for F ions.

Ion	Configuration	Term value (K)	Ion	Configuration	Term value (K)
F VIII	$(1s^2\,{}^1S)$	0	F III	$(1s^22p^5\,{}^2P)$	4 490 488
				$(1s^22s2p^4\,{}^2P)$	4 625 176
F VII	$(1s^22p\,{}^2P)$	1 380 747		$(1s^22s2p^4\,{}^2S)$	4 643 603
	$(1s^22s\,{}^2S)$	1 493 656		$(1s^22s2p^4\,{}^2D)$	4 681 617
				$(1s^22s2p^4\,{}^4P)$	4 739 766
F VI	$(1s^22p^2\,{}^1S)$	2 420 813		$(1s^22s^22p^3\,{}^2P)$	4 840 305
	$(1s^22p^2\,{}^1D)$	2 486 640		$(1s^22s^22p^3\,{}^2P)$	4 857 765
	$(1s^22p^2\,{}^3P)$	2 509 351		$(1s^22s^22p^3\,{}^4S)$	4 891 863
	$(1s^22s2p\,{}^1P)$	2 574 396			
	$(1s^22s2p\,{}^3P)$	2 664 085	F II	$(1s^22p^6\,{}^1S)$	(4 781 636)[a]
	$(1s^22s^2\,{}^1S)$	2 761 237		$(1s^22s2p^5\,{}^1P)$	4 934 448
				$(1s^22s2p^5\,{}^3P)$	5 009 098
F V	$(1s^22p^3\,{}^2P)$	3 335 256		$(1s^22s^22p^4\,{}^1S)$	5 129 134
	$(1s^22p^3\,{}^2D)$	3 375 442		$(1s^22s^22p^4\,{}^1D)$	5 153 180
	$(1s^22p^3\,{}^4S)$	3 406 030		$(1s^22s^22p^4\,{}^3P)$	5 173 885
	$(1s^22s2p^2\,{}^2P)$	3 467 495			
	$(1s^22s2p^2\,{}^2S)$	3 485 122	F I	$(1s^22s2p^6\,{}^2S)$	(5 146 052)[b]
	$(1s^22s2p^2\,{}^2D)$	3 529 802		$(1s^22s^22p^5\,{}^2P)$	5 314 471
	$(1s^22s2p^2\,{}^4P)$	3 596 260			
	$(1s^22s^22p\,{}^2P)$	3 682 190			
F IV	$(1s^22p^4\,{}^1S)$	(3 963 808)[a]			
	$(1s^22p^4\,{}^1D)$	(4 018 539)[a]			
	$(1s^22p^4\,{}^3P)$	4 037 908			
	$(1s^22s2p^3\,{}^1P)$	4 129 063			
	$(1s^22s2p^3\,{}^5S)$	4 148 156			
	$(1s^22s2p^3\,{}^1D)$	4 157 545			
	$(1s^22s2p^3\,{}^3P)$	4 211 212			
	$(1s^22s2p^3\,{}^3D)$	4 238 584			
	$(1s^22s2p^3\,{}^5S)$	4 311 946			
	$(1s^22s^22p^2\,{}^1S)$	4 332 909			
	$(1s^22s^22p^2\,{}^1D)$	4 361 212			
	$(1s^22s^22p^2\,{}^3P)$	4 386 038			

[a] Calculated by author.
[b] Estimated by Moore (reference 14).

TABLE III. Calculated energy levels for F ions.

Ion	Configuration	Calculated term values: From data of reference 14 (K)	Calculated term values: From reference 14 but with 1150K shift in quartet-doublet systems of F V (K)	Experimental term values from reference 14 (K)
F V	$(1s^22p^3\,{}^4S)$	3 385 812	3 385 812	3 406 030
F V	$(1s^22s2p^2\,{}^4P)$	3 582 371	3 582 371	3 596 260
F IV	$(1s^22p^4\,{}^1S)$	3 963 808	3 963 808	···
F IV	$(1s^22p^4\,{}^1D)$	4 018 539	4 018 539	···
F IV	$(1s^22p^4\,{}^3P)$	4 036 612	4 038 145	4 037 908
F II	$(1s^22p^6\,{}^1S)$	4 781 636	4 786 236	···
F I	$(1s^22s2p^6\,{}^2S)$	5 148 330	5 141 430	(5 146 052)[a]
F I	$(1s^22s^22p^5\,{}^2P)$	5 331 238	5 319 738	5 314 471
F^-	$(1s^22s^22p^6\,{}^1S)$	5 330 017[b]	5 336 967[b]	5 343 507[c]

[a] ( ) indicate estimated term value from reference 14.
[b] Average value computed using method of reference 9 to eliminate errors caused by unobserved terms.
[c] Computed using E_P = 83 Kcal/mole = 29 036K.

Determination of the electron affinity requires computation of the energy of the $(s^2p^6\,{}^1S)$ level and comparison of this energy with the observed energy for $(s^2p^5\,{}^2P)$. Formulas for this calculation may be developed by the method of Bacher and Goudsmit and are given by Wu. The accuracy of a calculated energy level depends, of course, on the reliability of the term values used in the calculation. Certain of the terms needed for the calculation of the energy of the $(s^2p^6\,{}^1S)$ level have not been observed experimentally but Wu was able to show that by use of a calculated value for $(sp^6\,{}^2S)$ one could eliminate the uncertainties caused by lack of knowledge about the $(p^4\,{}^1S)$, $(p^4\,{}^1D)$, and $(p^6\,{}^1S)$ levels. The major uncertainties in the pertinent experimental data concern the absolute positions of the $(sp^3\,{}^5S)$ level of F IV and the $(p^3\,{}^4S)$ and $(sp^2\,{}^4P)$ levels of F V. Any shifts in the absolute positions of these levels will markedly influence the calculated electron affinity. Moore gives the uncertainty in the position of the $(sp^3\,{}^5S)$ level of F IV as 50–100K and of the $(p^3\,{}^4S)$ and $(sp^2\,{}^4P)$ levels of F V as ±100K.

Calculations have been carried out with Moore's values and also values in which the position of the quartet system of F V has been shifted by 1150K with respect to the doublet system, approximately to the position first suggested by Edlen. No shift was tried for the $(sp^3\,{}^5S)$ level since its position appears more reliable. To check on the general reliability of the method it was thought advisable to calculate energies for levels in various fluorine ions. The results are listed in Table III

[14] C. Moore, "Atomic energy levels," Natl. Bur. Standards Circular No. 467, Vol. 1, June 15, 1949.
[15] R. Bacher and S. Goudsmit, Phys. Rev. **46**, 948 (1934).
[16] B. Edlen, Z. Phys. **89**, 179, 597 (1934); **92**, 19 (1934); **93**, 433 (1935).

where calculated values are compared with experimental values when possible.

From the results presented here it appears that better agreement between calculated and experimental values is obtained when the quartet-doublet position is shifted as described before. Energy levels calculated with Moore's data alone fail to indicate a stable F^- ion.

A shift in the quartet-doublet position is also indicated to be desirable on the basis of the calculated electron affinity. From Moore's data and the calculated term value for $(sp^6\,{}^2S)$, which corrects for uncertainties arising from the unobserved $(p^4\,{}^1S)$, $(p^4\,{}^1D)$, and $(p^6\,{}^1S)$ terms, one locates the position of $(s^2p^6\,{}^1S)$ so that the electron affinity is found to be 44 kcal/mole. A completely similar treatment with the relative position of the quartet and doublet system of F V shifted by 1150K gives the value 64 kcal/mole for the electron affinity. If the shift is taken as 1500K the electron affinity is calculated to be 70 kcal/mole and also, calculated and observed energy levels for F I and F^- agree within 3000K. The results obtained by this method only indicate the likelihood of a low value for the electron affinity, but definitely do not indicate a value as high as 95 kcal/mole.

ACKNOWLEDGMENT

The author wishes to thank Professor Leo Brewer, Department of Chemistry, University of California at Berkeley, for many helpful discussions of this problem.

THE JOURNAL OF CHEMICAL PHYSICS VOLUME 22, NUMBER 4 APRIL 1954

Absorption Intensities of the Isomeric Pentenes in the Vacuum Ultraviolet*

DOROTHY SEMENOW, ANNA J. HARRISON, AND EMMA P. CARR
Department of Chemistry, Mount Holyoke College, South Hadley, Massachusetts

(Received July 10, 1953)

Quantitative measurements of the absorption spectra of the six isomeric pentenes in vapor phase have been made in the region 45 000–65 000 cm^{-1}. The maximum of the intense band ($N\rightarrow V$) is the same for 1-pentene, *cis*-2-pentene, and 2-methyl-2-butene, with one, two, and three alkyl substituents, respectively. The results show that in a series of hydrocarbons, where the molecular weight is unchanged and the number of alkyl groups is the only variable, the position of the $N\rightarrow V$ maximum is not a function of the number of alkyl substituents. From the standpoint of methyl substituents, there is no shift between *cis*-2-pentene with one methyl group and 2-methyl-2-butene with three. In the absence of such a shift, spectral evidence in support of hyperconjugation in the substituted ethylenes is lacking.

The $N\rightarrow V$ maximum for *trans*-2-pentene is less intense and at somewhat longer wavelength than for the *cis*-isomer. The greatest shift in this band is with 2-methyl-1-butene, where the two alkyl groups are on the same carbon atom. These results indicate the importance of molecular shape in determining the energy of the $N\rightarrow V$ transition in the monoolefins.

The positions of the shallow bands ($N\rightarrow R$) on the long wave side of the $N\rightarrow V$ band are in substantial agreement with earlier measurements and confirm the conclusion that the energy of this transition is dependent on the number of alkyl substituents on the carbon atoms of the double bond. The possibility of other Rydberg bands on the short wave side is discussed briefly. Oscillator strengths for the $N\rightarrow V$ band are given for the six pentenes; these vary from 0.26 in 2-methyl-1-butene to 0.45 in *cis*-2-pentene but their value for testing theoretical predictions is doubtful because of the overlapping of different electronic transitions.

INTRODUCTION

IN earlier work from this laboratory the position of the absorption bands of the isomeric pentenes were measured[1] but there was no method available at that time for the accurate measurements of absorption intensities in this spectral region. Measurements of a few monoolefins in heptane solution have been made,[2] but a quantitative study of the absorption spectra of all the possible isomers of a given monoolefin has not been reported. Such measurements on a single group of isomeric hydrocarbons containing only one carbon-carbon double bond, each member of which has the same number of carbon and hydrogen atoms, reduce the number of variable factors which must be considered in the interpretation of absorption spectra in their relation to molecular structure. The theoretical analysis of the electronic spectra of simple organic molecules has made extraordinary progress in the last fifteen years, particularly in the work of Mulliken,[3] but the quantitative experimental data which are necessary to test the theoretical predictions for the ethylenic derivatives remain extremely limited.

The six pentenes which were measured previously were synthesized and purified in this laboratory.[4] Vapor phase measurements in the vacuum ultraviolet demand a very high degree of purity and hydrocarbons of the necessary purity are now obtainable from the American Petroleum Institute.[5] With the development in this laboratory of a method for the quantitative

* Supported in part by the National Science Foundation.

[1] E. P. Carr and H. Stücklen, J. Chem. Phys. **4**, 762 (1936); J. Am. Chem. Soc. **59**, 2138 (1937).

[2] Platt, Rusoff, and Klevens, J. Chem. Phys. **11**, 535 (1943); Platt, Klevens, and Price, J. Chem. Phys. **17**, 466 (1949).

[3] For ethylene derivatives especially, see R. S. Mulliken, Revs. Modern Phys. **14**, 265 (1942).

[4] These compounds were prepared under the direction of Professor M. L. Sherrill.

[5] The samples were made available for this investigation by the American Petroleum Institute Research Project 44 at the Carnegie Institute of Technology.

determination of extinction coefficients in the vacuum ultraviolet, it seemed advisable to repeat and extend the earlier measurements.

EXPERIMENTAL

The compounds used for these measurements were API Research hydrocarbons, supplied in glass ampoules which had been sealed "in vacuum."[6] The impurity in mole percent was reported as follows: 1-pentene 0.18 $\pm$0.12; *cis*-2-pentene 0.04$\pm$0.03; 2-methyl-1-butene 0.11$\pm$0.08; *trans*-2-pentene 0.07$\pm$0.05; 3-methyl-1-butene 0.22$\pm$0.12; 2-methyl-2-butene 0.055$\pm$0.046. Where the sealed tube was fitted for a magnetic hammer (the first three), the ampoules were sealed directly to the vacuum line. With the others, the cooled sample tube was broken open and poured quickly into a nitrogen-filled tube which was immediately placed in the vacuum system.

The apparatus and method used in the spectral measurements were substantially those described previously.[7] A Hilger fluorite prism spectrograph was used with a hydrogen lamp and flowing vapor absorbing system. Calculations of intensity were made from microphotometer records of plates on which had been photographed an accurately timed exposure through the compound (3–4 minutes) and four exposures through the empty cell for calibration. The length of the absorption tube was 32.5 cm, and the range of pressures varied from 0.02 to 6.46 mm. From 9–12 different pressures, showing a two- to threefold change of pressure were used for each compound. Each absorption curve was determined by measurements at 70–100 wavelengths. Two to six measurements were made at each wavelength and in general the average deviation of logϵ did not exceed 0.03. On the side of a steep curve the average deviation was occasionally larger, 0.04 to 0.05. In the line region of the hydrogen spectrum, beyond 60 000 cm^{-1}, one or two values showed a deviation of 0.14. The average deviation in calculated values at the maximum of the intense band was in each case less than 0.03.

To minimize exposure time, the slit width of the spectrograph is somewhat larger than in the earlier work where band maxima were measured with the comparator. This, together with the slit width of the microphotometer tended to reduce the sharpness of the bands and a number of the shallow bands for which band maxima were given are evident only as "stepouts" in the microphotometer tracings.

Measurements on *cis*-2-pentene and 2-methyl-2-butene were made below 48 000 cm^{-1} with the Beckmann spectrophotometer using a 1 cm cell and the vapor handling system described by Harrison and co-workers.[7] Pressures up to 30.5 mm were used in these measurements. The values of logϵ did not overlap those obtained with the vacuum spectrograph but gave a smooth curve with those obtained with the latter.

RESULTS

The identification in the microphotometer tracings, either as shallow bands or stepouts, of all of the bands reported by Carr and Stücklen[1] gives satisfactory confirmation of the purity of those earlier preparations. In the narrow shallow bands between 48 000 and 52 000 cm^{-1}, the present readings are in satisfactory agreement with their readings; in the broad shallow bands there was greater deviation because of the difficulty in reading band maxima. The agreement was, however, within this probable error.

The spectrum of 3-methyl-1-butene shows a very shallow band at 51 340 cm^{-1} which was not evident in the earlier work and it seems probable that this may be due to an impurity in the sample. The analysis reported for this isomer showed the highest impurity for any of the pentenes (0.22$\pm$0.12 mole percent) and the spectral results at high pressure indicate quite conclusively the presence of 1-3-butadiene. A group of three bands, with maxima at 46 260, 47 730, and 49 100 cm^{-1} appear at a pressure of 4.8 cm (logϵ=1.62 $-$1.73).[8] The presence of these bands at quite high pressures was noted by Carr and Stücklen. They were believed to be due to an impurity but were not identified, as the diene spectra in this region had not been measured at that time. Three samples of 3-methyl-1-butene were examined in those earlier experiments; two were prepared in this laboratory by different synthetic methods and one at Pennsylvania State College. All showed these three absorption bands but at much higher pressures (50 mm) than in the present work. This would indicate a higher degree of purity in those earlier preparations and since the band at 51 340 cm^{-1} was not noted in those measurements it seems reasonable to conclude that this band in the present work is due to an unidentified impurity and is not a character-

[6] These compounds were purified by the American Petroleum Institute Research Project 6, of the Carnegie Institute of Technology, from material obtained from the following sources:
1-pentene, by the Phillips Petroleum Company, Bartlesville, Oklahoma.
cis-2-pentene, by the API Research Project 45 at the Ohio State University, Columbus, Ohio and the Phillips Petroleum Company, Bartlesville, Oklahoma.
trans-2-pentene, by the API Research Project 45 at the Ohio State University, Columbus, Ohio.
2-methyl-1-butene and 2-methyl-2-butene, by the General Motors Corporation, Detroit, Michigan.
3-methyl-1-butene, by the Houdry Process Corporation, Marcus Hook, Pennsylvania.
The purification and purity of these compounds have been described in papers of the API Research Project 6. Streiff, Murphy, Sedlak, Willingham, and Rossini, J. Research Natl. Bur. Standards **37**, 331 (1946); Streiff, Zimmerman, Saule, Butt, Sedlak, Willingham, and Rossini, J. Research Natl. Bur. Standards **41**, 323 (1948).

[7] Harrison, Gaddis, and Coffin, J. Chem. Phys. **18**, 221 (1950).

[8] The identification is based on measurements by W. C. Price and A. D. Walsh (Proc. Roy. Soc. (London) **174A**, 220 (1940) and unpublished work of this laboratory. Quantitative determination of the amount present was made from the optical density curve in the Natl. Bur. Standards publication of the API Project 44 and gives approximately 0.20 mole percent. This indicates that the reported impurity must be chiefly butadiene.

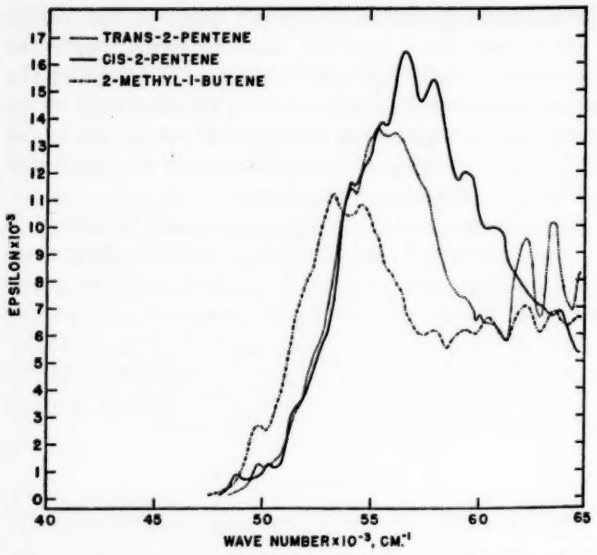

FIG. 1. Absorption curves of isomeric pentenes with two aklyl substituents. The molar extinction coefficient, epsilon, is defined by the relation: $\epsilon cL = \log_{10}(I_0/I)$, where c is concentration in moles per liter, L is path length in centimeters.

istic of 3-methyl-1-butene. Except for two very sharp bands, at 53 650 and 56 990 cm^{-1}, respectively, the absorption of butadiene is so small that it makes a negligible contribution to the total intensity of the broad, high-intensity band of the olefin in this region. The presence of minute amounts of butadiene in so many samples of highly purified 3-methyl-1-butene is of considerable chemical interest.

The possibility of photodecomposition during irradiation was investigated to a limited extent for several of the hydrocarbons. It was found that decomposition occurs after prolonged irradiation of the *static* vapor at high pressures. However, the results indicate that, in general, photodecomposition is not appreciable under the experimental conditions employed, i.e., flowing vapor and exposure time of 3–4 minutes.

The absorption curves for the three pentenes with two alkyl substituents on the carbon atoms of the double bond are shown in Fig. 1; the curve for *cis*-2-pentene is also given in Fig. 2 for comparison with the isomers containing one and three alkyl groups. It will be noted that in five of the curves, but particularly where there are two alkyl substituents (Fig. 1), the broad, intense band has two fairly sharp maxima of almost equal intensity. The difference in the values of $\log\epsilon$ is within the limit of possible experimental error but in each curve the long wave maximum is slightly higher and we have taken that as the maximum of the strong allowed transition, the $N \rightarrow V$ transition.

The complexity of these vapor spectra was recognized in the earlier work but becomes more pronounced in these curves based on quantitative measurements. The shallow diffuse bands which are superimposed on the long wave side of the $N \rightarrow V$ band have been identified previously as Rydberg transitions.[9] In the isomers having only one alkyl substituent the first Rydberg band appears only as a sharp stepout, the center of which is in good agreement with the value of the maximum of the shallow band in the earlier report. Measurements of 2-methyl-2-butene were made below 48 000 cm^{-1} with the Beckman spectrophotometer and nine very shallow, equally spaced bands were measured between 45 600 cm^{-1} and 47 750 cm^{-1} ($\log\epsilon = 2.16 - 2.48$). Five bands between 45 850 and 47 120 cm^{-1} were identified in the earlier measurements with the vacuum spectrograph. The wide slits necessary for the readings on the Beckman instrument in this region make the values of band positions less reliable but give important data on intensities. According to the present measurements the first band is at 45 600 cm^{-1} and the second band coincides with the first of the other measurements. Values for the longest wavelength band in the $N \rightarrow R$ transition and the maximum of the $N \rightarrow V$ band are given in Table I.

DISCUSSION

Examination of the curves in Fig. 2, together with the values of Table I, show that the maximum of the $N \rightarrow V$ band is the same for 1-pentene, *cis*-2-pentene, and 2-methyl-2-butene, with one, two, and three alkyl substituents, respectively. For the same compounds the position of the first narrow band ($N \rightarrow R$), in relation to 1-pentene is shifted toward the visible by 4250 cm^{-1} for two alkyl groups and 7450 cm^{-1} for three. The progressive decrease in ionization potential,[10] in heats of hydrogenation,[11] and in the energy

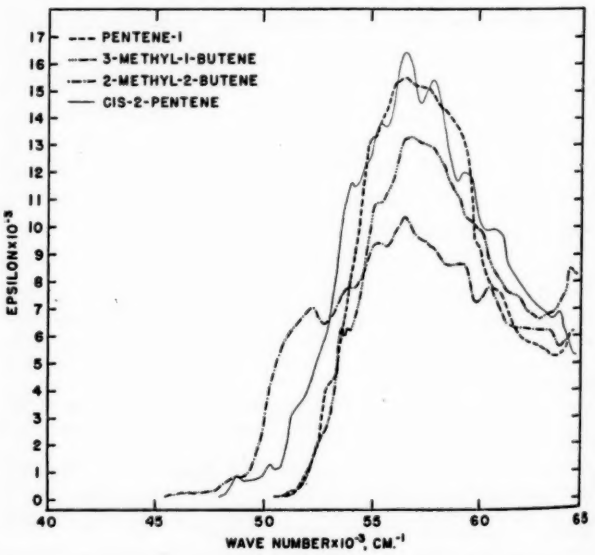

FIG. 2. Absorption curves of four isomeric pentenes with one, two, and three alkyl substituents.

[9] E. P. Carr and H. Stücklen, J. Chem. Phys. **7**, 631 (1939). See also R. S. Mulliken, Revs. Modern Phys. **14**, 265 (1942).

[10] W. C. Price and W. T. Tutte, Proc. Roy. Soc. (London) **A174**, 207 (1940).

[11] G. B. Kistiakowsky *et al.*, J. Am. Chem. Soc. **39**, 137 (1936).

of the first band of the Rydberg transition,[1] have been shown by experiment to be dependent primarily on the number of alkyl groups bound to the carbon atoms of the double bond and only to a limited extent related to the molecular weight or position of the substituent.[12]

Quantitative measurements of the position of the $N \rightarrow V$ band have been lacking and it has been assumed from the qualitative data available that there is a comparable shift toward the visible in this band with methyl substitution. This conclusion has been based on data for an homologous series of olefins in which the hydrogen atoms of ethylene are progressively replaced by methyl groups.[13] Two difficulties are involved in drawing conclusions from these data. The first is that in such a series the comparison is made between molecules of different molecular weight as well as different numbers of methyl groups. Although not definitely established by the earlier spectral measurements of the butenes and pentenes, the results at that time indicated a small shift of this band toward the visible with molecules of similar configuration but higher molecular weight. The observation has been recently confirmed by quantitative intensity measurements of the butenes.[14] The $N \rightarrow V$ band of 1-pentene shows a shift of 500 cm^{-1} in relation to 1-butene while the band of 2-methyl-2-butene, with three methyl groups is displaced 425 cm^{-1} in relation to *cis*-2-butene, with two methyl substituents. Evidently a part of any observed shift of this $N \rightarrow V$ band in an homologous series must be due to this difference in molecular weights.

A more series difficulty in basing conclusions on the data of Mulliken's table is the uncertainty of the experimental values. There were no quantitative measurements of intensities for any of the molecules available at the time of its publication. The maxima for propylene and tetramethylethylene were estimated values from Price and Tutte's photographic plates[10] and the values for 2-butene and 2-methyl-2-butene were interpolated between these values for one and four methyl groups. A further difficulty in a comparison based on ethylene lies in the lack of agreement in the values for the maximum of the $N \rightarrow V$ band. Recent quantitative determinations give values from 1614A to 1700A which represent a variation of 0.4 electron volt.[15] Although it is not possible at this time to make a rigorous test of methyl substitution alone, the curves of Fig. 2 show that there is no appreciable shift of the $N \rightarrow V$ maximum between *cis*-2-pentene and 2-methyl-2-butene with one and three methyl groups, respectively.

TABLE I. Position and intensity of characteristic bands.

Compound	Maximum $N \rightarrow V$ band			1st band $N \rightarrow R$		
	cm^{-1}	ev	log ϵ	cm^{-1}	ev	log ϵ
1-pentene	56 600	7.01	4.19	53 050	6.57	3.59
3-methyl-1-butene	56 800	7.03	4.12	52 700	6.53	3.39
cis-2-pentene	56 600	7.01	4.22	48 800	6.05	2.93
trans-2-pentene	55 500	6.88	4.13	49 800	6.17	3.10
2-methyl-1-butene	53 200	6.60	4.05	49 800	6.17	3.42
2-methyl-2-butene	56 575	7.01	4.02	45 600	5.65	2.16

These results are of particular interest in connection with the significance of hyperconjugation in the interpretation of the energy relations of the ethylenic hydrocarbons. According to Mulliken's theoretical computations it is the red shift in the $N \rightarrow V$ band by methyl substitution which may be explained by hyperconjugation. In the absence of this shift, where methyl or alkyl substitution is the only variable, it must be concluded that hyperconjugation does not play a significant role in explaining the energy relations of the monoolefins.

The decrease in ionization potential may be accounted for by the charge transfer or inductive effect brought about by the additional alkyl groups, as suggested by Price and Tutte.[10] According to Coulson's analysis of the methyl substituted ethylenes, the inductive effect should change the energy of the ground and excited state in nearly the same way. It is clear that this is the case in the four pentenes where the energy of the $N \rightarrow V$ transition remains practically constant while the number of alkyl groups varies from one to three. There is a slight shift toward the ultraviolet in 3-methyl-1-butene where the isopropyl group is substituted for the *n*-propyl of 1-pentene. In the absence of spectral evidence for hyperconjugation in the pentenes, the interpretation of the progressive decrease in the heat of hydrogenation with alkyl substitution from that point of view would lack justification.[16]

Consideration of the curves for the three isomers, having two alkyl substituents (Fig. 1), indicates that molecular shape must be an important factor in determining the position and intensity of the $N \rightarrow V$ maximum. The relative positions and intensities of the *cis*- and *trans*-isomers are not in accord with the results of Platt and co-workers[17] for the corresponding isomers of octene-2 in heptane solution. They are, however, in agreement with the results reported by Walsh[18] with regard to the relation in positions and intensities of the corresponding bands in the vapor phase spectra of *cis*- and *trans*-dichlorethylene, where the $N \rightarrow V$ band in the *trans*- form is of lower intensity and at longer wavelengths than the *cis*- form. Walsh reports ionization

[12] The *cis*- and *trans*-isomers show small differences in each of these quantities.

[13] R. S. Mulliken, Revs. Modern Phys. **14**, 265 (1942); these values are used by Coulson in the discussion of hyperconjugation. C. A. Coulson, *Valence* (Clarendon Press, Oxford, 1952) pp. 308–310.

[14] J. T. Gary and L. W. Pickett, J. Chem. Phys. **22**, 599 (1954).

[15] P. G. Wilkinson and H. L. Johnston, 1614A, J. Chem. Phys. **18**, 190 (1950); Platt, Klevens, and Price, 1625A, J. Chem. Phys. **17**, 466 (1949); M. Zelikoff and K. Watanabe. Paper presented at meeting of the Optical Society of America, New York, March, 1953. Maximum absorption index reported as near 1700A.

[16] L. N. Ferguson, *Electron Structure of Organic Molecules* (Prentice-Hall, Inc., New York, 1952), p. 165.

[17] Platt, Kelvens, and Price, J. Chem. Phys. **17**, 466 (1949).

[18] A. D. Walsh, Trans. Faraday Soc. **41**, 35 (1945).

TABLE II. Values of oscillator strength.

Substance	Wave number range	f value
cis-2-pentene	53 360–61 700 cm^{-1}	0.45
2-methyl-2-butene	50 690–63 850	0.44
1-pentene	54 000–60 730	0.38
3-methyl-1-butene	54 250–62 850	0.38
trans-2-pentene	52 880–59 750	0.32
2-methyl-1-butene	51 200–58 350	0.26

potentials of 9.66 and 9.99 electron volts for *cis*- and *trans*-dichlorethylene, respectively. The first Rydberg band of *cis*-2-pentene (Table I) is shifted 1000 cm^{-1} to the red in relation to *trans*-2-pentene; a corresponding difference in the photoionization limit would give the ionization potential of *cis*-2-pentene about 0.12 electron volt less than the *trans*-isomer. The value for the ionization potentials of *trans*-2-butene and cyclohexene, reported by Price and Tutte,[10] were based on the value determined for benzene since it was found that the spectrum of these two molecules in the vacuum ultraviolet fell very close to that of benzene. The bands due to the more highly excited states of the monoolefins are too diffuse to be extrapolated with accuracy to the photoionization limit; whereas this is possible for benzene and the ionization potential was taken as the same for the three molecules and was believed to be correct to within 0.05 ev. However, the difference of 0.12 ev between *cis*- and *trans*-2-pentene, indicated by our Rydberg measurements would seem resonable in view of the values for the dichlorethylenes.

Comparison of the curves of *trans*-2-pentene and 2-methyl-1-butene illustrates most strikingly the effect of molecular shape on the spectrum, particularly on the position of the $N \rightarrow V$ band. The first Rydberg band is at exactly the same position for each compound while the $N \rightarrow V$ band of the isomer where both alkyl groups are on the same carbon atom is shifted 2300 cm^{-1} toward the visible and the intensity shows a sharp decrease. Since the energy of the $N \rightarrow R$ band is the same for the two isomers, the ionization potential would probably be identical and would differ very slightly from the *cis*-2-pentene. Thus, there is an *increase* in term value, or a so-called stabilization of the excited state ($N \rightarrow V$) of the *trans*-2-pentene in relation to *cis*-2-pentene and a very much greater increase with the isomer where the two alkyl groups are on the same carbon atom. This unsymmetrical substitution increases markedly the polarity of the molecule. These results point to the conclusion that molecular shape would seem to be the most important factor in determining the intensity and frequency of the $N \rightarrow V$ transition in the monoolefins.

The parallelism between the Rydberg states of *trans*-2-pentene and 2-methyl-1-butene is evident not only in the first Rydberg band but also in what would seem to be the second member at 62 200 cm^{-1}, which is practically identical in both isomers (Fig. 1). The narrow band at 63 500 cm^{-1} is also common to both spectra; the separation of 1300 cm^{-1} is probably the excited C=C valence vibration which is reported from Raman measurements[19] to be 1674 cm^{-1} for *trans*-2-pentene in the ground state. This vibrational frequency cannot be measured accurately in the first Rydberg transition as it appears only as a stepout in the present measurements. Carr and Stücklen noted a band at 51 360 cm^{-1} giving a separation of 1580 cm^{-1} as the corresponding vibrational frequency in the first Rydberg state.

When the position of the second member of the Rydberg series is calculated from the series formula for benzene[20] the value is 62 050 cm^{-1}. Our value of 62 200 cm^{-1} for *trans*-2-pentene would be in accord with this assignment. These Rydberg bands are evidently superimposed on a region of general absorption which would account for the higher intensity of this transition in relation to the first bands of this series. This is the region at which the saturated hydrocarbons absorb. There are no quantitative measurements of pentane but the epsilon values for cyclopentane, between 62 000 and 65 000 cm^{-1}, are from 1000–6000.[21]

The superposition of other electronic transitions on the short wave side of the $N \rightarrow V$ band is indicated by the general shape of all the curves. In the earlier study of the butenes[1] the sudden appearance of sharply defined fine structure in the spectrum of isobutylene at 55 500 cm^{-1} indicates a new electronic transition superimposed on the $N \rightarrow V$ band. A group of sharp bands in benzene, beginning at 55 860 cm^{-1}, has been assigned[22] to a second Rydberg series converging to the same photoionization limit as Series I. In view of the general spectral resemblences, it seems reasonable to assume a comparable $N \rightarrow R$ transition in the butenes. The actual appearance of bands with the characteristic fine structure of Rydberg bands is evident only in isobutylene but analogous transitions would be expected in the other butenes and pentenes. The superposition of such bands on the short wave side of the $N \rightarrow V$ band is a complicating factor in the calculation of the oscillator strength of this band. Table II gives the oscillator strengths for the six pentenes, calculated from the curves; because of the overlapping of different electronic transitions their value in testing theoretical predictions is questionable. Our values are of the same order as the f value for ethylene (0.34 ± 0.15) reported by Platt and co-workers but in general higher than their values for the heptane solutions of the monoolefins.

[19] Bourgel, Grèdy, and Piaux, Compt. rend. **195**, 129 (1932).
[20] Hammond, Price, Teegan, and Walsh, Discussions Faraday Soc. **9**, 53 (1950).
[21] Pickett, Muntz, and McPherson, J. Am. Chem. Soc. **75**, 4862 (1951).
[22] W. C. Price and A. D. Walsh, Proc. Roy. Soc. (London) **A191**, 22 (1947).

Structural Investigations by Means of Nuclear Magnetism. III. Ammonium Halides*

H. S. GUTOWSKY, *Noyes Chemical Laboratory, University of Illinois, Urbana, Illinois*
G. E. PAKE, *Department of Physics, Washington University, St. Louis, Missouri*

AND

R. BERSOHN, *Department of Chemistry, Cornell University, Ithaca, New York*

(Received November 18, 1953)

The proton magnetic resonance absorption has been measured in NH_4Cl, NH_4Br, and NH_4I crystal powders from $-195°C$ to room temperature, and for NH_4Cl to 200°C. Line width transitions were found at -144, -171, and about $-198°C$ in the chloride, bromide, and iodide, respectively. The N−H distance in the ammonium ion was determined to be 1.035 ± 0.01A from the second moments of the broad, low-temperature absorption lines observed in NH_4Cl and NH_4Br, with allowance for broadening by modulation effects and narrowing by zero-point torsional oscillations. The relatively narrow room temperature line shapes are consistent with the broadening estimated for inter-NH_4^+ interactions, the intra-NH_4^+ interactions averaging to zero over the hindered rotational motions of the NH_4^+ ions. No appreciable line shape changes were found at the λ temperatures. An electrostatic calculation is made of the potential barriers to rotation of the NH_4^+ ion giving values comparing favorably with experimental inferences. The results clarify the motions which narrow the absorption line at low temperatures and emphasize the dynamic aspects of the order-disorder process.

1. INTRODUCTION

IN papers I[1] and II[2] methods were presented by means of which nuclear magnetic resonance absorption line shapes, widths, and second moments can give information about internuclear distances and motions in solids. In I a brief analysis was made of the broad proton resonance in several ammonium halides at low temperatures, giving a value of 1.025A for the N−H distance in the ammonium ion. At higher temperatures, the proton resonance lines in ammonium salts are narrower, suggesting[3] low-frequency rotational motions of the ammonium ions. This article includes detailed experimental results on polycrystalline ammonium halides, at temperatures of $-195°C$ and higher. The determination of the N−H distance in the ammonium ion is treated more exactly, and the motions responsible for narrowing the resonance lines are considered. In addition, the article[4] following this one gives results obtained with a single crystal of ammonium chloride, for which a more complete analysis and more comprehensive conclusions are possible.

Since the discovery by Simon[5] in 1922 of the anomaly in the specific heat of ammonium chloride at $-30.4°C$, an enormous amount of experimental data and theoretical discussion has been published on the properties and nature of this and similar transitions in other ammonium salts. The infrared spectra of several of the ammonium halides,[6,7] as well as the analysis by Lawson[8] of the specific heat, indicate strongly that the room temperature modifications contain NH_4^+ tetrahedra which are randomly oriented in the two possible equilibrium positions in the unit cells, with the hydrogen atoms directed essentially toward four of the surrounding eight halide ions at the unit cube corners. In the low-temperature phase, the NH_4^+ orientations are ordered, suggesting that the transitions are of an order-disorder type. Conclusive confirmation of this model has since been provided by the more direct neutron diffraction studies[9,10] of the structures of the hydrogen and deutero-ammonium chlorides and bromides. However, the details of the order-disorder process are still not understood, and in particular interesting questions remain concerning the motion of the ions.

Prior to our earlier nuclear resonance studies of the ammonium salts, qualitative observations on NH_4Cl were made by Bitter[11] and by Alpert.[12] Since then, Sachs and Turner[13] have measured proton spin-lattice relaxation times in NH_4Cl, NH_4Br, NH_4I, and NH_4IO_3 from -195 to $25°C$. Soutif[14] has reported line width *versus* temperature data on a single crystal of NH_4Cl, and Cooke and Drain[15] have made some line width and relaxation time observations on NH_4Cl, NH_4Br, and

* Supported in part by the U. S. Office of Naval Research.

[1] Gutowsky, Kistiakowsky, Pake, and Purcell, J. Chem. Phys. **17**, 972 (1949).
[2] H. S. Gutowsky and G. E. Pake, J. Chem. Phys. **18**, 162 (1950).
[3] H. S. Gutowsky and G. E. Pake, J. Chem. Phys. **16**, 1164 (1948).
[4] R. Bersohn and H. S. Gutowsky, J. Chem. Phys. **22**, 651 (1954).
[5] F. Simon, Ann. Physik **68**, 241 (1922). The next few references serve as an introduction to the literature on this subject.
[6] E. L. Wagner and D. F. Hornig, J. Chem. Phys. **18**, 296, 305 (1950).
[7] L. F. H. Bovey, J. Opt. Soc. Am. **41**, 836 (1951).
[8] A. W. Lawson, Phys. Rev. **57**, 417 (1940).
[9] H. A. Levy and S. W. Peterson, Phys. Rev. **86**, 766 (1952); J. Am. Chem. Soc. **75**, 1536 (1953).
[10] G. H. Goldschmidt and G. D. Hurst, Phys. Rev. **83**, 88 (1951); **86**, 797 (1952).
[11] Bitter, Alpert, Poss, Lehr, and Lin, Phys. Rev. **71**, 738 (1947).
[12] N. L. Alpert, Phys. Rev. **75**, 398 (1949).
[13] The results are summarized by E. M. Purcell, Physica **17**, 282 (1951); details are given by A. M. Sachs, Ph.D. thesis, Harvard University, 1949.
[14] M. Soutif, Rev. sci. **89**, 203 (1951).
[15] A. H. Cooke and L. E. Drain, Proc. Phys. Soc. (London) **A65**, 894 (1952).

NH_4I. The results generally agreed upon can be summarized as follows. For each ammonium salt there is a characteristic temperature range above which the resonance absorption line is relatively narrow and structureless and below which the line is very broad with unresolved fine structure. The resonance absorption does not change significantly at the λ temperatures. The width of the broad proton resonance arises from the magnetic dipole-dipole interaction of a given proton with the other three protons in the same NH_4^+ ion and also with all other neighboring magnetic nuclei in the crystal. A conclusion supported by the present work is that the narrowing of the line marks the disappearance of the intra-NH_4^+ interactions and a slight modification of the smaller, inter-ionic interactions. The disappearance of the intra-NH_4^+ interactions results from random reorientations of the NH_4^+ ions at an average frequency comparable to the inverse, proton spin-spin interaction time ($\sim 10^5$ cps).

This frequency is much too low to contribute appreciably to the specific heat or most of the other physical observables, and one main advantage of nuclear magnetic resonance is that the presence of such low-frequency processes can be detected. The measurements raise the problem of interpreting the low-frequency motions in terms of the crystalline potential barriers. The barriers are calculated electrostatically with results comparing favorably with the values deduced from the observed torsional frequencies.[6] The electrostatic calculations, relaxation times, and line shape studies combine to give a physically reasonable dynamical model for the rotational motions of the NH_4^+ ions and for the order-disorder process.

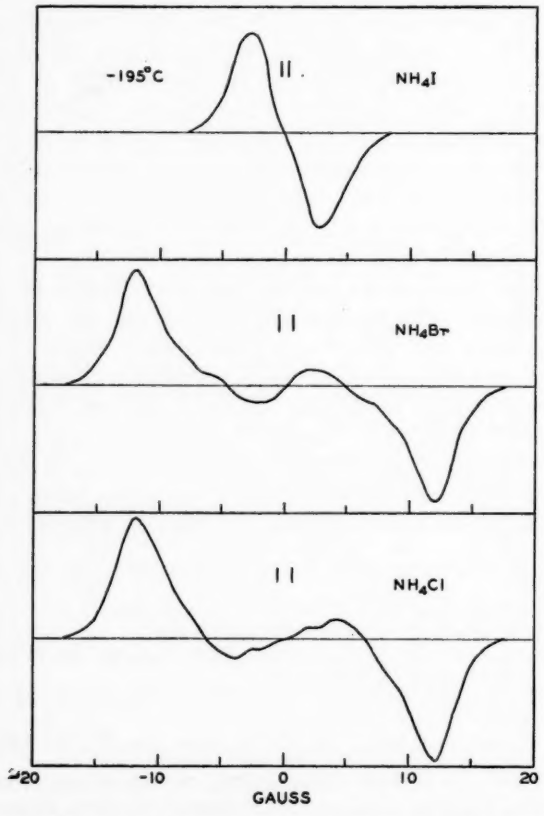

FIG. 1. Derivatives of the proton magnetic resonance absorption lines observed in the ammonium halide powders at liquid nitrogen temperatures. The absorption intensities are arbitrary. The pairs of vertical lines represent the field modulation.

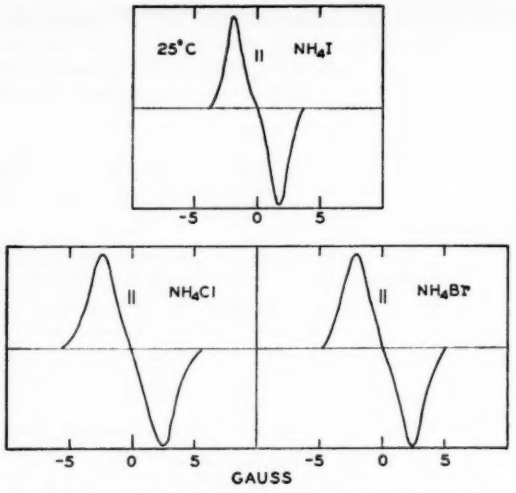

FIG. 2. Derivatives of the proton magnetic resonance absorption lines observed in the ammonium halide powders at room temperature. The absorption intensities are arbitrary. The pairs of vertical lines represent the field modulation.

2. EXPERIMENTAL METHOD

The data reported here were obtained with the automatic recording rf spectrometer and cryostat described elsewhere.[16] In general, these observations agree with the earlier ones,[1,3] the main differences arising from more effective temperature control in the present arrangement. A fixed radio-frequency of about 27.2 mc was used. The applied magnetic field was modulated a small fraction of the line width, and the derivative of the proton resonance line was plotted automatically as a function of applied field by a recording potentiometer, preceeded by a narrow-band amplifier.

The samples were polycrystalline, reagent grade, from commercial sources. An arbor press was used to make cylindrical pellets $\frac{3}{8}$ inch in diameter and $\frac{3}{4}$ inch long. The temperature was measured with a copper-constantan thermocouple imbedded in a small hole drilled in one end of the pellet. Complete line shapes were obtained at fixed temperatures over the temperature range investigated. There were significant differences in the line shapes observed upon warming and cooling through the line-width transition region. The differences could arise from a lag in attaining temperature equilibrium, most likely from the less effective temperature control upon cooling; however, there might be a true hysteresis. In any event, all data re-

[16] Gutowsky, Meyer, and McClure, Rev. Sci. Instr. 24, 644 (1953).

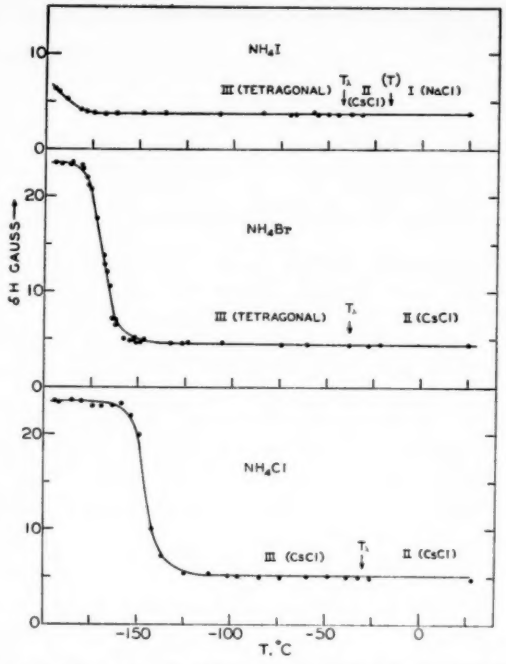

FIG. 3. Line widths of the proton magnetic resonance absorption in the ammonium halide powders plotted against temperature. The curves drawn for NH_4Cl and NH_4Br were calculated from T_1 results as described in Sec. 3c.

ported in the line-width transition region were obtained upon warming.

Second moments of the absorption lines were obtained by numerically integrating the observed first derivatives. The errors given in the text for second moments are the statistical errors of the observations. In addition, nonlinearity and systematic error in the biasing current-field change calibration introduce a further uncertainty of no more than one percent of the observed second moment values. *Both* errors are taken into consideration in calculating the N−H bond distance. The experimental errors in the line widths depend somewhat on the line shape; usually the statistical and maximum systematic errors together were no more than two percent of the values reported.

3. RESULTS AND DISCUSSION

The absorption line shapes observed at liquid nitrogen temperature are given in Fig. 1 and those at room temperature in Fig. 2. The line widths δH, defined as the separation in gauss between the maximum and minimum of the derivative of the absorption line, are plotted against temperature in Fig. 3; also included are the various phases of the ammonium salts and their transition temperatures. Second moments ΔH_2^2, obtained from some of the better observed derivatives, are plotted against temperature in Fig. 4. With the exception of the room temperature and liquid nitrogen temperature data, the points in Figs. 3 and 4 usually represent single observations. The line widths and second moments given in Table I for those two temperatures are averages of at least three different plotted line shapes. Ammonium fluoride is not included in this report as its structure differs significantly from that of the other halides.

a. Low Temperature Line Shapes and the N−H Distance in the Ammonium Ion

Figure 4 shows that the second moments in the chloride, and probably the bromide as well, have reached limiting values at −195°C. These values no doubt correspond to "rigid lattices" and can be used to evaluate the N−H distance in the ammonium ion. Van Vleck's theoretical result[17] for the second moment may be written for the proton resonance in the ammonium halides as[1]

$$\Delta H_2^2 = (9/32)g^2\beta^2\{\sum_{j<j'}(3\cos^2\theta_{jj'}-1)^2 r_{jj'}^{-6} + (1/2)\sum_{j,k}(3\cos^2\theta_{jk}-1)^2 r_{jk}^{-6}\} + (1/12)I_f(I_f+1)g_f^2\beta^2\sum_{j,f}(3\cos^2\theta_{jf}-1)^2 r_{jf}^{-6}; \quad (1)$$

g is the proton gyromagnetic ratio; β is the nuclear magneton; the indices j and j' refer to the four protons

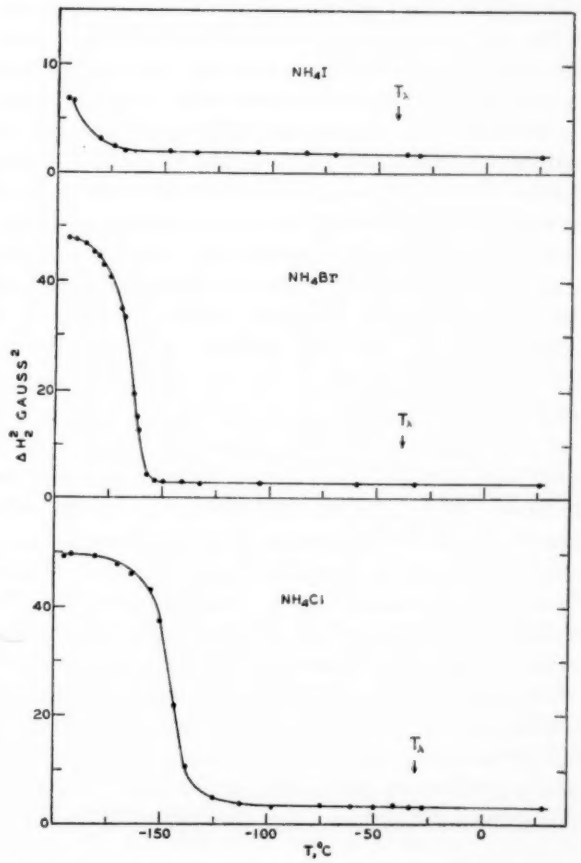

FIG. 4. Second moments of the proton magnetic resonance absorption in the ammonium halide powders plotted against temperature.

[17] J. H. Van Vleck, Phys. Rev. **74**, 1168 (1948).

TABLE I. Proton absorption line widths and second moments observed for the ammonium halide powders at −195°C and 25°C.

Compound	Line width, δH 25°C	Line width, δH −195°C	Second moment, ΔH_2^2 25°C	Second moment, ΔH_2^2 −195°C	N−H distance
NH_4Cl	4.8 gauss	23.4 gauss	3.35±0.05 gauss^2	49.5±0.5 gauss^2	1.038±0.004A
NH_4Br	4.6	23.7	2.70±0.03	48.0±0.5	1.031±0.004
NH_4I	3.8	5.9	1.55±0.02	6.85±0.2	

in a given NH_4^+, k to all other protons and f to all other magnetic nuclei in the sample; r_{jk} is an internuclear distance and θ_{jk} is the angle between $\mathbf{r}_{jk}$ and the applied magnetic field. If the crystal structure is known except for the N−H distance r, Eq. (1) is essentially a one-parameter equation, and r can be computed from it and the observed second moment. In the earlier calculation[1] two factors were neglected: (a) the possible broadening of the experimental absorption line by the field modulation; and (b) the effect of zero-point torsional vibrations of the ammonium ion in the calculation of the theoretical second moment. It turns out that the two effects nearly cancel, giving corrected values for the N−H distance agreeing with the original results.[1]

Relatively large modulation amplitudes were used initially. Perlman and Bloom[18] showed by an approximate method that this introduces an appreciable error in the second moments. Andrew[19] has given a direct calculation of the effect, obtaining the true second moment by subtracting $h_m^2/4$ from the observed, while the Perlman and Bloom correction is $h_m^2/3$. h_m is the modulation amplitude, i.e., one-half the values shown in Figs. 1 and 2. An experimental check was made of the correction by plotting the room temperature proton resonance in ammonium bromide as a function of modulation amplitude, at amplitudes less than the line width. The resultant second moments, which are averages of several plots at the two smallest modulations, are plotted against h_m in Fig. 5, and, for comparison, curves are given corresponding to $h_m^2/4$ and $h_m^2/3$. It is seen that the data are in better agreement with the $h_m^2/4$ correction term. It is of interest to note that the line width δH was 4.6 gauss independent of h_m, even at the maximum $2h_m$ of 3.35 gauss. The second moments reported here and in the following article as well have either been corrected for the modulation or else the modulation amplitude was small enough that the correction is well within the other experimental errors.

The correction for the zero-point torsional vibration is obtained by averaging the angular dependence in Eq. (1) over the motion, instead of assuming a completely rigid lattice and averaging only over the random crystalline orientations. By the spherical harmonic addition theorem, we can write

$$\langle 3\cos^2\theta_{jk}-1\rangle_{\text{torsional motion}} = (3\cos^2\theta_{jk}{}^0-1)\langle\tfrac{1}{2}(3\cos^2\theta-1)\rangle, \quad (2)$$

where $\theta_{jk}{}^0$ is the equilibrium value of θ_{jk} and θ is the angle between $\mathbf{r}_{jk}$ and its equilibrium position. θ is appreciable only for the intra-NH_4^+ interactions; and as the ammonium ion behaves like an isotropic oscillator (see Sec. 3d), we find

$$\langle\tfrac{1}{2}(3\cos^2\theta-1)\rangle = \langle 1-\tfrac{3}{2}\theta^2+\cdots\rangle = 1-\frac{3h}{8\pi^2 cI\nu}, \quad (3)$$

where I is the moment of inertia of the ion and ν is the torsional frequency in cm^{-1}. The correction factor $(1-\epsilon)$ is the square of Eq. (3) and introducing it into Eq. (1), averaging over the crystal powder and simplifying, there results

$$\Delta H_2^2 = \left\{\frac{5832}{81\,920}g^2+\frac{8}{15}g_N^2\right\}\beta^2 r^{-6}(1-\epsilon) + \frac{9}{80}g^2\beta^2\sum_{j,k}r_{jk}^{-6}+\frac{1}{15}I_f(I_f+1)g_f^2\beta^2\sum_{j,f}r_{jf}^{-6}. \quad (4)$$

The first term is the intra-NH_4^+ broadening; the second gives the interactions between protons in neighboring

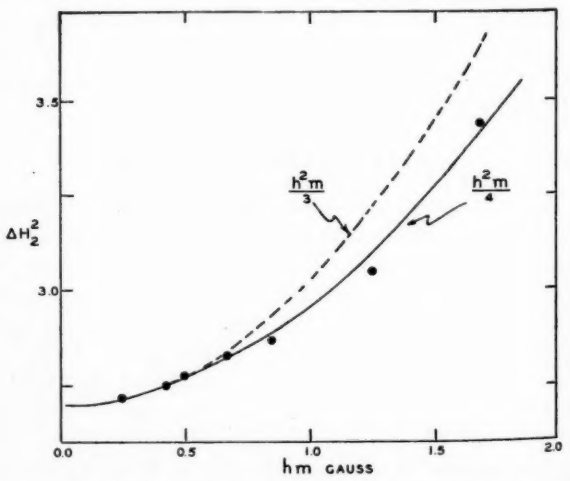

FIG. 5. The second moment of the proton magnetic resonance absorption in NH_4Br powder at room temperature plotted against modulation amplitude h_m. The limiting value at zero modulation is 2.70 gauss^2. The solid and dotted lines are theoretical values obtained by adding $h_m^2/4$ and $h_m^2/3$, respectively, to 2.70.

[18] M. M. Perlman and M. Bloom, Phys. Rev. **88**, 1290 (1952). We wish to thank Mr. Bloom who, prior to publication of their results, pointed out to us the importance of this correction in our original data.

[19] E. R. Andrew, Phys. Rev. **91**, 425 (1953).

NH_4^+, and the last represents the effects of the halogen and nitrogen nuclei external to the given NH_4^+.

For NH_4Cl, the second term in Eq. (4) was found to be approximately 6.5 gauss[2] by calculating correctly the interactions of an NH_4^+ with its thirty two nearest neighbors and replacing the remaining ions by points on a simple cubic lattice. The NH_4^+ ions were assumed ordered *a–a–a–a*; an ordering *a–b–a–b*; where *b* is the inverted configuration of *a*, would give values about 5 percent higher. The results depend on *r*, which was taken to be 1.04A, and on the size of the CsCl-type unit cell, which has been reported[20] to be 3.820A at −195°C. The last term in Eq. (4) is 0.1 gauss[2] for NH_4Cl, determined by computing the actual distances to the nearest eight chlorine and six nitrogen nuclei, replacing the remaining nuclei by points on CsCl and simple cubic lattices, respectively, and using partial summations readily obtained from the total summations given elsewhere.[21] The torsional oscillation frequency of NH_4^+ has been reported[6] to be 390 cm^{-1} in the chloride. With an *r* of 1.04A, the moment of inertia of NH_4^+ is 4.826×10^{-40} g cm^2. These values in Eq. (3) give 0.913 for $(1-\epsilon)$. As a final result, the observed second moment of 49.5±0.5 gauss[2] leads to a value of 1.038±0.004A for the N−H distance.

For NH_4Br, the calculation of the inter-NH_4^+ broadening is complicated by the tetragonal structure[9] at low temperatures. However, the distortion from a CsCl structure is slight, and the distances are such that only small errors are introduced by assuming the CsCl structure, for which the arithmetic is much simpler. A CsCl lattice constant of 4.11A was adopted, the average of $c+a/(2)^{\frac{1}{2}}$ as reported[9] for −145°C. The ordering of the NH_4^+ ions appears[9] to be such that they are parallel along a given *c* axis of the tetragonal structure, with those along adjacent axes oppositely oriented. This corresponds to an ordering *a–b–a–b* in the CsCl lattice used. The large lattice constant for NH_4Br permitted the proton-proton distance summations to be approximated by points on a simple cubic lattice after calculations to the six nearest NH_4^+. Otherwise the computations were analogous to those for NH_4Cl. The inter-NH_4^+ broadening was found[22] to be 3.9 gauss[2] and the broadening by bromine and nitrogen nuclei outside the given NH_4^+, 0.4 gauss.[2] The NH_4^+ torsional frequency is reported[6] as 319 cm^{-1}, giving a value for $(1-\epsilon)$ of 0.894. Combining these results with the observed second moment of 48.0±0.5 gauss[2] yields a value of 1.031±0.004 for the N−H distance.

The 1.038±0.004A value for the N−H distance in NH_4Cl powder is within experimental error of the values 1.031±0.007A and 1.033±0.004A from the (1,0,0) and (1,1,0) single crystal orientations.[4] The 1.031±0.004A value from NH_4Br powder appears to be identical with those from NH_4Cl. These proton magnetic resonance values are to be compared with the neutron diffraction results[9] of 1.03±0.02A for both ND_4Cl and NH_4Cl and for ND_4Br. Bernal[23] has implied that a change in environment of the NH_4^+ ions might produce a change in bond length. However, any such effect is small, even in NH_4Br where the tetragonal structure suggests the importance of Br^--proton attractions.

b. Resonance Absorption at Temperatures Above the Line-Width Transitions

The relatively narrow absorption lines shown in Fig. 2 persist without significant change from the line-width transitions in the neighborhood of −150°C to room temperature and higher. If the motions of the NH_4^+ ions associated with the line-width transition were restricted to reorientations about a single specific axis, such as a C_2 or C_3 symmetry axis, the intra-NH_4^+ broadening would still be an appreciable fraction[2] of the "rigid-lattice" value. Moreover, for the NH_4Cl single crystal[4] the angular dependence and magnitude of the room temperature second moments are given satisfactorily by a model in which the intra-NH_4^+ broadening is averaged to zero by reorientations effectively about all three of the C_2 axes. The observed line broadening is mainly from inter-NH_4^+ interactions which are reduced only partially by the reorientations, with a small contribution from proton-halogen interactions. This model predicts a value of about 3.40 gauss[2] for NH_4Cl powder, with disordered orientations of the NH_4^+ ions; the observed second moment is 3.35±0.05 gauss[2].

A similar model also appears reasonable for NH_4Br and NH_4I. The distance between NH_4^+ ions is large compared to the N−H distance so the numerical values for NH_4Cl given in Eq. (8) and Table VIII of the following article[4] should yield good approximations for the other halides simply by using their unit cell dimensions. In this manner the inter-NH_4^+ broadening from NH_4Br with a unit cell[9] of 4.060A is 2.50 gauss[2]. The observed room temperature second moment is 2.69±0.05 gauss[2] which compares very well with the calculated value when consideration is given to the proton-bromine broadening of 0.4 gauss[2] in the rigid lattice. The case of NH_4I is somewhat different in that the CsCl phase is stable only between −17.6 and −41.6°C, with a unit cell of[24] 4.37A. Using the same procedure as for NH_4Br, an inter-NH_4^+ broadening of 1.58 gauss[2] was estimated. This is to be compared with a second moment of 1.75 ±0.05 gauss[2] observed at −35°C, with allowance for proton-iodine broadening which is about 0.5 gauss[2] in the rigid lattice.

Once the intra-NH_4^+ broadening disappears, the

[20] L. Vegard and S. Hillesund, Anhandl. Norske Videnskaps-Akad. Oslo. I. Mat-Naturv. Kl. No. 8 (1942); Chem. Zentr. **I**, 930 (1943).

[21] H. S. Gutowsky and B. R. McGarvey, J. Phys. Chem. **20**, 1472 (1952).

[22] These values are somewhat smaller than those given in I, which were based on a smaller lattice constant 4.03A.

[23] M. J. M. Bernal, Proc. Phys. Soc. (London) **A66**, 514 (1953).

[24] A. Smits and D. Tollenaar, Z. physik. Chem. **B52**, 222 (1942).

theoretical second moments for the crystal powders are insensitive to the state of motion or ordering of the NH_4^+ ions; and even in a single crystal the angular dependence of the line shape is only slightly different for spherical rotation, and for disordered and ordered reorientations.[4] In agreement with this prediction, the second moments observed for NH_4Cl powder are constant[25] between 3.35 and 3.40 gauss^2 from room temperature to above 150°C. However, NH_4Cl undergoes a phase transition from a CsCl to a NaCl lattice at 184.3°C, and about this temperature the second moment is definitely smaller, for instance, 2.75 gauss^2 at 186.5°C. Detailed calculations were not made for the NaCl lattice, but the observed decrease is qualitatively consistent with the change in lattice structure and dimensions. In the case of NH_4I, the transition between the CsCl and NaCl structures occurs at −17.6°C. The second moment in the NaCl phase at room temperature is 1.55 gauss^2 which is also smaller than the value found in the CsCl phase, 1.75 gauss^2 at −35°C. Cooke and Drain[15] have mentioned a line width change from 4.5 to 5.8 gauss at −17.6°C, which we did not observe although the second moment changed as indicated. However, there is some possibility that the NaCl phase supercooled in our experiments.

From these results we conclude that the intra-NH_4^+ interactions become averaged out during the line-width transition and remain so at higher temperatures. This requires that the reorientations of the NH_4^+ ions, at temperatures above the line-width transitions, do not remain correlated with any specific axis of rotation for times greater than about 10^{-4} sec. Accordingly, some modification is required in the model postulating[26] one dimensional rotation of the NH_4^+ ions in the NaCl phase of NH_4I, on the basis of the infrared spectrum. Rotation of the NH_4^+ ion can occur about one of its C_3 axes, but there must be interchange in the orientation of the axis about which the rotation occurs. The relatively low interchange frequency required would not affect the infrared spectrum or heat capacity. Three models for the NaCl phase of ND_4Br and ND_4I were found satisfactory by Levy and Peterson[9] in their neutron diffraction studies; of these the single approach model appears to be the only one consistent with all the available evidence.

TABLE II. Frequency factors and activation energies for reorientations of the NH_4^+ ion.

Compound	T_1 measurements[a] $(\tau_c)_0$	E	Line-width transitions T_t[b]	E
NH_4Cl	2.6×10^{-14} sec	4740 cal	−144.1°C	4740[c] cal
NH_4Br	2.0×10^{-13}	3280	−170.6	3340
NH_4I	1.3×10^{-13}	2900	−198.1[d]	2550

[a] These values are from Sachs, reference 13; $\nu_0=1/2\pi(\tau_c)_0$.
[b] At this temperature the line width is half way between the limiting values.
[c] Assumed in calculating E values for NH_4Br and NH_4I.
[d] This value was extrapolated by assuming the line-width transition for NH_4I to be of the same general shape as for NH_4Cl and NH_4Br.

[25] In addition to the main resonance, with a width of 4.8 gauss, several samples exhibited a narrow central line gradually increasing in intensity at temperatures above about 50°C; the sharp line was found to originate in adsorbed moisture which could catalyze narrowing by self-diffusion.
[26] R. C. Plumb and D. F. Hornig, J. Chem. Phys. **21**, 366 (1952).

c. The Line-Width Transitions

The narrowing of the absorption line depends upon the correlation frequency ν_c, the average reorientation rate of the NH_4^+ ions. In the case of a change from a broad line to a narrower line,[2] the frequency width of the line $\delta\nu$ is given as a function of ν_c by the equation

$$(\delta\nu)^2=B^2+C^2(2/\pi)\tan^{-1}[\alpha(\delta\nu/\nu_c)]; \qquad (5)$$

where B is the width of the narrow line, $(B^2+C^2)^{\frac{1}{2}}$ is the width of the broad line, and α is a parameter depending upon the line shape with the value unity for a Gaussian shape. The reorientations are presumably thermally activated so the variation with temperature of ν_c is of the form

$$\nu_c=\nu_0 e^{-E/RT}, \qquad (6)$$

which when combined with Eq. (5) should describe the line-width transition. In principle Eqs. (5) and (6) can be combined with the observed line widths to compute E, the activation energy required for reorientation, and ν_0, the frequency factor. However, α is also unknown, complicating the analysis, so a simpler approach is followed.

It is physically reasonable that the NH_4^+ reorientations should be the most effective spin-lattice relaxation process. Sachs[13] and also Cooke and Drain[15] have observed the temperature dependence of the spin-lattice relaxation time T_1 and thereby evaluated E in the different ammonium halides, and also ν_0. The results are summarized in Table II. These E and ν_0 values can be used to compute ν_c values in Eq. (6), and the results, substituted in Eq. (5), should reproduce the line-width transition. The line shape parameter α was evaluated by fitting Eq. (6) to the T, $\delta\nu$, and ν_c values at the center of the transition, giving 4.88 and 10.4 for NH_4Cl and NH_4Br, respectively. In this manner, the lines drawn in Fig. 3 were computed for these compounds. The fit is generally quite good; the deviations for NH_4Br at the ends of the transition are outside experimental error. However, the line shapes change during the transition, (compare Figs. 1 and 2), and this may change α from the assumed constant value. In view of this uncertainty the agreement is as good as one might expect and is surely adequate to demonstrate that the NH_4^+ reorientations determine T_1, as well as the line widths in the transition region.

Wert and Marx[27] have described a procedure which can be adapted to give activation energies for reorientation from the line-width transition temperatures T_t. The correlation frequencies ν_c should be very nearly the same at the line width transition in the different

[27] C. Wert and J. Marx, Acta Metallurgica **1**, 113 (1953).

halides, and also the frequency factors ν_0 are only slightly different. Accordingly, Eq. (6) may be written as $E=AT_t$ where the constant A equals $R\ln(\nu_0/\nu)$ and can be evaluated from a known E and T_t. The E value for NH_4Cl of 4740 cal mole^{-1}, from T_1 data, combined with the observed T_t of 129°K, gives a value for A of 36.8 cal deg^{-1}. On this basis the transition temperatures of 102.5 and 75°K for NH_4Br and NH_4I give activation energies of 3340 and 2550 calories. Small corrections have been made for the differences in ν_0, using the T_1 results; if the infrared torsional frequencies are used for ν_0, the results are not affected significantly. The value for NH_4I from the transition temperature is a bit lower than the 2900 calories obtained by Sachs from T_1; however, Cooke and Drain suggest from their T_1 data an approximate, lower value of 1700 to 2200 calories.

The two interpretations given above depend more or less upon the T_1 results. A completely independent evaluation of E could be based upon the second moments observed as a function of temperature, which would eliminate the uncertainties associated with the line shape parameter α. This is touched upon indirectly in a discussion given in the following paper.[4]

d. The Motion of the Ammonium Ion

The experimental evidence presented and reviewed above demonstrates the existence of hindered rotational motion of the ammonium ions. In this section a phenomenological treatment is given which clarifies the nature of the rotational motion.

A phenomenological potential for the ammonium ion can be obtained following a method of Nagamiya.[28] The ammonium ion is assumed electrically to be a system of four point charges of $+e/4$ at the vertices of a rigid, regular tetrahedron. The potential energy of each proton, at a point (x_i,y_i,z_i) in a CsCl-type lattice, with respect to all charges outside of its own ion, is

$$V=\frac{1}{d}\left\{c_0+c_4\left(\frac{r}{d}\right)^4\left(\frac{x_i^4+y_i^4+z_i^4}{4}-\frac{3}{5}\right)+\cdots\right\}, \quad (7)$$

where d is the unit cell size and r is the N−H distance, taken to be 1.04A. The first term is very much larger than the second, but the second has an angular dependence which is the chief hindrance to rotation of the ammonium ion. Therefore, a suitable potential for the rotation is

$$V=\frac{V_0}{2}\sum_{i=1}^{4}\left(\frac{x_i^4+y_i^4+z_i^4}{r^4}-\frac{3}{5}\right). \quad (8)$$

For the specific model of the ion proposed above

$$V_0=\frac{35}{36}\left(\frac{e}{4}\right)^2\sum_j\frac{(\pm1)}{r_j^5}=46.8\left(\frac{e}{4}\right)^2\frac{r^4}{d^5}, \quad (9)$$

where r_j is the distance from a given nitrogen nucleus to a chloride ion or another nitrogen nucleus, the sign being + or − respectively. Values of V_0 computed with Eq. (9) for the different halides are given in Table III.

TABLE III. Potential barriers to rotation of the NH_4^+ ion in the ammonium halides (CsCl modification), evaluated by an electrostatic calculation.

Compound	ν(obs[a])	V_0 (Eq. 9)	V_0 (Eq. 14)[a]	E_0[b]
NH_4Cl	390 cm^{-1}	5400 cal	5250 cal	6410 cal
NH_4Br	319	3730	4180	4645
NH_4I	279	2910	2850	4100

[a] These values are obtained from the observed torsional frequencies ν, while the V_0 (Eq. 9) results are entirely from an electrostatic calculation.
[b] $E_0=E$ (from T_1 in Table II) $+(3/2)h\nu_{obs}$.

The potential in Eq. (8) is more general than the particular model used in obtaining Eq. (9). To demonstrate this generality the summation in Eq. (8) is carried out by introducing new coordinates. An x', y', z' system is fixed in the ion such that at equilibrium the z' axis coincides with the z cubic axis, but the x', y' axes are rotated by $\pi/4$ with respect to the x, y cubic axes. θ, ϕ are the polar coordinates of the z' axis and ψ measures rotation of the ion about the z' axis. In terms of these angular coordinates Eq. (8) becomes

$$\begin{aligned}V=\tfrac{1}{2}V_0\{&-(49/8)\cos^4\theta+(21/4)\cos^2\theta-(21/40)\\&+(7/8)\sin^4\theta\,(\cos4\psi-\cos4\phi)\\&+(\cos^2\theta+\tfrac{1}{8}\sin^4\theta)\cos4\phi\cos4\psi\\&-\tfrac{1}{2}(\cos\theta+\cos^3\theta)\sin4\phi\sin4\psi\}.\end{aligned} \quad (10)$$

This is the simplest nontrivial potential having the cubic symmetry of the lattice and the tetrahedral symmetry of the ion. The general solution of the Schrödinger equation for a spherical top moving in such a potential is formidable and we confine ourselves to the limit of small oscillations.[29]

For small, commuting rotations we can choose as coordinates

$$\begin{aligned}\xi&=\theta\cos\phi\\\eta&=\theta\sin\phi\\\zeta&=\phi+\psi+\pi/4,\end{aligned} \quad (11)$$

the angles of rotation about the cubic x, y, z axes. Developing the potential energy in a power series of small rotations about the equilibrium position, we obtain

$$V\cong\frac{V_0}{2}\left\{-\frac{12}{5}+8(\xi^2+\eta^2+\zeta^2)-\frac{32}{3}(\xi^4+\eta^4+\zeta^4)-8(\xi^2\eta^2+\xi^2\zeta^2+\eta^2\zeta^2)+\cdots\right\}. \quad (12)$$

Using first-order perturbation theory the energy levels

[28] T. Nagamiya, Proc. Phys. Math. Soc. Japan 24, 137 (1952).

[29] In so doing we give up the possibility of calculating tunnelling frequencies.

of this anharmonic isotropic oscillator are computed to be

$$E_{n_1n_2n_3}=-\frac{6}{5}V_0+(n_1+n_2+n_3+3/2)\hbar\omega$$
$$-\frac{1}{16}[\sum_{i=1}^{3}(2n_i^2+3n_i+5/4)$$
$$+n_1n_2+n_1n_3+n_2n_3](\hbar\omega)^2/V_0, \quad (13)$$

where $\hbar\omega=(16V_0(\hbar^2/2I))^{\frac{1}{2}}$ and I is the moment of inertia of the ammonium ion. If ν is the observed torsional frequency, i.e., $h\nu=E_{100}-E_{000}$, then from the energy levels we deduce that

$$V_0=\frac{1}{16}\frac{(h\nu+5\hbar^2/2I)^2}{\hbar^2/2I}. \quad (14)$$

The experimental torsional frequencies, from spectral data, are listed in Table III with the corresponding V_0 values calculated using Eq. (14). These experiment based V_0 values agree well with those determined by Eq. (9). So the simple model used in the electrostatic calculation of Eq. (9) gives reasonable results, supporting Pauling's view[30] that the charge on a polyatomic ion is distributed on the surface of the ion.

We turn now to the essential meaning of V_0. If an NH_4^+ ion rotates from one equilibrium configuration to another around a fourfold cubic axis it passes over a barrier of total height V_0. On the other hand, if an ion rotates around a threefold cubic axis (with one proton fixed) the barrier is (16/9) V_0, as may be seen from Eq. (8). The activation energy E, as given by the T_1 and line-width transition analyses, corresponds to the energy, above the ground state, of the NH_4^+ ions in their reorientations. If the values of E are corrected by adding the zero point torsional energy of the ground state, the total barrier height E_0 is obtained. These experimentally inferred values are listed in Table III; they are larger than V_0 but less than (16/9) V_0 and thus are between the barriers for rotation about a cubic fourfold axis and a cubic threefold axis. Therefore, the motion of the ion which is most important in relaxing the proton spins and in narrowing the absorption line is a motion which classically is partially free and partially hindered. This type of motion accounts for the averaging completely to zero of the intra-NH_4^+ contribution to the line width. Moreover, the experimental values of ν_0 given in Table II are the right order of magnitude for classical rotation frequencies of the ions.

[30] L. Pauling, J. chim. phys. **45**, 142 (1948).

e. The Order-Disorder Process

The preceding results and conclusions emphasize the dynamic nature implicit in the order-disorder process at T_λ, as was pointed out some time ago by Purcell.[13] Even at low temperatures in the ordered phase the ammonium ions experience occasional random reorientations, but return to the stable, ordered configuration. As the temperature is increased, the rate of the reorientations and the fraction of ions reorienting at a given instant increase. The slightly lower energy of the ordered phase results[28] mainly from the electrostatic interactions of neighboring NH_4^+ ions. When too large a fraction of the NH_4^+ ions are in motion, the coherency of these electrostatic interactions and the return of the ions to the ordered configuration break down, producing a cooperative order-disorder process. The over-all motions of the ions are not modified appreciably by the degree of order primarily because a reorienting ion is in a highly excited energy level, while the order-disorder energy is small, i.e., $RT_\lambda \ll E$.

Proton Magnetic Resonance in an Ammonium Chloride Single Crystal*†

R. BERSOHN, *Department of Chemistry, Cornell University, Ithaca, New York*

AND

H. S. GUTOWSKY, *Noyes Chemical Laboratory, University of Illinois, Urbana, Illinois*

(Received November 18, 1953)

The nuclear resonance absorption spectrum has been calculated theoretically for a tetrahedral 4-spin system, with I of $\frac{1}{2}$, for orientations in which the external magnetic field coincides with a two- or three-fold symmetry axis of the tetrahedron or with a tetrahedral edge. Comparison of the theoretical results with the proton resonance observed at −195°C in a single crystal of ammonium chloride demonstrates that the NH_4^+ ion is oriented with the N−H bonds pointed essentially towards corners of the unit cube. An N−H distance of 1.032±0.005A is determined from the low-temperature second moments of the resonance line with the applied magnetic field in the (1,0,0) and (1,1,0) directions. At room temperature, the anisotropy of the resonance results from inter $-NH_4^+$ interactions, with intra $-NH_4^+$ interactions averaged to zero by hindered rotational motions; free rotation of the ammonium ions does not occur. A small *decrease* with temperature of the second moment of the resonance line at the λ-point agrees with the order-disorder model for the transition. The motion of the NH_4^+ ion is discussed.

1. INTRODUCTION

THE preceeding article[1] gives the results of some proton magnetic resonance absorption experiments on ammonium halide crystal powders. However, the data obtained from a crystal powder consist of a single line shape and its second moment. Accordingly, more than one structural parameter can seldom be evaluated from the powder data, in this case the N−H distance in the ammonium ion. But, if a single crystal is available (about 1 cm³), the angular dependence of the resonance absorption provides additional data which permit a much more detailed analysis of the structure of the sample and of the nuclear magnetic dipole interactions themselves. This is exemplified by Pake's study[2] of a gypsum single crystal, and also by some recent research on $K_2HgCl_4 \cdot H_2O$ and $K_2SnCl_4 \cdot H_2O$ single crystals.[3]

In the case of the ammonium halides, the experiments by Soutif[4] and this work are apparently the only magnetic resonance experiments in which single crystals were used. The present work, believed to be more comprehensive than that of Soutif, leads to the following main results: (a) the orientation and size of the NH_4^+ ion are determined with results in complete agreement with those obtained from neutron diffraction;[5] (b) at temperatures for which the line breadth has reached its narrow value, the remaining breadth is due exclusively to interionic broadening. The first conclusion is based upon a theoretical calculation of the absorption spectrum for the tetrahedral 4-proton system in the ammonium ion and a comparison with the low temperature line shapes and second moments. The second conclusion is obtained by using Van Vleck's procedure[6] to calculate the second moments for several models and comparing the results with the anisotropy observed in the room temperature resonance.

Relatively little direct information is obtained on the order-disorder transition itself.[7] Firstly, an ion in a disordered position differs from an ion in an ordered position only by an inversion; a "disordered" ion therefore has the same discrete spectrum as an "ordered" ion. Secondly, the small interionic interactions are not very sensitive to the degree of order.

2. EXPERIMENTAL METHOD AND RESULTS

The general experimental procedure was identical with that described or referred to in the preceding article. The single crystal on which the reported measurements were made was rectangular in shape, 14 by 14 by 7 mm; it was supplied by Dr. H. A. Levy and Dr. S. W. Peterson. Some preliminary experiments were performed, with similar results, on a smaller crystal very kindly supplied by Mr. Meyer Bloom. The crystal was oriented visually in the applied magnetic field; line shapes were then plotted at several small angular displacements to ascertain the orientation giving the maximum or minimum line width, and this orientation was undisburbed in the record runs. The crystal shape caused some difficulty in orienting the applied magnetic field in the (1,1,1) direction; it was primarily for this reason that line shapes were not obtained as a function of temperature for this orientation, particularly as the other two orientations gave data sufficient for the present purposes.

The observed derivatives of the proton absorption line are given in Figs. 1 and 2 for the applied magnetic

* Assisted by the U. S. Office of Naval Research.

† Presented in part at the Washington Meeting of the American Physical Society, May, 1952; R. Bersohn, Phys. Rev. **87**, 226(A) (1952).

[1] Gutowsky, Pake, and Bersohn, J. Phys. Chem. **22**, 643 (1954).

[2] G. E. Pake, J. Chem. Phys. **16**, 327 (1948).

[3] Itoh, Kusaka, Yamagata, Kiriyama, and Ibamoto, J. Phys. Soc. Japan **8**, 293 (1953).

[4] M. Soutif, Rev. sci. **89**, 203 (1951).

[5] H. A. Levy and S. W. Peterson, Phys. Rev. **86**, 766 (1952); J. Am. Chem. Soc. **75**, 1536 (1953).

[6] J. H. Van Vleck, Phys. Rev. **74**, 1168 (1948).

[7] An erroneous statement to the contrary was made by one of us (R.B.) in the first reference (†) cited.

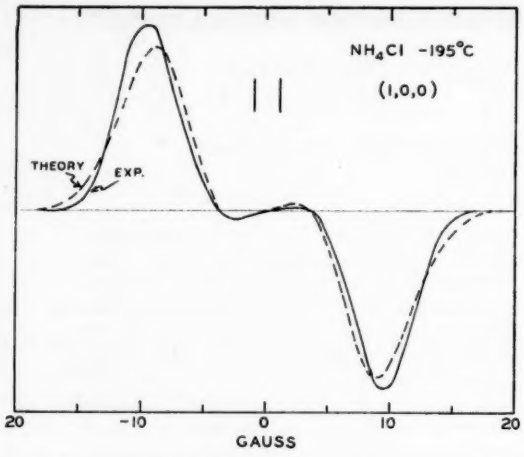

FIG. 1. Derivative of the proton magnetic resonance absorption line in a single crystal of ammonium chloride at −195°C with the magnetic field applied in the (1,0,0) direction. The dashed line is the result of a theoretical calculation described in the text. The vertical pair of lines represents the field modulation.

field in the (1,0,0) and (1,1,0) orientations, respectively, at −195°C, and in Fig. 3 for the (1,0,0), (1,1,0), and (1,1,1) orientations at room temperature. The dashed lines in Figs. 1 and 2 are theoretical line shapes; the details of the comparison are discussed later. The experimental data in Figs. 1 to 3 have been replotted; a direct reproduction of an original recording for the (1,1,0) orientation at −160°C has been given in the article[8] describing the instrumentation. The line widths, defined as the separation in gauss of the maximum and minimum of the derivative, are plotted in Fig. 4 as a function of temperature for the (1,0,0) and (1,1,0) orientations. A similar plot of the second moments, computed numerically from some of the better line

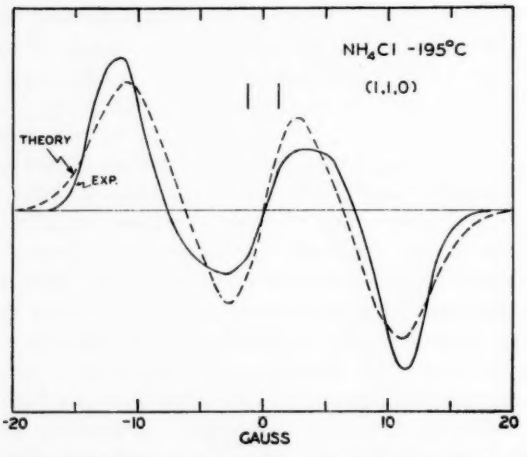

FIG. 2. Derivative of the proton magnetic resonance absorption line in a single crystal of ammonium chloride at −195°C with the magnetic field applied in the (1,1,0) direction. The dashed line is the result of a theoretical calculation described in the text. The vertical pair of lines represents the field modulation.

[8] Gutowsky, Meyer, and McClure, Rev. Sci. Instr. **24**, 644 (1953).

shapes, is given in Fig. 5. Table I gives values of the line widths and second moments observed at −195°C, room temperature, and just above and below the λ point, for various orientations of the crystal with respect to the applied magnetic field. These values are averages of at least three separate observations; the experimental errors are discussed in the preceeding article.[1]

3. THEORETICAL COMPUTATION OF THE SPECTRUM OF THE FOUR PROTON SYSTEM

(a) Introduction

The most striking confirmation of the assumed orientation[1] of the ammonium ions comes from examination of the actual line shape. A discrete spectrum for a system of four protons is calculated. The smaller inter-

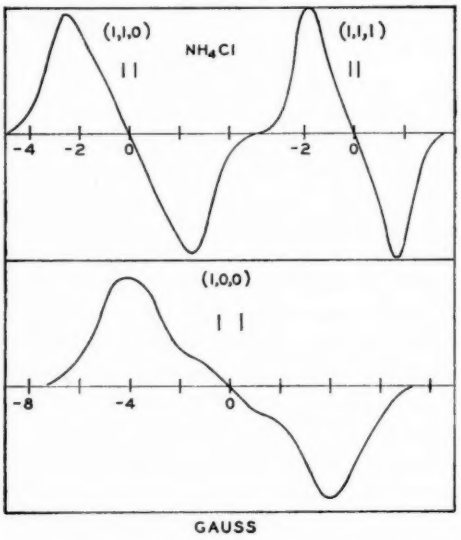

FIG. 3. Derivatives of the proton magnetic resonance absorption line in a single crystal of ammonium chloride at room temperature with the magnetic field applied in the (1,0,0), (1,1,0), and (1,1,1) directions. The vertical pairs of lines represent the field modulation.

actions with other neighboring nuclei are then introduced approximately by smearing the discrete lines so that the second moment agrees with experiment. This procedure is in the spirit of Pake's[2] and Andrew's[9] work on the two- and three-proton systems. Although the resulting line has structure, unlike the two-proton system the structure is unresolved and has qualitative rather than quantitative significance; one cannot use a separation between peaks as a measure of an internuclear distance.

The magnetic Hamiltonian for the four-proton system is

$$\mathcal{H}=-\sum_{i=1}^{4} g\beta H I_{zi}+\sum_{i<j} A_{ij}(\mathbf{I}_i\cdot\mathbf{I}_j-3I_{iz}I_{jz}), \qquad (1)$$

where

$$A_{ij}=g^2\beta^2 r_{ij}^{-3}[(3/2)\cos^2\theta_{ij}-\tfrac{1}{2}],$$

[9] E. R. Andrew and R. Bersohn, J. Chem. Phys. **18**, 159 (1950).

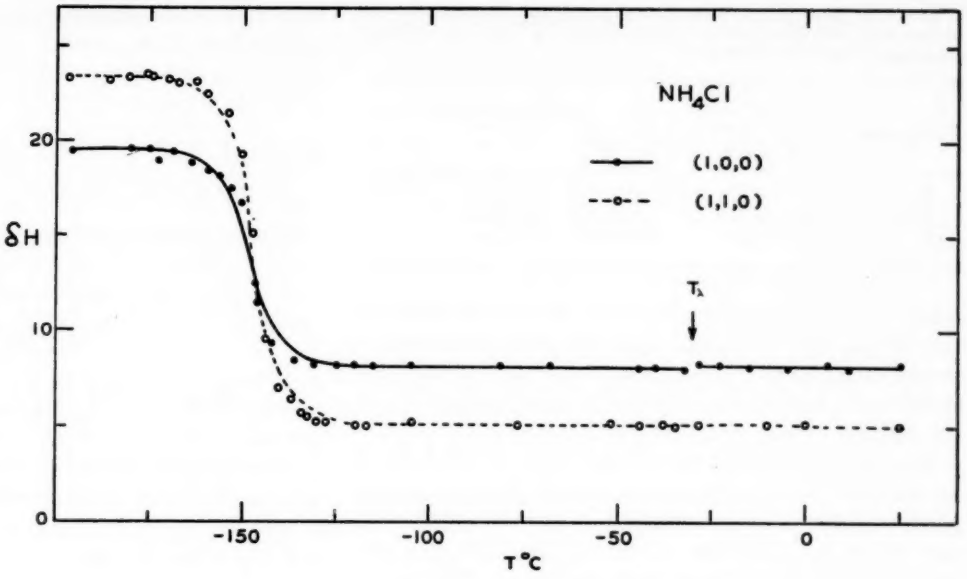

FIG. 4. The width of the proton magnetic resonance absorption line in a single crystal of ammonium chloride as a function of temperature with the magnetic field applied in the (1,0,0) and (1,1,0) directions.

and θ_{ij} is the angle between the field $\mathbf{H}$ and $\mathbf{r}_{ij}$, the vector connecting dipoles i and j; g is the proton gyromagnetic ratio and β the nuclear magneton.

Because we are interested only in transitions in which angular momentum components change by $\pm\hbar$, only that part of the dipole-dipole interaction has been included which commutes with the Zeeman energy. If M is the quantum number associated with the z component of the total angular momentum, we expect two singlets ($M=\pm 2$), two quartics ($M=\pm 1$), and a sextic ($M=0$). Actually the sextic will factor into two cubics if the states are labelled by I, the total angular momentum quantum number. For an arbitrary orientation of the external magnetic field no further factoring is possible.

(b) Conservation Conditions for Factoring the Secular Equation

For the purpose of seeing whether further factoring is possible, a representation is introduced which diagonalizes the squares of the operators

$$\mathbf{L}=\mathbf{I}_1+\mathbf{I}_2, \quad \mathbf{S}=\mathbf{I}_3+\mathbf{I}_4, \quad \text{and} \quad \mathbf{I}=\mathbf{L}+\mathbf{S}.$$

It is appropriate to introduce the quantum number I, because I^2 commutes with all terms of the form $\mathbf{I}_j\cdot\mathbf{I}_k$. The matrix elements for the general case are most easily calculated in an $M_1M_2M_3M_4$ representation which makes necessary the transformation (given in Table II) from the LSIM basis to the $M_1M_2M_3M_4$ basis.

Table III shows the matrix elements of the Hamil-

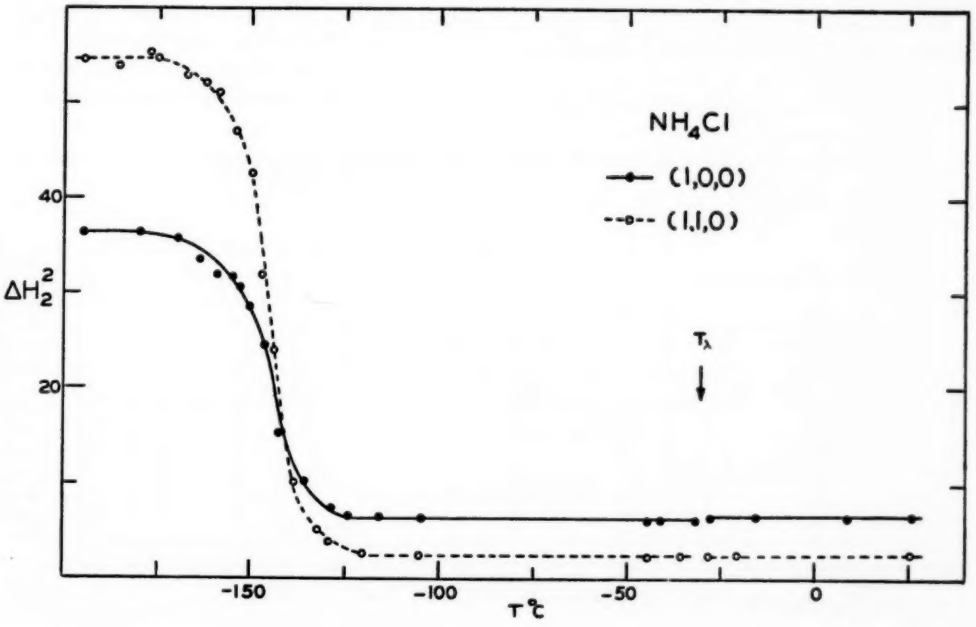

FIG. 5. The second moment of the proton magnetic resonance absorption line in a single crystal of ammonium chloride as a function of temperature with the magnetic field applied in the (1,0,0) and (1,1,0) directions.

TABLE I. Line widths and second moments observed for the proton magnetic resonance in a single crystal of NH_4Cl at different orientations and temperatures.

Temperature °C	Line width, δH in gauss (1,0,0)	(1,1,0)	(1,1,1)	Second moment, ΔH_2^2 in gauss^2 (1,0,0)	(1,1,0)	(1,1,1)
25	8.2	5.05	3.55	6.70±0.10	2.63±0.03	1.35±0.02
−28	8.3	5.10	...	6.62±0.15	2.64±0.05	...
−32 to −36	8.05	5.10	...	6.35±0.15	2.57±0.05	...
−195	19.5	23.3	...	36.5±0.7	54.6±0.6	...

tonian in the LSIM representation. Now a conservation law for any set of angular momenta will correspond to the factoring of the secular equations because they are cubic and quartic by virtue of the nonconservation of the angular momentum operator L^2, S^2, and I^2.

The Hamiltonian can be written down in the form of an operator which will commute with the square of a given angular momentum and an operator which will not commute. Sufficient conditions for factoring the secular equation will result from setting the latter operator equal to zero. For example we can write the interaction Hamiltonian in the form

$$\begin{aligned}\mathcal{H}=&A_{12}(\mathbf{I}_1\cdot\mathbf{I}_2-3I_{1z}I_{2z})+A_{34}(\mathbf{I}_3\cdot\mathbf{I}_4-3I_{3z}I_{4z})\\&+\tfrac{1}{2}(A_{13}+A_{23})[(\mathbf{I}_1+\mathbf{I}_2)\cdot\mathbf{I}_3-3(I_{1z}+I_{2z})I_{3z}]\\&+\tfrac{1}{2}(A_{14}+A_{24})[(\mathbf{I}_1+\mathbf{I}_2)\cdot\mathbf{I}_4-3(I_{1z}+I_{2z})I_{4z}].\\&+\tfrac{1}{2}(A_{13}-A_{23})[(\mathbf{I}_1-\mathbf{I}_2)\cdot\mathbf{I}_3-3(I_{1z}-I_{2z})I_{3z}]\\&+\tfrac{1}{2}(A_{14}-A_{24})[(\mathbf{I}_1-\mathbf{I}_2)\cdot\mathbf{I}_4-3(I_{1z}-I_{2z})I_{4z}]\end{aligned}\qquad(2)$$

When $A_{13}=A_{23}$ and $A_{14}=A_{24}$, the Hamiltonian will commute with L^2; and from Table III one can see that the cubics will factor and the quartic will factor into a cubic and a singlet. There are five other equivalent conditions corresponding to the six different ways of choosing a pair of angular momenta. If the tetrahedron is regular, these conditions correspond to having the magnetic filed in one of the six planes of symmetry.

If one asks that L^2 and S^2 be simultaneously conserved, we obtain as necessary conditions

$$A_{13}=A_{14}=A_{23}=A_{24},\qquad(3)$$

with two other equivalent conditions. For a regular tetrahedron, these conditions correspond to having the field along one of the three twofold axes or along one of the six edges. In this case we find

$$\begin{aligned}\mathcal{H}=&A_{12}(\mathbf{I}_1\cdot\mathbf{I}_2-3I_{1z}I_{2z})+A_{34}(\mathbf{I}_3\cdot\mathbf{I}_4-3I_{3z}I_{4z})\\&+A_{13}(\mathbf{I}_1+\mathbf{I}_2)\cdot(\mathbf{I}_3+\mathbf{I}_4)-3(I_{1z}+I_{2z})(I_{3z}+I_{4z}).\end{aligned}\qquad(4)$$

If $S^2=(I_1+I_2+I_3)^2$ is to be conserved, then we have

$$\begin{aligned}A_{12}&=A_{13}=A_{23}\\A_{14}&=A_{24}=A_{34},\end{aligned}\qquad(5)$$

with three other equivalent conditions corresponding to orientation of the field along one of the four threefold symmetry axes of a regular tetrahedron.

On inspecting Table III one sees that the conservation conditions in Eq. (3) result in the factoring of the secular equation into quadratics and singlets. Equation (5) is equally effective although it is not obvious in the LSIM representation.

(c) Spectra for Three Orientations of the Magnetic Field

(i) C_3 Orientation

For the C_3 orientation the proper representation is LSIM where $\mathbf{S}=\mathbf{L}+\mathbf{I}_3$. Tomita[10] analyzed the nuclear resonance spectrum of methane by an independent study of the four-spin system. His paper contains the wave functions and Hamiltonian matrix appropriate for the C_3 orientation. Tables IV and V give the energy levels and relative intensity of the ten-line spectrum; in these and subsequent tables, R is the length of the tetrahedral edge.

(ii) C_2 and Edge Orientations

At some expense of complexity in notation the C_2 and edge orientations of the external field can be treated together because they are both cases in which L^2 and S^2 are conserved [condition of Eq. (3)]. The

TABLE II. Transformation from LSIM basis to $M_1M_2M_3M_4$ basis. α_i and β_i are spin functions for an individual nucleus i.

	L	S	I											
ψ_1	1	1	2	1									$\alpha_1\alpha_2\alpha_3\alpha_4$	$M=2$
$2\psi_2$	1	1	2		1	1	1	1					$\beta_1\alpha_2\alpha_3\alpha_4$	
$2\psi_3$	1	1	1		−1	−1	1	1					$\alpha_1\beta_2\alpha_3\alpha_4$	$M=1$
$\sqrt{2}\psi_4$	1	0	1		0	0	−1	1					$\alpha_1\alpha_2\beta_3\alpha_4$	
$\sqrt{2}\psi_5$	0	1	1		−1	1	0	0					$\alpha_1\alpha_2\alpha_3\beta_4$	
$\sqrt{6}\psi_6$	1	1	2	=					1	1	1	1	$\beta_1\beta_2\alpha_3\alpha_4$	
$\sqrt{2}\psi_7$	1	1	1						1	0	0	0	$\alpha_1\beta_2\beta_3\alpha_4$	
$2\psi_8$	1	0	1						0	−1	−1	1	$\beta_1\alpha_2\beta_3\alpha_4$	$M=0$
$2\psi_9$	0	1	1						0	1	−1	−1	$\beta_1\alpha_2\alpha_3\beta_4$	
$2\psi_{10}$	0	0	0						0	−1	1	−1	$\alpha_1\beta_2\alpha_3\beta_4$	
$2\sqrt{3}\psi_{11}$	1	1	0						−2	1	1	1	$\alpha_1\alpha_2\beta_3\beta_4$	

[10] K. Tomita, Phys. Rev. **89**, 429 (1953).

Hamiltonian in Eq. (4) is equivalent to

$$\mathcal{H}=\tfrac{1}{2}(A_{12}-A_{13})(L^2-3L_z^2)+\tfrac{1}{2}(A_{34}-A_{13})(S^2-3S_z^2)+\tfrac{1}{2}A_{13}(I^2-3I_z^2). \quad (6)$$

By means of the matrix[11] $\langle LSIM|LM_LSM_S\rangle$, one can very conveniently calculate the matrix elements and the energy levels with results which are given in Table III and VI, respectively. The spectrum consists of seven lines if the magnetic field is in the C_2 orientation and twenty lines if it is parallel to a tetrahedral edge. The intensities of the lines are given in Table VII. Note that $\sum_{j<k} A_{jk}$ is zero for a regular tetrahedron.

4. ABSORPTION IN NH_4Cl BELOW THE LINE-WIDTH TRANSITION

(a) Comparison of Observed Line Shapes with Calculated Spectra

From the plot in Fig. 5 of second moment *versus* temperature, it is clear that at −195°C the line has reached its broadest possible value. At this temperature motions other than zero-point vibrations are negligible and we will assume that the ammonium ion is a rigid torsional oscillator.

The observed and calculated absorption derivatives at −195°C for the (1,0,0) and (1,1,0) orientations of the magnetic field are shown in Figs. 1 and 2. The calculated derivatives were obtained by replacing each component of the absorption line with the derivative of a Gaussian function whose width corresponded to the broadening computed in Eq. (7) for interactions outside the four-proton system. In order to obtain agreement between the experimental and computed line shapes, it is necessary to assume that the three C_2 axes of the NH_4^+ tetrahedron are parallel to the cubic axes.

That the agreement is not quite so good for the (1,1,0) curve as the (1,0,0) curve is perhaps to be explained by the smearing approximation used. The (1,1,0) curve consists of 20 separate transitions as compared to the 7 transitions of the (1,0,0) curve. If the different transitions were smeared differently much better agreement could be obtained. It does not seem worth while to pursue this point because NH_4Cl is a poor example to use for this comparison. In most crystals where the XH_4 or XF_4 groups are further apart the components of the line would be partially resolved.

In the case of solid methane the question has been raised[12] as to whether or not the molecules exist in *ortho* ($I=2$), *meta* ($I=1$), and *para* ($I=0$) states of total proton spin. The nuclear magnetic resonance

TABLE III. Matrix elements in LSIM representation.

$M=2$

$\langle 1122|H|1122\rangle=-\tfrac{1}{2}p$

$M=1$ (quartic)

diagonal elements

$\langle 1121|H|1121\rangle=\tfrac{1}{4}p$ $\qquad$ $\langle 1011|H|1011\rangle=-\dfrac{A_{12}}{2}$

$\langle 1111|H|1111\rangle=\tfrac{1}{2}(A_{12}+A_{34})-\tfrac{1}{4}p$ $\qquad$ $\langle 0111|H|0111\rangle=-\dfrac{A_{34}}{2}$

off-diagonal elements

$\langle 1121|H|1111\rangle=-\tfrac{3}{4}(A_{12}-A_{34})$

$\langle 1121|H|1011\rangle=\dfrac{3}{4\sqrt{2}}(A_{13}+A_{23}-A_{14}-A_{24})=3\langle 1111|H|1011\rangle$

$\langle 1121|H|0111\rangle=\dfrac{3}{4\sqrt{2}}(A_{23}+A_{24}-A_{13}-A_{14})=-3\langle 1111|H|0111\rangle$

$\langle 1011|H|0111\rangle=\tfrac{1}{4}(A_{13}+A_{24}-A_{23}-A_{14})$

$M=0$

$I=0,2$ (cubic)

$\langle 1120|H|1120\rangle=\tfrac{1}{2}p$
$\langle 0000|H|0000\rangle=\langle 1100|H|1100\rangle=0$

$\langle 1120|H|0000\rangle=\dfrac{\sqrt{6}}{4}(A_{14}+A_{23}-A_{24}-A_{13})$

$\langle 1120|H|1100\rangle=\dfrac{-1}{2\sqrt{2}}(3A_{12}+3A_{34}-p)$

$\langle 0000|H|1100\rangle=\dfrac{\sqrt{3}}{4}(A_{24}-A_{14})$

$I=1$ (cubic)

$\langle 0110|H|0110\rangle=A_{34}$; $\langle 1010|H|1010\rangle=A_{12}$
$\langle 1110|H|1110\rangle=\tfrac{1}{2}p-(A_{12}+A_{34})$

$\langle 1110|H|1010\rangle=\dfrac{1}{2\sqrt{2}}(A_{14}+A_{24}-A_{13}-A_{23})$

$\langle 1010|H|0110\rangle=\tfrac{1}{2}(A_{14}+A_{23}-A_{13}-A_{24})$

$\langle 1110|H|0110\rangle=\dfrac{1}{2\sqrt{2}}(A_{13}+A_{14}-A_{23}-A_{24})$

$p=\Sigma_{j<k} A_{jk}$

TABLE IV. Energy levels when external field is along a C_3 axis.

State in LSIM representation	Energy
$\langle 1\tfrac{3}{2}22\|$	$2g\beta H$
$I=(\tfrac{1}{2}+\sqrt{7}/4)^{\frac{1}{2}}\langle 1\tfrac{3}{2}21\|+(\tfrac{1}{2}-\sqrt{7}/4)^{\frac{1}{2}}\langle 1\tfrac{3}{2}11\|$	$g\beta H+(\tfrac{1}{4}+\sqrt{7}/2)g^2\beta^2R^{-3}$
$II=(\tfrac{1}{2}-\sqrt{7}/4)^{\frac{1}{2}}\langle 1\tfrac{3}{2}21\|-(\tfrac{1}{2}+\sqrt{7}/4)^{\frac{1}{2}}\langle 1\tfrac{3}{2}11\|$	$g\beta H+(\tfrac{1}{4}-\sqrt{7}/2)g^2\beta^2R^{-3}$
$\langle 1\tfrac{1}{2}11\|$, $\langle 0\tfrac{1}{2}11\|$	$g\beta H-\tfrac{1}{4}g^2\beta^2R^{-3}$
$\langle 1\tfrac{3}{2}20\|$, $\langle 0\tfrac{1}{2}00\|$, $\langle 1\tfrac{1}{2}00\|$	0
$\langle 1\tfrac{3}{2}10\|$	$-g^2\beta^2R^{-3}$
$\langle 1\tfrac{1}{2}10\|$, $\langle 0\tfrac{1}{2}10\|$	$\tfrac{1}{2}g^2\beta^2R^{-3}$

[11] E. U. Condon and G. H. Shortley, *The Theory of Atomic Spectra* (Cambridge University Press, London, reprinted 1951).
[12] T. Nagamiya, Progr. Theoret. Phys. (Japan) 6, 702 (1951).

TABLE V. Intensities of the lines in the C_3 orientation.

$\Delta E=\pm(E_M-E_{M-1}+g\beta H)$	Relative intensity
$\pm(5/4-\sqrt{7/2})g^2\beta^2R^{-3}=\pm0.073g^2\beta^2R^{-3}$	0.0744
$\pm\frac{3}{4}g^2\beta^2R^{-3}$	0.2500
$\pm(-\frac{1}{4}+\sqrt{7/2})g^2\beta^2R^{-3}=\pm1.073g^2\beta^2R^{-3}$	0.2534
$\pm(\frac{1}{4}+\sqrt{7/2})g^2\beta^2R^{-3}\ =\pm1.573g^2\beta^2R^{-3}$	0.3716
$\pm(5/4+\sqrt{7/2})g^2\beta^2R^{-3}=\pm2.573g^2\beta^2R^{-3}$	0.0506

data for methane,[10] and also for solid hydrogen,[13] are consistent with the existence of nuclear spin isomers. Now the line shape agreement in NH_4Cl depends on the existence of matrix elements between states of different total proton spin, which proves that individual ions do not exist in spin states of definite permutation symmetry. In view of the exclusion principle the normal vibrational modes must be such that the motions of neighboring ions are highly correlated in contrast to the molecules of solid methane or solid hydrogen.

(b) Second Moments and the N−H Bond Distance

With the assumption that the ions are ordered so that the N−H bonds point in the (1,1,1), $(\bar{1},\bar{1},1)$, $(1,\bar{1},\bar{1})$, and $(\bar{1},1,\bar{1})$ directions, Van Vleck's formula[6] for the second moment becomes

$$\Delta H_2{}^2=\frac{3{,}645}{32{,}768}\frac{g^2\beta^2}{r^6}\{1-\tfrac{3}{5}(\lambda_1{}^4+\lambda_2{}^4+\lambda_3{}^4)\}(1-\epsilon)$$
$$+\frac{4}{3}\frac{g'^2\beta^2}{r^6}\{1-(\lambda_1{}^4+\lambda_2{}^4+\lambda_3{}^4)\}(1-\epsilon)$$
$$+\frac{g^2\beta^2}{d^6}\{8.7+28.0(\lambda_1{}^4+\lambda_2{}^4+\lambda_3{}^4)\}+0.1\ \text{gauss}^2. \quad (7)$$

Here r is the N−H bond distance, g' is the nitrogen gyromagnetic ratio, d is the unit cell size, and λ_i is the direction cosine of the external field with respect to the ith cubic axis. The factor $(1-\epsilon)$ takes into account[1] the torsional oscillation of the ammonium ion. The first two terms in Eq. (7) give the intra $-NH_4{}^+$ interactions. The third term represents the interactions between neighboring $NH_4{}^+$ ions; the coefficients were computed[1] assuming $r/d=1.040/3.820$. The 0.1-gauss^2 term is the broadening from the chlorine and nitrogen nuclei outside a given $NH_4{}^+$ ion.

The experimental second moments at low temperature, given in Table I, when substituted in Eq. (7) result in N−H distances of 1.031 ± 0.007 and 1.033 ± 0.004A for the (1,0,0) and (1,1,0) orientations, respectively. These values are in excellent agreement with the neutron diffraction values[5] of 1.03 ± 0.02A. This agreement, as well as the agreement of the values for the two different crystal orientations, confirms the orientation assumed for the $NH_4{}^+$ ion in the unit cell.

[13] F. Reif and E. M. Purcell, Phys. Rev. **91**, 631 (1953).

5. ABSORPTION IN NH_4Cl ABOVE THE LINE-WIDTH TRANSITION TEMPERATURE

(a) Room Temperature Results

Above -125°C the line width is anisotropic but very slowly varying up to room temperature. The theory given in Sec. 3 is no longer applicable as the measured second moments are consistent with the assumption that the line broadening is due solely to interionic interactions.

Even these interactions are affected by the motion of the ions, and one can try using the dependence to investigate the motion. The second moment in general has the form

$$\Delta H_2{}^2=g^2\beta^2d^{-6}\{c_1(\lambda_1{}^4+\lambda_2{}^4+\lambda_3{}^4)-c_2\}+0.1\ \text{gauss}^2, \quad (8)$$

where the second term is an estimate of the contributions of the nitrogen and chlorine nuclei. The angular dependence of this term has been neglected.

Three models were considered. In model a each proton is distributed with equal probability over the four vertices of the tetrahedron; in model b each proton is distributed with equal probability over the four vertices of the tetrahedron as well as over the four vertices of the inverted tetrahedron. In model c each proton is distributed uniformly over the sphere circumscribing the tetrahedron.

Table VIII contains the values of c_1 and c_2 calculated for each model. The observed values at room temperature of c_1 and c_2 were obtained by varying the data, given in Table I for the different crystal orientations, within the limits set by experimental errors so as to obtain a completely consistent set of values of c_1 and c_2.

TABLE VI. Energy levels when external field is along an edge or a C_2 axis.

State in LSIM representation	Energy
$\langle1122\vert$	$2g\beta H$
$I=S_{11}\langle1121\vert-S_{12}\langle1111\vert$	$g\beta H+\frac{1}{4}(A_{12}+A_{34})+h$
$II=S_{12}\langle1121\vert+S_{11}\langle1111\vert$	$g\beta H+\frac{1}{4}(A_{12}+A_{34})-h$
$\langle1011\vert$	$g\beta H-\frac{A_{12}}{2}$
$\langle0111\vert$	$g\beta H-\frac{A_{34}}{2}$
$\langle0000\vert$	0
$III=\frac{1}{\sqrt{2}}\{\langle1120\vert-\langle1100\vert\}$	$\frac{3}{2\sqrt{2}}(A_{12}+A_{34})$
$IV=\frac{1}{\sqrt{2}}\{\langle1120\vert+\langle1100\vert\}$	$-\frac{3}{2\sqrt{2}}(A_{12}+A_{34})$
$\langle0110\vert$	A_{34}
$\langle1010\vert$	A_{12}
$\langle1110\vert$	$-(A_{12}+A_{34})$

If $A_{12}=A_{34}$, $S_{11}{}^2=1$, $S_{12}=0$ If $A_{12}=-2A_{23}$, $S_{11}{}^2=\frac{81}{162+2(82)^{\frac{1}{2}}}$, $S_{12}{}^2=1-S_{11}{}^2$

$h\equiv\frac{1}{4}\{10(A_{12}-A_{34})^2+4A_{12}A_{34}\}^{\frac{1}{2}}$

A comparison of the values in Table VIII makes it clear that the second moment is not very sensitive to the nature of the motion taking place. However, subject to this limitation the room temperature second moments show that not only is the crystal disordered but that the frequency with which an ordered ion becomes a disordered ion (or *vice versa*) is greater than the frequency associated with the line width, which is about 10^5 cps.

(b) Results in the Vicinity of the λ Point

The great changes in the crystal in the vicinity of the λ point are accompanied by almost negligible changes in the absorption. The disordered model *b* shows a larger line width than the ordered model *a* because in the disordered crystal the average proton-proton distance is smaller. However, when the crystal becomes disordered, it also expands anomalously[14] and the second moment is sensitive to the size of the crystal through the factor d^6. The two effects almost cancel so that the line width increases only slightly through the phase transition.

However, Eq. (8) can be applied to the observed second moments given in Table I for temperatures just below and above the λ point. With 3.84 and 3.85A assumed for the unit cell sizes,[14] c_1 and c_2 values of 30.5 and 5.3 are found below the phase transition and 32.6 and 5.9 above. The experimental errors are such that these results are not conclusive in themselves, but upon comparison with the theoretical values in Table VIII they provide an interesting confirmation of the order-disorder process.

TABLE VII. Intensities of the lines in the edge or C_2 orientations.

$\Delta E=\pm(E_M-E_{M-1}-g\beta H)$	Relative intensity
$\pm[\frac{1}{4}(A_{12}+A_{34})+h]$	$\frac{1}{4}S_{11}^2$
$\pm[-\frac{1}{4}(A_{12}+A_{34})+h]$	$\frac{1}{4}S_{12}^2$
$\pm\left[\left(\frac{1}{4}-\frac{3\sqrt{2}}{2}\right)(A_{12}+A_{34})+h\right]$	$\frac{3}{16}S_{11}^2$
$\pm\left[\left(\frac{1}{4}+\frac{3\sqrt{2}}{2}\right)(A_{12}+A_{34})+h\right]$	$\frac{3}{16}S_{11}^2$
$\pm\left[\left(\frac{1}{4}+\frac{3\sqrt{2}}{2}\right)(A_{12}+A_{34})-h\right]$	$\frac{3}{16}S_{12}^2$
$\pm\left[\left(\frac{1}{4}-\frac{3\sqrt{2}}{2}\right)(A_{12}+A_{34})-h\right]$	$\frac{3}{16}S_{12}^2$
$\pm[(5/4)(A_{12}+A_{34})+h]$	$\frac{1}{8}S_{12}^2$
$\pm[(5/4)(A_{12}+A_{34})-h]$	$\frac{1}{8}S_{11}^2$
$\pm\frac{3}{2}A_{12}$	$\frac{1}{8}$
$\pm\frac{3}{2}A_{34}$	$\frac{1}{8}$

If $A_{12}=A_{34}=-\frac{1}{2}g^2\beta^2R^{-3}$, $h=\frac{1}{4}g^2\beta^2R^{-3}$ (C_2 orientation)

If $A_{12}=-2A_{34}=g^2\beta^2R^{-3}$, $h=\frac{(82)^{\frac{1}{2}}}{8}g^2\beta^2R^{-3}$ (edge orientation)

[14] L. Vegard and S. Hillesund, Chem. Zentr. **1**, 930 (1943); P. Dinichert, Helv. Phys. Acta **15**, 462 (1943).

TABLE VIII. The anisotropy of the second moment, described by the parameters in Eq. (8), computed for three structural models and compared with the room temperature measurements.

	c_1	c_2
Model *a* (ordered)	30.97	4.86
Model *b* (disordered)	33.08	5.65
Model *c* (spherical rotation)	34.56	6.14
Experimental values	33.25	5.88

6. THE LINE-WIDTH TRANSITION AND THE MOTIONS OF THE AMMONIUM ION

The observed variation with temperature of the line widths and second moments for the different crystal orientations suggests that the motions of the NH_4^+ ions are essentially isotropic. There is no significant dependence upon crystal orientation of the character of the line-width transition.

The change in line width with temperature was calculated for the (1,0,0) and (1,1,0) crystal orientations using the same procedure, frequency factor (ν_0), and activation energy (E) as for the crystal powder.[1] The line shape factor α was 4.53 for the (1,0,0) and 3.98 for the (1,1,0) orientation. The curves drawn in Fig. 4 give the results of the calculation. The agreement with experiment is reasonably good; certainly there is no significant difference for the two crystal orientations.

The second moments measured along the (1,0,0) and (1,1,0) crystal axes are plotted in Fig. 5 against the temperature. An analysis of these data discloses the general nature of the motions responsible for narrowing the absorption. If we let S_T be the contribution to the second moment at absolute temperature T of the proton-proton interactions on a given NH_4^+, then it is found that S_T/S_0 is independent of crystal orientation, within experimental error. In Fig. 5, the curve drawn through the transition for the (1,0,0) orientation was calculated from the S_T/S_0 values for the (1,1,0) orientation. S_T is given by $(\Delta H_2^2)_T-(\Delta H_2^2)_{233°}$.

The independence of S_T/S_0 upon orientation can be derived by considering the motion of an NH_4^+ ion during the time required for rf absorption. In particular, assume a model in which any given edge of the ammonium ion tetrahedron is at its initial position a fraction $(1-5a)$ of the absorption period and a fraction a at each of the other five possible positions, i.e.,

$$A_{ij}=(1-5a)A_{ij}{}^0+a\{\textstyle\sum_{k<l}A^0{}_{kl}-A^0{}_{ij}\}$$
$$=(1-6a)A^0{}_{ij} \quad (9)$$

where A_{ij}, defined as for Eq. (1), is understood to be averaged over the motion of the ion and $A^0{}_{ij}$ is the value of A_{ij} when no motion occurs. Also, we have[6]

$$S_T=(9/4)\textstyle\sum_{i<j}A_{ij}{}^2=(9/4)(1-6a)^2\sum_{i<j}A^0{}_{ij}{}^2,$$

and

$$S_0=(9/4)\textstyle\sum_{i<j}A^0{}_{ij}{}^2.$$

Therefore, we obtain the result, which is independent of

orientation, that

$$S_T/S_0=(1-6a)^2. \tag{10}$$

An equivalent physical description of this model is the following. A given ion spends a certain fraction of its time in a nonrotating low-energy state. During the remaining time it is randomly excited to states with higher energy in which reorientations occur. These reorientations must produce in the high-energy state a uniform spatial distribution of the ion among the possible orientations in order to give the isotropic result of Eq. (10). The temperature dependence of the second moment arises from the larger fraction of time spent in the high-energy states at higher temperatures.

A crude classical picture is that the ion undergoes a Brownian motion from one equilibrium configuration to all other equilibrium configurations with the same probability. We infer that the state or states in which line narrowing occurs must lie above most of the potential barriers of the system. The same conclusion was reached in the preceding paper[1] by a comparison of the potential barriers deduced from the torsional frequency and from the variation of line width and relaxation time with temperature. Finally we note that the isotropy of S_T/S_0 implies that only one correlation time τ_c is important for this frequency range.

7. ACKNOWLEDGMENT

The excellent single crystal on which these experiments were performed was provided by Dr. H. A. Levy and Dr. S. W. Peterson. We are very grateful to them for their assistance in this research.

Infrared Spectrum of σ_2 for $B^{10}F_3$ and $B^{11}F_3$*†‡

ALVIN H. NIELSEN§
Department of Physics, The University of Tennessee, Knoxville, Tennessee
(Received January 4, 1954)

The infrared grating spectra of σ_2 for $B^{10}F_3$ and $B^{11}F_3$ have been reexamined from 650 to 750 K. Two samples of BF_3, one composed of 93.4 percent $B^{10}F_3$ and 6.6 percent of $B^{11}F_3$, and the other of the normal abundance ratio 20 percent $B^{10}F_3$ and 80 percent $B^{11}F_3$ were secured for the investigation. Complete resolution of the rotational fine structure of this parallel-type band was achieved. The following constants were obtained by means of the usual sort of rotational analysis: for $B^{10}F_3$, $\sigma_0=718.23$ K, $B_0=0.3527_2$ K, $B(v_2=1)=0.3528_8$ K, $D_J=13.72\times10^{-7}$ K. For $B^{11}F_3$, $\sigma_0=691.45$ K and the rotational constants are the same for the two isotopic species.

I. INTRODUCTION

THE infrared spectrum of boron trifluoride was investigated under high dispersion by Gage and Barker[1] in 1939. They observed the fundamental vibration frequencies, and partially resolved the rotational fine structure of the antisymmetric vibration $\sigma_2(A_2'')$. Boron trifluoride is a planar symmetric top molecule of symmetry D_{3h}. The fluorine atoms are situated at the corners of an equilateral triangle, and the boron atom is located at the center. In the normal mode σ_2 the motion is out of the plane and produces an oscillation of the electric moment parallel with the unique axis of the top.

Gage and Barker were, however, able to resolve only some twenty lines between 720 and 740 K from which they obtained the average line spacing, the moment of inertia I_B about an axis in the plane of the model, and the boron-fluorine internuclear distance. Their inability to resolve the band more completely was probably caused by the overlapping of the two isotopic bands. The natural abundances of the boron isotopes are about 20 percent B^{10} and 80 percent B^{11}, and the absorption by σ_2 of $B^{10}F_3$ should therefore be about one-fourth as intense as that for $B^{11}F_3$. The separation of the Q branches for the two bands is only about 27 K which causes the lines of the two species to overlap badly, and consequently to get into and out of phase periodically. As the rotational spacing is only about 0.7 K, these phase changes interfere with the resolution of the lines.

Past experience with the corresponding vibration in the planar molecule F_2CO[2] in which the lines have about the same spacing suggested that it should be possible to resolve completely the spectrum of boron trifluoride, particularly if samples enriched in one or the other isotope were available. Fortunately, boron trifluoride enriched to 93.4 percent B^{10} and 6.6 percent B^{11} is commonly used in neutron counters, and samples were obtained from the Oak Ridge National Laboratory, Isotopes Division, for this experiment. With samples of this purity it was anticipated that the band overlap would not be serious enough to interfere with resolution of the lines.

This paper concerns itself with the high-dispersion measurements of σ_2 for two samples of boron trifluoride; one with an abundance ratio of 93.4 percent B^{10} and 6.6 percent B^{11}, and the other with the natural ratio of 20 percent B^{10} and 80 percent B^{11}.

II. EXPERIMENTAL DETAILS AND RESULTS

The spectra described herein were recorded on The University of Tennessee prism-grating spectrometer[3] equipped with a 1200 lines-per-inch grating, ruled by Professor E. F. Barker of the University of Michigan, and a Perkin-Elmer 13-cps thermocouple-amplifier system. The samples of $B^{10}F_3$ and $B^{11}F_3$ were contained in 10-cm long fluorothene absorption cells, closed with KBr windows, at pressures of 23 and 38 mm of mercury, respectively. Because these bands fall in the region of the atmospheric CO_2 band at 15μ, the spectrometer box was carefully sealed and the CO_2 and water vapor were removed by means of trays of Ascarite and P_2O_5 placed within. At the same time a rapid flushing of the spectrometer box by dry nitrogen was carried on for about thirty minutes. This was so effective that upon standing overnight no trace of CO_2 or H_2O was observable in the background.

Figure 1 shows a tracing of a record made of the 93.4 percent $B^{10}F_3$ sample in the spectral region from 680 to 750 K with the slits including a spectral interval of about 0.4 K. In all, some 102 lines were observed, and the P and R branches of the bands are completely resolved. The weak Q branch, D, of $B^{11}F_3$ at about 691 K may be seen overlapping the P branch and obscuring a few lines. The Q branches degrade toward higher frequencies indicating that $B(v_2=1)$ is larger than $B(v_2=0)$. In the close vicinity of the Q branch, D', of $B^{10}F_3$ may be seen five fairly intense lines labeled A', B', C', E', and F'

* Presented at the Symposium on Molecular Structure, The Ohio State University, Columbus, Ohio, June 1953.
† This work was supported in part by the U. S. Army Office of Ordnance Research.
‡ This work was supported in part by the K-25 Laboratories, operated by Carbide and Carbon Chemicals Company, a Division of Union Carbide and Carbon Chemicals Corporation, Oak Ridge, Tennessee.
§ Consultant at the K-25 Laboratories, Carbide and Carbon Chemicals Company, Oak Ridge, Tennessee.
[1] D. M. Gage and E. F. Barker, J. Chem. Phys. 7, 455 (1939).
[2] A. H. Nielsen, J. Chem. Phys. 19, 98 (1951).
[3] A. H. Nielsen, J. Tenn. Acad. Science 22, 241 (1947).

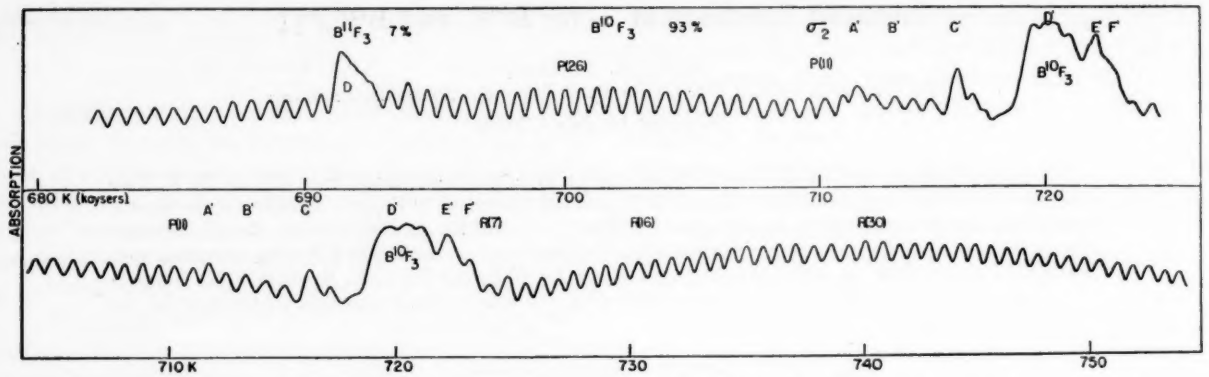

FIG. 1. Trace of records of σ_2 for $B^{10}F_3$ (93.4 percent sample). A', B', C', D', E' and F' are the Q branches associated with $B^{10}F_3$, and D is the Q branch of σ_2 for $B^{11}F_3$.

at 711.60, 713.2, 716.1, 722.1, and 722.9 K which are probably Q branches of the fundamental σ_2 arising from populated excited states. The record shows that little, if any, confusion results from the two overlapping bands. Table I gives a list of the frequencies of the observed lines, their rotational assignments, and the frequencies calculated from the molecular constants derived in a later section.

The spectrum of $B^{11}F_3$ in the region from 650 to 750 K is shown in Fig. 2, which was recorded using a sample of normal abundance ratio. Because the concentration of B^{10} in this sample is about three times as large as the concentration of B^{11} in the sample from which Fig. 1 was made, $\sigma_2(B^{10}F_3)$ in Fig. 2 is about three times as intense relative to $\sigma_2(B^{11}F_3)$ as $\sigma_2(B^{11}F_3)$ is to $\sigma_2(B^{10}F_3)$ in Fig. 1. The effect of this is to cause more serious interference between the overlapping bands. Though the bands shown in Fig. 2 are well resolved, the line frequencies are somewhat displaced by the lines of the two interfering bands coming into and out of phase. This spectral region is also about 30 K wider than for $\sigma_2(B^{10}F_3)$ showing that on the high-frequency side of the band the $B^{10}F_3$ lines are still quite intense because of the relatively large concentration of $B^{10}F_3$. In fact, near the high-frequency extremity of the region shown in Fig. 2 the observed wave numbers agree very nearly with the $B^{10}F_3$ wave numbers given in Table I. The Q branch region in Fig. 2 resembles almost exactly the corresponding region in Fig. 1. The satellite Q branches at 684.3, 688.3, 693.9, and 694.6 K are labeled B, C, E, and F as in Fig. 1 and are interpreted in the same manner. Table II lists the observed wave numbers, the calculated wave numbers, and the rotational assignments of the lines measured for this sample.

III. ROTATIONAL ANALYSIS

The energy of a nonrigid symmetric top, as given by Slawsky and Dennison,[4] is given by the relation

$$F(J,K)=BJ(J+1)+(A-B)K^2 - D_J J^2(J+1)^2 - D_{JK}J(J+1)K^2 - D_K K^4.$$

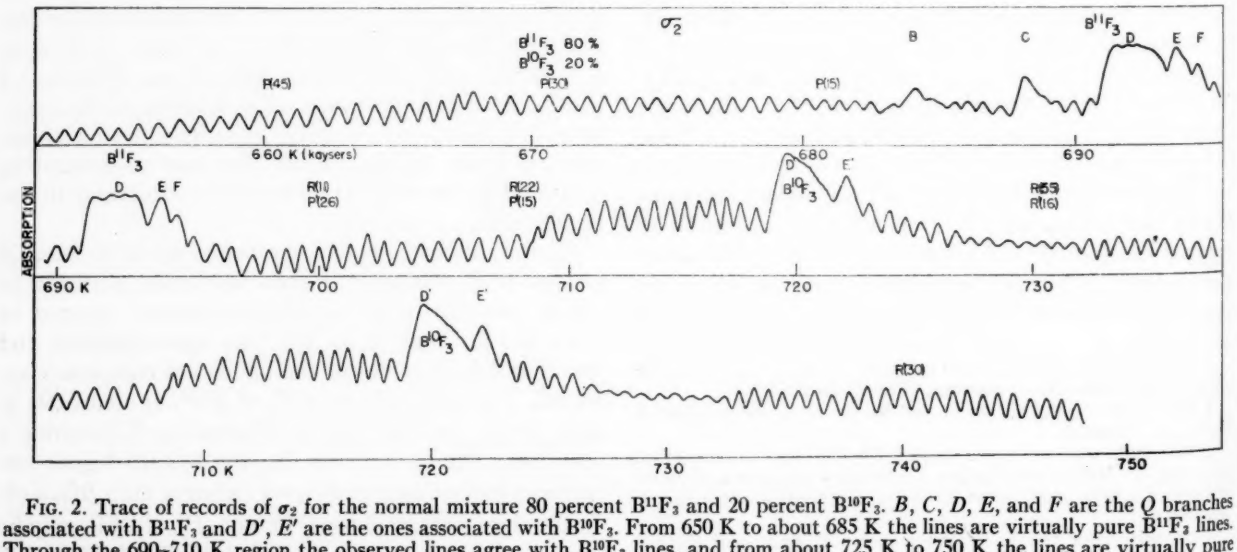

FIG. 2. Trace of records of σ_2 for the normal mixture 80 percent $B^{11}F_3$ and 20 percent $B^{10}F_3$. B, C, D, E, and F are the Q branches associated with $B^{11}F_3$ and D', E' are the ones associated with $B^{10}F_3$. From 650 K to about 685 K the lines are virtually pure $B^{11}F_3$ lines. Through the 690–710 K region the observed lines agree with $B^{10}F_3$ lines, and from about 725 K to 750 K the lines are virtually pure $B^{10}F_3$ lines. The unprimed R and P lines are $B^{11}F_3$.

[4] Z. I. Slawsky and D. M. Dennison, J. Chem. Phys. 7, 509 (1939).

As boron trifluoride is a planar molecule, and, therefore, an oblate symmetrical top, the vibration σ_2 is the only parallel-type vibration. The rotational selection rules for such a vibration are $\Delta J=\pm 1$, 0, and $\Delta K=0$. By substituting these into $F(J,K)$ and applying the Bohr frequency relation, the following expressions for $R(J)$, $Q(J)$, and $P(J)$ are obtained:

$$\begin{aligned} R(J)&=\sigma_0+(B'+B'')(J+1)+(B'-B'')(J+1)^2 \\ &\quad -2(D'+D'')(J+1)^3, \\ Q(J)&=\sigma_0+(B'-B'')J(J+1), \qquad (1) \\ P(J)&=\sigma_0-(B'+B'')J \\ &\quad +(B'-B'')J^2+2(D'+D'')J^3, \end{aligned}$$

where J takes values 1, 2, 3, $\cdots$. The term $D'-D''$ is negligibly small and has been omitted. From these expressions it is possible to derive the following combination relations which serve to give σ_0, B', B'', D', and D'' by graphical methods:

$$\begin{aligned} (1/2)[R(J)+P(J)]&=(\sigma_0+B')+(B'-B'')(2J+1), \\ \Delta_2'F(J)/2(2J+1)&=(1/2)[R(J)-P(J)]/(2J+1) \\ &=B'+D'(2J+1)^2, \qquad (2) \\ \Delta_2''F(J)/2(2J+1)&=(1/2)[R(J-1) \\ &\quad -P(J+1)]/(2J+1)=B''+D''(2J+1)^2. \end{aligned}$$

For an A_2-type vibration in a planar XY_3 molecule (D_{3h} symmetry) in which the nuclear spin I of the identical nuclei is $\frac{1}{2}$, the levels of even J, for $K=0$, do not occur; and the levels with K divisible by 3, including zero, have larger statistical weights than those not divisible by 3. The effect of this upon the rotational structure should be that $R(0)$ does not occur, and there should be no R and P transitions among the J values for $K=0$. Furthermore, there should be a weak, weak, strong, etc., type of intensity alternation. Such an alternation was not observed because it would be relatively largest for the first few lines which are obscured by the wide Q branches.

Analysis of $\sigma_2(B^{10}F_3)$

As the sample of $B^{10}F_3$ was the more pure, the observed line positions in the spectrum should be less disturbed by overlapping than those for the other sample. The rotational constants determined from this band should, therefore, be the more accurate. Graphs of the Eqs. (2) yield the following constants: $\sigma_0=718.23$ K, $B'-B''=0.00015_4$ K, $B'=0.3528_8$ K, $B''=0.3527_2$ K, and $D'\cong D''=13.7_2\times 10^{-7}$ K. It should be noted that, as expected, $B'-B''$ is quite small and positive. From Eqs. (2) it may be seen that for positive $B'-B''$ the Q branch degrades in the direction of higher frequencies as shown in Fig. 1. The $B'-B''=0.00015_4$ K obtained from the slope of the first of the relations (2) is also in quite good agreement with the actual difference between the two intercepts B' and B'' (0.0001_6 K) obtained from the second and third of the relations (2). These constants, when substituted into (1), give the following equations from which the calculated wave numbers of Table I were obtained:

$$\begin{aligned} R(J)&=718.23+(0.7056)(J+1) \\ &\quad +(0.00015_4)(J+1)^2-(54.8_8\times 10^{-7})(J+1)^3, \\ P(J)&=718.23-(0.7056)J+(0.00015_4)J^2 \\ &\quad +(54.8_8\times 10^{-7})J^3. \end{aligned} \qquad (3)$$

The band center obtained in this analysis differs, by 1.3 K, from the value 719.5 K quoted by Gage and Barker,[1] but as the present value was obtained from a band analysis it is believed to be more reliable.

TABLE I. Observed and calculated wave numbers for σ_2 in $B^{10}F_3$. K (vacuum), $\sigma_0=718.23$ K.

Assignment	Obs wave number	Calc wave number	Δ $(O-C)$	Assignment	Obs wave number	Calc wave number	Δ $(O-C)$
$R(50)$	753.99	753.88	+0.11	$P(1)$		717.52	
$R(49)$	753.18	753.20	−0.02	$P(2)$		716.81	
$R(48)$	752.54	752.52	+0.02	$P(3)$		716.11	
$R(47)$	751.89	751.84	+0.05	$P(4)$		715.41	
$R(46)$	751.22	751.16	+0.06	$P(5)$		714.70	
$R(45)$	750.50	750.47	+0.03	$P(6)$		714.00	
$R(44)$	749.80	749.79	+0.01	$P(7)$		713.29	
$R(43)$	749.10	749.10	0.00	$P(8)$		712.59	
$R(42)$	748.39	748.41	−0.02	$P(9)$		711.89	
$R(41)$	747.73	747.73	0.00	$P(10)$	711.03	711.19	−0.16
$R(40)$	747.00	747.04	−0.04	$P(11)$	710.34	710.49	−0.15
$R(39)$	746.30	746.34	−0.04	$P(12)$	709.65	709.79	−0.14
$R(38)$	745.58	745.65	−0.07	$P(13)$	709.01	709.09	−0.08
$R(37)$	744.94	744.96	−0.02	$P(14)$	708.26	708.39	−0.13
$R(36)$	744.24	744.27	−0.03	$P(15)$	707.62	707.69	−0.07
$R(35)$	743.53	743.57	−0.04	$P(16)$	706.93	707.00	−0.07
$R(34)$	742.86	742.87	−0.01	$P(17)$	706.28	706.30	−0.02
$R(33)$	742.14	742.18	−0.04	$P(18)$	705.56	705.61	−0.05
$R(32)$	741.48	741.48	0.00	$P(19)$	704.91	704.91	0.00
$R(31)$	740.78	740.78	0.00	$P(20)$	704.19	704.22	−0.03
$R(30)$	740.06	740.08	−0.02	$P(21)$	703.52	703.53	−0.01
$R(29)$	739.36	739.38	−0.02	$P(22)$	702.81	702.84	−0.03
$R(28)$	738.69	738.68	+0.01	$P(23)$	702.16	702.14	+0.02
$R(27)$	738.04	737.98	+0.06	$P(24)$	701.47	701.46	+0.01
$R(26)$	737.28	737.28	0.00	$P(25)$	700.78	700.77	+0.01
$R(25)$	736.61	736.58	+0.03	$P(26)$	700.09	700.08	+0.01
$R(24)$	735.89	735.88	+0.01	$P(27)$	699.44	699.39	+0.05
$R(23)$	735.21	735.17	+0.04	$P(28)$	698.73	698.71	+0.02
$R(22)$	734.52	734.47	+0.05	$P(29)$	698.00	698.03	−0.03
$R(21)$	733.79	733.76	+0.03	$P(30)$	697.33	697.34	−0.01
$R(20)$	733.06	733.06	0.00	$P(31)$	696.70	696.67	+0.03
$R(19)$	732.34	732.36	−0.02	$P(32)$	696.03	695.98	+0.05
$R(18)$	731.67	731.65	+0.02	$P(33)$	695.30	695.30	0.00
$R(17)$	731.00	730.99	+0.01	$P(34)$	694.64	694.63	+0.01
$R(16)$	730.32	730.24	+0.08	$P(35)$	693.94	693.95	−0.01
$R(15)$	729.62	729.53	+0.09	$P(36)$	693.31	693.28	+0.03
$R(14)$	728.96	728.83	+0.13	$P(37)$		692.61	
$R(13)$	728.25	728.12	+0.13	$P(38)$		691.94	
$R(12)$	727.54	727.41	+0.13	$P(39)$		691.27	
$R(11)$	726.82	726.71	+0.11	$P(40)$	690.68	690.60	+0.08
$R(10)$	726.11	726.00	+0.11	$P(41)$	690.02	689.93	+0.09
$R(9)$	725.39	725.29	+0.10	$P(42)$	689.26	689.27	−0.01
$R(8)$	724.66	724.59	+0.07	$P(43)$	688.63	688.61	+0.01
$R(7)$	723.88	723.88	0.00	$P(44)$	687.91	687.94	−0.03
$R(6)$	723.07	723.17	−0.10	$P(45)$	687.28	687.29	−0.01
$R(5)$		722.46		$P(46)$	686.68	686.63	+0.05
$R(4)$		721.76		$P(47)$	686.00	685.97	+0.03
$R(3)$		721.05		$P(48)$	685.35	685.32	+0.03
$R(2)$		720.34		$P(49)$	684.65	684.67	−0.02
$R(1)$		719.64		$P(50)$	684.00	684.02	−0.02
				$P(51)$	683.35	683.37	−0.02
				$P(52)$	682.67	682.72	−0.05
				$P(53)$	682.01	682.08	−0.07

TABLE II. Observed and calculated wave numbers for σ_2 in $B^{11}F_3$. K (vacuum).

Assignment	Obs wave numbers	Calc wave numbers	Δ (O−C)	Wave numbers of $B^{10}F_3$ lines from Table I	Assignment	Obs wave numbers	Calc wave numbers	Δ (O−C)	Wave numbers of $B^{10}F_3$ lines from Table I
R(59)	733.07	733.16	−0.09	733.06	P(1)		690.75		690.68
R(58)	732.40	732.49	−0.09	732.34	P(2)		690.04		690.02
R(57)	731.72	731.82	−0.10	731.67	P(3)		689.34		689.26
R(56)	730.98	731.15	−0.17	731.00	P(4)		688.63		688.63
R(55)	730.34	730.48	−0.14	730.32	P(5)		687.93		687.91
R(54)		729.81		729.62	P(6)		687.22		687.28
R(53)		729.14		728.96	P(7)		686.52		686.68
R(52)		728.46		728.25	P(8)		685.82		686.00
R(51)		727.79		727.54	P(9)		685.13		685.35
R(50)		727.11		726.82	P(10)		684.42		684.65
R(49)	726.56	726.43	+0.13	726.82	P(11)		683.78		684.00
R(48)	725.93	725.75	+0.18	726.11	P(12)	682.84	683.01	−0.17	683.35
R(47)	725.20	725.07	+0.13	725.39	P(13)	682.21	682.32	−0.11	682.67
R(46)	724.52	724.38	+0.14	724.66	P(14)	681.48	681.62	−0.14	682.01
R(45)	723.81	723.70	+0.11	723.88	P(15)	680.72	680.92	−0.20	
R(44)	723.10	723.01	+0.09	723.07	P(16)	680.12	680.22	−0.10	
R(43)		722.33			P(17)	679.45	679.53	−0.08	
R(42)		721.64			P(18)	678.76	678.83	−0.07	
R(41)		720.95			P(19)	678.06	678.14	−0.08	
R(40)		720.26			P(20)	677.46	677.44	+0.02	
R(39)		719.57			P(21)	676.78	676.75	+0.03	
R(38)		718.88			P(22)	676.12	676.06	+0.06	
R(37)	718.34	718.18	+0.16		P(23)	675.41	675.37	+0.04	
R(36)	717.62	717.49	+0.13		P(24)	674.70	674.68	+0.02	
R(35)	716.96	716.80	+0.16		P(25)	674.07	673.99	+0.08	
R(34)	716.25	716.10	+0.15		P(26)	673.42	673.31	+0.11	
R(33)	715.70	715.40	+0.30		P(27)	672.72	672.62	+0.10	
R(32)	714.83	714.71	+0.12		P(28)	672.07	671.94	+0.13	
R(31)	714.15	714.01	+0.14		P(29)	671.41	671.25	+0.16	
R(30)	713.50	713.30	+0.20		P(30)	670.70	670.57	+0.13	
R(29)	712.82	712.61	+0.21		P(31)	669.99	669.89	+0.10	
R(28)	712.10	711.91	+0.19		P(32)	669.38	669.21	+0.17	
R(27)	711.43	711.21	+0.22		P(33)	668.68	668.53	+0.15	
R(26)	710.72	710.51	+0.21		P(34)	668.00	667.85	+0.15	
R(25)	710.02	709.80	+0.22		P(35)	667.34	667.18	+0.16	
R(24)	709.29	709.10	+0.19		P(36)	666.70	666.50	+0.20	
R(23)	708.59	708.40	+0.19		P(37)	665.92	665.83	+0.09	
R(22)	707.92	707.69	+0.23	707.62	P(38)	665.23	665.16	+0.08	
R(21)	707.24	706.99	+0.25	706.93	P(39)	664.58	664.49	+0.09	
R(20)	706.46	706.29	+0.15	706.28	P(40)	663.94	663.82	+0.12	
R(19)	705.82	705.58	+0.24	705.56	P(41)	663.25	663.16	+0.09	
R(18)	705.04	704.87	+0.17	704.91	P(42)	662.59	662.49	+0.10	
R(17)	704.36	704.17	+0.19	704.19	P(43)	661.95	661.83	+0.12	
R(16)	703.58	703.46	+0.12	703.52	P(44)	661.30	661.17	+0.13	
R(15)	702.93	702.76	+0.17	702.81	P(45)	660.58	660.51	+0.07	
R(14)	702.26	702.05	+0.21	702.16	P(46)	659.90	659.85	+0.05	
R(13)	701.54	701.34	+0.20	701.47	P(47)	659.27	659.20	+0.07	
R(12)	700.82	700.64	+0.18	700.78	P(48)	658.58	658.54	+0.04	
R(11)	700.17	699.93	+0.24	700.09	P(49)	657.91	657.89	+0.02	
R(10)	699.45	699.22	+0.23	699.44	P(50)	657.25	657.24	+0.01	
R(9)	698.74	698.52	+0.22	698.73	P(51)	656.63	656.59	+0.04	
R(8)	698.05	697.81	+0.24	698.00	P(52)	655.97	655.95	+0.02	
R(7)	697.35	697.11	+0.24	697.33	P(53)	655.24	655.30	−0.06	
R(6)	696.66	696.40	+0.26	696.70	P(54)	654.63	654.66	−0.03	
R(5)	696.11	695.69	+0.42	696.03	P(55)	653.93	654.02	−0.09	
R(4)	695.36	694.98	+0.38	695.30	P(56)	653.27	653.38	−0.11	
R(3)	694.68	694.28	+0.40	694.64	P(57)	652.65	652.75	−0.10	
R(2)	693.97	693.57	+0.40	693.94	P(58)	652.01	652.11	−0.10	
R(1)		692.86							

Analysis of $\sigma_2(B^{11}F_3)$

As the boron atom is situated at the center of mass of the molecule, a change in its isotopic mass should not affect the moments of inertia of the molecule. Only the band center should be affected by such a change. The overlapping of the $B^{11}F_3$ and $B^{10}F_3$ spectra in Fig. 2 is of such a nature that, though the lines appear to be well resolved, they are actually composite lines with their frequencies distorted, in some cases, by as much as 0.4–0.5 K. It was, therefore, concluded that a band analysis like the one discussed in the previous section would not provide as accurate a σ_0 as some other method which might take advantage of the identity of the two spectra except for band center.

Upon examination of the observed line frequencies it was noted that the lines beyond 723.10 cm^{-1} in Fig. 2

(Table II) agreed almost exactly with the lines shown in Fig. 1 (Table I) for $B^{10}F_3$. It was further noted that between 690 and 708 K the observed line positions of Fig. 2 agreed quite well with the observed line positions of Fig. 1. These facts may be verified from Tables I and II where separate columns have been included to demonstrate the near coincidences.

Figure 1 shows that the intensity maxima of the P and R branches of the nearly pure $B^{10}F_3$ band lie between $J=20$ and $J=40$, or 733.06 K and 747.00 K for the R branch. This same spectral range in Fig. 2 includes lines of $B^{11}F_3$ from about $R(59)$ to $R(75)$, which must be quite weak. Thus, in the region where the $B^{10}F_3$ R branch spectrum is most intense the overlapping $B^{11}F_3$ lines are extremely weak. It is evident that from about 723.07 K the lines shown in Fig. 2 are virtually pure $B^{10}F_3$ lines.

The other region, 690–708 K, shown in Fig. 2 corresponds to the maximum region of the P branch of $B^{10}F_3$ ($J=15$ to $J=40$). For $B^{11}F_3$ this region corresponds to the interval between $P(1)$ and $R(22)$. Despite the fact that there are about four times the number of $B^{11}F_3$ molecules as $B^{10}F_3$ present in this sample these lines will be weaker or, at most, of about the same intensity as the lines of maximum intensity in $B^{10}F_3$. It may be seen in Table II that the agreement between the observed lines and the $B^{10}F_3$ lines is extremely good, and these lines must probably be ascribed to $B^{10}F_3$ with a small amount of distortion from overlapping. At the same time, the intensity of the $B^{10}F_3$ lines of $J>50$ in the normal sample is probably quite low, which means that the lines in Fig. 2 with wave numbers lower than 682 K are principally of $B^{11}F_3$ origin with almost no distortion from $B^{10}F_3$ overlapping.

Two separate graphs were made plotting the observed line positions and band center for $B^{10}F_3$, and the observed line positions for the normal sample leaving the exact location of the band center undetermined. These two plots were laid over each other over a light box so that they could be matched. Because the two spectra should be identical except for band center, and because the lines between 650 and 680 K in Fig. 2 are virtually pure $B^{11}F_3$ lines, it is possible to match the two spectra line for line. This makes it possible to fix the band center for $B^{11}F_3$ at 691.45 K and to assign proper J values throughout. By replacing 718.23 K by 691.45 K in Eqs. (2), the calculated wave numbers shown in Table II for $B^{11}F_3$ may be obtained. The agreement between observed and calculated wave numbers is satisfactory. Gage and Barker[1] quote the band center for $B^{11}F_3$ as 691.3 K.

IV. CONCLUSIONS

As the geometric form of BF_3 is that of an equilateral triangle with the boron atom located at the center, the moment of inertia in the ground state about an axis in the plane of the model, and the B–F internuclear distance are easily calculated from B'', the rotational constant of the ground state. These constants are found to be $I_B=79.34\times10^{-40}$ g cm^2 and 1.295_1A, respectively, as compared with 79×10^{-40} g cm^2 and 1.29A given by Gage and Barker from their average line spacings. The present r(B–F) is in excellent agreement with the electron diffraction measurements by Levy and Brockway[5] who quote r(B–F)$=1.30\pm0.02$A, and by Braune and Pinnow[6] who quote r(B–F)$=1.31\pm0.03$A.

The Teller-Redlich product rule for BF_3 is given by Herzberg[7] as

$$\frac{\omega_2(B^{10}F_3)}{\omega_2(B^{11}F_3)}=\frac{(\omega_3\omega_4)(B^{10}F_3)}{(\omega_3\omega_4)(B^{11}F_3)}=\left[\frac{m_{B^{11}}(m_{B^{10}}+3m_F)}{m_{B^{10}}(m_{B^{11}}+3m_F)}\right]^{\frac{1}{2}}=1.0405, \quad (4)$$

where the ω_i represent the wave numbers of the harmonic vibrations with infinitesimal amplitude. Insufficient information is presently available with which to compute the ω_i and it would not be expected that the band centers substituted into (4) would give perfect agreement. Gage and Barker, however, did substitute their observed band centers in order to verify their assignments and found $\sigma_2{}^{10}/\sigma_2{}^{11}=1.0408$ and $\sigma_3\sigma_4{}^{10}/\sigma_3\sigma_4{}^{11}=1.0388$. The present new values of the band centers for σ_2 give the ratio $\sigma_2{}^{10}/\sigma_2{}^{11}=1.0387$, which agrees perfectly with Gage and Barker's[1] $\sigma_3\sigma_4$ ratio.

It does not appear to be possible at the present time to assign unambiguously the satellite Q branches discussed in an earlier section. Table III lists all the observed Q branches for both molecules including the 0–1. An interesting, though perhaps not significant, fact may be pointed out in column 6 of Table III which shows that with the exception of $\sigma_2{}^{10}/\sigma_2{}^{11}$ for B and D the ratios are in nearly perfect agreement with the Teller-Redlich prediction.

TABLE III. Observed Q branches for $B^{10}F_3$ and $B^{11}F_3$.

Designation in Figs. 1 and 2	$B^{10}F_3$ observed wave number	$\Delta\sigma$	$B^{11}F_3$ observed wave number	$\Delta\sigma$	Ratio $\sigma_2{}^{10}/\sigma_2{}^{11}$
A	711.6				
		1.6			
B	713.2		684.3		1.0422
		2.9		4.0	
C	716.1		688.3		1.0404
		2.1		3.2	
D	718.23		691.45		1.0387
		3.9		2.4	
E	722.1		693.9		1.0406
		0.8		0.7	
F	722.9		694.6		1.0407

[5] H. Levy and L. O. Brockway, J. Am. Chem. Soc. **59**, 2085 (1937).
[6] H. Braune and P. Pinnow, Z. physik. Chem. **B35**, 239 (1937).
[7] G. Herzberg, *Infrared and Raman Spectra of Polyatomic Molecules* (D. Van Nostrand Company, Inc., New York, 1945), p. 298.

It appears that any assignments which can be made are uncertain because there are seven possible transitions arising from excited states for which the Boltzmann factor is not negligibly small, which will fall very close to the 0–1 for both molecules. The excited levels are $v_4=1$ at 480 K, $v_2=1$ at about 700 K, $v_1=1$ at 888 K, $v_4=2$ at 960 K, $v_2=2$ at 1400 K, $v_4=3$ at about 1440 K, and $v_3=1$ at 1450 K. The difference bands arising from these levels are $2\sigma_2-\sigma_2$, $\sigma_2+\sigma_4-\sigma_4$, $\sigma_1+\sigma_2-\sigma_1$, $\sigma_2+2\sigma_4-2\sigma_4$, $3\sigma_2-2\sigma_2$, $\sigma_2+3\sigma_4-3\sigma_4$, and $\sigma_2+\sigma_3-\sigma_3$. Of these seven bands, the first four are the most likely from the point of view of population. Of the Q branches listed in Table III the ones which are quite certainly observed are A', C', D', and E' for $B^{10}F_3$, and B, C, D, and E for $B^{11}F_3$. B' for $B^{10}F_3$ is also believed to be certain as there were indications of it in most of the records. For $B^{11}F_3$ Q branch A was not observed. As may be seen from columns 3 and 5 of Table III the Q branches B, C, and D are about equally spaced in both molecules. The Q branches E and F fall at slightly higher wave numbers than 0–1. This indicates that the x_{ij} associated with these transitions is positive.

ACKNOWLEDGMENT

The author gratefully acknowledges the aid of Mr. A. V. Faloon and Mr. T. G. Burke of K-25 Laboratories who, respectively, prepared the sample of nearly pure $B^{10}F_3$ and the cells which were used in the experiment.

THE JOURNAL OF CHEMICAL PHYSICS VOLUME 22, NUMBER 4 APRIL 1954

Scattering of High-Velocity Neutral Particles. II. Helium-Helium

I. AMDUR AND A. L. HARKNESS
Department of Chemistry, Massachusetts Institute of Technology, Cambridge, Massachusetts
(Received December 11, 1953)

Total collision cross sections have been measured for helium atoms, with energies between 500 and 2100 ev, scattered in room temperature helium. Measurements were made with two detectors of different geometric aperture, 13.4 and 0.96 minutes. In order to obtain meaningful potential energy information from such results, it is necessary to determine effective apertures by taking into account beam shape, intensity distribution, and for the case where the beam is wider than the detector, scattering to the detector from external regions of the beam. Potential energy functions have been derived from the cross sections obtained with the two detectors. The functions agree within a factor of about 1.3 as compared with 0.17 when geometric apertures are used directly. The results from both detectors have been represented by an average function, namely,

$$V(r)=7.55\times10^{-12}/r^{5.94}\ \text{ergs}$$

for values of r between 1.27A and 1.59A.

The potential energy information obtained from the present experiments is in agreement with theoretical calculations of P. Rosen and H. Margenau within the uncertainty of such calculations. The information also appears to be consistent with that derived from measurements of gaseous compressibility and viscosity, for values of r between 1.90A and 2.30A.

RESULTS on the scattering of beams of high-velocity helium atoms in room-temperature helium have been reported previously in connection with the experimental determination of molecular interactions at small distances of separation.[1,2] Additional results for this system have been obtained with a different molecular beam apparatus which has been described in detail in a publication[3] hereafter referred to as Paper I. The new measurements extend considerably the range of internuclear distance over which the potential energy may be evaluated. The extension results from a decrease in the effective angular aperture of the detector system, and the use of a recording potentiometer instead of a microammeter in the dc amplifier which is part of the detector system. The increased accuracy with which beam intensities can be estimated with the recording potentiometer makes it possible to extend measurements to lower beam energies and correspondingly larger cross sections. In the present experiments, total collision cross sections, for beam energies between 500 and 2100 electron volts were obtained from ratios of scattered and unscattered beam intensities. Two different detectors were used: a special, five-junction thermopile, kindly supplied by Harris,[4] and a butt-welded, single-junction, vacuum thermocouple, referred to in Paper I as detector C. The five-junction thermopile, hereafter referred to as the wide detector, was masked so that its effective width and length were 2.03×10^{-2} and 5.08×10^{-2} cm, respectively. It was located 2.600 cm from the midpoint of the scattering chamber and had a geometric aperture, based on its narrow dimension, of 13.4 minutes. Detector C, hereafter referred to as the

[1] I. Amdur and H. Pearlman, J. Chem. Phys. **9**, 503 (1941).
[2] I. Amdur, J. Chem. Phys. **17**, 844 (1949).
[3] Amdur, Glick, and Pearlman, Proc. Am. Acad. Arts Sci. **76**, 101 (1948).
[4] L. Harris, J. Opt. Soc. Am. **36**, 597 (1946).

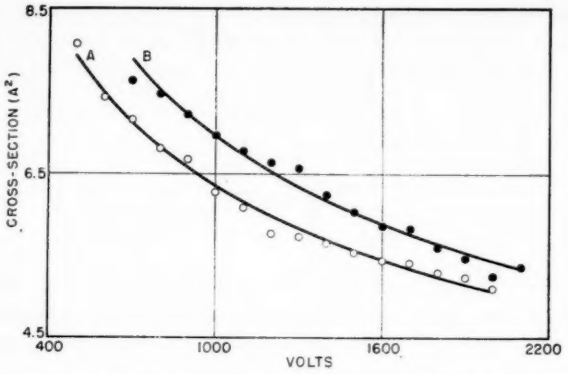

FIG. 1. Total collision cross-sections: A. Wide detector; B. Narrow detector.

narrow detector, had an average width of 1.40×10^{-3} cm and a masked length of 5.08×10^{-2} cm. Its geometric aperture, with respect to its width, was incorrectly given in Paper I as 1.21 minutes, due to an error in the distance from the midpoint of the scattering chamber to the detector. The correct value for this distance, 2.493 cm, leads to a geometric aperture of 0.96 minute.

Total collision cross sections, as a function of the beam energy, E, are summarized in Table I where observed values $\bar{S}_w$, $\bar{S}_n$, and smoothed values S_w, S_n, read from curves in Fig. 1, are listed for each detector, along with the percentage deviations between the observed and smoothed values. The values of $\bar{S}_w$ or $\bar{S}_n$ at each energy are, in general, averages of several determinations made at different scattering pressures to insure the absence of multiple scattering, and to increase the probable accuracy of the results. For both detectors, observed cross sections were calculated from the relation

$$\bar{S}_w(\text{or } \bar{S}_n)=[4.82\times10^{-3}T\log(I_0/I)]/P_{sc} \times(P_{sc}\text{ in mm of Hg};\ \bar{S}_w,\ \bar{S}_n\text{ in }A^2), \quad (1)$$

where T is the absolute temperature, and P_{sc}, the pressure, of the scattering gas. I_0 and I are the unscattered and scattered beam intensities, respectively. Equation (1) yields values of $\bar{S}_w$ or $\bar{S}_n$ which are within 0.5 percent of those given by Eq. (36) in Paper I. The present equation results from a more rigorous analysis of the scattering in various regions of the scattering section. It also corrects for the error in the scattering chamber to detector distance previously mentioned. Upon completion of the present experiments, the Pirani gauge in the scattering chamber was recalibrated to obtain the best possible values of P_{sc}. The average deviation between scattering pressures corresponding to the original and new calibrations was of the order of one percent.

Previous calculations of interaction potentials from total collision cross sections as a function of energy[1,2,5–7] have assumed that the critical dimension[8] of the beam is negligibly small compared with the corresponding detector dimension. In reality, however, beams have finite width across which the intensity varies, as illustrated in Fig. 2 where typical profiles, as measured with the narrow detector, are shown. Thus, in the case of the wide detector, particles in the unscattered beam which originally struck near the outer edges of the detector, require smaller angular deflections to barely miss the detector than unscattered beam particles which originally struck nearer the center. It is, therefore, necessary to consider an *effective* angular aperture, rather than the geometric angular aperture. The calculation of this effective aperture involves averaging, over the width of the detector, the scattering probabilities, weighted for intensity, of the particles in the unscattered beam. In the case of the narrow detector, there are two major effects which produce a large difference between the geometric and effective angular apertures. One is the variation in intensity across the width of the beam; the other, the scattering of particles to the detector from portions of the beam beyond the detector. The effect of scattering to the detector may be described qualitatively by considering an ideal beam whose intensity is constant across its width (a so-called square beam) which impinges upon a detector whose width is negligible in comparison with that of the beam. For this idealized situation, the probability that a particle will be scattered from the beam axis to regions beyond the detector is equal to the probability that a particle from regions of the beam beyond the detector will be scattered to the detector, if the scattering angle for the two events is the same and does not exceed the half-angle subtended by the beam width with respect to the detector. The effective aperture, or minimum angle through which a beam particle must be scattered

TABLE I. Summary of collision cross section results.

	Wide detector			Narrow detector		
E ev	$\bar{S}_w$ A^2	S_w A^2	Percent deviation	$\bar{S}_n$ A^2	S_n A^2	Percent deviation
500	8.08	7.93	+1.9			
600	7.43	7.48	−0.7			
700	7.15	7.12	+0.4	7.63	7.87	−3.1
800	6.80	6.81	−0.1	7.47	7.51	−0.5
900	6.68	6.56	+1.2	7.21	7.21	0.0
1000	6.28	6.34	−1.0	6.95	6.94	+0.1
1100	6.09	6.15	−1.0	6.77	6.72	+0.7
1200	5.78	5.98	−3.5	6.63	6.51	+1.2
1300	5.73	5.82	−1.6	6.57	6.33	+3.7
1400	5.66	5.69	−0.3	6.25	6.17	+1.3
1500	5.54	5.56	−0.4	6.04	6.02	+0.3
1600	5.45	5.45	0.0	5.87	5.89	−0.3
1700	5.42	5.34	+1.5	5.83	5.76	+1.2
1800	5.30	5.24	+1.1	5.60	5.64	−0.7
1900	5.23	5.15	+1.5	5.47	5.54	−1.2
2000	5.10	5.07	+0.6	5.25	5.44	−3.6
2100				5.36	5.35	+0.2

[5] I. Amdur, J. Chem. Phys. **11**, 157 (1943).
[6] Amdur, Davenport, and Kells, J. Chem. Phys. **18**, 525 (1950).
[7] Amdur, Kells, and Davenport, J. Chem. Phys. **18**, 1676 (1950).

[8] When, as in the present case, the beam cross section at the plane of the detector is approximately a long narrow rectangle, the beam width is the critical dimension.

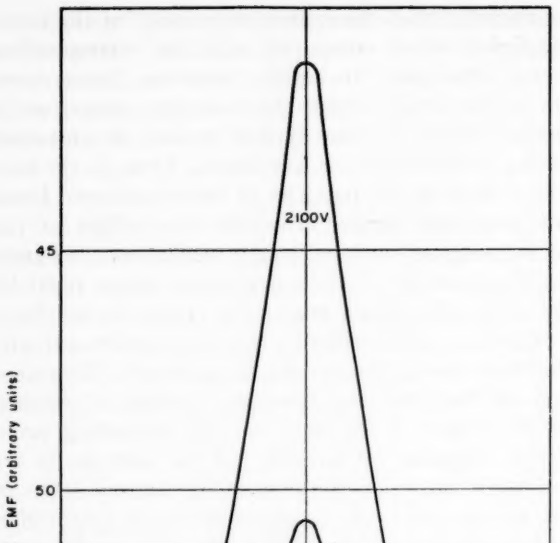

FIG. 2. Typical intensity profiles of unscattered beams.

to be permanently lost to the detector, therefore, must exceed this half-angle. Thus, the effective aperture is the same as the geometric aperture of the reciprocal beam-detector system, namely, a beam of negligible width which impinges upon the midpoint of a detector whose width is equal to that of the square beam. The above considerations may be applied to the present case by taking into account the variation of intensity across the beam width and the finite width of the narrow detector.

To analyze quantitatively the effect of the shape and intensity distribution of the beam on total collision cross sections measured with the wide detector, it is necessary to know the form of the interaction potential between the beam and scattering particles, the geometry of the scattering chamber-detector system, shown in Fig. 3, and details of the shape and intensity distribution of the unscattered beam, represented in Figs. 3 and 2, respectively.

If the interaction potential is of the form $V(r)=K/r^s$, the total collision cross section as measured with the wide detector may be written

$$\bar{S}_w=\frac{\pi(KC/E)^{2/s}}{\int_0^{d_w} I_0(x)dx}\left\{\int_0^{d_w} I_0(x)[\theta_w(x)]^{-2/s}dx - \frac{m_1+m_2}{m_2C}\int_0^{d_w} I_0(x)[\theta_w(x)]^{1-2/s}dx\right\}, \quad (2)$$

where C is a constant, $\pi^{\frac{1}{2}}\Gamma(s/2+\frac{1}{2})/\Gamma(s/2)$; E, the kinetic energy of the beam particle; d_w, the half-width of the detector; $I_0(x)$, the intensity of the unscattered beam at a point x along the half-width of the detector; $\theta_w(x)$, the angle, in apparatus coordinates, through which beam particles, originally incident on x, must be scattered to be lost to the detector; m_1, the mass of the beam particle; and m_2, the mass of the scatterer. Equation (2) which may be derived from relations for small angle scattering,[9,10] assumes negligible beam intensity beyond the edges of the detector, a condition which is fulfilled in the present case. Because of the extremely small values of $\theta_w(x)$ which are characteristic of the present geometry, the second term in Eq. (2) is extremely small compared to the first term, about 0.1 percent. It is therefore possible, with an error of less than 0.5 percent, to use only the first term in calculating numerical values of the constant K in the interaction potential. Although both terms have been given for the sake of completeness, for the purposes of the present paper, Eq. (2) will hereafter be considered as a single term expression.

For any selected position along the half-width of the detector, $[\theta_w(x)]^{-2/s}$ is an average quantity which is a function not only of the index s, but of the scattering chamber-detector geometry. For example, by referring to Fig. 3, it can be seen that particles from the unscattered beam which impinge upon the detector at x, will be scattered by collisions which occur in the region RS_1S_2T of the scattering chamber. These collisions can result in losses to the detector by deflecting the beam particles through angles which will cause them to strike the base AA of the scattering chamber at points beyond the edges of the exit slits S_1, S_2, or to pass beyond the edges of the detector D_1, D_2. Integrals for $[\theta_w(x)]^{-2/s}$ corresponding to these different scattering possibilities lead to the relation

$$\begin{aligned}[\theta_w(x)]^{-2/s}=&\alpha\{\beta d^{1+2/s}-[(2+2/s)b]^{-1}(\beta-e)\\&\times(d^{2+2/s}-c^{2+2/s})-ec^{1+2/s}\}+\gamma\{db^{1+2/s}\\&+(b-w)(d-w)[(1+\delta)^{1-2/s}(d-w)^{2/s}\\&-(b-w)^{2/s}]+(2+2/s)^{-1}\\&\times[(b-w)^{2+2/s}-b^{2+2/s}]-(1-2/s)\\&\times(1+\delta)^{-2/s}c^{2+2/s}-(2+2/s)^{-1}(1+2\delta/s)\\&\times(1+\delta)^{-2/s}[(d-w)^{2+2/s}-c^{2+2/s}]\},\end{aligned} \quad (3)$$

[9] E. H. Kennard, *Kinetic Theory of Gases* (McGraw-Hill Book Company, Inc., New York, 1938), pp. 115 ff.
[10] M. C. Kells, J. Chem. Phys. **16**, 1174 (1948).

where α, β, and δ are functions of x, and γ is a constant independent of x. These quantities are related to s, x, and the fixed dimensions in Fig. 3 as follows:

$$\alpha=(1+2/s)^{-1}(f-x)^{-2/s}c[be(b+2c)]^{-1};$$
$$\beta=(2c)^{-1}[b(2x+e)+2ac]+b(f-x)[c(1-2/s)]^{-1};$$
$$\gamma=(1-4s^2)^{-1}e^{1-2/s}[be(b+2c)]^{-1};$$
$$\delta=(f+x-e)/e.$$

Equation (3) has been so arranged that the term which includes the α factor takes account of scattering with respect to D_2 and S_2, while the remaining term, which includes the γ factor, takes account of scattering with respect to D_1 and S_1. Values of $[\theta_w(x)]^{-2/s}$ for negative values of w, corresponding to $0<x<2.89\times10^{-3}$ cm, cannot be calculated from Eq. (3) as written above, but must be obtained by extrapolation or by making modifications in the equation. These modifications can be obtained from geometrical considerations which apply when $w<0$, but in view of the small magnitude of the change in $[\theta_w(x)]^{-2/s}$ produced by extrapolation, it does not seem desirable to present a detailed discussion of the procedure.

The procedure for using Eq. (2) to obtain numerical values of the potential parameters involves the following steps:

(1) Values of $[\theta_w(x)]^{-2/s}$ are calculated for a number of values of x and of s. For convenience, integral values of s are chosen.

(2) For each value of x, the average quantity, $\langle\theta_w^{-2/s}\rangle_{Av}$, defined as $\{\int_0^{d_w}I_0(x)[\theta_w(x)]^{-2/s}dx\}/\int_0^{d_w}I_0(x)dx$, is obtained by graphical integration. Since $\langle\theta_w^{-2/s}\rangle_{Av}$ is insensitive to the choice of function for $I_0(x)$, an approximate relation is adequate. The actual function which was chosen was

$$I_0(x)=I_0(0)(1-x/d_w), \tag{4}$$

where $I_0(0)$ is the axis intensity of the unscattered beam. The values of $\langle\theta_w^{-2/s}\rangle_{Av}$ for the selected integral values of s are fitted with an empirical analytical function which can be used to compute $\langle\theta^{-2/s}\rangle_{Av}$ for any given value of s.

(3) The wide detector results of Table I are used to obtain a plot of $\log\bar{S}_w$ *vs* $\log E$. The index s of the potential energy function is determined from the slope and the parameter K from the intercept, which may be written $\log\pi(KC)^{2/s}\langle\theta_w^{-2/s}\rangle_{Av}$.

Strictly, in deriving Eq. (2), classical mechanics should not be used when the scattering angles are sufficiently small to introduce significant diffraction effects,[11] for example, for angles corresponding to unscattered beam particles striking the detector near $x=f$. In the present case, however, where the scattering probability for a given angle is weighted according to the unscattered beam intensity, classical mechanics has been used throughout. This is permissible because $I_0(x)$ approaches zero as x approaches d_w (or f), and the contribution of $I_0(x)[\theta_w(x)]^{-2/s}$ to $\langle\theta_w^{-2/s}\rangle_{Av}$ also approaches zero as x approaches f.

The above calculation procedure with the wide detector results in Table I, leads to the following numerical results:

$$\langle\theta_w^{-2/s}\rangle_{Av}=(440.9+1957/s^2)^{2/s}$$
(θ in radians, $4\leqq s\leqq10$),
$$\log\pi(KC)^{2/s}\langle\theta_w^{-2/s}\rangle_{Av}=-2.0397;$$
$s=6.19$ from $\log\bar{S}_w(A^2)$ *vs* $\log E$(ergs),
$$\langle\theta_w^{-2/6.19}\rangle_{Av}=7.409;\quad C=2.995,$$
$$V(r)=K/r^s=9.56\times10^{-12}/r^{6.19}\text{ ergs}(r\text{ in }A). \tag{5}$$

Equation (5), which is valid for r between 1.27A and 1.59A, is shown in Fig. 4 as curve A.

In order to obtain numerical values of the potential parameters from the narrow detector results in Table I, Eq. (2) is written in the form

$$\bar{S}_n=\pi(KC/E)^{2/s}\langle\theta_n^{-2/s}\rangle_{Av}, \tag{6}$$

where $\langle\theta_n^{-2/s}\rangle_{Av}$ now involves the geometry of the beam with respect to the narrow detector. In deriving a rela-

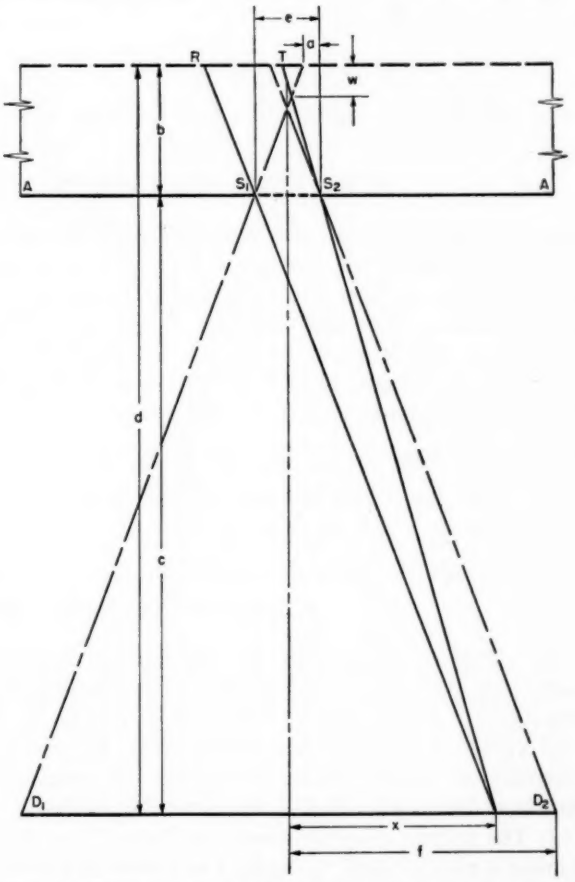

FIG. 3. Geometry of scattering chamber-detector system. Fixed dimensions (in cm): scattering chamber $\cdots a=6.223\times10^{-4}$; $b=0.506$; $e=2.540\times10^{-3}$; wide detector (half-width, $d_w=1.016\times10^{-2}$) $\cdots d=b+c=2.853$; $f=1.016\times10^{-2}$; narrow detector (half-width, $d_n=6.985\times10^{-4}$) $\cdots d=b+c=2.746$; $f=9.754\times10^{-3}$.

[11] H. S. W. Massey and C. B. O. Mohr, Proc. Roy. Soc. (London) A141, 434 (1933).

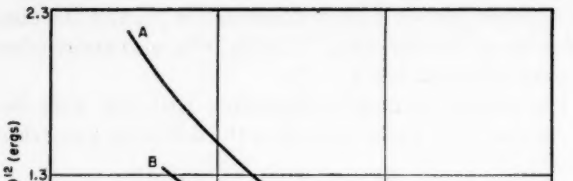

FIG. 4. Potential energy between two helium atoms: A. Wide detector results; B. Narrow detector results.

tion for it, it is necessary to take account of the variation of intensity across the width of the beam and the scattering of particles to the detector from the portions of the beam beyond the detector, as indicated earlier in the qualitative discussion of the reciprocal features of the beam-detector system. The formal expression may be written

$$\langle\theta_n^{-2/s}\rangle_{Av}=(2b)^{-1}\int_0^b(d-z)^{2/s}dz \times\left[\int_0^{d_n}\int_{d_n}^{f}I_0(x)dxdy\right]^{-1}\int_0^{d_n}\int_{d_n}^{f}I_0(x) \times[(x-y)^{-2/s}+(x+y)^{-2/s}]dxdy, \quad (7)$$

where x, y, and z are variable positions along the half-width of the beam, the half-width d_n of the detector, and the length of the scattering chamber, respectively. If the distance from the midpoint of the scattering chamber to the detector, $d-b/2$, is set equal to L, and if $I_0(x)$ is set equal to $I_0(0)(1-x/d_w)$, to the second order of small quantities, Eq. (7) reduces to

$$\langle\theta_n^{-2/s}\rangle_{Av}=L^{2/s}s^2[dn(f-d_n)(2d_w-f-d_n)(s-2) \times(2s-2)]^{-1}\{[(f+d_n)^{2-2/s}-(f-d_n)^{2-2/s}] \times(d_w-f)-(2d_n)^{2-2/s}(d_w-d_n) +s[(f+d_n)^{3-2/s}-(f-d_n)^{3-2/s} -(2d_n)^{3-2/s}](3s-2)^{-1}\}. \quad (8)$$

The calculation procedure for the narrow detector results is similar to that described in connection with the wide detector results and is carried out as follows:

(1) Values of $\langle\theta_n^{-2/s}\rangle_{Av}$ are computed from Eq. (8) for a number of integral values of s, and an empirical analytical function is used to represent the results.

(2) The narrow detector results in Table I are used to make a plot of $\log\bar{S}_n$ *vs* $\log E$. The potential parameters are determined from the slope and intercept of the plot, as in the case of the wide detector.

The numerical results obtained from the above procedure may be summarized in the following manner:

$$\langle\theta_n^{-2/s}\rangle_{Av}=(797.0+554.5/s)^{2/s} \quad (\theta \text{ in radians}, 4\leqq s\leqq 11),$$

$$\log\pi(KC)^{2/s}\langle\theta_n^{-2/s}\rangle_{Av}=-2.2551;$$

$s=5.68$ from $\log\bar{S}_n(A^2)$ *vs* $\log E(\text{ergs})$,

$$\langle\theta^{-2/5.68}\rangle_{Av}=10.95; \quad C=2.859,$$

$$V(r)=K/r^s=5.96\times10^{-12}/r^{5.68}\ \text{ergs}(r \text{ in } A). \quad (9)$$

Equation (9), which is valid for r between 1.30A and 1.58A, is shown in Fig. 4 as curve B. The ratio of the value of $V(r)$ calculated from Eq. (5) to that calculated from Eq. (9) varies from 1.37 to 1.27 as r increases from 1.30A to 1.58A. A single relation which gives values intermediate between those of Eq. (5) and Eq. (9) may be written

$$V(r)=7.55\times10^{-12}/r^{5.94}\ \text{ergs}(r \text{ in } A). \quad (10)$$

Calculated values of S_w based on Eq. (10) are between 4.3 and 6.1 percent lower than the smoothed values in Table I. In the case of S_n, the calculated values are between 4.8 and 6.2 percent higher than the corresponding tabulated values.

Derived values of $V(r)$ are very sensitive to the magnitude of the experimental values of the cross sections, and to deviations of the actual system from an ideal system in which an unscattered beam, whose critical dimension is negligible compared with the corresponding detector dimension, impinges normally upon the midpoint of the detector; that is, to the difference between the effective and geometric angular apertures. For example, if instead of considering effective apertures by taking into account beam shape, intensity distribution, and scattering to a narrow detector from a relatively wide beam, simple geometric apertures were used, the ratio of $V(r)$ values obtained from the wide-detector results to those obtained from narrow-detector results would be about 0.17 instead of about 1.3 as found above. In view of this, the agreement between Eqs. (5) and (9) is considered satisfactory, and Eq. (10) will be taken as an adequate representation of the potential derived from both wide and narrow detector results.

The present investigation increases considerably the information available from experimental measurements, concerning the interaction potential of helium atoms at small distances. The potential in the range 0.52A to 1.02A has been derived from previous scattering experiments,[1,2] while Mason and Rice[12] have used experimental values of the compressibility[13] and viscosity[14] of

[12] E. A. Mason and W. E. Rice (private communication).

[13] J. D. A. Boks and H. Kammer Onnes, Commun. Kammerlingh-Onnes Lab. Univ. Leiden No. 170a (1924); L. Holborn and J. Otto, Z. Physik **33**, 1 (1925); **38**, 359 (1926); G. P. Nijhoff and W. H. Keesom, Commun. Kammerlingh-Onnes Lab. Univ. Leiden No. 188b (1927); Nijhoff, Keesom, and Iliin, Commun. Kammerlingh-Onnes Lab. Univ. Leiden 188c (1927); Tanner and Masson, Proc. Roy. Soc. (London) **A122**, 283 (1929); A. Michels and H. Wouters, Physica **8**, 923 (1941); W. G. Schneider and J. A. H. Duffie, J. Chem. Phys. **17**, 751 (1949); J. L. Yntema and W. G. Schneider, J. Chem. Phys. **18**, 641 (1950).

[14] Y. Ishida, Phys. Rev. **21**, 550 (1923); M. N. States, Phys. Rev. **21**, 662 (1923); A. G. Nasini and C. Rossi, Gazz. chim. ital.

helium to derive a relation for $V(r)$ for the range 1.90A to 2.30A. Their results may be represented by

$$V(r)=[2.87\exp(-3.96r)-0.0232/r^6]\times10^{-10}\text{ ergs}(r\text{ in }A). \quad (11)$$

The range of r for which Eq. (10) is valid, 1.27A to 1.59A is sufficient to permit interpolation between 1.02A and 1.27A, and between 1.59A and 1.90A to obtain intermidate values of $V(r)$. Such values obtained by interpolation between terminal points of two derived potential curves would be expected to be more reliable than values obtained by extrapolation from a single curve. Although it was not possible to find a relatively simple analytical form to represent $V(r)$ over the complete range 0.52A to 2.30A, the potential derived from the present scattering experiments as well as that obtained from compressibility and viscosity measurements can be represented within 7 percent (with an average absolute deviation of about 3 percent) by the relation

$$V(r)=6.18\times10^{-10}\exp(-4.55r)\text{ ergs}(r\text{ in }A). \quad (12)$$

It is suggested, therefore, that within the limits indicated, Eq. (12) may be used to represent the interaction potential between 1.27A and 2.30A.

In view of the small separation distances involved in the scattering experiments, it seems reasonable to assume that only repulsive forces are involved between 0.52A and 1.59A, and to compare the theoretical values calculated by Rosen[15] for the repulsive energy between two helium atoms with the corresponding values obtained from the scattering experiments. Between 0.52A and 1.02A Rosen's values differ by about 25 percent from those derived from the earlier scattering measurements. In the range 1.27A to 1.59A the discrepancy is about 50 percent. Since Margenau and Rosen[16] have shown that the inherent uncertainty in the theoretical values may be very much larger than the above discrepancies, it is felt that the repulsive potentials calculated from theory and those derived from experiment are in accord.

In summary, therefore, it would appear that the combination of scattering experiments and measurements of gaseous compressibility and viscosity lead to values of the potential energy between two helium atoms at separation distances from 0.52A to 2.30A which appear to be self-consistent and reasonably accurate.

ACKNOWLEDGMENT

The authors are deeply indebted to the Research Corporation which has generously supported the work with grants-in-aid.

58, 433, 898 (1928); M. Trautz and H. Binkele, Ann. Physik **5**, 561 (1930); M. Trautz and R. Zink, Ann. Physik **7**, 427 (1930); M. Trautz and R. Heberling, Ann. Physik **20**, 118 (1934); M. Trautz and I. Husseini, Ann. Physik **20**, 121 (1934); M. Trautz and H. Zimmermann, Ann. Physik **22**, 189 (1935); A. van Itterbeek and W. H. Keesom, Physica **5**, 257 (1938); A. van Itterbeek and O. van Paemel, Physica **7**, 265 (1940); R. Wobser and Fr. Müller, Kolloid-Beih. **52**, 165 (1941); H. L. Johnston and E. R. Grilly, J. Phys. Chem. **46**, 948 (1942); van Itterbeek, van Paemel, and van Lierde, Physica **13**, 88 (1947).

[15] P. Rosen, J. Chem. Phys. **18**, 1182 (1950).

[16] H. Margenau and P. Rosen, J. Chem. Phys. **21**, 394 (1953).

Scattering of High-Velocity Neutral Particles. III. Argon-Argon

I. AMDUR AND E. A. MASON*
Department of Chemistry, Massachusetts Institute of Technology, Cambridge, Massachusetts
(Received December 11, 1954)

Total collision cross sections have been measured for argon atoms, with energies between 700 and 2100 ev, scattered in room temperature argon. Results obtained with two detectors of different geometric aperture are shown to be in accord when allowance is made for beam shape, intensity distribution, and scattering to a detector which is narrower than the beam, in accordance with procedures previously used for helium scattered in helium.

Potential energy information derived from the cross sections may be represented by

$$V(r)=1.36\times10^{-9}/r^{8.33} \text{ ergs}$$

for values of r between 2.18A and 2.69A, and appears to be consistent with that derived from measurements of gaseous compressibility, viscosity, and crystal properties.

ADDITIONAL measurements of the scattering of high-velocity argon atoms in room temperature argon have been obtained in an apparatus which has been previously described.[1] As in the case of recent measurements on helium,[2] two detectors, referred to as wide and narrow, were used. Details for converting the geometric apertures of these detectors, 13.4 and 0.96 minutes, to effective apertures are discussed in the helium paper, hereafter referred to as Paper II. The nomenclature and symbolism in the present paper are the same as in Paper II. Potential energy information derived from the present measurements is valid for a range of interaction distance which lies between that associated with earlier scattering measurements[3,4] and that associated with measurements of gaseous compressibility,[5] viscosity,[6] and crystal properties.[7]

The experimental results are shown in Table I where values of $\bar{S}_w$ and $\bar{S}_n$, the experimental total collision cross sections, were computed from Eq. (1) in Paper II. The smoothed values, S_w and S_n, have been calculated from the following equations, obtained by the method of least squares:

$$\log S_w=-0.23595\log E-0.82472, \quad (1)$$

$$\log S_n=-0.24440\log E-0.83193, \quad (2)$$

where S_w and S_n are in A^2 and E, in ergs. The percentage deviations are referred to the experimental values. The results shown in Table I appear graphically in Fig. 1 where the smooth curves have been computed from Eqs. (1) and (2).

As shown in Paper II, if the interaction potential is assumed to be of the form $V(r)=K/r^s$, the index s is obtained from the slope, and the constant K, from the intercept of Eq. (1) or Eq. (2). Specifically, for the wide detector, $s=2/0.23595=8.48$, and for the narrow detector, $s=2/0.24440=8.18$. The intercepts of Eqs. (1) and (2) are related to K through the expressions

$$-0.82472=\log\pi(KC)^{2/8.48}\langle\theta_w^{-2/8.48}\rangle_{Av}, \quad (3)$$

$$-0.83193=\log\pi(KC)^{2/8.18}\langle\theta_n^{-2/8.18}\rangle_{Av}, \quad (4)$$

where $C=\pi^{\frac{1}{2}}\Gamma(s/2+\frac{1}{2})/\Gamma(s/2)$, and $\langle\theta_w^{-2/8.48}\rangle_{Av}$ and $\langle\theta_n^{-2/8.18}\rangle_{Av}$ are the effective apertures of the detectors. General expressions for $\langle\theta_w^{-2/s}\rangle_{Av}$ and $\langle\theta_n^{-2/s}\rangle_{Av}$ in Paper I lead to $\langle\theta_w^{-2/8.48}\rangle_{Av}=4.264$ and $\langle\theta_n^{-2/8.18}\rangle_{Av}=5.225$. Equations (3) and (4) and the values of s obtained from Eqs. (1) and (2) combine to give the following potential energy functions characteristic of the wide and narrow detector results:

$$V(r)=K/r^s=1.50\times10^{-9}/r^{8.48} \text{ ergs } (r \text{ in A}) \quad (5)$$

and

$$V(r)=K/r^s=1.22\times10^{-9}/r^{8.18} \text{ ergs } (r \text{ in A}). \quad (6)$$

TABLE I. Summary of collision cross section results.

E ev	Wide detector $\bar{S}_w$ A^2	Wide detector S_w A^2	Wide detector Percent deviation	Narrow detector $\bar{S}_n$ A^2	Narrow detector S_n A^2	Narrow detector Percent deviation
700	19.66	19.37	+1.5	22.76	22.67	+0.4
800	18.74	18.77	−0.2	22.13	21.97	+0.8
900	18.08	18.25	−0.9	21.09	21.32	−1.1
1000	17.82	17.80	+0.1	20.80	20.78	+0.1
1100	17.25	17.41	−0.9	20.29	20.30	0.0
1200	17.06	17.06	0.0	19.72	19.87	−0.8
1300	16.82	16.74	+0.5	19.48	19.49	−0.1
1400	16.38	16.45	−0.4	18.97	19.14	−0.9
1500	16.18	16.18	0.0	18.91	18.82	+0.5
1600	15.90	15.94	−0.3	18.74	18.53	+1.1
1700	15.55	15.71	−1.0	18.18	18.25	−0.4
1800	15.42	15.50	−0.5	18.10	18.00	+0.6
1900	15.40	15.30	+0.6	17.81	17.77	+0.2
2000	15.22	15.12	+0.7	17.55	17.54	+0.1
2100	15.06	14.95	+0.7	17.25	17.53	−0.5

* Present address: Department of Chemistry, Pennsylvania State University, State College, Pennsylvania.

[1] Amdur, Glick, and Pearlman, Proc. Am. Acad. Arts Sci. **76**, 101 (1948).
[2] I. Amdur and A. L. Harkness, J. Chem. Phys. **22**, 664 (1954).
[3] Amdur, Davenport, and Kells, J. Chem. Phys. **18**, 525 (1950).
[4] H. W. Berry, Phys. Rev. **75**, 913 (1949).
[5] H. Kammerlingh Onnes and C. A. Crommelin, Commun. Kammerlingh-Onnes Lab. Univ. Leiden No. 118b (1910); L. Holborn and J. Otto, Z. Physik **23**, 77 (1924); **30**, 320 (1924); **33**, 1 (1925); Michels, Wijker, and Wijker, Physica **15**, 627 (1949).
[6] Y. Ishida, Phys. Rev. **21**, 550 (1923); M. Trautz and W. Ludewigs, Ann. Physik **3**, 409 (1929); M. Trautz and H. E. Binkele, Ann. Physik **5**, 561 (1930); M. Trautz and R. Zink, Ann. Physik **7**, 427 (1930); A. van Itterbeek and O. van Paemel, Physica **5**, 1009 (1938); R. Wobser and Fr. Müller, Kolloid-Beih. **52**, 165 (1941); H. L. Johnston and E. R. Grilly, J. Phys. Chem. **46**, 948 (1942); V. Vasilesco, Ann. phys. **20**, 137, 292 (1945).
[7] G. Kane, J. Chem. Phys. **7**, 603 (1939).

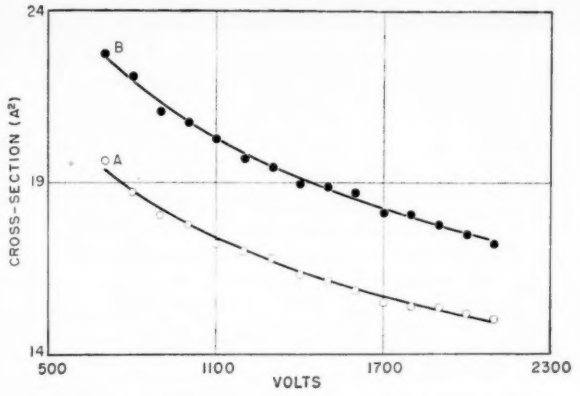

FIG. 1. Total collision cross sections: A. Wide detector; B. Narrow detector.

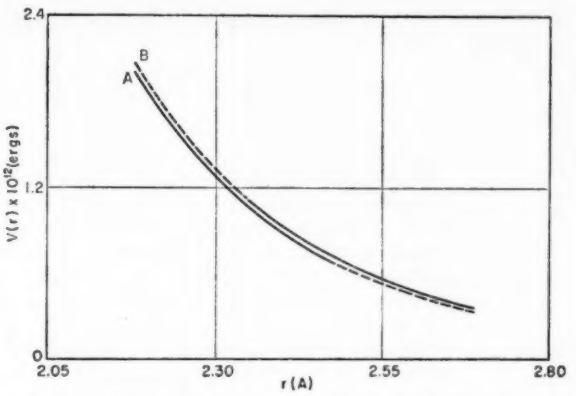

FIG. 2. Potential energy between two argon atoms: A. Wide detector results; B. Narrow detector results.

Equation (5), which is valid for r between 2.18A and 2.48A and Eq. (6), which is valid for r between 2.35A and 2.69A, are shown in Fig. 2 as curves A and B, respectively. The ratio of the value of $V(r)$ calculated from Eq. (5) to that calculated from Eq. (6) varies from 0.951 to 0.936 as r increases from 2.35A to 2.48A, the range of interaction distance which is common to both wide and narrow detector cross sections. When Eq. (5) is used for r values as high as 2.69A and Eq. (6) for values as low as 2.18A, the ratio of the potentials decreases from 0.972 to 0.913 as r increases from 2.18A to 2.69A. A relation, valid for the full range of r, which gives values of $V(r)$ intermediate between those of Eq. (5) and Eq. (6), and which will be taken as the potential function derived from both wide and narrow detector results may be written in the form

$$V(r)=1.36\times10^{-9}/r^{8.33} \text{ ergs } (r \text{ in } A). \quad (7)$$

Calculated values of S_w based on Eq. (7) are between 0.50 and 0.05 percent higher than the smoothed values in Table I, and calculated values of S_n are between 0.50 and 0.05 percent lower than the corresponding tabulated values.

The present results again illustrate the need, as discussed in Paper II, for considering effective, rather than geometric, apertures. If simple geometric apertures had been used, the ratio of $V(r)$ values obtained from wide detector results to those obtained from narrow detector results would have been about 0.12 instead of about 0.94.

The ranges of interaction distance involved in earlier scattering measurements[3,4] are 0.6A to 1.2A and 1.37A to 1.84A, while the range associated with measurements of gaseous compressibility, viscosity, and crystal properties is 2.98A to 4.83A. The range involved in the present measurements, 2.18A to 2.69A, is sufficiently wide and in the proper region to permit reasonably accurate graphical interpolations. The only interpolation region for which an analytical form could be found of sufficient simplicity for calculation purposes was 2.69A to 2.98A. The relation

$$V(r)=9.03\times10^{-10}/r^{7.87} \text{ ergs } (r \text{ in A}) \quad (8)$$

represents the present results from 2.18A to 2.69A within 5 percent (with an average absolute deviation of less than 3 percent) and at 2.98A is within 3.5 percent of the value given by the relation

$$V(r)=[153\exp(-3.62r)-0.994/r^6]\times10^{-10} \text{ ergs } (r \text{ in } A), \quad (9)$$

which is valid for r between 2.98A and 4.83A. Equation (9) has been derived by Mason and Rice[8] from the experimental results on gaseous compressibility, viscosity, and crystal properties. It is suggested that Eq. (8) be used to represent the interaction potential between 2.18A and 2.98A, and that Eq. (9) be used from 2.98A to 4.83A.

No experimental values of $V(r)$ in the range between 2.18A and 2.69A exist for comparison with the present results. Kunimune[9] has calculated the repulsive portion of the interaction energy between two argon atoms at separation distances of 3.70A, 2.64A, and 2.12A. At 3.70A his value is threefold greater than that calculated from the first term of Eq. (9), whereas at 2.64A and 2.12A his values are eightfold greater than the total potential obtained from the present scattering experiments. (The experimental value of $V(r)$ at 2.12A is obtained by extrapolation from 2.18A.) In view of the relatively small contribution of the attractive potential at 2.64A and 2.12A, it is estimated that Kunimune's repulsive potentials are about sixfold too great at these distances. However, it is felt that these theoretical values are not necessarily in disagreement with the present results, because of the approximations involved in Kunimune's calculations and the known magnitude of the error in his results at 3.70A.

ACKNOWLEDGMENT

The authors wish to thank the Research Corporation for its generous support of the work with grants-in-aid.

[8] E. A. Mason and W. E. Rice (private communication).
[9] M. Kunimune, J. Chem. Phys. 18, 754 (1950); Progr. Theoret. Phys. (Japan) 5, 412 (1950).

Reaction of Cyclohexane with Mercury-6($^3P_1$) Atoms*

P. W. Beck, D. V. Kniebes† and H. E. Gunning
Department of Chemistry, Illinois Institute of Technology, Chicago, Illinois

(Received October 20, 1953)

An investigation has been made of the mercury-6($^3P_1$)-photosensitized decomposition of cyclohexane at 29.30±0.01°C, under static conditions. The products of the reaction are hydrogen, bicyclohexyl, and cyclohexene, in order of decreasing importance. The mean quantum yields of cyclohexane disappearance, hydrogen formation, and cyclohexene formation were found to increase slightly with increasing substrate pressure; at 90-mm cyclohexane pressure, the values are 0.83, 0.43, and 0.03, respectively. Extrapolation to initial conditions of data on the variation of mean quantum yield with time at constant substrate pressure gave 0.55 for the initial quantum yield of hydrogen formation, and 0.17 for cyclohexene formation, independent of substrate pressure. From the foregoing initial quantum yield data, taken in conjunction with the stoichiometry of the reaction, a value of 0.93 was obtained for the initial quantum yield of cyclohexane consumption.

Absence of hexane, dodecanes, *n*-hexylcyclohexane, and low molecular weights products was taken as evidence of the stability of the cyclohexane ring during reaction.

The results of the investigation can be adequately accounted for by the following simple mechanism:

(1) cyclo C_6H_{12}+Hg 6($^3P_1$)→cyclo C_6H_{11}+H+Hg 6($^1S_0$),

(2) H+cyclo C_6H_{12}→H_2+cyclo C_6H_{11},

(3) 2 cyclo C_6H_{11}→cyclo C_6H_{10}+cyclo C_6H_{12},

(4) 2 cyclo C_6H_{11}→bicyclo $C_{12}H_{22}$,

(5) H+cyclo C_6H_{10}→cyclo C_6H_{11}.

Steps (1) to (4) describe the reaction under initial conditions.

From the initial quantum yield data the ratio k_4/k_3, the ratio of the rates of recombination to disproportionation for cyclohexyl radicals, was evaluated at 2.2. In short, recombination is approximately twice as fast as disproportionation for cyclohexyl radicals.

INTRODUCTION

In the study of the reactions of hydrocarbons with Hg-6($^3P_1$) atoms in the gas phase, a great deal of evidence has now accumulated which points fairly unequivocally to the fact that the primary process involves C—H bond scission exclusively. Investigations on the cycloparaffins in this laboratory indicate that they also conform to the aforementioned generalization.[1–3] Earlier published data on the complex cyclopropane reaction led to the conclusion that ring cleavage occurred in the primary process.[4,5] However a detailed study[6] which has recently been completed on this reaction suggests that the seemingly exceptional behavior of this molecule arises from the rapid isomerization of cyclopropyl radicals formed in the primary process, rather than by primary C—C bond rupture.

The present investigation on cyclohexane formed part of our general program on the mercury-6($^3P_1$) reactions of the cycloparaffins. The results follow.

EXPERIMENTAL

The general experimental technique used in this series of investigations on the cycloparaffins has been previously described.[2,7]

The cylindrical fused quartz reaction cell was 8.5 cm long and 5 cm in diameter. The thermostat, wherein the cell was immersed, was maintained at 29.30±0.01°C. The connecting tubing of the reaction system was constructed entirely of heavy-walled 3-mm i.d. capillary, to minimize the effects of ambient temperature fluctuations on the pressure readings. The Pearson differential manometer was maintained at the same temperature as the reaction cell.[2] Condensable products for mass spectral analysis and chemical characterization were removed from the system by freezing them in a small detachable finger trap which was connected to the reaction cell.

The resonance lamp[2] was operated from a Sola Luminous Tube Transformer supplying 3000 v at 30 ma. Primary input to the lamp transformer was stabilized as before with a Sola Constant Voltage Transformer.

* This work was supported by the U. S. Atomic Energy Commission under Contract AT(11–1)–43. This paper formed part of a dissertation submitted by one of us (P.W.B.) in partial fulfillment of the requirements for the Ph.D. degree at Illinois Institute of Technology. A portion of this paper was presented before the Division of Physical and Inorganic Chemistry at the 122nd meeting of the American Chemical Society, Atlantic City, New Jersey, September, 1952.

† Institute of Gas Technology, Illinois Institute of Technology, Chicago, Illinois.

[1] Allen, Kantro, and Gunning, J. Am. Chem. Soc. **72**, 3588 (1950).

[2] M. Schlochauer and H. E. Gunning, J. Chem. Phys. **19**, 474 (1951).

[3] D. L. Kantro and H. E. Gunning, J. Chem. Phys. (to be published).

[4] H. E. Gunning and E. W. R. Steacie, J. Chem. Phys. **17**, 351 (1949).

[5] R. Scott and H. E. Gunning, J. Phys. Chem. **56**, 156 (1952).

[6] Ford, Mori, and Gunning (unpublished work).

[7] G. A. Allen and H. E. Gunning, J. Chem. Phys. **16**, 1146 (1948).

The 1849A radiation from the lamp was removed with a Vycor 7910 filter.

For the generation of larger quantities of condensable products, an auxiliary apparatus was employed similar to that described in our work on the cyclopropane reaction.[5] Here the tubular reaction cell, which was inserted axially through the coils of the quartz resonance lamp, was fashioned of 30-mm i.d. Vycor 7910 tubing.

The cyclohexane used in the investigation was National Bureau of Standards sample No. 209a-8s. Stated limits of impurity were 0.010±0.006 mole percent. The ampoules of cyclohexane were connected to the reaction system, via Fugassi valves.[2]

The hydrogen (Mathieson Reagent Grade) was 99.9 percent pure. The cyclopropane (Ohio U.S.P. Grade) used in the actinometric runs was purified by several trap-to-trap distillations. Mass spectral analysis of the purified material gave cyclopropane 99.9 percent, propane 0.1 percent.

The bicyclohexyl used was obtained by fractional distillation of Monsanto Technical Grade material on a Podbielniak Hypercal column. Density, refractive index, and boiling point of the purified material were in accordance with reported values on this compound.

The *n*-hexylcyclohexane was synthesized by standard methods and purified in a similar manner to the bicyclohexyl.

The mass spectral data were obtained with a Consolidated Engineering Model 21-103 instrument. For the infrared data a Perkin-Elmer double-beam instrument was employed.

TABLE I. Quantum yield of pressure decrease at various initial pressures of cyclohexane.

Initial cyclohexane pressure mm	Duration of exposure min	Quantum yield of pressure decrease mole/einstein
3.6	20	0.048
10.3	50	0.172
10.3	60	0.160
15.0	60	0.216
18.7	30	0.25
26.7	48	0.31
27.6	34	0.35
28.0	60	0.32
28.6	60	0.31
39.6	30	0.34
40.8	30	0.40
50.4	30	0.46
51.6	60	0.48
52.0	30	0.46
54.0	30	0.50
61.8	50	0.58
62.0	60	0.60
64.5	30	0.68
66.0	30	0.63
69.0	30	0.63
70.6	60	0.70
74.1	30	0.70
77.5	30	0.81
78.6	156	0.83
79.2	60	0.84
85.1	60	0.93

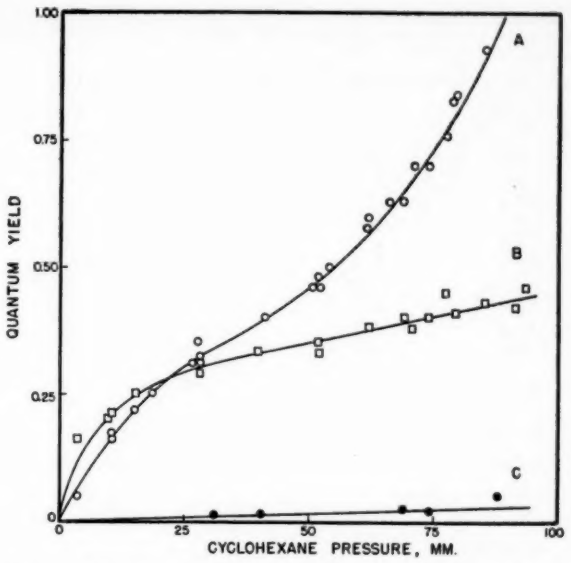

FIG. 1. Curve *A*, quantum yield of pressure decrease. Curve *B*, quantum yield of hydrogen formation. Curve *C*, quantum yield of cyclohexene formation.

RESULTS

The reaction is pressure-decreasing, with the rate of pressure decrease reaching a maximum and constant value after two to three minutes of exposure. After approximately thirty minutes of exposure, the rate was observed to fall off with increasing rapidity. During the irradiation, minute droplets of a colorless liquid were noted to form on the incident face of the cell. The pressure decrease is due to the condensation of this product.

In order to ascertain whether the falling-off in the rate of pressure decrease, upon prolonged exposure, arose from absorption of the incident radiation by the liquid product, several runs were carried out as follows: at the end of a run, the system was evacuated, but the cell was not removed for cleaning. A new charge of cyclohexane was admitted at the same pressure as in the preceding run, and the lamp was turned on. For this run the rate of pressure decrease was found to coincide with the final rate of pressure decrease in the clean cell. As an example, at a pressure of 45 mm of cyclohexane, the rate of pressure decrease, during the first thirty minutes of exposure in a cleaned cell, was 0.233 mm/min. After an hour of exposure, the slope of the pressure-time curve corresponded to 0.164 mm/min. When the run was resumed with a fresh charge of cyclohexane, the constant rate of pressure decrease was 0.168 mm/min. From data such as these it was concluded that the reduced rate at long exposures could be attributed to the screening effect of the condensed product.

The light intensity was checked at regular periods during the course of the investigation, using the cyclopropane reaction as the actinometer.[2] The mean value of the light intensity at 2537A was $2.5\pm0.05\times10^{-6}$ einstein/min.

TABLE II. Mean quantum yield of hydrogen formation as a function of cyclohexane pressure for runs of 30 to 60 minutes' duration.

P_0 mm	Q_{H_2}	P_0 mm	Q_{H_2}
3.6	0.16	54.0	0.41
9.6	0.20	62.0	0.38
10.3	0.21	69.0	0.40
10.3	0.20	70.5	0.38
15.0	0.25	74.1	0.40
28.0	0.29	77.5	0.45
28.5	0.29	79.2	0.41
39.6	0.33	85.1	0.43
51.6	0.35	91.2	0.42
51.9	0.33	93.3	0.46

The data on the quantum yield of pressure decrease as a function of initial substrate pressure are given in Table I and Fig. 1.

Analysis of the gas, noncondensable in liquid nitrogen, remaining after reaction, showed that it consisted of at least 99 percent mole percent hydrogen. The average rate of hydrogen formation was determined as a function of both cyclohexane pressure and of duration of exposure. The data on the mean quantum yield of hydrogen formation Q_{H_2}, as a function of substrate pressure, P_0, for runs of 30 to 60 minutes duration are given in Table II and Fig. 1.

The dependence of the mean quantum yield of hydrogen formation on exposure time is shown for three substrate pressures in Table III.

The values of $Q_{H_2}^0$, i.e., Q_{H_2} at zero time, given in Table III, were obtained by linear extrapolation on a semilog plot of the 10-, 4-, and 2-min values. It is seen from Table III that the primary quantum yield of hydrogen formation $Q_{H_2}^0$ is independent of cyclohexane pressure in the complete quenching region, at a mean value of 0.55 mole/einstein.

TABLE III. Mean quantum yield of hydrogen formation as a function of exposure time at three substrate pressures.

P_0 mm	Duration of run minutes	Q_{H_2} mole/einstein
...	0	0.50
27.9	2	0.46
28.1	4	0.43
27.9	10	0.36
28.0	60	0.29
28.5	60	0.29
...	0	0.56
51.5	2	0.54
52.3	4	0.50
52.8	10	0.43
51.6	60	0.36
...	0	0.58
73.5	2	0.58
72.0	4	0.54
74.6	4	0.54
72.4	10	0.50
72.7	10	0.48
69.0	30	0.40
70.6	60	0.39

In some of the 60-min runs, small particles of a translucent, wax-like solid were found intermingled with the droplets of liquid, indicating, presumably, a decomposition of the liquid product.

The mass spectra of the liquid nitrogen condensates showed unequivocally the presence of two condensable products, cyclohexene and bicyclohexyl. Cleavage of the cyclohexane ring would be expected to lead to the formation of *n*-hexane, dodecanes, *n*-hexylcyclohexane, and perhaps products with carbon numbers lower than six. The foregoing products were specifically sought for, and found absent. Hence it would seem reasonable to conclude that the cyclohexane ring remains stable during reaction.

In order to gain additional information on the heavy products of the reaction, larger quantities of material were prepared on the auxiliary system. Under these conditions some photolysis of the bicyclohexyl could occur. Two series of runs were performed, and in each case the heavy product was isolated by removal of the C-6 fraction by distillation. In Table IV, the physical properties of the heavy product are compared with those of pure bicyclohexyl.

TABLE IV. Physical properties of heavy product from two series of runs on the auxiliary system.

	Mol. wt.	C (Wt. %)	H (Wt. %)	n_D^{20}	Density (20°C)
Condensable product:					
A-4	184	...	...	1.4881	0.900
A-5	...	86.69	13.25	1.4846	0.902
Bicyclohexyl					
Theor.	166.3	86.66	13.34	...	...
Lit.[a]	...	...	...	1.4796	0.8846

[a] G. Egloff, *Physical Constants of Hydrocarbons* (Reinhold Publishing Corporation, New York, 1940), Vol. II.

From Table IV, it is apparent that hydrocarbons with carbon numbers greater than 12 are present. Recombination of radicals formed by the removal of a hydrogen atom from bicyclohexyl, either by photolysis or radical abstraction reactions, would result in the formation of quater-cyclohexyls, i.e., $C_{24}H_{42}$. Unfortunately, none of the quater-cyclohexyls has been prepared.

The mass spectra of the accumulated heavy product were found to correspond precisely to that for bicyclohexyl. Hence we may conclude that no other C-12 product than bicyclohexyl is present. Any C-24 compounds present in the heavy fraction would, of course, be too involatile for ordinary mass spectrometric detection. In order to circumvent this difficulty, a sample of the heavy product (A-4 series) was run on a Consolidated Engineering Corporation Mass Spectrometer with a special heated inlet system. The results of the analysis, using the "parent peak" method,[8] may be summarized as follows:

[8] M. J. O'Neal and T. P. Wier, Anal. Chem. **23**, 830 (1951).

(1) The predominant molecular type is a C-12 bicycloalkyl, i.e., bicyclohexyl. This compound formed *ca* 80 mole percent of the mixture.

(2) All the compounds present have two to four rings.

(3) The following types of compounds are absent: (a) normal paraffins. (b) Isoparaffins. (c) Monocyclo paraffins. (d) Mono olefins.

In Fig. 2, the infrared absorption spectra of pure bicyclohexyl and heavy product from the A-5 series are compared. The spectra are essentially the same, apart from the absorption peak present at 13.83 mμ in the product but absent in bicyclohexyl. Consequently the solid product present must be structurally very similar to bicyclohexyl.

From the above analytical data, as well as the kinetic data, it is assumed here that the solid products are quater-cyclohexyls.

From the mass spectra of the condensable products from each run, information on the dependence of the mean quantum yield of cyclohexene formation, Q_u, on substrate pressure and exposure time was obtained. The results are summarized in Table V (see Fig. 1). Since cyclohexene is only a very minor constituent of the condensed mixture of undecomposed substrate and products, the quantum yield data could be in error as much as 20 percent. Extrapolation of these data on a semilog plot led to a value of 0.17 ± 0.02 for the primary quantum yield of cyclohexene formation, independent of substrate pressure.

Since the only products of the cyclohexane reaction would seem to be cyclohexene, hydrogen, and bicyclohexyl, the stoichiometry of the reaction can be represented by the two equations

$$\text{Cyclo } C_6H_{12}=\text{Cyclo } C_6H_{10}+H_2,$$
$$\text{Cyclo } C_6H_{12}=\tfrac{1}{2}C_{12}H_{22}+\tfrac{1}{2}H_2.$$

Hence, the rate of bicyclohexyl formation and the rate of cyclohexane consumption can be calculated from the data on the hydrogen and cyclohexene rates.

Direct determination of the rates of bicyclohexyl formation from the mass spectral data gave somewhat lower values than those calculated from the stoichiometry. The reason for the discrepancy became apparent in experiments with synthetic mixtures of cyclohexane, cyclohexene, and bicyclohexyl. The low volatility of the bicyclohexyl prevented its quantitative recovery by liquid nitrogen condensation in the small freezeout trap attached to the reaction cell. Attempts to desorb the bicyclohexyl from the walls by warming the reaction cell increased the amount recovered, but the results were still 10 to 20 percent short of quantitative. Similar difficulties were encountered in the mass spectrometer.

From the stoichiometry of the reaction, taken in conjunction with the fact that the pressure decrease arises essentially from the condensation of the bicyclohexyl from the gas phase, the following relations among

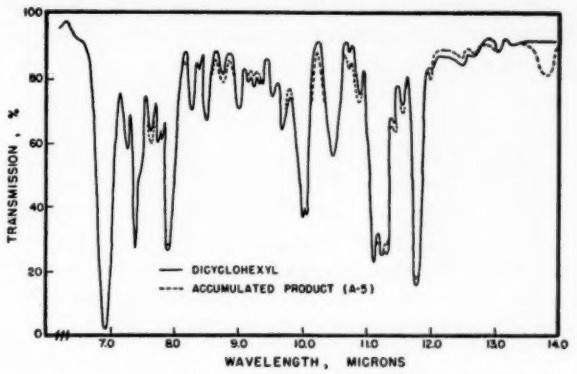

FIG. 2. Infrared absorption spectrum of dicyclohexyl and accumulated product.

the quantum yield should exist:

$$Q_C{}^P=Q_P+Q_{H_2}+Q_u,$$
$$Q_C=2Q_{H_2}-Q_u,$$
$$Q_{C_2}=Q_{H_2}-Q_u.$$

The meanings of the symbols are given in Table VI. In Fig. 1, the experimental quantities, Q_P (curve A), Q_{H_2} (curve B), and Q_u (curve C) are represented as functions of substrate pressure. From the best curves through the experimental points, interpolated values for decadic multiples of the pressure have been obtained and recorded in Table VI.

It is quite apparent from Table VI that the values of $Q_C{}^P$ and Q_C diverge rapidly with increasing substrate pressure. Experiments with liquid bicyclohexyl in the presence of cyclohexane vapor showed very clearly that the discrepancies in the values of the quantum yields of cyclohexane consumption calculated by the two methods were due almost exclusively to the solubility of cyclohexane in the bicyclohexyl formed during reaction.

In the next-to-the-last column of Table VI, the ideal solubilities of cyclohexane in Q_{C_2} moles of bicyclohexyl

TABLE V. Mean quantum yield of cyclohexene formation.

Initial cyclohexane pressure mm	Duration of run min	Mean quantum yield
31.0	30	0.012
40.2	30	0.012
51.5	2	0.11
52.23	4	0.092
52.0	15	0.028
51.6	60	0.008
69.0	30	0.024
70.6	60	0.008
72.4	10	0.052
73.6	2	0.123
74.1	30	0.016
79.2	60	0.004
80.0	15	0.044
81.5	5	0.092
85.2	60	0.012
87.8	30	0.048
91.2	60	0.016
93.3	50	0.040

TABLE VI. Quantum yield data for 30-min runs.[a]

P_0 mm	Q_P	Q_{H_2}	Q_u	Q_{C_2}	$Q_C{}^P$	Q_C	$Q_C{}^P - Q_C$	S moles	$(Q_C{}^P - Q_C)/S$
0	0	0	0	0	0	0	0	0	...
10	0.16	0.21	0	0.21	0.37	0.42	[−0.05]	0.02	...
20	0.26	0.27	0.005	0.26	0.53	0.53	0	0.05	...
30	0.33	0.31	0.010	0.30	0.65	0.61	0.04	0.10	0.4
40	0.39	0.33	0.010	0.32	0.73	0.65	0.08	0.17	0.5
50	0.46	0.35	0.015	0.33	0.82	0.69	0.13	0.23	0.6
60	0.55	0.37	0.020	0.35	0.94	0.72	0.22	0.35	0.6
70	0.67	0.39	0.020	0.37	1.08	0.76	0.32	0.52	0.6
80	0.82	0.41	0.025	0.39	1.26	0.80	0.46	0.78	0.6
90	1.02	0.43	0.030	0.40	1.48	0.83	0.65	1.20	0.5

[a] Explanation of symbols:

P_0 = Initial pressure of cyclohexane.
Q_P = Quantum yield of pressure decrease.
Q_{H_2} = Quantum yield of hydrogen formation.
Q_u = Quantum yield of cyclohexene formation.
Q_{C_2} = Quantum yield of bicyclohexyl formation = $Q_{H_2} - Q_u$.
$Q_C{}^P$ = Quantum yield of cyclohexane consumption from rate of pressure decrease = $Q_P + Q_{H_2} + Q_u$.
Q_C = Quantum yield of cyclohexane consumption from stoichiometry = $2Q_{H_2} - Q_u$.
S = Ideal solubility of cyclohexane in Q_{C_2} moles of bicyclohexyl.

are given for each pressure. In the last column of the table it is seen that $Q_C{}^P - Q_C$ only amounts to about 50–60 percent of the quantity of cyclohexane which could be taken up by the bicyclohexyl at equilibrium.

DISCUSSION

Before proposing a mechanism, the salient features of this investigation of the mercury-6($^3P_1$)-photosensitized decomposition of cyclohexane will be summarized.

(a) The reaction is pressure-decreasing, with the pressure decrease arising from the condensation of heavy product.

(b) The products of the cyclohexane reaction are hydrogen, bicyclohexyl, and cyclohexene. Upon prolonged irradiation, secondary reactions occur which result in the formation of high molecular weight material. From physical, mass spectral, and infrared data on the heavy product, it is concluded that the high molecular weight material is probably a mixture of quater-cyclohexyls, $C_{24}H_{42}$.

(c) Using a light intensity of 2.5×10^{-6} einstein/min, it was found that no appreciable secondary decomposition took place during 30-min exposures.

(d) In the 30-min runs, it was found that the mean quantum yields of cyclohexane disappearance, cyclohexene formation, and hydrogen formation increased slowly with increasing substrate pressure in the complete quenching region. At 90-mm cyclohexane pressure, the aforementioned mean quantum yields were found to be 0.83, 0.03, and 0.40, respectively.

(e) The mean quantum yield of hydrogen formation Q_{H_2} at constant substrate pressure was found to rise rapidly with decreasing exposure time. Extrapolation of Q_{H_2} to zero time, at three different substrate pressures, led to the value 0.55 for the initial quantum yield of hydrogen formation. A similar treatment of the cyclohexene data gave 0.17 for the initial quantum yield of cyclohexene formation.

(f) No mass spectral evidence was found for the presence of hexane, dodecanes, *n*-hexylcyclohexane, or products of carbon number less than 6. From this fact it is concluded that the cyclohexane ring remains stable during decomposition.

From the nature of the products, a mechanism similar to that which has been well established in the mercury-photosensitized reactions of the paraffins immediately suggests itself.

Under initial conditions, the following sequence is proposed:

$$C + \text{Hg } 6(^3P_1) \rightarrow R + \text{H} + \text{Hg } 6(^1S_0), \quad (1)$$

$$\text{H} + C \rightarrow \text{H}_2 + R, \quad (2)$$

$$2R \rightarrow U + C, \quad (3)$$

$$2R \rightarrow C_2, \quad (4)$$

where C represents cyclohexane; R, cyclohexyl radical; U, cyclohexene; and C_2, bicyclohexyl. The assumption of the steady state for (H) and (R) leads to the following primary quantum yield relations:

$$Q_C{}^0 = K\left[\frac{1+2r}{1+r}\right], \quad (5)$$

$$Q_{H_2}{}^0 = K, \quad (6)$$

$$Q_u{}^0 = K\left[\frac{1}{1+r}\right], \quad (7)$$

where $r = k_4/k_3$, the ratio of the rates of recombination to disproportionation for cyclohexyl radicals. The constant K is assumed to represent the fraction of quenching which leads to reaction. The fraction $1-K$ may well represent quenching to the metastable Hg-6($^3P_0$) state.

Since from Table III, $Q_{H_2}{}^0 = 0.55$, Eq. (6) gives $K = 0.55$. Using $K = 0.55$, and $Q_u{}^0 = 0.17$, we obtain from Eq. (7)

$$r = k_4/k_3 = 2.2.$$

Hence the proposed mechanism predicts that cyclohexyl

radicals recombine a little over twice as fast as they disproportionate.

From Eq. (5), the primary quantum yield of cyclohexane can be calculated:

$$Q_C^0 = (0.55)\left[\frac{1+2(2.2)}{1+2.2}\right] = 0.93.$$

From Table VI it can be seen that Q_C has attained the value 0.83 at 90 mm. The mechanism predicts that $Q_C \rightarrow Q_C^0$ with increasing substrate pressure.

From the sharp decline in Q_{H_2} and Q_u with increasing exposure time, it is assumed that under these conditions the cyclohexene rapidly reaches a steady-state concentration by the step

$$H + U \rightarrow R. \tag{8}$$

The sequence (1), (2), (3), (4), and (8) would, therefore, describe the reaction in the 30-min runs. The five-step mechanism yields the following relations:

$$Q_C^S = K\left[\frac{2r}{1+r}\right], \tag{9}$$

$$Q_{H_2}^S = K\left[\frac{r}{1+r}\right], \tag{10}$$

where the superscript indicates the instantaneous quantum yields when the cyclohexene has reached its steady-state concentration. Substituting the numerical values for K and r in (9) and (10), we obtain

$$Q_C^S = 0.76,$$
$$Q_{H_2}^S = 0.38.$$

The mean values of the quantum yields should fall between the initial and steady-state values. Since the onset of the complete quenching region begins at a substrate pressure of approximately 30 mm, the values of Q_C and Q_{H_2} at this pressure should lie, respectively, in the ranges 0.76–0.93, and 0.38–0.55. From Table VI, at 30 mm, $Q_C = 0.61$ and $Q_{H_2} = 0.31$; both somewhat lower than the values allowed by the mechanism. It is not felt, however, that this discrepancy represents an inadequacy in the proposed mechanism, but rather that it reflects errors in the extrapolation of the quantum yields to initial conditions.

CONCLUSIONS

From this investigation it would appear reasonable to conclude that cyclohexyl radicals are remarkably stable, showing little tendency either to isomerize or become hydrogenated. Their reactions seem to be limited to recombination and disproportionation. No evidence was found for atomic cracking reactions, and in this respect they differ from paraffinic free radicals.

In a publication shortly to be submitted to this journal, new data on the cyclopentane reaction will be presented and, in addition, our earlier work on cyclopentane and methylcyclopentane[2] will be reevaluated in the light of our present findings.

ACKNOWLEDGMENT

The authors would like to express their appreciation to Dr. A. C. Hogge and his staff at the Research Laboratories of the Shell Oil Company, Houston, for their kindness in performing the special mass spectral analysis of the high molecular weight products of the cyclohexane reaction.

Further Studies on the Reaction of Cyclopentane with Mercury-6($^3P_1$) Atoms*

P. W. Beck, D. V. Kniebes,† and H. E. Gunning
Department of Chemistry, Illinois Institute of Technology, Chicago, Illinois

(Received October 20, 1953)

A further investigation has been made of the reaction of cyclopentane with Hg6($^3P_1$) atoms at 29.30 ±0.01°C, under static conditions. Analyses, using mass spectrometric techniques, confirm that the only direct products of the reaction are hydrogen, bicyclopentyl, and cyclopentene. No evidence was found for decomposition of the cyclopentane ring.

The kinetics of the reaction can be satisfactorily explained in terms of the following general mechanism:

(1) cyclo C_nH_{2n}+Hg6($^3P_1$)→cyclo C_nH_{2n-1}+H+Hg6($^1S_0$),

(2) H+cyclo C_nH_{2n}→H_2+cyclo C_nH_{2n-1},

(3) 2(cyclo C_nH_{2n-1})→cyclo C_nH_{2n-2}+cyclo C_nH_{2n},

(4) 2(cyclo C_nH_{2n-1})→bicyclo $C_{2n}H_{4n-2}$,

(5) H+cyclo C_nH_{2n-2}→cyclo C_nH_{2n-1}.

Reaction (5) can be ignored at high substrate pressures or low extents of decomposition. The limiting high-pressure values for the quantum yields of cyclopentane disappearance, hydrogen formation, and cyclopentene formation are 0.90, 0.49, and 0.078, respectively.

From the steady-state treatment of the mechanism coupled with the quantum yield data, the ratio k_4/k_3, the ratio of the rates of recombination to disproportionation for cyclopentyl radicals, was determined to be 5.3.

INTRODUCTION

In a recent investigation by the present authors[1] of the reaction of cyclohexane with Hg6($^3P_1$) atoms at 30°C in a static system, it was shown that the kinetics of the reaction could be satisfactorily accounted for by a simple paraffinic free radical mechanism. The cyclopentane reaction has been the subject of a previous investigation from this laboratory.[2] The present work was undertaken to provide data which, when taken in conjunction with the earlier findings, could be used to evaluate the extent to which the cyclopentane reaction conforms to the aforementioned paraffinic sequence. The results of the investigation follow.

EXPERIMENTAL

For a description of the general experimental technique, reference should be made to earlier papers in this series.[2–4] The cyclopentane runs were performed in the same system as that used for the cyclohexane study.[1]

The cyclopentane used in the investigation, together with the cyclopentene and bicyclopentyl used to calibrate the mass spectrometer, was a standard hydrocarbon sample from the National Bureau of Standards. Pertinent data on the materials are given in Table I.

The light intensity at 2537A for this investigation[1] was 2.5×10^{-6} einsteins/min.

RESULTS

Mass spectrometric analyses repeatedly confirmed that the only direct condensable products of the reaction were cyclopentene and bicyclopentyl, in agreement with previous deductions[2] based upon the physical constants of the products. Combustion over heated copper oxide also confirmed that hydrogen was the only product non-condensable in liquid nitrogen.

The new rate data, from the mass spectral analyses, expressed in quantum yields are listed in Table II and represented graphically in Fig. 1. It will be noted that the mean quantum yields of hydrogen formation Q_{H_2}, cyclopentene formation Q_u, and cyclopentane consumption Q_C, all attain constant maximum values at substrate pressures greater than approximately 160 mm. The limiting high-pressure values are taken as follows: $Q_{H_2}=0.49$, $Q_u=0.07$, and $Q_C=0.90$. In the cyclohexane studies it was not possible to attain the high-pressure plateaus in the quantum yields owing to vapor pressure limitations.

In Fig. 1, the solid circles represent values of Q_{H_2} calculated from the data in reference 1 for runs of 90 minutes' duration. It will be noticed that the earlier values are some 10–15 percent lower than the present

Table I. Hydrocarbons used in the present investigation.

Compound	NBS sample No.	Impurity limits mole %
Cyclopentane	219-5S	0.05 ±0.02
Cyclopentene	288-5S	0.034±0.02
Bicyclopentyl	583-5S	0.05 ±0.03

* This work was supported by the U. S. Atomic Energy Commission. This paper formed part of a dissertation submitted by one of us (P.W.B.) in partial fulfillment of the requirements for the degree of Doctor of Philosophy at Illinois Institute of Technology.

† Institute of Gas Technology, Illinois Institute of Technology, Chicago, Illinois.

[1] Beck, Kniebes, and Gunning, J. Chem. Phys. **22**, 672 (1954).

[2] Allen, Kantro, and Gunning, J. Am. Chem. Soc. **72**, 3588 (1950).

[3] M. Schlochauer and H. E. Gunning, J. Chem. Phys. **19**, 474 (1951).

[4] G. A. Allen and H. E. Gunning, J. Chem. Phys. **16**, 1146 (1948).

ones. Since the data reported herein on hydrogen yield are the result of improved techniques, it is believed that they are more reliable than those previously reported.

From the stoichiometry of the reaction the following relations result:

$$Q_C{}^P = Q_P + Q_{H_2} + Q_u,$$
$$Q_C = 2Q_{H_2} - Q_u,$$
$$Q_{C_2} = Q_{H_2} - Q_u,$$

where Q_P represents the quantum yield of pressure decrease and Q_{C_2} the quantum yield of bicyclopentyl formation. The significance of the remainder of the symbols will be found in Table II.

From the last two columns of Table II, it is apparent that the differences between the quantum yields of substrate disappearance calculated from the pressure decrease ($Q_C{}^P$) and the true values (Q_C) are not as great as in the cyclohexane reaction.[1] The reasons for this difference in behavior between the two molecules are not far to seek. The solubility effect would naturally become more marked as the substrate pressure approaches the equilibrium vapor pressure at the temperature at which the reaction is being studied. At 30°C the vapor pressure of cyclopentane is 385 mm, while that for cyclohexane is 122 mm. The highest pressure used in the cyclopentane reaction, i.e., 212 mm, represents only 55 percent of the vapor pressure, while in the cyclohexane reaction the highest pressure, 93 mm, is equal to 76 percent of the vapor pressure.

TABLE II. Quantum-yield data for the cyclopentane decomposition.[a]

P_0 mm	t min	Q_{H_2} obs	Q_u obs	Q_C calc	$Q_C{}^P$ calc
41.6	30	0.38	0.024	0.74	...
58.0	60	0.37	0.013	0.73	...
110.7	60	0.40	0.044	0.76	0.71
145.7	60	0.46	0.079	0.84	0.91
170.0	60	0.49	0.070	0.91	1.07
200.3	60	0.50	0.076	0.92	1.12
212.0	60	0.49	0.079	0.90	1.12

[a] Symbols. P_0 = Initial cyclopentane pressure. t = Duration of exposure. Q_{H_2} = Mean quantum yield of hydrogen formation. Q_u = Mean quantum yield of cyclopentene formation. Q_C = Mean quantum yield of cyclopentane disappearance = $2Q_{H_2} - Q_u$. $Q_C{}^P$ = Mean quantum yield of cyclopentane disappearance calculated from pressure decrease.

In order to facilitate comparison with the cyclohexane reaction, interpolated values for all quantum yields for 20 mm-increments in the initial cyclopentane pressure are given in Table III.

DISCUSSION

As in the treatment of the cyclohexane reaction[1] the paraffinic mechanism will be symbolized as follows:

$$C + Hg6(^3P_1) \rightarrow R + H + Hg6(^1S_0), \quad (1)$$
$$H + C \rightarrow H_2 + R, \quad (2)$$
$$2R \rightarrow U + C, \quad (3)$$

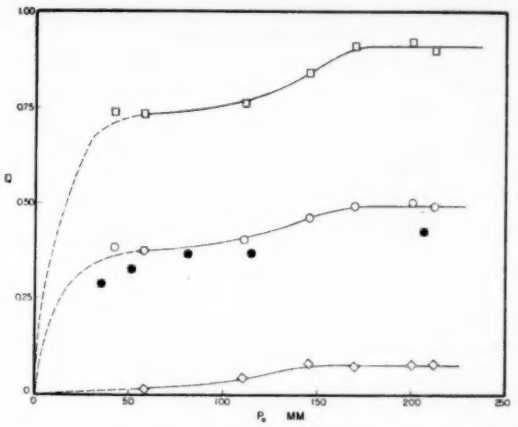

FIG. 1. Quantum-yield data for cyclopentane reaction. □, Q_C; ○, Q_{H_2}; ●, Q_{H_2} calculated from reference 2 (90-min runs); ◇, Q_u.

$$2R \rightarrow C_2, \quad (4)$$
$$H + U \rightarrow R, \quad (5)$$

where, in this case, C represents cyclopentane; R, cyclopentyl radicals; U, cyclopentene; and C_2, bicyclopentyl. Step (5) can be neglected when the ratio $(U)/(C)$ becomes negligibly small. Such conditions would obtain at $t=0$, and also at high substrate pressures. Quantum-yield expressions derived from steps (1) to (4) will be designated as initial quantum yields (Q^0). The five-step sequence would describe the reaction when the cyclopentene concentration has been reduced to a steady-state value by hydrogenation. The steady-state would be approached with increasing extent of reaction. These quantum-yield expressions will be referred to as steady-state quantum yields (Q^S). Using the conventional steady-state treatment the following quantum-yield expressions are obtained:

$$Q_C{}^0 = K\left[\frac{1+2r}{1+r}\right], \quad (6)$$
$$Q_C{}^S = K\left[\frac{2r}{1+r}\right], \quad (7)$$
$$Q_{H_2}{}^0 = K, \quad (8)$$
$$Q_{H_2}{}^S = K\left[\frac{r}{1+r}\right], \quad (9)$$
$$Q_u{}^0 = K\left[\frac{1}{1+r}\right], \quad (10)$$

where $r = k_4/k_3$. The constant K is assumed to represent the fraction of the quenching which leads to decomposition.

Owing to the high vapor pressure of cyclopentane it has been possible to follow the reaction to substrate pressures sufficiently high to evaluate the initial quantum

TABLE III. Interpolated quantum-yield data for the cyclopentane reaction.

P_0 mm	Q_{H_2}	Q_u	Q_{C_2}	Q_C
60	0.37	0.015	0.35	0.72
80	0.38	0.02	0.36	0.74
100	0.39	0.03	0.36	0.75
120	0.42	0.05	0.37	0.79
140	0.45	0.07	0.38	0.83
160	0.48	0.08	0.40	0.88
180	0.49	0.08	0.41	0.90
200	0.49	0.08	0.41	0.90
220	0.49	0.08	0.41	0.90

yields by direct measurement. This procedure was not possible in cyclohexane[1] where the initial quantum yields could only be obtained by extrapolation of mean quantum yields to zero time.

From the data of Tables II and III it follows that $Q_{H_2}^0=0.49=K$; and $Q_C^0=0.90$. The quantities in Eqs. (6) to (10) will therefore have the following values:

$$Q_C^0=0.90;\ K=0.49;\ r=5.3;\ Q_C^S=0.82;$$
$$Q_{H_2}^0=0.49;\ Q_{H_2}^S=0.41 \text{ and } Q_u^0=0.078.$$

The mean quantum yields listed in Table III should lie between the initial and the steady-state values. Inspection of Table II indicates that this is true for substrate pressures greater than 120 mm.

Extrapolation, using a semilogarithmic plot, of the Q_{H_2} data of Allen, Kantro, and Gunning[2] to zero time, gave the value $Q_{H_2}^0=0.57\pm0.02$. The agreement between the two values for $Q_{H_2}^0$ from the two completely independent investigations would appear to be satisfactory considering the inherent uncertainties in the extrapolation method.

Since r represents the ratio of the rates of recombination to disproportionation for cyclopentyl radicals, again, as in cyclohexane, a small value, 5.3, is obtained for this ratio.

In the light of the fact that it has now been shown[1] that quantum yields of substrate disappearance calculated from pressure-rate data are in error owing to the solubility of the substrate in the heavy products, the work of Schlochauer and Gunning on methylcyclopentane[3] must needs be extended using mass spectrometric methods of analysis. However, from their data certain quantities can be obtained which are pertinent to the present discussion. Thus these authors found that the initial rate of hydrogen formation in the complete quenching region was 1.7×10^{-6} mole/min. Since their light intensity was 4.1×10^{-6} einstein/min, it follows that $Q_{H_2}^0=K=0.41$. The value of Q_u^0 can only be roughly estimated. Thus for runs of 3 minutes' average duration, titration yielded 0.5×10^{-6} mole/min for the rate of methylcyclopentene formation. If we take $0.5/4.1=0.12$ as a minimum value for Q_u^0, we obtain, by Eq. (10), $r=2.4$. The results of our calculations for the three molecules under discussion are summarized in Table IV.

TABLE IV. A comparison of cyclopentane, methylcyclopentane, and cyclohexane in terms of the paraffinic mechanism.

	K	$Q_{H_2}^0$	Q_u^0	Q_C^0	$r=k_4/k_3$
Cyclopentane	0.49	0.49	0.078	0.90	5.3
Methylcyclopentane	0.41	0.41	0.12	0.70	2.4
Cyclohexane	0.55	0.55	0.17	0.93	2.2

Certain interesting correlations become apparent from an examination of Table IV. Thus the primary efficiency constant K would seem to be related to the number of secondary C—H bonds in the molecules. If we divide K by the number of secondary C—H bonds, the values 0.046, 0.049, and 0.046 are obtained for cyclohexane, cyclopentane, and methylcyclopentane, respectively. Furthermore, if we correct for the inefficiency in the primary quenching act, the initial quantum yields of substrate disappearance are essentially the same. Thus Q_C^0/K is 1.8 for cyclopentane, 1.7 for methylcyclopentane, and 1.7 for cyclohexane.

An Investigation of the Microwave Spectrum of Pyridine*

K. E. McCulloh and Gilbert F. Pollnow
Department of Chemistry, State University of Iowa, Iowa City, Iowa
(Received August 17, 1953)

The microwave spectrum of pyridine has been observed in the region from 22 140 to 27 300 mc. One hundred twenty-four lines have been found, while measured frequencies have been assigned to thirty-one Q transitions and three R branch transitions. From these data the molecular constants, including those pertaining to an approximate treatment of centrifugal distortion, have been evaluated.

INTRODUCTION

OBSERVATION of the microwave spectrum of pyridine, in a somewhat lower-frequency region than that covered in the present investigation, has already been reported by Bak and Rastrup-Andersen.[1] However, the interpretation of the spectrum proposed by these workers has been questioned by the present authors[2] in a preliminary report of this investigation. It is the purpose of this article to present a more complete account of the results of this study and to discuss these findings in their relation to the structure of the pyridine molecule.

EXPERIMENTAL METHODS

Details of the recording-type spectrometer used in this work, constructed by Dr. C. D. Cornwell and coworkers, and similar to that described by McAfee, Hughes and Wilson,[3] have been given by Robinson.[4] Although this instrument is inherently capable of giving frequency measurements to within ± 0.05 mc, the observed width of pyridine lines limited the accuracy of the measurements to ± 0.1 mc. While the design is not such as to yield exact intensities, line heights taken from recorder traces were sufficient to confirm the existence of nuclear-spin statistical weights.

Two samples of pyridine were used, with consistent results. One was obtained from Eastman Kodak Company; the other from Coleman-Bell (C.P. grade). Both samples were purified by repeated fractional distillations in a vacuum system, with the distilling flask at room temperature and the receiver at the temperature of dry ice.

The absorption cell was maintained at room temperature in order to obtain sufficient vapor pressure for observation of the spectrum. Optimum pressures were found to be of the order of $10^{-2}-10^{-3}$ mm Hg. The entire range of frequencies from 22 140 to 27 300 mc was covered in these measurements.

EXPERIMENTAL RESULTS AND INTERPRETATION

Of the 124 observed absorption lines, only those which have been assigned to specific rotational transitions are reported. These frequencies, together with calculated values, appear in Table I. Hyperfine structure due to the nitrogen nuclear quadrupole was unresolved in all cases.

The approach to the problem of line classification proceeded from the electron diffraction results given by Pauling and Schomaker.[5] Preliminary estimates of rotational constants based on this work indicated that the

TABLE I. Microwave frequencies of pyridine.

Transition	Observed frequency, mc	Calculated frequency, mc
$2_{11} - 3_{12}$	26926.3	26926.3
$3_{13} - 4_{14}$	26634.8[a]	26634.5
$3_{03} - 4_{04}$	26634.8[a]	26635.0
$5_{05} - 5_{24}$	26636.9[b]	26637.0
$5_{15} - 5_{14}$	26636.9[b]	26636.8
$6_{15} - 6_{34}$	26624.4	26624.5
$6_{25} - 6_{24}$	26623.7	26623.8
$7_{25} - 7_{44}$	26605.2	26605.2
$7_{35} - 7_{34}$	26602.6	26602.6
$8_{35} - 8_{54}$	26577.8	26577.6
$8_{45} - 8_{44}$	26569.7	26569.7
$9_{45} - 9_{64}$	26540.6	26540.6
$9_{55} - 9_{54}$	26520.2	26520.1
$10_{55} - 10_{74}$	26494.1	26494.1
$10_{65} - 10_{64}$	26446.7	26446.6
$11_{65} - 11_{84}$	26439.9	26439.9
$11_{75} - 11_{74}$	26338.8	26338.8
$12_{75} - 12_{94}$	26382.3	26382.3
$12_{85} - 12_{84}$	26182.4	26182.5
$13_{85} - 13_{10,4}$	26328.9	26329.0
$13_{95} - 13_{94}$	25958.0	25958.0
$14_{95} - 14_{11,4}$	26292.3	26292.3
$14_{10,5} - 14_{10,4}$	25640.1	25640.0
$15_{10,5} - 15_{12,4}$	26290.2	26290.3
$15_{11,5} - 15_{11,4}$	25198.9	25198.8
$16_{11,5} - 16_{13,4}$	26347.5	26347.5
$16_{12,5} - 16_{12,4}$	24602.0	24602.0
$17_{12,5} - 17_{14,4}$	26495.8	26495.8
$17_{13,5} - 17_{13,4}$	23820.8	23820.7
$18_{13,5} - 18_{15,4}$	26775.7	26775.6
$18_{14,5} - 18_{14,4}$	22834.8	22835.0
$16_{12,4} - 16_{14,3}$	23781.4	23781.5
$17_{12,4} - 17_{15,3}$	25209.6	25209.6
$18_{14,4} - 18_{16,3}$	27033.0	27032.9
$2_{21} - 3_{22}$	[c]	26292.2

[a,b] Unresolved doublets.
[c] Obscured by stronger line at 26292.3. Excluded from data used in evaluating molecular constants.

* Work supported by the U. S. Office of Naval Research.
[1] B. Bak and J. Rastrup-Andersen, J. Chem. Phys. **21**, 1305 (1953).
[2] K. E. McCulloh and G. F. Pollnow, J. Chem. Phys. **21**, 2082 (1953).
[3] McAfee, Hughes, and Wilson, Rev. Sci. Instr. **20**, 821 (1949).
[4] G. W. Robinson, III, Ph.D. thesis, State University of Iowa, 1952 (unpublished).
[5] L. Pauling and V. Schomaker, J. Am. Chem. Soc. **61**, 1769 (1939).

TABLE II. Molecular constants of pyridine.

$\kappa=0.84777\pm0.00001$
$(a-c)/2=1539.94\pm0.01$ mc
$(a+c)/2=4499.19\pm0.02$ mc
$I_a=83.701$ amu A^2
$I_b=87.081$ amu A^2
$I_c=170.814$ amu A^2
$I_c-I_a-I_b=0.032$ amu A^2
$D_J=-3.57$ kc
$D_{JK}{}^a=-1.94$ kc
$D_K{}^a=5.87$ kc

[a] The subscript K refers to K_1, the quantum number of the limiting oblate symmetric top.

molecule would be a near-oblate asymmetric rotor, but it was impossible to predict with conviction whether the dipole moment should lie in the axis of least or intermediate moment of inertia. In either case, two prominent sub-branches ($^aQ_{0\mathrm{I}}$ and $^aQ_{2\mathrm{I}}$ in the former case; two $^bQ_{1\mathrm{I}}$ sub-branches in the latter),[6] involving transitions from $K_1=5$ to $K_1=4$,[7] were expected to exhibit a conspicuous accumulation of lines somewhere in the region between 26 000 and 27 000 mc. In the observed spectrum such a grouping was found to extend from about 26 640 mc toward lower frequencies. By tentatively assigning the $J=5$ members of these sub-branches to the higher-frequency side of this group, and employing the value of $(a-c)/2$ required to bring the calculated frequencies of these transitions to about 26 640 mc, spectral patterns were computed to the extent of the rigid rotor approximation for both orientations of the dipole moment relative to the principal axes of inertia and for several values of the asymmetry parameter κ. Comparing calculated with observed spectra, the possibility of $^bQ_{1\mathrm{I}}$ sub-branches was eliminated, measured frequencies were assigned to the $^aQ_{0\mathrm{I}}$ and $^aQ_{2\mathrm{I}}$ transitions, and κ was found to lie between 0.847 and 0.848. In order to arrive at a final value of this asymmetry parameter, use was made of frequency separations for pairs of lines of the general type $J_{J-5,5}-J_{J-3,4}$, $J_{J-4,5}-J_{J-4,4}$, correlating with the unresolved K doublets of the limiting accidental oblate symmetric top. To the extent that the small observed centrifugal distortion effects can be approximated by means of the formula applying to symmetric rotors[8] (in the present case, within the accuracy of the measurements), these doublet splittings depend only upon $(a-c)/2$ and κ. The value of κ consistent with these splittings for $J=15$, 16, 17, and 18 was found to be 0.84777.

After locating all other lines corresponding to $J<20$ falling within the observed range of frequencies, the remaining molecular constants, including D_J, D_K, and D_{JK} in the Slawsky-Dennison formula,[8] were fitted to the experimental data. The resulting values are listed in Table II. All such calculations were based on reduced energies, $E(\kappa)$, obtained by solving the continued-fraction form of the secular equation.[7]

The assumption that pyridine is a planar molecule belonging to the point group C_{2v} is consistent with modern theories of valence. Since the derived moments of inertia, appearing in Table II, indicate a planar structure, then in order to establish this point group it is only necessary to prove the existence of the symmetry element C_2, coincident with the axis of least moment of inertia. A twofold symmetry axis leads to the hydrogen nuclear-spin statistical weights of 10 for even K_{-1} and 6 for odd K_{-1}; for lower symmetry this weight factor is independent of the parity of K_{-1}. Observed intensities confirm the first of these possibilities, and the C_{2v} point group is established. This result clearly eliminates the possibility of a static arrangement of alternate single and double bonds between ring atoms.

DISCUSSION OF STRUCTURE

Since the present study yields only two independent moments of inertia, while the geometric structure of the molecule involves ten parameters, structural considerations are based on a combination of these results with those of electron diffraction. By taking Pauling and Schomaker's[5] values, $r(\mathrm{C-H})=1.08$A and $r(\mathrm{C-C})=1.39$A, and further assuming that the C−H bonds bisect the exterior ring-bond angles, several structures have been fitted to the observed moments of inertia. Ring-bond angles and C−N distances for three such models appear in Table III. The smallest allowed C−N distance, occurring in Model I, is 1.35_1A. For any assumed value of $r(\mathrm{C-N})$ exceeding this minimum, two different sets of ring-bond angles are possible. This situation is illustrated by Models II and III, with $r(\mathrm{C-N})=1.36$A. Comparison of these three structures indicates that Model I leads to the most reasonable values for the ring-bond angles and to closest consistency with the sharpness of the unresolved meta-distance peak at 2.39A in Pauling and Schomaker's[5] radial distribution curve. These considerations tend to favor a C−N distance of about 1.35A, a value falling within the limits of error, 1.37 ± 0.03A, for the electron diffraction results.

TABLE III. Some structural models for pyridine.[a]

Model	r(C−N)	∠CNC	∠NCC	∠$C_2C_3C_4$[b]	∠$C_3C_4C_5$[b]
I	1.35_1A	117.0°	123.0°	119.8°	117.4°
II	1.36	108.2	131.4	111.9	125.3
III	1.36	126.8	112.7	130.0	107.7

[a] Based on certain parameters as given in the text of the article.
[b] *Chemical Abstracts* numbering of ring atoms is followed except where its omission does not lead to ambiguity in designating the angles.

[6] The notation employed is that used by Cross, Hainer, and King, J. Chem. Phys. **12**, 210 (1944).
[7] As here employed, K_1 refers to the quantum number K of the limiting oblate symmetric top. See King, Hainer, and Cross, J. Chem. Phys. **11**, 27 (1943).
[8] Z. I. Slawsky and D. M. Dennison, J. Chem. Phys. **7**, 509 (1939).

Theory of Electromagnetophoresis. I. Magnetohydrodynamic Forces Experienced by Spherical and Symmetrically Oriented Cylindrical Particles*

DANIEL LEENOV AND ALEXANDER KOLIN
University of Chicago, Chicago, Illinois

(Received July 20, 1953)

This paper is the first of a series dealing with the theory of the electromagnetokinetic effect. This effect consists of the exertion of a force upon a body submerged in a fluid which is traversed by an electric current and a transverse magnetic field. In this communication the conditions for equilibrium of an homogeneous fluid are established and forces upon particles suspended in the fluid are determined. The computations are carried out for spherical bodies and long cylindrical bodies oriented parallel to the magnetic field, to the electric current, and to the exerted force. It is shown that the effect could be observed with suspended particles which differ from the surrounding fluid in the value of their electrical conductivity or dielectric constant, and/or their magnetic permeability.

DEFINITIONS OF SYMBOLS

a	radius of sphere or of circular cylinder
$\mathbf{B}$	magnetic flux density
$d\mathbf{S}$	surface element
$\partial/\partial n$	normal derivative at a boundary of discontinuity
$\partial/\partial\tau$	tangential derivative at a boundary of discontinuity
$\mathbf{E}$	electric field strength
$\mathbf{e}_x$, $\mathbf{e}_r$,	etc. unit vector in the direction of increase of the corresponding coordinate
ϵ	dielectric constant
$\mathbf{F}$	total force on a body
$\mathbf{F}_s$	integrated surface force
$\mathbf{F}_v$	integrated volume force
$\mathbf{f}$	electromagnetic force per unit volume
$\mathbf{H}$	magnetic field strength
η	viscosity
$\mathbf{j}$	current density at any point
J	limiting magnitude of $\mathbf{j}$ at large distance from suspended object
L	length of cylinder
μ	magnetic permeability
n	as a subscript, indicates the normal component of a vector at a boundary
p	fluid pressure
ρ	fluid density
σ	electrical conductivity
T	viscous stress tensor
τ	as a subscript, indicates the tangential component of a vector at a boundary
V	electric potential, or volume
$\mathbf{v}$	fluid velocity
ϕ	general symbol for potential, defined specifically in the text
$'$	indicates a property of a suspended object
$''$	indicates a property of the fluid in which the object is suspended

* This publication has been supported by a research grant from the Abbott Laboratories fund and, in part, by a grant from the Office of Naval Research.

I. INTRODUCTION

As has been shown by one of the authors,[1] it is possible to exert forces by electromagnetic means upon particles suspended in a conducting fluid. The particles may be electrically neutral. The essential prerequisite for the occurrence of the effect is that the electrical conductivity of the suspended particles should differ from that of the fluid in which they are suspended. The effect is expected, however, to occur also in cases where the particle differs from the surrounding fluid in the value of its magnetic permeability or its dielectric constant. In the initial exposition of the effect we shall confine ourselves to the consideration of differences in electrical conductivities.

In an homogeneous conducting fluid traversed by a uniform electric current and a uniform magnetic field perpendicular to the current, each volume element ΔV experiences an electromagnetic force $\Delta\mathbf{f}=\mu(\mathbf{j}\times\mathbf{H})\Delta V$ at right angles to $\mathbf{H}$ and $\mathbf{j}$. Since the fluid remains in equilibrium under these conditions, it is evident that this volume force must be neutralized by an equal and opposite force. This neutralizing force is provided by the surface force (analogous to gravitational hydrostatic buoyancy) exerted upon the volume element by the surrounding fluid. This surface force is due to a pressure gradient (analogous to the gravitational hydrostatic pressure gradient) established in the fluid by the force exerted upon this current in the magnetic field.

Let us now assume that we disturb the homogeneity of the local current field by altering, say, the electrical conductivity of a volume element. Then the equilibrium between the volume and surface force will be destroyed, and the volume element will experience a resultant force, partly due to the current traversing it, partly to the quasi-buoyant surface force, and in part to a hydrodynamic force exerted upon the volume element by the liquid streaming which is engendered in its surrounding owing to the inhomogeneity in the field. Such a volume element represents in fact a particle suspended in a liquid of different electrical conductivity. It will be

[1] A. Kolin, Science **117**, 134–137 (1953).

caused to migrate at right angles to H and to j. The rate of migration will depend on its volume, shape, orientation, and on its electrical properties as well as on those of the surrounding fluid. It is the objective of this investigation to determine the forces and torques exerted in appropriate electromagnetic fields upon suspended particles and to compute the rates of migrations. In this first communication we limit ourselves to the consideration of spherical and cylindrical bodies suspended in a viscous fluid. The suspension is considered to be diluted to a point where the distortion of the field and liquid streaming caused by a particle can be neglected at the location of the neighboring particles.

II. SIMPLIFYING ASSUMPTIONS

Before proceeding with the discussion of forces on suspended bodies under ideal conditions, some remarks on experimental limitations will be in order. These remarks will deal with factors which affect the accuracy of measurements, and the extent to which they can be controlled.

(a) Magnetic Field Inhomogeneity

The electromagnetic force per unit volume at any point in the liquid is given by $\mathbf{f}=\mu(\mathbf{j}\times\mathbf{H})$. A circulation in the liquid will result, even in the absence of suspended particles, if there is nonuniformity in either $\mathbf{j}$ or $\mathbf{H}$ such that $\nabla\times(\mathbf{j}\times\mathbf{H})\neq 0$. On the other hand, the vanishing of this quantity will be the condition for no circulation. This may be accomplished in principle either by having completely uniform current and field, or by only permitting such spatial variations of these quantities as will keep $\nabla\times\mathbf{f}=0$. In the calculations to follow in Part III it will be assumed that such circulation is absent.

(b) Change in Ion Concentration

In most investigations of the effect under discussion, the conducting liquid may be expected to be an electrolytic solution. One might ask whether the electromagnetic force on the ions, which are the current carriers, will cause a nonuniformity in the ion concentration, and hence in the current density. Calculation of the effect, for conditions which would normally obtain, shows it to have negligible importance.

(c) Effect of a Finite Cell

In the calculations discussed in Part III, we shall make use of expressions for the current distribution in the neighborhood of a suspended sphere or cylinder, assuming the current to be uniform at great distances from the suspended particle. Under actual experimental conditions the surrounding medium is a conducting liquid contained in a cell in which two opposite walls are used as electrodes. In order that future calculations be valid, it is evident that the cell must be much larger than the suspended particle; otherwise the current density near the particle will deviate from the assumed distribution.

III. FORCES UPON SUBMERGED BODIES

We shall deal here only with the forces arising as a result of difference in conductivity between the sussuspended body and the liquid. In Part IV it will be shown that the results obtained here are applicable to situations in which there is a difference in magnetic permeability, or when dealing with dielectrics and rapidly alternating fields, to cases in which there is a difference in the dielectric constants.

(a) Force upon a Sphere

The methods used for the sphere will be representative of the procedure to be used for objects of any shape. The symmetry of the sphere, of course, eliminates the possibility of a torque, which could exist in other cases.

The problem at hand consists of calculating the force on the sphere due to, first, the direct force on it due to the current it carries, and, second, the surface force exerted by the liquid. The force density being given (assuming $\mu=1$) by

$$\mathbf{f}=\mathbf{j}\times\mathbf{H}, \tag{1}$$

it is necessary to find the distribution of the current inside and outside the sphere, assuming the imposition of a uniform electric as well as a uniform magnetic field.

The current distribution is obtained by solving La Place's equation for the electric potential,

$$\nabla^2 V=0, \tag{2}$$

subject to the boundary conditions[2]

$$\begin{aligned} &j_n'=j_n'' \quad \text{or} \quad \sigma'\frac{\partial V'}{\partial n}=\sigma''\frac{\partial V''}{\partial n} \\ &E_\tau'=E_\tau'' \quad \text{or} \quad \frac{\partial V'}{\partial \tau}=\frac{\partial V''}{\partial \tau}. \end{aligned} \tag{3}$$

For the electric field in the x direction, solution of (2) for the current gives, in spherical coordinates,

$$\begin{aligned} &\mathbf{j}'=A\mathbf{e}_x, \\ &\mathbf{j}''=J\mathbf{e}_x-\frac{C}{r^3}(2\mathbf{e}_r\cos\theta+\mathbf{e}_\theta\sin\theta). \end{aligned} \tag{4}$$

Here

$$A=\frac{3\sigma'}{2\sigma''+\sigma'}J, \quad C=\frac{\sigma''-\sigma'}{2\sigma''+\sigma'}Ja^3. \tag{5}$$

The force density at any point being given by (1), the total force on the sphere will be

$$\mathbf{F}=\mathbf{F}_s+\mathbf{F}_v, \tag{6}$$

[2] W. R. Smythe, *Static and Dynamic Electricity* (McGraw-Hill Book Company, Inc., New York, 1950).

where $\mathbf{F}_s$ is the surface force and $\mathbf{F}_v$ is the volume force. The latter may be computed immediately. Take $\mathbf{H}$ in the z direction; then

$$\mathbf{F}_v=\int\int\int \mathbf{j}'\times\mathbf{H}dV$$

$$=AH\int\int\int \mathbf{e}_x\times\mathbf{e}_z dV=-AHV\mathbf{e}_y. \quad (7)$$

The surface force will be caused by two effects, the ordinary pressure contribution, and the viscous stress due to motion of the fluid. The latter will produce a force on a surface element on the suspended body given by $T\cdot d\mathbf{S}$, where T is a tensor defined by

$$T=2\eta(\nabla\mathbf{v})^{\text{sym}}$$

and where by $(\nabla\mathbf{v})^{\text{sym}}$ is meant the symmetric part of the tensor. In tensor notation, $(\nabla\mathbf{v})_{ij}{}^{\text{sym}}=\frac{1}{2}(\partial v_i/\partial x_j+\partial v_j/\partial x_i)$. In terms of this, the surface force may be written

$$\mathbf{F}_s=\int\int (p d\mathbf{S}+T\cdot d\mathbf{S}). \quad (8)$$

For this integral, the pressure and velocity are to be calculated by the methods of hydrodynamics, taking into consideration the viscosity of the liquid. We start with the Navier-Stokes differential equation

$$\rho d\mathbf{v}/dt=\rho\partial\mathbf{v}/\partial t+\rho\mathbf{v}\cdot\nabla\mathbf{v}=-\nabla p+\mathbf{f}+\eta\nabla^2\mathbf{v}. \quad (9)$$

To avoid the difficulties connected with the quadratic term in v, we shall, as is customary, restrict ourselves to consideration of small fluid velocities, and hence neglect the term $\rho\mathbf{v}\cdot\nabla v$. The limits within which this approximation may be made will be discussed at the end of this section. Another simplification comes from the fact that we are considering only steady-state conditions, hence $\rho\partial\mathbf{v}/\partial t=0$. This leaves

$$\nabla p=\mathbf{f}+\eta\nabla^2\mathbf{v}, \quad (10)$$

which is to be solved subject to the additional condition that the liquid is incompressible; that is

$$\nabla\cdot\mathbf{v}=0. \quad (11)$$

The problem will then consist of finding a solution for $\mathbf{v}$ and p subject to the above conditions and to the boundary conditions: $\mathbf{v}(r=a)=0$ and $\mathbf{v}(r=\infty)=0$.

Another condition on the velocity $\mathbf{v}$ may be found by taking the curl of (10), namely

$$\nabla\times\mathbf{f}+\eta\nabla\times\nabla^2\mathbf{v}=\nabla\times\mathbf{f}_{\text{rot}}+\eta\nabla\times\nabla^2\mathbf{v}=0. \quad (12)$$

By the symbol $\mathbf{f}_{\text{rot}}$ is meant the rotational part of $\mathbf{f}$. To determine it we first note that according to (4), $\mathbf{j}''$ is made up of two parts, a constant field and a dipole field. The latter may just be represented by the gradient of the dipole potential: $\nabla(Cx/r^3)$. Then for $\mathbf{f}$ we have, according to (1),

$$\mathbf{f}=\mathbf{j}''\times\mathbf{H}=-HJ\mathbf{e}_y+\nabla(Cx/r^3)\times\mathbf{H}\equiv\mathbf{f}_0+\mathbf{f}_{\text{rot}}. \quad (13)$$

In order to solve for the vector function $\mathbf{v}$, it is convenient to set $\mathbf{v}=\mathbf{v}_1+\mathbf{v}_2+\mathbf{v}_3$, where we define these parts in the following way. Let $\mathbf{v}_1$ satisfy

$$\eta\nabla^2\mathbf{v}_1=-\mathbf{f}_{\text{rot}} \quad (14)$$

and $\mathbf{v}_2$ satisfy

$$\nabla^2\mathbf{v}_2=0 \quad \text{and} \quad \nabla\cdot\mathbf{v}_2=-\nabla\cdot\mathbf{v}_1. \quad (15)$$

Then $\mathbf{v}_1+\mathbf{v}_2$ is a particular solution of (11) and (12) and represents the fluid motion induced by $\mathbf{f}_{\text{rot}}$. To meet the boundary conditions at the surface of the sphere and at infinity, it is necessary to add an additional term, $\mathbf{v}_3$, which, according to (11) and (12), satisfies

$$\nabla\cdot\mathbf{v}_3=0; \quad \nabla\times\nabla^2\mathbf{v}_3=0. \quad (16)$$

The quantity $\mathbf{v}_3$ may be thought of as the change in the velocity field brought about by the presence of the boundaries.

In terms of the above definitions, we may now write (10) as follows:

$$\nabla p=\mathbf{f}_0+\mathbf{f}_{\text{rot}}+\eta\nabla^2(\mathbf{v}_1+\mathbf{v}_2+\mathbf{v}_3)=\mathbf{f}_0+\eta\nabla^2\mathbf{v}_3. \quad (17)$$

Let us now determine $\mathbf{v}_1$, making use of (13) and (14). We have

$$\eta\nabla^2\mathbf{v}_1=-\nabla(Cx/r^3)\times\mathbf{H}.$$

A solution of this is seen to be

$$\mathbf{v}_1=(Cx/2\eta r^3)\mathbf{H}\times\mathbf{r}. \quad (18)$$

[In order to demonstrate this, it is helpful to make use of the identity $\nabla^2(uv)=u\nabla^2v+2\nabla u\cdot\nabla v+v\nabla^2u$.]

To find $\mathbf{v}_2$, we have, from (15) and (18),

$$\nabla\cdot\mathbf{v}_2=-\nabla\cdot\mathbf{v}_1=(CH/2\eta)(y/r^3) \quad \text{and} \quad \nabla^2\mathbf{v}_2=0,$$

from which

$$\mathbf{v}_2=-(CH/2\eta r)\mathbf{e}_y. \quad (19)$$

It remains to find the vector $\mathbf{v}_3$, specified by (16), which must be added to the particular solution $\mathbf{v}_p=\mathbf{v}_1+\mathbf{v}_2$ in order to satisfy the boundary conditions. Writing $\mathbf{v}_p$ in terms of its rectangular components, we have, with $\mathbf{H}=H\mathbf{e}_z$, $\mathbf{r}=x\mathbf{e}_x+y\mathbf{e}_y+z\mathbf{e}_z$,

$$\mathbf{v}_p=(k/r^3)(-xy\mathbf{e}_x+(x^2-r^2)\mathbf{e}_y), \quad (20)$$

where

$$k=CH/2\eta. \quad (20')$$

Let us separate $\mathbf{v}_3$ into two parts: $\mathbf{v}_3=\mathbf{v}_3'+\mathbf{v}_3''$, where first we choose $\mathbf{v}_3'$ so that $\mathbf{v}_p+\mathbf{v}_3'$ meets the boundary condition at $r=a$, and also that $\nabla^2\mathbf{v}_3'=0$, and $\nabla\cdot\mathbf{v}_3'=0$:

$$\mathbf{v}_3'=k[(a^2xy/r^5)\mathbf{e}_x+\{2/3a-(a^2/r^5)(x^2-r^2/3)\}\mathbf{e}_y]. \quad (21)$$

However, it is seen that at large distances

$$\mathbf{v}_3'\rightarrow(2k/3a)\mathbf{e}_y,$$

whereas the total velocity is required to vanish at large distances. Hence $\mathbf{v}_3''$ must be chosen to meet the conditions

$$\mathbf{v}_3''\rightarrow-(2k/3a)\mathbf{e}_y \quad \text{as} \quad r\rightarrow\infty, \quad v_3=0 \quad \text{at} \quad r=a,$$

as well as the requirements in (16). Such a velocity distribution, however, is just the solution to Stokes' problem for a liquid moving at a velocity of $-2k/3a$ with respect to the sphere. Taking the known result, we have for v_3''

$$\mathbf{v}_3''=k[(xy/2r^3)(1-a^2/r^2)\mathbf{e}_x+\{-2/3a+1/2r+a^2/6r^3+(y^2/2r^3)(1-a^2/r^2)\}\mathbf{e}_y+(yz/2r^3)(1-a^2/r^2)\mathbf{e}_z]. \quad (21')$$

To find the pressure, we refer to Eq. (17). Since $\nabla^2\mathbf{v}_3'=0$, we have

$$\nabla p=-JH\mathbf{e}_y+\eta\nabla^2\mathbf{v}_3''=(-JH+k\eta(1-3y^2/r^2)/r^3)\mathbf{e}_y-(3k\eta/r^5)(xy\mathbf{e}_x+yz\mathbf{e}_z).$$

Hence,

$$p=-JHy+k\eta y/r^3. \quad (22)$$

The values for $\mathbf{v}$ and p which have been obtained are to be substituted into (8) to calculate the surface force. Combining (20), (21), and (21'), and simplifying, we find for the velocity

$$\mathbf{v}=(k/2r^3)(a^2/r^2-1)(xy\mathbf{e}_x+(z^2-x^2)\mathbf{e}_y-yz\mathbf{e}_z). \quad (23)$$

The contribution of the second term in (8) can be found by first noting that

$$T\cdot d\mathbf{S}\equiv 2\eta(\nabla\mathbf{v})^{\text{sym}}\cdot d\mathbf{S}=2\eta\tfrac{1}{2}[(d\mathbf{S}\cdot\nabla)\mathbf{v}+\nabla\mathbf{v}\cdot d\mathbf{S}]. \quad (24)$$

By symmetry, the surface force will be in the y direction. Hence the contribution by the viscous stress will be, using the result of (24),

$$\mathbf{e}_y\cdot\int\int T\cdot d\mathbf{S}=\eta\int\int\mathbf{e}_y\cdot[(d\mathbf{S}\cdot\nabla)\mathbf{v}+\nabla\mathbf{v}\cdot d\mathbf{S}]=\eta\int\int\left(\nabla v_y+\frac{\partial\mathbf{v}}{\partial y}\right)\cdot d\mathbf{S}. \quad (25)$$

Substituting the expression for $\mathbf{v}$ in (23), and setting $r=a$, and $d\mathbf{S}=\mathbf{e}_r dS=1/a(x\mathbf{e}_x+y\mathbf{e}_y+z\mathbf{e}_z)dS$, gives

$$\mathbf{e}_y\cdot\int\int T\cdot d\mathbf{S}=-\eta\frac{k}{2a^3}\frac{2}{a}\int\int(z^2-x^2)dS. \quad (26)$$

On integrating over the surface of the sphere the integrand will be averaged over all directions. It is easily seen that the resulting force vanishes exactly. This leaves only the surface force due to the pressure. Using (22), it is seen that

$$\begin{aligned}\mathbf{F}_s&=-\int\int p\,d\mathbf{S}\\&=-\int\int\left(-JH+\frac{k\eta}{a^3}\right)y(x\mathbf{e}_x+y\mathbf{e}_y+z\mathbf{e}_z)\frac{dS}{a}\\&=-\left(-JH+\frac{k\eta}{a^3}\right)\mathbf{e}_y\frac{1}{a}\int\int y^2dS\\&=-\frac{4\pi}{3}a^3\left(-JH+\frac{k\eta}{a^3}\right)\mathbf{e}_y. \quad (27)\end{aligned}$$

Substituting $k=CH/2\eta$, and

$$C=\frac{\sigma''-\sigma'}{2\sigma''+\sigma'}Ja^3,$$

we find

$$\mathbf{F}_s=JHV\left(1-\frac{1}{2}\frac{\sigma''-\sigma'}{2\sigma''+\sigma'}\right)\mathbf{e}_y.$$

For the total force, we have from (7) and (5),

$$\mathbf{F}=\mathbf{F}_v+\mathbf{F}_s=\left[-\frac{3\sigma'}{2\sigma''+\sigma'}+1-\frac{1}{2}\frac{\sigma''-\sigma'}{2\sigma''+\sigma'}\right]HJV\mathbf{e}_y;$$

$$\mathbf{F}=\tfrac{3}{2}HJV\frac{\sigma''-\sigma'}{2\sigma''+\sigma'}\mathbf{e}_y. \quad (28)$$

Equation (28) gives the force on a sphere of arbitrary conductivity in a conducting liquid, subject to the limitation that the fluid velocity is small. This approximation will be discussed below. First, however, we express the predictions of (28) for three particular values of conductivity of the sphere, corresponding to very low conductivity, high conductivity, and conductivity near that of the liquid.

Conductivity	Force		
$\sigma'\ll\sigma''$	$3/4HJV$		
$\sigma'\gg\sigma''$	$-3/2HJV$		
$\sigma'\approx\sigma''$	$\Delta\sigma/2\sigma HJV$	where	$\Delta\sigma=\sigma''-\sigma'$
		and	$\sigma\approx\sigma'\approx\sigma''$.

(29)

Because of the choice of field directions, the negative direction is that in which the force acts on the liquid itself.

As mentioned previously, Eq. (28) has been derived by neglecting the quadratic term in (9), which gives the effect of the inertial forces of the liquid. To find what limitation this puts on the validity of our result, we may use the following dimensional type of analysis. For the neglect of the quadratic term we must have

$$\rho\mathbf{v}\cdot\nabla\mathbf{v}\ll\eta\nabla^2\mathbf{v},$$

which, by the methods of dimensional analysis, may be approximated by

$$\rho\frac{v^2}{a}\ll\frac{\eta v}{a^2}, \quad \text{or} \quad va\ll\frac{\eta}{\rho}, \quad (30)$$

where a is the radius of the sphere. Putting in for v, as an order of magnitude,

$$v\approx CH/\eta a,$$

Eq. (30) becomes

$$CH\rho\ll\eta^2, \quad \text{or} \quad F\rho\ll\eta^2, \quad (31)$$

since, from (5) and (28), it is seen that CH is of the order of the total force F on the suspended sphere. For an ordinary situation we may choose the following values:

$\rho=1$ g/cm^3, $H=10^3$ oersteds, $J=10^{-2}$ abs amp/cm^2, $\eta=10^{-2}$ cgs. For the extreme case of either a good or a poor conductor, $C\approx Ja^3$, and we find the above condition equivalent to

$$F\rho=HJV\rho=10^3\cdot 10^{-2}V\ll 10^{-4}, \quad V\ll 10^{-5}\text{ cm}^3,$$

giving the following condition on the radius of the sphere in order for Eq. (28) to hold:

$$a\lesssim 10^{-2}\text{ cm}.$$

It is interesting to note that so long as the condition (31) is satisfied, the force on the sphere will be independent of viscosity; Eq. (28) will then hold for any particle size within the allowable range.

(b) Force upon a Circular Cylinder

In this case the force will depend on the orientation of the cylinder axis. In the following discussion three directions of the axis are considered for reasons of symmetry. These are: 1. axis parallel to $\mathbf{H}$; 2. parallel to $\mathbf{j}$; 3. parallel to the force, hence perpendicular to $\mathbf{H}$ and $\mathbf{j}$. The solution in each case may be easily found for cylinders of infinite length; the problem of the finite cylinder has not yet been rigorously considered.

(1) The method of solution is analogous to the case of the sphere, except that in this instance there is no fluid motion, since, for the axis parallel to $\mathbf{H}$

$$\nabla\times f=\nabla\times(\mathbf{j}\times\mathbf{H})$$
$$=\mathbf{H}\cdot\nabla\mathbf{j}-\mathbf{j}\cdot\nabla\mathbf{H}+\mathbf{j}\nabla\cdot\mathbf{H}-\mathbf{H}\nabla\cdot\mathbf{j}=0. \quad (32)$$

The second term vanishes again because $\mathbf{H}$ is assumed uniform, the first because of cylindrical symmetry. Hence, in place of (10), there is only

$$\nabla p=\mathbf{f}. \quad (33)$$

Following the method used for the sphere, solution of (2), subject to conditions (3), gives, in cylindrical coordinates,

$$\mathbf{j}'=A\mathbf{e}_x,$$

$$\mathbf{j}''=J\mathbf{e}_x-\frac{C}{r^2}(\mathbf{e}_r\cos\theta+\mathbf{e}_\theta\sin\theta), \quad (34)$$

where

$$A=\frac{2\sigma'}{\sigma''+\sigma'}J, \quad C=\frac{\sigma''-\sigma'}{\sigma''+\sigma'}Ja^2.$$

Again, the electric field is taken in the x direction and the magnetic field in the z direction. From (1), (33), and (34)

$$\mathbf{f}=\nabla p=-JH\mathbf{e}_y-(CH/r^2)(\mathbf{e}_r\sin\theta-\mathbf{e}_\theta\cos\theta);$$
$$p=-JHy+(CH/r)\sin\theta.$$

From (7) and (8), with $T=0$,

$$\mathbf{F}_v=-HJV\frac{2\sigma'}{\sigma''+\sigma'}\mathbf{e}_y,$$

$$\mathbf{F}_s=HJV\frac{2\sigma'}{\sigma''+\sigma'}\mathbf{e}_y, \quad (35)$$

$$\mathbf{F}=\mathbf{F}_s+\mathbf{F}_v=0.$$

(2) For a long cylinder whose conductivity σ' satisfies the condition

$$L/a\gg\sigma'/\sigma'', \quad (36)$$

the currents inside and outside the cylinder will be related by

$$j'/j''=\sigma'/\sigma''. \quad (37)$$

This statement may be justified by using the boundary condition $E_\tau'=E_\tau''$, and observing that, except near the ends, E'' is uniform and parallel to the cylinder axis. Hence, along most of the cylinder, $E'=E''$, and (37) follows. From this, the force on the cylinder is easily calculated. The volume force is obtained in the usual way, and the surface force may be considered as the electromagnetic buoyant force due to the liquid displaced. Thus

$$F_v=-Hj'V,$$
$$F_s=Hj''V, \quad (38)$$
$$F=HV(j''-j')=HV(\sigma''-\sigma')E=HJV\frac{\sigma''-\sigma'}{\sigma''},$$

where $J=\sigma''E$, as usual.

(3) We now consider the cylinder axis perpendicular to both $\mathbf{j}$ and $\mathbf{H}$. Hence, for $\mathbf{j}'$ the value given in (34) may be used:

$$j'=\frac{2\sigma'}{\sigma'+\sigma''}J.$$

The force F_v will be the same as given in (35); on the other hand, F_s for a long cylinder will be determined by the pressure at the ends. Neglecting distortion of the current lines there, the pressure difference will just be $\Delta p=Hj''L$, and the surface force will be

$$F_s=Hj''LA=Hj''V=HJV. \quad (39)$$

Then

$$F=F_s+F_v=\frac{\sigma''-\sigma'}{\sigma''+\sigma'}HJV.$$

IV. GENERALIZATION OF THE EFFECT TO MATERIALS DIFFERING IN MAGNETIC OR DIELECTRIC PROPERTIES

Since electromagnetic forces have been observed in the case of difference in electrical conductivity between

liquid and suspended body, one might also expect to find such forces in certain analogous situations. One example would be that of a dielectric body suspended in a dielectric medium, in which case the constant current and magnetic field used previously would have to be replaced by a displacement current produced by a rapidly alternating electric field used in conjunction with an alternating magnetic field of equal frequency and phase. Another case would be one in which a difference in magnetic permeability existed between the suspended body and the liquid; in this instance, the current could be either an ionic or a displacement current.

To calculate the anticipated forces on suspended bodies, in the two cases, we may almost directly make use of the results obtained in *III*, owing to the analogy between the conditions satisfied by current density, magnetic induction, and electrical displacement. Thus we have

$$\nabla\cdot\mathbf{j}=0, \quad \mathbf{j}=\sigma\mathbf{E}, \quad \nabla\times\mathbf{E}=0 \tag{40a}$$

$$\nabla\cdot\mathbf{B}=0, \quad \mathbf{B}=\mu\mathbf{H}, \quad \nabla\times\mathbf{H}=0 \tag{40b}$$

$$\nabla\cdot\mathbf{D}=0, \quad \mathbf{D}=\epsilon\mathbf{E}, \quad \nabla\times\mathbf{E}=0. \tag{40c}$$

(Note that in (40b) the **H** referred to is the externally applied field; the field produced by the current is comparatively negligible.) From the analogy between the above equations, it is easily seen that equations of the type of (2) and (3) will apply in all three cases. As an example, we may calculate the force to be expected for a sphere in the case of differences in μ, and in either σ or ϵ. The expressions for **B** and **D** will be similar to Eqs. (4) and (5); it will only be necessary to replace σ by μ or ϵ, respectively, and **j** by **B** or **D**, respectively. In a given situation we can predict the force if, alternately, μ and σ, or μ and ϵ, differ for the two materials. It is necessary that the relative differences be small, i.e., $\Delta\sigma/\sigma\ll 1$, $\Delta\mu/\mu\ll 1$, $\Delta\epsilon/\epsilon\ll 1$, in order to be able to neglect second-order effects. Then the predicted forces will be [compare (29)]

$$F=BJV\left(\frac{\Delta\mu}{2\mu}+\frac{\Delta\sigma}{2\sigma}\right) \tag{41a}$$

$$F=BJV\left(\frac{\Delta\mu}{2\mu}+\frac{\Delta\epsilon}{2\epsilon}\right), \tag{41b}$$

where in the latter case J represents the displacement current $\partial D/\partial t$.

V. CONCLUSIONS

This treatment extends the theoretical foundation for several interesting applications which have been previously suggested.[1] For example, the effect could be used to provide a substitute for the gravitational field for certain purposes. While gravity, in connection with the effect of buoyancy, may be employed to separate substances of different density (one may include in this category a quasi-gravitational field such as a centrifugal force field), the phenomena discussed here would make possible a separation dependent on other properties of matter, namely electrical conductivity, and perhaps magnetic permeability and dielectric properties. In addition, the shape of the objects to be separated would be a factor; compare, for instance, the force on a sphere with that on a cylinder with its axis in different orientations.

Another basic application lies in the possibility of measuring conductivities of small suspended objects by a null method,[1] if liquids exist with conductivities of the same order of magnitude as that of the suspended object. The example which suggests itself is that of living cells suspended in solutions of electrolytes.

The calculations in this paper have served to illustrate methods for computing forces on bodies of various shapes, though no attempt has been made to treat the subject exhaustively. Various factors have been neglected, for example: 1. the end corrections for the cylinder; 2. the effect of finite cell size on the current distribution and on the circulation of the liquid, which is important whenever the circulation may produce a pronounced effect, as in the case of the sphere; and 3. the inertial forces due to circulation of the liquid.

It was shown that the force exerted upon small spherical particles is independent of the viscosity of the fluid. It was also demonstrated that the force exerted upon a long cylinder vanishes when its axis is parallel to the magnetic field but not for other orientations. Expressions are given for the force exerted upon cylinders oriented parallel to the current and to the force.

The authors wish to thank the Abbott Laboratories of North Chicago for a generous research grant.

Kinetics of the Fast Gas Phase Reaction between Ozone and Nitric Oxide*

HAROLD S. JOHNSTON AND HARVEY J. CROSBY
Department of Chemistry, Stanford University, Stanford, California

(Received July 13, 1953)

The rate of reaction between ozone and nitric oxide was followed optically at −43 and −75°. The reaction appears to be elementary bimolecular

$$NO+O_3=NO_2+O_2$$

and the rate constant is

$$k=0.8\times10^{12}e^{-2500/RT} \text{ cc mole}^{-1} \text{ sec}^{-1}.$$

The pre-exponential factor for this reaction is compared with those of six other elementary gas phase reactions of the type

$$X+Y=Z+W+\cdots$$

involving the oxides of nitrogen for which the energies of activation were higher. For this series of similar reactions the molecular complexity of the reactants is about constant (five or six atoms), and there appears to be no systematic difference in pre-exponential factor between the fast and the slow reactions.

EXPERIMENTAL

THE rate of this fast reaction was followed by the method of Johnston and Yost.[1] Several modifications were necessary in order to attain the low pressures of reactants and the low temperatures necessary to bring the rate into a measurable range, even for the photoelectric and oscilloscopic method. The storage bulbs, glass-diaphragm gauge, and method of preparation of nitric oxide were identical with the intermediate pressure apparatus described by Mills and Johnston.[2] Ozone was prepared pure and free of oxygen by the method of Karrer and Wulf.[3] Prepurified nitrogen from the Matheson Company was sometimes used untreated except for passage through phosphoric anhydride, and sometimes it was passed through a hot tube full of copper wool. By successive dilutions and expansions a 3-liter storage bulb was filled to the desired partial pressure of ozone (about 0.1 to 0.2 mm) and about 700 mm of nitrogen; the other 3-liter storage bulb was filled with a comparable amount of nitric oxide and nitrogen. Over a series of runs these pressures were reduced to about one-fifth of the initial value.

The new modifications of the apparatus are shown in Fig. 1. The reactants flowed separately through 70-cm cooling coils and were mixed in a Hartridge and Roughton type mixing chamber. The mixed reactants flowed through a stainless steel needle valve, into a stainless steel reaction cell (0.8 cm i.d. and 10.0 cm long), through another needle valve, through a capillary critical orifice, and into a 12-liter vacuum reservoir. A sample of mixed but not completely reacted gases was trapped in the reaction cell by the rapid simultaneous closing of the coupled needle valves. The cooling coils and mixing chamber were Pyrex glass. The glass was joined to the needle valves at first by means of de Khotinsky sealing wax and later through a graded seal to Kovar[4] metal which was soldered to the stainless steel needle valve. The needle valve was packed with Teflon and was vacuum-tight. At the ends of the reaction cell quartz windows were held against Teflon gaskets by a threaded plug and a rubber washer on the outside of the window. At the outer edge of the quartz window there was applied a thin film of chloro-trifluorocarbon stopcock grease;[5] these windows were vacuum-tight. Another pair of quartz windows were mounted on the outside of the threaded plug, and a stream of warm dry air was directed against them in order to prevent frosting of the windows. A low-pressure mercury arc served as radiation source, and the 2537A line was isolated by means of two chemical filters,[6] 3 cm of nickel and cobalt sulfate solution and 1 cm thickness of a continuously flowing solution of potassium iodide and iodine. A quartz lens was used to focus the radiation so that it was convergent inside the reaction cell. In some

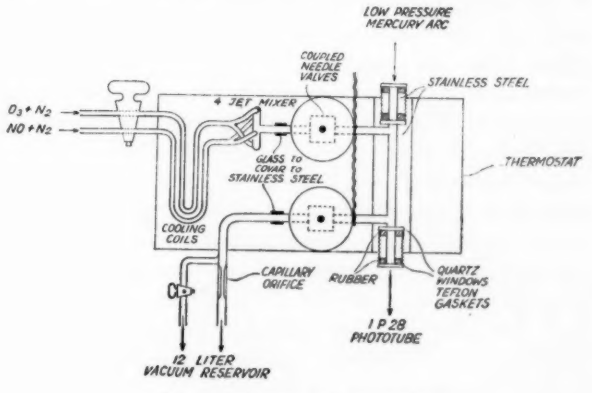

FIG. 1. Diagram of apparatus.

* This work was supported in part by a fellowship from the American Cyanamid Company. See also J. Chem. Phys. **19**, 799 (1951).

[1] H. S. Johnston and D. M. Yost, J. Chem. Phys. **17**, 386 (1949).

[2] R. L. Mills and H. S. Johnston, J. Am. Chem. Soc. **73**, 938 (1951).

[3] S. Karrer and O. R. Wulf, J. Am. Chem. Soc. **44**, 2391 (1922).

[4] Stupakopf Ceramic and Manufacturing Company, Latrobe, Pennsylvania.

[5] Halocarbon Products Corporation, 2010-88th Street, North Bergen, New Jersey.

[6] A. Noyes and P. A. Leighton, *Photochemistry of Gases* (Reinhold Publishing Corporation, New York, 1941).

cases the beam was chopped every 1/20 sec by a rotating sector turned by a synchronous motor, and at other times the 120-cycle radiation pulse frequency was used as time scale. The thermostat was built of copper, and it was surrounded and covered with a one-inch layer of plumber's magnesia insulation. The reaction cell was bolted to a lead brick inside the thermostat, and the brick was bolted through the copper base to a heavy laboratory table. In this system mechanical vibrations did not produce detectable fluctuations in the phototube readings. Temperature was maintained near $-43°$ by a stirred slush bath of dry ice and chlorobenzene, and it was held near $-75°$ by a stirred bath of dry ice and acetone. Temperature was measured by a pentane thermometer, which was calibrated against a copper-constantan thermocouple, and they were calibrated together against the sublimation point of dry ice, the melting point of mercury, and the freezing point of water.

Radiation intensity I was measured as the output of the RCA *1*P28 electron multiplying photoelectric tube on the screen of the oscilloscope (DuMont 304-H); this datum was recorded as the time exposure photograph of a single sweep of the oscilloscope. When the reaction cell is evacuated, this reading is written I_0; during a run or a calibration, it is called I; and I_∞ is used to describe the reading after the reaction has proceeded for at least 100 half-lives. The reaction cell was calibrated against ozone by flowing a highly diluted oxygen-ozone mixture through the cell, through a bubbler containing neutral potassium iodide solution, and into a wet test meter. The potassium iodide solution was acidified and titrated in the usual manner. From the expression $\ln I_0/I=\alpha CL$, the value of α was found to be 6.3×10^6 cc mole^{-1} cm^{-1}. The calibration was made at room temperature and at $-75°$. Nitrogen tetroxide also absorbs this radiation, and the cell was calibrated to give $\alpha=0.28\times10^6$ cc mole^{-1} cm^{-1}. During a series of runs, the optical density of the gas from each 3-liter bulb was determined. For each run, the reactants flowed through the system for about 3 sec, the two needle valves were closed, and this closed an electrical contact which caused the oscilloscope to sweep once. Delay time from mixing chamber to the reaction cell was 0.1 sec, the needle valves could be closed somewhat faster than this, and the sweep frequency of the oscilloscope was from 0.2 to 2 sec. As the reactants and diluent nitrogen flowed through the leads, cooling coils, needle valves, and reaction cell, there was a pressure drop of 8 percent. This valve was reproducible and constant over the pressure range used. It was applied as a correction for reactant concentrations during the runs.

RESULTS

The stoichiometry of the reaction was established under conditions somewhat different from those of the rate studies. Reactant concentration and temperatures ($-45°$ up to room temperature) were usually higher. Under these conditions the rate was too fast to follow, but the precision of making up known amounts of nitric oxide was considerably improved. At room temperature some optical analyses were made for nitrogen dioxide, using 436 mμ radiation. These preliminary runs were made both with excess ozone and with excess nitric oxide. With excess ozone it was found that one ozone immediately disappeared for each nitric oxide present, and eventually more ozone disappeared at a much slower rate. With excess nitric oxide it was found that one nitrogen dioxide (corrected for nitrogen tetroxide) was immediately produced for each ozone originally present, and eventually more nitrogen dioxide appeared at a very much slower rate. Other preliminary studies proved that under conditions of these experiments the equilibrium

$$2NO_2=N_2O_4 \tag{1}$$

was attained much faster than this apparatus was capable of following. From these studies it was concluded that the fast initial rate was

$$\begin{matrix} NO+O_3\rightarrow NO_2+O_2 \\ \Downarrow\Uparrow \\ 1/2N_2O_4 \end{matrix} \tag{2}$$

and the negligibly slow secondary reactions with excess ozone and with excess nitric oxide were, respectively,

$$2NO_2+O_3=N_2O_5+O_2, \tag{3}$$

$$2NO+O_2=2NO_2. \tag{4}$$

Another factor contributing to the slowness of (3) is that at the low temperatures of the rate studies, most of the nitrogen dioxide is associated to nitrogen tetroxide, and results obtained in these preliminary studies confirm the previous statement[1] that nitrogen tetroxide does not react directly with ozone.

The rate of reaction was followed by optical analyses using 2537A radiation. The studies of stoichiometry and the relative rates of (2) with (1) and with (3) and (4) show that one must consider three absorbing species at this wavelength, that is, ozone, nitrogen tetroxide, and nitrogen dioxide. Fortunately the effect of nitrogen dioxide is completely negligible and that of nitrogen tetroxide is almost negligible,[7] compared to ozone. The small correction for the effect of nitrogen tetroxide on the optical density was made. Thus the concentration of ozone as a function of time could be followed. It proved to be much more difficult to know the nitric oxide concentration at each time. Attempts to prepare known concentrations of nitric oxide at these low pressures from successive expansions and dilutions revealed poor precision for the process. At the higher temperature and higher pressures, the reaction was about 75 percent complete by the time the needle valves were closed and observations started, and thus small errors in the initial concentration could introduce large errors in computed

[7] T. C. Hall and F. E. Blacet, J. Chem. Phys. **20**, 1745 (1952).

rate constants. All successful runs were made with a slight excess of ozone, and the difference in ozone present at any time and that remaining at the end of the run was assumed to be equal to the nitric oxide present.

In determining the order of a reaction, it is desirable to vary reactant concentrations widely and to see how the initial rate depends on such variation. This reaction was too fast to be treated in this way, and so order was deduced by the much weaker method of comparing the curves of *concentration versus time* with the various integrated rate expressions. The integrated rate expression for a second-order reaction was found to fit the data

$$kt=\frac{1}{X_\infty}\log\frac{X_0-X_\infty}{X-X_\infty}\frac{X}{X_0}, \tag{5}$$

where X is the concentration of ozone at the time t. The initial value X_0 was based on blank analyses taken before and after each run, and the final value X_∞ was based on pictures taken up to 30 sec after the run ended. A plot of (5) for a typical run is shown in Fig. 2. By extrapolation of the logarithmic function back to zero, one finds how long the reaction had been progressing before observations started, 0.07 sec for this run.

In the same manner second-order rate constants were found for each run, 65 in all. The total range of initial nitric oxide concentration was 0.17 to 1.85×10^{-8} m cc^{-1}, and for ozone 0.27 to 2.13×10^{-8} m cc^{-1}; the ratio of initial ozone to initial nitric oxide was varied from 1.1 to 2.2. The logarithms of these second-order rate constants are plotted against reciprocal temperature in Fig. 3, and the line drawn there was found by the method of least squares. The energy of activation was 2.5 kcal, and twice the standard error of estimate was 0.3 kcal. If the rate constant is written as $k=Ae^{-E/RT}$, the value of A is 0.80×10^{12} cc mole^{-1} sec^{-1}.

From Fig. 3 it can be seen that the individual rate constants were subject to severe scatter, but in view of the large number of points the standard error of the energy of activation was quite low. The principal source of error seems to be due to rapid fluctuations in the light source, photoelectric tube, and oscilloscope trace. A large source of error was uncertainty in the knowledge

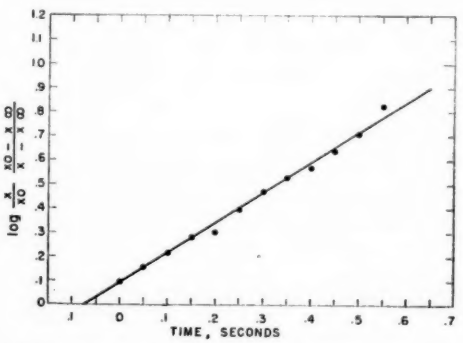

FIG. 2. Test of integrated second-order rate expression. Initial concentrations: Ozone, 0.78×10^{-8} m/cc; nitric oxide, 0.68×10^{-8} m/cc. Pressure of nitrogen, 565 mm. Temperature, $-75.5°$.

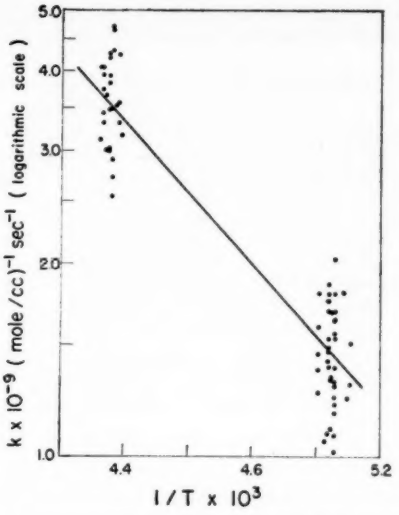

FIG. 3. Temperature dependence of the rate constants.

of nitric oxide concentration. Any error in temperature came probably from the highly exothermic nature of the reaction rather than from nonuniformity in the well-stirred thermostat. Reaction (2) is 48 to 55 kcal exothermic (depending on what fraction of the nitrogen dioxide associates to form nitrogen tetroxide). If the reaction occurred adiabatically with no heat exchange with the walls of the cell, the temperature of the reaction mixture plus nitrogen would have risen about 6° in the most unfavorable case. Other studies with thermocouple probes have indicated that under these conditions the temperature rise is only about one-fifth of that estimated from adiabatic conditions.

MECHANISM

The reaction was a very fast second-order process, and the reactants and products are simple molecules of well-known kinetic properties. The authors were unable to think of any reasonable mechanism other than the elementary bimolecular one

$$NO+O_3=NO_2+O_2 \tag{6}$$

followed by (1). Thus the proposed mechanism is a simple bimolecular process whereby a single oxygen atom was transferred from ozone to nitric oxide.

COMPARISON OF FAST AND SLOW BIMOLECULAR REACTIONS OF THE OXIDES OF NITROGEN

The directly observed energy of activation for this reaction was the extremely low value of 2.5 ± 0.3 kcal. In view of this low energy of activation, it is interesting to compare the pre-exponential factor with those for similar bimolecular processes which have a higher energy of activation.[8] This comparison is restricted to homogeneous gas-phase reactions of the type

$$X+Y=Z+W+\cdots. \tag{7}$$

[8] In this discussion A and E are regarded strictly as empirical quantities based on the Arrhenius equation $k=Ae^{-E/RT}$.

TABLE I. Pre-exponential factors for elementary bimolecular gas phase reactions involving oxides of nitrogen with only five or six atoms.

Reaction	Activation energy kcal	Pre-exponential factor $\times 10^{-12}$ cc mole^{-1} sec^{-1}	Temp range °K	Ref.
$NO_2+CO=NO+CO_2$	27.8	0.48	500–800	a
$2NO_2=2NO+O_2$	26.6	1.8	470–660	b
$2NOCl=2NO+Cl_2$	24.5	9.4	423–523	c
$NO_2+F_2=NO_2F+F$	10.4	1.6	300–343	d
$NO_2+O_3=NO_3+O_2$	7.0	5.9	286–302	e
$NO_2Cl+NO=NO_2+NOCl$	6.9	0.83	273–343	f
$NO+O_3=NO_2+O_2$	2.5	0.80	198–230	

[a] F. B. Brown and R. H. Crist, J. Chem. Phys. **9**, 840 (1941).
[b] M. Bodenstein and H. Ramstetter, Z. physik. Chem. **100**, 106 (1922).
[c] G. Waddington and R. C. Tolman, J. Am. Chem. Soc. **57**, 689 (1935).
[d] R. L. Perrine and H. S. Johnston, J. Chem. Phys. **21**, 2202 (1953).
[e] See reference 1.
[f] Freiling, Johnston, and Ogg, J. Chem. Phys. **20**, 327 (1952).

Bimolecular associations are qualitatively different from reactions of type (7), and these are excluded. Also excluded, of course, are unimolecular reactions in their second-order region.

In going from one reaction to another it is almost impossible to vary only one feature at a time, especially for inorganic reactions. There is a concurrent change of size, mass, vibration frequencies, bond energies, polarizability, dipole moment, etc., and the experimenter has no way to separate the effect of these variables. In an effort to keep the range of such variables at a minimum, the reactions compared with (6) are restricted to those of the oxides and oxyhalides of nitrogen and including ozone and carbon monoxide. In a further effort to make the reactions comparable, the number of atoms in the transition state is held almost constant at 5 or 6 atoms. It is possible to find 7 elementary bimolecular reactions, involving 6 different reactants, and containing only C, N, O, F, and Cl. These 7 reactions are listed in Table I according to decreasing energy of activation (note that there is a strong correlation between temperature and energy of activation). It can be seen that the cases fall into two groups, those with energy of activation of about 25 kcal and those below 10 kcal. There is no conspicuous difference in pre-exponential factor between the fast and the slow reactions, that is, the variation inside each group is greater than any difference between the groups.

THE JOURNAL OF CHEMICAL PHYSICS VOLUME 22, NUMBER 4 APRIL 1954

Calculation of the Moments of the Vibrational Frequency Distributions of Simple Crystals

THOMAS H. WALNUT
Syracuse University, Syracuse, New York
(Received December 22, 1953)

A method of obtaining moments of frequency distributions of vibrations of simple crystal lattices is demonstrated. The moments are obtained directly from corresponding powers of the dynamical matrices in terms of simple displacement coordinates.

THE purpose of this paper is to demonstrate a method that can be used in obtaining an explicit numerical expression for the frequency distribution of the vibrations of a simple crystal lattice.

The procedure employed here is very similar to that used by Montroll[1] and consists of obtaining the moments of the frequency distribution. The moments are then used to express the frequency distribution as a linear combination of orthogonal functions.

The moments are obtained by determining the average values of the diagonal elements of the matrices H^n, where H is the dynamical matrix of a lattice. In the form of H^n prior to symmetry factoring for simple crystals, all of the diagonal elements are equal. Hence, any diagonal element of H^n is the $2n$th moment of the circular frequency distribution. (It is $2n$ because the dimensions of H are frequency squared.)

The difference between this procedure and Montroll's method lies in the use of the original H matrix instead of the form partially diagonalized by use of translational symmetry coordinates.[2]

Two examples of the method, applied to a linear and a square monatomic lattice, will be given instead of a detailed description of the procedure.

A linear monatomic lattice with nearest neighbor forces has a dynamical matrix where

$$H(x,x)=2\alpha, \quad H(x,x\pm1)=-\alpha \quad \text{and} \quad H(x,x+x_1)=0, \quad x_1\neq\pm1 \text{ or } 0.$$

It is readily verified that

$$H^n(x,x+x_1)=\alpha^n(-1)^{x_1}\binom{2n}{n+x_1}$$

and, hence, that the $2n$th moment is $\alpha^n\binom{2n}{n}$.

[1] E. Montroll, J. Chem. Phys. **10**, 218 (1942); **11**, 481 (1943); E. Montroll and D. Peaslee, J. Chem. Phys. **12**, 98 (1944).

[2] The original H matrix has also been used in calculation of frequency distributions by W. Nierenberg, J. Chem. Phys. **19**, 659 (1951).

For the case of a square lattice with first and second nearest neighbor central forces, the problem is more difficult. The difficulty arises primarily from the fact that an atom can vibrate in both the x and y direction. A simple way of writing the dynamical matrix is

$$H=H_{10}+H_{01}+H_{11}+H_{1\bar{1}},$$

where

$$\begin{aligned}
&H_{10}(x,y;x,y)=2\alpha\mathbf{ii},\\
&H_{10}(x,y;x\pm1,y)=-\alpha\mathbf{ii},\\
&H_{01}(x,y;x,y)=2\alpha\mathbf{jj},\\
&H_{01}(x,y;x,y\pm1)=-\alpha\mathbf{jj},\\
&H_{11}(x,y;x,y)=\gamma(\mathbf{ii}+\mathbf{ij}+\mathbf{ji}+\mathbf{jj}),\\
&H_{11}(x,y;x\pm1,y\pm1)=-\tfrac{1}{2}\gamma(\mathbf{ii}+\mathbf{ij}+\mathbf{ji}+\mathbf{jj}),\\
&H_{1\bar{1}}(x,y;x,y)=\gamma(\mathbf{ii}-\mathbf{ij}-\mathbf{ji}+\mathbf{jj}),\\
&H_{1\bar{1}}(x,y;x\pm1,y\mp1)=-\tfrac{1}{2}\gamma(\mathbf{ii}-\mathbf{ij}-\mathbf{ji}+\mathbf{jj}),
\end{aligned}\tag{1}$$

and all of the other elements of each matrix are zero.

The major difficulty in computing moments with this matrix is that the matrices in the sum do not always commute. To obtain the moments conveniently the matrix H can be written

$$H=A\mathbf{ii}+C\mathbf{ij}+C\mathbf{ji}+B\mathbf{jj}=\begin{pmatrix}A & C\\ C & B\end{pmatrix}.$$

The matrices A, B, and C commute because it is possible to convert each into a diagonal matrix by utilizing the translational symmetry.[3]

$$\begin{aligned}
S^{+}AS&=A_{\text{diag}}\\
S^{+}BS&=B_{\text{diag}}\\
S^{+}S&=E\\
A_{\text{diag}}B_{\text{diag}}&=B_{\text{diag}}A_{\text{diag}}=S^{+}ABS=S^{+}BAS\\
SS^{+}ABSS^{+}&=SS^{+}BASS^{+}=AB=BA.
\end{aligned}$$

Similarly $AC=CA$, $BC=CB$. While A, B, and C commute, the matrices

$$\begin{pmatrix}0 & C\\ C & 0\end{pmatrix}\equiv F \quad\text{and}\quad \begin{pmatrix}A & 0\\ 0 & B\end{pmatrix}\equiv D$$

do not commute.

The first diagonal element of H^n must consist of a sum of matrices of the form $A^kB^lC^m$. It is also clear that a term of this form is derived from a term of the form $D^{\beta_1}F^{\delta_1}D^{\beta_2}F^{\delta_2}\cdots F^{\delta_j}D^{\beta_{j+1}}$ where the total number of F's is m. The first diagonal element becomes

$$\sum_k\sum_m A^kB^{n-m-k}C^mW(nkm),\tag{2}$$

where $W(nkm)$ is a weighting factor derived from the products of F and D. Some of these products are

$$\begin{aligned}
D^{\beta}F&=\begin{pmatrix}0 & A^{\beta}C\\ B^{\beta}C & 0\end{pmatrix},\\
FD^{\beta}&=\begin{pmatrix}0 & B^{\beta}C\\ A^{\beta}C & 0\end{pmatrix},\\
D^{\beta}F^2&=\begin{pmatrix}A^{\beta}C^2 & 0\\ 0 & B^{\beta}C^2\end{pmatrix}=F^2D^{\beta},\\
FDF&=\begin{pmatrix}B^{\beta}C^2 & 0\\ 0 & A^{\beta}C^2\end{pmatrix}.
\end{aligned}\tag{3}$$

From these relations it is apparent that when m is odd the weighting factor is zero. It is also apparent from Eqs. (3) that in the first diagonal element of H^n an A will be changed to a B and vice versa when followed by an F raised to an odd power. Consequently, in any of the terms of $(D+F)^n$ the values of the exponents k and l of A and B, respectively, can be found by knowing the position and value of each of the odd δ_i's. For convenience we shall call the number of odd δ_i's the number, j, of F sites.

When m is even the number of F sites must also be even. It is apparent from Eqs. (3) that the value of k, the exponent of A, is equal to the sum of the exponents of D on the left of the first F site, on the right of the last F site, and between sites 2ν and $2\nu+1$ where ν is an integer. The value of l is then the sum of the exponents of D between sites $2\nu-1$ and 2ν.

To calculate the $W(nkm)$ the number of terms in H^n consistent with given values of k, l, m must be found. Each possible set of β_i's and δ_i's occurs only once. When there are j F sites, there are $j/2$ B sites and $j/2+1$ A sites as can be seen from the expression $AFBFAFBFA$.

The problem of finding $W(nkm)$ resolves into three separate problems, finding the number of distinguishable arrangements of the A's in the A sites, B's in the B sites, and F^2's in the whole product.

The number of indistinguishable ways of arranging the l B's in the $j/2$ B sites is equal to the number of ways of placing $l-j/2$ identical particles in $j/2$ boxes, i.e.,

$$\binom{l-1}{l-j/2}.$$

The number of ways of arranging the A's in the A sites is equal to the number of ways of arranging $k-j/2+1$ particles in $j/2+1$ boxes, or

$$\binom{k+1}{k-j/2+1}.$$

The number of sites available for the F^2's is $k+l+1$, the number of F^2's is $\frac{1}{2}(m-j)$. The number of possible

[3] F. Seitz, *Modern Theory of Solids* (McGraw-Hill Book Company, Inc., 1940), pp. 125–133.

arrangements of the F^{2}'s is

$$\binom{k+l+m/2-j/2+1}{m/2-j/2}.$$

The value of $W(nkm)$ is the product of these quantities or

$$W(nkm)=\binom{n-k-m-1}{n-k-m-j/2}\binom{k+1}{k-j/2+1}\times\binom{n-m/2-j/2+1}{m/2-j/2} \quad (4)$$

since $l=n-k-m$.

The next problem is to find the scalar diagonal elements of $\sum_k \sum_m A^k B^{n-m-k} C^m W(nkm)$. This involves finding the diagonal elements of each of the terms $A^k B^{n-k-m} C^m$.

From Eqs. (1),

$$A=A_{10}+C,$$
$$B=B_{01}+C,$$
$$C=C_{11}+C_{1\bar{1}},$$

where

$$A_{10}(x,y;xy)=2\alpha,$$
$$A_{10}(x,y;x\pm1,y)=-\alpha,$$
$$B_{01}(x,y;x,y)=2\alpha,$$
$$B_{10}(x,y;x,y\pm1)=-\alpha,$$
$$C_{11}(x,y;x,y)=\gamma,$$
$$C_{11}(x,y;x\pm1,y\pm1)=-\tfrac{1}{2}\gamma,$$
$$C_{1\bar{1}}(x,y;x,y)=\gamma,$$
$$C_{1\bar{1}}(x,y;x\pm1,y\pm1)=-\tfrac{1}{2}\gamma,$$

and all of the other elements are zero.

From the binomial theorem,

$$A^k B^l C^m=\sum_d \sum_f \binom{k}{d}\binom{l}{f} A_{10}{}^{k-d} B_{01}{}^{l-f} C^{d+f+m}.$$

An element of A^{k-d} is

$$A_{10}{}^{k-d}(x,y;x+x_1,y+y_1)=\alpha^{k-d}(-1)^{x_1}\binom{2k-2d}{k-d+x_1}\delta(y_1,0)$$

and

$$B_{01}{}^{l-f}(x,y;x+x_2,y+y_2)=\alpha^{l-f}(-1)^{y_2}\binom{2l-2f}{l-f+y_2}\delta(x_2,0).$$

An element of the product $A^{k-d}B^{l-f}$ is

$$A^{k-d}B^{l-f}(x,y;x+x_3,y+y_3)=\sum_{x_1y_1} A^{k-d}(x,y;x+x_1,y+y_1)\times B^{l-f}(x+x_1,y+y_1;x+x_3,y+y_3),$$

where $x_3=x_1+x_2$ and $y_3=y_1+y_2$. Consequently,

$$A_{10}{}^{k-d}B_{01}{}^{l-f}=\alpha^{k-d+l-f}(-1)^{x_3+y_3}\binom{2k-2d}{n-d+x_3}\binom{2l-2f}{l-f+y_3}.$$

In a similar way, since

$$C^{d+f+m}=\sum_e \binom{d+f+m}{e} C_{11}{}^{e} C_{1\bar{1}}{}^{d+f+m-e},$$

$$C^{d+f+m}(x,y;x+x_4-x_5,y+x_4-x_5)=\sum_e (-1)^{x_4+x_5}(\gamma/2)^{d+f+m}\times\binom{d+f+m}{e}\binom{2e}{e+x_4}\binom{2d+2f+2m-2e}{d+f+m-e+x_5}.$$

By further matrix multiplication

$$A_{10}{}^{k-d}B_{01}{}^{l-f}C^{d+f+m}(x,y;x+x_6,y+y_6)=\sum_{def} x_4y_4(-1)^{x_4+x_5+x_7+y_7}\alpha^{k-d+l-f}\left(\frac{\gamma}{2}\right)^{d+f+m}\times\binom{d+f+m}{e}\binom{2e}{e+x_4}\binom{2d+2f+2m-2e}{d+f+m-e+x_5}\times\binom{2k-2d}{k-d+x_6-x_4-x_5}\binom{2l-2f}{l-f+y_6-x_4+x_5}.$$

When this is substituted back into the expression for $H^n(x,y;x,y)$, i.e., where x_6 and y_6 are zero, using Eqs. (2) and (4), we obtain on simplifying the summation indices

$$H^n(x,y;x,y)=\sum_R (-1)^{d+f+u_1+u_2}\alpha^{n-d-f-2r}\times(\gamma/2)^{d+f+2r}\binom{k}{d}\binom{d+f+2r}{e}\binom{n-k-2r}{f}\binom{2e}{u_1}\times\binom{2d+2f+4r-2e}{u_2}\binom{2k-2d}{\xi(R)}\binom{n-k-2r-2f}{\eta(R)}\times\binom{n-k-2r-1}{r-v}\binom{k+1}{r-v+1}\binom{n-2r+v}{v}.$$

The indices of summation R are all of the italic letters except n.

$$\xi(R)=k+f+2r+u_1+u_2,$$
$$\eta(R)=n-k-4r-d+2e-2f+u_1-u_2.$$

The value of $H^n(x,y;x,y)$ is the $2n$ moment of the circular frequency.

The moments may now be used to expand the frequency distribution in terms of Legendre polynomials. The advantage of the explicit expressions for the moments is that they can be used for calculation of frequency distribution by digital computers and that large moments can be closely approximated by integrals of continuous functions.

The method may be applied without excessive complexity to more complex lattices and to cases where the forces are not central.

Hybridization and Ionic Character in the Hydrogen Chloride Molecule

PAUL N. SCHATZ*
Gates and Crellin Laboratories of Chemistry, California Institute of Technology, Pasadena, California†
(Received July 22, 1953)

Hybridization in the HCl molecule has been studied in terms of an *spd* hybrid valence bond function including an ionic term (H^+-Cl^-). The results indicate that the quadrupole coupling constant for gaseous HCl (not known experimentally) may be of the order of 100 percent larger than the value reported for the solid. It is found that the quadrupole coupling constant depends principally on the amount of ionic character and does not distinguish among various possible hybridizations.

The sign of the dipole moment is discussed briefly.

INTRODUCTION

A STUDY has been made of the nature of the hybridization in the HCl molecule in terms of an *spd* hybrid valence bond function including an ionic term (H^+-Cl^-). The hybridization was determined using the known dipole moment of gaseous HCl ($\pm 1.10d$),[1] and the quadrupole coupling constants corresponding to various hybridizations were calculated.

Robinson[2] has shown that it is very difficult to come to conclusions about the ionic character in the HCl molecule using the measured dipole moment. He studied the behavior of the dipole moment as a function of the hybridization (assumed to be $s-p$) and found that the moment was very sensitive to the exact amount of s character present in the chlorine bonding wave function.

The present treatment will show that using the known dipole moment and quadrupole coupling constant (if a reliable experimental value were available) may permit one to obtain an estimate of the amount of ionic character but will not permit one to draw any definite conclusions about the exact nature of the hybridization. It will also be shown that the quadrupole coupling constant of gaseous HCl is possibly very much larger (in absolute value) than the value reported for the solid, in contrast with other molecules where the difference does not seem to exceed about ten percent.

All calculations were carried out using three different sets of wave functions, and the qualitative conclusions were found to be largely independent of the exact wave functions used.

CALCULATIONS AND RESULTS

The bonding wave function used was

$$\psi_b=A[\psi_{Cl}(1)\psi_h(2)+\psi_{Cl}(2)\psi_h(1)+\lambda\psi_{Cl}(1)\psi_{Cl}(2)], \quad (1)$$

where

$$\psi_{Cl}=a\psi_{3s}+b\psi_{3p_z}+c\psi_{3d_z},$$
$$\psi_h=\alpha\psi_{1s}+\beta\psi_{2p}.$$

A is the normalization factor given by

$$A=[2+2S^2+4\lambda S+\lambda^2]^{-\frac{1}{2}},$$

where S is the overlap integral defined by

$$S=\int\psi_{Cl}(1)\psi_h(1)d\tau(1).$$

In order that the individual wave functions be normalized, we have

$$a^2+b^2+c^2=1, \quad (2)$$

$$\alpha^2+\beta^2=1. \quad (3)$$

When a and c are not both equal to zero, a pair of electrons will occur in a nonbonding hybrid orbital on the Cl atom which will make an important contribution to the dipole moment and quadrupole coupling constant.[2] This wave function will be of the form

$$\psi_{nb}=a'\psi_{3s}+b'\psi_{3p_z}+c'\psi_{3d_z}.$$

The following relations will be apparent:

$$a'^2+b'^2+c'^2=1, \quad (4)$$

$$a'a+b'b+c'c=0. \quad (5)$$

Equation (5) expresses the requirement that the bonding and nonbonding chlorine wave functions be orthogonal.

The dipole moment of HCl will be given by the expression

$$\mu=e[r_0-2\bar{Z}_b-2\bar{Z}_{nb}], \quad (6)$$

where e is the protonic charge (4.803×10^{-10} esu), r_0 is the internuclear distance (1.2746A), $\bar{Z}_b$ is the average value of the Z coordinate of a bonding electron, and $\bar{Z}_{nb}$ is the same quantity for a nonbonding electron. The HCl molecule is taken to lie along the z axis with the Cl atom at the origin. Throughout it will be assumed that the $3p_x$ and $3p_y$ electrons make no contribution to the dipole moment.

The expressions for $\bar{Z}_b$ and $\bar{Z}_{nb}$ are easily shown to be

$$\bar{Z}_b=\frac{M[1+\lambda^2+2\lambda S]+\dfrac{r_0}{2}+(S+\lambda)P}{1+S^2+2\lambda S+\lambda^2/2}, \quad (7)$$

$$\bar{Z}_{nb}=2a'b'M_{sp}+2b'c'M_{pd}+2a'c'M_{sd}; \quad (8)$$

* Present address: Metcalf Research Laboratory, Brown University, Providence 12, Rhode Island.
† Contribution No. 1827.
[1] R. Rollefson and A. H. Rollefson, Phys. Rev. **48**, 779 (1935).
[2] D. Z. Robinson, J. Chem. Phys. **17**, 1022 (1949).

where

$$M=abM_{sp}+acM_{sd}+bcM_{pd},$$

$$S=aS_{hs}+bS_{hp}+cS_{hd}, \quad P=aM_{hs}+bM_{hp}+cM_{hd},$$

and

$$M_{sp}=\int\psi_{3s}(1)Z(1)\psi_{3p_z}(1)d\tau(1),$$

$$M_{hs}=\int\psi_h(1)Z(1)\psi_{3s}(1)d\tau(1),$$

$$S_{hs}=\int\psi_h(1)\psi_{3s}(1)d\tau(1),$$

with exactly analogous definitions for the remaining M's and S's.

The chlorine quadrupole coupling constant in HCl may be regarded as arising from the following three factors: (1) the electron pair forming the bond; (2) the pairs of $3p_x$ and $3p_y$ electrons, assumed to remain in nonbonding orbitals as in the chlorine atom; (3) the remaining nonbonding electron pair, which makes a nonzero contribution whenever hybridization occurs.

For the first factor we obtain

$$eq_bQ=2eQ\int\psi_b^2(1)\left(\frac{3\cos^2\theta-1}{r^3}\right)d\tau(1), \qquad (9)$$

where eq_b is twice the average value of $(\partial^2V/\partial Z^2)_{Z=0}$ for a bonding electron, V being the electrostatic potential, and Q is the chlorine nuclear quadrupole moment. $\psi_b^2(1)$ is the square of the bonding wave function integrated over electron (2), and θ and r are the coordinates of electron (1). If we substitute from Eq. (1), we obtain

$$eq_bQ=\frac{eQ(1+\lambda^2+2\lambda S)q_{ClCl}+q_{hh}+2(S+\lambda)q_{Clh}}{1+S^2+2\lambda S+\lambda^2/2}, \qquad (10)$$

where

$$q_{ClCl}=\int\psi_{Cl}^*(1)\left[\frac{3\cos^2\theta-1}{r^3}\right]\psi_{Cl}(1)d\tau(1),$$

with similar definitions for q_{Clh} and q_{hh}. (Hereafter, quantities such as q_{ClCl}, q_{hh}, etc., will be abbreviated as q_{Cl}, q_h, etc.)

To evaluate the second factor, we note that

$$2q_{p_x}+2q_{p_y}+2q_{p_z}=0. \qquad (11)$$

Hence the contributions of the pairs of $3p_x$ and $3p_y$ electrons will be just $-2eQq_{p_z}$.

For the third factor we obtain

$$eq_{nb}Q=2eQ\int\psi_{nb}^2(1)\left(\frac{3\cos^2\theta-1}{r^3}\right)d\tau(1). \qquad (12)$$

The expression for the total chlorine quadrupole coupling constant is then

$$eq_TQ=eQ[q_b-2q_{p_z}+q_{nb}]. \qquad (13)$$

This equation may be simplified in the following way. q_s, q_{sp_z}, and $q_{p_zd_z}$ will always be zero[3] due to the symmetry properties of the angular wave functions. Furthermore, q_{d_z} and q_{sd_z} are roughly one percent of q_{p_z}. For all hybridizations considered, b will be considerably larger than a or c so that the terms involving q_{d_z} and q_{sd_z} may be neglected. It has been customary to assume that an integral of the type q_{Clh} will be small.[3] Since the overlap integral for hydrogen chloride is quite large, it seemed interesting to actually evaluate an integral of this type. Consequently, the integral $\int\psi_{3p_z}b(1)\psi_{1s}(1)\times(3\cos^2\theta-1/r^3)d\tau(1)$ was evaluated using the methods of Barnett and Coulson.[4] $\psi_{3p_z}b$ is defined below. ψ_{1s} is just a hydrogen $1s$ wave function. This integral was found to be less than one percent of the integral $q_{3p_z}b$. It seems clear that the integral q_h will be even smaller. Hence, for the hybridization considered in this work, Eq. (13) may be written to an over-all accuracy of about one percent as

$$eq_TQ=110.4\ \text{Mc}\left[\frac{(1+\lambda^2+2\lambda S)b^2}{1+S^2+2\lambda S+\lambda^2/2}-2(1-b'^2)\right]. \qquad (14)$$

The quantity eQq_{p_z} was taken as 110.4 Mc,[3] the experimental quadrupole coupling constant of atomic chlorine.

It is true that q_{p_z} could be evaluated explicitly from the wave functions used in this work. However, such a procedure would be of little significance, since this quantity would depend almost entirely (and very sensitively) on the r term in a hydrogen-like $3p$ function, and the r term is quite unimportant with regard to chemical binding in comparison with the r^2 term.

The following three sets of wave functions were used in all of the calculations: (1) Slater nodeless functions[5] (with $\beta=0$); (2) hydrogen-like functions for chlorine using Pauling and Sherman screening constants[6] ($Z_p=6.5$, $Z_s=8.4$, $Z_d=4.0$), and a Rosen function for hydrogen;[7] (3) the same as set (2) except that

$$\psi_{3p_z}(\text{bonding})\equiv\psi_{3p_zb}=\frac{\sqrt{3}}{2(\pi)^{\frac{1}{2}}}[Are^{-8.98r}-r^2(Be^{-1.18r}+Ce^{-2.53r})]\cos\theta,$$

$$\psi_{3p_z}(\text{nonbonding})\equiv\psi_{3p_znb}=\frac{\sqrt{3}}{2(\pi)^{\frac{1}{2}}}[A're^{-7.368r}-r^2(B'e^{-0.865r}+C'e^{-1.992r})]\cos\theta.$$

Here A is 59.82; B, 0.1517; C, 9.4684; A', 36.76; B', 0.05192; C', 4.1247; and the unit of r is the Bohr radius. These functions were obtained as follows. An analytic wave function was fitted to the Hartree-Fock

[3] C. H. Townes and B. P. Dailey, J. Chem. Phys. **17**, 782 (1949).
[4] M. P. Barnett and C. A. Coulson, Trans. Roy. Soc. (London) **243**, 221 (1951).
[5] J. C. Slater, Phys. Rev. **36**, 57 (1930).
[6] L. Pauling and J. Sherman, Z. Krist. **81**, 1 (1932).
[7] N. Rosen, Phys. Rev. **38**, 2099 (1931).

function for the chloride ion[8] in the manner described by Slater,[9] and 0.35 was added to the screening constants so obtained to convert the function to that of atomic Cl. The function thus obtained is $\psi_{3p_z nb}$. The function $\psi_{3p_z b}$ was then obtained by increasing the screening constants an additional 20 percent in an attempt to take account of the fact that bonding electrons tend to have higher screening constants than nonbonding electrons. It has been assumed that q_{p_z} is the same for $\psi_{3p_z b}$ and $\psi_{3p_z nb}$.‡ It was necessary to make a correction in Eq. (5) to take account of the fact that $\int \psi_{3p_z b}\psi_{3p_z nb} d\tau$ is now not quite equal to unity.

The results of the calculations are shown in Figs. 1, 2, and 3. The curves represent values of the hybridization for which it is possible to fit the known dipole moment of HCl (assumed to be of polarity $H^+ - Cl^-$) using a *positive* value of λ. Numerical values of λ are indicated at various points on the curves. The solid and dotted horizontal lines represent, respectively, the experimental quadrupole coupling constant for solid HCl and this quantity increased by 50 percent.

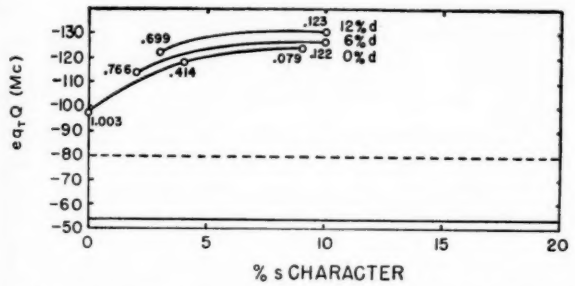

FIG. 1. Quadrupole coupling constant as a function of hybridization and ionic character using Slater nodeless functions. Numbers on the curves are the values of λ at the indicated points. The solid line is the experimental quadrupole coupling constant for solid HCl, and the dotted line is this quantity increased by 50 percent.

The amount of *d* character occurring in the nonbonding wave function would be expected to be very small; it was estimated from spectroscopic promotion energies[10] to be of the order of a few hundredths of a percent. The calculations are not at all sensitive to the exact value of this quantity.

The numerical values of all of the integrals are listed in Table I.

CONCLUSIONS

The qualitative features of the three graphs are similar. The somewhat different behavior of the curves

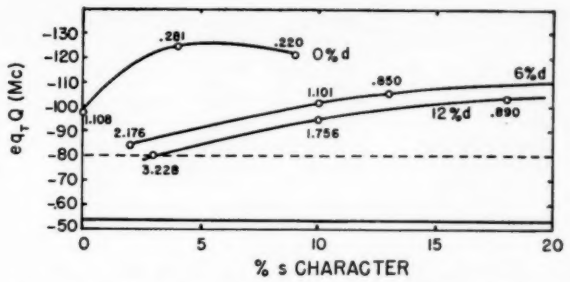

FIG. 2. Quadrupole coupling constant as a function of hybridization and ionic character using hydrogenlike functions. Numbers on the curves are the values of λ at the indicated points. The solid line is the experimental quadrupole coupling constant for solid HCl, and the dotted line is this quantity increased by 50 percent.

obtained using Slater functions is due principally to the unreasonably small values obtained for the integrals involving the *3d* function. It would seem that Figs. 2 and 3 are more reliable than Fig. 1.

It appears that either the quadrupole coupling constant for gaseous HCl is drastically different from that of the solid (of the order of 100 percent greater), or the contribution of the ionic term is very much greater than has previously been supposed. It will be noted that it is not possible to have either λ greater than about 1.1 or the amount of *s* character greater than about 11 percent without the presence of an appreciable amount of *d* character.

In those cases where it has been possible to compare the quadrupole coupling constant for the same substance in the gaseous and solid states, the difference has usually been no greater than about ten percent.[11,12] Thus, for CH_3Cl, the gas value is about 10 percent higher (in absolute value) than that of the solid.[11] Nevertheless it is quite possible that the polarization effects occurring in the HCl crystal are much greater than those in the CH_3Cl crystal, and this seems a more reasonable explanation of the results of the present work than the assignment of a very large value to λ.

It is also entirely possible that some polarization of the $3p_x$, $3p_y$, and inner core electrons of the chlorine

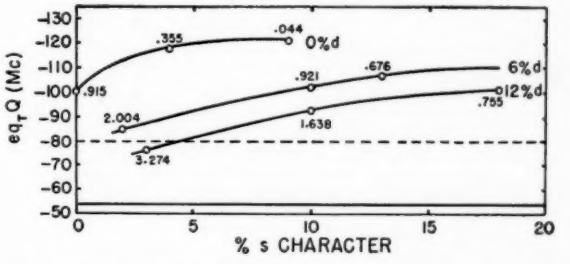

FIG. 3. Quadrupole coupling constant as a function of hybridization and ionic character using modified hydrogenlike functions. Numbers on the curves are the values of λ at the indicated points. The solid line is the experimental quadrupole coupling constant for solid HCl, and the dotted line is this quantity increased by 50 percent.

[8] D. R. Hartree and W. Hartree, Proc. Roy. Soc. (London) A156, 45 (1936).

[9] J. C. Slater, Phys. Rev. **42**, 33 (1932).

‡ This appears to be a serious inconsistency, since q_{p_z} would differ greatly if determined explicitly from these two different functions. However, $\psi_{3p_z b}$ should have been formed by increasing the screening constants of only the r^2 terms, leaving the coefficient and screening constant of the r term unchanged. Had this been done, the above assumption would be justified to within a few percent, and the numerical values of the molecular integrals would remain essentially unchanged.

[10] Charlotte E. Moore, "Atomic energy levels," Natl. Bur. Standards U. S. Circ. **467** (1949).

[11] B. P. Dailey, J. Phys. Chem. **57**, 490 (1953).

[12] H. C. Allen, Jr., J. Phys. Chem. **57**, 501 (1953).

TABLE I. Values of molecular integrals.

Wave function	M_{hs} (A)	M_{hp} (A)	M_{hd} (A)	S_{hs}	S_{hp}	S_{hd}	M_{sp} (A)	M_{pd} (A)	M_{sd} (A)
(1) Slater	0.3132	0.5043	0.2263	0.5007	0.4562	0.09513	0.5257	0.07133	0
(2) Hydrogen-like	0.2689	0.5760	0.6065	0.4164	0.5087	0.4122	0.5031	0.5366	0
(3) Modified hydrogen-like	0.2689	0.4638	0.6065	0.4164	0.4422	0.4122	0.4825	0.5947	0

atom occurs. Townes and Dailey have indicated that this would probably have only a small effect on the quadrupole coupling constant.[3] However, the occurrence of polarization could have an appreciable indirect effect on the present calculations since the calculated dipole moment (*and hence the value of* λ) is sensitive to such effects. It is difficult to make an accurate estimation of the importance of polarization but it is possible to get some rough idea of the magnitudes involved by assuming that the effective value of λ is really considerably larger than that calculated in the present simple treatment. Thus suppose, for example, that at the point corresponding to 0 percent d character, 9 percent s character (Fig. 3) the value of λ were 0.5 instead of 0.044. It is found that the quadrupole coupling constant would then be -107.6 Mc rather than -120.9 Mc indicated by Fig. 3. Similarly, at the point corresponding to 4 percent s character and 0 percent d character (Fig. 3) using a value of λ equal to 0.6 rather than 0.355 gives a quadrupole coupling constant of -109.6 Mc instead of -117.9 Mc. Thus, we see that it is possible to get an appreciable decrease in the quadrupole coupling constant if one assumes quite drastic inaccuracies in the value of λ caused by polarization, but even in that case it does not seem that the qualitative conclusions drawn in the present paper would be changed.§

It will be observed that the quadrupole coupling constant depends chiefly on the value of λ and only very little on the exact nature of the hybridization (the dipole moment always being held fixed at the experimental value). Thus, for example, from Fig. 2 we find that the following three widely differing hybridizations all yield a quadrupole coupling constant of about -100 Mc. (1) 0 percent d, 0 percent s, 100 percent p; (2) 6 percent d, 10 percent s, 84 percent p; (3) 12 percent d, 16-percent s, 72 percent p. In each of these cases, however, the value of λ is about 1.1. Hence it would appear, at least in the case of HCl, that using both the experimental dipole moment and quadrupole coupling constant (unfortunately not known for gaseous HCl) may permit one to obtain a fairly reliable value for λ, but will not distinguish among a variety of possible hybridizations. Consequently, care should be exercised in drawing conclusions from quadrupole coupling constants about the nature of the hybridization whenever it is possible to have more than one type of hybridization. In the case of chlorine, it seems reasonable to assume that the amount of d character occurring in the bonding wave function may be quite appreciable.[13]

Finally, one might consider the dipole moment of HCl to be of opposite polarity from that usually assumed. Examination of Eq. (14) shows that for any particular hybridization this would have the effect of increasing the quadrupole coupling constant (in absolute value). Such a state of affairs seems unlikely but is not definitely ruled out in the absence of a reliable value for the quadrupole coupling constant.

ACKNOWLEDGMENTS

I wish to thank Professor L. Pauling and Professor V. Schomaker for many helpful and stimulating discussions. I would also like to thank the American Telephone and Telegraph Company for the award of a Frank B. Jewett postdoctoral fellowship under which this work was carried out.

§ *Note added in proof.*—Kastler [Compt. rend. **232**, 2323 (1951)] recently calculated the dipole moments of the hydrogen halides using wave functions antisymmetrized in all seven outer-shell electrons of the halogen atoms. He was able to account for the observed dipole moments using pure p bonds for the halogen atoms without the use of an unreasonable amount of ionic character. However, calculation of the quadrupole coupling constant of HCl using his model gives about -125 Mc, a value which seems unreasonably large (in absolute value).

[13] See, for example, the treatment of phosphorus, L. Pauling and M. Simonetta, J. Chem. Phys. **20**, 29 (1952). A similar treatment for HCl indicates that there will be about four times as much d character as s character in the chlorine bonding wave function. However, for a given amount of s character, the addition of d character requires the inclusion of a larger amount of ionic character in order that one may obtain the observed dipole moment. Therefore, the relative amount of d character present in the bonding wave function may be considerably less than indicated by such a simple calculation.

Use of Electron Repulsion Integral Approximations in Molecular Quantum Mechanics*

ROLAND S. BARKER, HENRY EYRING, CHARLES J. THORNE, AND DON A. BAKER
Departments of Chemistry and Mathematics, University of Utah, Salt Lake City, Utah

(Received October 26, 1953)

Straightforward theoretical calculation for molecular systems using eigenfunctions built up from atomic orbitals and employing actual and approximate methods for the evaluation of certain integrals have recently been widely applied with considerable success. Most of these calculations have evaluated the difficult multicentered electron repulsion integrals by use of an approximate formula suggested by Mulliken, in terms of Coulombic and overlap integrals. Previous work has indicated the general utility of this relationship. Here, direct numerical comparison is made of actual and approximate values of the multicenter 1*s* orbital integrals. The comparisons indicate that this approximation of integrals is moderately accurate over a wide range of internuclear configurations. Direct calculations of the energy of the linear triatomic hydrogen complex molecule with this approximate integral formula disclose that the total binding energy obtained by the two procedures is different by several kcal/mole. However the energy variation with internuclear separations obtained from the approximate calculations has its minimum very near that obtained using actual integrals. This indicates that energy minimization by variation of the parameters included in the trial eigenfunction may be accomplished using these approximate integrals. Single calculations may then be made using these "best" parametric values.

1. INTRODUCTION

THE difficulty of obtaining numerical values of many of the two-, three-, and four-center integrals arising in molecular quantum mechanics has given rise to certain approximate formulas.[1-4] The degree to which such evaluations correspond to actual integral calculations is not clear. Mulliken[1] gives a general approximate formula for multicenter repulsion integrals in terms of two-center overlap and Coulombic integrals. His expression may be written,

$$L_{AB,CD}=\int \chi_A(1)\chi_B(1)(1/r_{12})\chi_C(2)\chi_D(2)d\tau_1 d\tau_2$$

$$\approx\tfrac{1}{4}S_{AB}S_{CD}\{L_{AA,CC}+L_{AA,DD}+L_{BB,CC}+L_{BB,DD}\}, \quad (1.1)$$

where

$$S_{AB}=\int \chi_A(1)\chi_B(1)d\tau_1,$$

$$L_{AA,CC}=\int \chi_A(1)\chi_A(1)(1/r_{12})\chi_C(2)\chi_C(2)d\tau_1 d\tau_2,$$

χ_A, χ_B, χ_C, χ_D = functions representing general AO's (atomic orbitals) on nuclei "*A*," "*B*," "*C*," and "*D*,"

$d\tau_1$ and $d\tau_2$ = volume elements of electrons 1 and 2,

r_{12} = distance between electrons 1 and 2.

This general approximate integration formula (1.1) may be specialized to approximate expressions for exchange, ionic and three- and four-center hybrid integrals of all kinds. Thus for the two-center ionic integral (1.1) becomes

$$L_{aa,ab}=\int \chi_a(1)\chi_a(1)(1/r_{12})\chi_a(2)\chi_b(2)d\tau_1 d\tau_2$$

$$\approx\tfrac{1}{2}S_{ab}\{L_{aa,aa}+L_{aa,bb}\}. \quad (1.2)$$

This expression follows at once on noticing that $S_{aa}=1$ and on replacing "*A*," "*B*," and "*C*" by "*a*" and "*D*" by "*b*" in (1.1). The two-center exchange integral is similarly easily written as

$$L_{ab,ab}=\int \chi_a(1)\chi_b(1)(1/r_{12})\chi_a(2)\chi_b(2)d\tau_1 d\tau_2$$

$$\approx\tfrac{1}{2}S_{ab}^2\{L_{aa,aa}+L_{aa,bb}\}\approx S_{ab}\cdot L_{aa,ab}. \quad (1.3)$$

Mulliken states[1] that "the at least rough validity of these relations can be seen pictorially." He further adds "that they are *rather exact* has been verified for two examples by reference to numerical computations" using 1*s* and $2p\pi$ orbitals.[1,2] Rudenberg[5] justifies the above relations first assumed intuitively by Mulliken by showing that they follow on the basis of neglect of all but the largest term of certain expansions. He further cites analogous formulas in terms of two-center exchange and overlap integrals useful when *A* and *C*, and *B* and *D* are close together. How exact any of these approximate relations are is, however, still open to question. Rudenberg states that "correct information can be obtained only by calculating concrete cases" and that "in these cases, the approximate values obtained could be compared with actual values" if available. Mulligan[4] made extensive use of Mulliken's approximate formulas in his calculations on CO_2. However the first complete numerical comparison, to our knowledge, of the quantum-mechanical treatment of a polyatomic molecule using Mulliken's approximate formulas and a similar treatment using actual formulas is given in a following

* Sponsored by the Office of Ordnance Research, U. S. Army.

[1] R. S. Mulliken, J. chim. phys. **46**, 500 and 521 (1949).

[2] R. G. Parr and B. L. Crawford, Jr., J. Chem. Phys. **16**, 526 (1948).

[3] K. Rudenberg, J. Chem. Phys. **19**, 1433 (1951).

[4] J. F. Mulligan, J. Chem. Phys. **19**, 347 (1951).

[5] K. Rudenberg, J. Chem. Phys. **19**, 1433 (1951).

section of this paper for the H_3 activated complex molecule.

2. APPROXIMATE AND ACTUAL VALUES OF MULTICENTERED INTEGRALS

Few "actual" numerical values for multicenter integrals are readily available and most of these few are for integrals involving 1*s* AO's (atomic orbitals). A few quantum-mechanical problems, however, do involve only 1*s* AO's. Thus, Taylor[6] in his treatment of the linear H_4 system calculated three four-center integral values. For this system with nuclei *a*, *b*, *c*, *d* spaced at equal intervals ($R=1.4a_0$), the equilibrium internuclear separation in H_2, he obtained the values of integrals $L_{ab,\,cd}$, $L_{ac,\,bd}$, and $L_{ad,\,bc}$. The numerical calculations were made using formulas of Barnett and Coulson[7] requiring generalized exponential integrals and Bessel functions of half-integral order and imaginary argument. Values of these three four-center integrals and six values for unsymmetric configurational three-center ones are used in the calculations of Taylor and are given in Tables I and II. Atomic units are used throughout this but not Taylor's paper. That is, distances are in units of the first Bohr radius $a_0=0.5292$A, energies in units of e^2/a_0. The units employed by Taylor for these integrals are electron volts. His values are listed below in both these units and the appropriately calculated A.U. (atomic units). The approximate values listed were obtained using the particularized form of (1.1) applicable. All the necessary 1*s* orbital two-center Coulombic and overlap integrals used in Mulliken's general multicenter electronic repulsion formula (1.1) have recently been tabulated[8] over a large range of internuclear separations and effective nuclear orbital charge. Approximate values for all multicenter 1*s* orbital integrals, $\psi_{1s}=(Z^3/\pi)^{\frac{1}{2}}e^{-Zr}$, may thus be readily obtained in the tabulated parametric ranges.

TABLE I. Four-center integrals.

Integral	Actual values (Taylor)		Approximate value
$L_{ab,\,cd}$	5.033 ev	0.1859 A.U.	0.2007 A.U.
$L_{ac,\,bd}$	1.903	0.0703	0.0664
$L_{ad,\,bc}$	1.776	0.0656	0.0527

TABLE II. Three-center unsymmetrical configurational integrals.

Integral	Actual values (Taylor)		Approximate value
$L_{aa,\,bd}$	3.589 ev	0.1326 A.U.	0.1443 A.U.
$L_{ac,\,cd}$	5.583	0.2062	0.2163
$L_{ab,\,ad}$	1.481	0.0547	0.0533
$L_{ac,\,ad}$	0.776	0.0287	0.0276
$L_{bb,\,ad}$	2.113	0.0780	0.0699
$L_{ab,\,bd}$	3.207	0.1185	0.1250

TABLE III. $L_{aa,\,bc}\approx\frac{1}{2}S_{ab}\{L_{aa,\,bb}+L_{aa,\,cc}\}$.

R	Hirschfelder's[a] actual value	Value using Mulliken's[b] approx.
1.0	0.417 063 A.U.	0.421 A.U.
1.5	0.286 059	0.294
2.0	0.188 392	0.197
2.5	0.121 9667	0.130
3.0	0.078 4356	0.085
4.0	0.032 225	0.035
6.0	0.005 3549	0.006

[a] Reference 9.
[b] Reference 1.

TABLE IV. $L_{bb,\,ac}\approx S_{ac}\cdot L_{aa,\,bb}$.

R	Hirschfelder's[a] actual value	Value using Mulliken's[b] approx.
1.0	0.335 838 A.U.	0.325 A.U.
1.5	0.186 210	0.175
2.0	0.094 214	0.081
2.5	0.044 874	0.036
3.0	0.020 491	0.015
4.0	0.003 9228	0.0025
6.0	0.000 117844	0.00006

[a] Reference 9.
[b] Reference 1.

The cited integral values in Tables I and II indicate the accuracy of approximation (1.1) for only a single configurational distance ($R=1.4$ A.U.). Comparisons over a considerable range of "R" values, however, may be made with the symmetrical three-center integrals evaluated by Hirschfelder[9] in his treatment of the symmetrical linear activated complex H_3. Tables III, IV, V, and VI contain values calculated with the approximation (1.1) and those found by Hirschfelder by more elaborate methods. Hirschfelder's values are stated by him to be "accurate to five figures after the decimal point."

A comparison over a large range of internuclear distances of the two-center specialized approximate formulas (1.2) and (1.3) with actual calculations for integrals occurring in the H_3 problem is made in Tables VII and VIII.

3. USE OF MULLIKEN'S APPROXIMATE INTEGRALS IN OBTAINING "BEST" VALUES FOR ENERGY MINIMIZATION PARAMETERS

One of the most important problems in molecular quantum mechanics as well as one of the simplest to formulate mathematically is the energy calculation of the triatomic hydrogen complex. This neutral molecule is of particular interest because it is intermediate in reactions of the type $D+H_2\rightarrow D\cdot H\cdot H\rightarrow D-H+H$.

Various approximations for calculating the energy of this linear symmetrical molecule from first principles

[6] R. Taylor, Proc. Phys. Soc. (London) **A64**, 249 (1951).
[7] M. P. Barnett and C. A. Coulson, Trans. Roy. Soc. (London) **A243**, 221 (1951).
[8] Thorne, Barker, and Eyring, *Studies in Applied Mathematics No. 10* (University of Utah, Salt Lake City), "Tables of Quantum Mechanical Integrals. 1. Some Two Parameter Integrals," (1953). The integrals of all tables in the above publication are tabulated for the ranges $R=1.0(0.1)1.5$, $1.50(0.05)2.00$, $2.0(0.1)5.0$; $Z=0.70(0.05)1.00$, $1.00(0.02)1.50$.
[9] J. O. Hirschfelder, PhD thesis, Princeton University, 1935.

have been considered. London[10] tried the calculation using an eigenfunction built up of hydrogen atomic orbitals. Resulting from the neglect of all multicenter integrals in his calculation an energy value very much greater than the known value as determined by experiment was obtained. Coolidge and James[11] used a similar eigenfunction to calculate the energy of this lowest homopolar state for the single configurational distance ($R=1.7a_0$). Their value in terms of present-day constants ($e^2/a_0=627.23$ kcal/mole) was -39.91 kcal/mole. Hirschfelder, Eyring, and Rosen[12] also carried through the evaluation for this eigenfunction (so-called Heitler-London approximation). They determined the energy for a number of different internuclear distances. Using the variational method a "best" value of -53.39 kcal/mole for the configurational distance $R=2.0a_0$ was obtained. These workers also obtained other first principle approximations (Wang, valence-bond plus ionic terms, etc.) which gave still better values. However all these treatments necessitate an energy parameter minimization procedure which involves calculation of multicenter integrals for several configurational distances. Indeed if Coolidge and James had been able to secure the "best" parametric value $R=2.0$ and had carried through their integral evaluations exactly for this value instead of for $R=1.7$ they would have obtained the "best" Heitler-London approximation -53.39 kcal/mole. Similarly if Hirschfelder, Eyring, and Rosen had known in advance that this was the "best" value for "R" they could have obtained their results with a fraction of the effort expended.

TABLE V. $L_{ab,ac}\approx\frac{1}{4}S_{ab}\cdot S_{ac}\{L_{aa,aa}+L_{aa,cc}+2L_{ca,bb}\}$. $L_{aa,aa}=0.625$.

R	Hirschfelder's[a] actual value	Value using Mulliken's[b] approx.
1.0	0.278 798 A.U.	0.272 A.U.
1.5	0.127 762	0.122
2.0	0.051 214	0.048
2.5	0.018 7244	0.017
3.0	0.006 41576	0.0059
4.0	0.000 65391	0.00060
6.0	0.000 0047688	0.000046

[a] Reference 9.
[b] Reference 1.

TABLE VI. $L_{ab,bc}\approx\frac{1}{4}S_{ab}^2\{L_{aa,aa}+L_{aa,cc}+2L_{aa,bb}\}$.

R	Hirschfelder's[a] actual value	Value using Mulliken's[b] approx.
1.0	0.399 463 A.U.	0.398 A.U.
1.5	0.247 086	0.253
2.0	0.141 207	0.148
2.5	0.075 091	0.082
3.0	0.039 101	0.043
4.0	0.009 128	0.011
6.0	0.004 3635	0.0058

[a] Reference 9.
[b] Reference 1.

[10] F. London, Z. Physik **46**, 455 (1928); **50**, 24 (1928).
[11] A. S. Coolidge and H. M. James, J. Chem. Phys. **2**, 811 (1934).
[12] Hirschfelder, Eyring, and Rosen, J. Chem. Phys. **4**, 121 (1936).

TABLE VII. The ionic integral $(L_{aa,ab}\approx\frac{1}{2}S_{ab}\{L_{aa,aa}+L_{aa,bb}\})$.

R	Actual value	Value using Mulliken's[a] approx.
1.00	$5.070\,4485\times10^{-1}$ A.U.	5.062×10^{-1} A.U.
1.50	$4.053\,6896\times10^{-1}$	4.044×10^{-1}
2.00	$3.080\,3646\times10^{-1}$	3.082×10^{-1}
2.50	$2.255\,9548\times10^{-1}$	2.276×10^{-1}
3.00	$1.607\,4246\times10^{-1}$	1.646×10^{-1}
4.00	$7.698\,167\times10^{-2}$	8.3×10^{-2}
5.00	$3.495\,3043\times10^{-2}$	4.0×10^{-2}
6.00	$1.531\,1456\times10^{-2}$	1.9×10^{-2}
8.00	$2.738\,7379\times10^{-3}$	3.8×10^{-3}
12.00	$7.465\,8581\times10^{-5}$	1.3×10^{-4}

[a] Reference 1.

TABLE VIII. The exchange integral $(L_{ab,ab}\approx\frac{1}{2}S_{ab}^2\{L_{aa,aa}+L_{aa,bb}\})$.

R	Actual value	Value using Mulliken's[a] approx.
1.00	$4.366\,51\times10^{-1}$ A.U.	4.34×10^{-1} A.U.
1.50	$2.968\,35\times10^{-1}$	2.93×10^{-1}
2.00	$1.841\,56\times10^{-1}$	1.81×10^{-1}
2.50	$1.066\,22\times10^{-1}$	1.04×10^{-1}
3.00	$5.850\,83\times10^{-2}$	5.74×10^{-2}
4.00	$1.562\,72\times10^{-2}$	1.56×10^{-2}
5.00	$3.717\,04\times10^{-3}$	3.85×10^{-3}
6.00	$8.140\,27\times10^{-4}$	8.8×10^{-4}
8.00	$3.289\,59\times10^{-5}$	3.9×10^{-5}
12.00	$3.548\,36\times10^{-8}$	5.0×10^{-8}

[a] Reference 1.

The energy calculations of the next section for the H_3 system indicate that the use of Mulliken's approximate integrals give results which are several kcal/mole different from those using actual integral values. However comparison of the energy variation with the internuclear configurational distance disclosed that the approximate calculation minimum is very near that obtained using actual integrals. This suggests that the "best" value of energy minimization parameters may be selected with the use of approximate integral calculations. The complete first principle calculations giving the "best" energy can then be carried through with only a single evaluation of the actual integrals.

4. ENERGY CALCULATIONS OF THE TRIATOMIC HYDROGEN MOLECULE USING APPROXIMATE AND ACTUAL INTEGRALS

Several first principle approximate methods[13] have been employed for the H_3 calculation. For the purpose of this paper, however, the simple Heitler-London approximation will be used.

The Hamiltonian operator for H_3 expressed in atomic units (A.U.) is

$$H=-\tfrac{1}{2}(\nabla_1^2+\nabla_2^2+\nabla_3^2)+1/R_{ab}+1/R_{ac}+1/R_{bc}-1/r_{a1}-1/r_{a2}-1/r_{a3}-1/r_{b1}-1/r_{b2}-1/r_{b3}-1/r_{c1}-1/r_{c2}-1/r_{c3}+1/r_{12}+1/r_{13}+1/r_{23}.$$

The nuclei "a," "b," and "c" are equally spaced and collinear. The electrons are designated as 1, 2, and 3.

[13] J. M. Walsh and F. A. Matsen, J. Chem. Phys. **19**, 526 (1951).

TABLE IX. Summary of H_3 calculations.[a]

R	Using true binding energy (integral values)	Using approx. binding energy (integral values)
1.5	15.07 kcal/mole	1.65 kcal/mole
2.0	53.39 kcal/mole	45.82 kcal/mole
2.5	44.29 kcal/mole	40.29 kcal/mole

[a] The numerical values of Table IX were calculated on the basis of $e^2/a_0 = 27.206$ ev $= 627.23$ kcal/mole.

Application of the variational principle to quantum mechanics gives for the energy of a molecule

$$E \leqq \frac{\int \psi^* H \psi d\tau}{\int \psi^* \psi d\tau}.$$

The integrations, $\int \cdots d\tau$, imply an integration over all the spacial and spin coordinates of all the electrons. ψ is the trial function for the molecule and is taken as a linear combination of products of atomic orbitals of the type

$$a(1) = (Z^3/\pi)^{\frac{1}{2}} e^{-Zr_{a1}} \quad \text{and} \quad b(1) = (Z^3/\pi)^{\frac{1}{2}} e^{-Zr_{b1}}.$$

Such eigenfunctions must satisfy the Pauli principle and must belong to one of the irreducible representations of the molecular point group. The eigenfunction for the covalent structure (Heitler-London approximation) is

$$\psi_{\text{cov}} = 2\begin{pmatrix} a & b & c \\ \alpha & \beta & \alpha \end{pmatrix} - \begin{pmatrix} a & b & c \\ \beta & \alpha & \alpha \end{pmatrix} - \begin{pmatrix} a & b & c \\ \alpha & \alpha & \beta \end{pmatrix}.$$

The notation $\begin{pmatrix} a & b & c \\ \alpha & \beta & \alpha \end{pmatrix}$ represents the Slater determinant

$$\begin{pmatrix} a & b & c \\ \alpha & \beta & \alpha \end{pmatrix} = \frac{1}{\sqrt{3!}} \begin{vmatrix} a(1)\alpha(1) & b(1)\beta(1) & c(1)\alpha(1) \\ a(2)\alpha(2) & b(2)\beta(2) & c(2)\alpha(2) \\ a(3)\alpha(3) & b(3)\beta(3) & c(3)\alpha(3) \end{vmatrix}.$$

Use of the orthonormal properties of the spin functions α and β enables one to reduce the energy expression for E to

$$E_{\text{cov}} \leqq \frac{6(a^2b^2c^2 + a^2\, bc\, cb = ac\, b^2\, ac - ab\, bc\, ac)}{6(1 + S_{ab}^2 - S_{ac}^2 - S_{ab}^2 \cdot S_{ae})}.$$

Orbital integral notation such as

$$ab\ \ bc\ \ ac = \int a(1)b(2)a(3)\,|H|\,b(1)c(2)c(3)d\tau_1 d\tau_2 d\tau_3$$

has been used in the above expression for the energy. The orbital integrals $a^2b^2c^2$, $a^2\, bc\, cb$, $ac\, b^2\, ac$, and $ab\, bc\, ac$ are easily reduced to the elemental integral expressions,

$$a^2\ \ b^2\ \ c^2 = \left(\frac{5}{2R} - 1.5\right) - 4G_{a,\,b^2}(R) - 2G_{a,\,c^2}(2R) + 2L_{aa,\,bb} + L_{aa,\,cc},$$

$$a^2\ \ bc\ \ cb = \left(\frac{5}{2R} - 1.5\right) \cdot S_{ab}^2 - 2S_{ab}(K_{a,\,bc} + J_{a,\,ab} - L_{aa,\,bc}) - S_{ab}^2(G_{a,\,c^2} + G_{a,\,b^2}) + L_{ab,\,ab},$$

$$ac\ \ b^2\ \ ac = \left(\frac{5}{2R} - 1.5\right) \cdot S_{ac}^2 - 2S_{ac}(K_{b,\,ac} + J_{a,\,ac}) - 2S_{ac}^2 \cdot G_{a,\,b^2} + 2S_{ac} \cdot L_{bb,\,ac} + L_{ac,\,ac},$$

$$ab\ \ bc\ \ ac = \left(\frac{5}{2R} - 1.5\right) \cdot S_{ab}^2 \cdot S_{ac} - S_{ab}^2(J_{a,\,ac} + K_{b,\,ac}) - 2S_{ab} \cdot S_{ac}(K_{a,\,bc} + J_{a,\,ab}) + 2S_{ab} \cdot L_{ab,\,ac} + S_{ac} \cdot L_{ab,\,bc}.$$

The two-center integrals employed in these expressions are defined and tabulated.[8,14] The indicated evaluations of the Heitler-London treatment of H_3 for the approximate and actual integral calculation are given in Table IX.

[14] J. O. Hirschfelder and J. W. Linnett, J. Chem. Phys. 18, 130 (1950).

Light Scattering by Tobacco Mosaic Virus Nucleic Acid

THEODORE G. NORTHROP* AND ROBERT L. SINSHEIMER
Department of Physics, Iowa State College, Ames, Iowa

(Received June 18, 1953)

The molecular weight of ribonucleic acid separated from tobacco mosaic virus by heat denaturation of the protein has been measured by light-scattering techniques and found to correspond to the weight of all the nucleic acid in a virus rod. The nucleic acid disintegrated rapidly at room temperature, most probably by enzymatic action.

INTRODUCTION

THE molecular weight of ribonucleic acid (RNA) isolated from tobacco mosaic virus (TMV) has been determined in the past by measuring various physical properties of its solutions. Among the properties measured[1] have been osmotic pressures, sedimentation constants, viscosities, and diffusion constants. The weight obtained has varied with the method of separating the nucleic acid and with the physical method employed. The highest weight reported by Cohen and Stanley[1] was 2.9×10^5. Their preparations disintegrated spontaneously. In the present work, the weight of the virus RNA has been determined by light-scattering techniques and the instability studied.

THEORY

The theory of the angular distribution of light scattered from solutions of optically isotropic large or small particles can be found in review articles by Oster[2] and by Doty and Edsall.[3] In addition, an expression for the angular distribution of light scattered by a gas of small, anisotropic, randomly oriented particles has been given by King.[4] His expression is

$$\frac{I(r,\theta)r^2}{I_0V}=\frac{\pi^2(n_e^2-1)^2}{2\lambda^4 v}\cdot\frac{6(1+\rho_u)}{6-7\rho_u}\left\{1+\frac{1-\rho_u}{1+\rho_u}\cos^2\theta\right\}. \quad (1)$$

$I(r,\theta)$ = intensity of scattered light at a distance r from the scattering gas; θ is the angle between the scattering direction and the direction of incident light.
I_0 = intensity of light incident on the gas.
V = volume of scattering gas.
n_e = index of refraction of the gas.
λ = vacuum wavelength of incident light.
v = number of gas particles per unit volume.
ρ_u = depolarization ratio for unpolarized incident light, and equals H_u/V_u, where H_u is the intensity of horizontally polarized scattered light at θ equal to 90°, and V_u is the intensity of the vertically polarized component.

In a solution n_e^2-1 must be replaced by $n_e^2-n_0^2$, where n_e is the index of the solution and n_0 that of the solvent. Martin[5] proves that $\rho_u=2\rho_v/(1+\rho_v)$, where ρ_v is the depolarization ratio for vertically polarized incident light. In addition $v=cN_0/M$, where c = concentration of solute in gm/ml, N_0 is Avogadro's number, and M is the molecular weight of the solute particles. $(n_e^2-n_0^2)^2/v$ can be replaced by a derivative. With these changes, expression Eq. (1) becomes

$$Kc(1+\cos^2\theta)/R(\theta)=F(\theta,\rho_v)/M \quad (2)$$

where

$$K=2\pi^2n_0^2\left[\frac{\partial n_e}{\partial c}\right]^2\lambda^{-4}N_0^{-1} \quad \text{and} \quad R(\theta)=I(r,\theta)r^2/I_0V,$$

$$F(\theta,\rho_v)=(3-4\rho_v)(1+\cos^2\theta)/3[1+3\rho_v+(1-\rho_v)\cos^2\theta].$$

A correction to Eq. (2) must be made if the particles are not small compared to the wavelength. This can be done approximately by multiplying the numerator of the left member of Eq. (2) by a particle form factor, usually denoted by $P(\theta)$. Numerical values of $P(\theta)$ have been given by Doty and Steiner[6] for several shapes. It can be shown that for $\theta\neq0°$, Eq. (2) is not quite correct, even with the form factor, when the particles are both large and anisotropic; the correction to the scattering cannot be expressed exactly by the ratio of the two factors $P(\theta)/F(\theta,\rho_v)$. Horn and Benoit[7] have carried out the exact calculation for the case of anisotropic rods.

The error in using Eq. (2) with the form factor is probably negligible in the case of RNA from TMV. Horn and Benoit[8] have published data which gives a rough idea of the possible magnitude of this error. They have studied how H_v and V_v vary with θ for solutions of TMV. A plot of H_v/V_v from their data shows about a 10 percent increase in this ratio from $\theta=0°$ to 90°. For small anisotropic particles this ratio would be constant. Thus, even for particles as large as TMV the size effect is negligible as far as correcting scattering curves for depolarization is concerned, for the size effect is a correction to a correction. In addition, the RNA was found to be both smaller and more isotropic than TMV.

In deriving Eq. (2) corrected by the form factor $P(\theta)$, it is necessary to assume that the polarizability tensor is

* National Cancer Institute Predoctorate Fellow (1951–1952), National Institutes for Health, Public Health Service, Federal Security Agency.

[1] S. Cohen and W. Stanley, J. Biol. Chem. **144**, 589 (1942).
[2] G. Oster, Chem. Revs. **43**, 319 (1948).
[3] P. Doty and J. Edsall, Advances in Protein Chem. **6**, 35 (1951).
[4] L. V. King, Nature **111**, 667 (1923).
[5] W. H. Martin, Trans. Roy. Soc. Can. **17**, 151 (1923).
[6] P. Doty and R. Steiner, J. Chem. Phys. **18**, 1211 (1950).
[7] Horn, Benoit, and Oster, J. chim. phys. **48**, 530 (1951).
[8] P. Horn and H. Benoit, J. Polymer Sci. **10**, 29 (1953).

not a function of position within the molecule. Hence, it cannot be assumed without further justification that the expression holds for example in the case of a stiff, kinked polymer chain, each monomer of which is more polarizable along its axis than at right angles to the axis.

APPARATUS

The 4358A mercury line isolated from the spectrum of an AH-4 lamp by Corning filters No. 3389 and No. 5113 was used for all the scattering measurements. An image of the AH-4 arc was formed in the center of the scattering cell by a lens. The cell[9] consisted of a hemi-cylinder 4 cm in diameter with a narrow solution compartment separated from the hemi-cylinder by a glass partition. The hemi-cylinder was filled with solvent. The advantage of such a cell over just a cylinder or hemi-cylinder is the much smaller volume of solution required. The lens and appropriately dimensioned stops were so placed that the following conditions were fulfilled: (1) No ray could get into the cell which made a greater angle with the axis in the horizontal plane than 1.1°, or greater than 2.0° in the vertical plane. (2) No ray could strike the inside of the cell. (3) The image, formed at the center of the cell with water in the cell, was 0.3 cm wide and 0.5 cm high.

The photometer used a 1P21 photomultiplier and had two stops. One stop was as near as possible to the 1P21 and slightly smaller than the cathode; the other was as near as possible to the scattering cell. The vertex angle of the cone of light from the scattering volume accepted by the photometer was less than 4° horizontally and less than 9.4° vertically. The current from the 1P21 was read on a sensitive galvanometer. Scattering could be observed at all angles from $\theta=20°$ to 155°.

The instrument was calibrated with "Ludox," a 30 percent colloidal dispersion of silica,[10] by making use of the relation $R(90°)=3T/(16\pi)$, which applies to dilute solutions of particles small compared to λ. T is the turbidity of the solution. This expression is derived by Doty and Steiner.[6] The calibration constant Q of the instrument was the ratio of R(90°) to the corresponding galvanometer deflection. By observing the scattering from a clean, dilute Ludox solution, it was verified that the scattering obeyed the small particle formula from 20° to 155°. Calibration consisted then of determining the galvanometer current due to the scattered light from a dilute Ludox solution of known T. The scattering by water was subtracted to get the scattering by the silica particles alone.

For scattering measurements 0.01 ml of the 30 percent Ludox stock solution was mixed into about 10 ml of dust-free water in the scattering cell. Mixing of the Ludox and the water was accomplished with a small piece of iron wire (1 mm diam) coated with fingernail polish to prevent rusting. The wire was moved about in the solution by means of an external magnet.

The turbidity T of the scattering solutions was much too low to measure directly. Scattering could not be successfully carried out with higher Ludox concentrations because i(45°)/i(135°) became less than unity, indicating multiple scattering and particle interactions. It was therefore necessary to calculate the T of a dilute solution from its concentration, the T of a solution of higher concentration, and a knowledge of the manner in which T varies with concentration. Mommaerts[11] has made a study of the variation of T with concentration, c, and found that c/T is a linear function of c for Ludox—i.e., $c/T=A+Bc$.

By swinging the photometer to $\theta=0°$, it was possible to use the light scattering instrument to measure T. A dense photographic plate was placed in the beam to avoid overloading the photomultiplier tube. Mommaerts' finding that c/T is a linear function of c was verified for the entire range of c from 30 percent down to the smallest concentration giving measurable turbidity (about 2 percent).

In all, seventeen plots of c/T against c were made. These were excellent straight lines, but for unknown reasons the slopes were not reproducible. Values of B varied from 1.25 cm to 2.18 cm as compared to Mommaerts' value of 1.20 cm (for 4358A). The intercepts A were, however, reproducible, and these were used for the calibration. The average value of A was 12.0 cm-percent, based upon the assumption that the stock solution was 30 percent as labelled. This assumption does not influence the calibration constant Q, which is defined as:

$$Q=\text{limit}\ (c\to 0)3T/[16\pi\cdot i(90°)]=3/[16\pi A\sigma], \quad (3)$$

where σ is a constant equal to i(90°)/c. Both A and σ contain c implicitly (that is, the number representing each depends upon assumed Ludox concentration), but the product σA does not, so that a knowledge of the stock Ludox concentration is unnecessary.[12]

Refractive increments $\partial n_e/\partial c$ were measured with a differential refractometer somewhat similar to the one described by Brice and Halwer.[13,14] Data given by Stamm[15] for the refractive indices of NaCl and KCl solutions at 4358A were used to calibrate the refractometer.

[9] Obtained on special order from the Pyrocell Corporation of New York.

[10] Kindly furnished by Dr. H. H. Snyder of E. I. duPont de Nemours and Company.

[11] W. F. H. M. Mommaerts, J. Colloid Sci. **7**, 71 (1952).

[12] A check on the calibration constant was attempted by measuring the scattering of clean benzene and using the refractive correction described by Brice, Halwer, and Speiser (see reference 13). The authors' value of 48.4×10^{-6} for R(90°) of benzene was used. The resulting calibration constant was 25 percent higher than that obtained with Ludox. It is believed that this higher result was obtained because no refractive correction was made for the beam entering the scattering cell from the source, which was no longer imaged at the center of the cell. The refractive correction mentioned above applies only to the scattered light.

[13] Brice, Halwer, and Speiser, J. Opt. Soc. Am. **40**, 768 (1950).

[14] B. A. Brice and M. Halwer, J. Opt. Soc. Am. **41**, 1033 (1951).

[15] R. F. Stamm, J. Opt. Soc. Am. **40**, 788 (1950).

PREPARATION OF TMV RIBONUCLEIC ACID FOR LIGHT SCATTERING

TMV[16] was cultured on Havana tobacco plants and separated from the plant juice by differential centrifugation as described by Rawlins, Roberts, and Utech.[17] Their procedure prevents aggregation of the virus during purification. The molecular weight of the TMV was determined by the extrapolation method to be 40.0×10^6 after correction for depolarization. This value agrees with that of Oster, Doty, and Zimm[18] and shows that the virus preparation was mostly monomeric. A total of 6 g of virus was separated from 300 plants and found to be infective.

The protein of the virus was denatured by heating as described by Cohen and Stanley[1] and by Knight.[19] About 80 mg of TMV suspended in 4 ml of 0.1M sodium acetate buffer of *p*H 5.7, to which 0.2M of NaCl per liter had been added, was placed in a Pyrex test tube (2-mm wall thickness) at 2°C. This test tube was immersed in boiling water with constant stirring for the desired time and then immediately cooled in ice water with stirring. The coagulated protein was removed by about five two-minute centrifugations at 700 g. The RNA, which remained in the supernatant, showed a characteristic nucleic acid ultraviolet absorption spectrum, with a maximum at 2570A.

Corning ultrafine porosity sintered glass filters 1 cm in diameter were used to clean the solutions for light scattering. The best method found was to force the RNA solution through the filter directly into the scattering cell with compressed nitrogen. The solution was then poured back into the filter and refiltered into the cell. This process, which gradually washes dust from the cell into the filter,[20] was repeated as often as necessary to obtain dust-free solution in the cell. Usually the cell was first well cleaned of dirt by use of buffer solution in the above manner. Then, the RNA solution was filtered through three or four times. Specks of dust in a solution could be easily seen by looking through it almost directly towards a bright light.

The concentration of each RNA solution was determined from the ultraviolet absorption after the scattering of the solution had been measured. After an aliquot for absorption measurement had been removed from the scattering cell, the contents were poured back into the filter and enough buffer added to give approximately the desired dilution for the next scattering reading. Three or four more filtrations were needed to get the new dilution clean and well mixed with the few drops which always remained in the cell.

Optical density at 2570A was related to concentration by means of phosphorus analyses. From data given by Markham and Smith[21] for the nucleotide composition of RNA separated from TMV by heating, it can be shown that 8.97 percent by weight of the sodium salt of RNA is phosphorus. This figure, plus phosphorus analysis of an RNA solution whose optical density was known, showed that $c/D_{2570A}=0.0387$ at *p*H 8.0, and 0.0396 at *p*H 5.7. c is the concentration of sodium ribonucleate in mg/ml, and D_{2570A} is the optical density in a 1-cm path at 2570A. Markham and Smith[21] obtained approximately 0.035 at *p*H 7 to 8.

A sensitive test for protein was necessary to insure that the observed scattering was due to RNA and not to undenatured virus or protein. A modification of the biuret test has been described by Smith and Markham[22] which gives greater sensitivity by extracting the color into an alcohol layer. The minimum detectable protein from virus with this method was 40 mg/ml. The more concentrated the RNA preparation, the smaller the upper bound which could be set on the protein-to-RNA ratio. The table of results (Table I) shows that in one case this ratio was less than 0.7 percent by weight. Knight[19] detected no amino acids by paper chromatography and could have detected 2 percent or more. 0.7 percent by weight of whole TMV of molecular weight

TABLE I. Molecular weights[a] of the ribonucleic acid preparations.

Prep. No.	Prep. method from virus (heat time, centrifugation, etc.)	Upper lim. on protein (% of RNA)	No. of conc's. used	Average intercept $2c/R(0^\circ)$	Molecular wt. before correction	Molecular wt. corrected for depol.
1	60″ heat +1½ hr at 40 000 g	1.4	6	0.751	2.15×10^6	2.03×10^6
2	60″ heat +1½ hr at 40 000 g, top half of supernatant	0.7	4	0.751	2.15	2.03
3	70″ heat +1½ hr at 40 000 g	5.6	6	0.769	2.11	1.99
4	70″ heat	···	2	0.820	1.98	1.87
5	70″ heat	3.4	4	0.764	2.13	2.01
6	Prep. 5+½ hr at 40 000 g	3.4	4	0.779	2.08	1.96
7	Prep. 4 extracted once with $CHCl_3$	···	1	0.733	2.21	2.08
8	70″ heat, extracted 3 times with $CHCl_3$	···	1	0.748	2.16	2.03
9	70″ heat extracted 5 times with $CHCl_3$	···	1	0.711	2.28	2.15
10	80″ heat +1½ hr at 40 000 g	11.5	6	0.762	2.13	2.01
11	2 min heat	···	4	0.676	2.39	2.25
12	5 min heat	···	2	0.563	2.87	2.70
13	TMV washed 3 times, 70″ heat	···	1	0.687	2.36	2.22

[a] Of the sodium salt.

[16] The virus strain was kindly furnished by Dr. L. O. Kunkel of the Rockefeller Institute for Medical Research through Dr. W. J. Hooker of Iowa State College.

[17] Rawlins, Roberts, and Utech, Am. J. Botany **33**, 356 (1946).

[18] Oster, Doty, and Zimm, J. Am. Chem. Soc. **69**, 1193 (1947).

[19] C. A. Knight, J. Biol. Chem. **197**, 241 (1952).

[20] Initially the ultrafine filters were cleaned by soaking them for several hours in concentrated nitric acid; buffer was then forced through them until the filtrate showed the original buffer *p*H. Filters treated in this fashion were found to degrade RNA prepared from TMV by a detergent denaturation of the protein; for the scattering by a given solution decreased with each successive filtration. If, however, the filter was soaked in 1 N NaOH for twelve to twenty-four hours after the acid cleaning, degradation did not occur. RNA prepared by the heat method described in this paper was in some instances forced through one of these neutralized filters two or three dozen times with no change in molecular weight. The filter neutralization step takes time; merely forcing 1 N NaOH through the filter several times is not sufficient. The NaOH soaking must of course be followed by rinsing with buffer.

[21] R. Markham and J. D. Smith, Biochem. J. **46**, 513 (1950).

[22] J. D. Smith and R. Markham, Biochem. J. **46**, 509 (1950).

40×10^6 would change a RNA solution of true molecular weight 2.0×10^6 to one with a weight average molecular weight of 2.2×10^6.

The similarity of molecular weights obtained with and without centrifugation of solutions for $1\frac{1}{2}$ hours at 40 000 g (sufficient to sediment TMV) after removing coagulated protein, again showed that any residual virus was not influencing the scattering.

INSTABILITY OF TMV RIBONUCLEIC ACID

It was observed that the RNA prepared by heating TMV in boiling water disintegrated rapidly at room temperature. This breakdown could be halted for at least 24 hours by cooling the solution to 2°C. It was therefore necessary to keep solutions cold at all times after the preparative heating. The disintegration of a preparation of RNA (preparation 3, Table I) was followed for 62 hours by light scattering, after which time the rate of decrease of scattering had become very small. The scattering curves became concave down, indicative of polydispersity, and could not be extrapolated to $\theta=0°$ because of the rapid drop at low angles. The intensity of 90° scattering fell by a factor of 3.6 during this period, and the dissymmetry fell from 1.6 to 1.3.

The similarity of molecular weights (Table I) obtained by varying times of heating, ranging from 60 seconds to 5 minutes, shows that the disintegration observed at room temperature was not caused solely by a thermal collision process. If it had been, the molecular weights should have been lower the longer the RNA was heated. If anything, two-minute heating gave a higher molecular weight than the shorter times, while five-minute heating definitely gave a higher weight. The evidence therefore suggested an enzymatic action.

Several attempts were made to remove or inactivate the suspected enzyme. Repeated washing of the TMV with *p*H 7 phosphate buffer did not reduce the disintegration of the RNA prepared from it. Loring[23] found that pancreatic ribonuclease is absorbed to TMV and inactivates it. Four washings of the inactive virus with *p*H 7 phosphate buffer restored 70 percent of the virus infectivity. Therefore, if the enzyme in the RNA preparations came from the tobacco plant originally, it was tightly adsorbed to the virus. Neither Be^{+++}, Cu^{++}, nor a change in *p*H from 5.7 to 7.9 was effective in preventing enzymatic action. The only promising method found was to extract the RNA solution with half its volume of chloroform (containing 20 percent of octyl alcohol) by shaking for 15 minutes. After three such extractions, the scattering by the RNA at $\theta=90°$ decreased by only 25 percent at 20°C, instead of the 80 percent or more for unextracted RNA. More prolonged or additional extractions were useless in preventing this 25 percent reduction. However, after the 25 percent disintegration, the scattering curves were still monodisperse in appearance.[24]

Instability of RNA prepared by heating was reported by Cohen and Stanley,[1] who observed a slow degradation even at 4°C. Ultracentrifuge analysis showed that their RNA of molecular weight 2.9×10^5 was polydisperse. Degradation from an original weight of about 2×10^6 may have taken place either during handling or in the ultracentrifuge at 20°C. Knight[19] also had evidence for polydispersity of the RNA in his preparations. It, therefore, seems that several workers have had evidence of this enzymatic action.

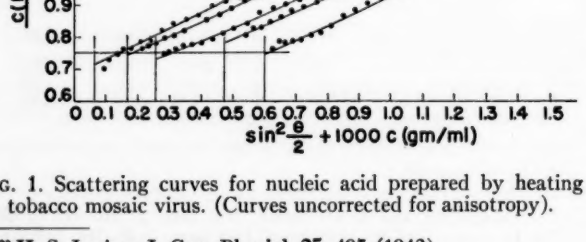

FIG. 1. Scattering curves for nucleic acid prepared by heating tobacco mosaic virus. (Curves uncorrected for anisotropy).

LIGHT SCATTERING RESULTS

The depolarization of the scattered light was measured at $\theta=90°$. ρ_v was found to be 0.0256 and ρ_h was 0.243. The refractive increment of the RNA was 0.194 ml-g^{-1}.

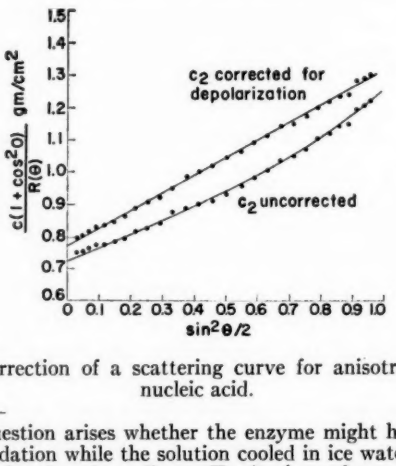

FIG. 2. Correction of a scattering curve for anisotropy of the nucleic acid.

[23] H. S. Loring, J. Gen. Physiol. 25, 497 (1942).

[24] The question arises whether the enzyme might have caused some degradation while the solution cooled in ice water after the preparative heating. According to Kunitz (see reference 25) a 0.01 percent solution of crystalline pancreatic ribonuclease retains 64 percent of its activity after 5 minutes at 100°C and *p*H 5.8. If the enzyme in the TMV RNA preparations is similar, it would not have been destroyed by the heating periods used. Kunitz did not attempt to determine whether the pancreatic ribonuclease remained active at elevated temperatures, but measured activities after cooling to room temperature for 30 minutes. However, trypsin which can also withstand brief periods at 100°C (see reference 26), is reversibly denatured and inactive at this temperature. It regains all its activity only after 10 minutes at 0°C. The enzyme present in the TMV RNA preparations may also show such a reversible denaturation. Hence, no definite conclusion can be drawn at present concerning possible enzymatic activity during the cooling period after the preparative heating.

[25] M. Kunitz, J. Gen. Physiol. 24, 15 (1940).

[26] J. H. Northrop, J. Gen. Physiol. 16, 323 (1932).

The scattering curves at five concentrations of RNA preparation 1 are shown in Fig. 1. The curves, which are uncorrected for depolarization, show a gentle upward curvature. Figure 2 shows the curve for concentration c_2, along with the same data corrected for depolarization by dividing the data points by $F(\theta, 0.0256)$. The corrected curve is straight, as would be expected for solutions having the observed dissymmetry of about 1.5. Theoretical scattering curves for spheres, monodisperse coils, and rods, all of such dimensions that their solutions have a dissymmetry of 1.5, deviate only slightly from straight lines.

Table I gives a complete list of the RNA preparations and the corresponding molecular weights, corrected for depolarization. These weights represent approximately the weight of all the RNA in one TMV rod. By phosphorus analyses of the virus it was found that the virus contained 5.6 ± 0.5 percent RNA by weight (expressed as the sodium salt). This figure is based on the assumption that all the phosphorus of TMV is in the RNA. 5.6 percent of 40.0×10^6 is 2.24×10^6, or about the RNA molecular weights observed. The molecular weight appeared to increase with prolonged preparative heating times (preparation 12, Table I). Since the RNA seems to be removed from the virus rod in one piece, it is likely that all of the nucleic acid is contiguous in the rod.

ACKNOWLEDGMENTS

One of us (T.G.N.) is pleased to acknowledge the assistance of a National Cancer Institute Predoctorate Research Fellowship in carrying out the above work.

We are indebted to Dr. W. J. Hooker of the Department of Botany and Plant Pathology of Iowa State College for assistance in culturing the tobacco mosaic virus, and to Dr. L. O. Kunkel of the Rockefeller Institute for Medical Research for supplying the virus strain.

THE JOURNAL OF CHEMICAL PHYSICS VOLUME 22, NUMBER 4 APRIL 1954

Structure of the Perrhenate Ion

HOWARD H. CLAASSEN* AND A. J. ZIELEN
Argonne National Laboratory, Lemont, Illinois

(Received November 18, 1953)

Raman and infrared spectra have been obtained for aqueous solutions of perrhenic acid and sodium perrhenate. The spectra are interpreted satisfactorily with the assumption that the perrhenate ion in dilute solutions is ReO_4^- and has tetrahedral symmetry.

INTRODUCTION

THE Raman spectra of solutions of perrhenic acid and sodium perrhenate, and of crystalline sodium and potassium perrhenate, have been investigated by Fonteyne.[1] He observed only three Raman bands for dilute perrhenic acid and for solutions of perrhenate and concluded that the anion in solution may be ReO_6^{-5} with an octahedral structure rather than ReO_4^- with a tetrahedral structure as the ion exists in alkali perrhenate crystals.[2] After a study of the ultraviolet absorption spectra of perrhenate solutions, as well as some of the chemical properties, J. C. Hindman suggested that the Raman spectra should be reinvestigated.

MATERIALS AND EXPERIMENTAL PROCEDURE

Rhenium heptaoxide was obtained from the Department of Chemistry of the University of Tennessee. Spectrochemical analysis[3] of a sample of this material did not reveal the presence of any impurities. Stock solutions of perrhenic acid were prepared by dissolving the heptaoxide in doubly distilled water. Weight analyses of the $HReO_4$ content were carried out by titration with standard sodium hydroxide to the methyl red end point. Utilizing a Cary recording spectrophotometer, absorption spectra of diluted aliquots of the perrhenic acid stock solutions were obtained. These did not indicate the presence of any lower oxidation states of rhenium and were in quantitative agreement with the results reported by Hindman and Wehner.[4]

The sodium perrhenate solution was prepared by adding a slight excess of perrhenic acid to CP grade sodium hydroxide pellets. The pH of the solution was then adjusted to 6 by the addition of dilute sodium hydroxide.

A Hilger E612 Raman spectrograph, having two 63° glass prisms, camera aperture $f/5.7$, and inverse dispersion on the plate of 16A per mm at 4358A, was used. The Raman excitation unit was obtained from Applied Research Laboratories; it has been described by Kemp, Jones, and Durkee.[5] A 21-ml Raman tube

* Department of Physics, Wheaton College, Wheaton, Illinois. Participating institution appointment.

[1] R. Fonteyne, Natuurw. Tijdschr. (Belg.) **20**, 20 (1938).
[2] J. Beintema, Z. Krist. **97A**, 300 (1937).
[3] Kindly performed by J. A. Goleb of this Laboratory.
[4] J. C. Hindman and P. Wehner, J. Am. Chem. Soc. **75**, 2869 (1953).
[5] Kemp, Jones, and Durkee, J. Opt. Soc. Am. **42**, 811 (1952).

TABLE I. Raman frequencies and the exciting Hg lines for which each was observed, for various perrhenate solutions.

$NaReO_4$, 25.4%	331±*e,k*	920 *e,k,i*	970.7 *e,k,i*
$HReO_4$, 6%	331±*e,k*	919 *e,k*	970.3±*e,k,i*
$HReO_4$, 10.0%	331±*e,k*	920 *e,k*	970.7±*e,k,i*
$HReO_4$, 28.5%	332±*e,k,i*	918 *e,k,i*	970.7±*e,k,i*
$HReO_4$, 70.0%	332±*e,k,i*	916 *e,k,i*	971.8±*e,k,i,l*
$HReO_4$, 80.1%	333±*e*	916 *e*	974.8 *e,k*

was used. It was filled by forcing the solutions through fine fritted glass filters by means of compressed air.

Raman spectra were recorded on Kodak 103*a-J* and III-*J* plates. Sodium nitrite solutions were used as light filters. Frequencies were determined by linear interpolation between nearby lines on an adjacent iron arc spectrum. Measurements were made with a Gaertner Model M1205C comparator modified by the addition of the photoelectric setting device described by Tomkins and Fred.[6] A Leeds and Northrup photoelectric microphotometer was used to trace some of the spectra. Qualitative information about the state of polarization of Raman bands was obtained by taking two equal exposures with polaroid sheets around the Raman tube, one transmitting the electric vector perpendicular to and one parallel to the axis of the tube.

Infrared spectra were obtained by means of a Model 21 Perkin-Elmer spectrophotometer with NaCl prism. Silver chloride windows 0.25 mm thick and coated with silver sulfide were used to contain the sample. A drop of solution was placed on one window, the other window was laid on, and they were held pressed together with thumb and finger and clamped between brass collars.

RESULTS AND DISCUSSION

Raman spectra were obtained for six different concentrations of perrhenic acid solutions and for one of sodium perrhenate. For all except the most concentrated acid only three Raman shifts were observed in addition to the diffuse scattering due to the water. The averages of the measured frequency shifts and the Kohlrausch designations of the exciting Hg lines for which each shift was observed are given in Table I. The relative intensities and widths of the bands may be estimated from Fig. 1A, a photograph of a microphotometer trace showing the three shifts from 4358A for the 70 percent perrhenic acid solution. The spectra for the more dilute solutions are essentially identical to this one. For the most concentrated solution, however, several new bands were observed. These are shown, and their frequencies listed, in Fig. 1B. An additional weak band, whose assignment must be considered doubtful, was observed shifted 1612 cm^{-1} from 4358A.

The great difference in exposure times for Figs. 1A and 1B was necessary because of absorption in the 87.7 percent sample. This solution appeared yellowish green; the 80.1 percent solution appeared slightly yellowish, but all the more dilute solutions were colorless. Because of the absorption, the relative intensity of the 338 cm^{-1} band is probably considerably greater than indicated in Fig. 1B.

Polarization exposures were made on a 10 percent $HReO_4$ solution. These showed the 971 cm^{-1} band to be polarized and indicated the other two to be depolarized. This is as one would expect by noting the high intensity and sharpness of the 971 cm^{-1} band.

The infrared spectrum was scanned from 700 to 1400 cm^{-1} for the sodium perrhenate solution and for three different concentrations of perrhenic acid. Only one absorption maximum due to the perrhenate ion was found in each case, a strong band at 914 cm^{-1}.

The data of Fonteyne[1] agree well with the present Raman data for dilute solutions, but some differences may be noted for the most concentrated solutions. Thus he lists a band at 1102 cm^{-1} which we did not observe, and we find bands at 886 and 989 cm^{-1} which he apparently did not resolve from the neighboring stronger bands. More puzzling is the disagreement in regard to the concentrations at which extra bands may be observed. Fonteyne lists a band at 840 cm^{-1} for 30 percent $HReO_4$, whereas we found the corresponding band only at 87.7 percent concentration. For example, in the case of the 70 percent solution, exposures 30 times as great as the one shown in Fig. 1A showed no evidence of this band.

STRUCTURE CONSIDERATIONS

Fonteyne[1] has suggested that the perrhenate ion in dilute solution may be octahedral rather than tetrahedral. The number of fundamental vibrations of each

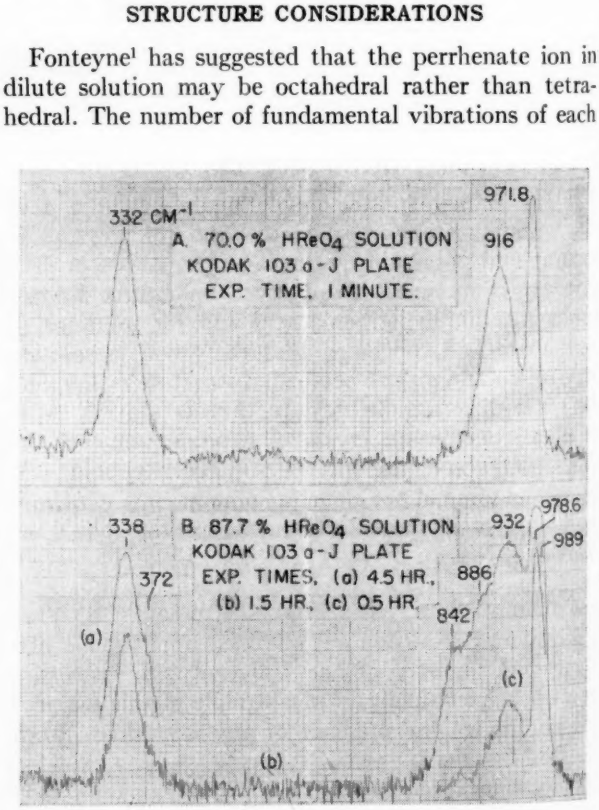

FIG. 1. Microphotometer traces of Raman spectra.

[6] F. S. Tomkins and M. Fred, J. Opt. Soc. Am. 41, 641 (1951).

symmetry species and the selection rules for their observation are listed in Table II both for XY_4 molecules of T_d symmetry and XY_6 molecules of O_h symmetry. Fonteyne[1] believed that only three Raman bands could be ascribed to the ion, and that therefore the O_h structure was most plausible. When the absence of a fourth Raman band, except in very concentrated solutions, was verified in the present work, an infrared investigation was attempted. The Raman band at 971 cm^{-1}, since it is polarized, sharp, and intense, must be due to a totally symmetric vibration, and would be observable by absorption neither for the T_d nor for the O_h structures. The band at about 918 cm^{-1}, on the other hand, must belong to species F_2 and be infrared active if the symmetry is T_d, but cannot be infrared active if it is O_h, since for that symmetry no vibrational mode can be active in both infrared and Raman spectra. Fortunately, water has no strong absorption bands in this region, and it was possible to observe an infrared band at 914 cm^{-1} due to the perrhenate ion. This is so close to the observed 918 cm^{-1} Raman band that it is quite plausible they are both due to the same vibrational mode.

The experimental data leave two choices: (1) The symmetry is T_d and the reason one does not observe four R bands is that the E and one of the F_2 vibrations happen to lie so close together that one cannot resolve them, or (2) The symmetry is O_h and the close agreement between the one Raman and the infrared band is accidental; they are actually due to vibrational modes of different species. Either choice requires the assumption of an accidental coincidence, the first perhaps more probable since the observed Raman band at 331 cm^{-1} is quite broad, as shown in Fig. 1.

Further light on this question may be obtained by calculation. Heath and Linnett[7] have shown that for several types and many individual molecules and anions it is possible to calculate frequencies to within one or two percent, using an intramolecular force field between bonded atoms in accordance with modern theories of directed valency plus an assumed Van der Waals type of repulsion between nonbonded atoms. They have given equations both for tetrahedral XY_4 and for octahedral XY_6 types of molecules. In either case the vibration frequencies for one molecule are given in terms of three potential constants. These equations have been used for the present problem.

First, assuming an O_h ion, ReO_6^{-5}, the three observed Raman bands at 971, 918, and 331 cm^{-1} were assigned to species A_{1g}, E_g, and F_{2g}, respectively, and three potential constants evaluated: $k_1=7.59$, $k_\beta=0.337$, and $A=0.162\times10^5$ dynes/cm. Then the two frequencies of species F_{1u}, which should be infrared active, were calculated. The result was 315 and 1000 cm^{-1}.

Second, assuming a T_d ion, ReO_4^-, the Raman bands at 971, 918, and 331 cm^{-1} were assigned to A_1, F_2, and E, respectively, and three potential constants evaluated: $k_1=6.52$, $k_\alpha'=0.400$, $A=0.295\times10^5$ dynes/cm. The other F_2 frequency could then be calculated. The result was 343 cm^{-1}.

These calculations seem definitely to favor the tetrahedral assumption. The fourth frequency calculated for this assumption is only 12 cm^{-1} from the observed peak at 331 cm^{-1}, so that it is very plausible that this observed Raman band at 331 cm^{-1} is a superposition of two bands too close to resolve, particularly in view of the width of the observed band. On the other hand, the octahedral assumption leads to a calculated value for the high infrared frequency of 1000 cm^{-1}, which is 86 cm^{-1} or 9 percent from the observed band at 914 cm^{-1}. This deviation between calculated and observed is much greater than Heath and Linnett[7] found in any of their examples.

On the basis of the spectroscopic evidence, then, it seems most likely that the perrhenate ion in dilute solution is tetrahedral. The source of the additional Raman bands and of the green color in concentrated solutions may well be the undissociated acid $HOReO_3$. The difference in Raman spectra of dilute and highly concentrated perchloric acid presents a very similar case.[8,9]

TABLE II. Selection rules for the two models considered.

Symmetry species	Number of vibrations	Selection rules: Raman	Selection rules: Infrared	Assignment
		T_d symmetry, ReO_4^-		
A_1	1	Allowed	Forbidden	971
E	1	Allowed	Forbidden	331
F_2	2	Allowed	Allowed	918,331
		O_h symmetry, ReO_6^{-5}		
A_{1g}	1	Allowed	Forbidden	(971)
E_g	1	Allowed	Forbidden	(918)
F_{2g}	1	Allowed	Forbidden	(331)
F_{1u}	2	Forbidden	Allowed	···
F_{2u}	1	Forbidden	Forbidden	···

ACKNOWLEDGMENTS

The authors are indebted to Dr. J. C. Hindman for suggesting the problem and to Dr. Sheffield Gordon for making available the infrared spectrophotometer.

[7] D. F. Heath and J. W. Linnett, Trans. Faraday Soc. **44**, 873, 878, 884 (1948); **45**, 264 (1949).

[8] J. H. Hibben, *The Raman Effect and its Chemical Applications* (Reinhold Publishing Corporation, New York, 1939), p. 376.

[9] Redlich, Holt, and Bigeleisen, J. Am. Chem. Soc. **66**, 13 (1944).

Carbon-13 Isotope Effect in the Thermodecomposition of Nickel Carbonyl

RICHARD B. BERNSTEIN*
Department of Chemistry, Illinois Institute of Technology, Chicago, Illinois
(Received November 2, 1953)

The $C^{12}-C^{13}$ fractionation factor in the decomposition of gaseous nickel carbonyl has been measured from 30–105°C, using samples of normal isotope abundance. Assuming that the rate-determining step is the rupture of a Ni–C bond, the rate constants are defined as follows:

$$\begin{aligned} &Ni(CO)_4 \longrightarrow Ni(CO)_3\cdot + CO \quad k_1, \\ &Ni(CO)_3C^*O- \begin{cases} \rightarrow Ni(CO)_3\cdot + C^*O & k_2, \\ \rightarrow Ni(CO)_2C^*O\cdot + CO & k_3. \end{cases} \end{aligned}$$

The C^{12} enrichment of the first fraction of CO from decomposition gives, over the temperature range studied,

$$k_1/(k_2+k_3)=1.0222-6.7\times10^{-5}t(°C).$$

The intramolecular and intermolecular isotope effects are defined as $k_3/3k_2$ and $k_1/4k_2$, respectively. The magnitude of the intramolecular effect was assumed to be given by the square root of the usual reduced mass ratio, with a value of 1.0345. Thus the intermolecular effect calculated from the data becomes,

$$k_1/4k_2=1.0481-6.7\times10^{-5}t(°C).$$

A theoretical estimate of the magnitude of the intermolecular effect was made using the method of Bigeleisen. Isotopic shifts in vibrational frequencies were computed, and the usual assumptions regarding the vibrations of the activated complex were made. The calculated isotope effect was somewhat smaller than that observed.

INTRODUCTION

MOST of the previous studies of carbon isotope effects in reaction rates have dealt with the decarboxylation reactions of various carboxylic acids.[1] This report is concerned with the $C^{12}-C^{13}$ fractionation in the thermal decomposition of gaseous nickel carbonyl. It was thought of interest to study the isotope effects for a somewhat simpler molecule where the vibrational analysis is subject to less uncertainty than in the case of the relatively complex organic compounds.

The kinetics of the decomposition have been studied by several workers.[2–4] The rate law was found to be

$$-\frac{d}{dt}[Ni(CO)_4]=\frac{K_1[Ni(CO)_4]}{1+K_2[CO]}. \quad (1)$$

The rate-limiting step for the homogeneous decomposition is presumed to be the rupture of a single Ni–C bond. Unfortunately, the reaction proceeds partly by a heterogeneous mechanism, and is therefore not a simple one. From measurements of the temperature coefficient of the over-all reaction, values for the apparent activation energy of 10 250 and 12 000 cal/mol have been reported.[2,3]

Previous measurements of the isotope effect in the thermal decomposition of nickel carbonyl were carried out in a flow system at high extent of reaction.[5] From the C^{13} enrichment in the undecomposed $Ni(CO)_4$ it was possible to make an estimate of the isotope effect. However, because of the possibility that the mechanism of the reaction may be altered under these conditions in such a way as to influence the isotopic effect, it was thought desirable to measure the fractionation at low extent of decomposition in a conventional static system.

In the present study, the C^{12} enrichment in the first fraction of CO obtained from the decomposition of a normal sample of $Ni(CO)_4$ was determined, and ratios of certain isotopic rate constants were computed from the data and compared with the theory of Bigeleisen.[6]

EXPERIMENTAL

Figure 1 shows a schematic diagram of the apparatus. Nickel carbonyl (International Nickel Company, Mond process, stated to contain <0.004 percent Fe, other metals and sulfur absent) was freed of carbon monoxide by a trap-to-trap distillation immediately before use. A sample was introduced from one of the reservoirs into the Pyrex reaction vessel, maintained at the appropriate temperature by a glycerin bath. After a suitable time, the reaction was stopped by quenching with liquid nitrogen. The CO was separated from the $Ni(CO)_4$ by passage through the spiral trap at −195°C. After measurement of the CO pressure in a known volume (thus determining the percent decomposition of the $Ni(CO)_4$), the CO was quantitatively oxidized to CO_2 for subsequent mass spectrometric isotopic analysis by repeated passage through the copper oxide tube at 300°C. Samples of "normal" $Ni(CO)_4$ were taken for each experiment. They were quantitatively pyrolyzed at

* Present address: Department of Chemistry, University of Michigan, Ann Arbor, Michigan.

[1] For a review, see J. Bigeleisen, J. Chem. Phys. **56**, 823 (1952).
[2] A. P. Garratt and H. W. Thompson, J. Chem. Soc. **1934**, 1822.
[3] C. E. Bawn, Trans. Faraday Soc. **31**, 440 (1935).
[4] K. Tonosaki and B. Suginuma, Bull. Inst. Phys. Chem. Research (Tokyo) **22**, 1014 (1943).
[5] R. B. Bernstein, J. Phys. Chem. **56**, 893 (1952).
[6] J. Bigeleisen, J. Chem. Phys. **17**, 675 (1949).

200–300°C in small Pyrex sample tubes, and the CO was then similarly oxidized to CO_2.

The decompositions were carried out over a range of initial pressures from 60–300 mm Hg. Although the over-all rate of decomposition was dependent on the pressure, no trend in the fractionation factor with respect to pressure was noted. The extent of decomposition for most experiments was <10 percent. Small corrections were applied to the observed fractionation factors to bring all data to the basis of infinitesimal extent of reaction.

Isotopic assays were carried out with a Consolidated-Nier Isotope Ratio Mass Spectrometer, Model 21-201; in certain cases, isotopic analyses were performed by the Analytical Service of the Consolidated Engineering Corporation, Pasadena, California. The enrichment factor was taken to be the ratio of the mass spectrometer isotope ratios $(45/44)_1/(45/44)_2$, where the subscripts 1 and 2 refer to CO_2 from "normal" $Ni(CO)_4$ and product CO, respectively. In certain experiments the CO was not oxidized; the isotopic analyses were carried out directly on the CO. Here the enrichment factor was taken to be the ratio of the isotope ratios $(29/28)_1/(29/28)_2$. The estimated error in the fractionation factor for a given experiment due to uncertainty in the mass spectrometric assay was ±0.1 percent, corresponding to an error of ±0.001 in the ratio $k_1/(k_2+k_3)$.

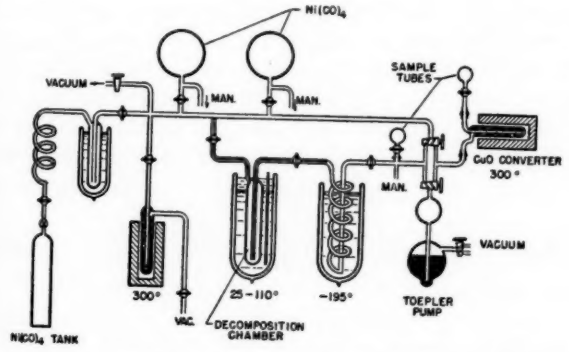

FIG. 1. Apparatus for study of isotope effect in thermodecomposition of nickel carbonyl.

RESULTS

Figure 2 shows a graph of the enrichment factor *S versus* temperature (°C) for eighteen experiments.† A least-squares line has been drawn through the data:

$$S \equiv k_1/(k_2+k_3) = 1.0222 - 6.7\times10^{-5}t(°C). \qquad (2)$$

The average deviation from the line is ±0.002, which is approximately twice that anticipated on the basis of the analytical imprecision. No significant differences are noted between experiments in which CO rather than CO_2 was used for the C^{13} isotopic assay.

† These results differ somewhat with the preliminary values[5] obtained at high extent of reaction. It is believed that the present results are more reliable because the possible complication of a reversible isotopic exchange reaction has been eliminated by operation at low extent of decomposition.

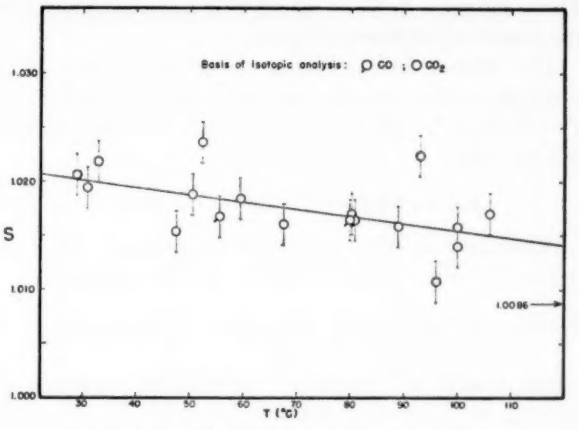

FIG. 2. Enrichment factor *vs* temperature.

DISCUSSION

Upon the assumption that the rate-determining step in the decomposition is the rupture of a single Ni–C bond, the relevant rate constants have been defined[5] as follows:

$$\begin{aligned} &Ni(CO)_4 \longrightarrow Ni(CO)_3\cdot + CO \quad k_1,\\ &Ni(CO)_3C^*O \begin{cases} \longrightarrow Ni(CO)_3\cdot + C^*O & k_2,\\ \longrightarrow Ni(CO)_2C^*O\cdot + CO & k_3. \end{cases} \end{aligned}$$

Thus,

$$\frac{d}{dt}[CO] = 4k_1[Ni(CO)_4] + 3(k_2+k_3)[Ni(CO)_3C^*O],$$

and

$$\frac{d}{dt}[C^*O] = (k_2+k_3)[Ni(CO)_3C^*O],$$

so that

$$\frac{[CO]}{[C^*O]} = 3+4\left(\frac{k_1}{k_2+k_3}\right)\frac{[Ni(CO)_4]}{[Ni(CO)_3C^*O]}.$$

One may define the observed separation factor

$$S \equiv 1+\epsilon = \frac{[CO]}{[C^*O]} \Big/ \left(\frac{(1-\alpha)}{\alpha}\right), \qquad (3)$$

where α represents the "normal" abundance of C^{13} in the nickel carbonyl and $[CO]/[C^*O]$ is the C^{12}/C^{13} ratio in the product CO. Upon substitution one finds that the desired ratio of the rate constants is $k_1/(k_2+k_3) = 1+\epsilon(1+3\alpha+\cdots)$. Since α is approximately 0.011 for natural carbon, and ϵ is of the order of 0.02 for this reaction, to a good approximation one may write

$$k_1/(k_2+k_3) = S. \qquad (4)$$

Thus, the ratio $k_1/(k_2+k_3)$ may be taken to be equal to the observed separation factor.

The intramolecular isotope effect is written, in accordance with conventional usage, as $k_3/3k_2$. Defining $\epsilon^*=k_3/3k_2-1$, one obtains for the intermolecular isotope effect

$$k_1/4k_2=1+\epsilon+(3/4)\epsilon^*=S+(3/4)\epsilon^*. \quad (5)$$

According to the theory of Bigeleisen,[6] the intermolecular effect would be given by the expression

$$k_1/4k_2=(m^*/m)^{\frac{1}{2}}[1+\sum_i G(u_i)\Delta u_i-\sum_i G(u_i^\ddagger)\Delta u_i^\ddagger], \quad (6)$$

where m and m^* represent the reduced masses of the normal and isotopic activated complexes along the decomposition coordinate and the other quantities have their usual significance. Here $(m^*/m)^{\frac{1}{2}}$ is taken[5] to be 1.0345, based on the Ni—C^{12}, Ni—C^{13} reduced masses, as suggested by Slater's[7] treatment of the rupture of an isolated bond. The intramolecular isotope effect should be given directly by $k_3/3k_2=(m^*/m)^{\frac{1}{2}}$. Substituting this value of $\epsilon^*=k_3/3k_2-1=0.0345$ in Eq. (5), and combining with the equation for the least-squares line of Fig. 2 (Eq. (2)), one obtains the empirical expression

$$k_1/4k_2=1.0481-6.7\times10^{-5}t(°C). \quad (7)$$

For this decomposition it is not possible to measure separately the intramolecular and intermolecular effects, since the $Ni(CO)_3\cdot$ radical is an unstable species which cannot be isolated for C^{13} assay. However, a review of the literature[1] on intramolecular effects involving C^{13} substitution has indicated that the Slater approximation is a fairly satisfactory one. With this assumption, one may compute the intermolecular effect using the Bigeleisen[6] Eq. (6) and compare with the results derived from the experimental data.

Letting the difference in the free energy functions be defined

$$\delta=\sum_i G(u_i)\Delta u_i-\sum_i G(u_i^\ddagger)\Delta u_i^\ddagger, \quad (8)$$

one obtains

$$k_1/4k_2=(1+\epsilon^*)(1+\delta)=1+\epsilon+(3/4)\epsilon^*. \quad (9)$$

Thus,

$$\epsilon=\delta+\epsilon^*/4. \quad (10)$$

This implies that as the temperature increases and $\delta\to0$, ϵ approaches a lower limit of 0.0086. In Fig. 2, an arrow indicates the value of this lower limit of 1.0086 on the separation factor, S.

In order to evaluate δ, it is necessary to postulate a model for the isotopic activated complexes.

The simplest model for the activated complex is that which has usually been chosen for similar calculations. All vibrational frequencies of the activated complex are considered identical with those of the reactant molecule except for vibrations involving the stretching of the fissile bond; these frequencies are assumed to be zero. The use of this model (designated "model A") would seem to give rise to an upper limit for the isotope effect. In the case of $Ni(CO)_4$, therefore, it has been assumed that the only terms in δ which require evaluation are those associated with the two Ni—C stretching vibrations, $\omega_1(a_1)$ and $\omega_6(t_2)$; the symbols are those of Crawford and Cross.[8]

In order to compute the frequencies for $Ni(CO)_3C^*O$ from those of $Ni(CO)_4$, one must consider the change in the symmetry of the molecule from T_d to C_{3v} due to isotopic substitution. Thus, the triply degenerate vibration ω_6 would split into a singly degenerate frequency $\omega_{6a}(a_1)$ and a double degenerate frequency $\omega_{6b}(e)$. It was thought desirable to simplify the problem by computing the frequencies ω_1 and ω_6 corresponding to the tetra-C^{13}-substituted molecule, $Ni(C^*O)_4$. Thus, the same array of potential constants may be used for the two sets of calculations; one merely substitutes the mass of C^{13} for C^{12} in the appropriate elements of the determinants.

TABLE I. Ni—C and C—O stretching frequencies (cm^{-1}) for C^{12}- and C^{13}-tetrasubstituted nickel carbonyl.

	Ni—C stretching		C—O stretching	
	$\omega_1(a_1)$	$\omega_6(t_2)$	$\omega_2(a_1)$	$\omega_8(t_2)$
Observed (reference 8)	380	300	2040	2050
Calc. $Ni(C^{12}O)_4$	382.1	339.5	2043.6	2044.9
Calc. $Ni(C^{13}O)_4$	376.0	331.7	1994.6	1998.7
$\Delta\omega$ (calc.)	6.1	7.8	49.0	46.2

TABLE II. Comparison of "experimental" δ with δ calculated (model A).

T(°C)	δ calc	δ exp (smoothed)
25	0.0044	0.0119
50	0.0037	0.0103
75	0.0032	0.0086
100	0.0028	0.0069
125	0.0025	0.0052

Using force constants modified slightly from those of Crawford and Cross,‡ frequencies for C^{12}- and C^{13}-tetrasubstituted nickel carbonyl were computed.

In Table I are listed four of the observed[8] frequencies for the normal molecule, the frequencies for the C^{12} and C^{13} molecules calculated using the revised force constants, and the isotopic frequency shifts.

The desired difference in the free-energy functions is then:

$$\delta=\tfrac{1}{4}[G(u_1)\Delta u_1+3G(u_6)\Delta u_6], \quad (11)$$

[7] N. B. Slater, Proc. Roy. Soc. (London) **A194**, 112 (1948).

[8] B. L. Crawford, Jr., and P. C. Cross, J. Chem. Phys. **6**, 525 (1938).

‡ A numerical error in the calculations of reference 8 was found by Mr. Fred L. Voelz. His revised set of constants was therefore used for the present calculations for the pair of isotopic molecules. Unfortunately, the revised constants of Voelz do not satisfactorily reproduce all the observed frequencies. It is thought by Professor Crawford that the potential energy expression of reference 8 is too simple for this molecule. (Private communication.)

where $u=hc\omega/kT$. The factor $\frac{1}{4}$ is introduced on the assumption that the free energy function of a molecule is additively changed by a constant increment upon the substitution of isotopic atoms successively into equivalent positions in the molecule,[9] i.e., the "rule of the geometric mean."

Values of δ were calculated using observed frequencies (ω_1 and ω_6) and calculated shifts (Table I). These are compared with the smoothed "experimental" values in Table II.

It is to be noted that the calculated δ's are appreciably smaller than the experimental values.

It is difficult to understand why the calculated isotope effect should be smaller than the experimental one, considering the nature of the limiting assumptions employed in the calculations. Two possibilities have been considered. First, the heterogeneous component of the reaction may be partially responsible for the larger observed isotope effect. Second, in the activated complex the carbon-oxygen bond may be slightly weakened.

TABLE III. Comparison of "experimental" δ with δ calculated (Model B).

T(°C)	δ calc	δ exp (smoothed)
25	0.0101	0.0119
50	0.0088	0.0103
75	0.0079	0.0086
100	0.0072	0.0069
125	0.0066	0.0052

Evaluation of the former possibility does not seem feasible in the light of present knowledge. However, with regard to the latter it is quite simple to estimate the degree of weakening of the C—O bond required in order to make the calculated δ agree with the experimental one. Because of the high frequencies of the C—O vibrations and the correspondingly high values for the isotopic shifts, the C—O stretching force constant in the activated complex would need to be reduced by only a small amount below that in the normal molecule.

Table III gives the calculated δ's on the basis of an assumed 5 percent reduction of the frequencies ω_2 and ω_8 in the activated complex; a 5 percent reduction in the isotopic frequency shifts was likewise assumed. The Ni—C contribution to the δ, taken from Table II, has been included in the total δ calculated for Model B.

Since the C—O bond in $Ni(CO)_4$ is a relatively "tight" bond, the possibility of weakening in the activated complex may not be entirely unreasonable.

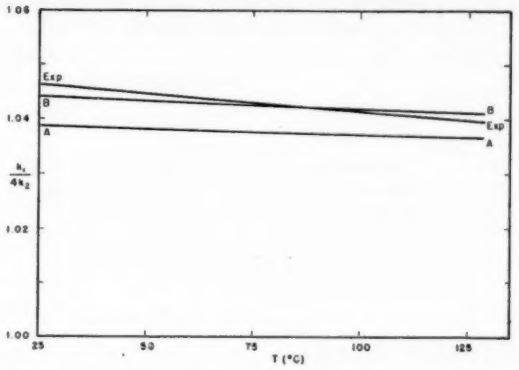

FIG. 3. Intermolecular isotope effect *vs* temperature. A—Theoretical model A. B—Theoretical model B. Exp—Smoothed experimental.

Figure 3 shows a graph of the temperature dependence of the intermolecular isotope effect $k_1/4k_2$. The curve labelled "smoothed experimental" represents Eq. (7). The curves labelled "theoretical" were obtained by substituting the calculated δ's of Table II and Table III, respectively, into Eq. (9).

It is believed by many of the workers in the field that the study of isotopic effects on reaction rates will eventually lead to a better understanding of the properties of the activated complex. However, it appears that the results of such studies often do not allow for unequivocal deductions, because of the following basic problem of indeterminancy: the measured isotope effect alone cannot, even in principle, reveal the multiple individual vibrational terms in the summation involved in the free energy functions for polyatomic molecules.

It is, of course, to be hoped that with the eventual accumulation of a sufficiently large body of experimental data, certain limitations on the allowable properties of the activated complex may be established.

ACKNOWLEDGMENTS

The author is grateful to Professor Henry Taube and Dr. Otto Forchheimer of the University of Chicago for their kind cooperation with regard to the mass spectrometer. Thanks are due to Mr. F. L. Voelz for assistance with the calculations of the vibrational frequencies. The author appreciates the support of the U. S. Atomic Energy Commission.

[9] It is of interest to examine the validity of this assumption for the case of the deuterated methanes, where all the isotopic frequencies are known. Considering the two stretching vibrations $\omega_1(a_1)$ and $\omega_3(t_2)$, for the pair CH_4 and CD_4, one computes a value of $\delta=6.07$ at 300°K. For CH_4 and CH_3D, the calculated δ is 1.42. Thus the ratio of the δ's is 0.234 compared to $\frac{1}{4}$.

Raman Spectra and Potential Constants for CF_3Cl, CF_3Br, and CF_3I

ROBERT COOPER TAYLOR
Department of Chemistry, University of Michigan, Ann Arbor, Michigan
(Received October 30, 1953)

Raman frequencies have been obtained for gaseous CF_3Cl and CF_3Br and for liquid CF_3I at $-40°C$. The assignments are in agreement with previous investigations. The spectra have been analyzed using a simplified, six-constant potential function of the Urey-Bradley type without the assumption of tetrahedral angles around the central carbon atom. In all three cases, it was found possible to reproduce the experimental frequencies to within less than their experimental error.

PREVIOUS workers have reported the infrared[1–6] and Raman[6,7] spectra of the various trifluoromethyl halides. However, in view of the fact that the region of the two lowest fundamentals has been inaccessible in the infrared work and the Raman investigations have dealt with the liquid state, it appears desirable to have information on the gaseous Raman spectra.

Since data have recently become available giving reliable values for bond angles in CF_3Cl, it was considered of interest to carry through a vibrational analysis using observed values instead of assuming tetrahedral angles. A Urey-Bradley type of potential function which has not been tried yet with these molecules was selected and calculations were extended to the bromide and iodide for comparison.

EXPERIMENTAL

The spectra were obtained with a Gaertner Raman spectrograph with an $f/3.5$ camera lens. The light source consisted of 12 type *AH*-11 mercury arc lamps arranged concentrically around the Raman tube and backed by a circular chrome plated reflector. Although this source had been designed primarily for liquid samples, its performance was satisfactory. The gaseous CF_3Cl and CF_3Br samples were contained in sealed heavy walled Pyrex tubes approximately 18-mm o.d. No internal baffles were used and the background consequently was heavier than desirable on some of the exposures. It was found, however, that the background could be reduced quite appreciably by lengthening the Raman tube and blackening the portion next to the window for several inches. No filters were used for the chloride and bromide but saturated sodium nitrite solution helped to reduce the photochemical decomposition of the iodide.

Both the trifluoromethyl chloride and bromide were supplied by the Jackson Laboratory of E. I. du Pont de Nemours Company and had been specially purified for PVT work. The iodide was prepared from the silver salt of trifluoroacetic acid[8,9] and purified by bulb to bulb distillation. In all cases, the samples were condensed into the Raman cell after passing through several inches of dried activated alumina followed by an ultrafine Pyrex sintered glass filter. The gas pressures of the bromide and chloride were 6–8 atmospheres. Photochemical decomposition of the vapor made it difficult to obtain the gas spectrum of the iodide and consequently it was obtained only for the liquid state at $-40°C$.

Exposure times varied from six to forty hours using 103*a*-*J* plates. In general, six hours was sufficient to show all fundamentals clearly. Wavelength shifts were measured on tracings made by a Leeds and Northrup microphotometer and the positions of the sharp lines were measured in addition with a comparator. The values reported represent the means of observations from several plates, excitation being by the 4046A 4358A, and sometimes the 4078A lines of mercury except for the iodide. Semiquantitative polarization data for the iodide were obtained by the two-exposure method using polaroid cylinders.

EXPERIMENTAL RESULTS

The observed frequencies, estimated relative intensities, and assignments are given in Table I.

In general, the standard deviations of the mean for the sharp bands were less than one reciprocal centimeter while those for the broader bands were about two cm^{-1}. The band maxima were measured in all cases. The

TABLE I. Observed Raman frequencies in cm^{-1} for CF_3Cl, CF_3Br, and CF_3I.

CF_3Cl (gas) Freq.	Assign.		CF_3Br (gas) Freq.	Assign.		CF_3I (liq.) Freq. (cm^{-1})	Assign.		Pol.
351 *w, br*	ν_6	e	305 *w, br*	ν_6	e	267 *w, br*	ν_6	e	···
475 *s*	ν_3	a_1	350 *s*	ν_3	a_1	285 *vs*	ν_3	a_1	pol.
559 *w, br*	ν_5	e	549 *w, br*	ν_5	e	541 *w, br*	ν_5	e	dp.
782 *s*	ν_2	a_1	762.5 *s*	ν_2	a_1	739 *s*	ν_2	a_1	pol.
1104 *ms, br*	ν_1	a_1	1081 *ms, br*	ν_1	a_1	1058 *mw, br*	ν_1	a_1	pol.
1217 *w, br*	ν_4	e	1209 *w, br*	ν_4	e	1177 *w, br*	ν_4	e	dp.
						1024 *vw*	$\nu_2+\nu_3$	A_1	···

[1] H. W. Thompson and R. B. Temple, J. Chem. Soc. **1948**, 1422.
[2] E. K. Plyler and W. S. Benedict, J. Research Natl. Bur. Standards **47**, 202 (1951).
[3] E. K. Plyler and N. Acquista, J. Research Natl. Bur. Standards **48**, 92 (1952).
[4] S. R. Polo and M. K. Wilson, J. Chem. Phys. **20**, 1183 (1952).
[5] McGee, Cleveland, Meister, Decker, and Miller, J. Chem. Phys. **21**, 242 (1953).
[6] W. F. Edgell and C. E. May, J. Chem. Phys. **20**, 1822 (1952).
[7] L. Kahovec and J. Wagner, Z. physik. Chem. **B48**, 188 (1941).
[8] A. L. Henne and W. G. Finnegan, J. Am. Chem. Soc. **72**, 3806 (1950).
[9] Hauptschein, Nodiff, and Grosse, J. Am. Chem. Soc. **74**, 1347 (1952).

assignments given above are in agreement with those previously proposed[4–6] and are further substantiated by the nature of the bands. With the exception of ν_1, all A_1 bands showed a sharp and intense Q branch, while the E bands were much weaker and of a broad and diffuse character. The ν_1 band associated with the symmetrical stretching motion of the fluorine atoms was an exception, being rather broad, only moderately intense, and without the pronounced Q branch observed for the other A_1 frequencies. Similar observations have been made by J. Rud Nielsen and others for symmetrical fluorine stretching motions in other molecules. The semiquantitative polarization data for CF_3I also are in agreement with previous assignments and do not agree with the suggestion by Pitzer and Gelles[10] that the values for ν_3 and ν_6 be interchanged.

FORCE CONSTANT TREATMENT

The vibrational spectra of these molecules have been analyzed previously[5,11] using valence force coordinates and a complete quadratic potential function. However, the simplicity and ease of interpretation of the Urey-Bradley type of potential field favor its use in those cases where it can be applied successfully; it has been found particularly suitable for halogenated methane derivatives.[12,13] In the present case, a simplified potential function of this type containing only six force constants, the same as the number of vibrational frequencies, was found adequate to reproduce all of the observed data.

The potential function employed for the CF_3X molecule is

$$2V=k_R\Delta R^2+k_r\sum\Delta r_i^2+k_\alpha\sum(r\Delta\alpha_i)^2+k_\beta\sum(r\Delta\beta_i)^2+k_D\sum\Delta D_i^2+k_d\sum\Delta d_i^2, \quad (1)$$

where R represents the $C-X$ distance, r the $C-F$ distance, D the $X-F$ distance, d the $F-F$ distance, α the $F-C-F$ angle, and β the $F-C-X$ angle. Since these coordinates are not all independent, the potential energy expression was converted to a form involving bond angles and distances alone by means of the following relationships:

$$\Delta D_i=\frac{1}{D}[(r_i-R\cos\beta_i)\Delta r_i+(R-r_i\cos\beta_i)\Delta R+r_iR\sin\beta_i\Delta\beta_i], \quad (2)$$

$$\Delta d_{ij}=\sin\frac{\alpha_{ij}}{2}\Delta r_i+\sin\frac{\alpha_{ij}}{2}\Delta r_j+(r_i+r_j)/2\cos\frac{\alpha_{ij}}{2}\Delta\alpha_{ij}. \quad (3)$$

These expressions are adequate to a first degree of approximation. The analysis was made by the familiar $F-G$ matrix method of Wilson, the symmetry coordinates employed being identical with those chosen by Meister and Cleveland.[14] The elements of the symmetry factored F matrix are given below:

$$F_{11}=k_R+3k_DA^2,$$
$$F_{12}=3^{\frac{1}{2}}k_DAB,$$
$$F_{13}=-(3/2)^{\frac{1}{2}}rRk_dAC,$$
$$F_{22}=k_r+4k_d\sin^2\alpha/2+k_DB^2,$$
$$F_{23}=2^{-\frac{1}{2}}rk_d\sin\alpha-2^{-\frac{1}{2}}rRk_DBC,$$
$$F_{33}=\tfrac{1}{2}r^2[k_\alpha+k_\beta+k_d\cos^2\alpha/2+R^2k_DC^2],$$
$$F_{44}=k_r+k_d\sin^2\alpha/2+k_DB^2,$$
$$F_{45}=rRk_DBC,$$
$$F_{46}=-\tfrac{1}{2}rk_d\sin\alpha,$$
$$F_{55}=r^2k_\beta+r^2R^2k_DC^2,$$
$$F_{56}=0,$$
$$F_{66}=r^2k_\alpha+r^2k_d\cos^2\alpha/2,$$

$$A=\frac{(R-r\cos\beta)}{D},\quad B=\frac{(r-R\cos\beta)}{D},\quad C=\frac{\sin\beta}{D}.$$

Practically all normal coordinate treatments of methane derivatives carried out up to now have assumed tetrahedral angles around the central carbon atom. Electron diffraction and infrared investigations have shown that, in some cases, deviations from the tetrahedral figure may be appreciable. A recent sector electron diffraction investigation by Dr. L. S. Bartell[15] has furnished reliable values for all the parameters of CF_3Cl. Although microwave data are available for both CF_3Br and CF_3I, the situation is not quite as satisfactory since it was necessary to assume values for at least one of the molecular parameters in each case in order to calculate the rest. Unequivocal values for the angles consequently could not be obtained. For the purpose of these calculations, suitable values for the angles in CF_3Br and CF_3I were chosen to be consistent with the microwave data and to reflect the increased steric effect to be expected for the Br and I atoms as compared to Cl. The numerical values of the various parameters are listed in Table II.

TABLE II. Molecular parameters for CF_3Cl, CF_3Br, and CF_3I used in force constant calculations.

	CF_3Cl[a]	CF_3Br	CF_3I
$C-F$ dist.	1.328 A.U.	1.328 A.U.	1.332 A.U.
$C-X$ dist.	1.753	1.918	2.134
$\angle F-C-F$	108° 42′	108° 25′	108° 0′
$\angle F-C-X$	110° 18′	110° 31′	110° 55′
$F-F$ dist.	2.158	2.154	2.155
$F-X$ dist.	2.540	2.688	2.891

[a] Reference 15. Atomic weights (phys. scale):
C = 12.0039 F = 19.0045 I = 126.932
Cl = 34.9787 Br = 79.941
Avogadro's number: $N=6.02544\times10^{23}$ (DuMond and Cohen, 1951).

[10] K. S. Pitzer and E. Gelles, J. Chem. Phys. **21**, 855 (1953).
[11] Decker, Meister, and Cleveland, J. Chem. Phys. **19**, 784 (1951).
[12] T. Simanouti, J. Chem. Phys. **17**, 245 (1949).
[13] T. Simanouti, J. Chem. Phys. **17**, 848 (1949).
[14] A. G. Meister and F. F. Cleveland, Am. J. Phys. **14**, 13 (1946).
[15] L. S. Bartell and L. O. Brockway (to be published).

TABLE III. Calculated and observed values for the vibrational frequencies of the trifluoromethyl halides (in cm^{-1}).

CF_3Cl		CF_3Br		CF_3I	
Obs	Calc	Obs	Calc	Obs[a]	Calc
1104	1104	1081	1081	1074	1074
782	782	762.5	762.2	741	741
475	475	350	350	285	285
1217	1217	1209	1209	1185	1185
559	559	549	549	540	540
351	351	305	305	264	264

[a] Selected as most probable values from the infrared measurements on CF_3I vapor. References 3, 4, 5, and 6.

TABLE IV. Force constants for the trifluoromethyl halides.

	($\times 10^{-5}$ dynes/cm)		
	CF_3Cl	CF_3Br	CF_3I
k_R	2.977	2.596	2.593
k_r	4.528	4.596	4.420
k_α	0.531	0.426	0.456
k_β	0.305	0.345	0.352
k_d	1.168	1.368	1.241
k_D	0.732	0.465	0.209

Expressions for the inverse kinetic energy matrix elements in terms of bond distances and atom masses have been tabulated by Decius for nontetrahedral angles.[16] These were evaluated and the inverse kinetic energy matrix transformed to the symmetry factored G matrix. The values of the force constants were then systematically adjusted as usual until the roots of the secular equation, $|FG-\lambda I|=0$, coincided with the experimental values. No attempt was made to transfer force constants from one molecule to another. In all three cases, it was possible to obtain agreement to within less than one wave number of the experimental values as shown in Table III. The force constants are listed in Table IV.

The good agreement between the observed and calculated frequencies obtained with such a simple potential function gives additional emphasis to the usefulness of the Urey-Bradley type of field. The success achieved in this case cannot be considered particularly unusual, however, since central force fields have in the past been most successful with completely halogenated methane derivatives. The present disfavor of such fields has been chiefly due to their inadequacy when hydrogen atoms are present in the molecule, and in this connection it is interesting to speculate whether the fit obtainable might not be improved by the use of correct angle parameters instead of assuming tetrahedral. No indication of this was given in the present work since the CF_3Cl frequencies could be fitted equally well using either observed or tetrahedral angles. The effect of this change in parameters on the force constants is shown in Table V. Similar calculations were not carried out for the other two molecules.

Inspection of the force constants in Table IV shows that those constants primarily associated with the CF_3 group, k_r, k_α, and k_d, have approximately the same values in all three molecules indicating that the CF_3 radical is little affected by the particular halogen to which it is attached. The remaining three constants, as might be expected, vary systematically as the halogen is changed from Cl to Br to I. A more detailed comparison does not seem warranted in view of the uncertainty in the angle values in the bromide and iodide and the lack of information on the anharmonicities.

ACKNOWLEDGMENT

The author is indebted to Dr. J. J. Martin of the Department of Chemical Engineering through whom the CF_3Cl and CF_3Br samples were obtained, and to Drs. L. S. Bartell and L. O. Brockway for permission to use their data on the molecular parameters of CF_3Cl in advance of publication.

TABLE V. Effect of angle parameters on force constants of CF_3Cl.[a]

	Observed angles	Tetrahedral angles	Difference
k_R	2.977	3.197	7.4%
k_r	4.528	4.453	−1.7
k_α	0.531	0.562	5.8
k_β	0.305	0.311	2.0
k_d	1.168	1.070	8.4
k_D	0.732	0.730	−0.3

[a] Force constants in 10^5 dynes per centimeter.

Note added in proof:—The Raman spectrum of gaseous CF_3Cl has been reported quite recently by H. H. Claassen [J. Chem. Phys. **22**, 50 (1954)] while the present article was in press. The agreement between the two sets of experimental data for this molecule is excellent. Claassen in addition observed ν_3 for the Cl^{37} isotopic species, the shift being 7.6 cm^{-1} from the value for the Cl^{35} species. This may be compared with a shift of 6.8 cm^{-1} calculated from the present treatment.

[16] J. C. Decius, J. Chem. Phys. **16**, 1025 (1948).

Eckart Conditions in Wilson's Treatment of Molecular Vibrations

ROBERT J. MALHIOT* AND SALVADOR M. FERIGLE
Spectroscopy Laboratory,† Illinois Institute of Technology, Chicago 16, Illinois
(Received December 14, 1953)

The consistency of Wilson's treatment of molecular vibrations with the Eckart conditions is discussed in detail. The necessary conditions for this consistency are written in vector form and the applicability of the equations, thus derived, to the calculation of **s** vectors is indicated.

WHEN the kinetic energy corresponding to the nuclear motions of a polyatomic molecule is written in general form, there are terms corresponding to the interaction between external coordinates—describing vibration and rotation—and internal coordinates—describing small displacements of the nuclei from the equilibrium configuration. The Eckart conditions[1] are introduced to insure the smallness of these interactions and they define a system of coordinates in which the vibrations of the nuclei are described. In the treatment of molecular vibrations the Eckart conditions are usually written explicitly for each molecular type, therefore providing some equations of constraint between the cartesian displacements.[2] However, in the treatment of Wilson[3] these conditions are contained only implicitly in a way which is not immediately obvious. It is the purpose of this paper to show the consistency of Wilson's method with the Eckart conditions when properly chosen internal coordinates are used, and also to indicate the usefulness of this explicit formulation for the calculation of Wilson's **s** vectors.

VIBRATIONAL KINETIC ENERGY

The kinetic energy of vibration T of a polyatomic molecule is given by

$$2T=\delta_{ab}\dot{\rho}^a\dot{\rho}^b, \tag{1}$$

where

$$\rho^a=(m_a)^{\frac{1}{2}}x^a \tag{2}$$

is a mass-reduced Cartesian displacement coordinate.

The summation convention will be used in the first part of this paper; that is, whenever an index appears in a product as superscript and subscript, summation over that index is implied. For consistency in the notation, the following indices will be used:

a, b, c, d for the range 1 to $3N$ where N is the number of atoms in the molecule.
i, j, k for the range 1 to $3N-6$ (or 1 to $3N-5$ for linear molecules).
p, q for the range $3N-5$ (or $3N-4$) to $3N$.

A set of independent internal coordinates R^i can be chosen to describe the small vibrations of the nuclei, corresponding to the $3N-6$ degrees of internal freedom of the molecule.

Since the internal motions are small, they may be expressed as linear combinations of the $3N$ mass reduced displacements, giving

$$R^i=D_a{}^i\rho^a. \tag{3}$$

Along with the $3N-6$ internal coordinates, we introduce six additional coordinates $R^p(R^p\equiv 0)$ corresponding to the six Eckart conditions,[1] so that

$$R^b=D_a{}^b\rho^a. \tag{4}$$

$D_a{}^b$ corresponds then to a square matrix and will have an inverse since the transformation is nonsingular because of the independence of the R^b, giving

$$\rho^a=Q_b{}^aR^b \tag{5a}$$

or

$$\rho^a=Q_i{}^aR^i+Q_p{}^aR^p=Q_i{}^aR^i, \tag{5b}$$

where the summation has been split in Eq. (5b).

Substitution of Eq. (5b) in Eq. (1) gives

$$2T=g_{ij}\dot{R}^i\dot{R}^j,$$

where

$$g_{ij}=Q_i{}^aQ_j{}^b\delta_{ab}. \tag{6}$$

THE ORTHOGONALITY CONDITION FOR THE INTERNAL COORDINATES

We consider now the properties of the transformation matrices $\mathbf{Q}=(Q_b{}^a)$ and $\mathbf{D}=(D_b{}^d)$. Since they are inverse matrices we have

$$Q_d{}^aD_b{}^d=\delta_b{}^a \tag{7}$$

and

$$D_c{}^aQ_b{}^c=\delta_b{}^a. \tag{8}$$

The matrix $\mathbf{D}$ is formed from $(D_a{}^i)$ by adding six additional rows containing the elements for transforming from mass reduced displacements to the Eckart coordinates. The elements corresponding to the Eckart coordinates for the inverse transformation matrix $\mathbf{Q}$ are contained in the last six columns. The multiplication taken in the order of Eq. (8), i.e., $\mathbf{DQ}$, gives rise to a $3N$ matrix which may be subdivided into 4 blocks. There will be two diagonal blocks, one $3N-6\times 3N-6$ corresponding to elements for internal coordinates only, and one 6×6 corresponding to elements for Eckart

* One of the investigations carried out in partial fulfillment of the requirements for the Master of Science degree.
† Publication No. 96.
[1] C. Eckart, Phys. Rev. **47**, 552 (1935). For a detailed derivation of Eckart conditions see S. M. Ferigle and A. Weber, Am. J. Phys. **21**, 102 (1953).
[2] H. H. Nielsen, Revs. Modern Phys. **23**, 90 (1951), and references given therein.
[3] E. B. Wilson, Jr., J. Chem. Phys. **7**, 1047 (1939); **9**, 76 (1941).

conditions only. The other two blocks will correspond to mixed elements. Since **DQ** is a unit matrix, then each diagonal block will also be a unit matrix; in particular,

$$D_c{}^i Q_j{}^c = \delta_j{}^i. \tag{9}$$

The summation of Eq. (7) may be split giving

$$Q_j{}^a D_b{}^j + Q_p{}^a D_b{}^p = \delta_b{}^a. \tag{10}$$

Multiplying Eq. (10) by $D_c{}^i \delta^{cb} Q_k{}^d \delta_{ad}$ and reducing the right-hand side by using Eq. (9) one obtains

$$(D_c{}^i D_b{}^j \delta^{cb})(Q_j{}^a Q_k{}^d \delta_{ad}) + (D_c{}^i D_b{}^p \delta^{cb})(Q_p{}^a Q_k{}^d \delta_{ad}) = \delta_k{}^i. \tag{11}$$

If the internal coordinates are chosen with the requirement that

$$D_c{}^i D_b{}^p \delta^{cb} = 0, \tag{12}$$

then Eq. (11) reduces to

$$g^{ij} g_{jk} = \delta_k{}^i, \tag{13}$$

where

$$g^{ij} = D_c{}^i D_b{}^j \delta^{cb}, \tag{14}$$

and g_{jk} was defined in Eq. (6).[4]

Equation (12) requires that the internal coordinates be orthogonal to the Eckart conditions, when expressed in terms of mass-reduced Cartesian displacements. It is Eq. (12) which makes unnecessary the explicit formulation of Eckart conditions for particular molecular types. If Eq. (12) is not satisfied, the inverse of g_{ij} will contain $Q_p{}^a$ elements.

VECTOR REPRESENTATION

The aforementioned condition of Eq. (12) is more easily expressed in terms of the **s** vectors introduced by Wilson.[3] The summation convention will be dropped in the vector equations and summation signs will be used instead.

The following nomenclature will be used:

$\mathbf{r}_n{}^0$ = equilibrium position vector of the nth atom with respect to the center of mass, where n ranges from 1 to N;

$\mathbf{d}_n$ = displacement vector of the nth atom from the equilibrium position;

$\mathbf{e}_t$ = unit vector along the t axis of Cartesian coordinates, where t ranges from 1 to 3.

If the index a used in previous sections is split into n and t with the meaning given above, Eqs. (2) and (3) give

$$R^i = D_{nt}{}^i \sqrt{m_n} x^{nt}. \tag{15}$$

Since

$$x^{nt} = \mathbf{e}_t \cdot \mathbf{d}_n, \tag{16}$$

Eq. (15) becomes

$$R^i = \sum_n \mathbf{s}_n{}^i \cdot \mathbf{d}_n, \tag{17}$$

where

$$\mathbf{s}_n{}^i = \sum_t D_{nt}{}^i \sqrt{m_n} \mathbf{e}_t \tag{18}$$

is the **s** vector corresponding to the ith internal coordinate and the nth atom.

In vector representation the orthogonality condition of Eq. (12) becomes, by using Eq. (18),

$$D_{nt}{}^i D_{lu}{}^p \delta^{nl} \delta^{tu} = \sum_{nt} \frac{1}{m_n} (\mathbf{s}_n{}^i \cdot \mathbf{e}_t)(\mathbf{s}_n{}^p \cdot \mathbf{e}_t) = \sum_n \frac{1}{m_n} \mathbf{s}_n{}^i \cdot \mathbf{s}_n{}^p = 0. \tag{19}$$

In Eq. (19), **s** vectors corresponding to the Eckart coordinates are implied. The Eckart conditions are[1]

$$\sum_n m_n \mathbf{d}_n = 0$$

and

$$\sum_n m_n \mathbf{r}_n{}^0 \times \mathbf{d}_n = 0,$$

with corresponding coordinates

$$R^p = \mathbf{e}_p \cdot \sum_n m_n \mathbf{d}_n = 0 \quad p = 1,2,3$$

and

$$R^q = \mathbf{e}_q \cdot \sum_n m_n \mathbf{r}_n{}^0 \times \mathbf{d}_n = 0 \quad q = 1,2,3,$$

which give the following **s** vectors:

$$\mathbf{s}_n{}^p = m_n \mathbf{e}_p \tag{20}$$

$$\mathbf{s}_n{}^q = m_n \mathbf{e}_q \times \mathbf{r}_n{}^0. \tag{21}$$

Substitution of Eqs. (20) and (21) in Eq. (19) gives

$$\sum_n \mathbf{e}_p \cdot \mathbf{s}_n{}^i = 0$$

and

$$\sum_n \mathbf{e}_q \cdot \mathbf{r}_n{}^0 \times \mathbf{s}_n{}^i = 0.$$

Since the last equations must hold for every value of p and q, the **s** vectors for any internal coordinate must satisfy the following two equations:

$$\sum_n \mathbf{s}_n{}^i = 0 \tag{22}$$

and

$$\sum_n \mathbf{r}_n{}^0 \times \mathbf{s}_n{}^i = 0. \tag{23}$$

INTERNAL COORDINATES

Decius[5] has given a detailed discussion of the four types of internal coordinates which are sufficient to describe all the vibrational degrees of freedom for any molecule. These are bond stretching, interbond bending, bond torsion, and out of plane bending. Each of these may be defined as the difference between a scalar function of position vectors in a distorted configuration and

[4] The elements designated here as g^{ij} are defined as g_{ij} in the papers of Wilson and others. The notation has been changed to make it more consistent with the general nomenclature used in mechanics.

[5] J. C. Decius, J. Chem. Phys. **17**, 1315 (1949).

the same function in the equilibrium configuration. The internal coordinates defined in this way will be zero for an infinitesimal translation or an infinitesimal rotation of the molecule as a whole. This immediately implies that Eqs. (22) and (23) are satisfied for these four types of internal coordinates; as a consequence the orthogonality condition of Eq. (12) is satisfied and the Eckart conditions need not be written explicitly when carrying out a normal coordinate treatment.

Let us consider an internal coordinate,

$$R^i = f^i(\mathbf{r}_l) - f^i(\mathbf{r}_l^0), \quad l = 1,2 \cdots N.$$

By expanding $f^i(\mathbf{r}_l)$ in a Taylor series about the equilibrium position, and neglecting terms higher than first order—which approximation was already implied in the definition of the internal coordinates as a linear combination of displacements—we have

$$f^i(\mathbf{r}_l) = f^i(\mathbf{r}_l^0) + \sum_n (\mathbf{r}_n - \mathbf{r}_n^0) \cdot \frac{\partial}{\partial \mathbf{r}_n^0} f^i(\mathbf{r}_l^0), \qquad (24)$$

where the symbol $\partial/\partial \mathbf{r}_n^0$ is used for the gradient with respect to the coordinates of the nth atom at the equilibrium position.

Rearranging Eq. (24) we obtain

$$R^i = f^i(\mathbf{r}_l) - f^i(\mathbf{r}_l^0) = \sum_n \mathbf{d}_n \cdot \frac{\partial}{\partial \mathbf{r}_n^0} f^i(\mathbf{r}_l^0). \qquad (25)$$

By comparison of Eqs. (17) and (25) we can redefine the **s** vectors in the form

$$\mathbf{s}_n{}^i = \frac{\partial}{\partial \mathbf{r}_n^0} f^i(\mathbf{r}_l^0). \qquad (26)$$

It is possible to derive analytically expressions for the **s** vectors using Eqs. (26) and appropriate scalar functions. However, making use of the properties of a gradient along with Eqs. (22) and (23), it is possible to give a straightforward derivation of the **s** vectors, as will be shown in a subsequent paper.

ACKNOWLEDGMENTS

This work was part of a research program aided by a contract with the Office of Ordnance Research, U. S. Army. The authors also wish to acknowledge the continuous inspiration given by Professor Forrest F. Cleveland in their research work.

Infrared Studies of Solutions Involving Aromatics and Halogens*

WOLFGANG HALLER,† GEORGE JURA, AND GEORGE C. PIMENTEL
Department of Chemistry and Chemical Engineering, University of California, Berkeley, California
(Received August 17, 1953)

Infrared studies were made in the region 640–1400 cm^{-1} to investigate the effect of adding iodine to benzene, toluene, mesitylene, hexamethylbenzene, naphthalene, cyclohexane, and methylcyclohexane. Spectral changes were observed for each of the aromatics except for naphthalene. The enhancement of the mesitylene band at 1300 cm^{-1} was observed for mesitylene purified in five distinct ways. The enhancement of the hexamethylbenzene band at 1298 cm^{-1} was studied as a function of the concentrations in carbon disulfide solutions and correlates with the product of hexamethylbenzene and iodine concentrations. The effect of bromine on the spectrum of benzene was noted also. The results can be discussed in terms of weak complex formation or strong solvent perturbations.

I. INTRODUCTION

In the past few years, considerable application has been made of the Lewis acid-base theory to explain the apparently anomalous behavior of certain solution systems. Such systems were considered by Benesi and Hildebrand[1] and Keefer and Andrews.[2] The former studied the ultraviolet spectra of solutions of iodine in various aromatic hydrocarbons. The appearance of a new band at approximately 3200A was attributed to complex formation between iodine and the aromatic hydrocarbon. From a study of the solubility of various aromatic hydrocarbons in aqueous solutions of salts of Ag^+, Keefer and Andrews conclude that complexes are formed between the ion and the aromatic hydrocarbon.

Neither of the above investigations throws light on the structure of the compound which is formed. Rundle[3] has found in the silver perchlorate-mesitylene complex that the silver ion is not on the symmetry axis of the mesitylene. The result was obtained by an analysis of the x-ray diffraction pattern of the solid. Mulliken[4] has reached a similar conclusion concerning the structure from theoretical considerations.

Pimentel, Jura,[5] and Grotz made a report of infrared studies which seemed to indicate that the complexing group was not on the symmetry axis of the aromatic molecule. A portion of this work was repeated by Ham, Rees, and Walsh.[6] Those authors were not able to duplicate the iodine-mesitylene spectra and suggest that impurities in mesitylene may have caused spurious spectral changes. It is the purpose of this paper to report further investigations of these systems including repetition of the work reported earlier. The results indicate that neither of the previous articles concerning the infrared studies[5,6] is completely correct. Some of the spectral changes reported earlier are indeed spurious, but other changes which were not detected by Ham, Rees, and Walsh have been corroborated. Other systems have been studied as well.

II. EXPERIMENTAL PROCEDURE

The spectra were determined using a Perkin-Elmer Model 21 spectrophotometer with a NaCl prism. The region investigated was 1400 to 640 cm^{-1}. The cell thickness was 0.2 mm. The spectral slit width at 1400 cm^{-1} was 2 cm^{-1}.

The iodine was sublimed several times before use. Bromine, Merck N.F.V. was used without purification. The hydrocarbons used in the experiments were all purified and, except for hexamethylbenzene and naphthalene, the final step in each purification was a fractional distillation using a 20-plate column. The benzene used was Baker's analytic grade purified by a fractional crystallization before the final distillation. Toluene, Baker's analytical grade, was first fractionally distilled, then sulfonated, the sulfonate was fractionally recrystallized, hydrolyzed, and then distilled. Five different samples of mesitylene were used in this work: (1) a sample supplied by the Bureau of Standards; (2) a sample obtained from Keefer and Andrews which had been purified by the method prescribed by Ham, Rees and Walsh;[6] (3) Eastman Kodak mesitylene which was distilled, sulfonated, the sulfonate recrystallized, hydrolyzed and then distilled; (4) Eastman Kodak mesitylene which was distilled, treated with excess iodine, extracted, treated with mercury, and then finally distilled; and (5) Eastman Kodak mesitylene fractionally recrystallized at the freezing point. Eastman Kodak hexamethylbenzene was recrystallized from pure benzene and then sublimed in high vacuum. Baker's analytical grade naphthalene was sublimed. Matheson cyclohexane was purified by fractional distillation and crystallization at the freezing point. Methylcyclohexane was purified by distillation. The infrared spectrum of the carbon disulfide which was used as a solvent was checked for evidence of impurity.

* We wish to acknowledge support of this work by the U. S. Office of Naval Research.
† Present address: Institute of Silicate Research, University of Toledo, Toledo 6, Ohio.
[1] H. A. Benesi and J. H. Hildebrand, J. Am. Chem. Soc. **71**, 2703 (1949).
[2] L. J. Andrews and R. M. Keefer, J. Am. Chem. Soc. **74**, 640 (1952) and references there cited.
[3] R. E. Rundle and J. H. Goring, J. Am. Chem. Soc. **72**, 5337 (1950).
[4] R. S. Mulliken, J. Am. Chem. Soc. **72**, 600–608 (1950).
[5] Pimentel, Jura, and Grotz, J. Chem. Phys. **19**, 513 (1951).
[6] Ham, Rees, and Walsh, J. Chem. Phys. **20**, 1337 (1952). See also, Nature **169**, 110 (1952).

III. RESULTS AND DISCUSSION

Four series of experiments were performed. In the first, iodine was added to the liquid hydrocarbon or to a solution of the hydrocarbon in carbon disulfide. These exploratory experiments were performed to observe the spectroscopic changes caused by the addition of the halogen. In the spectrum of each of the aromatic hydrocarbons, benzene, toluene, mesitylene, and hexamethylbenzene, the intensity of at least one band which normally is only Raman active for the gas phase was enhanced on the addition of iodine. Under the conditions studied, no effect was detected with cyclohexane, methylcyclohexane, or naphthalene. The mesitylene band at 1300 cm^{-1} was found to be intensified on addition of iodine in the spectrum of each of the five purified samples mentioned earlier. Glusker, Thompson, and Mulliken[7] obtained a similar result with mesitylene but did not detect the changes reported here in the benzene and toluene spectra.

The remaining experiments consist of semiquantitative studies of the systems which show spectral changes. The next series of experiments involved the determination of the spectra of solutions of the hydrocarbons and iodine in carbon disulfide. The hydrocarbon and iodine concentrations were $0.015M$ and $0.36M$, respectively, in each of the solutions. The pertinent spectral regions are shown in Figs. $1A''$, $1B''$, $1C''$, $1D''$, and $1E''$. Also included in Figs. $1A'$, $1B'$, $1C'$, and $1D'$ are the spectra of the pure aromatics containing iodine (without control of the concentrations). Table I shows the frequencies of the bands whose intensities are enhanced on addition of iodine. In each case, the band considered to be caused by the totally symmetric skeletal stretching vibration has been enhanced. The hydrocarbons are given in order of increasing base strength and for the solutions of fixed concentrations, the spectral changes seem to correlate.

The next series involved the determination of the spectra of iodine and hexamethylbenzene as the concentrations were varied in carbon disulfide solution. Figure $2A$ shows the influence of the concentration of the hydrocarbon and Fig. $2B$ that of the iodine. The enhancement of the band at 1298 cm^{-1} correlates with the product of the concentrations of the hexamethylbenzene and iodine. The intensity accuracy and limited concentration range do not permit calculation of an equilibrium constant.

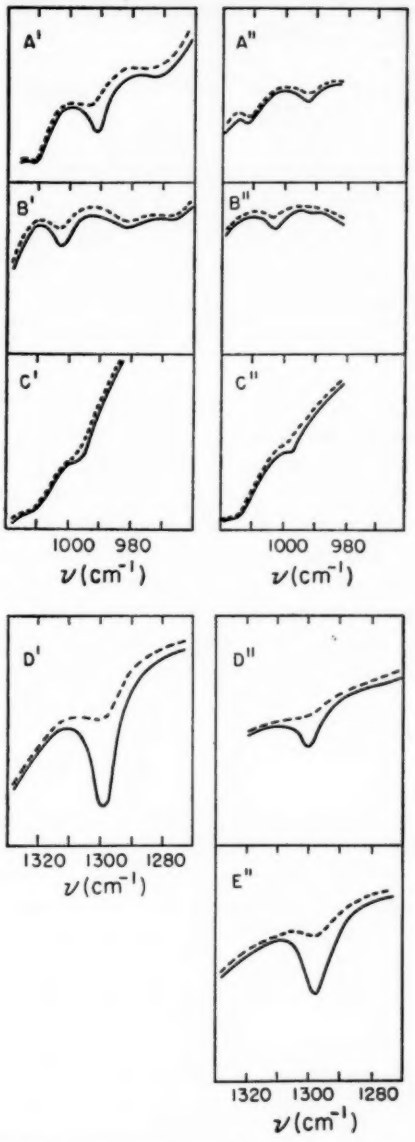

FIG. 1. Influence of iodine on the IR spectra of aromatics. - - - - aromatic without iodine; —— aromatic with iodine; A', B', C',D': spectra of pure aromatic or aromatic plus iodine; A'', B'', C'', D'', E'': spectra of CS_2 solutions, aromatic $1.5M$ (except for E'', where all of the aromatic did not dissolve), I_2 $0.36M$; A: benzene; B: toluene; C: mesitylene; D: mesitylene; E: hexamethylbenzene.

TABLE I. The effect of iodine on the intensities of infrared bands of aromatic hydrocarbons.

Hydrocarbon	Frequency (cm^{-1})	Relative intensity without I_2	Relative intensity with I_2
benzene	992	1/2(shoulder)	1
toluene	1003	1/2	1
mesitylene	1300	1/2(shoulder)	3
	998	1/2(shoulder)	1
hexamethyl-benzene	1298	1	4

Finally the spectra of solutions of iodine or bromine in pure benzene were compared in the spectral region near 992 cm^{-1}. The concentration of the halogen was $0.25M$. The enhancement of the 992 cm^{-1} band was about the same for the two halogens.

Attempts to duplicate the earlier spectral changes reported for the magnesium laurate-mesitylene system[5] indicated that these changes were spurious. No spectral

[7] Glusker, Thompson, and Mulliken, J. Chem. Phys. **21**, 1407 (1953).

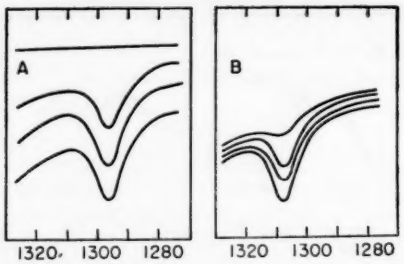

FIG. 2. Influence of concentration on the IR spectra of hexamethylbenzene-iodine solutions. *A*: I_2: 0.36*M*, HMB: 0*M*; 0.50*M*; 0.75*M*; 1.0*M*. *B*: HMB: 1.0*M*, I_2: 0*M*; 0.18*M*; 0.27*M*; 0.36*M*.

changes were observed upon addition of either 0.02M magnesium laurate or silver laurate to mesitylene. This requires reconsideration of the earlier conclusions regarding the symmetry of the mesitylene complex. If the corroborated spectral changes are attributed to complex formation, the only conclusion which can be drawn concerning the structure of the complex species is that it has lower symmetry than mesitylene itself. This eliminates one structure, a mesitylene complex with two complexing groups on opposite sides of the aromatic ring.

It is difficult and often somewhat arbitrary to distinguish between spectral changes caused by complex formation and those which are better termed solvent perturbations. In the present work, complex formation is suggested by the magnitude of the spectral changes compared to the spectra in other solvent environments, the pure aromatic hydrocarbon or carbon disulfide. Also there were no noticeable effects with saturated hydrocarbons, suggesting some specificity in the aromatic-halogen interaction. Finally, the usually accepted base strengths of the aromatics appear to be correlated with the magnitudes of the spectral changes. There are two observations which may be used to argue against the formation of complexes. No spectral changes were detected upon addition of iodine to naphthalene, and no new bands, only intensity changes, have been observed in the systems under investigation. However, the choice between the two models is probably one of convenience. These systems probably involve molecular interactions of a magnitude such that it is neither possible nor necessary to differentiate between weak complex formation and strong solvent perturbation.

Investigations of the "Vapor Snake" Phenomenon

R. VERSCHINGEL AND H. I. SCHIFF
Department of Chemistry, McGill University, Montreal, Quebec, Canada
(Received Oct. 23, 1953)

The "vapor snake" phenomenon, originally reported for cyclohexane, has been found to occur with some twenty compounds. The ease of occurrence increases with the triple point pressure of the compound. The tubule tip was always at the freezing point of the compound although the surrounding liquid may be above the freezing point. Although the presence of a crust on the surface of the liquid is not essential for the occurrence of the phenomenon, transport of heat by vapor to a cold portion of the sample must occur in order to produce a tubule sheath of the thickness observed.

IN a previous communication[1] an unusual phenomenon was reported to occur when an ampule of pure degassed cyclohexane was immersed in a freezing mixture. A solid crust first formed on the liquid surface below which a small bubble appeared. This bubble then grew in the form of a thin snake-like tubule which extended rapidly into the liquid. The liquid meanwhile gradually solidified from the walls of the ampule so that the final appearance of the sample was that of a clear solid in which was imbedded an interwoven pattern of tubule, from the walls of which white crystals extended into the clear solid for several millimeters.

Seki has also reported the phenomenon[2] and has suggested a connection between its occurrence and the formation of plastic crystals.

Frank has offered a different explanation for the phenomenon[3] from that given in our previous communication. His mechanism for the formation and propagation of the tubule involves the transfer of heat from the tip of the tubule by means of vapor to the crust and thence, by sublimation, to the "cold upper walls" of the ampule. Although the presence of a crust and cold upper walls is an essential part of Frank's mechanism, they were not found to be necessary experimentally. The fact that our photographs were inverted on publication may have been misleading.

EXPERIMENTAL

We have subsequently observed the phenomenon with a number of other substances. Over fifty compounds were investigated with a view to determining the effect of the following properties: (1) symmetry of chemical structure, (2) vapor pressure at the melting point, (3) heat and entropy of fusion, (4) the occurrence of solid-solid transitions. Table I lists those compounds which showed the phenomenon, along with a sufficient number of those which do not, to show the dependence on these properties.

It will be seen that the higher the triple-point pressure of the compound the more readily will it produce the phenomenon. With none of the compounds having a triple-point pressure greater than 2 mm Hg was it necessary to cool the walls of the ampule above the liquid surface. Indeed for those compounds having triple point pressures greater than 50 mm Hg great care had to be taken to prevent cooling the upper walls. Otherwise the pressure inside the tubule was so much greater than that above the crust that the latter was blown off and tubule formation prevented. For those compounds having triple-point pressures in the range of 1 to 2 mm Hg it was necessary to cool the upper walls or even to pump on the sample in order to form the crust and produce tubules.

In order to determine whether the crust is necessary for tubule formation the following experiments were performed:

1. A sample of cyclohexane was confined over mercury so that a closed volume was provided which had no vapor space. This sample was immersed into a bath whose temperature was below the freezing point of mercury. As soon as the mercury froze, a bubble formed at the top of the cyclohexane and developed into a tubule whose behavior was identical in every respect to that previously described.

2. An ampule of cyclohexane was immersed in a freezing bath in the usual manner. However, as soon as the crust had formed the ampule was quickly inverted before the bubble had formed. The bubble then appeared at the top of the sample and then produced a tubule which made no contact with the crust.

3. When a sample was allowed to melt after the conclusion of one experiment a vapor bubble occasionally emerged when the melting surface crossed the tubule, and rose to the surface of the liquid.* On several occasions it was possible to form a crust by reimmersing the sample in the bath just as one of these bubbles was emerging from a small amount of remaining solid. On each such occasion a new tubule developed from this bubble and grew in the usual manner, but having no contact with the crust. At no time was it possible to produce two tubules simultaneously.

Thus it appears that the sole function of the crust is to provide a closed volume for the system.

[1] M. K. Phibbs and H. I. Schiff, J. Chem. Phys. **17**, 843 (1949).
[2] S. Seki, J. Chem. Phys. **18**, 397 (1950).
[3] F. C. Frank. J. Chem. Phys. **18**, 231 (1950).

* These bubbles have been identified as being composed of the vapor of the compound and not of any foreign gas.

TABLE I.

Compound	Triple point pressure mm Hg	Melting point °K	Fusion entropy eu	Transition temp. °K	Transition entropy eu	Comments
Hexachloro-ethane	760	460	4.35	345	7.2	Very good snakes, fine temp. control required
Hexamethyl-ethane	710	377	4.5	148	3.2	Very good snakes, fine temp. control required
Camphor	385	453	2.8	250	7.6	Very good snakes, fine temp. control required
Neopentane	230	253	3.0	140	4.4	Very good snakes, fine temp. control required
Ammonia	46	195.3	9.4	...	...	Very good snakes
2-butyne	44	240.9	9.16	153.8	2.0	Very good snakes
Bromine	42	265.9	4.87	...	...	Very good snakes
Tert-butyl alcohol	41	298.6	3.4	...	...	Very good snakes
Cyclohexane	40	279.8	2.24	186.0	8.59	Very good snakes
Benzene	35	278.7	8.46	...	...	Very good snakes
Tert-butyl chloride	24	244.7	2.0	219.3	3.0	Good snakes
Carbon tetrachloride	9	250.3	2.3	225.7	4.8	Good snakes
Naphthalene	7	353.4	12.75	...	...	Good snakes
Tetranitro-methane	6	286.7	...	...	...	Good snakes
1,1,1,-trichloro-ethane	5	240.5	4.5	224.3	5.0	Good snakes
Trichloro-acetic acid	1	332	4.2	...	...	Poor snakes, pumping and wall cooling required
Phenol	1	313.9	8.6	...	...	Poor snakes, pumping and wall cooling required
Cyclohexanol	1	297	1.4	263	7.45	Poor snakes, pumping and wall cooling required
Chloroform	Less than 1 mm	209.6	10.8	...	...	No snake formation
1-butyne	Less than 1 mm	192.9	...	...	...	No snake formation
Methyl-cyclohexane	Less than 1 mm	146.6	11.0	...	...	No snake formation
Chloro-cyclohexane	Less than 1 mm	230	2.9	218	7.8	No snake formation
Cyclohexene	Less than 1 mm	169.7	4.6	138.7	7.2	No snake formation
Cyclopentene	Less than 1 mm	138.1	5.8	87.1	1.31	No snake formation
Cyclopentane	Less than 1 mm	179	0.8	122.4	9.6	No snake formation
Cyclohexanone	Less than 1 mm	169	4.6	139	...	No snake formation
Toluene	Less than 1 mm	177.9	9.3	...	...	No snake formation
Methyl alcohol	Less than 1 mm	175.3	4.3	157.8	1.0	No snake formation
2,2-dimethyl butane	Less than 1 mm	172.1	0.64	127.4	8.6	No snake formation

The phenomenon was found to occur at all bath temperatures from 0.1°C below the melting point to −196°C. For a given ampule the colder the bath the greater the velocity of the tubule and the smaller its diameter. At a given bath temperature a decrease in the diameter of the ampule resulted in an increase in the velocity and a decrease in the diameter of the tubule. For a given ampule size and bath temperature repeated experiments indicated that both the velocity and the cross section of the tubule were essentially constant. In the limiting case of a bath temperature less than 0.2°C below the freezing point the bubble grew in a spherical shape. The sheath in this case was too thin to withstand distortion although its presence could be observed. The existence of a thick sheath at lower bath temperatures could best be seen if the sample was warmed after the tubule had progressed for some distance. Expansion then forced liquid back into the tubule whereupon the sheath could be seen to be up to 1 mm thick. Upon reimmersing this sample into the bath the liquid was again expelled from the tubule which then continued in its previous direction.

Temperature measurements were made at various positions in the sample by means of a copper-constantan thermocouple. This thermocouple was made of number 32 gauge wire in order to minimize its heat capacity and thermal conductivity, and was introduced into the sample through an atmospheric leg of mercury. The tip of the tubule was always found to be at the freezing point of the compound while the liquid through which it travelled was at or above the freezing point. If the removal of heat from the sample was very rapid, the tubule was able to travel through liquid whose temperature could be as high as 10°C above the freezing point although the tip was always at the freezing point.

Previous history of the sample had no effect upon the phenomenon. A sample of cyclohexane kept at 100°C for two months showed the same behavior as one freshly purified or previously frozen. One notable exception, however, was observed. When cyclohexane was kept at less than 0.1°C above its freezing point for at least one-half hour and then immersed in a bath at least at −40°C no tubule formation occurred. Instead the crust extended downward until the entire sample became an opaque mass of small crystals. This may be due to some degree of orientation attained by the liquid under these conditions.

In the case of benzene a small hole was noticed in the crust directly above the origin of the tubule. The size of the hole increased with increasing cooling rate. Smaller holes were also noticed in some of the other compounds when the rate of cooling was sufficiently rapid.

The effect of impurities was investigated. Air or nitrogen introduced into the ampule at pressures in excess of 2 cm Hg prevented the occurrence of the phenomenon. More than 1 percent by volume of miscible liquids (even those which themselves produced the phenomenon), or trace amounts of solid impurities

also caused crystallization to occur throughout the sample with no tubule formation.

DISCUSSION

The observations shown in Table I are not in agreement with Seki's suggestions. According to Timmermans,[4] plastic crystals are produced only by those compounds which have low entropies of fusion and relatively high entropies of transition. However, no allotropic forms of benzene have been reported while naphthalene has a relatively high entropy of fusion; yet both of these compounds produce the phenomenon readily. On the other hand, cyclopentane has both a low entropy of fusion and a high entropy of transition but does not show the phenomenon.

A simple mechanism for the formation and propagation of the tubule can be formulated. Removal of heat from the system causes volume contraction. If the volume of the system is fixed, this contraction produces a negative pressure sufficiently high to produce a bubble which immediately fills with vapor to the vapor pressure of the liquid. Because of the high triple point pressures of these compounds, considerable mass transfer will occur from the liquid to the vapor phase per unit change in volume of the system. Since the heats of evaporation of these compounds are normal while their heats of fusion are low, this large mass transfer will result in solidification at the liquid-vapor interface, if the temperature of the liquid is near the freezing point. Consequently, the vapor bubble will become incased in a solid sheath. As contraction continues the bubble must grow since it possesses a positive pressure. It is prevented from growing spherically by the sheath and so grows in the direction of the weakest part of the sheath—that which has been last formed. Hence, it will grow in the form of a tubule, expanding only at its tip. It will travel at a rate governed by the rate of volume contraction until all the liquid has solidified. This is in agreement with the constancy of the product of tubule velocity and cross section observed for a given rate of heat removal. The same explanation will apply to those substances where a hole was noticed, since the liquid is still confined to a closed system.

However, simple calculation shows that the thickness of the sheath which would be formed if this mechanism alone were operative is quite small. Thus, if we consider a small spherical bubble of radius r, it can be readily shown that on the basis of this mechanism the thickness of the sheath t would be

$$t=\frac{rMPL_e}{3dRTL_f},$$

where M is the molecular weight, P the triple point pressure, R the gas constant, T the freezing point, d the density of the solid, L_e and L_f the latent heats of evaporation and fusion, respectively.

The thickness of the sheath for a bubble of 1-mm radius in cyclohexane would be 0.001 mm. For a tubule of radius 1 mm the sheath would be even thinner. Although the sheath may be as thin as this at the tip of the tubule it is thicker a short distance behind the tip. Since it has been shown that the liquid need not be supercooled, additional heat cannot be removed by conduction through the liquid. The only other possibility is transport of heat by the vapor, as suggested by Frank.[3] Although we have shown that the conduction need not take place to the crust, it may take place to a portion of the sample which is below the freezing point. Thus in experiments 1 and 2 the tubule originated at the glass wall. In experiment 3 the tubule may have had a very thin sheath until it approached the glass wall where it would acquire a cold spot. When the rate of cooling was increased either by using a colder bath or a narrower ampule the velocity of propagation increased because of the faster contraction while the diameter of the tubule decreased because of the more rapid sheath formation.

The main discrepancy between Frank's explanation and our observations lies in the velocity of propagation of the tubule. Frank argued that the tubule cannot travel at a rate greater than the linear crystallization velocity of the material. On this basis he predicted that a change in the diameter of the ampule would not alter the velocity of the tubule. This is contrary to what was found. Moreover, he stated that our reported velocity of 3 cm/sec constituted a new "record" for crystallization velocities. Our observations indicated that the true crystallization velocity was not much greater than the rate at which the crystals grew out from the sheath, and the rate at which the crust grew downwards, which never exceeded 1 mm/sec. Crystals were formed directly after a fresh liquid-vapor surface was produced which suggests that the tubule velocity is governed solely by the rate of liquid contraction. The fact that crystallization does occur at a rate in excess of the linear crystallization velocity may perhaps be taken as evidence for nucleation preconditioned by a liquid-vapor interface.

ACKNOWLEDGMENT

The authors would like to express their gratitude to Dr. Adrian Booth for his helpful suggestions and to the National Research Council (Canada) for the granting of an award to one of us (R.V.).

[4] J. Timmermans, J. chim. phys. **35**, 331 (1938).

Reduction of SrO by Methane

GEORGE E. MOORE, H. W. ALLISON, AND K. B. WOLFSTIRN
Bell Telephone Laboratories, Inc., Murray Hill, N. J.

(Received July 20, 1953)

The reduction of SrO supported on purified platinum or nickel filaments was investigated over the range 1050 to 1700°K. Reduction is rapid, and at least part occurs in two major steps: (1) the methane dissociates, depositing carbon in the oxide, which (2) then reacts with SrO to give Sr and CO.

When SrO is supported on platinum filaments a major part of the Sr enters the platinum. This is far less pronounced in nickel supports. Possible significance for the oxide cathode is discussed. Calculations indicate that SrC_2 may also be formed.

INTRODUCTION

SEVERAL observers have studied the reduction of alkaline earth oxide to free metal by two general methods. In the first,[1–4] the reducing agent forms all, or part, of the metallic support for the oxide. In the second,[2,5] the oxide is treated in a reducing gas, such as methane. Measurements of kinetics and equilibria of a few reactions between metal filaments and oxide have been reported,[1,3,4,6,7] but no corresponding data have been published for reactions with gaseous reducing agents.

The Prescott-Morrison[5] experiments in methane were probably the earliest investigations of chemical reduction of either type. Prescott first showed (in unpublished calculations) that the reaction

$$CH_4+BaO\rightarrow CO+2H_2+Ba, \qquad (1)$$

could be expected under experimentally realizable conditions. They gave no measurements on kinetics, but showed that the reaction occurred and emphasized principally the effect of methane treatment on the thermionic emission of their system. The object of the present experiments was to investigate the reaction between CH_4 and SrO, using a simpler system than that employed by Prescott. Neglecting intermediate processes, the reaction was presumably:

$$CH_4+SrO\leftrightarrows CO+2H_2+Sr. \qquad (2)$$

Previous work[8] has shown that SrO can be heated in vacuum in contact with carefully purified platinum without perceptible reduction. Furthermore, in the reduction[4] of SrO coatings by *W* filaments, essentially all Sr produced left the coat and deposited on the walls of the experimental tube, where it was measured radiochemically. Therefore, the present plan was to reduce a SrO coat, supported on Pt wire, by heating in methane and to measure reduction by the bulb deposit. SrO is more suitable than BaO because (1) the vapor pressure of SrO is lower relative to its reducibility, and (2) the radioactive isotopes of Sr are more convenient.

EXPERIMENTAL

Figure I shows the experimental tube. The glass is Pyrex (Corning 774). Filament *A* is a platinum,* or 499 Nickel† wire, 0.010 in. in diameter, supporting the SrO. End-cooling reduces the effective length to approximately $2\frac{1}{4}$ in., making the effective coated area about 0.55 cm^2; the coating density is very nearly 5 mg/cm^2. The platinum (or nickel) wire was treated in wet H_2 at 1200°C (or 1000°C) before coating, to oxidize any impurities capable of reducing SrO. The coating consisted of nonradioactive $SrCO_3$ of high purity mixed with fission $SrCO_3$‡ applied by B. A. Diggory,[8] in a mixture of nitrocellulose and amyl acetate.

Filament *B*, used for auxiliary purposes, is a tungsten ribbon 0.40 in.×0.0005 in. with its plane face toward *A*. For example, before admitting methane, it could be stabilized by heating in high vacuum so that a given heating current corresponded to a definite temperature; the error introduced in pyrometer measurements by a film of Sr on the glass was evaluated by observing the heated tungsten both before and after methane reaction. Such observations showed that pyrometer measurements were unaffected by the film; therefore, *B* was generally used to receive Sr deposit for experiments described later.

Temperatures were measured pyrometrically and corrected for emissivity by reflectometer.[8] Constant

[1] G. E. Moore, J. Chem. Phys. **9**, 327 (1941).
[2] A. H. White, J. Appl. Phys. **20**, 856 (1949).
[3] C. Brown, J. Chem. Phys. **18**, 1311 (1950).
[4] Moore, Allison, and Morrison, J. Chem. Phys. **18**, 1579 (1950).
[5] C. H. Prescott and J. Morrison, J. Am. Chem. Soc. **60**, 3047 (1938).
[6] L. T. Aldrich, J. Appl. Phys. **22**, 1168 (1951).
[7] Hughes, Coppolla, and Evans, Phys. Rev. **85**, 388 (1952).
[8] Moore, Allison, and Struthers, J. Chem. Phys. **18**, 1572 (1950).

* Copper, the only spectroscopically detectable impurity, was present to less than 0.03 percent.

† Driver-Harris 499 nickel wire, Lot 6550, B.T.L. analysis

Element	Weight %	Element	Weight %
Al	0.011	Mg	<0.01
B	<0.005	Mn	<0.01
Cr	<0.004	Si	0.011
Cu	0.085	Ti	<0.009
Fe	0.016		

‡ Obtained from Oak Ridge National Laboratories of the U. S. Atomic Energy Commission.

pyrometer temperature was maintained throughout methane treatment.

For dissociation of $SrCO_3$ and methane treatment, the tube was sealed to a system which could readily be evacuated to pressures below 10^{-7} mm. Matheson cp grade methane, supplied in tanks, was purified and admitted as described previously,[9] with the entire system at room temperature, and pressure observed with a McLeod gauge. This initial reading ranged from 0.06 to 1.30 mm and never varied by more than 10 percent during an experiment. The tubes were processed in groups of 2 or 3, each group being exposed to a constant methane pressure, and either the temperature or duration of treatment was varied.

For convenience, treatment was made from tube to tube in one or more definite charges of methane, rather than by continuous flow. The observed rate of reaction seemed unaffected whether performed in one charge, or by repeatedly introducing fresh charges. At the lower pressures, the numbers of methane molecules in the system and of SrO molecules on a

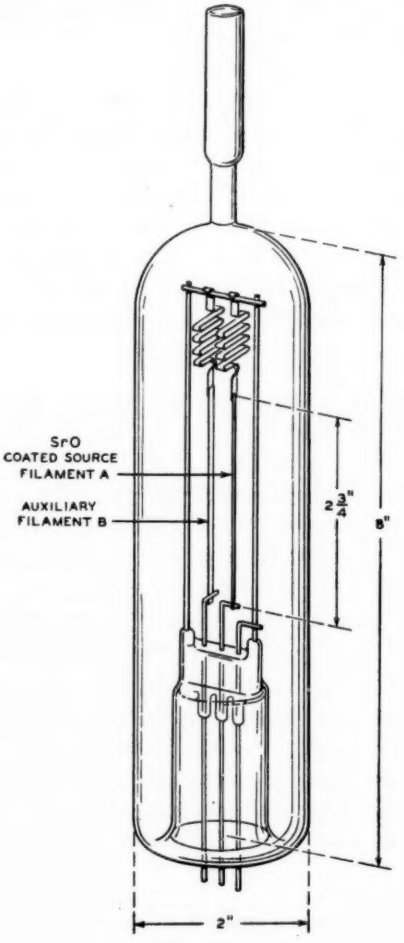

FIG. 1. Experimental tube.

[9] Hannay, MacNair, and White, J. Appl. Phys. **20**, 669 (1949).

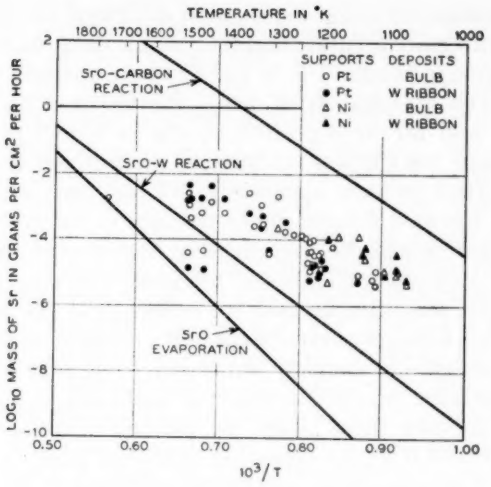

FIG. 2. Production of Sr metal during heating in methane.

filament were approximately equal; only a small fraction of each was consumed in any experiment.

Sr was measured by comparing radioactive counts of the tungsten ribbons (both sides), or of washings from the bulb with counts from aliquots of the mixture used to coat the source filaments. Because of β-particle reflection, calibration deposits must be mounted on the same material as experimental samples.

RESULTS

1. Blank Tests

Blank tests were made by measuring the deposit, on bulbs and ribbons, evaporated from 6 coated filaments which were heated only in vacuum. The deposits corresponded to the physical vaporization of SrO molecules. Therefore, the organic binder in the coating and inpurities in the platinum or nickel support metal cause no appreciable chemical reduction. The rates of evaporation computed from bulb and ribbon deposits agreed within a factor of 2 for each tube.

2. Production of Sr by Treatment in Methane

Figure 2 shows all tests in which deposits on the bulb and auxiliary filament measure reaction occurring while the coated filament was heated in methane. Rate of Sr evolution in grams per *hour* per square centimeter of coated filament surface is plotted logarithmically against reciprocal temperature. Figures 2 and 3 show three *reference* lines; the lowest represents the physical evaporation of SrO molecules.[8,10] The central line shows the observed[4] rate of Sr produced by reaction between SrO and tungsten. The third shows the expected rate of reduction by graphite carbon. This curve is entirely computed, by extending slightly the method which predicted the rate for the *W* reduction; the equilibrium constant for the reaction products, CO and Sr, was

[10] Claassen and Veenemans, Z. Physik **80**, 343 (1933).

first computed using the method described by White[2] but with more accurate thermodynamic data than were available to White. The Sr and CO were assumed to be produced at equal rates, while the CO was pumped away and the Sr deposited on the bulb and ribbon. Although the CO was not pumped away in our system, its partial pressure apparently did not limit reaction rate. The rate for the direct reaction (2) of SrO with methane would be considerably higher and would depend on the pressures of methane and of gaseous reaction products. Because we believe that the actual reaction involves several steps and because the rate of (2) cannot be uniquely expressed as a function of temperature, no calculated curve is shown.

Each open point gives the rate of Sr production determined from the deposit on bulb and mount of one individual tube. Each closed point represents the rate determined from the deposit on one *W* ribbon. Although the two determinations always agreed within a factor of 3 in each tube, the results from tube to tube scatter too widely to justify a curve. Although many refinements were introduced, reproducibility was not improved. This lack of reproducibility made the expected pressure dependence undetectable and was the most surprising feature of these tests. Despite the scatter, nearly all points are above the line for SrO evaporation by orders of magnitude and are also higher than for the reaction with *W*.

3. Reaction with Carbon Residues

The possibility that methane first dissociated with liberation of hydrogen and deposit of carbon on the oxide surface, was examined in other tubes, for which the results are shown in Fig. 3. The coated filament was heated in methane, which was then pumped out. Reaction rate during this period *in* methane as deduced from *bulb* deposit is shown for these tubes in Fig. 2. The tungsten filaments were then cleaned by heating, and filament *A* was again heated in vacuum. Ribbon deposits were thus a measure of any reaction in the source filament *after* exposure to methane. If the direct reaction (2) caused all reduction shown in Fig. 2, the ribbon deposits in Fig. 3 should correspond to the relatively slow physical evaporation of SrO molecules. But if reduction occurred in the two-step process:

$$CH_4 \rightarrow C + 2H_2 \quad \text{(a)}$$

(with carbon depositing on the SrO)

$$C + SrO \rightarrow Sr + CO \quad \text{(b)}, \qquad (3)$$

a more rapid reduction by carbon residues should occur, although possibly not as rapid as while heating in methane. Rapid reaction is evident, although the rate is roughly an order of magnitude less than that shown in Fig. 2. The rate is far more rapid than for evaporation of SrO and is usually more rapid than for reduction of SrO by *W*, indicating that at least some of the

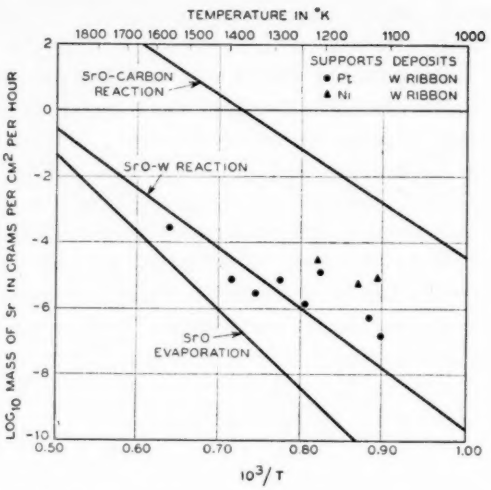

FIG. 3. Production of Sr metal by carbon residues remaining in coat after methane treatment.

reaction of Fig. 2 was caused by carbon (and possibly hydrocarbon) residues.§

For this group of tubes, no Sr was detected on the back surface of the tungsten, indicating no migration around the ribbon and a reflection coefficient less than 0.2 for Sr atoms from the bulb.

CO as a reaction product does not appreciably retard (3b). Thus, after removing the methane, reaction with carbon residues can be measured either by heating the filament in a closed system, or by continuous pumping. In the former case, the CO pressure rapidly builds up to the order of 10^{-2} mm; in the latter method this never exceeds 10^{-5} mm. The rate of (3b) seems substantially independent of CO pressure over this range.

4. Diffusion of Sr Into the Source Filament

(*a*) *General*

Figures 2 and 3 are plotted with the tacit assumption that all Sr produced leaves filament A. However, the amount of Sr metal diffusing into platinum supports is comparable to the total leaving the filament. Diffusion into nickel was very much less; this probably explains a result of Fig. 2—that the rate of reduction seems greater when the coating is applied to nickel. Presumably reaction really occurs at the same rate with either support metal; the greater amount of Sr diffusing into the platinum accounts for the smaller amount moving outward and registering in Fig. 2. These and other results are demonstrated in 3 experiments.

§ The Sr could scarcely have been present in the coat because CO was formed on heating and the amounts of Sr in Table II are much larger than the quantities of Ba or Sr observed in oxide coatings. See Jenkins and Newton, J. Sci. Instr. **26**, 172 (1949). Similar data on Ba or Sr content were presented orally by L. A. Wooten, Phys. Rev. **69**, 248 (1946).

(b) *Amounts of Sr in Pt and Ni Support Wires*

The source filaments were removed after the blank tests and the experiments shown in Figs. 2 and 3, and treated to remove all coating and interface, without removing any nickel or platinum. Boiling in water removed substantially all coating. Nickel filaments were then washed in acetic acid which readily dissolves the Sr compounds, but affects nickel only slightly. With platinum filaments, repeated washings in HCl reduce the count to a definite value not decreased by additional HCl treatment.

Results are shown in Table I. Column 2 gives the Sr found on, or in, the filament after acid wash, determined from radioactive count on the filament itself; because of β absorption, this is a lower limit but relative amounts from one filament to another are accurate. Column 3 gives the ratio of Sr in the wire to the amount which had been found on bulb and supports. The table contains four parts, each dealing with one combination of support metal and environment for previous treatment. The following features are clear: (1) the mean amount of Sr entering platinum filaments is approximately twice that found on bulb and structure, *if* the filament had been treated in methane. (2) In the blank tests, where the coated platinum had been heated only in vacuum, the mean amount of Sr (or SrO) entering the platinum is only about 1/40 of that found on the bulb. (3) The total Sr in the nickel filaments is only a small fraction of that found on the bulb, regardless of whether the filament had been heated in methane or vacuum. (4) An asterisk in column 3 marks tubes in which reaction with deposited carbon had been studied. The ratio for these is not significantly different from the ratio for tubes in the same grouping, which had not undergone this additional treatment. The conclusion that Fig. 3 shows reaction between deposited carbon and SrO, is based partly on the results of this table. For example, one might object that Sr found on the tungsten receivers in Fig. 3 could have simply vaporized out of the support metal, and that there is really no appreciable reaction with deposited carbon. However, this would require that (a) tubes marked by asterisk show less Sr than those not so marked, and (b) Sr deposit in nickel (as well as in Pt) be greater than the amount leaving the filament during test for reaction with deposited carbon. Neither condition was satisfied. The mean amount of Sr in the four platinum filaments which had been tested for reaction with deposited carbon was actually slightly greater than in those not so tested. The Sr found in nickel filaments is not nearly sufficient to account for all Sr produced in the reaction shown by Fig. 3.

TABLE I. Sr in support metal.

Tube No.	μg of Sr in stripped support filament	Ratio Filament content Bulb deposit
Part A: Platinum supports treated in methane.		
497	335	4.68*
498	55.5	1.93*
513	176	3.10
514	221	1.95
516	151	2.57
517	175	3.18*
526	25.2	0.88
527	32.5	0.98*
528	38.5	0.98
530	143	2.92
	Mean	2.32±1.15 rms
Part B: Platinum supports treated in vacuum		
515	0.415	0.011
518	1.09	0.035
580	3.55	0.023
583	0.34	0.011
584	0.49	0.010
	Mean	0.018±0.010rms
PartC: Nickel supports treated in methane.		
592	1.39	0.0061
593	8.85	0.102
594	1.55	0.114
595	1.50	0.075
596	0.85	0.049
599	0.71	0.072
600	0.49	0.052
602	3.04	0.024*
603	1.91	0.027*
604	3.19	0.042*
	Mean	0.047±0.031rms
Part D: Nickel support treated in vacuum.		
601	1.70	0.135

* Tested for reaction with carbon residues.

(c) *Experiment No. 2. Vaporization of Sr out of Stripped Pt Filaments*

Stripped filaments were remounted and then heated in high vacuum; vaporized Sr was measured radiochemically. In all filaments previously treated in methane, this rate, shown in Fig. 4, was much higher than the rate at which SrO could vaporize. The rate at which Sr diffuses out of the platinum and vaporizes was assumed constant throughout treatment (1 hr to 18 hrs). This rate, on a logarithmic scale, is plotted against reciprocal temperature. Vapor pressure of SrO is plotted as a solid line; its slope is considerably greater than that of any line that one could draw for filaments treated in methane. The dotted line represents a least squares fit, the slope corresponding to 24 kcal, but the processes are sufficiently complex that this should not be related to any single process, such as diffusion. Sr is obviously lost from the platinum much more rapidly than SrO vaporizes, especially at lower temperatures. This and the fact that the four filaments which had been heated only in vacuum (triangular points) lose Sr much *less* rapidly, suggest that Sr enters the platinum and leaves as metal atoms, despite long exposure to air (10–20 days) and washing in water and acids experienced by these filaments between treatments in methane and vacuum. More than 25 percent of the Sr left the platinum filaments previously treated in methane, but only $\frac{3}{4}$ percent (of the SrO) left the filaments previously treated only in vacuum.

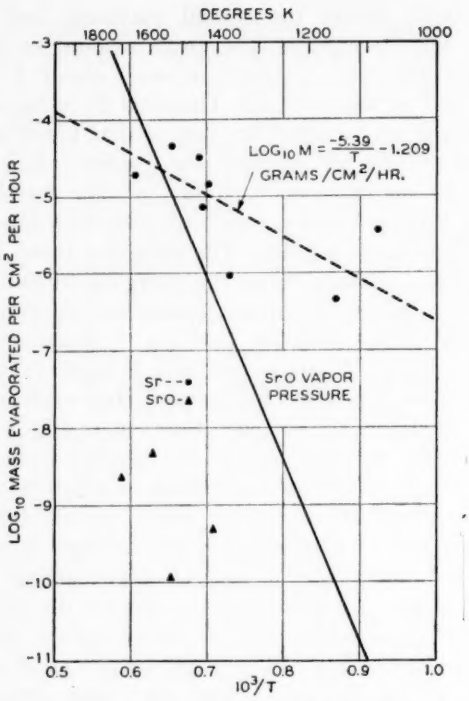

FIG. 4. Vaporization of Sr from stripped filaments.

(d) *Experiment No. 3. Diffusion Coefficients for Sr in Pt and Ni*

Several filaments were etched to determine the distribution of dissolved Sr. Figure 5 shows typical results for tube 530, one of three platinum filaments etched, and for tube 596, one of six nickel filaments etched. The density C_0 of Sr at the surface of the support metal is taken as 2.58 grams per cc, its bulk density, because the curves indicate that the true value cannot be less than 1.9. On the ordinate scale used for the solid curves, the concentration drops essentially to zero within 2.5×10^{-5} cm for Ni, and 2.5×10^{-4} cm for Pt, distances only 1/500 and 1/50 of the respective radii of the wires. Absorption of radially directed β particles should not be serious at these small depths. Repeated washing of platinum filaments in acetic or hydrochloric acids did not decrease the count; this decreased only on etching in aqua regia. The count on the nickel filament was not affected by repeated washings in hot water, but decreased slowly on washing with acetic acid. The decrease represented by the first point for nickel is the sum of six washings in acetic acid. Continuity of the dotted curves, which show concentration multiplied by appropriate factors to indicate diffusion at greater depths, demonstrates the high sensitivity of the radioactive method. The theoretical relationship between diffusion and depth is given[11] by

$$C=C_0\left[1-\varphi\left(\frac{x}{2(Dt)^{\frac{1}{2}}}\right)\right].$$

TABLE II. Mass spectrometer tests of methane reactant and gaseous reaction products.

Gas	Methane as reactant	Tube 667 Reaction at 1350°K	Tube 668 Reaction at 1200°K
	Content in percent by volume		
CH_4	90.5	39.6	40.4
CO	0.76	17.3	20.8
H_2	7.96	41.3	38.6
C_2H_6	0.38	0.87	0.18
C_2H_4	0.21	0.44	<0.01
C_2H_2	0.03	0.28	<0.01
Higher Hydrocarbons	0.15	0.19	0.02
		Initial Pr=0.60 mm	0.57 mm
		Final Pr=0.91	0.70
Spectral emissivity of filament		0.58	0.36

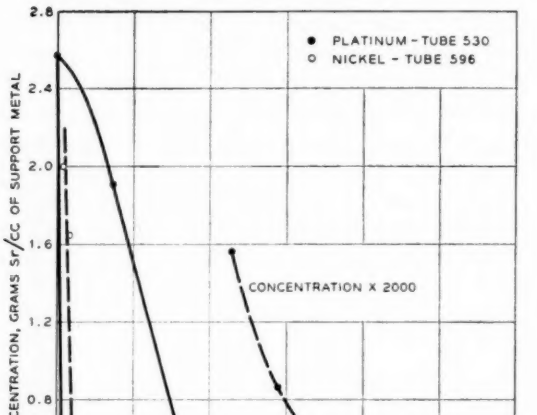
● PLATINUM - TUBE 530
○ NICKEL - TUBE 596
CONCENTRATION X 2000
CONCENTRATION X 20
MEAN CONCENTRATION, GRAMS Sr/CC OF SUPPORT METAL
MEAN DEPTH IN CM

FIG. 5. Diffusion of Sr into support metals.

One computes the diffusion coefficient D from the error function φ, the depth x, and time t. For the platinum filament, D varies from 0.3×10^{-11} to 3×10^{-11} cm² per sec. Setting[11] $D=Ae-Q/RT$ where $A\sim1$, gives 69 kcal for the activation energy for diffusion of Sr in Pt at 1448°K. The value of Q is not sensitive to the 10-fold range in D, nor reduced by assuming that A has the lowest values previously[11] measured (~0.01) for diffusion in metals like Pt. The value of Q is increased if we assume $C_0<2.58$ g/cm³.

For the nickel filament, $D\sim1.3\times10^{-15}$ cm²/sec and $Q=75$ kcal at 1108°K.

5. Analysis of Methane and Gaseous Reaction Products

Table II shows mass spectrometer tests, by E. E. François, of the methane as introduced, and of the

[11] See for example Robert F. Mehl, Trans. Am. Inst. Mining Met. Engrs. **122**, 14 (1936). We assume plane parallel geometry here to avoid complication.

gases remaining after a reaction about 3 times as extensive as those at the corresponding temperatures in Figs. 2 and 3. For one test, the filament was operated at 1350°K, and for the other at 1200°K; reaction at 1350° tends to increase the concentration of ethane, ethylene, acetylene, and higher hydrocarbons, while reaction at 1200° tends to remove these gases. The higher spectral emissivity of the former filament indicates a large carbon deposit; the spectral emissivity of the latter filament does not differ significantly from that of similar filaments never exposed to methane.

DISCUSSION

1. General

The preceding measurements (a) determine roughly how fast SrO reacts with methane, (b) indicate that it occurs in two steps designated as (3a), and (3b), and (c), trace the Sr produced. Methane reduces SrO at a rate which is rapid relative to that for *W*, but far less reproducible.

Dissociation with deposit of carbon on the oxide is generally neglected in experiments emphasizing the thermionic behavior of oxide cathodes exposed to methane. Yet equilibria for 3a[12] show that under present conditions, substantially complete dissociation could be expected at any temperature above 600°K. Early measurements of equilibria have been summarized[13,14]. Catalysis by alkaline earth oxide, with deposit of carbon on the oxide, has been observed by Schwab and Pietsch[15] and others.[9] Measurements of mechanism and kinetics for 3a are in a much less satisfactory state than measurements of equilibria. In our opinion, the literature favors a five-step process, proposed by Kassel,[16] in which the methane forms, in order, the radical CH_2, ethane, ethylene, and acetylene, which then dissociates to carbon and H_2. During four of the 5 steps, H_2 is also formed and it inhibits further reaction. There remain important disagreements‖ in the literature on mechanism and kinetics. Until 3a can be controlled reproducibly, the kinetics of SrO reduction by methane will probably remain erratic.

2. Relation to Theories of Thermionic Activity in Oxide Cathodes

Experimental determinations of the physical and chemical state of emitting oxide cathodes are extraordinarily difficult, but necessary for interaction with theory. While the present work gives definite answers to some questions, it accentuates the difficulty in answering others.

For example, these experiments, and those of Prescott and Morrison, establish that methane reduces alkaline earth oxide. From current theories, with their emphasis on excess alkaline earth metal as essential for high thermionic activity, one might expect at least a statistical thermionic advantage for cathodes treated in methane. Yet cathodes so treated have never been especially active. Thus the *optimum* emission of Prescott's filaments (obtained with about 30μg of Ba per cm^2) was approximately an order of magnitude less than that obtained without methane in most of the commercial product over the last 20 years The increased carbon content following methane treatment, observed in these experiments, might somehow explain a deactivation which should only be temporary in view of reaction 3b. Yet the low emission of Prescott's cathodes treated in methane persisted[5] indefinitely.

Similarly Figs. 4 and 5 show that platinum supports dissolve Sr during methane treatment, but readily give up this Sr on subsequent heating. This suggests that, in contrast to nickel, platinum supports could serve as a reservoir of alkaline earth metal. Therefore, platinum might be an ideal support metal for cathodes treated in methane, at least for the duration of Sr evolution, which would continue for many hours. However, this is not observed. Originally Prescott supported his cathodes on pure platinum. The thermionic activity was very low and decayed rapidly with time. This behavior was improved by the addition of nickel powder to the coating. Such results require theoretical explanation; this is difficult in terms of the present simple theory of emission which attaches no fundamental importance to the support metal.

Figure 5 shows that the concentration of Sr at the interface is nearly equal to that for the bulk metal. This suggests that most of the Sr may be formed at the interface, diffusing both inward and outward. The concentration of Sr in the coat might therefore approximate its solubility limit.

3. Formation of Strontium Carbide

Brown[3] utilized plausible theoretical arguments to conclude that the reaction

$$BaO+3C\rightarrow BaC_2+CO \qquad (4)$$

was very improbable. However the available thermodynamic data do not justify strong reliance on calculations involving either SrC_2 or BaC_2. Data *are* available for calculating equilibria between CaO, CaC_2, Ca, and CO. The method of Kelly[17] applied to more recent publications[12,18,19] of specific heat and equilibria indicate

[12] F. D. Rossini, "Selected values of chemical thermodynamic properties," National Bureau of Standards (1950–1951).
[13] M. Randall and Ali Mohammad, Ind. Eng. Chem. **21**, 1048 (1929).
[14] H. H. Storch, Information Circular, U. S. Bureau of Mines, No. 6549, (January, 1932).
[15] Schwab and Pietsch, Z. Elektrochem. **32**, 430 (1926).
[16] Louis S. Kassel, J. Am. Chem. Soc. **54**, 3949 (1932).
‖ See for example: H. H. Storch, J. Am. Chem. Soc. **54**, 4188 (1932); Alvin S. Gordon, J. Am. Chem. Soc. **56**, 2381 (1934); Rice and Glasebrook, J. Am. Chem. Soc. **70**, 395 (1948); Barrow, Pearson, and Purcell, Trans. Faraday Soc. **35**, 880 (1939); G. C. Eltenton, J. Chem. Phys. **10**, 403 (1942); J. O. Smith and H. S. Taylor, J. Chem. Phys. **1**, 390 (1939).
[17] K. K. Kelley, Bureau of Mines Bulletin, No. 407 (1937), p. 6.
[18] K. K. Kelley, Ind. Eng. Chem. **33**, 1314 (1941).
[19] G. E. Moore, Ind. Eng. Chem. **35**, 1292 (1943).

that carbide formation is probable in experiments such as ours.

The writers acknowledge their indebtedness to H. C. Geissler for cooperation in the methane processing, to N. B. Hannay for discussion, and to both Conyers Herring and Howard Reiss for suggestions along theoretical lines.

APPENDIX. DIFFUSION OF Sr THROUGH METHANE

At the methane pressures used, the mean free path of a Sr atom is short compared to the distance travelled before depositing on filament *B* or bulb. This diffusion process must be considered in translating deposits into the rates of Fig. 2. Evidence for it is clear; e.g., Sr is deposited with equal density on both sides of the ribbon during methane treatment, but on only one side during the blank or carbon residue tests. If diffusion severely limited the flow of reaction products away from filament *A*, our measurements might not give the true rate of the forward reaction, but only the small net difference between forward and reverse rates under arbitrary conditions, and therefore would have no significance.

In the reverse reaction, two H_2 molecules, a CO molecule, and a Sr atom must interact to form the CH_4 and the SrO molecule, the latter returning to filament *A*. This sequence is much less probable than collision of a CH_4 molecule and Sr atom, such that the Sr atom returns to the filament, for which the probability is not over 0.03 even with CH_4 and Sr at the same temperature.

Herring considered diffusion effects in a more general way. If forward and reverse reactions occur at approximately equal rates, the system is in approximate equilibrium, by definition, and the equilibrium constant (which was computed) relates the pressures of gaseous reagents, including Sr. The requirement of steady state further specifies individual pressures, since the relative effusion rates of reaction products must be given by (2). Assuming that the Sr pressure just outside the coat is only 0.1 its equilibrium value, he calculated that Sr atoms would diffuse to the bulb at a rate much greater than observed under any present experimental conditions. Similarly, equilibrium could not have existed *throughout* the pores; these occupy far more area than the apparent surface[20] and the Sr pressure at the apparent surface would in effect have been the equilibrium pressure measured by thermal effusion from many small orifices.

If it occurs at all, diffusion limitation of Sr deposits would occur in the depths of the pores. Herring therefore assumed that equilibrium existed at the depths of pores of diameter 2μ and length 75μ, and calculated the rate of Sr diffusion. He found that the deposits would be significantly larger than observed except possibly at the lowest experimental temperatures and highest pressures. Herring's method therefore indicates that Fig. 2 gives the rates of the forward reaction.

[20] L. A. Wooten and C. Brown, J. Am. Chem. Soc. **65**, 113 (1943).

Theory of Laminar Flame Stability. I. Analytic Stability Condition*

J. B. ROSEN
Forrestal Research Center, Princeton University, Princeton, New Jersey
(Received July 20, 1953)

The stability of propagation of a laminar flame or combustion wave is studied for a general type of flame propagating medium. This is done by investigating the stability of the steady-state solution of the flame equations for such a system. The method is to solve the linearized system of partial differential equations resulting from an instantaneous heat release perturbation of the steady-state solution. An approximate solution in analytic form to this linearized partial system is obtained. This permits the statement of an analytic stability condition, and shows the existence of stability limits. The existence of stability limits is suggested as an explanation of inflammability limits.

1. INTRODUCTION

A THEORETICAL study of the stability of the laminar combustion wave or flame is most conveniently started by consideration of the steady-state solutions to the flame equations. It has been shown by Boys and Corner[1] and Friedrichs[2,3] that the solution of the flame equations is essentially an eigenvalue problem for the determination of the flame velocity. The most complete statement of these equations as well as detailed techniques and numerical solutions for specific cases have been given by Hirschfelder and Curtiss.[4–6,†] It is found that a definite value of the mass flow M ($M=\rho_0 v_0$, v_0=flame velocity) is required in order that a solution will exist which satisfies both the cold and hot boundary conditions. Furthermore, it appears that for reasonably simple systems a steady-state solution will always exist, i.e., a value of M can always be found such that the equations and boundary conditions are satisfied.[7] The steady-state theory does not appear to predict any discontinuity in the solutions as a function of the equation parameters or to limit the existence of solutions to certain ranges of these parameters.

Experimental evidence, such as inflammability limits, detonation limits and the dual possibility of a flame or detonation in a given combustible mixture, apparently contradicts the continuous nature of the theoretical steady-state results. It is proposed here that the explanation for this apparent contradiction is that the steady-state solution is not necessarily a stable solution, and in fact becomes unstable when certain definite conditions are violated.

This hypothesis is based on the results presented in this paper and summarized below. These results can be applied directly to explain the phenomenon of inflammability limits. A detailed picture of how these limits depend on the kinetic scheme and on the physical parameters such as activation energy, heat of combustion, initial gas temperature and composition, and the rate constants is implicit in the stability condition obtained but has not yet been studied for specific cases. While the results given here represent a possible mechanism by which a flame can go over into a detonation, the relation of this stability criterion to experimental detonation limits is not yet clear.

The results obtained in the present investigation will be briefly stated:

(a) A description is given of the nature of possible instabilities in the steady-state solutions to the flame equations.

(b) A sufficient condition for a stable steady-state solution is stated.

(c) The following approximate condition for stability in terms of the steady-state parameters is obtained from (b). Let E be the activation energy and r the order of the reaction rate $\mathfrak{R}$ in the rate determining step. Let the subscript i denote steady-state values at the inflection point on the temperature-distance curve ($k=0$ in Fig. 1). Then the approximate stability condition is

$$\frac{E}{RT_i}-r\leq\tfrac{1}{4}\left(\frac{\rho c_p}{\lambda}\right)_i\frac{T_i}{T_\infty}\left(\frac{v^2}{\mathfrak{R}}\right)_i.$$

The flame is stable if this condition is satisfied and unstable if it is violated.

In terms of (c), an explanation of the occurrence of an inflammability limit due to dilution is that as diluent is added, T_i decreases until the point is reached where the above condition is no longer satisfied. This point is the

* This research was supported in whole by the United States Air Force under Contract No. AF 33(038)-23976 monitored by the Office of Scientific Research.

[1] S. F. Boys and J. Corner, Proc. Roy. Soc. (London) **A197**, 90–106 (1949).

[2] K. O. Friedrichs, "On the mathematical theory of deflagrations and detonations," Naval Report 79–46, Bureau of Ordnance (1946).

[3] R. Courant and K. O. Friedrichs, *Supersonic Flow and Shock Waves* (Interscience Publishers, Inc., New York, 1948), Sec. 96.

[4] J. O. Hirschfelder and C. F. Curtiss, J. Chem. Phys. **17**, 1076–1081 (1949).

[5] Hirshfelder, Curtiss, and Campbell, *Fourth Symposium on Combustion* (Williams and Wilkins Company, Baltimore, 1953), pp. 190–210.

[6] Hirschfelder, Curtiss, and Campbell, J. Phys. Chem. **57**, 403–414 (1953).

† See also T. v. Karman and S. S. Penner, *Proceedings AGARD Combustion Colloquium* (Butterworth Scientific Publications, London, 1954).

[7] See reference 3, p. 235. Also, Y. B. Zeldovich, Zhur. Fiz. Khimii **22** (1948). English translation Natl. Advisory Comm. Aeronaut. Tech. Mem. 1282 (1951).

inflammability limit since a stable flame is no longer possible.

2. DESCRIPTION OF INSTABILITY

Before proceeding to the detailed theory it is necessary to describe what is meant by stability and instability and to discuss the method used to determine under what conditions a steady-state solution will become unstable. Previous work on instability has been largely devoted to what might be called "hydrodynamic instability" of flame fronts in that the instability is essentially hydrodynamic in origin and involves a two or three dimensional distortion of the flame front.[8–10]

In these previous investigations the flame front is considered as a surface of discontinuity. The reaction zone structure therefore does not appear explicitly and the kinetics enter by their effect on the boundary conditions. It has also been assumed in these investigations that temperature perturbations are always stable and can therefore be neglected.

The results presented here relate the question of stability directly to the kinetics and the steady-state solution through the use of a rate function $\mathfrak{R}$ which can be made quite general. The stability criterion obtained depends only on certain general assumptions about $\mathfrak{R}$ and its partial derivatives with respect to temperature and the mixture components. Furthermore, the results show that instability can exist in a strictly one-dimensional flame and is in fact a temperature instability which causes a temperature perturbation to grow in size. The significant results are obtained using a single spatial coordinate taken in the direction of the gas flow velocity. We therefore limit consideration to a one-dimensional planar flame; the independent variables of the problem being the distance x and the time t.

The complete mathematical description of the problem[11] will consist of the system of nonlinear partial differential equations representing the conservation and diffusion relations together with the boundary conditions and the equation of state. The complete solution will give the system variables, temperature, composition, mass flow, and density as functions of time and distance.

The steady-state solution is defined as the solution to the system of equations obtained from the original system by making all time derivative terms identically zero. If we take a coordinate system fixed with respect to the flame this steady-state system will consist of ordinary differential equations in the variable x, with the cold and hot boundary conditions specified at $x=-\infty$ and $x=\infty$, respectively. The gas flow is thus taken in the direction of increasing x.

Suppose now that a steady-state solution to these ordinary differential equations has been obtained. We wish to obtain an answer to the following question: If the steady-state solution is disturbed by an infinitesimal amount, will the disturbance die out or will it build up as a function of time? As a first step in answering this question we observe that since we are dealing with an infinitesimal perturbation, the original nonlinear system can be linearized in terms of the steady-state solution to give a linear system of partial differential equations. The magnitude and sign of the assumed disturbance to this new system will now affect the solution only linearly, so that these quantities can be chosen arbitrarily in the most convenient manner. The solution to this linearized system and therefore the stability results may, however, depend on the form of the initial perturbation so that this cannot be taken arbitrarily, but is chosen in the light of the following considerations.

We are dealing with a free flame so that the boundary conditions on the perturbation must be specified as asymptotic values; in particular we want its value to approach zero as $x\rightarrow\pm\infty$. In addition, the disturbance must be initiated in a physically realizable manner. A disturbance meeting these requirements is that caused by the release of an instantaneous source of heat over some small region of the flame. This corresponds physically to a momentary increase in this region of the steady-state rate of heat production, and is a type of disturbance which will certainly occur. Furthermore, because of the linearity of the equations the negative of the heat source solution is the heat sink solution. This corresponds to a momentary decrease in heat production, and is an event which is equally likely to occur.

It therefore seems justified to limit the investigation to the instantaneous heat source temperature perturbation, and at the same time to claim that the stability results obtained in this way are the important ones in terms of physical significance. Mathematically this perturbation has the distinct advantage that it permits an approximate solution to be obtained in analytic form, as will be discussed in Sec. 4. A typical steady-state solution for temperature, product concentration, and free radical concentration is shown in Fig. 1. The temperature perturbation due to an instantaneous heat sink is also shown.

We are interested now in the time-dependent behavior of the solution to the linearized system of equations for the heat source initial condition. The coefficients of this system are given in terms of the steady-state solution and are therefore functions of the distance x only. The solution of such a system must, in general, be obtained numerically, but offers considerably less difficulty than the original nonlinear system.

The linearized system is of the parabolic type, and for a short interval of time following the release of the source of heat the solution is essentially the same as that for a much simpler problem; namely, the temperature distribution following the release of a heat source in an infinite conducting medium. The heat release takes

[8] G. H. Markstein, J. Aeronaut. Sci. **18**, 199–209 (1951).
[9] G. H. Markstein, *Fourth Symposium on Combustion* (Williams and Wilkins Company, Baltimore, 1953), pp. 44–59.
[10] H. Einbinder, J. Chem. Phys. **21**, 480–489 (1953).
[11] See Appendix II.

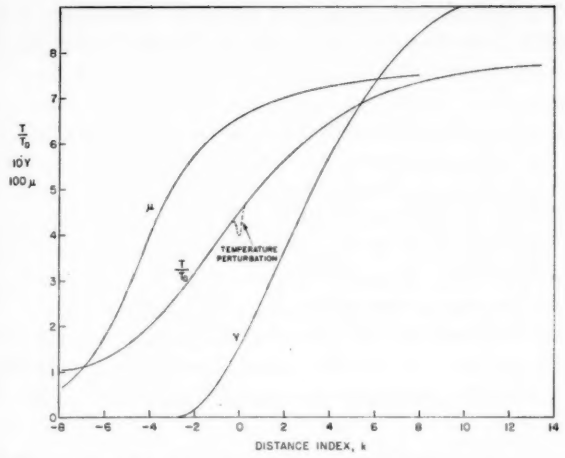

FIG. 1. Steady-state solution for typical parameter values. T=temperature, Y=main product concentration, μ=free radical concentration $\times 10^4$.

place over a small volume element and will spread out in all directions, so that we are actually faced with a problem involving two spatial dimensions (a cylindrical coordinate system is applicable because of the symmetry). In order to permit numerical solutions to be carried out with a reasonable amount of work it is necessary to reduce the problem to one involving a single space coordinate, the distance x. This is most easily accomplished by assuming a disk-like volume element for the region in which heat release takes place. In a one-dimensional picture this region will consist of an element of length along the x axis, the length representing the thickness of the disk. It is shown in Appendix I that at least in so far as the approximate analytic solution is valid, the stability condition obtained for the one-dimensional case is identical with that obtained by considering the complete problem in cylindrical coordinates. The following discussion is therefore limited to the one-dimensional case.

Since we do not want the behavior of the perturbation to depend on the size of the small region in which the heat release takes place, we let the size of this region approach zero as a limit. If we were to attempt to maintain a constant value for the total quantity of heat released this would lead to an infinite initial temperature at the point of release, violating the linearization condition. Therefore, we maintain a constant value for the heat release per unit length as the region shrinks. This leads to a constant initial temperature in the region of heat release, and a temperature distribution outside of the heat release region which approaches that of the finite point source. A rigorous discussion of this question is given in Appendix I.

In what follows we will consider the one-dimensional problem and take the initial condition to be the release of a point source of heat. For a short interval of time following the release the effect of mass flow will be small, and the solution of the problem[12] will be given approximately by

$$\tau=\frac{1}{\sqrt{t}}\exp\left(-\frac{x^2}{4t}\right)$$

for the point source released at $t=0$ at the space point $x=0$. Immediately following the heat release the energy will diffuse away from the source due to heat conduction, with a resulting decrease in the temperature at $x=0$. If the steady-state solution is stable this process will continue and the temperature will eventually approach zero everywhere. On the other hand, if the solution is not stable the temperature at $x=0$ will drop initially, but will reach a minimum and then start to increase.

Physically, the unstable situation for the point source results from the fact that the initial "pip" in the steady-state temperature causes the local rate of heat release to become greater than its steady-state value. This may lead to heat being released by the chemical reaction at a rate greater than it is being transported away. If this occurs the temperature will rise, causing an acceleration of the process and a growth of the original perturbation which will continue at least until the linearized approximation ceases to be valid. The situation for the point sink in the unstable case is identical except that the temperature "pip" now points downward, causing a local decrease in heat release. In this case a growth of the initial perturbation means that the temperature is continually decreasing.

On the basis of the preceding discussion we now classify steady-state solutions as stable or unstable according to the following definition:

> A steady-state solution to the flame equations is *stable* or *unstable*, respectively, depending on whether the solution to the linearized system with the point source initial condition *dies out* or *grows continually* with time.

The question of stability therefore is determined by the coefficients of the linearized equations and thus depends on the steady-state solution to the original system and the parameters in the original system. On the basis of this definition it is possible to obtain a sufficient condition for stability in terms of the steady-state solution, i.e., the steady-state solution is stable if this condition is satisfied. The condition and the method by which it is obtained are discussed in detail in Sec. 4.

A few remarks on the physical interpretation of an unstable solution will complete this section. The decay or growth of the initial infinitesimal perturbation is determined by the linearized system. If it decays the solution obtained is valid for all time. If it grows, it will eventually reach a size such that the linearization is no longer valid, and it becomes necessary to consider the original nonlinear system to follow the solution further.

[12] H. S. Carslaw and J. C. Jaeger, *Conduction of Heat in Solids* (Oxford University Press, London, 1947), Sec. 103.

The behavior of the solution may now become quite different than it was in the vicinity of its steady-state value. In particular, the solution may be such that the initial increase in size of the disturbance comes to a halt and may even reverse its direction of growth in some spatial regions. Furthermore, we no longer have the previous symmetry for the source and sink solutions, so that the continuous growth in the nonlinear region for one case does not imply it for the other. The following three possibilities for an unstable solution are suggested.

(a) The point source solution ceases to grow in the nonlinear region while the point sink solution continues to grow. Since both types of perturbation occur, the latter will cause the temperature to decrease throughout the flame toward its cold zone value, i.e., the flame goes out. This corresponds to the situation at or outside the inflammability limits.

(b) The source solution grows and the sink stops growing. The continued local temperature rise causes a readjustment of temperature, pressure, and velocity until a stable steady-state solution is reached at a much higher velocity (additional terms in the original equations must now be considered because of the supersonic velocity). This corresponds to the transition from a normal flame to a detonation.

(c) Both source and sink solutions stop growing when they reach some finite amplitude, which however does not represent a steady-state solution. They cannot remain in this new unstable situation and the amplitude of the perturbation at this point in space will decrease. This leads to oscillations of finite amplitude about the steady-state solution and may represent the situation as the inflammability limit is approached.

It is worth noting that the condition of the unburned combustible mixture at the ambient temperature will normally represent a stable steady-state solution as defined here. Therefore, an energy source of finite size is required to go from this stable state to that represented by the normal flame. The size of the energy source required represents the ignition energy, and should be calculable from the original system of nonlinear equations.

In the following section a complete description is given of the method by which the coefficients a_i of the linearized partial differential equations (system II) are obtained from the steady-state solution. It is most convenient to write the original steady-state equations in dimensionless form with the physical constants appearing as dimensionless parameters. The coefficients of the linearized system (also dimensionless) are then obtained directly from the solution of the steady-state equations. A typical steady-state system in dimensionless form is described and solved in Part II of this investigation.[13] Its numerical solution for a particular choice of parameters is shown in Fig. 1.

[13] J. B. Rosen, J. Chem. Phys. **22**, 743 (1954). Denoted hereinafter as Part II.

The use of a dimensionless form for the steady-state equations makes it easier to study the effect of changes in such physical parameters as activation energy, heat of combustion, initial gas composition and temperature, and rate constant. Changing the value of one or more of the dimensionless parameters will alter the steady-state solution and the effect will appear in the a_i in system (II). This procedure makes it possible to determine the effect of any of these physical parameters on stability, or to put it another way, to determine the regions of stability in a multidimensional parameter space.

With proper care it should also be possible to determine the effect on stability of such boundary conditions as heat or radical loss to a flame holder. The altered boundary conditions are applied to the steady-state equations only, and the results will be valid in so far as the a_i are changed and not the form of Eqs. (II).

3. SYSTEM EQUATIONS

Starting with the complete time-dependent equations for a one-dimensional, constant pressure, laminar flame the general system of linearized equations for the temperature, mass flow, and concentration perturbations are given in Appendix II. The assumption of no diffusion is then made, and the original complete equations are simplified to a smaller number of equations where the dependent variables are T, M, ρ and the weight fractions Y_i. These equations are denoted by (1), (2a), (3), and (4a) and represent, respectively, the conservation of energy, the continuity of individual components, the conservation of mass, and the equation of state.

In order to permit a detailed investigation of the stability of these equations to be carried out without undue complication, it is desirable to simplify them further. In particular we wish to reduce the number of continuity equations to one, and deal with a single weight fraction which for convenience we denote as the *main product concentration* Y. This can be done by making two additional assumptions.

(a) Choose one of the main chemical components, the concentration of which increases[14] during the course of the reaction, say $i=1$. The mole fraction of this component is denoted by X_i. We assume that the mole fractions of all other components are given in terms of T and X_1. That is, we assume that $X_i=f_i(T,X_1)$, $i=1, 2, \cdots s$, where $f_1\equiv X_1$ and $\sum f_i=1$.

(b) The mean molecular weight, $\nu=\sum m_iX_i$, is assumed to be constant.

In general, the mole fraction and the weight fraction are related by $Y_i=m_iX_i/\nu$, so that with these two assumptions we can readily express all of the X_i and the Y_i in terms of the temperature and the single weight fraction $Y\equiv Y_1$. We thus obtain $X_i=f_i(T,\nu Y/m_1)$, and similarly for the Y_i. It follows that $h=\sum h_iY_i$ can be

[14] A similar development can be made for the case where the chosen component decreases during the reaction.

expressed as a function $h=(T,Y)$ of T and Y only. Furthermore, we can define a rate function of T and Y.

$$\mathfrak{R}=\mathfrak{R}(T,Y)=(m_1RT/p\nu)K_1(T,f_j).$$

The value of Y increases from its initial value Y_0 to its final value Y_∞ during the reaction, where $0\leq Y_0<Y_\infty\leq 1$. By the proper choice of the main product component we can always insure that $\mathfrak{R}(T_\infty,Y_\infty)=0$ and that the partial derivative $h_Y\equiv\partial h/\partial Y<0$. We assume these relations to hold. In addition, although not essential to what follows, it will almost always be true that $\mathfrak{R}>0$ for $Y<Y_\infty$, and that for the partial derivatives we have $\mathfrak{R}_Y\leq 0$ and $h_T>0$.

Using the additional assumptions (a) and (b) and the rate function $\mathfrak{R}$, the Eqs. (1), (2a), (3), and (4a) in Appendix II reduce the following system of four equations for the quantities T, Y, M, and ρ.

$$\text{(I)}\qquad \begin{aligned} &\rho h_t+Mh_x-(\lambda T_x)_x=0, &(1)\\ &Y_t+(M/\rho)Y_x-\mathfrak{R}=0, &(2)\\ &\rho_t+M_x=0, &(3)\\ &\rho T=\rho_0T_0=\text{constant}. &(4)\end{aligned}$$

The corresponding steady-state equations are obtained by making the time derivatives in (1), (2), and (3) identically zero. Equation (3) then gives $M=$ constant, while integrating (1) once and combining with (2) gives the single equation

$$\frac{dY}{dT}=\frac{\lambda\rho\mathfrak{R}}{M^2(h-h_0)}, \tag{5}$$

where $h_0=h(T_0,Y_0)$ is the enthalpy of the reactants at the cold temperature. The relation

$$h(T_\infty,Y_\infty)=h_0,$$

determines the adiabatic hot temperature T_∞, for no heat loss by the system. The eigenvalue problem is to find M so that the solution $Y=Y(T)$ of (5) with $Y(T_0)=Y_0$ takes the value $Y(T_\infty)=Y_\infty$.

A difficulty is encountered in determining M if a finite rate[15] is assumed at T_0, since T_0 is then a singular point of Eq. (5). This does not appear to be a fundamental difficulty insofar as the over-all problem is concerned. It apparently results from the fact that the continuous Eqs. (1) and (2) do not apply as $x\to-\infty$, since T_x and $\mathfrak{R}$ become so small that the statistical averaging process implicit in (1) and (2) is no longer valid.

It is proposed here that the proper method of dealing with this difficulty is to choose a suitable small positive constant ϵ, and to define a new rate function

$$\mathfrak{R}^*\equiv\begin{cases}\mathfrak{R}, & \mathfrak{R}\geq\epsilon,\\ 0, & \mathfrak{R}<\epsilon.\end{cases}$$

[15] J. B. Rosen, *Fourth Symposium on Combustion* (Williams and Wilkins Company, Baltimore, 1953), pp. 210–211.

The rate function $\mathfrak{R}^*$ may now be used in (5) without difficulty. The size of the quantity ϵ must, in general, be determined by probability considerations, but if properly chosen an increase or decrease in its size by a factor of 10 will not appreciably alter the steady-state solution.

The steady-state solution is discussed in greater detail in Part II, where certain general properties of the solution of (5) are obtained.

For the remainder of Part I it will be assumed that a steady-state solution has been obtained so that we have available as known functions of x; $[T(x)]$, $[Y(x)]$, $[\rho(x)]=\rho_0T_0/[T(x)]$, and $[M]=M_0=$ constant, as well as their x derivatives. The square bracket will be used to denote the steady-state solution. Since h and $\mathfrak{R}$ are known functions of Y and T we also know $[h]$ and $[\mathfrak{R}]$ as functions of x.

The investigation of stability is carried out by assuming perturbations $T_0\tau$, y, and M_0m in the quantities T, Y, and M, respectively, so that

$$\begin{aligned} &\frac{T}{T_0}=\frac{[T(x)]}{T_0}+\tau,\\ &Y=[Y(x)]+y,\\ &\frac{M}{M_0}=1+m,\\ &\rho=[\rho(x)]-\frac{[\rho(x)]^2}{\rho_0}\tau.\end{aligned} \tag{6}$$

When these quantities are substituted in the system equations the steady-state terms cancel out, and if second-order terms in the perturbations are neglected a linear system in τ, y, and m results. We will use the fact that

$$h_x=h_TT_x+h_YY_x$$

and similarly for h_t. Also to terms of second order

$$\mathfrak{R}(T,Y)=\mathfrak{R}([T],[Y])+\mathfrak{R}_TT_0\tau+\mathfrak{R}_Yy.$$

The linearized system obtained from (I) in this way consists of 3 equations.

$$\begin{aligned} F_1(\tau_t,\tau,\tau_x,\tau_{xx},y_t,y,y_x,m)&=0,\\ F_2(y_t,y,y_x,\tau,m)&=0,\\ F_3(\tau_t,m_x)&=0,\end{aligned}$$

where the F_i are linear functions in their arguments with coefficients which are known functions of x involving the steady-state solutions and their derivatives. It is more instructive to obtain the equations in a somewhat different form. This is done by eliminating y_t between F_1 and F_2 and multiplying the resulting equation as well as the original F_2 and F_3 by $-1/K\rho h_Y$. In this, K is the rate constant (independent of temperature) in $\mathfrak{R}$. Finally the variables t and x are replaced by

the dimensionless variables

$$z=K\frac{\rho_0}{M}x, \qquad \theta=Kt. \tag{7}$$

The point $z=x=0$ is chosen as the inflection point of the steady-state temperature, i.e., the point at which $[T_{xx}]=0$.

The following system of equations is obtained:

$$-a_1\tau_{zz}+a_2\tau_z+a_3\tau+a_4\tau_\theta+a_5m+a_6y=0, \tag{8}$$

(II)
$$\tau_\theta-a_7m_z=0, \tag{9}$$

$$y_\theta+a_8y_z+a_9y+a_{10}\tau+a_{11}m=0. \tag{10}$$

The dimensionless coefficients $a_i=a_i(z)$ are defined by

$$a_1=\left[-\frac{\lambda T_0K\rho_0^2}{\rho h_Y M^2}\right]>0,$$

$$a_2=\left[-\frac{h_TT}{h_Y}-2a_1\frac{d\log\lambda}{dz}\right]>0,$$

$$a_3=\left[\frac{T_0}{K}\left(\frac{\Re}{T}-\Re_T\right)-\frac{T}{h_Y}\frac{dh_T}{dz}\right],$$

$$a_4=\left[\frac{-h_TT_0}{h_Y}\right]>0,$$

$$a_5=\left[-\frac{h_TT}{h_YT_0}\frac{dT}{dz}\right]\geq 0,$$

$$a_6=\left[-\frac{\Re_Y}{K}-\frac{T}{h_YT_0}\frac{dh_Y}{dz}\right]\geq 0,$$

$$a_7=\left[\frac{T}{T_0}\right]^2>0,$$

$$a_8=\left[\frac{T}{T_0}\right]>0,$$

$$a_9=\left[-\frac{\Re_Y}{K}\right]\geq 0,$$

$$a_{10}=\left[\frac{T_0}{K}\left(\Re_T-\frac{\Re}{T}\right)\right],$$

$$a_{11}=\left[\frac{T}{T_0}\frac{dY}{dz}\right]\geq 0.$$

The term d/dz is the total derivative of the steady-state solution, so that

$$\frac{dh_T}{dz}=h_{TT}\frac{dT}{dz}+h_{TY}\frac{dY}{dz}$$

and similarly for dh_Y/dz. These two terms therefore depend on the second partials of h, and may be neglected if the second partials are sufficiently small. The indicated signs of these coefficients are based on the previous assumptions and the resulting properties of the steady-state solution.

4. APPROXIMATE SOLUTION

We wish to solve the system of Eqs. (II) for the release of a point source of heat at $z=0$ with the initial conditions $y=m=0$ for all z and $\tau=0$ for $z\neq 0$. Since the coefficients a_j, $j=1, 2, \cdots 11$ are complicated functions of z the system (II) must in general be solved numerically. A suitable method for obtaining numerical solutions and its application to a typical system are described completely in Part II.

On the basis of these numerical results it appears that the essential features of the solution can be obtained by means of a greatly simplified system. The simplification consists first of neglecting the effect of the last two terms in (8), so that the history of the temperature "pip" is given by the single Eq. (8) with $m=y=0$. This means that the changes caused in composition and mass flow by the initial temperature perturbation are sufficiently small so that their effect on stability can be neglected. The kinetics of the reaction thus enter into the stability condition by determining the steady-state solution and therefore the coefficients of the temperature perturbation terms, rather than by the direct effect of the concentration term y in the linearized equations.

Secondly, the coefficients are taken to be constants, the value of these constants being given by a spatial average of the ratios of the appropriate a_i. The equation for τ now becomes

$$-\tau_{zz}+2B\tau_z+C\tau+\tau_\xi=0, \tag{11}$$

where

$$B=\left(\frac{a_2}{2a_1}\right)_{Av}>0, \quad C=\left(\frac{a_3}{a_1}\right)_{Av},$$

$$D=\left(\frac{a_4}{a_1}\right)_{Av}>0, \qquad \xi=\frac{\theta}{D}.$$

The motivation for simplifying the equation in this way is that a simple analytic solution for the point source initial condition can now be obtained. The desired solution of (11) for a unit point source is

$$\tau=u(z,\theta)=\frac{1}{2(\pi\xi)^{\frac{1}{2}}}\exp\left[-(B^2+C)\xi-\frac{z^2}{4\xi}+Bz\right]. \tag{12}$$

This solution exhibits in a clear manner the nature of the possible instability, and gives a simple stability condition.

If we define the quantity

$$S=-\left(\frac{B^2+C}{D}\right), \tag{13A}$$

then the approximate stability condition is

$$S<0 \rightarrow \text{stable}, \qquad S>0 \rightarrow \text{unstable}. \tag{IIIA}$$

Since $D>0$, the sign of S depends on the term C, the system becoming unstable when C is a sufficiently large negative quantity. This will happen only if the average value of the partial derivative of the rate function, $\Re_\tau$, is large enough. *Thus, the important quantity from the point of view of stability is the magnitude of the temperature dependence of the rate function.*

For θ small (short times) the solution (12) is very close to the previously mentioned solution for the infinite conducting medium. However, for large values of the time and for $S>0$, the value of u will grow exponentially with time at any fixed point in space. In particular at $z=0$, we have

$$u(0,\theta)=\frac{e^{S\theta}}{2\left(\frac{\pi}{D}\theta\right)^{\frac{1}{2}}},$$

so that for $\theta>\theta_m=1/2S$, the value of u will be increasing.

For $0<z^2<D/4S$ there will be two extremum points given by

$$\theta_m=\frac{1}{4S}\left[1\pm\left(1-\frac{4S}{D}z^2\right)^{\frac{1}{2}}\right].$$

In this region u, which is initially zero, will increase, then decrease and finally begin to grow again. For $z^2\geq D/4S$, u will increase monotonically with time.

The behavior of the analytic solution $u(z,\theta)$ given by Eq. (12) is illustrated for both a stable and unstable case in Figs. 2 and 3. The stable case chosen (Case No. 1, Fig. 2) is $C=0$, $S=-B^2/D=-0.442$. This corresponds to the point source solution for a flow system with no reaction. For the unstable case (Case No. 3, Fig. 3) a value of $S=5.22$ is used. The curve for $\theta=\theta_m=0.072$, for this unstable case is that for which $u(0,\theta)$ has a minimum, and as is shown, u is increasing everywhere for all greater values of time. These two figures show clearly the difference in behavior of the stable and the unstable solutions, since the stable case continues to decrease while the unstable case will always increase after a sufficient length of time has elapsed.

The usefulness of the solution $u(z,\theta)$ as an approximation to the solution $\tau(z,\theta)$ of the complete system (II) with variable coefficients will depend largely on the choice of the constants B, C, and D. The criterion used is that the two solutions shall be close together at $z=0$, namely that the difference $\tau(0,\theta)-u(0,\theta)$ shall be small.

If the solution $\tau(z,\theta)$ has been obtained numerically for a particular set of coefficients $a_i(z)$, values of S and D can be obtained directly by satisfying this criterion. In particular, if the solution $\tau(0,\theta)$ has a minimum value $\tau(0,\theta_m)=\tau_m$ at $\theta=\theta_m$, the function $u(0,\theta)$ can be made to take the same minimum value at $\theta=\theta_m$ by a proper

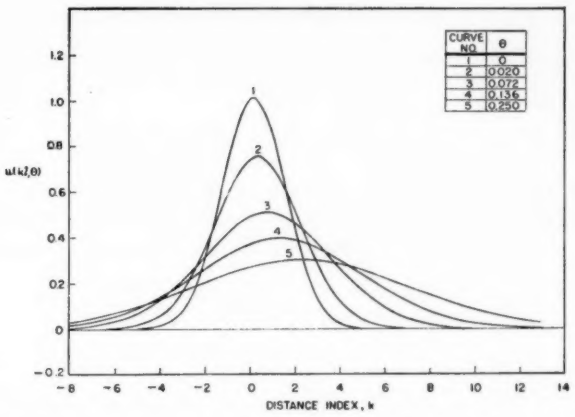

FIG. 2. Temperature perturbation behavior. Approximate solution $u(z,\theta)$. Stable, Case No. 1 ($S=-0.442$).

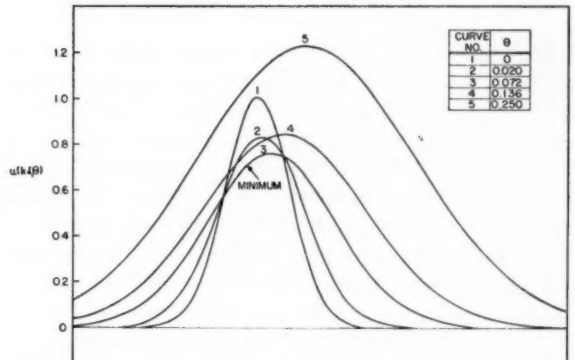

FIG. 3. Temperature perturbation behavior. Approximate solution $u(z,\theta)$. Unstable, Case No. 3 ($S=5.22$).

choice of S and D. The value of B can then be found, for example, so that $u(z,\theta_m)$ gives the best approximation to $\tau(z,\theta_m)$.

A comparison of the analytic solution $u(z,\theta)$ obtained in this way with the numerical solution $\tau(z,\theta)$ for two cases is given in Part II. The excellent agreement obtained with these two cases (chosen in so far as possible as typical steady-state solutions) leads one to believe that the stability condition which holds for the approximate equation can be used as a basis for an equivalent condition for the complete system (II). What is desired is a stability condition which involves only the coefficients $a_i(z)$, so that the question of stability can be answered without actually solving the system (II).

The nature of the problem is most clearly shown by looking at the variable terms corresponding to B, C, D, and S, namely:

$$B(z)=\frac{a_2}{2a_1}, \quad C(z)=\frac{a_3}{a_1}, \quad D(z)=\frac{a_4}{a_1}, \qquad S(z)=-\frac{a_2^2+4a_1a_3}{4a_1a_4}, \tag{13B}$$

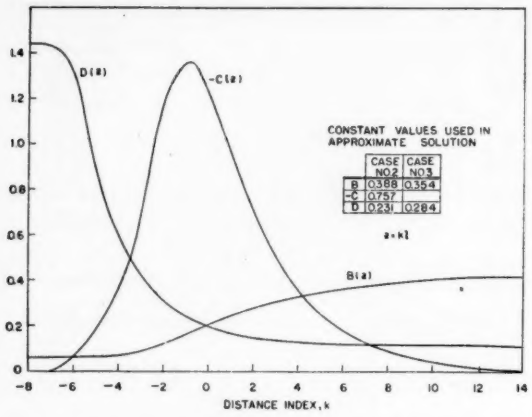

FIG. 4. Variable coefficients in approximate temperature perturbation equation

$$-\tau_{zz}+2B(z)\tau_z+C(z)\tau+D(z)\tau_\theta=0.$$

for the two unstable cases solved numerically. These are shown in Figs. 4 and 5 together with the constant values used in $u(z,\theta)$. The stability condition (IIIA) for the constant coefficient case suggests a somewhat weaker stability condition for the variable coefficient system (II), directly in terms of the $a_i(z)$. This is a *sufficient condition for stability*‡ and will be stated as follows:

The steady-state solution of the flame equations is stable if for all z, $-\infty<z<\infty$, *we have*

$$S(z)=-\left(\frac{a_2^2+4a_1a_3}{4a_1a_4}\right)\leq 0. \qquad \text{(IIIB)}$$

While violation of this condition does not necessarily mean unstable solutions, it is true that if $S(z)$ is positive over a sufficiently large interval the solutions will be unstable. Thus the "stability function" $S(z)$ gives a simple method for determining whether the steady-state solutions are stable or unstable for cases which are well within the regions of stability or instability. For borderline cases, or for steady-state solutions which differ in some essential way from the example considered here, it is necessary to solve the complete system (II) numerically, as described in Part II, in order to determine whether or not the solutions are stable.

It is clear from Fig. 5 that the approximate solution $u(z,\theta)$ will correspond most closely to $\tau(z,\theta)$ in a limited interval about $z=0$. For increasing values of $|z|$ the value of $S(z)$ decreases and in fact becomes negative in the cold and hot end zones. This indicates that the steady-state equations are stable in the end zones, as is to be expected since no reaction is taking place in these zones. Mathematically, the stability in the cold and hot end zones results from the fact that $a_3\to 0$ as the rate function $\mathfrak{R}\to 0$ in these zones.

In order to bring out more clearly the physical significance of the stability function $S(z)$ and the stability condition (IIIB), it is worth while to get $S(z)$ directly in terms of the quantities used in the original steady-state Eq. (5). If the small contribution of the term $d\lambda/dx$ is neglected we have

$$S(z)=-\frac{M^2h_T}{4K\lambda\rho}+\frac{h_Y}{Kh_T}\left(\frac{\mathfrak{R}}{T}-\mathfrak{R}_T\right). \qquad (14)$$

The maximum value of $|S(z)|$ will probably occur at or near the temperature inflection point $z=0$. This is a result of the fact that $\mathfrak{R}$ attains its maximum value near this point, and is illustrated by the results in Fig. 5. Therefore, if $S(z)$ becomes positive anywhere it will be at $z=0$, so that the stability condition can be written simply as $S(0)\leq 0$.

We write $\mathfrak{R}$ in the form

$$\mathfrak{R}=f(T,Y)T^{-r+1}e^{-E/RT},$$

where T^{-r+1} represents the density dependence for an rth-order reaction and $f(T,Y)$ includes all other temperature effects, as well as the Y dependence. We assume that the temperature dependence of f is small compared to that of the Arrhenius and density terms, so that

$$\mathfrak{R}_T\cong\frac{\mathfrak{R}}{T}\left[\frac{E}{RT}-(r-1)\right].$$

We will use the inflection point values in (14) and make use of the approximate relations

$$h_T\cong c_p, \quad -\frac{h_Y}{h_T}\cong\frac{\Delta h}{c_p}\cong T_\infty.$$

We then obtain the stability condition in the comparatively simple form

$$-\left(\frac{\rho c_p}{\lambda}\right)_i\left(\frac{v_i^2}{4}\right)\frac{T_i}{T_\infty}+\left(\frac{E}{RT_i}-r\right)\mathfrak{R}_i\leq 0,$$

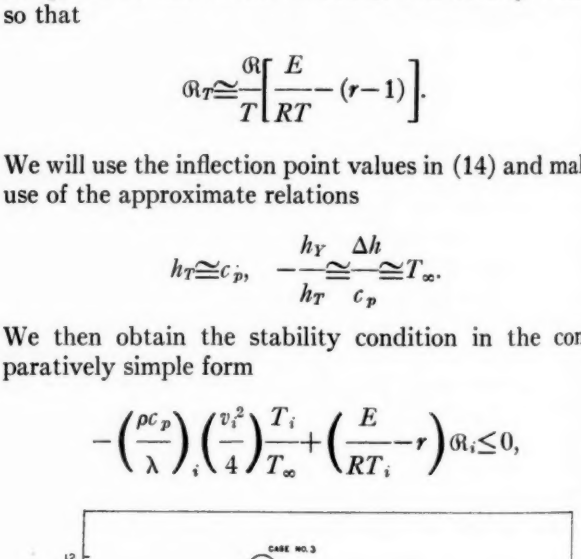

FIG. 5. Stability function $S(z)$ for unstable cases

$$S(z)=-\frac{B^2(z)+C(z)}{D(z)}.$$

‡ For a necessary and sufficient condition see J. B. Rosen, J. Chem. Phys. **22**, 743 (1954).

which leads directly to that previously stated in the introduction.

ACKNOWLEDGMENT

The author wishes to express his thanks to Professor Theodore von Karman for a discussion of certain aspects of this work, and to Professor R. H. Wilhelm, Department of Chemical Engineering, and Professor J. W. Tukey, Department of Mathematics, Princeton University, for helpful suggestions and comments.

NOMENCLATURE

Square brackets indicate a consistent system of units. [#] indicates a dimensionless quantity.

a_i = coefficients of linearized stability system, [#]
B, C, D = coefficients of approximate stability equation, [#]
c_p = specific heat, [cal/g deg]
E = activation energy in reaction rate $\mathfrak{R}$, [cal/mole]
h = total specific enthalpy, [cal/g]
Δh = specific heat of combustion, [cal/g]
k = distance index, [#]
K = rate constant in reaction rate $\mathfrak{R}$, [sec^{-1}]
$M = \rho v$ = mass flow, [g/cm^2 sec]
m = mass flow perturbation, [#]
n = moles mixture/unit vol., [mole/cm^3]
p = pressure, [dyne/cm^2]
r = order of reaction rate $\mathfrak{R}$, [#]
R = gas constant, [cal/mole deg] or [erg/mole deg]
$\mathfrak{R}$ = reaction rate for formation of Y, [sec^{-1}]
S = stability function, [#]
t = time, [sec]
T = temperature [deg]
u = approximate temperature perturbation, [#]
v = gas flow velocity, [cm/sec]
v_0 = flame velocity, [cm/sec]
x = distance coordinate (parallel to gas flow) [cm]
X_i = mole fraction ith component, [#]
Y = main product concentration, [#]
Y_i = weight fraction ith component, [#]
y = product concentration perturbation, [#]
$z = K(\rho_0/M)x$ = distance variable, [#]
$\theta = Kt$ = time variable [#]
λ = thermal conductivity, [cal/sec cm deg]
μ = free radical concentration, [#]
ν = mean molecular weight of mixture, [g/mole]
$\xi = \theta/D$, [#]
$n\nu$ = density, [g/cm^3]
τ = temperature perturbation, [#]
$\phi = T/T_0$, [#]

Subscripts

$_0$ = cold (unburned) zone values, $x \to -\infty$
$_\infty$ = hot (burned) zone values, $x \to \infty$

APPENDIX I

The constant coefficient approximate equation [see Eq. (11)] for τ in three dimensions is

$$-\nabla^2\tau + 2B\tau_z + C\tau + \tau_\xi = 0. \qquad \text{(11-3D)}$$

In cylindrical coordinates with angular symmetry we have $\tau = \tau(r,z,\xi)$, where r = radial distance from cylinder axis. The equation then becomes

$$-\frac{1}{r}(r\tau_r)_r - \tau_{zz} + 2B\tau_z + C\tau + \tau_\xi = 0.$$

The solution of this equation for a unit point source heat release at $z = r = \xi = 0$ is

$$\tau = u(r,z,\xi) = \frac{1}{8(\pi\xi)^{\frac{3}{2}}} \times \exp\left[-(B^2+C)\xi - \left(\frac{r^2+z^2}{4\xi}\right) + Bz\right]. \qquad \text{(12-3D)}$$

The stability condition for this 3D case is just that given by (IIIA). The stability condition for the constant coefficient equation is thus identical for the 1D and 3D cases.

The proper statement of the initial conditions for the 1D case, Eq. (11), will now be obtained. We assume an instantaneous heat source to be released at the time $\xi = \theta/D = 0$. The source has a strength of q per unit length and is assumed to extend from $z = -\epsilon/2$ to $z = \epsilon/2$. The solution for the finite source is obtained by integrating the product of the source strength and the appropriate Green's function[16] over the region of heat release. The desired Green's function is just the unit point source solution $u(z,\theta)$ given by Eq. (12). The finite source solution is therefore

$$w(z,\xi,\epsilon) = \frac{q}{2(\pi\xi)^{\frac{1}{2}}} e^{-C\xi} \int_{-\epsilon/2}^{\epsilon/2} \exp\left[-\left(\beta - \frac{\alpha}{2\sqrt{\xi}}\right)^2\right] d\alpha,$$

where $\beta = z/2\sqrt{\xi} - B\sqrt{\xi}$. Making a change of variable and performing the integration gives

$$w(z,\xi,\epsilon) = \frac{qe^{-C\xi}}{2}\left[\operatorname{erf}\left(\beta + \frac{\epsilon}{4\sqrt{\xi}}\right) - \operatorname{erf}\left(\beta - \frac{\epsilon}{4\sqrt{\xi}}\right)\right].$$

Since $\operatorname{erf}(\infty) = -\operatorname{erf}(-\infty) = 1$, we have that for a fixed value of $\epsilon > 0$,

$$\lim_{\xi \to 0} w(z,\xi,\epsilon) = \begin{cases} q, & |z| < \epsilon/2, \\ q/2, & |z| = \epsilon/2, \\ 0, & |z| > \epsilon/2. \end{cases}$$

Therefore $w(z,\xi,\epsilon)$ is finite everywhere as $\xi \to 0$. By expanding $w(z,\xi,\epsilon)$ in a finite Taylor's series about $\epsilon = 0$ it

[16] See reference 12, Sec. 130.

can be shown that for any fixed $\xi>0$,

$$w(z,\xi,\epsilon)=q\epsilon u(z,\xi)+q(\epsilon/\sqrt{\xi})^3N,$$

where $|N|\leq e^{-C\xi}/96\sqrt{\pi}$. Then for $\xi>0$ we can make $w(z,\xi,\epsilon)\to q\epsilon u(z,\xi)$ as closely as we please by taking a small enough value for ϵ. If we choose $q=1/\epsilon$, $w(z,\xi,\epsilon)$ will approach the unit point source solution. Alternately, we can make $w(0,\xi_0,\epsilon)=1$ by choosing $q\epsilon=2(\pi\xi_0)^{\frac{1}{2}}e^{(B^2+C)\xi_0}$. The latter procedure is used to obtain the initial value of $\tau(z,0)$ for a numerical integration.

APPENDIX II

The complete time-dependent equations for the propagation of a one-dimensional, constant pressure, laminar combustion wave may be written in the following form[17]:

$$(n\sum_i m_ih_iX_i)_t+(M\sum_i h_iG_i-\lambda T_x)_x=0,$$

$$m_i(nX_i)_t+(MG_i)_x-m_iK_i(T,X_j)=0,$$

$$n(X_i)_x-M\sum_j(m_iX_iG_j-m_jX_jG_i)/m_im_jD_{ij}=0,$$

$$n=p/RT.$$

These equations are the energy equations, the s continuity equations, the s diffusion equations, and the equation of state, respectively, for a chemical system of s chemical species.[18] Here, m_i=molecular weight, X_i=mole fraction, G_i=fraction of the mass rate of flow, $h_i=h_i^0+\int c_i dT$=specific enthalpy, and $K_i(T,X_j)$ =rate of production per unit volume [moles/sec cm^3]. All of these quantities refer to the ith chemical component.

A perturbation of the above system of equations about its steady-state solution leads to the following linearized system for the perturbations τ, x_i, and g_i in the quantities T/T_0, X_i and MG_i/M_0, respectively.

$$-A_1\tau_{xx}+A_2\tau_x+A_3\tau+A_4\tau_t+\sum_j A_{5j}x_j+\sum_j A_{6j}g_j=0,$$

$$A_{7i}\tau+A_{8i}\tau_t+n(x_i)_t+M_0(g_i/m_i)_x-\sum_j P_{ij}x_j=0,\qquad i=1,2,\ldots l+1,$$

$$A_{9i}\tau+n(x_i)_x+\sum_j a_{ij}x_j+\sum_j b_{ij}g_j/m_j=0,\qquad i=1,2,\ldots s-1.$$

This linear system of $l+s+1$ equations determines the $l+s+1$ linearly independent quantities τ, $l+1$ of the g_i and $s-1$ of the x_i. The coefficients are defined in terms of the steady-state values by:

$$A_1=\lambda T_0,$$

$$A_2=M_0T_0\sum_i c_iG_i-2T_0\lambda_T T_x,$$

$$A_3=T_0\sum_i m_ih_iK_{iT}+M_0T_0\sum_i(c_iG_i)_x-T_0\lambda_T T_{xx},$$

$$A_4=nT_0\sum_i m_ic_iX_i,$$

$$A_{5j}=\sum_i m_ih_iP_{ij},$$

$$A_{6j}=c_jM_0T_x,$$

$$A_{7i}=-T_0K_{iT},$$

$$A_{8i}=-nT_0X_i/T,$$

$$A_{9i}=(\eta-1)(nT_0/T)(X_i)_x,$$

$$a_{ij}=(M_0G_i/m_iD_{ij})-\delta_{ij}\sum_k M_0G_k/m_kD_{ik},$$

$$b_{ij}=-(M_0X_i/D_{ij})+\delta_{ij}\sum_k M_0X_k/D_{ik},$$

where $P_{ij}\equiv\partial K_i/\partial X_j$, $K_{iT}\equiv\partial K_i/\partial T$ and η is the exponent of the temperature dependence of D_{ij} which is assumed the same for all D_{ij}. All summations are taken from 1 to s.

For the limiting case of no diffusion ($D_{ij}\to 0$), the equations can be simplified. Let $Y_i=m_iX_i/\nu$=weight fraction, and $h=\sum_i h_iY_i$=total specific enthalpy, where

$$\nu=\sum_i m_iX_i=(\sum_i Y_i/m_i)^{-1}=\text{mean molecular weight.}$$

The diffusion equations are now replaced by the limiting relations $G_i\to Y_i$. The original system of equations now reduces to the $l+3$ equations

$$\rho h_t+Mh_x-(\lambda T_x)_x=0, \tag{1}$$

$$\rho(Y_i)_t+M(Y_i)_x-m_iK_i(T,X_j)=0,\quad i=1,2,\cdots l, \tag{2a}$$

$$\rho_t+M_x=0, \tag{3}$$

$$\rho T=p\nu/R, \tag{4a}$$

for the $l+3$ linearly independent quantities T, M, ρ, and l of the Y_i. Use of the limiting relation $g_i\to y_i+[Y_i]m$, where y_i is the perturbation in the steady-state value $[Y_i]$, will give the equivalent simplification in the linearized perturbation system for no diffusion.

[17] See reference 4, Appendix A; and reference 5, Sec. A.

[18] Only $l+s+2$ of the $2s+2$ equations are linearly independent, where $l\leq s-1$ is the number of independent K_i.

THE JOURNAL OF CHEMICAL PHYSICS VOLUME 22, NUMBER 4 APRIL 1954

Theory of Laminar Flame Stability. II.* General Numerical Method and Application to Typical System

J. B. ROSEN
Forrestal Research Center, Princeton University, Princeton, New Jersey
(Received July 20, 1953)

The steady-state flame equations for a system which may include the effect of a free radical are obtained in dimensionless form and solved for a typical choice of parameter values. A general numerical method for determining the stability of such a system is described. This method is applied to the chosen steady-state solution which is shown to be unstable. The growth of the temperature, concentration, and mass-flow perturbations are shown, and the temperature perturbation is compared with that given by the corresponding approximate analytic solution obtained in Part I.

1. INTRODUCTION

A GENERAL formulation of the problem of the stability of laminar flame propagation and the resulting derivation of a stability condition in analytic form have been presented in Part I of this paper.[1] This stability condition is based on an approximate analytic solution to the linearized system of partial differential equations denoted in Part I as the system (II) and repeated hereinafter. Two simplifying assumptions were necessary in order that the analytic solution $u(z,\theta)$ could be obtained. These assumptions were that the contribution to the temperature perturbation equation of the terms involving the concentration perturbation y and the mass-flow perturbation m could be neglected, and that constant average values could be assumed for the coefficients of the remaining terms. Since these are not trivial assumptions, some justification for them is necessary.

The best procedure is to choose one or more specific cases and obtain the solution $\tau(z,\theta)$ of the complete system (II) with the appropriate boundary conditions. A comparison of $\tau(z,\theta)$ so obtained, with the corresponding approximate solution $u(z,\theta)$, will determine the validity of the latter. In particular, for an unstable system near the stability limit the solution $\tau(z,\theta)$ and the approximate solution $u(z,\theta)$ should grow in size in the same manner.

Because of the complicated nature of the system (II) and in particular because of the variable coefficients $a_i(z)$, it is necessary to obtain $\tau(z,\theta)$ by means of a numerical solution. This solution is desired for the initial condition of the release of a point source of heat at $z=0$, and for the boundary conditions that τ and y approach zero as $z\to\pm\infty$. The system (II) is parabolic, and, as a result, an improperly chosen numerical method may lead to an unstable solution even though the system (II) is actually stable. For this reason as well as because of the nature of the initial and boundary conditions, it is essential to exercise considerable care in choosing a numerical method of solution which will yield satisfactory results. The large amount of computation required to determine whether or not a solution is stable means that a high-speed digital computer is essential if an answer is to be obtained in a reasonable length of time. This imposes the additional requirement on the numerical method that it must be suitable for automatic programming on a high-speed machine.

A numerical method of solving the system (II) which meets these requirements is described below and is applied to two specific cases of a typical flame-propagating medium. This numerical method can be used to determine the stability of a steady-state solution whether or not the approximate analytic methods given in Part I are applicable. It thus represents a general procedure for determining the stability of the perturbed steady-state solution. It should also be emphasized that a complete numerical solution is the only method of determining the behavior of the concentration and mass-flow perturbations for an unstable system.

In the next section the steady-state flame equations are derived in dimensionless form and the solution obtained for a particular choice of the dimensionless parameters. In Sec. 3 the general numerical method for determining stability is described. This general method is applied to two cases in Sec. 4; one of which is found to be just outside the stability limit (case No. 2), the other of which is found to be definitely unstable (case No. 3). The numerical solutions obtained for these two cases are given in Figs. 1 through 5, inclusive. In Figs. 1 and 2 the temperature perturbation $\tau(z,\theta)$ is shown and is compared with the approximate solution $u(z,\theta)$ in Fig. 3. Figures 4 and 5 show the concentration and mass-flow perturbations, respectively, for the definitely unstable case.

2. DIMENSIONLESS STEADY-STATE EQUATIONS

The steady-state equations considered here represent a three component system, the chemical composition of which is therefore specified by the two concentrations Y and μ. Y is the main product concentration,[2] and μ represents a free radical concentration. We assume that

* This research was supported in whole by the United States Air Force under Contract No. AF 33(038)-23976 monitored by the Office of Scientific Research.

[1] J. B. Rosen, J. Chem. Phys. **22**, 733 (1954), preceding paper, denoted hereinafter as Part I.

[2] See Sec. 3, Part I.

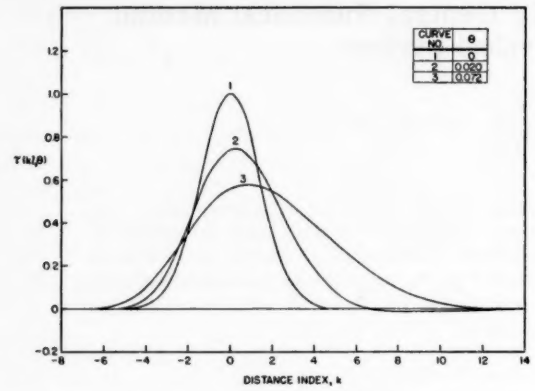

FIG. 1. Temperature perturbation behavior. Numerical solution $\tau(z,\theta)$. Unstable, Case No. 2 ($S=2.625$).

μ can be specified in terms of the temperature[3] by means of the relation $\gamma\mu=\exp(-E_1/RT)$, where γ is a constant depending on the particular system considered. We take the rate function $\mathfrak{R}$ for the formation of Y to be

$$\mathfrak{R}=\kappa\gamma\mu(Y_\infty-Y)\phi^{-1}\exp(-E_2/RT)$$
$$=\kappa(Y_\infty-Y)\phi^{-1}\exp(-E/RT), \quad (1)$$

where $E=E_1+E_2$ is the effective activation energy, and the constant term $\gamma\kappa$ is essentially a frequency factor. The total specific enthalpy is assumed to be given by

$$h-h_0=c_{p1}(T-T_0)+c_{p2}(T-T_0)^2-\Delta h(Y-Y_0), \quad (2)$$

where Δh is the specific heat of combustion. We also take $\lambda=\lambda_0\phi^{\frac{1}{2}}$.

In addition to those previously defined, we now define the following dimensionless parameters:

$$c_1=\frac{c_{p1}T_0}{\Delta h}, \quad c_2=\frac{c_{p2}T_0^2}{\Delta h}, \quad r_1=\frac{E_1}{E},$$
$$\alpha=\frac{\kappa\rho_0\lambda_0T_0}{\Delta hM^2}, \quad \sigma=\frac{E}{RT_0}.$$

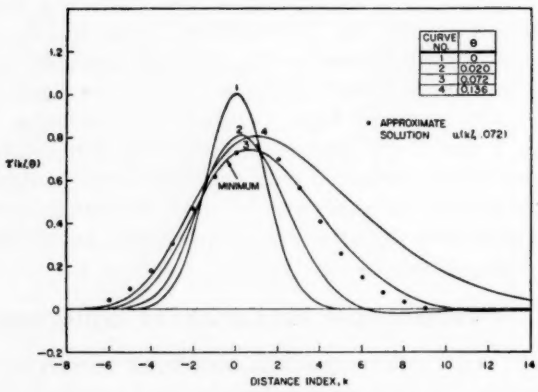

FIG. 2. Temperature perturbation behavior. Numerical solution $\tau(z,\theta)$. Unstable, Case No. 3 ($S=5.22$).

[3] This has been shown to be the case for the O atom concentration in an ozone decomposition flame. See T. v. Karman and S. S. Penner, *Proc. AGARD Combustion Colloquium* (Butterworth, London, 1954).

Also let $\phi=T/T_0$, and

$$Q(\phi,Y)=\phi^{-\frac{1}{2}}[c_1(\phi-1)+c_2(\phi-1)^2-(Y-Y_0)]$$
$$P(\phi,Y)=(Y_\infty-Y)\phi^{-2}\exp(-\sigma/\phi). \quad (3)$$

Finally, we define P^* by

$$P^*=\begin{cases}P, & P\geq\epsilon\\ 0, & P<\epsilon\end{cases}.$$

Taking ϕ as the independent variable we obtain the steady-state equations in the dimensionless form

$$Y_\phi=\alpha\frac{P^*(\phi,Y)}{Q(\phi,Y)}, \quad (4)$$

$$\gamma\mu=\exp(-r_1\sigma/\phi). \quad (5)$$

Equation (4) corresponds to Eq. (5) in Part I, where now the value of α is the eigenvalue required, so that $Y=Y_0$ at $\phi=1$ and $Y=Y_\infty$ at $\phi=\phi_\infty$. The value of ϕ_∞ is

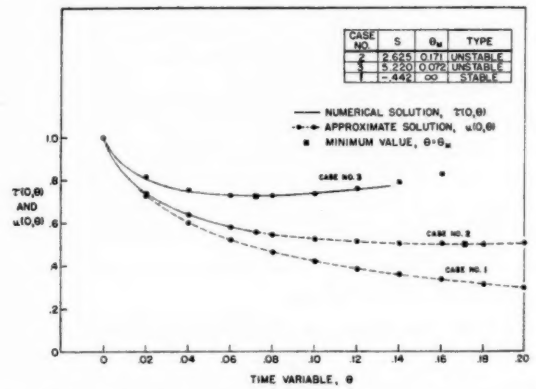

FIG. 3. Temperature perturbation behavior. Comparison of approximate and numerical solutions for $z=0$.

determined by $Q(Q_\infty,Y_\infty)=0$. Equation (4) was solved numerically, using a successive approximation method to get the eigenvalue α. After the solution $Y=Y(\phi)$ was obtained from (4), the value of z was calculated from the expression

$$z=(\alpha/\omega)\int_{\phi_i}^{\phi}\frac{d\phi}{Q(\phi,Y)}, \quad (6)$$

where ω is an appropriate scale factor.

The values of the dimensionless parameters appearing in these equations were chosen using typical experimentally measured values wherever possible. The parameter α, involving the mass flow M is, of course, an eigenvalue of the equations and cannot be chosen in advance. The values chosen were: $c_1=0.1$, $c_2=0.007$, $Y_0=0$, $Y_\infty=1$, $\sigma=20$, $\gamma=10^4$, $r_1=0.8$, and $\epsilon=10^{-8}$. These give $\phi_\infty=7.733$ and $\alpha=765$. The constant K used in Part I is defined in these terms by $K=\kappa/\omega$.

The steady-state solution for T/T_0, Y, and μ as

functions of z, obtained for these parameter values, is that given in Fig. 1 of Part I. This solution is investigated by the method described in the following sections and is found to be unstable.

3. NUMERICAL SOLUTION OF COMPLETE SYSTEM

We will now obtain a general numerical procedure for determining the stability of the complete linearized system:

$$-a_1\tau_{zz}+a_2\tau_z+a_3\tau+a_4\tau_\theta+a_5m+a_6y=0, \quad (7)$$

(II)

$$\tau_\theta-a_7m_z=0, \quad (8)$$

$$y_\theta+a_8y_z+a_9y+a_{10}\tau+a_{11}m=0. \quad (9)$$

In order to obtain a numerical solution to (II) it is necessary to replace the system of partial differential equations by an appropriate system of difference equations. This is done by constructing a rectangular grid

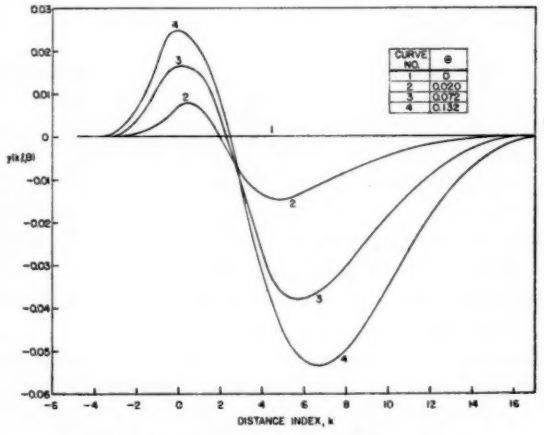

FIG. 4. Concentration perturbation behavior. Numerical solution, Case No. 3.

in the z,θ plane and considering the values of τ,y, and m at the grid points. Such a grid is shown in Fig. 6 and is considered to cover the infinite space-time region $-\infty<z<\infty$, $\theta\geq0$. We will denote the z interval by l and the θ interval by h, so that the grid points are located at

$$z=kl, \quad k=0,\pm1,\pm2,\cdots,$$
$$\theta=jh, \quad j=0,1,2,\cdots.$$

The values of the dependent variables τ, y, and m at a particular grid point will be denoted by subscripts, e.g.,

$$\tau_{k,j}=\tau(kl,jh).$$

In deciding on a suitable difference equation system with which to replace (II), the initial and boundary conditions to be satisfied must be taken into account. Since immediately following the release of heat the derivatives in the neighborhood of $z=0$ are very large,[4]

[4] See Appendix I, Part I.

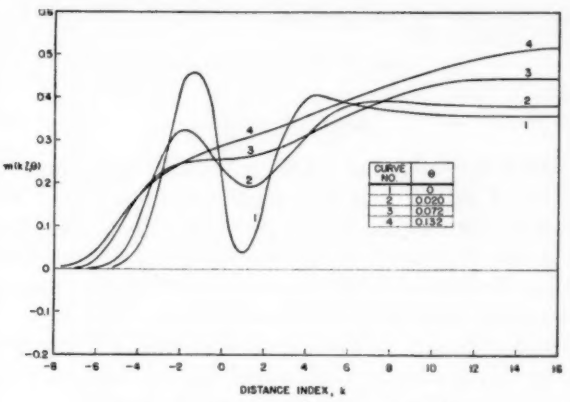

FIG. 5. Mass-flow perturbation behavior. Numerical solution, Case No. 3.

a modification must be made in order to start a numerical solution. The modification consists of assuming that the heat source is released at a small negative value of time $\theta=-D\eta_0$, and that at $\theta=0$ the solution of (II) is given by

$$\tau(z,0)=\exp(-z^2/4\eta_0),$$
$$y(z,0)=0. \quad (10)$$

It has been shown[4] that these represent correct solutions provided the constant coefficient equation applies for $-D\eta_0\leq\theta\leq0$ and the spatial region involved, and the heat source density q is correctly chosen. The choice of η_0 is determined so that the initial derivatives of $\tau(z,0)$ can be approximated numerically with good accuracy and will depend on the value of the space interval l. The boundary conditions appropriate to the heat source are that $\tau\to0$ and $y\to0$ as $z\to\pm\infty$ and $m\to0$ as $z\to-\infty$.

Returning to the system (II), we substitute the value of τ_θ given by (8) into (7). The resulting equation is of the form

$$m_z+bm=F(\tau_{zz},\tau_z,\tau,y), \quad (11)$$

where $b=b(z)=a_5/a_4a_7$, is a known function of z, and F is a linear function of its arguments involving the coefficients $a_i(z)$, $i=1,2,3,4,6,7$. Then if $\tau(z,jh)$ and $y(z,jh)$ are known for any fixed value, $\theta=jh$, this is an ordinary first-order equation for $m(z,jh)$. The remaining

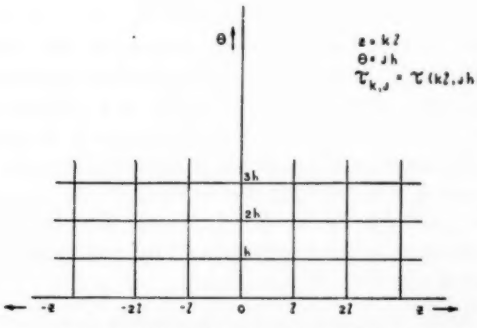

FIG. 6. Distance-time grid used in numerical integration of complete system.

Eqs. (8) and (9) are written

$$\tau_\theta = g(F,m) \equiv a_7[F - bm], \tag{12}$$

and

$$y_\theta = G(y_z, y, \tau, m). \tag{13}$$

Since the values of $\tau(z,0)$ and $y(z,0)$ are given, the value of $m(z,0)$ can be calculated from (11). This permits the calculation of the time derivatives from (12) and (13) and thus the values of $\tau(z,h)$ and $y(z,h)$ along the line $\theta = h$. The process can thus be repeated for any desired number of time intervals, $j = 1, 2, 3, \cdots$.

It is necessary to evaluate the functions F and G in terms of the values of the variables τ, y, and m at the grid points. This is done by approximating each of the variables with a 4th degree polynomial,[5] so that, for example, the derivatives τ_z and τ_{zz} at $z = kl$ are given in terms of the five quantities τ_{k-2}, τ_{k-1}, τ_k, τ_{k+1}, τ_{k+2}. The function g is defined by (12) and is evaluated using F and m, when the latter has been found from (11). We denote the values of F, g, and G obtained in this way at the point (kl, jh) by $F_{k,j}$, $g_{k,j}$, and $G_{k,j}$.

The integration of (11) is accomplished by the implicit use of Simpson's rule,[6] while (12) and (13) are replaced by the simplest difference equation in the variable θ. The resulting system of difference equations corresponding to (II) is given by

$$m_{k+1,j} = \frac{1}{3 + lb_{k+1}}[l(F_{k-1,j} + 4F_{k,j} + F_{k+1,j}) + (3 - lb_{k-1})m_{k-1,j} - 4lb_k m_{k,j}], \tag{14}$$

(IV)

$$\tau_{k,j+1} = \tau_{k,j} + hg_{k,j}, \tag{15}$$

$$y_{k,j+1} = y_{k,j} + hG_{k,j}. \tag{16}$$

The explicit expressions for b_k, $F_{k,j}$, $g_{k,j}$, and $G_{k,j}$ in terms of the coefficients $a_i(kl)$ and the values of τ, y, and m at the appropriate grid points are given in the Appendix.

In applying these equations we must deal with a finite z interval although the boundary conditions are actually specified at $z = \pm\infty$. Starting with the known initial values $\tau_{k,0}$ and $y_{k,0}$, the values of $m_{k,0}$ are found from (14), starting at $k = -N$ with

$$m_{-(N+1),0} = m_{-(N+2),0} = 0.$$

Equation (14) is applied repeatedly until the values $m_{k,0}$, $-N \leq k \leq N$, have been obtained. Simultaneously, Eqs. (15) and (16) are used to give $\tau_{k,1}$ and $y_{k,1}$ for the same z interval. The positive integer N is chosen sufficiently large so that within a permissible error we can let $\tau_k = y_k = m_k = 0$ for $k = -N-2$, $-N-1$, $-N$, and $\tau_k = y_k = 0$ for $k = N$, $N+1$, $N+2$. The boundary conditions at $\pm\infty$ are thus replaced by equivalent conditions at $k = \pm N$.

[5] W. E. Milne, *Numerical Calculus* (Princeton University Press, Princeton, New Jersey, 1949), p. 97.
[6] See reference 5, p. 135.

The numerical process thus consists of moving from left to right in Fig. 6 along a fixed time line, and moving upward line by line for increasing time. With the provision that the value of N may be increased as required, the process can be continued until the question of the growth or decay of the initial disturbance is definitely decided.

The replacement of the system (II) by the finite difference Eqs. (IV) introduces certain errors which may, in some cases, build up and lead to unstable (in particular, oscillating) numerical solutions even though the system (II) is itself stable.[7] For the variable coefficient parabolic equation

$$-\tau_{zz} + 2B\tau_z + c\tau + D\tau_e = 0,$$

namely, the approximate temperature perturbation equation, it has been shown[8] that stability of the numerical method depends on the ratio of the difference steps h and l. In particular, if D_m is the minimum value of $D(z)$, we require for computational stability that

$$\frac{h}{l^2} \leq \frac{D_m}{2}. \tag{17}$$

The largest value of l which can be used is determined by the truncation errors in the Simpson integration formula and the polynomial approximation. These errors will be proportional to $l^4 f^{(5)}(z)$, where $f^{(5)}(z)$ is the fifth derivative of the function approximated. The value of the allowable truncation error and an estimate of the maximum value of $f^{(5)}(z)$ will determine l.

Although the actual system (II) is more complicated than that used to get (17), this simple relation for h proved satisfactory. In the numerical cases carried out, a value close to the maximum permissible value of $h = l^2 D_m/2$ was used with no trouble because of computational instability of the finite difference approximation. The use of the 4th degree as compared to a lower-degree polynomial approximation permitted a larger value of l to be used for a specified truncation error. In view of the relation (17), the number of grid points and, therefore, the cost of the computation will vary inversely as l^3, so that the additional complication of the 4th degree polynomial is well worth while.

4. SOLUTION FOR TYPICAL CASES

The method of the preceding section will now be applied to the steady-state solution obtained in Sec. 2. The coefficients $a_i(z)$ are evaluated at the grid points $z = kl$ using the previously given definitions[9] of these coefficients and the steady-state values of ϕ and Y as functions of z. The coefficients obtained in this manner are given in Table I.

[7] O'Brien, Hyman, and Kaplan, J. Math. Phys. **29**, 223-51 (1951).
[8] F. John, Commun. Pure Appl. Math. **5**, 155–211 (1952).
[9] See Sec. 3, Part I.

TABLE I. Coefficients for complete system (II), case No. 2.

k	a_1	a_2	a_3	a_4	a_5	$a_6=a_9$	a_7	a_8	a_{10}	a_{11}
$k\leq -7$	0.077	0.015	0	0.110	0.080	0	1.000	1.000	0	0
−6	0.077	0.010	−0.005	0.110	0.144	0	1.000	1.000	0	0
−5	0.129	0.019	−0.025	0.115	0.256	0	2.008	1.417	0	0
−4	0.202	0.032	−0.073	0.119	0.419	0	3.641	1.908	0	0
−3	0.300	0.051	−0.211	0.125	0.670	0.064	6.180	2.486	−0.152	0.064
−2	0.426	0.093	−0.502	0.132	0.977	0.313	9.866	3.141	−0.428	0.307
−1	0.573	0.176	−0.782	0.138	1.254	0.878	14.661	3.829	−0.692	0.821
0	0.731	0.294	−0.895	0.145	1.452	1.724	20.286	4.504	−0.795	1.466
1	0.882	0.429	−0.848	0.151	1.521	2.665	26.030	5.102	−0.748	1.987
2	1.022	0.572	−0.727	0.156	1.495	3.662	31.708	5.631	−0.631	2.289
3	1.147	0.711	−0.581	0.161	1.292	4.409	36.966	6.080	−0.495	2.337
4	1.255	0.839	−0.444	0.165	1.224	5.053	41.693	6.457	−0.370	2.169
5	1.337	0.930	−0.335	0.167	1.129	5.578	45.374	6.736	−0.289	2.008
6	1.417	1.040	−0.253	0.170	0.882	6.061	49.000	7.000	−0.201	1.638
7	1.480	1.115	−0.193	0.173	0.739	6.350	51.700	7.190	−0.155	1.400
8	1.520	1.175	−0.146	0.175	0.605	6.600	54.020	7.350	−0.115	1.100
9	1.560	1.225	−0.105	0.175	0.480	6.800	55.800	7.470	−0.080	0.850
10	1.580	1.265	−0.073	0.176	0.369	7.000	56.850	7.540	−0.050	0.630
11	1.605	1.300	−0.047	0.176	0.270	7.120	57.610	7.590	−0.030	0.400
12	1.620	1.320	−0.025	0.176	0.181	7.200	58.370	7.640	−0.010	0.250
13	1.630	1.335	−0.010	0.176	0.112	7.250	58.980	7.680	−0.002	0.150
14	1.640	1.350	−0.001	0.176	0.060	7.349	59.290	7.700	0	0.050
15	1.645	1.360	0	0.177	0.021	7.349	59.600	7.720	0	0
$k\geq 16$	1.645	1.371	0	0.177	0	7.349	59.800	7.733	0	0

A spatial range of $-3.185\leq z\leq 5.211$ was used, based on the size of the interval in which the $a_i(z)$ were nonconstant. Consideration of the truncation errors led to dividing this into 30 intervals of length $l=0.2895$ each, so that the index k runs from $k=-11$ to $k=18$ in traversing the spatial range of interest. The minimum value of $D(z)$ occurs for large positive z, namely, $D_m=0.108$, so that the maximum value of h as given by the inequality (17) is $h=0.0045$. The value of $h=0.002$ was used at the start of the integration when τ_θ has its maximum value, and was increased to $h=0.004$ after a suitable number of time steps.

The numerical integration of the complete system (II) using the values of the $a_i(kl)$ in Table I was obtained by the method of the previous section, starting with the initial condition (10) with $\eta_0=l^2=0.0838$. We denote this as case No. 2. It was found that this case was apparently unstable, but was so close to the stability limit that the amount of computation required for a definite decision would have been excessive. The numerical solution was carried out to a value of $\theta=0.072$ and the results are presented in Figs. 1 and 3. On the basis of these results the values of $S=2.625$, $D=0.231$, and $B=0.388$ were obtained for the approximate solution $u(z,\theta)$. The predicted minimum point is $\theta_m=0.171$, so that the computation would have to be carried out at least to $\theta=0.20$ to give a definite answer. The continuation as given by the approximate solution $u(0,\theta)$ is shown in Fig. 3.

In view of this it was very desirable to treat a case for which instability could clearly be shown in the numerical solution of the complete system. Based on the approximate solution this should be accomplished most easily by making the average value of $a_3(z)$ more negative, thereby increasing the value of S. This was done by simply doubling a_3 and using a new value of $a_3'(z)=2a_3(z)$ with all other $a_i(z)$ unchanged. This is called case No. 3. Physically, this might correspond to a doubling of the activation energy or a lowering of the average flame temperature, keeping in mind, however, that such changes would alter the steady-state solution and, therefore, would cause changes in some or all of the other $a_i(z)$.

Since the a_3 term represents the largest contribution to $S(z)$ in the central zone, the value of $S(z)$ is also approximately doubled in this zone.[10] Thus it is to be expected that the new value $S'\cong 2S$, and that the minimum point for $\tau(0,\theta)$ should occur in half the time previously required. These expectations were fulfilled and the computation was carried far enough past the minimum point $\theta_m=0.072$ to show clearly that the system is unstable. The results are shown in Figs. 2, 3, 4, and 5. The corresponding values in the approximate solution are $S=5.22$, $D=0.284$, and $B=0.354$.

Certain interesting features of the mass-flow perturbation m and the concentration perturbation y are brought out by Figs. 4 and 5. Figure 5 shows how the mass flow increases as the gas passes through the reaction zone. Because of the transient heating and the resulting density decrease, the amount of gas flowing out of the reaction zone is greater than that flowing in. Because of Eq. (8), for large positive z the quantity m represents a weighted spatial average of the time rate of change of τ over the reaction zone. Figure 5 shows clearly how this average value of τ_θ is increasing with time for case No. 3.

In Fig. 4, it is shown that y remains small throughout the time interval considered. Since we have $|y|<0.055$, the effect of the last term in Eq. (7) will be small com-

[10] See Fig. 5, Part I.

pared to the other terms. The direct effect of the concentration perturbation is, therefore, small. The fact that y becomes negative on passing through the reaction zone is a result of the increased mass flow just discussed.

The excellent agreement between $u(z,\theta)$ and $\tau(z,\theta)$ for case No. 3 is shown in Figs. 2 and 3 and indicates that the approximate solution is quite good if S and D are properly chosen. A good idea of the behavior of a stable case is given by the analytic solution for $C=0$ shown in Fig. 3 and previously denoted as case No. 1.[11] Since the detailed solution for a stable case does not have as great interest as the unstable case, it was not felt worth while in this initial investigation to carry out a numerical solution for a system which was definitely stable.

A few brief remarks should be made on the actual method by which the numerical work was carried out. The computations were done using an automatic digital computer, the IBM Card Programmed Calculator.[12] The calculations required by the difference equations (IV) are carried out at electronic speed. The instructions, the coefficients, and the required values of τ, y, and m are taken from cards which are fed through the machine at approximately 90 cards per minute. Forty-four cards are required for the calculations at a given grid point, namely, at the point (k,j), the computation of $m_{k,j}$, $\tau_{k,j+1}$, and $y_{k,j+1}$. Thus, for any given time cycle a deck of 1320 cards is required for a spatial traverse of 30 points. Approximately 15 minutes is required for such a traverse.

The same deck of 1320 cards is used repeatedly, it being necessary to replace the 30 cards containing the values $\tau_{k,j}$ and $y_{k,j}$ by the new values $\tau_{k,j+1}$ and $y_{k,j+1}$ before proceeding to the next time cycle. This replacement operation is done automatically by means of a standard collating machine. An estimate of the cost of a computation can easily be obtained on the basis of a nominal figure of \$25 an hour for machine time. Assuming no wasted effort (a very optimistic assumption) an integration like those carried out here can be performed for about \$300.

[11] See also Fig. 2, Part I.

[12] International Business Machines, "The Card-Programmed Electronic Calculator," Form No. 22-8686-1, New York (1951).

ACKNOWLEDGMENT

The author wishes to thank Mr. R. Goerss, Forrestal Research Center, Princeton University, for assistance in programming for the machine computation.

APPENDIX

The details of the difference equations (IV) used for the numerical solution of the system (II) are as follows. The system (II) is written in the form

$$m_z+bm=F, \tag{11}$$

$$\tau_\theta=g, \tag{12}$$

$$y_\theta=G, \tag{13}$$

where

$$b=\frac{a_5}{a_4a_7}, \quad g=a_7[F-bm],$$

$$F=\frac{1}{a_4a_7}[a_1\tau_{zz}-a_2\tau_z-a_3\tau-a_6y],$$

$$G=-[a_8y_z+a_9y+a_{10}\tau+a_{11}m].$$

The corresponding functions in the difference system (IV) are given by

$$b_k=\frac{a_5}{a_4a_7},$$

$$g_{k,j}=a_7[F_{k,j}-b_km_{k,j}],$$

$$G_{k,j}=-\frac{a_8}{12l}[y_{k-2,j}-8y_{k-1,j}+8y_{k+1,j}-y_{k+2,j}] - a_9y_{k,j}-a_{10}\tau_{k,j}-a_{11}m_{k,j},$$

$$F_{k,j}=\frac{1}{12l^2a_4a_7}[d_1(kl)\tau_{k-2,j}+d_2(kl)\tau_{k-1,j}+d_3(kl)\tau_{k,j} +d_4(kl)\tau_{k+1,j}+d_5(kl)\tau_{k+2,j}]+d_6(kl)y_{k,j},$$

where

$$d_1(kl)=-a_1-la_2 \qquad d_2(kl)=16a_1+8la_2$$

$$d_3(kl)=-30a_1-12l^2a_3 \qquad d_4(kl)=16a_1-8la_2$$

$$d_5(kl)=-a_1+la_2 \qquad d_6(kl)=-\frac{a_6}{a_4a_7}.$$

All of the quantities $a_i(z)$ above are evaluated at $z=kl$.

Letters to the Editor

THIS section will accept reports of new work, provided these are terse and contain few figures, and especially few half-tone cuts. The Editorial Board will not hold itself responsible for opinions expressed by the correspondents. Contributions to this section should not exceed 600 words in length and must reach the office of the Editor not later than the 15th of the second month preceding that of the issue in which the Letter is to appear. No proof will be sent to the authors. A publication charge of $10.00 per Letter is made which, when honored, will entitle the Institution to 100 free reprints.

Anomalous Rotatory Dispersion of Quartz Above 3.7μ?

C. D. WEST
Polaroid Corporation, Cambridge, Massachusetts
(Received June 22, 1953)

GUTOWSKY[1] concluded that quartz exhibits a real anomalous rotatory dispersion beginning at 3.68μ and extending up to the limit of his measurements at 9.71μ (see Fig. 1). These were made with a Perkin-Elmer 12B (single) monochromator through crystal sections about 25 mm thick. We question whether the observations were correctly interpreted in arriving at this conclusion on the following grounds.

The relative energy in each wavelength interval transmitted by a basal quartz section of thickness t can be calculated approximately from the relation

$$I/I_0=\exp(-K_0t).$$

The absorption constant K_0 for the ordinary ray through quartz was measured by Drummond[2] for the range 1–7.5μ, and by Stein[3] for the adjoining range 7.5–20.0μ. These curves are also shown in the figure where the unit of K_0^{-1} and t is taken as one mm.

In the equation, since we know t and can estimate from experience a value of I/I_0 below which polarimetric settings become questionable or meaningless, we can solve for the corresponding level of K_0 after introducing these two numerical values. By taking logarithms once, we have

$$K_0=\ln(I_0/I)/t$$

and again (since the graph is logarithmic in K_0)

$$\log K_0=\log\log(I_0/I)-\log t+\log\ln 10,$$

which equals

$$\log\log(I_0/I)-1.036$$

for $t=25$ mm and $\log\ln 10=0.3622$.

Taking into account the slit widths shown by Gutowsky, the further loss of energy in the two polarizers, and other pertinent facts, we consider an I/I_0 of 10^{-3} to be a generous estimate for the relative energy required. The K_0 corresponding to this energy is 0.276 mm^{-1}, and the $\log K_0$ is -0.559. This level of K_0 is shown on Fig. 1 as Level A. To take the argument to an absurdity, we would only need to select an I/I_0 of 10^{-6}, an amount of energy far below the capacity of the Perkin-Elmer instrument, and get a relatively small rise of $\log K_0$ to the -0.258 level.

The conclusion from a study of the figure is that, above about wavelength 4μ, Gutowsky has insufficient spectrally pure energy to make significant polarimetric settings for the section thickness in question. Further, since he does not mention steps to exclude stray radiations from reaching the detector we conclude that the rotation constants, reported from 9.71μ down to some wavelength around 4μ, all certainly correspond to spectrally indeterminate stray radiations, in this case comprising wavelengths shorter than those indicated. The figure shows an interesting similarity in the trends of the apparent rotation constant and the actual absorption constant in the interval 3.68 to 4.13μ. Since this anomalous trend of the apparent rotation constant could here also reflect effects of stray radiations, the reported constants in this range invite confirmation before they can claim an unreserved acceptance.

The previous measurements of the quartz rotation constant by Lowry and Snow[4] were made essentially with a double monochromator (prism and grating in series) with a very thick crystal section of 495 mm. For the same I/I_0 of 10^{-3} the K_0 level for this section comes out 0.0138, or a log K_0 of -1.86. This level (B) is also shown in Fig. 1, together with a few of the numerous reported points which are seen to agree tolerably with those of Gutowsky. Lowry and Snow could not get enough radiation through their

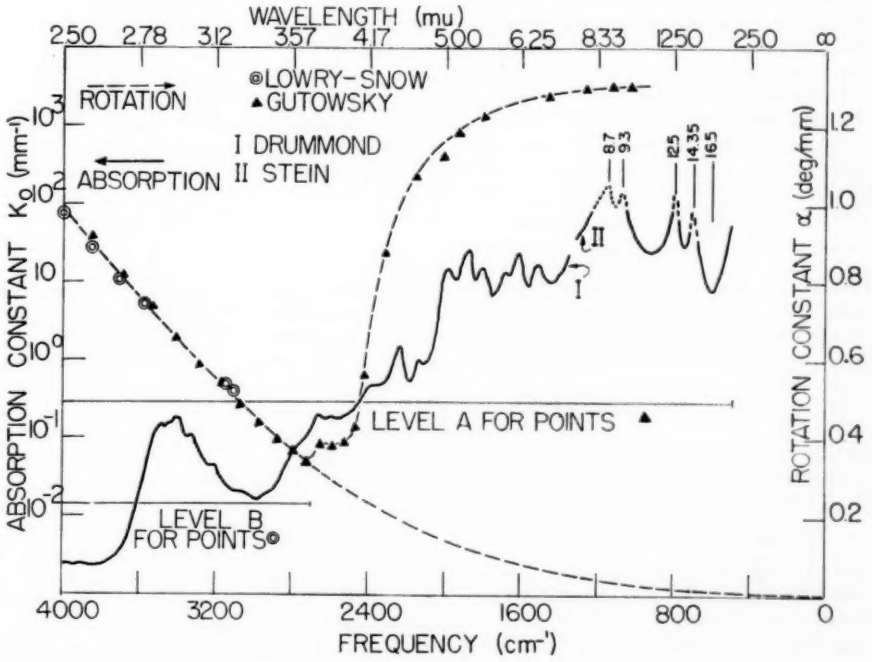

FIG. 1. Superposition of two independent sets of absorption constants, two independent sets of rotation constants, and levels of $I/I_0=10^{-3}$ for the two quartz sections used for the rotation measurements.

system between 2.79 and 3.18μ, nor above 3.21μ, to detect. These three points are included on the figure because in our opinion they lend independent support to our argument.

It is also pertinent to recall the rotation measurements of Ingersoll, Rudnick, Slack, and Underwood[5] for the tetragonal $NiSO_4 \cdot 6H_2O$ crystal in the neighborhood of the vibration band of the water molecule at 2.0μ, where the absorption constant rises to nearly 10 mm^{-1}. The thicker crystals examined show an apparent anomaly of the rotation curve through this band, similar in character to that of Gutowsky; but the "anomaly" substantially disappears when a thin crystal with a transmission of 10 percent at the band peak is measured. The authors conclude that the 1.5 and 2.0μ vibrational bands of water, "as expected, make no appreciable contribution to the rotatory power" of the crystal. Their measurements extend to 2.2μ.

In conclusion, we believe that the rotation of quartz is reliably known only up to and including Gutowsky's value of 0.34 ± 0.02 deg/mm at 3.676μ. A long extrapolation through this point to the expected zero at zero frequency is included in Fig. 1. We recommend a level diagram of the kind illustrated here as a method for testing the plausibility of measurements of any property of specularly transmitted radiation such as rotation or ellipticity.

This work was supported by contract with the U. S. Office of Naval Research and was lightened through the cooperation of my associates A. S. Makas and L. Baxter, II.

[1] H. S. Gutowsky, J. Chem. Phys. **19**, 438 (1951).
[2] Drummond, Proc. Roy. Soc. (London) **A153**, 318 (1936).
[3] Stein, Ann. Physik **36**, 462 (1939).
[4] Lowry and Snow, Proc. Roy. Soc. (London) **A127**, 271 (1930).
[5] Ingersoll, Rudnick, Slack, and Underwood, Phys. Rev. **57**, 1145 (1940).

Combustion Wave Stability and Flammability Limits*

J. B. ROSEN
The James Forrestal Research Center, Princeton University, Princeton, New Jersey
(Received December 15, 1953)

IT has been shown[1] that an essentially thermal instability of s.s. (steady-state) solutions to equations for a laminar combustion wave can occur. A simplified stability condition has now been obtained[2] which permits investigation of stability as a function of fundamental physical parameters. This condition is used here to determine the region of stability in the parameter space of a model flame-propagating medium with simple kinetics.

In the general case[1] the complete time-dependent equations are linearized about their s.s. solution, and the stability of the system is determined for certain initial perturbations. Here, only the linearized one-dimensional energy equation is considered, and further, only terms involving the temperature perturbation τ. This gives the parabolic equation

$$-\tau_{zz}+2B\tau_z+C\tau+D\tau_\theta=0; \tag{1}$$

z and θ are dimensionless variables representing distance and time, respectively, in a coordinate system fixed in the s.s. flame.[3] The time dependence of τ is given by $\exp(-\delta\theta)$, where δ is an eigenvalue of (1) such that $\tau \to 0$ as $z \to \pm\infty$. Thus, Eq. (1) is stable if, and if, we have $\delta \geq 0$ for all eigenvalues δ.

This eigenvalue problem can be transformed so as to be formally equivalent to the one-dimensional Schrödinger equation for a particle in a potential field V. The transformation is accomplished by letting $\tau=\Psi \exp[-\delta\theta+\int_0^z P dz]$, $\xi=B_\infty \int_0^z (D/D_\infty)^{\frac{1}{2}} dz$, and $P=B-(D_z/4D)$. Then (1) becomes

$$\Psi_{\xi\xi}+[\delta-V(\xi)]\Psi=0, \tag{2}$$

where $V=(D_\infty/B_\infty{}^2D)[B^2+C-P_z-(D_z{}^2/16D^2)]$. The shape of the "potential function" $V(\xi)$ completely determines the eigenvalues δ; two typical examples are shown (Fig. 1). A simple and useful procedure is to approximate $V(\xi)$ by a square-well potential in the manner shown by the dashed line. An explicit solution of (2) for the square potential is known,[4] and leads to the condition that the s.s. solution is stable if, and only if

$$2la^{\frac{1}{2}} \leq \tan^{-1}(1/a)^{\frac{1}{2}}+\tan^{-1}(b/a)^{\frac{1}{2}}, \tag{3}$$

where a, b, and l are defined in Fig. 1.

This condition has been applied to solutions of a s.s. system with a reaction rate $\Re = k(1-Y)\phi^{-1}\exp(-\sigma/\phi)$, and an enthalpy linear in T and Y.[5] This leads to the s.s. equation

$$dY/d\phi = P/\beta Q, \tag{4}$$

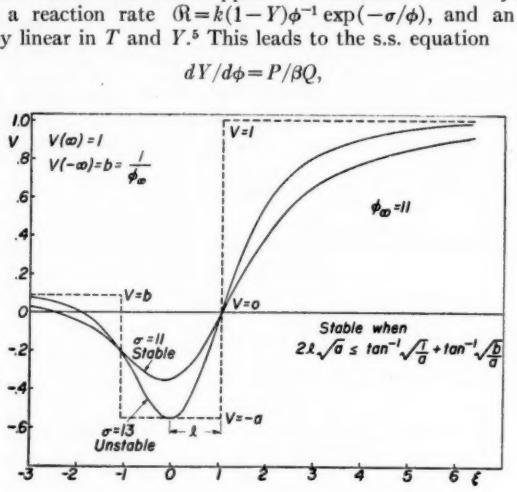

FIG. 1. Two typical functions $V(\xi)$ and the square-well approximation for $\sigma = 13$.

where $P=\Re/k\phi$, $Q=(\phi-1)-(\phi_\infty-1)Y$, and β is the eigenvalue to be determined. This system is completely determined by the parameters σ and ϕ_∞. Values of V and ξ for this system are given by $V\phi_\infty=\phi-(4/\beta)(\phi_\infty-1)[(\sigma/\phi)-2]P$ and $2\xi=\int_{\phi_i}^{\phi}(\phi_\infty/\phi)^{\frac{1}{2}}Q^{-1}d\phi$. Numerical solutions of (4) were obtained using an IBM card-programmed calculator, and β and the corresponding $Y(\phi)$ calculated for points throughout the σ, ϕ_∞ plane. For each point the function $V(\xi)$ was computed and the stability condition (3) applied, with the result shown (Fig. 2). The σ,ϕ_∞ plane is divided into two regions: solutions corresponding to points in the upper left region are unstable, those in the lower right stable. The boundary between these two regions is the stability limit.

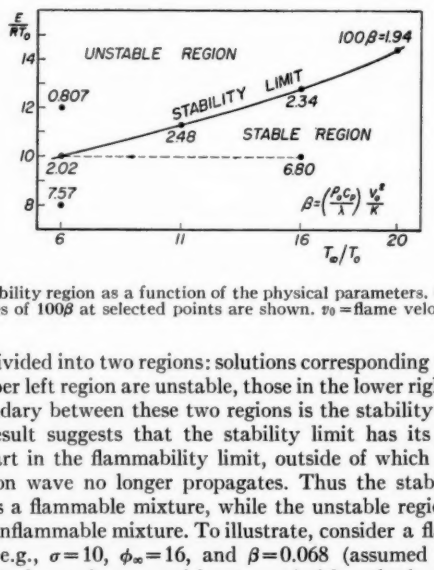

FIG. 2. Stability region as a function of the physical parameters. Computed values of 100β at selected points are shown. v_0 = flame velocity.

This result suggests that the stability limit has its physical counterpart in the flammability limit, outside of which a steady combustion wave no longer propagates. Thus the stable region represents a flammable mixture, while the unstable region represents a nonflammable mixture. To illustrate, consider a flammable mixture, e.g., $\sigma=10$, $\phi_\infty=16$, and $\beta=0.068$ (assumed stoichiometric). A change in composition toward either the lean or rich limits causes a lowering of the adiabatic flame temperature T_∞. Eventually the stability (flammability) limit is reached as shown at $\phi_\infty=6$ if σ is assumed unchanged. Flame velocity, as represented by β, decreases during this process in agreement with the physical fact.[6]

Direct comparison with experiment will require introduction of

more detailed kinetics. However, a simple model, as here presented serves to explore the general outlines of flame stability behavior.

* This research was supported by the United States Air Force under contract No. AF 33(038)-23976 monitored by the Office of Scientific Research.

[1] J. B. Rosen, J. Chem. Phys. **22**, 733 and 743 (1954).

[2] This result is based largely on very helpful suggestions made by Professor John von Neumann, Institute for Advanced Study, Princeton, New Jersey.

[3] The coefficients $B>0$, $D>0$, and C are determined by the s.s. solution and are functions of z only. $-C$ is approximately the temperature derivative of the reaction rate and $\to 0$ as $z\to\pm\infty$ ($z=0$ at s.s. temperature inflection point with gas flow from $-\infty$ to $+\infty$).

[4] L. I. Schiff, *Quantum Mechanics* (McGraw-Hill Book Company, Inc., New York, 1949), Section 9.

[5] In this, T = temperature, Y = product concentration, k = rate constant, $\phi=T/T_0$, $\sigma=E/RT_0$, and the subscript zero and ∞ refer to cold and hot conditions, respectively.

[6] It should be noted that the limit occurs at a nonzero value of flame velocity.

Thermodynamics of the Hydrogenation of Benzene

GEORGE J. JANZ
Walker Laboratory, Department of Chemistry, Rensselaer Polytechnic Institute, Troy, New York

(Received February 8, 1954)

THE hydrogenation of benzene in addition to the direct over-all reaction a to cyclohexane may be regarded as proceeding in three steps b, c, d, one for each mole of hydrogen added. Qualitative calculations on the equilibria in these systems

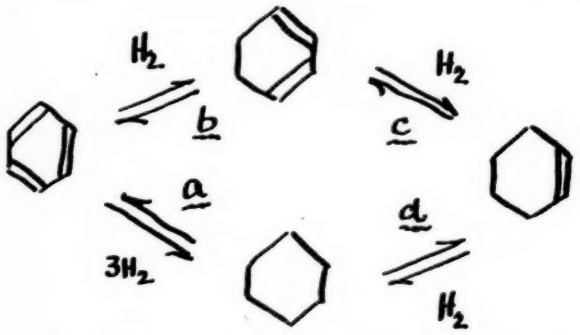

at 600°K have been reported by Taylor,[1] and direct experimental measurements of the over-all reaction equilibrium, by Burrows and Lucarni,[2] and Zharkov and Frost.[3] In the present communication these are re-examined in the light of more recent thermodynamic data.

For benzene and cyclohexane, the thermodynamic data are well established.[4] The statistical thermodynamic functions[5] and experimental heat capacities[6,7] for cyclohexene have also been reported.

The heat of combustion of cyclohexene has been recently measured by Pergiel and Prosen.[8] Using these data [$\Delta H_C°$ (25°C) (liquid), -896.20 ± 0.17 kcal/mole, $\Delta H_f°$ (25°C) (liquid), -9.70 ± 0.19] and the heat of vaporization[9] corrected to the present definition of the calorie, gives $\Delta H_f°$ (25°C) (gas), -1.72 ± 0.22 kcal/mole, for cyclohexene. A second value calculated from the heat of hydrogenation of cyclohexene to cyclohexane[10] is -1.2 ± 0.1 kcal/mole. Of the two values, the former has been used in the present work. For cyclohexadiene no recent heat of combustion data are available. Using the heat of hydrogenation of cyclohexadiene to benzene,[10] the heat of formation for cyclohexadiene, $\Delta H_f°$ (25°C) (gas), 25.6 ± 0.1 kcal/mole, was obtained.

The entropy of cyclohexadiene was estimated from that of cyclohexadiene.[5] An increment of 5.3 eu accompanies the hydrogenation of one double bond in aliphatic olefins (e.g., *cis*-butene-1,3-butadiene, $71.90-66.62=5.28$; *cis*-2-pentene-*cis*-1,3-pentadiene, $82.76-77.5=5.26$). Accordingly the entropy of cyclohexadiene (assuming a symmetry number of 2) is 68.9 eu. The heat capacities were calculated by the method of Dobratz[11] using the tables of bonding frequencies reported by Stull and Mayfield.[12]

TABLE I. Thermodynamic data for benzene, cyclohexadiene, cyclohexene, and cyclohexane.

	$\Delta H_{f298}°$ kcal/mole	$\Delta S_{298}°$ cal/deg/mole	$C_p=a+bT+cT^2$ (cal) a	$b\times10^3$	$c\times10^6$
Benzene	19.82	64.3	−3.54	90.37	−36.67
Cyclohexadiene-1,3	25.6	68.9	−1.35	97.6	−37.3
Cyclohexene	−1.72	74.2	−9.14	131.9	−57.1
Cyclohexane	−29.43	71.3	−12.46	143.2	−54.94

The thermodynamic data for benzene, cyclohexane, cyclohexene, and cyclohexadiene are listed in Table I. The free energy changes were calculated using the modified form of the van't Hoff Isochore,

$$\Delta F_T°=I_H+(\Delta a-I)T-\Delta aT\ln T-\tfrac{1}{2}\Delta bT^2-\tfrac{1}{6}\Delta cT^3,$$

where the constants I_H and I_s are evaluated from the data at 25°C, and Δ signifies $(p-r)$ for each property, and are summarized in Table II and Fig. 1. It follows that over the whole temperature range considered, cyclohexadiene is thermodynamically unstable relative to the other three compounds. The earlier prediction of

TABLE II. Change in free energy per molecule of hydrogen added in the hydrogenation of benzene.

Reaction	T°K 298.16	400	550	700	1000
			ΔF (kcal)		
a[a]	−23.40	−14.35	0.00	+13.62	+41.97
b	13.2	15.7	19.6	23.5	31.3
c	−17.9	−14.8	−10.2	−5.5	+4.2
d	−18.7	−15.2	−9.4	−4.4	+6.5

[a] For the over-all reaction, the free energy tables in reference 4 were used.

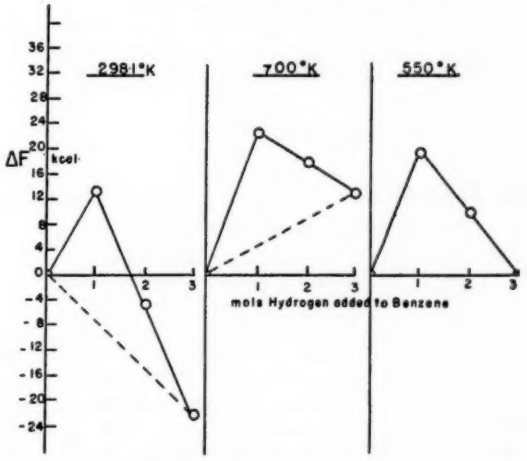

FIG. 1. Thermodynamic free energy change in the hydrogenation of benzene per molecule of hydrogen added.

Taylor at 600°K based on very qualitative calculations, is in accord with these results. It has been known experimentally for a long time that cyclohexadiene and cyclohexane react to form benzene and cyclohexane even by passage through heated tubes without any catalysts. It is clear from the thermodynamic conclusions that at moderately high temperatures, cyclohexadiene and cyclohexene could never be isolated, even in trace amounts in the hydrogenation of benzene.

A comparison of the results reported by Burrows and Lucarni[2] and Zharkov and Frost[3] by direct measurement in this temperature region with the values calculated using precise thermodynamic data is shown in Fig. 2. The free energy change, from the data of Burrows and Lucarni, is -23.43 kcal/mole at 25°C, whereas the value calculated thermodynamically is 23.40 kcal/mole. The agreement leaves little to be desired, especially in view of the various difficulties in the direct experimental measurement of equilibrium data.

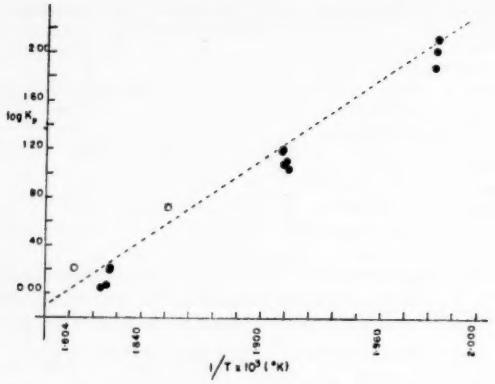

FIG. 2. Comparison of experimental data and thermodynamic values for the benzene-cyclohexane hydrogenation reaction at equilibrium. ○ G. H. Burrows and C. Lucarni, J. Am. Chem. Soc. **49**, 1157 (1927). ● V. R. Zharkov and A. V. Frost, J. Gen. Chem. U. S. S. R. **2**, 534 (1932). – – – – Values predicted themodynamically from data in reference 4.

The author thanks Dr. E. J. Prosen for his very helpful comments on these calculations, and for the most recent data on cyclohexene prior to publication.

[1] H. S. Taylor, J. Am. Chem. Soc. **60**, 627 (1938).
[2] G. H. Burrows and C. Lucarni, J. Am. Chem. Soc. **49**, 1157 (1927).
[3] V. R. Zharkov and A. V. Frost, J. Gen. Chem. U. S. S. R. **2**, 534 (1932).
[4] "Selected Values of Properties of Hydrocarbons," Circular Natl. Bur. Standards. C461, U. S. Dept. Commerce, Washington, D. C. (1947).
[5] Beckett, Freeman, and Pitzer, J. Am. Chem. Soc. **70**, 4227 (1948).
[6] Huffman, Eaton, and Oliver, J. Am. Chem. Soc. **70**, 2991 (1948).
[7] J. B. Montgomery and T. DeVries, J. Am. Chem. Soc. **64**, 2375 (1942).
[8] F. Y. Pergiel and E. J. Prosen, National Bureau of Standards Thermochemical Laboratory, unpublished data.
[9] J. H. Mathews, J. Am. Chem. Soc. **48**, 562 (1926).
[10] Kistiakowsky, Ruhoff, Smith, and Vaughan, J. Am. Chem. Soc. **58**, 137 (1936).
[11] C. Dobratz, Ind. Eng. Chem. **33**, 759 (1941).
[12] D. R. Stull and F. D. Mayfield, Ind. Eng. Chem. **35**, 639 (1943).

The Radical Pair Yield of Ionizing Radiation in Sulfuric Acid Solution*

EVERETT R. JOHNSON AND JEROME WEISS †
Chemistry Department, Brookhaven National Laboratory, Upton, Long Island, New York
(Received July 1, 1953)

SOLUTIONS of ceric sulfate in 0.8*N* H_2SO_4 were irradiated in the presence and absence of various gases under two different conditions: In one case the gases were constantly bubbled through the solution under irradiation (flow system), while in the other, the solutions were initially saturated with the gas (CO and air only) and then irradiated (static system). In both the flow and static systems Ce^{+4} analyses were performed; however, gas analyses were also done in the static system.

Flow system.—Ceric sulfate solutions (10^{-1}–10^{-3}M in 0.8*N* H_2SO_4) were irradiated in the presence of N_2, He, H_2, air, and CO, in a cylindrical CO^{60} source. Highest-purity tank gases were used when possible and these were further purified by passage through an appropriate gas train. Carbon monoxide, made by the method of Thompson,[1] was carefully purified and found to contain less than 0.5 percent of fixed gases (O_2, N_2, H_2) and no hydrocarbons, by mass spectrographic analysis. The gases were bubbled through the solution (flow rate 300 cc/min) during irradiation and the solution analyzed at various intervals. All solutions were carefully preflushed before irradiation. Since sources of different intensity were used, all results have been normalized to a constant dose rate of 3576±36μM of air sat $FeSO_4$ oxidized/hr. The results are summarized in Fig. 1. In the presence of CO or H_2 the rate of Ce^{4+} reduction was 1190±12.5μM/hr and 1202±μM/hr, respectively. In the presence of air, N_2, or He the rate of Ce^{4+} reduction was 601±6.1, 596±4.0, and 595±6.3 μM/hr, respectively.

Static system.—In Fig. 2 is summarized the rate of CO_2 formation obtained by irradiating solutions of 0.8*N* H_2SO_4 (with and without added Ce^{4+}) initially saturated with CO at 300–500m pressure, with hard x-rays (dose rate 234.5μM Fe oxid/1000 sec).

These solutions were prepared by variation in a method previously described.[2] The method consists essentially of saturating a

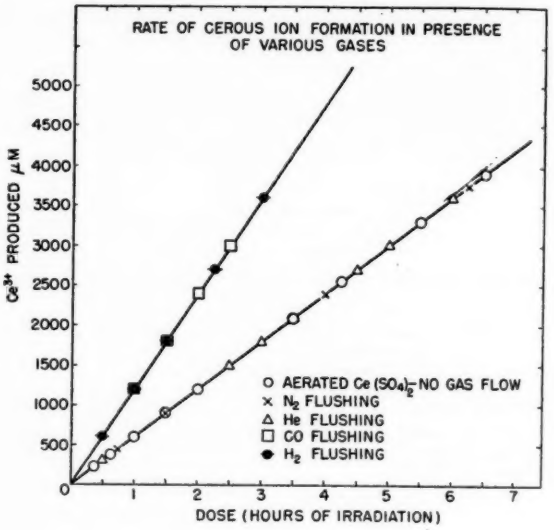

FIG. 1.

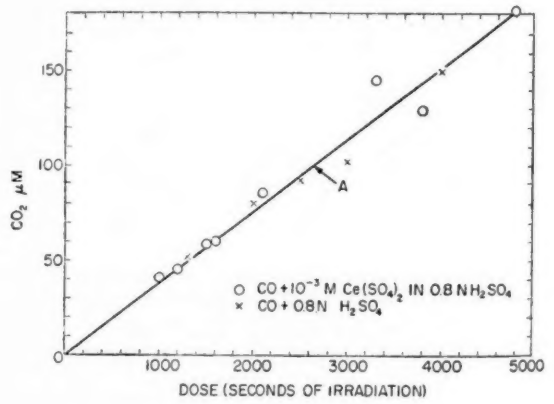

FIG. 2.

de-aerated solution with CO and pouring this solution into 10-cc bulbs sealed to a manifold with 4-mm heavy walled tubing, partially evacuating and then sealing off the bulbs. Curve A, Fig. 2 is the normal rate of ceric sulfate reduction (aerated and de-aerated mM solutions of $Ce(SO_4)_2$ in 0.8*N* H_2SO_4) and is equal to 38.0±1.9 μM Ce^{4+} reduced/1000 sec. The rate of CO_2 formation from all solutions was 38.3±1.8 μM/1000 sec. The rate of Ce^{4+} reduction in the presence of CO, in this system was 75.5±1.5 μM/1000 sec. These results indicate the following stoichiometry for the reduction of Ce^{4+} in the presence of CO:

$$H_2O+CO+2Ce^{4+}=2Ce^{3+}+CO_2+2H^+.$$

From these results it would appear that the molecular H_2O_2 formed in reaction (1) is either destroyed or does not exist as such. We believe that these data can be explained by assuming the following reactions:

$$2H_2O \rightarrow H_2+H_2O_2 \text{ (or } 2H_2+O_2) \quad (1)$$

$$H_2O \rightarrow H+OH \quad (2)$$

$$CO \text{ (or } H_2) + OH \rightarrow CO_2 \text{ (or } H_2O) + H \quad (3)$$

$$Ce^{4+} + H \rightarrow Ce^{3+} + H^+. \quad (4)$$

Reactions (1), (2), (4) occur in the aerated, de-aerated N_2 or He saturated solutions while (1)–(4) occur in the presence of CO or H_2. On the basis of this mechanism the radical pair yield is found to be 2.54/100 ev.

* Research carried out under the auspices of the U. S. Atomic Energy Commission.

† Health Physics Division, Brookhaven National Laboratory, Upton, Long Island, New York.

[1] J. G. Thompson, Ind. Eng. Chem. **21**, 389 (1929).

[2] E. R. Johnson and A. O. Allen, J. Am. Chem. Soc. **74**, 4147 (1952).

The Velocity of Sound in Hydrazine-Water Mixtures at 500 Kilocycles

GEORGE G. KRETSCHMAR
Michelson Laboratory, U. S. Naval Ordnance Test Station
Inyokern, China Lake, California

(Received January 29, 1954)

ULTRASONIC waves have been used to determine the sound velocities in a large number of liquids.[1] Such sound velocity determinations enable one to compute the adiabatic compressibilities of the liquids from the well-known relation $\beta = 1/\rho c^2$. Recently such sound velocity data have been used to determine the compressibilities of a number of rocket propellant liquids.[2,3] One of these, hydrazine, is of particular interest because it has a higher sound velocity than any of the 138 liquids listed in the table[1] in Bergman's book. The very high sound velocity in hydrazine and the fact that it is soluble in water in all proportions has made it desirable to measure sound velocities of hydrazine-water mixtures.

It has been shown that the freezing-point curve for the hydrazine-water system has two discontinuities at approximately 40 and 69 weight percent of hydrazine,[4] and the present experiment on hydrazine-water mixtures was undertaken partly to see if similar anomalies might appear in the velocity of sound data.

The sound velocities were obtained with an ultrasonic interferometer and associated electronic circuits which have been described in a previous publication.[3] The data were obtained by starting with a concentrated sample of hydrazine, which was poured into the interferometer with the whole operation carried on in a gloved box, under dry nitrogen. At the time of filling the interferometer, a sample was placed in a closed weighing bottle, and this was later used for obtaining the hydrazine concentration by the direct iodate method.[5] The velocity of sound was obtained for the contents of the interferometer, giving one point on the curve. The interferometer was then transferred back into the dry box, and the contents diluted to a previously calculated new dilution point, and the process repeated. In this way a large number of points were determined at different dilutions ranging from about 98 weight percent of hydrazine down to 5 percent.

The measurements were taken at a temperature of 25°C. This temperature was maintained by surrounding the interferometer with water pumped and circulated from a 30-liter tank in which the temperature was regulated by an electronic temperature control circuit.[6] The precision of the sound velocity measurements was a little better than one percent.

The data are plotted in Fig. 1, which gives the relation between the velocity of sound and various concentrations of hydrazine from 0 to 100 weight percent of hydrazine. It will be seen that the velocity of sound of the various hydrazine-water mixtures plotted against the concentrations form a smooth curve without the anomalies which occur in the freezing point curve. The freezing-point curve for the hydrazine-water system is given for comparison.

A large number of points were taken about the higher eutectic point (69 weight percent of hydrazine), and the data here show considerable scatter. It was noted that it was very difficult at times to get the interferometer to peak at this point. The tuning was broad and at times quite unreliable. This was attributed to small bubbles due to decomposition or cavitation. It may be that there is some sort of anomalous effect here, but the data taken so far are inconclusive. It is planned to repeat the experiment to check this point using redesigned equipment capable of higher precision.

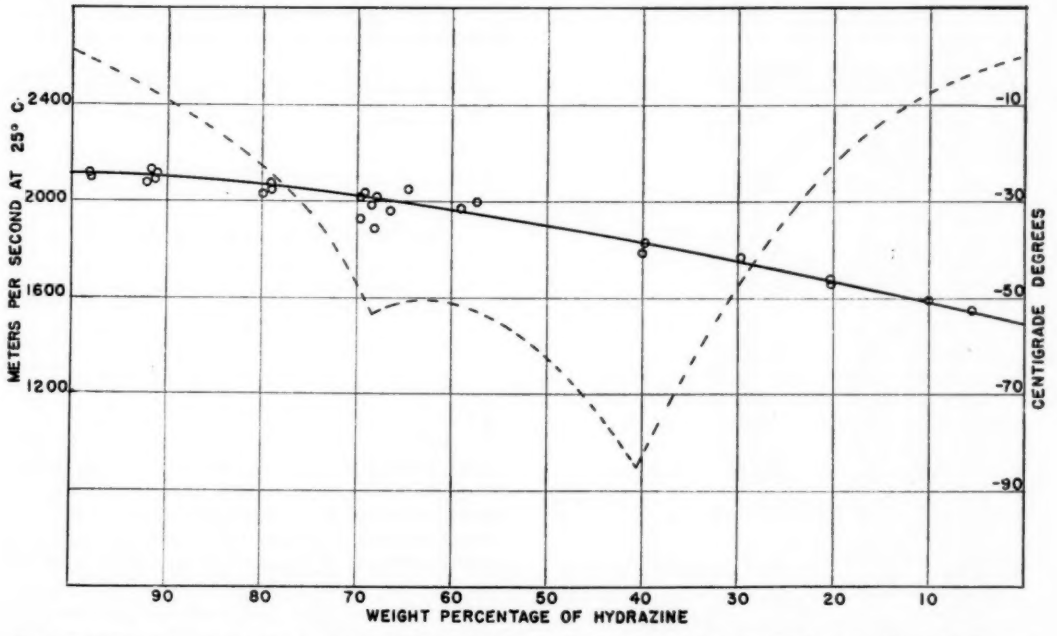

FIG. 1. Velocity of sound in hydrazine-water mixtures. Solid line—velocity of sound data. Broken line—freezing-point diagram.

[1] Ludwig Bergmann, *Der Ultraschall* (J. W. Edwards, Ann Arbor, Michigan, 1942), 3rd ed., p. 175.

[2] K. R. Stehling and A. A. Kovitz, Am. Rocket Soc. J. **23**, 374 (1953).

[3] George G. Kretschmar, Am. Rocket Soc. J. **23**, 82 (1953).

[4] T. C. H. Hill and J. F. Summer, J. Am. Chem. Soc. **838** (1951), Part I.

[5] L. F. Andrieth and Betty Ackerson Ogg, *The Chemistry of Hydrazine* (John Wiley and Sons, Inc., New York, 1951), p. 157.

[6] I. Sucher and H. S. Anker, Rev. Sci. Instr. **20**, 321 (1949).

Conversion of *Ortho-* to *Para*-Hydrogen in the Liquid Phase

G. L. SQUIRES * AND A. T. STEWART †
Cavendish Laboratory, Cambridge, England
(Received February 9, 1954)

ONE of the difficulties in the storage of liquid hydrogen is that the hydrogen converts spontaneously into the *para*-modification, and the heat evolved in the process increases the evaporation rate of the liquid. One solution of the problem is to convert the hydrogen into the *para*-form in the liquifier by means of a suitable catalyst.

In the course of an experiment[1] to measure the scattering cross section of *para*-hydrogen for slow neutrons, we have made *para*-hydrogen in the liquid phase on many occasions. Charcoal and oxygen were used to catalyze the conversion which was found to proceed exponentially. As our values for the half-life of the conversion differ markedly from those previously published,[2] a description of our method is given.

The apparatus used is shown in Fig. 1. Approximately 45 g of

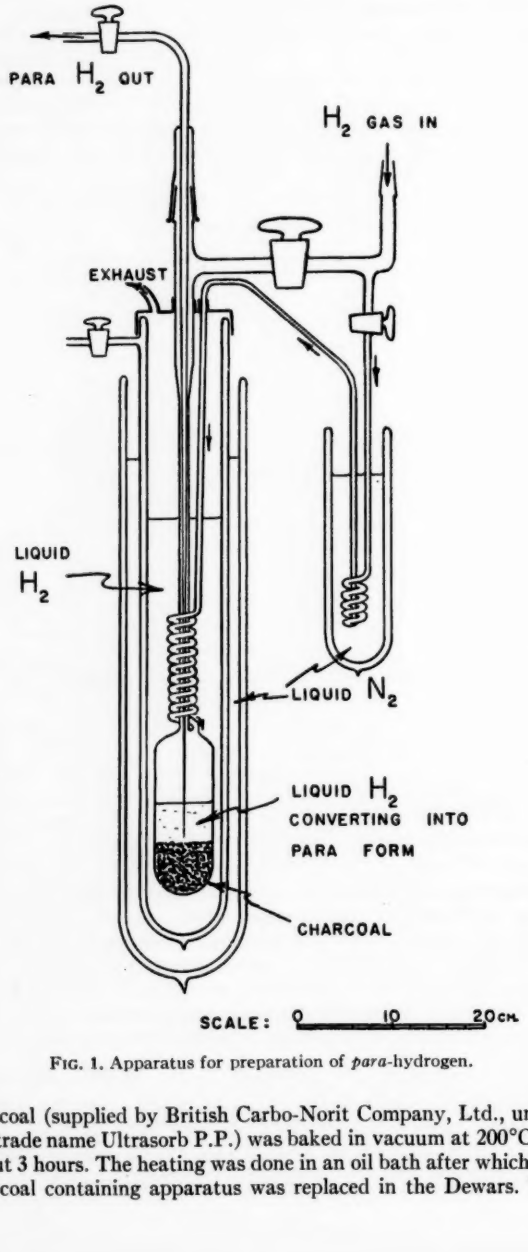

FIG. 1. Apparatus for preparation of *para*-hydrogen.

charcoal (supplied by British Carbo-Norit Company, Ltd., under the trade name Ultrasorb P.P.) was baked in vacuum at 200°C for about 3 hours. The heating was done in an oil bath after which the charcoal containing apparatus was replaced in the Dewars. The outer Dewar was then filled with liquid nitrogen. This precooled the charcoal through the "soft" inner Dewar. (The space between its walls contained air at a pressure of 2 mm). About 200 ml of oxygen at N.T.P. were admitted to the charcoal and the inner Dewar was then filled with 2 liters of liquid hydrogen.

Hydrogen gas, precooled in liquid nitrogen, was forced into the apparatus at a pressure sufficient to condense about 140 ml of liquid hydrogen in 20 minutes. The hydrogen gas flow was shut off and the rate of conversion of the isolated liquid hydrogen followed by the thermal conductivity method of *ortho-para* analysis.

Our value for the conversion half-life varied between 10 and 20 minutes, depending chiefly on the amount of oxygen added. When the conversion was carried out without adding oxygen, the other conditions being unchanged, the half-life was about 18 hours. The only other published data for the conversion in the liquid phase are those of Swenson.[2] With almost the same ratio of charcoal to liquid hydrogen, he obtained a value of 25 minutes for the conversion half-life, which is to be compared with our value of 18 hours. It is not thought likely that the discrepancy can be explained by the different charcoals that were used because we have measured the conversion rates for several different charcoals without oxygen and the half-lives have not differed by more than a factor of five. A possible explanation is that Swenson inadvertently exposed the charcoal to air and thereby increased its catalytic efficiency.

The catalytic efficiency of the charcoal plus adsorbed oxygen does not appear to change during the conversion. We concluded this from a measurement of the conversion rate of a second quantity of liquid hydrogen condensed on the charcoal after the first had been removed, the charcoal remaining at liquid hydrogen temperature. The conversion rates of both batches were the same.

* Now at Atomic Energy Research Establishment, Harwell, England.
† Now at Dalhousie University, Halifax, Nova Scotia, Canada.
[1] A. T. Stewart and G. L. Squires, Phys. Rev. **90**, 1125 (1953).
[2] C. A. Swenson, J. Chem. Phys. **18**, 520 (1950).

The Boron Arrangement in a B_6 Hydride

K. ERIKS AND WILLIAM N. LIPSCOMB, *School of Chemistry, University of Minnesota, Minneapolis, Minnesota*
AND
RILEY SCHAEFFER, *Department of Chemistry, Iowa State College, Ames, Iowa*
(Received February 12, 1954)

THE boron skeleton of a hydride containing six boron atoms has been derived from an x-ray diffraction study of a single crystal. Probable delay of our final results until we obtain sufficient data to locate hydrogen atoms has prompted us to make a preliminary report of this boron arrangement.

The B_6 hydride was separated by fractional condensation from a complex mixture of boron hydrides which was formed when diborane was carried through a silent electrical discharge by a stream of dry nitrogen. Details will be published elsewhere. Evidence that the molecule contains six boron atoms includes (1) the vapor pressure of 7 mm at 0°C, which is close to the expected value for six boron atoms, (2) a mass spectroscopic study,[1] which showed that the highest dominant mass peaks correspond to expected hydride molecules containing six boron atoms, and (3) the final agreement obtained in our x-ray diffraction study.

Analysis of 144 observed reflections, hkl with $k=0$, 1, 2, and 3, was made by Patterson, trial and error, Fourier projection along b, and one cycle of complete least-squares techniques. The unit cell is *ortho*-rhombic, $a=7.50$, $b=9.23$, and $c=8.50$A, and contains four molecules. The space group is $Cmc2_1$. Since the structure is ordered the molecule is required to have a plane of symmetry. The boron arrangement is very nearly a pentagonal pyramid (Fig. 1), with the central boron atom about 0.9A above the approximate plane of the pentagon. Thus the boron arrangement is a fragment[2] of the icosahedron. Distances, which are surely very close to our final

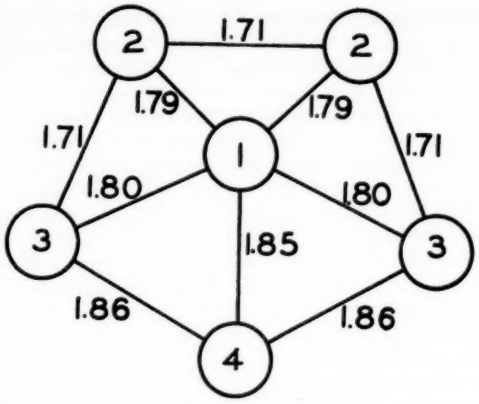

FIG. 1. Boron skeleton in a B_6 hydride, presumably B_6H_{10}.

values, are $B_1B_2=1.79$, $B_1B_3=1.80$, $B_1B_4=1.85$, $B_2B_3=1.71$, $B_3B_4=1.86$, and $B_2B_2=1.71$A. The present agreement shows that $R=\Sigma||F_0|-|F_c||/\Sigma|F_0|=0.16$ for the 144 observed reflections, which are 90 percent of the observable reflections on our photographs. Only boron atoms have been included so far in the calculations; no doubt inclusion of hydrogen atoms will decrease further this already satisfactory value of R.

The assumption of ten hydrogen atoms is, of course, consistent with the best characterized of the known B_6 hydrides. However, we hope to obtain more direct evidence from the x-ray diffraction data about both the number and positions of these hydrogen atoms, if possible from the Fourier maps, but at least from the packing contacts in the crystal.

It is a pleasure to thank the U. S. Office of Naval Research for financial aid.

[1] We are indebted to Professor A. O. C. Nier and Mr. B. L. Donnally, Jr., for the mass-spectroscopic results.
[2] *Systematic Inorganic Chemistry*, Edited by Sneed, Maynard, and Brasted (D. Van Nostrand Company, Inc., New York, 1953), p. 48.

Deductions About Hybridization from Nuclear Quadrupole Coupling Constants*

PAUL N. SCHATZ
Metcalf Chemical Laboratories, Brown University, Providence, Rhode Island
(Received December 15, 1953)

IT has been customary to assume that an atom in a given configuration has the same quadrupole coupling constant whether the atom is free or is forming a bond.[1] For example, it is supposed that a Cl^{35} atom which utilizes a pure $3p_\sigma$ orbital in forming a purely covalent bond has just the nuclear quadrupole coupling constant (−110.4 Mc) of a free Cl^{35} atom.[1] It is the purpose of this note to show that such an assumption is not generally justified and may lead to incorrect conclusions about hybridization.

According to this assumption one interprets the measured quadrupole coupling constant of Cl_2 (∼−108.5 Mc) as implying that the Cl bonding orbitals in this molecule are essentially pure $3p_\sigma$ in nature.[2] The following calculations, based on a very simple model, indicate that, in fact, a very considerable amount of hybridization must occur if the quadrupole coupling constant of gaseous Cl_2 is to be in the vicinity of −108.5 Mc.

The Cl—Cl bond is described by a simple Heitler-London covalent wave function containing Cl bonding orbitals of the form

$$\psi_{Cl}=\alpha\psi_{3s}+\beta\psi_{3p_z}, \qquad (1)$$

with $\alpha^2+\beta^2=1$. It is assumed that the $3p_x$ and $3p_y$ electron pairs remain unpolarized. It is also assumed that the charges on one chlorine atom do not appreciably affect the quadrupole coupling constant of the other chlorine atom and that the distortions of nonbonding closed shells around the nuclei likewise have negligible effects. (Actually, these two effects tend to cancel.)[3] These assumptions are usually made in interpreting quadrupole coupling data.[1,3] Using these assumptions and the experimental relationship

$$eQ\int\psi_{3p_z}^2\left(\frac{3\cos^2\theta-1}{r^3}\right)d\tau=+110.4\text{ Mc},$$

it is easy to obtain the following expression for the quadrupole coupling constant ($\equiv eqQ$) of a chlorine atom in Cl_2:

$$eqQ=110.4\text{ Mc}\left(\frac{\beta^2}{1+S^2}-2\beta^2\right). \qquad (2)$$

In this expression S is the overlap integral. It was evaluated using Slater functions[4] and Mulliken's tables.[5]

The results of the calculations are shown in Fig. 1. The observed

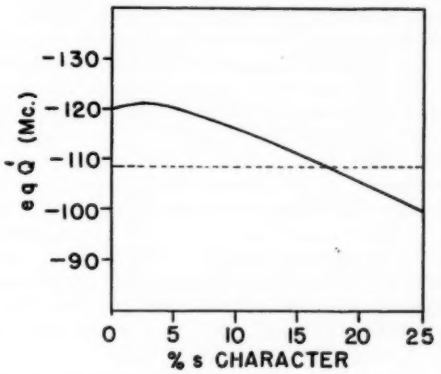

FIG. 1. Calculated quadrupole coupling constant of Cl_2 as a function of hybridization. The dotted horizontal line is the experimental value (for the solid).

quadrupole coupling constant of −108.5 Mc is obtained only if a very substantial amount of hybridization occurs. For the Slater functions used, about 17 percent s character is required in the bonding wave function. Inspection of Eq. (2) shows that for a pure $3p_z$ bond ($\alpha=0$, $\beta=1$), a quadrupole coupling constant as small (in absolute value) as −110.4 Mc (the quadrupole coupling constant of atomic Cl^{35}) could be obtained only if S were equal to zero, which would mean that no bond existed. The use of more accurate wave functions would give somewhat different values for S, but the qualitative results would be unchanged.

Similar results are found with other molecules. Thus some calculations made on CH_3Cl, which will be reported at a later date, indicate that a hypothetical purely covalent CH_3Cl molecule which contained a pure $3p_\sigma$ chlorine orbital would have a quadrupole coupling constant of about −127 Mc. For the same situation in HCl one finds a value of about −128.5 Mc.[6] This type of result may be expected on simple physical grounds. The formation of a covalent bond shifts electronic charge from the atoms forming the bond into the region between the two atoms with consequent changes of the field gradient at the nuclei.

In view of the present calculations, a tentative conclusion that the Cl orbital in a molecule such as CH_3Cl has about 18 percent s character[1] does not seem justified. In fact, it will be shown in some future work on HCl[6] and CH_3Cl that it is quite difficult, using quadrupole coupling constants, to come to even rough quantitative conclusions about the amount of hybridization occurring in such molecules.

I would like to thank Professor D. F. Hornig for several helpful suggestions.

* Research supported by the U. S. Office of Naval Research, Contract N6ori-88, task 1.
[1] C. H. Townes and B. P. Dailey, J. Chem. Phys. **17**, 782 (1949).
[2] R. Livingston, J. Phys. Chem. **57**, 496 (1953).
[3] C. H. Townes and B. P. Dailey, J. Chem. Phys. **20**, 35 (1952).
[4] J. C. Slater, Phys. Rev. **36**, 57 (1930).
[5] Mulliken, Rieke, Orloff, and Orloff, J. Chem. Phys. **17**, 1248 (1949).
[6] P. N. Schatz, J. Chem. Phys. **22**, 695 (1954).

Dielectric Anomaly of Ammonium Sulfate at Its Transition Temperature

KAN-ICHI KANIYOSHI AND TOSHIHIKO MIYAMOTO
Research Institute for Scientific Measurements, Tohoku University, Sendai, Japan
(Received February 12, 1954)

PHASE transition phenomena have been found in many ammonium salts. Among these, the transition temperature of ammonium sulfate has been reported by the measurement of specific heat by Grenshaw and Ritter[1] to be −50.7°C, but according to Hettner and Simon's result[2] of studies on the infrared transmission of the thin single crystal, it was around −40°C. Three results have been reported on the dielectric anomaly accompanied by this phase transition, namely, the sharp peak of λ type observed by Guillien[3] at −53.4°C at the wavelength of 2700 m, the peak, but of different type, observed by Freymann[4] at −52°C in the microwave region, and a broad peak with the maximum at about −40°C found by Bayley[5] at 3 kc/sec. These results were from experiments made with the crystalline powder sample.

Several measurements were made on the dielectric properties at 1440 kc/sec in three axial directions of the single crystal of $(NH_4)_2SO_4$ (*ortho*-rhombic) grown from aqueous solution. The results are shown in Fig. 1, where the cooling or warming rate is about 10°C per hour. The anomaly characterized by a sharp peak in dielectric constant was found in the direction of *a* axis (applied electric field being parallel to *a* axis). The transition temperatures are about −36°C on cooling curve and about −29°C on warming curve, respectively. Rapid cooling or warming shifts the transition temperature. For instance, −80°C on cooling and −10°C on warming were observed in extreme cases. But the difference between the transition temperature obtained by the previous workers and those of present work does not seem to be due only to the difference in warming rate.

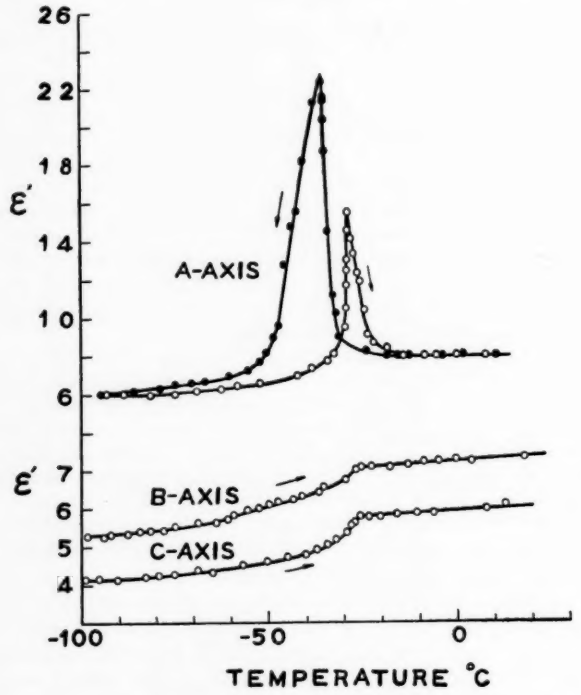

FIG. 1. Temperature dependence of the dielectric constant of $(NH_4)_2SO_4$ in three axial directions at 1440 kc/sec.

Measurements were also made on the sample of crystalline powder. The transition temperature is roughly between −55° and −40° on warming curve; slower warming produces the lower temperature value. This temperature is considerably lower than that for the single crystal but is rather in accordance with those of previous workers. Therefore, it may be concluded from the previously mentioned results that the transition temperature for the single crystal has a tendency to be higher than that for crystalline powder. It was also observed that once the transition begins the dielectric constant gradually increases to the maximum value without any further change in temperature or even when the temperature reverses a little. In crystalline powder this was not so remarkable. This feature is manifest in Fig. 1, where the curves are nearly perpendicular to the temperature axis. The descending sides of the peaks are rather broad but this is due to bad temperature control, and the true shape of the peak is expected to be very sharp and narrow.

As is seen in the figure, a sharp kink but not a peak appears when the applied electric field is parallel to *b* or *c* axis. Measurements were also made at other frequencies ranging from 6 Mc/sec to 1 kc/sec, but no essential difference was observed.

The details of these results will be published in *Science Reports of the Research Institutes*, Tohoku University. Thanks are due Onahama Fertilizer Factory, Nihon Suiso Kogyo Company for preparing some of the single crystals used in this experiment.

[1] J. L. Grenshaw and I. Ritter, Z. physik. Chem. **B16**, 143 (1932).
[2] G. Hettner and F. Simon, Z. physik. Chem. **B1**, 293 (1928).
[3] R. Guillien, Compt. rend. **208**, 980 (1939).
[4] M. Freymann, Compt. rend. **233**, 1449 (1951).
[5] S. T. Bayley, Trans. Faraday Soc. **47**, 518 (1951).

The Reaction between Fluorine and Chlorine Dioxide, a Homogeneous, Bimolecular Reaction

P. J. AYMONINO, J. E. SICRE, AND H. J. SCHUMACHER
Instituto de Investigaciones, Facultad de Química y Farmacia, Universidad Nacional de Eva Perón, Argentina
(Received February 2, 1954)

THE compound $FClO_2$ was discovered and first prepared by Schumacher and Schmitz.[1] These authors found that it was the only compound formed when dry fluorine and chlorine dioxide, diluted by inert gases, reacted at low temperatures with each other.

We investigated this reaction in a more thorough manner. We worked at a temperature range of −46 to −26°C, and a pressure range of approximately 50 to 500 torr. The concentrations of fluorine and chlorine dioxide were varied by a factor of more than 10 and as inert gases were added nitrogen, oxygen, and the $FClO_2$ itself. We used three reaction vessels, two of Pyrex glass and another of clear Vycor. The Pyrex vessels differed in the surface-to-volume ratio by a factor of 2.3; the first one (I) was a cylinder of the following dimensions: length, 16.5 cm; diameter, 7.0 cm; volume, 575 ml; and the other one (II) was a cylinder with a length of 21 cm, a diameter of 2.9 cm, and a volume of 114 ml. The Vycor vessel was a sphere with a diameter of 8.7 cm.

The experimental results obtained could be represented by the following reaction scheme:

$$(1)\quad F_2+ClO_2=FClO_2+F$$
$$(2)\quad F+ClO_2\longrightarrow FClO_2$$
$$(3)\quad F+F+M=F_2+M$$
$$(4)\quad F\xrightarrow{\text{wall}}\tfrac{1}{2}F_2.$$

All the experiments carried out in the reaction vessel II and those in the vessels I and III at low concentrations of ClO_2 and at a low total pressure, could be represented by the simple equation,

$$\frac{d[FClO_2]}{dt}=2\frac{dp}{dt}=k_1[F_2][ClO_2].$$

Under these conditions practically only the reactions (1) and (4) occurred. Almost all the fluorine atoms were carried to the

walls by diffusion or, more probably, by convection processes. Reaction (1) was absolutely homogeneous.

At high concentrations of chlorine dioxide and high total pressures, reactions (2) and (3) occurred to a certain degree. The effect of reaction (2) was greater at high temperatures caused by its considerable heat of activation.

For k_1 we got the following values (as mean values of more than one hundred experiments):

$$k_1(-46°C)=0.23 \text{ mole}^{-1} \text{ liter}\cdot\text{sec}^{-1}$$
$$k_1(-36°C)=0.52 \text{ mole}^{-1} \text{ liter}\cdot\text{sec}^{-1}$$
$$k_1(-26°C)=1.05 \text{ mole}^{-1} \text{ liter}\cdot\text{sec}^{-1}.$$

The heat of activation of reaction (1) obtained from these values is 8.5±0.4 kcal; for α, the steric factor, calculating with a diameter[2] of 3.0A for the fluorine molecule, and with one of 4.3A for the chlorine dioxide molecule,[3] results a value of 3.0×10^{-4}. This value of α is of the same order as the steric factors of numerous reactions, recently investigated by Steacie and co-workers.[4]

The complete work will be published in the *Anales de la Asociación Química Argentina*.

[1] H. Schmitz and H. J. Schumacher, Z. anorg. u. allgem. Chem. **249**, 238 (1942).
[2] E. Kanda, Bull. Chem. Soc. Japan, **12**, 463 (1937).
[3] From data given by L. O. Brockway, Proc. Natl. Acad. Sci. **19**, 868 (1933).
[4] R. Rebbert and E. W. R. Steacie, J. Chem. Phys. **21**, 1723 (1953). See also, H. J. Schumacher, *Chemische Gasreaktionen* (Th. Steinkopff, Dresden und Leipzig, 1938), p. 298.

"Smoothed Potential" Theory of Chemical Binding

JAMES R. ARNOLD
Institute for Nuclear Studies, University of Chicago, Chicago, Illinois
(Received February 18, 1954)

THIS note introduces an attempt at a model for ordinary covalent bonds, based on considerations similar to those used in the so-called "free electron" model for aromatic systems,[1] ignoring details of the potential field. As in the latter case, we draw on the more exact theories for basic descriptive facts. The existence of the additivity rules[2,3] for bond energies and distances encouraged the attempt. This model, starting from distance parameters only, yields values for the nonpolar part of the bond energy. This polar contribution is computed using the electronegativity scale.

The model is based on the following assumptions:

1. The eigenfunctions of the valence electrons in the atom are represented by those of electrons in a simple potential, whose extension is measured by the nonbonding radius of the atom.

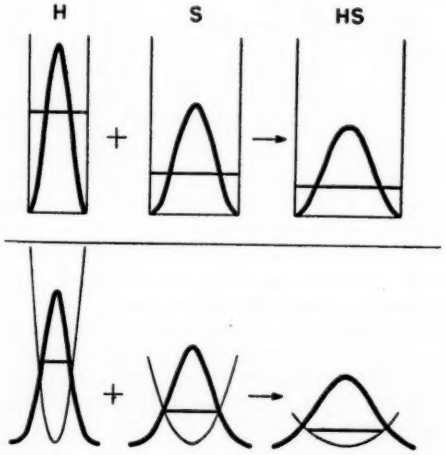

FIG. 1. Potentials, energy levels, and eigenfunctions for the H—S bond: (a) square-well model, (b) harmonic oscillator model.

2. The eigenfunctions of the valence electrons in a diatomic molecule are the same as in the atom, except along the bond axis. Here the extension is increased by the bond distance, so that the energy is lowered, resulting in binding.

3. In a polyatomic molecule the bonding electrons are localized between pairs of atoms. This is the familiar G. N. Lewis assumption. The calculation of a bond energy then reduces to that for the (often hypothetical) single-bonded diatomic molecule.

Two examples allowing separation of coordinates are the cylindrical square well and the harmonic oscillator. For the first case, if l is the radius of the well the binding energy of a two-electron bond is

$$E_{\text{bond}}=219\left(\frac{1}{l_A^2}+\frac{1}{l_B^2}-\frac{2}{l_{AB}^2}\right)+23.06(x_A-x_B)^2 \text{ kcal/mole}, \quad (1)$$

where l_A and l_B correspond to the atoms, and l_{AB} to the molecule, being given by $(l_A+l_B+r_{AB})/2$ where r_{AB} is the bond distance.

The bond energy in the harmonic oscillator case is

$$E_{\text{bond}}=88.6\left(\frac{1}{a_A^2}+\frac{1}{a_B^2}-\frac{2}{a_{AB}^2}\right)+23.06(x_A-x_B)^2 \text{ kcal/mole}, \quad (2)$$

where a_A and a_B refer to atoms, and $a_{AB}=(a_A+a_B+r_{AB})/2$ to the molecule. These two equations have the same form. Other smooth potentials will show similar behavior, a fact ultimately due to the Heisenberg principle.

Treating Eqs. (1) and (2) as single-parameter equations, l and a can be fixed at 1.185 and 0.822 times the nonbonding radius, respectively, to give best agreement throughout the table.

Comparison of these equations with experiment does not give agreement for N, O, and F. The energies of single N—N, O—O, and F—F bonds calculated on this model are almost twice too high. No quantitative theoretical explanation of the weakness of these bonds is known to the author; in our model the fact is equivalent to the statement that there is a trough in the bond eigenfunction between the nuclei, so that the electrons are still largely localized.

Excluding bonds containing these elements, the comparison is given in Table I for all entries in Huggins' table.[3] Huggins' bond distances are also used, while the nonbinding radii are taken from Pauling,[2] with an extrapolation to the fourth row of the periodic table.

The resemblance of the two models, shown in Fig. 1, illustrates how the long wavelength of the electron irons out major changes in the shape of the potential.

TABLE I. Comparison of calculated and experimental single bond energies.

Bond	$E_{(1)}$	$E_{(2)}$	E_{exp}	Bond	$E_{(1)}$	$E_{(2)}$	E_{exp}
H—H	81.0 kcal	90.5 kcal	104 kcal	S—S	50.6	49.3	49
H—C	83.1	85.8	91	S—Cl	57.8	57.3	61
H—Si	85.9	82.1	81	S—As	53.3	52.2	50
H—P	84.0	81.2	76	S—Br	50.8	50.0	51
H—S	86.6	84.2	81	Cl—Cl	51.7	51.8	58
H—Cl	102.4	101.4	103	Cl—Ge	82.3	82.2	80
H—As	85.3	81.1	59	Cl—As	73.1	72.9	73
H—Se	87.3	85.1	66	Cl—Se	55.8	55.7	58
H—Br	96.3	93.2	88	Cl—Br	49.5	49.5	52
H—Te	87.9	81.0	57	Cl—Sn	80.3	79.6	77
H—I	90.7	84.7	71	Cl—Sb	73.7	72.6	74
C—C	60.2	62.3	65	Cl—I	52.0	51.2	50
C—Si	64.7	64.8	66	Ge—Ge	41.2	40.9	42
C—Cl	63.9	64.7	70	Ge—I	52.3	52.1	55
C—Br	58.2	58.0	58	As—As	44.0	43.5	38
C—I	54.3	52.8	43	As—Br	60.9	60.8	58
Si—Si	42.9	42.9	50	As—I	48.4	47.7	42
Si—S	56.1	55.5	60	Br—Br	45.1	45.1	46
Si—Cl	82.2	82.6	90	Br—Sn	65.4	65.1	65
Si—Br	67.9	68.4	73	Br—Sb	59.9	59.5	62
Si—I	53.3	53.0	53	Br—I	44.4	43.8	42
P—P	47.5	47.4	51	Sn—Sn	35.0	34.6	36
P—Cl	71.9	72.3	79	Sb—Sb	37.7	36.8	35
P—Br	60.8	60.8	64	Sb—I	46.0	45.4	44
P—I	49.6	48.9	49	I—I	38.3	37.7	34

To summarize, a model which ignores details of atomic and molecular potentials seems to have considerable success in predicting covalent bond energies. Its justification, like that of other

so-called "free electron" theories, must rest on the overriding importance of distance parameters in calculating energies in these systems.

Details, together with a discussion of multiple bonds, ionic species, activation energies, and metallic binding, will be treated in a forthcoming paper.

[1] K. Ruedenberg and C. W. Scherr, J. Chem. Phys. **21**, 1565 (1953); C. W. Scherr, J. Chem. Phys. **21**, 1582 (1953); J. R. Platt, J. Chem. Phys. **21** 1597 (1953).
[2] L. Pauling, *The Nature of the Chemical Bond* (Cornell University Press, Ithaca, 1939).
[3] M. L. Huggins, J. Am. Chem. Soc. **41**, 4123, 4126 (1953). These two references give a key to the earlier literature.

The Oxidation of Nitrogen by Ozone to Form Nitrous Oxide

P. HARTECK AND S. DONDES
Rensselaer Polytechnic Institute, Troy, New York
(Received December 28, 1953)

IN the gaseous state, nitrogen is one of the most inert elements (with the exception of the noble gases). Thus, only at very high temperatures or by catalysis is nitrogen capable of undergoing chemical reactions with other substances. Recently, we have utilized molecular nitrogen in a homogeneous reaction at 295°C.

The decomposition of nitrous oxide into nitrogen and oxygen is a first-order reaction.[1] The heat of activation of this reaction is 53 kcal. The heat of formation of nitrous oxide from nitrogen is 17.17 (latest value 19.49) kcal. The heat of dissociation of oxygen is 117.3 kcal. Thus, of the 53 kcal heat of activation, 41 are endothermic and the remaining 12 kcal considered as the true heat of activation. In the reverse process of the thermal dissociation of nitrous oxide

$$N_2+O+M=N_2O+M,$$

an approximate efficiency may be obtained from the reaction coefficient in the following equation:

$$K_4=2\times10^{-33}e^{-12\,000/RT}.$$

Thus, it should not be too difficult to find a method of bringing about this reaction. In our special case, a mixture of nitrogen, and oxygen containing 5 percent ozone, was passed through a furnace which was heated to 295°C, with the ozone practically completely thermally decomposed in less than a minute. The following reactions occurred:

$$O_3+M=O_2+O+M\cdots K_1, \quad (1)$$
$$O_2+O+M=O_3+M\cdots K_2, \quad (2)$$
$$O_3+O=2O_2\cdots K_3, \quad (3)$$
$$O+N_2+M=N_2O+M\cdots K_4, \quad (4)$$
$$O_3^*+N_2=N_2O+O_2\cdots, \quad (4a)$$
$$O_3+N_2^*=N_2O+O_2\cdots, \quad (4b)$$
$$K_3=k_3e^{-6160/RT};\quad K_4=k_4e^{-12\,000/RT};\quad k_3=2\times10^{-10};\quad k_4=2\times10^{-33}. \quad (4c)$$

The steady-state concentration of atoms is given by reaction (1) and (2). Reactions (3) and (4) indicate the manner in which oxygen atoms are consumed. The fraction of oxygen atoms which oxidize nitrogen into nitrous oxide, according to Eq. (4), [with possibly (4a)] and (4b) in the ozonizer, is small but readily detected in the presence of the reaction of oxygen atoms with ozone as indicated in Eq. (3). The rates of the above reactions may be represented by the following equations:

$$-\frac{d[O]}{dt}=2k_3[O_3][O]e^{-6160/RT}+k_4[O][N_2][M]e^{-12\,000/RT}, \quad (5)$$

$$+\frac{d[N_2O]}{dt}=k_4[O][N_2][M]e^{-12\,000/RT}, \quad (6)$$

$$-\frac{d[N_2O]}{d[O]}=\frac{k_4[N_2][M]e^{-5840/RT}}{2k_3[O_3]+k_4[N_2][M]e^{-5840/RT}}. \quad (7)$$

The integration of Eq. (7) gives the total amount of nitrous oxide formed

$$N_2O=\frac{k_4[N_2][M]e^{-5840/RT}}{2k_3}\ln\left(\frac{2k_3[O_3]}{k_4[N_2][M]e^{-5840/RT}}\right). \quad (8)$$

If the values of (4c) are introduced in Eq. (8), and the concentrations expressed in number of particles per cubic centimeter, a value of 5×10^{13} nitrous oxide molecules formed per cubic centimeter, is obtained (if the gas has a composition of 50 percent nitrogen, 47.5 percent oxygen, and 2.5 percent ozone). This corresponds to a conversion of about 10^{-4} ozone into nitrous oxide. Actually, 3×10^{13} nitrous oxide molecules per cubic centimeter were observed. (It should be indicated that partly estimated numerical values were used in Eq. (8) and that mixing of the gases during the reaction not shown in Eq. (8) would give higher yields.)

Experimentally, nitrous oxide condensed in liquid oxygen was sensitively measured by physico-chemical means. Blanks indicated a small percentage of N_2O produced in the ozonizer, from the small amount of nitrogen (which may have become activated) found in the tank oxygen (an effect not indicated in the literature) which was readily detected in our mode of analysis.

[1] L. Kassel, *The Kinetics of Homogeneous Gas Reaction* (1932), American Chemical Society Monograph Series. (Actual values in this volume used.)

Isotopic Exchange of Oxygen in the Systems Water-Silica and Oxygen-Silica

DWIGHT A. HUTCHISON
Chemistry Division, Argonne National Laboratory, Lemont, Illinois
(Received February 18, 1954)

THE exchange of oxygen is being investigated in the systems silica-water and silica-oxygen. Isotopic exchange in the latter system has been found not to occur up to 1000°C. The former exchange may be represented by

$$H_2O^{18}+SiO_2{}^{16}=H_2O^{16}+SiO^{16}O^{18}. \quad (1)$$

Prime purposes of this work are the collection of rate data for the study of other exchange reactions as well as the intrinsic interests and applications to geochemical problems.[1]

The reaction was performed in 8-mm diameter silica tubes of about 1.3 cm³. The volumes were determined precisely, water of 1.1 atomic percent O^{18} was weighed in the tubes, and finally the tubes were sealed under vacuum with the water frozen. The tubes were introduced into a resistance-heated furnace with temperature

TABLE I. Data for H_2O-SiO_2 exchange experiments at 960°C.

Sample number	Time (minutes)	$[O_w]$ microgram atoms-cm^{-3}	$(f_w{}^{18})_t$ $\times10^3$	Experimental $(1-F)$	Corrected $(1-F)$
141	30	791 ±10	8.80	0.638 ±0.009	0.669
134	60	555	7.91	0.380	···
135	120	555	7.22	0.180	···
182	180	756.3 ±0.4	6.78	0.0522 ±0.0008	0.06867
136	240	555	6.76	0.0464	···
89	360	479.6 ±0.5	6.62	0.00580 ±0.00008	0.00473
Standard	0.0		10.05	1.000	···
91	990	576.6 +0.4	5.62	···	···

controlled to ±5°C. Water was analyzed for O^{18} content by equilibration[2] with normal isotopic CO_2 and subsequent mass spectrometric analyses[3] on the enriched CO_2.

It can be shown that the isotopic exchange reaction will follow first-order kinetics[4] with respect to water concentration if the rate is controlled by a homogeneous phase reaction in which chemical identity of the oxygen isotopes is assumed. For this case the rate equation is

$$-\frac{d[O_w{}^{18}]}{dt}=k_1[O_w][O_s](f_w{}^{18}-f_s{}^{18}), \quad (2)$$

where square brackets represent concentrations, f is an atomic fraction, k_1 is the specific rate constant, t is the time, and subscripts w and s refer to water and silica. Upon integration one obtains

$$\ln(1-F)=\frac{\ln(f_w^{18})_t-(f_w^{18})_\infty}{(f_w^{18})_0-(f_w^{18})_\infty}=-k_1\{[O_w]+[O_s]\}t, \qquad (3)$$

where the additional subscripts refer to zero and equilibrium times. Initial data are summarized in Table I.

A plot of $(f_w^{18})_t$ *vs* time yields a smooth curve from which one may obtain an extrapolated value for $(f_w^{18})_\infty$ equal to 0.00660. A semilog plot of $(1-F)$ *vs* time is shown in Fig. 1. The experimental

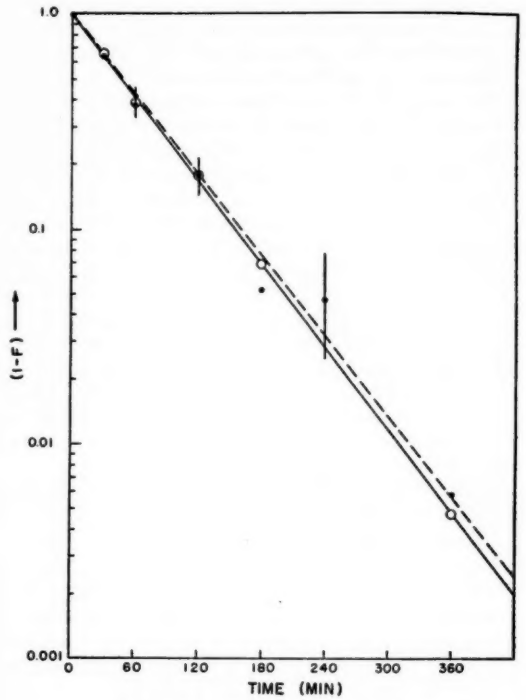

FIG. 1. Plot of $(1-F)$ *vs* time for H_2O-SiO_2 oxygen exchange reaction at 960°C.

points are represented by black dots while the circles were obtained from $(1-F)$ values corrected to a common value of $\{[O_w]+[O_s]\}$. The $[O_s]$ and k_1 values were obtained by solution of two equations resulting from the substitution of the precise data of experiments 182 and 89 into Eq. (4) together with the slope of the dashed curve through the experimental points. The vertical lines associated with the experimental points represent a best estimate of the error in the slope of the curve due to an error in $\{[O_w]+[O_s]\}$ of experiments 134, 135, and 136 wherein the water was weighed only approximately. It is seen that this concentration correction results in a straight line which goes through the point $(1-F)=1.00$ at zero time. This is taken as partial evidence of a homogeneous phase reaction between water and dissolved silica. Further evidence is found in the constancy of the reaction rate with variation in silica surface.

At 960°C, $k_1=0.78\times10^{-5}$ cm³ (microgram atoms)$^{-1}$ minute^{-1} and the half-time is 47 minutes. Experiments at 750°C yield $k^1=3.7\times10^{-5}$ and the half-time, 100 minutes. These values give an experimental activation energy of -4.6 kcal-mole^{-1} deg^{-1}. This negative value is interpreted in terms of a predominate surface rate-controlling reaction at 750°C. Evidence of a slow surface reaction at 960°C is indicated by the f_w^{18} of experiment 190 which falls below the extrapolated curve of the shorter time experiments.

A detailed account of work in progress will be published in the near future.

My acknowledgments are due L. F. Daum for technical assistance and L. G. Pobo for mass spectrometric analyses.

[1] G. W. Morey and J. M. Hesselgesser, Econ. Geol. **46**(8), 821 (1951).
[2] I. Dostrovsky and F. S. Klein, Anal. Chem. **24**, 414 (1952).
[3] Analyses were made on a 60° direction focusing instrument designed by and constructed under the direction of the writer. Details of the instrument will be published elsewhere.
[4] H. McKay, Nature **142**, 997 (1938).

Appendix: The Assignments of the Raman and Infrared Frequencies of 1,2-Dichloroethane Observed in the Gaseous, Liquid, and Solid States

[J. Chem. Phys. **21**, 2195 (1953)]

ICHIRO NAKAGAWA AND SAN-ICHIRO MIZUSHIMA
Chemical Laboratory, Faculty of Science, Tokyo University, Tokyo, Japan

THE potential function used in the calculation[7] of the normal frequencies of 1,2-dichloroethane is

$$V=\sum_i\{K_i'r_{0i}\Delta r_i-\tfrac{1}{2}K_i(\Delta r_i)^2\}$$
$$+\sum_{i<j}\{H_{ij}'r_{0i}r_{0j}\Delta\alpha_{ij}+\tfrac{1}{2}H_{ij}r_{0i}r_{0j}(\Delta\alpha_{ij})^2$$
$$+\sum_{i<j}\{F_{ij}'q_{ij}\Delta q_{ij}+\tfrac{1}{2}F_{ij}(\Delta q_{ij})^2\},$$

where r's are the bond lengths, α's the bond angles, and q's the distances between atoms not bonded directly. K, K', H, H', F, and F' are force constants of which F and F' are those of the repulsive terms. K' and H' can be expressed in terms of F' and intramolecular tension κ by the equilibrium conditions.[15] The values of the force constants are shown in Table III. They have been shown to

TABLE III. Force constants (in 10^5 dynes/cm) and intramolecular tension (in 10^{-11} dynes·cm).

K(C—C) =2.80	H(Cl—C—C) =0.10	F(C···Cl) =0.60
K(C—Cl) =1.81	H(Cl—C—H) =0.05	F(Cl···H) =0.80
K(C—H) =4.20	H(C—C—H) =0.15	FF(C···H) =0.40
	H(H—C—H) =0.40	F(H···H) =0.10
	$F'=-1/10$	$\kappa=0.10$

give calculated frequencies of CH_3Cl, CH_2Cl_2, $CHCl_3$, C_2H_6, and C_2Cl_6 in good agreement with the observed frequencies.

[7] I. Nakagawa, J. Chem. Soc. Japan **74**, 848 (1953).
[15] As for details, see: T. Shimanouchi, J. Chem. Phys. **17**, 245, 734, 848 (1949).

Reduction of Carbon Dioxide on Mercury Cathodes

TRUMAN E. TEETER AND PIERRE VAN RYSSELBERGHE
Department of Chemistry, University of Oregon, Eugene, Oregon
(Received January 25, 1954)

SEVERAL years ago one of us[1] described a polarographic wave due to carbon dioxide dissolved in aqueous solutions of quaternary ammonium salts. Reasons were given for ascribing this wave to an actual reduction of CO_2 rather than to hydrogen evolution. However, several authors[2] have presented arguments in favor of this latter interpretation, in one case, at least, on the basis of the *a priori* assumption that CO_2 would not be electrochemically reducible.

In order to settle the matter, the problem of the reduction of CO_2 on mercury cathodes was attacked along two additional lines: polarization curves and electrolysis, with cathodes of large area in both cases.

Polarization curves recorded with solutions of KCl, NH_4Cl, $NaHCO_3$, $N(CH_3)_4Br$, etc., through which purified CO_2 was passed continuously, exhibit sudden increases of current at cathodic potentials similar to those at which polarographic currents due to CO_2 begin to increase, but appreciably lower than the potentials at which the current begins to increase when CO_2 is replaced by

nitrogen, this being the case even with $NaHCO_3$ solutions. With CO_2 present the polarization curves can be closely reproduced in several successive cycles of increases and decreases of current. With CO_2 replaced by N_2, on the other hand, decrease of the cathodic potential after a certain current has been reached, results in the appearance of an anodic current, the amalgam formed during cathodic polarization then being oxidized. These experiments clearly show that, in the range of *p*H values covered, CO_2 enters into a reduction process at cathodic potentials lower than those of alkali or ammonium, or even hydrogen ion reduction. There was no visible hydrogen evolution in any of the runs with CO_2, except possibly at very large currents.

Numerous electrolysis experiments were carried out at various constant current strengths, with purified CO_2 passing through the solutions for several hours. The only detectable reduction product was in all cases formic acid, qualitatively identified in various ways, but chiefly by means of the chromotropic acid test,[3] and quantitatively determined by an electrometric titration procedure. The current efficiencies were in all cases large and often approached 100 percent. Comparative runs were made with various series of electrolytes: alkali halides, ammonium halides, symmetrical quaternary ammonium compounds, etc. Details will be given elsewhere.

Both the polarization curves and the electrolysis results indicate that, when the potentials are such that CO_2, the main cation and H^+ (or water) can be simultaneously reduced, the resulting amalgam and hydrogen (atomic at least in part) reduce additional amounts of CO_2 to the same product as that formed in the direct cathodic reduction, namely, HCOOH. This is also demonstrated by experiments on the direct reduction of CO_2 by alkali amalgams. The fact that current efficiencies are definitely lower with ammonium than with alkali ion solutions is explained on the basis of either decomposition or smaller reactivity of the amalgam. The high efficiencies observed with quaternary ammonium ion solutions fit in entirely with polarographic observations.

Electrolysis experiments were also run in sealed cells provided with both polarizing and polarographic sets of electrodes in order to demonstrate that, starting with a given initial CO_2 concentration in quaternary ammonium salt solutions, polarograms taken at intervals during electrolysis show a gradual decrease in the height of the CO_2 wave.

The identification as formic acid of the electrolytic reduction product of CO_2 on mercury cathodes (or on other high hydrogen overvoltage cathodes) has repeatedly been reported in the older literature.[4]

Other workers in this laboratory, particularly J. M. McGee and J. Weissbart, have made contributions to these investigations. Financial support of this work by the Graduate School of the University of Oregon is gratefully acknowledged.

[1] P. Van Rysselberghe and G. J. Alkire, J. Am. Chem. Soc. **66**, 1801 (1944); P. Van Rysselberghe, *ibid.* **68**, 2047 (1946); Van Rysselberghe, Alkire, and McGee, *ibid.* **68**, 2050 (1946).
[2] M. v. Stackelberg and W. Stracke, Z. Elektrochem. **53**, 118 (1949); O. H. Müller, Proc. 1st Intern. Polarograph. Congr. (Prague) 159 (1951); A. A. Vlček, Nature **172**, 861 (1953).
[3] F. Feigl, *Qualitative Analysis by Spot Tests* (Elsevier Publishing Company, New York, 1946), see pp. 395–7.
[4] E. Royer, Compt. rend. **70**, 731 (1870); N. Klobukow, J. prakt. Chem. **34**, 126 (1887); A. Lieben, Monatsh. Chem. **16**, 211 (1895), **18**, 582 (1897); A. Cohen and S. Jahn, Ber. deut. Chem. Ges. **37**, 2836 (1904); F. Fischer, *Praktikum der Elektrochemie* (Julius Springer, Berlin, 1912), see p. 99; M. Rabinowitsch and A. Maschowetz, Z. Elektrochem. **36**, 846 (1930).

Preparation and Isolation of Carrier-Free As^{74} from Germanium Cyclotron Targets*

MINO GREEN† AND JAMES A. KAFALAS†
Lincoln Laboratory, Massachusetts Institute of Technology, Cambridge, Masssachussetts
(Received January 27, 1954)

THE bombardment of germanium with 16-Mev deuterons gives As^{74} by the reaction, $_{32}Ge^{73}(d,n)_{33}As^{74}$. Other radionuclides are formed but these are short lived compared with As^{74}. The only long-lived species will be As^{73} and this is too weak to be detected by our counting arrangement. The germanium target is processed two weeks after irradiation when nearly all the activity is due to As^{74}.

The preparation of radioactive arsenic of high specific activity from germanium cyclotron targets has been reported by J. W. Irvine, Jr.;[1] but this method is not applicable to the preparation of carrier-free material. The preparation of carrier-free As^{74} reported here has the advantage that no special apparatus is required and, also, because of the simplicity of the procedure the radiation hazard is much reduced.

The target, a strip of germanium (~5 ohm-cm, *N* type) 4 in.$\times\frac{3}{8}$ in.$\times\frac{1}{32}$ in., was placed on a water-cooled holder and bombarded for 6 hours. After a period of two weeks the target was processed as follows: The germanium was dissolved in aqua regia (3:1, concentrated hydrochloric acid—concentrated nitric acid, by volume) using 20-ml aqua regia per gram of germanium—complete solution required about 1½ hours heating on a hot plate. The solution was then evaporated down to a final volume of about 1–2 ml. A precipitate of germanium dioxide was present at this point. This precipitate was dissolved by adding 5 ml of concentrated hydrochloric acid and heating on a steam bath to distill off the germanium tetrachloride formed. The volume of the solution was brought down to 2 ml and 8 ml of concentrated hydrochloric added to make the solution about 11*N*. Two drops of concentrated nitric acid were added, to keep the arsenic in the highest oxidation state, and the solution was then extracted with two 10-ml portions of benzene. The arsenic remains in the acid phase and the germanium is extracted into the benzene phase. $[As^{+5}]_{benzene}/[As^{+5}]_{11N\ HCl} \leqslant 0.003$ and $[Ge^{+4}]_{benzene}/[Ge^{+4}]_{11N\ HCl} \geqslant 260$.[2] These distribution coefficients are sensitive to the acid concentration and care should be taken to keep the acid 11*N* or higher.

The acid layer contained the arsenic in the pentavalent state in 11*N* HCl. The recoveries obtained were 90±5 percent. The measured half-life of the isolated activity was 17.5 days.

* The research in this document was supported by the U. S. Army, Navy, and Air Force under contract with the Massachusetts Institute of Technology.
† Staff member, Lincoln Laboratory, Massachusetts Institute of Technology.
[1] J. W. Irvine, Jr., J. Phys. Chem. **46**, 910 (1942).
[2] Irvine, Sharp, Kafalas, and Brink, 123rd National Meeting of the American Chemical Society, Los Angeles, March, 1953.

I_4: A Charge-Transfer Molecular Complex?

HARDEN MCCONNELL
Shell Development Company, Emeryville, California
(Received January 25, 1954)

NUMEROUS electron donor molecules with electronic ionization potentials in the *ca* 8–11 electron-volt range form donor-acceptor or *intermolecular charge-transfer* complexes with iodine which is an electron acceptor. Examples of such donor molecules are aromatics, olefins, cyclanes, ethers, alcohols, and alkyl halides.[1] Since iodine itself has, according to the recent electron impact measurements of Morrison and Nicholson,[2] the relatively low ionization potential of 9.41 ev, it is of interest to inquire whether or not iodine could serve as the donor partner in some molecular complex. The following discussion gives evidence that iodine may exhibit this amphoteric character as a *self-intermolecular charge-transfer complex* with the formula I_4.

Donor-acceptor complexes between various donor molecules and iodine frequently show strong intermolecular charge-transfer transitions. McConnell, Ham, and Platt[1] have pointed out the existence of a semiempirical correlation between the energies of these charge-transfer excited states and the ionization potentials of the donor partners in molecular complexes containing iodine as the acceptor. The equation expressing this correlation is

$$E = 0.67 I_p - 1.9 \text{ (in ev)}, \quad (1)$$

where *E* is the energy of the charge-transfer excited state (relative to the energy of the ground electronic state of the complex) and

I_p is the ionization potential of the donor partner in the complex. An essentially similar correlation has been noted by Hastings *et al.*[3]

Kortüm and Friedheim[4] have found an absorption band in the spectrum of iodine vapor at 2670A which they attribute to loosely bound I_4 molecules. If this absorption band is interpreted as an intermolecular charge-transfer transition, then the energy of the charge-transfer excited state is 4.66 ev. By taking $I_p=9.41$ ev for I_2,[2] Eq. (1) gives a calculated value of the excited-state energy E equal to 4.4 ev. These calculated and experimental values of E are equal to one another to within the accuracy of Eq. (1).[1] This agreement provides evidence that the 2670 band of I_4 is a charge-transfer band and that intermolecular charge-transfer forces are important in the interaction of two iodine molecules.

In connection with this proposal of intermolecular charge-transfer forces between two iodine molecules, it is of interest to point out that Townes and Dailey[5] have measured the pure nuclear quadrupole absorption spectrum of solid iodine and have concluded that "new bonds must occur in solid I_2 which do not occur in the isolated molecule." It is then entirely plausible that these "new bonds" are just the intermolecular charge-transfer interactions between iodine molecules discussed above.[6]

[1] McConnell, Ham, and Platt, J. Chem. Phys. **21**, 66 (1953).
[2] J. D. Morrison and A. J. Nicholson, J. Chem. Phys. **20**, 1023 (1952).
[3] Hastings, Franklin, Schiller, and Matsen, J. Am. Chem. Soc. **75**, 2900 (1953).
[4] G. Kortüm and G. Friedheim, Z. Naturforsch. **2a**, 20 (1947). See also R. S. Mulliken, J. Am. Chem. Soc. **72**, 600 (1950).
[5] C. H. Townes and B. P. Dailey, J. Chem. Phys. **20**, 35 (1952).
[6] A study of the nuclear quadrupole spectra of various solid donor-acceptor complexes containing iodine should give considerable information regarding the electronic structures of these complexes.

Reaction Velocity Near Equilibrium

PIERRE VAN RYSSELBERGHE
Department of Chemistry, University of Oregon, Eugene, Oregon
(Received February 15, 1954)

THE proportionality existing near equilibrium between reaction velocity and affinity[1-3] and the general problem of approach to equilibrium have recently been the object of several communications.[4-8] As a further contribution towards the clarification of this important question we present the following reasoning.

The reaction $A+B\rightarrow M+N$ can be regarded as involving a forward complex C_f and a reverse complex C_r with the same gross composition AB or MN, and the two component processes can be represented as

$$A+B\rightleftarrows C_f\rightarrow M+N$$
$$M+N\rightleftarrows C_r\rightarrow A+B.$$

There is no equilibrium between C_f and C_r since, otherwise, $A+B$ would be in equilibrium with $M+N$.

The net reaction velocity is

$$v=k_f a_A a_B/\gamma_{C_f}-k_r a_M a_N/\gamma_{C_r},$$

in which the a's are activities and the γ's are activity coefficients. Introducing the equilibrium activities we may write

$$v=k_f a_{Ae}a_{Be}\exp[\ln(a_A a_B/a_{Ae}a_{Be})]/\gamma_{C_f}$$
$$-k_r a_{Me}a_{Ne}\exp[\ln(a_M a_N/a_{Me}a_{Ne})]/\gamma_{C_r},$$

in which all a/a_e ratios are very close to unity.

For states very near equilibrium we may assume

$$\gamma_{C_f}=\gamma_{C_fe}\quad\text{and}\quad\gamma_{C_r}=\gamma_{C_re},$$

with

$$k_f a_{Ae}a_{Be}/\gamma_{C_fe}=k_r a_{Me}a_{Ne}/\gamma_{C_re};$$

and, expanding the exponentials to their first-order terms, we find

$$v=k_f a_{Ae}a_{Be}\ln(Ka_A a_B/a_M a_N)/\gamma_{C_fe},$$

in which K is the equilibrium constant. The logarithmic factor is nothing but the ratio of the affinity to RT:

$$v=k_f a_{Ae}a_{Be}A/RT\gamma_{C_fe}.$$

From the absolute rate theory we have

$$k_f=\kappa_f kTK_{C_f}/h,$$

in which K_{C_f} is the equilibrium constant for the formation of the complex C_f from $A+B$, and κ_f the transmission coefficient for the forward process.

We thus have

$$v=\kappa_f K_{C_f}a_{Ae}a_{Be}A/Nh\gamma_{C_fe}$$

or

$$v=\kappa_f C_{C_fe}A/Nh.$$

Although we thus arrive at the same final expression as that of Zwolinski and Marcus[8] (with $A=-\Delta F$), our derivation is more precise and shows clearly that their $C^{\pm}$ is actually the concentration of the forward complex at equilibrium.

We also have

$$v=\kappa_r C_{C_re}A/Nh.$$

[1] Th. De Donder and P. Van Rysselberghe, *Thermodynamic Theory of Affinity* (Stanford University Press, Stanford, 1936).
[2] I. Prigogine, *Etude Thermodynamique des Phénomènes Irréversibles* (Desoer, Liège, 1947).
[3] Prigogine, Outer, and Herbo, J. Phys. Chem. **52**, 321 (1948).
[4] C. A. Hollingsworth, J. Chem. Phys. **20**, 921, 1649 (1952).
[5] Gilkerson, Jones, and Gallup, J. Chem. Phys. **20**, 1182 (1952).
[6] M. Manes, J. Chem. Phys. **21**, 1791 (1953).
[7] S. H. Bauer, J. Chem. Phys. **21**, 1888 (1953).
[8] B. J. Zwolinski and R. J. Marcus, J. Chem. Phys. **21**, 2235 (1953).

A Vector Representation of Chemical Affinities

C. A. HOLLINGSWORTH, *Department of Chemistry, University of Pittsburgh, Pittsburgh, Pennsylvania*
AND
ROBERT L. POTTER, *Bell Aircraft, Buffalo, New York*
(Received July 16, 1953)

CHEMICAL affinities lend themselves well to a vector representation. One such representation is described in this letter. The vector spaces to be used are the following: (1) *mole space* with a dimension for each chemical species; (2) a two-dimensional *thermodynamic space* to represent such variables as temperature and pressure; (3) *total space* resulting from the combination of mole space and thermodynamic space.

The total mass of a system is the scalar product $\mathbf{X}\cdot\mathbf{n}$, where $\mathbf{X}$ is a vector in mole space with components X_i equal in magnitude to the molecular weight of the corresponding chemical species, and $\mathbf{n}$ is the position vector in mole space, i.e., the component n_i is the number of moles of the ith chemical species. It follows that all motions of a closed system must be normal to $\mathbf{X}$.

We define the *reaction vector* $\boldsymbol{\nu}_k$ of the kth reaction to be the vector in mole space with components ν_{ik} equal to the coefficients in the kth reaction. The chemical equation can then be expressed

$$\boldsymbol{\nu}_k\cdot\mathbf{X}=0. \tag{1}$$

The displacement in mole space caused by the kth reaction is $\boldsymbol{\nu}_k d\xi_k$, where ξ_k is the degree of advancement of the reaction. The velocity of the kth reaction is $\boldsymbol{\nu}_k\dot{\xi}_k$, and the "total" reaction velocity is $(\partial\mathbf{n}/\partial t)$.

The displacement $d\mathbf{n}$ of an open system can be separated into an "external" displacement $d\mathbf{n}_E$ caused by the exchange of matter with the surroundings and an "internal" displacement $d\mathbf{n}_I$ caused by the reactions. Also, $d\mathbf{n}$ can be resolved into a component $d\mathbf{n}_R$ in the reaction subspace and a component $d\mathbf{n}_N$ normal to the reaction subspace. The component $d\mathbf{n}_N$ is the component of $d\mathbf{n}_E$ normal to the reaction subspace. The component $d\mathbf{n}_R$ is the sum of $d\mathbf{n}_I$ and the component of $d\mathbf{n}_E$ in the reaction subspace.

The change $d\Phi$ of a thermodynamic quantity Φ can be expressed by

$$d\Phi=\nabla\Phi\cdot(d\mathbf{n}+d\mathbf{s}), \tag{2}$$

where $d\mathbf{s}$ is the displacement in thermodynamic space. When (T,P) space is used and Φ is an extensive property, we have

$$\Phi=\nabla_{(T,P)}\Phi\cdot\mathbf{n}, \tag{3}$$

where the subscript (T,P) indicates that temperature-pressure space is being used.

We define the *chemical potential vector* $\boldsymbol{\mu}$ to be the vector in mole space with components equal to the chemical potentials. The Gibbs-Duhem equation becomes

$$\mathbf{n}\cdot d\boldsymbol{\mu}=0. \tag{4}$$

The vector $d\boldsymbol{\mu}$ can be expressed by

$$d\boldsymbol{\mu}=\nabla_{(T,P)}\boldsymbol{\mu}\cdot d\mathbf{n}, \tag{5}$$

where $\nabla\boldsymbol{\mu}$ is a dyadic. The chemical affinity A_k of the kth reaction can be expressed by

$$A_k=-\boldsymbol{\mu}\cdot\boldsymbol{\nu}_k. \tag{6}$$

It is seen that $A_k/|\boldsymbol{\nu}_k|$ is the component of $-\boldsymbol{\mu}$ in the direction of the reaction. The system behaves like a mechanical body being acted upon by an attractive force in the direction $-\boldsymbol{\mu}$ and being constrained to move in the direction $\boldsymbol{\nu}_k$. When the system is in equilibrium $\boldsymbol{\mu}$ is normal to each reaction vector.

There will be paths along which the kth reaction is isoaffine; these directions must be normal to the vector ∇A_k. If the system is closed, and $d\mathbf{s}=0$, then a necessary and sufficient condition for the kth reaction to be isoaffine is

$$\nabla A_k\cdot\Sigma_j\boldsymbol{\nu}_j d\xi_j=0. \tag{7}$$

The more stringent condition that $d\xi_j=0$ for all j, which De Groot[1] considered to be necessary is actually sufficient but not necessary.

[1] S. R. De Groot, *Thermodynamics of Irreversible Processes* (Interscience Publishers, New York, 1951), p. 174.

The Vibrational Assignment and Thermodynamic Properties of *N*-Dimethylaminodiborane

D. E. Mann
National Bureau of Standards, Washington 25, D. C.
(Received February 8, 1954)

In a recent paper[1] the vibrational spectra and assignments of *N*-dimethylaminodiborane $(CH_3)_2NB_2H_5$ and its deuteriated relative $(CH_3)_2NB_2D_5$ were presented. Calorimetric and more extensive infrared data that have now become available for $(CH_3)_2NB_2H_5$ permit some refinements in the original assignment to be made, an estimate of the barrier to internal rotation of the methyl groups to be given, and a table of thermodynamic functions to be computed with greater reliability than was previously possible.

As part of a more general program now under way at the National Bureau of Standards the infrared spectrum of gaseous $(CH_3)_2NB_2H_5$ has been redetermined and extended down to about 400 cm^{-1} by Stewart,[2] and its third-law entropy evaluated from calorimetric data by Furukawa *et al.*[3] Stewart lists several bands not reported in I but most of them are weak bands, shoulders, and branches brought out at the higher vapor pressures used, and are easily interpreted. The bands found in the region not accessible in I are clustered in two broad, poorly resolved groups: 415(m), 424(m), 434(m), 440(m), and 596(w), 611(w), 616(w), 635(w).

The only changes in the original assignment warranted by the new data are confined to the four angular motions of the dimethylamino group, *viz.*, $\nu_{13}(\delta)$, $\nu_{20}(\tau)$, $\nu_{30}(\beta)$, and $\nu_{41}(\rho)$. In I these modes were assigned, respectively, the frequencies 399, 236, 279, and 399 cm^{-1}, obtained from the Raman spectrum of the liquid. The 415–440 cm^{-1} infrared cluster may be identified, in part at least, with the 399 Raman line, though the reason for the discrepancy is not clear. The appearance of the envelope suggests that it comprises at least two bands whose centers are probably near 434 and 424 cm^{-1}. The usefulness of 434 and 424 as well as 315 and 279 in various binary combinations, particularly those needed to explain some of the weak bands first reported by Stewart, suggests that they be ascribed to fundamental vibrations. The revised assignment is 434$(a_1;\delta)$, 315$(a_2;\tau)$, 279$(b_1;\beta)$, and 424$(b_2;\rho)$. The evidence in favor of 315 as a fundamental is somewhat ambiguous since the Raman line at 325 has already been assigned to the b_2 bridge hydrogen bending mode. It is, however, more useful and plausible than 236 for the present purpose. The 596–635 group of bands may be explained as 279+315=594, 896−279=617, 2×315=630, and 950−315=635.

The present assignment can now be used with the entropy value reported by Furukawa *et al.*[3] to estimate the restricting potential for the methyl groups. The experimental entropy for $(CH_3)_2NB_2H_5$ as an ideal gas at one atmos and 271.60°K is 72.25±0.14 eu. The structural data given by Hedberg and Stosick[4] were used for the calculation. The three principal moments of inertia are 145.904, 166.710, and 204.202×10^{-40} g cm^2. The reduced moment of inertia for internal rotation is 5.123×10^{-40} g cm^2. The total symmetry number is 18 with these factors: 3 for each internal rotation and 2 for the over-all rotation. The entropy of translation, over-all rotation, and free enternal rotation for *N*-dimethylaminodiborane in the ideal gaseous state at one atmos is then $S^0_{T+R+F.I.R.}=13.225+22.878\log_{10}T$ eu. The restricting potential V_0 required to give agreement with the experimental entropy is 3.9 kcal/mole. This result accords well with the barriers reported for neopentane,[5] $V_0=4.3$ kcal/mole, and 1,1-dimethylcyclopentane,[6] $V_0=5.3$ kcal/mole. The barrier just suggested would explain the Raman line at 236 cm^{-1}.

The restricting potential, modified assignment, and moments of inertia given in this note were used to compute the thermodynamic functions presented in Table I. The tables of Pitzer and Gwinn[7] were used to calculate the contributions from the hindered rotations. The uncertainty is probably no greater than 2 percent in the C_p^0/R entries and is less for the other functions.

TABLE I. Calculated thermodynamic functions in dimensionless units for $(CH_3)_2NB_2H_5$ for the ideal gaseous state at 1 atmos and a barrier of 3.9 kcal/mole.

T°K	C_p^0/R	$(H^0-E_0^0)/RT$	$-(F^0-E_0^0)/RT$	S^0/R
200	9.89	6.20	26.64	32.84
300	14.16	8.00	29.71	37.71
400	18.45	10.00	32.42	42.42
500	22.18	12.00	34.97	46.97
600	25.27	13.91	37.40	51.31
700	27.86	15.68	39.73	55.41
800	30.03	17.30	41.98	59.28
900	31.87	18.79	44.15	62.94
1000	33.44	20.15	46.23	66.38
1100	34.78	21.40	48.24	69.64
1200	35.93	22.44	50.17	72.71
1300	36.91	23.59	52.04	75.63
1400	37.76	24.55	53.85	78.40
1500	38.49	25.44	55.59	81.03

The author is grateful to Dr. C. W. Beckett for helpful discussions, and to Dr. G. T. Furukawa and Mr. J. E. Stewart for permitting him to use their data in advance of publication.

[1] D. E. Mann, J. Chem. Phys. **22**, 70 (1954). This paper will be denoted by I in the present note.
[2] J. E. Stewart (private communication).
[3] G. T. Furukawa (private communication).
[4] Hedberg and Stosick, J. Am. Chem. Soc. **74**, 954 (1952).
[5] K. S. Pitzer, Disc. Faraday Soc. No. 10, 66 (1951).
[6] Epstein, Barrow, Pitzer, and Rossini, J. Research Natl. Bur. Standards **43**, 245 (1949).
[7] Pitzer and Gwinn, J. Chem. Phys. **10**, 428 (1942).

The Effect of Channel Holes on the Force Exerted by Effusing Vapors*

Robert D. Freeman and Alan W. Searcy
Department of Chemistry, Purdue University, West Lafayette, Indiana
(Received February 8, 1954)

A method for determination of vapor pressures of 10^{-7} to 10^{-4} atmosphere has been developed by Mayer,[1] Vollmer,[2] and others.[3–5] In this method the force exerted by a vapor as it effuses from a small orifice is measured directly. For effusion from a hole of infinitesimal length, $P=2F/\pi r^2$, where P is the pressure

in the effusion cell, F is the force, and r is the radius of the hole. We shall derive the relationship between the pressure in the cell and the resultant force when a hole of finite length is used.

Clausing[6] has derived correction factors which are applicable to pressure determinations by the Knudsen method.[7] However, these factors cannot be used to calculate the pressure in a cell from the force exerted by vapor effusing from the cell because the force depends on the angular distribution of effusing molecules as well as on their number. The form of this angular distribution has also been derived by Clausing.[8] Changing his term for the solid angle $d\omega/\pi$ to polar coordinates with the axis of the hole as the reference axis gives

$$K_{(\theta)}d\theta=2\nu_1\pi r^2T\cos\theta\sin\theta d\theta. \quad (1)$$

Where θ is the angle measured from the reference axis, $K_{(\theta)}d\theta$ is the number of molecules effusing per second between θ and $\theta+d\theta$, ν_1 is the number of molecules incident on the walls of the container per cm² per second, and T is a complicated function of θ and the length L and radius r of the hole.

The resultant force F acting on the vapor container along the axis of the hole is

$$F=\int_0^{\pi/2}p\cos\theta K_{(\theta)}d\theta=2\nu_1\pi r^2p\int_0^{\pi/2}T\sin\theta\cos^2\theta d\theta, \quad (2)$$

where p is the mean momentum of the molecules. Equation (2) cannot, in general, be integrated analytically; it may, however, be evaluated to any desired degree of accuracy by Simpson's method.[9] In the limiting case $L/r=0$, T reduces to unity and Eq. (2) may be integrated to yield

$$F_0=2\nu_1\pi r^2p/3 \quad (3)$$

which is the result obtainable from elementary kinetic theory, F_0 designating the limiting case.

Division of Eq. (2) by Eq. (3) gives the ratio f of the force resulting from vapor effusing through a hole for which $L/r>0$, to the force expected under the same conditions except that $L/r=0$; thus,

$$f=\frac{F}{F_0}=3\int_0^{\pi/2}T\sin\theta\cos^2\theta d\theta. \quad (4)$$

From Eq. (4) it follows that the relation between the pressure in a cell and the force resulting from the effusion of vapor from the cell through a hole for which $L/r>0$ is

$$P=2F/\pi r^2f. \quad (5)$$

The correction factors f for values of L/r between 0.0 and 2.0 are given in column 4 of Table I. For the integration of Eq. (4) by Simpson's method, $T\sin\theta\cos^2\theta$ was calculated at $\theta=0$, 15, 30, 45, 60, 75, and 90° for each value of L/r. The equation

$$1/f=0.0147(L/r)^2+0.3490(L/r)+0.9982 \quad (6)$$

reproduces the tabulated values of f within ±0.2 percent over the range $0\leqslant L/r\leqslant 2.0$.

TABLE I. Correction factors for the effect of channel holes on the number and force of effusing molecules.

L/r	K	K'	f
0	1	1	1
0.2	0.9092	0.913	0.938
0.4	0.8341	0.831	0.877
0.6	0.7711	0.769	0.825
0.8	0.7177	0.719	0.778
1.0	0.6720	0.674	0.734
1.2	0.6320	0.633	0.694
1.4	0.5970	0.599	0.660
1.6	0.5659	0.567	0.627
1.8	0.5384	0.538	0.597
2.0	0.5136	0.512	0.570

For comparison, columns 2 and 3 of Table I list calculated probabilities that molecules entering one end of holes with L-to-r ratios between 0 and 2.0 will escape through the other end. The values K in column 2 were calculated by Clausing.[6] Values K' in column 3 were calculated by us from Clausing's equation for the angular distribution of effusing molecules [Eq. (1) in this note].

* Work supported by U. S. Office of Naval Research.

[1] H. Mayer, Z. Physik **67**, 240 (1931).
[2] M. Vollmer, Z. physik. Chem. Bodenstein Festband, 863 (1931).
[3] Neumann and Völker, Z. physik. Chem. **A161**, 33 (1932).
[4] K. Niwa, and Z. Shibata, J. Fac. Sci. Hokkaido Imp. Univ. **3**, 53 (1940).
[5] G. Wessel, Z. Physik. **130**, 539 (1951).
[6] P. Clausing, Ann. Physik. **12**, 961 (1932).
[7] S. Dushman, *Scientific Foundations of Vacuum Technique* (John Wiley and Sons, Inc., New York, 1949), pp. 18–24, 90–101.
[8] P. Clausing, Z. Physik. **66**, 471 (1930).
[9] See any standard calculus textbook.

Concentration Dependence of Differential Capacity in Electrolytes at the Electrocapillarity Maximum

J. ROSS MCDONALD
Texas Instruments Incorporated, Dallas, Texas
(Received January 18, 1954)

FROM an electrolyte such as aqueous NaF which exhibits no ionic adsorption on cathodic polarization at an ideal polarized electrode,[1] information concerning the structure of the double layer at this electrode can be obtained from the dependence of differential capacitance on concentration at the electrocapillarity maximum potential (abbreviated as "ecm" potential): the potential at which there is no charge on the electrode.[1]

When a negative potential numerically greater than the ecm potential is applied, the resulting double layer probably consists of a negative charge density on the metal electrode, a charge-free layer of thickness x_0 beginning at the electrode, and a diffuse space-charge layer of excess positive ions and fewer-than-normal negative ions extending from $x=x_0$ into the material. The total differential capacitance per unit area is $C_T{}^d=d\sigma_m/dV_a=d\sigma_m/dV_0$. Here σ_m is the charge density on the electrode, V_a is the applied potential, and V_0 is a (negative) potential referred to the ecm potential as zero. The distance x_0 may be interpreted as the sum of the ionic radius of the nearest positive ions and the diameter of any hydrated water molecules possibly present between the ions and the electrode.

Work of the author in progress is concerned with a theoretical treatment of the dependence of $C_T{}^d$ on V_0. The resulting expression for $C_T{}^d$ at $V_0=0$ is particularly simple and is $C_T{}^d=C_1{}^0/[1+\gamma]$. Here, $C_1{}^0=\kappa_1{}^0/4\pi x_0{}^0$ and $\gamma=\kappa_1{}^0L_D{}^0/\kappa_2{}^0x_0{}^0$. $\kappa_1{}^0$ and $\kappa_2{}^0$ are the differential dielectric constants[2] of the charge-free layer and the diffuse layer, respectively, for $V_0=0$, and $L_D{}^0$ is the Debye length for ions in the diffuse part of the double layer for $V_0=0$.[3] $C_1{}^0$ is the differential capacitance of the charge-free region for $V_0=0$; $C_T{}^d$ is therefore the series combination of this capacitance and that of the diffuse double layer.

If $C_T{}^d$, $L_D{}^0$, and $\kappa_2{}^0$ are known from experiment, $\kappa_1{}^0/x_0{}^0$ can be unambiguously obtained. Table I shows the results of such a calculation for five concentrations of NaF at 25°C. The data are recent accurate results of Grahame.[4] The value of $C_T{}^d$ at $V_0=0$ was obtained by graphical interpolation of Grahame's curves of $C_T{}^d$ *versus* V_a and from Grahame's results for the ecm potential.[4] In column three, $L_D{}^0$ was calculated from the known concentration and a static dielectric constant of 78.5;[5] the same value was used for $\kappa_2{}^0$. Small changes in these latter two quantities with electrolyte

TABLE I.

Normality	Experimental $C_T{}^d$ at $V_0=0$ (μf/cm²)	$\frac{L_D{}^0}{\kappa_2{}^0}$ (cm)	$\frac{x_0}{\kappa_1{}^0}$ (cm)	Theoretical $C_T{}^d$ at $V_0=0$ (μf/cm²)
10^{-3}	5.98	1.216×10^{-8}	2.64×10^{-9}	5.81
10^{-2}	13.04	3.842×10^{-9}	2.95×10^{-9}	12.80
10^{-1}	20.67	1.216×10^{-9}	3.060×10^{-9}	20.70
0.660	24.83	4.740×10^{-10}	3.086×10^{-9}	25.00
0.916	25.71	4.028×10^{-10}	3.037×10^{-9}	25.50

concentration were neglected. The first two quantities in column four represent small differences between large numbers and are thus rather inaccurate. It is apparent, however, that the ratio x_0^0/κ_1^0 is substantially independent of electrolyte concentration in the range here considered. The average of the last three quantities in this column is $x_0^0/\kappa_1^0=3.061\times10^{-9}$ cm. The resulting value of C_1^0 is 28.9μf/cm^2. This average value of x_0^0/κ_1^0, a single number derived from the experimental data, was then used to compute the values of $C_T{}^d$ shown in the final column of the table. Agreement between theoretical and experimental values of $C_T{}^d$ is excellent for all concentrations.

The value of x_0^0/κ_1^0 is the most interesting result of this analysis. If κ_1^0 is taken as 78.5, x_0^0 is 24A. This large a value of x_0^0 would require several water molecules between the nearest positive ion and the electrode. Such a distribution is unlikely. The most reasonable explanation of these results is that the ions are hydrated with single water molecules between nearest ions and the electrode. If we assume that κ_1^0 for the water molecule is partly saturated by the local field of the positive ion and has an initial value of 10 at $V_0=0$, then $x_0^0=3.1$A. This value is reasonable for the combined radius of a Na^+ ion and the diameter of the hydrated water molecule. Further, $\kappa_1^0\cong10$ allows the full curve *versus* V_0 to be explained theoretically, as will be demonstrated in a later paper. The author is greatly indebted to Professor Grahame for permission to use his fine data prior to publication.

[1] D. C. Grahame, Chem. Revs. **41**, 441 (1947).
[2] D. C. Grahame, J. Chem. Phys. **18**, 903 (1950).
[3] x_0^0 is the value of x_0 at $V_0=0$.
[4] Private communication.
[5] Dorsey, *Properties of Ordinary Water-Substance* (Reinhold Publishing Corporation, New York, 1940) p. 367.

The Application of a High-Speed Digital Computer to Molecular Vibration Problems*

D. E. Mann, L. Fano, and W. F. Cahill, *National Bureau of Standards, Washington, D. C.*

and

T. Shimanouchi,†‡ *The American University, Washington, D. C.*

(Received February 8, 1954)

We have devised and used a code with which the SEAC[1] has been applied to the solution of the characteristic equations common to all molecular vibration problems. An iteration procedure has been used to find all the eigenvalues of a matrix of order 12. The method has also been used to handle a large number of smaller matrices of order 6. The entire computation is quite rapid, and high accuracy is preserved throughout. The code is applicable not only to similar equations derived from other types of physical problems but also to much larger matrices. The time required to solve completely a typical 12 by 12 matrix is of the order of one to two hours. For a 6 by 6 matrix the time is around 15 minutes. Results are printed out directly and can be given to as many as 11 significant figures.

For computational convenience the familiar GF formulation,[2] $GFL=L\Lambda$, was replaced by its symmetrized equivalent,[3] $D'FDY=Y\Lambda$, where $L=DY$, D gives the transformation from mass-adjusted Cartesian to internal coordinates, the prime indicates matrix transposition, and the other symbols have their usual significance.[2] The use of $(D'FD-I\lambda_\alpha)y_\alpha=0$ has other practical advantages. It is easy to set up D directly, and the need for G is avoided. Symmetry factoring can still be applied with the aid of Cartesian symmetry coordinates; internal symmetry coordinates are not necessary. Characteristic vectors in terms of the mass-adjusted Cartesian coordinates are useful. If the l's are needed they can be obtained easily from $l=Dy$. It is not necessary to consider redundancies.

The iteration procedure used to solve $(D'FD-I\lambda_\alpha)y_\alpha=0$ is conventional.[4] Let $D'FD=A$, let y_α be the correct vector appropriate to A and λ_α, let $y_\alpha{}^{(n)}$ and $\lambda_\alpha{}^{(n)}$ be the nth approximations to y_α and λ_α, respectively, Then the iteration scheme proceeds essentially as follows. An arbitrary vector $y_\alpha{}^{(n)}$ is used to obtain an approximation to the largest root $\lambda_\alpha{}^{(n)}$ by means of the familiar Rayleigh quotient $\lambda_\alpha{}^{(n)}=y_\alpha{}'^{(n)}Ay_\alpha{}^{(n)}/y_\alpha{}'^{(n)}y_\alpha{}^{(n)}$. The vector $y_\alpha{}^{(n)}$ is then improved by $y_\alpha{}^{(n+1)}=Ay_\alpha{}^{(n)}/\lambda_\alpha{}^{(n)}$. This process is continued until convergence of successive approximations to y_α is obtained. This automatically ensures convergence to λ_α. After the largest root has been found the matrix A is modified by the scheme $A_\beta=A-[\lambda_\alpha(y_\alpha y_\alpha')/(y_\alpha'y_\alpha)]$, and the entire procedure is repeated with A_β, $y_\beta{}^{(n)}$, and $\lambda_\beta{}^{(n)}$. The iteration routine and matrix modifications are carried out until all the roots and vectors, including those which are zero, have been found. Normally an iteration is continued until the first nine significant figures of each element of the vector are stationary. Each complete iteration step, from the nth to the $(n+1)$th approximation, takes about $\frac{1}{3}$ to $\frac{1}{2}$ second. The number of iterations required increases sharply if two roots happen to be close but not degenerate. No difficulty was encountered in separating the vectors which correspond to fundamentals only a few wave numbers apart.

The present code has already been applied to the study of the planar and nonplanar vibrations of a large number of ethylenes. Other SEAC codes have been developed and used successfully for the calculation of the matrix products and reciprocals involved in statistical and least-squares techniques for finding best sets of force constants. Details of all these applications will be published later.

It is a pleasure to acknowledge the constant support and encouragement given us in this work by members of the Thermodynamics and Computation sections at the National Bureau of Standards.

* This work was supported in part by the U. S. Office of Naval Research under contract NAonr 112-51.
† Work performed under contract with the National Bureau of Standards.
‡ Present address: Chemistry Department, Faculty of Sciences, Tokyo University, Tokyo, Japan.
[1] SEAC is the designation for the National Bureau of Standards Eastern Automatic Computer. See: Natl. Bur. Standards Tech. News Bull. **34**, 121 (1950); Proc. Inst. Radio Engrs. **41**, 1300 (1953). See also: "The Incorporation of Sub-Routines into a Complete Problem on the NBS Eastern Automatic Computer," Math. Tables and Other Aids to Computation **4**, 164 (1950).
[2] E. B. Wilson, Jr., J. Chem. Phys. **7**, 1047 (1939); **9**, 76 (1941).
[3] P. Torkington, J. Chem. Phys. **17**, 1026 (1949).
[4] W. M. Kincaid, Quart. Appl. Math. **5**, 320 (1947).

Erratum: Studies by Infrared Spectra on the Initiation Process in Autoxidation of Methyl Linolenate

[J. Chem. Phys. **21**, 952 (1953)]

N. A. Khan
Hormel Institute, Austin, Minnesota

Page 952, third paragraph, line 15, "These unstable peroxides" should read: "These unstable hydroperoxides" and line 19 "structure of the peroxides,": "structure of the hydroperoxides."

This paragraph should also include: "1. These results along with the infrared absorption by hydroxyl group of hydroxylinolenate at 2.94μ indicate that methyl linolenate forms monomeric monohydroperoxide at the initial stage of autoxidation. 2. Oxygen-free nitrogen was bubbled through all the samples as a measure of precaution against further oxidation, wherever it was necessary."

Errata: A Study of Two-Center Integrals Useful in Calculations on Molecular Structure. I, II

[J. Chem. Phys. 19, 1445, 1459 (1951)]

C. C. J. ROOTHAAN AND KLAUS RUEDENBERG
Laboratory of Molecular Structure and Spectra, Department of Physics, University of Chicago, Chicago, Illinois

I—P. 1446, left column, the third equation in formula (10) should read:

$$\text{“}S_{l,-|m|}(\theta,\phi)=(i/\sqrt{2})\{\cdots\text{.”}$$

P. 1448, left column, line 23, the equation in this line should read:

$$\text{“}\int\Omega_b dv/r_a=[a|\Omega_b]\text{,”}$$

i.e., the factor Z should be omitted.

P. 1453, lower part of the page, the formula for $[2S_a|2S_b]$ should read:

$$(\zeta/\rho)[1-(1-\kappa)^2\{(1/12)(6-\kappa-8\kappa^2-4\kappa^3)+(1/3)(1-\kappa-\kappa^2)\rho_a$$
$$+(1/18)(1-2\kappa)\rho_a^2\}e^{-2\rho_a}-(1+\kappa)^2\{(1/12)(6+\kappa-8\kappa^2+4\kappa^3)$$
$$+(1/3)(1+\kappa-\kappa^2)\rho_b+(1/18)(1+2\kappa)\rho_b^2\}e^{-2\rho_a}].$$

P. 1456, upper part of the page, the formula for $[3S_a|2P\Sigma_b]$ should read:

$$[3S_a|2P\Sigma_b]=\frac{\zeta}{\rho^2}\left\{1-\left(1+2\rho+2\rho^2+\frac{83}{64}\rho^3\right.\right.$$
$$\left.\left.+\frac{19}{32}\rho^4+\frac{47}{240}\rho^5+\frac{2}{45}\rho^6+\frac{1}{180}\rho^7\right)e^{-2\rho}\right\},$$

Note: All expressions in Eqs. (34), (34_a), (34_b) have recently been rechecked by an entirely different method. No error or misprint was found except the two reported in these Errata.

II.—P. 1463, right column, third table from the bottom $(2p\pi_a 3d\pi_b\Sigma)$: The number “1” standing in the fifth row and first column *should stand* in the *fourth* row and *first* column.

P. 1464, right column: } The heading should read: “II-type dis-
P. 1465, left column: } tributions continued.”

P. 1466–1467: Additional note to Sec. 1, III: “The total number of exchange integrals between orbitals with quantum numbers 1, 2, and 3 is 1175. There are 577 exchange integrals of Σ type, 462 of Π type, 123 of Δ type, 12 of Φ type, and 1 of Γ type.”

P. 1467, left column, line 30, should read: “When the exponents $\zeta\cdots$.”

P. 1467, Table III: The right-hand side of the second equation in this table should read:

$$\text{“}\cdots=[\chi_a(1)\bar{\chi}_a(2)|1/r_{12}|\chi_b'(1)\bar{\chi}_b'(2)]\text{.”}$$

P. 1469, reference 13: The last line of this reference should read: “reference 13a) have given$\cdots$.”

P. 1469, right column, formula (2.33), the right-hand side of this equation should read:

$$\text{“}\cdots=(-1)^{l+M}\omega_n{}^l(-\beta)\text{.”}$$

P. 1470, left column, lines 9 and 10: The sentence in parentheses “(For ... inappropriate)” should be omitted.

P. 1471, left column, Eq. (3.23′) should read:

$$\text{“}\Phi_{n\bar{n}}=(1/\alpha\bar{\alpha})\{\bar{\alpha}n\Phi_{(n-1)\bar{n}}+\alpha\bar{n}\Phi_{n(\bar{n}-1)}-\cdots\text{.”}$$

P. 1473, reference 17, the last figure should read: “115.”

P. 1476, left column, add the following new references: “Calculations of exchange integrals with Σ-type charge distributions were reported by E. P. Wohlfahrt in Nature **163**, 57 (1949), and by H. Kaplan, Phys. Rev. **85**, 1038 (1952).”

Erratum: A Note on the Kinetics of Unitary Processes

[J. Chem. Phys. 21, 2227 (1953)]

STUART A. RICE
Gibbs Memorial Laboratory, Harvard University, Cambridge, Massachusetts

THE last equation should read

$$\langle s\rangle=k_0 t.$$

The Electronegativities and some Electron Affinities of Copper, Zinc, and Gallium Subgroup Elements

AUBREY P. ALTSHULLER
1911 Clover Street, Cleveland, Ohio

(Received February 2, 1954)

IN the present note, the electronegativities of the Cu, Zn, and Ga subgroup elements will be calculated by the thermochemical (T.C.) method. Gordy[1] has evaluated the electronegativities of these elements by means of his empirical method relating electronegativities (E.N.) to force constants and bond distances. The results of the two methods differ somewhat and there is some reason to believe that the T.C. results are somewhat more satisfactory. If Mulliken's relationship[2] is reversed, then the electron affinities (E.A.) of some of these elements may be calculated using the values of E.N. calculated thermochemically or by Gordy's method.

The dissociation energies of the halides and hydrides used for the T.C. calculations of the electronegativities given in Table I

TABLE I. Electronegativity and electron affinity values.

Element	$(E.N.)_a$	$(E.N.)_g$	E.N. (Gordy)	E.A. (T.C.)	E.A. (G)
Cu	1.6	1.2	2.0(1.7–2.3)	2.4 ev	4.9 ev
Ag	1.6	1.2	1.9(1.6–2.1)	2.5	4.4
Au	1.8	1.3	3.1(3.0–3.9)	2.1	10.3
Zn	1.7	1.6	1.2	...	...
Cd	1.9	1.7	1.1	...	...
Hg	...[a]	2.2	1.0	...	...
Ga	1.2	0.9	1.4	...	...
In	1.2	0.9	1.4	...	...
Tl	1.3	1.0	1.3	2.1	2.1

[a] $(E.N.)_a{}^2$ is negative.

are taken from Gaydon's compilation[3] and Landolt-Börnstein.[4] (It is assumed that Cu, Ag, Au and Ga, In, Tl have little, if any, tendency to form diatomic molecules M_2 in the gaseous state.) The quantities $(E.N.)_a$ and $(E.N.)_g$ given in columns 2 and 3 are the electronegativities calculated assuming the arithmetic and geometric mean of the dissociation energies of homopolar molecules. The electronegativities given by Gordy are listed in column 4 except for Cu for which Cu$-X$ distances given in Landolt-Börnstein[4] are used for recalculating the E.N. The values listed in column 4 are calculated from the halides and hydrides except that the limits listed in parenthesis are those calculated from the Cu subgroup hydrides by Gordy.

The electron affinities of Cu(I), Ag, Au(I), and Tl(I) given in columns 5 and 6 are calculated from E.A.$=6.3$ (E.N.)$-$I,[5] where E.N. is $(E.N.)_a$ or E.N.(G). (The ordinary ionization potentials are used.)

The E.N. values for Cu, Ag, Ga, In, and Tl calculated by the T.C. method $(E.N.)_a$ give fairly good agreement with Gordy's values. The $(E.N.)_g$ values are generally smaller than the values of $(E.N.)_a$ and in considerable disagreement with Gordy's values.[1] It does not seem too probable, on the basis of the general properties of the Cu and Ga subgroup elements and their compounds, that these elements would be as electropositive as indicated by the $(E.N.)_g$ values.[6]

The value of 3.1 for the E.N. of Au calculated by Gordy seems out of line with the other values listed. It does not seem likely that a Group I metal would be more electronegative than the Group VII nonmetals Cl, Br, and I.

The E.N. values calculated for Zn, Cd, and Hg are much higher than those calculated by Gordy[1] whose values seem somewhat small. For example, Hg has the same E.N. as Li on Gordy's scale. Using the ordinary ionization potential[4] and the electron affinity of Hg,[7] Mulliken's relationship gives E.N. = 1.9. If the valence state I and E.A. were available, E.N. would probably come out to be somewhat larger than 1.9. This estimate of E.N. for Hg is in good agreement with the T.C. value.

The electron affinities calculated from the T.C. data,[8] $(\text{E.N.})_a$, for Cu(I), Ag, Au(I), and Tl(I) of from 2.1 to 2.5 ev (50–60 kcal) are somewhat larger than those for the alkali metals[7] or mercury[7] but they are fairly reasonable. The electron affinities calculated from Gordy's values for the Cu subgroup elements range from 4.4 to 10.3 ev (100 to 240 kcal). These values seem excessively large for metallic elements. The assumption that the ordinary ionization potentials are satisfactory may be somewhat incorrect especially for Tl(I) which appears to have some $s-p$ hybridization.[9] The electron affinities of 50–60 kcal which have been calculated here may be regarded only as very approximate values which in some cases may only represent the upper limits for the electron affinities.

[1] W. Gordy, J. Chem. Phys. **14**, 305 (1946).
[2] R. S. Mulliken, J. Chem. Phys. **2**, 782 (1934).
[3] A. G. Gaydon, *Dissociation Energies and Spectra of Diatomic Molecules* (John Wiley and Sons, Inc., New York, 1947).
[4] Landolt-Börnstein, *Numerical Values and Functions from Physics, Chemistry, Astronomy, Geophysics and Technology* (Springer-Verlag, Berlin, 1950), Molecular Physics, Parts I and II.
[5] H. A. Skinner and H. O. Pritchard, Trans. Faraday Soc. **49**, 1254 (1953).
[6] If some of these elements should have small dissociation energies then the differences in $(\text{E.N.})_a$ and $(\text{E.N.})_g$ would be decreased. For example, if Tl formed Tl_2 with $D(Tl_2) = 0.2$ ev, then $(\text{E.N.})_a = 1.3$ and $(\text{E.N.})_g = 1.15$.
[7] H. O. Pritchard, Chem. Revs. **52**, 529 (1953).
[8] If the $(\text{E.N.})_g$ values for these elements were used, the E.A. values calculated would be zero or negative. If E.A. is approximately inversely proportional to the atomic radius for elements with the same outer valence shells, then the Cu subgroup elements with much smaller radii (Cu, 1.27A; Ag, 1.44A; Au, 1.45A) than the alkali metals (Li, 1.52A to Cs, 2.62A) should have somewhat larger values for their electron affinities.
[9] B. P. Dailey, J. Phys. Chem. **57**, 490 (1953).